

**AN INVESTIGATION OF SUPPORTED  
PLATINUM AND BIMETALLIC  
OXIDATION CATALYSTS**

by

Michael J. Tiernan, B.Sc.(Hons.)

A Thesis presented to Dublin City University for the degree of Doctor  
of Philosophy.

This work was carried out under the supervision of Dr. Odilla  
Finlayson, School of Chemical Sciences, at Dublin City University.

September, 1996.

**I hereby certify that this material, which I now submit for assessment on the programme of study leading to the award of Ph.D. is entirely my own work and has not been taken from the work of others save and to the extent that such work has been cited and acknowledged within the text of my work.**

Signed : Michael Tiernan  
**MICHAEL TIERNAN**

Date : 25/9/1996

## TABLE OF CONTENTS

<u>Section</u>	<u>Page</u>	
Abstract	i	
Acknowledgements	ii	
General Introduction	iii	
<b><u>Chapter 1:</u></b>	<b>Catalytic Combustion</b>	
<b>1.1</b>	<b>Introduction</b>	<b>2</b>
<b>1.2</b>	<b>Catalytic Combustion on Metal Oxides</b>	<b>3</b>
<b>1.3</b>	<b>Catalytic Combustion On Noble Metals</b>	<b>8</b>
	1.3.1 Oxidation of Methane	11
	1.3.2 Oxidation of Higher Hydrocarbons	32
	1.3.3 Automotive Exhaust Catalysts	48
<b>1.4</b>	<b>Use of Ceria in Supported Noble Metal Combustion Catalysts</b>	<b>53</b>
	1.4.1 Oxygen Storage Capacity and Water Gas Shift Activity	53
	1.4.2 Oxidation of Carbon Monoxide	59
	1.4.3 Oxidation of Hydrocarbons	77
<b>1.5</b>	<b>Summary</b>	<b>92</b>
	<b>References</b>	<b>98</b>

## **Chapter 2: Catalyst Preparation and Characterisation.**

<b>2.1</b>	<b>Introduction</b>	103
	2.1.1 Catalyst Preparation	103
	2.1.2 Catalyst Characterisation	104
<b>2.2</b>	<b>Experimental</b>	118
	2.2.1 Preparation of Catalysts	118
	2.2.2 BET Surface Area	120
	2.2.3 Total Metal Content	122
	2.2.4 Metal Surface Area	123
<b>2.3</b>	<b>Results and Discussion</b>	133
	2.3.1 BET Surface Areas	133
	2.3.2 Total Metal Content	133
	2.3.3 Metal Surface Areas	134
<b>2.4</b>	<b>Summary</b>	147
	<b>References</b>	148

## **Chapter 3: Study of Pt/Al<sub>2</sub>O<sub>3</sub>, Pt-Ce/Al<sub>2</sub>O<sub>3</sub> and Pt/CeO<sub>2</sub> Catalysts.**

<b>3.1</b>	<b>Introduction</b>	151
	3.1.1 Temperature Programmed Reduction (TPR)	153
	3.1.2 X-ray Photoelectron Spectroscopy (XPS)	171
<b>3.2</b>	<b>Experimental</b>	176
	3.2.1 X-ray Photoelectron Spectroscopy (XPS)	176
	3.2.2 H <sub>2</sub> Chemisorption Measurements	176
	3.2.3 Temperature Programmed Reduction (TPR)	176
	3.2.4 Activity Measurements	178
	3.2.5 Sample Analysis	180
<b>3.3</b>	<b>Results and Discussion</b>	182
	3.3.1 Characterisation of 'Fresh' Catalysts	182
	3.3.2 Oxidation Activity and its Effect on the Catalyst Surfaces	212
	3.3.3 Effect of Aging on Activity and Surface Features	261
<b>3.4</b>	<b>Conclusions</b>	283
	<b>References</b>	287

**Chapter 4:** Study of Pt-Mn/Al<sub>2</sub>O<sub>3</sub>, Pt-Cr/Al<sub>2</sub>O<sub>3</sub> and Pt-Zr/ Al<sub>2</sub>O<sub>3</sub>  
Catalysts.

<b>4.1</b>	<b>Introduction</b>	<b>291</b>
<b>4.2</b>	<b>Experimental</b>	<b>293</b>
<b>4.3</b>	<b>Results and Discussion</b>	<b>294</b>
<b>4.4</b>	<b>Conclusions</b>	<b>324</b>
	<b>References</b>	<b>326</b>

<b>5</b>	<b>Conclusions</b>	<b>328</b>
----------	--------------------	------------

**Appendix A**

**Appendix B**

## **ABSTRACT**

A variety of supported Pt and bimetallic catalysts were investigated for the combustion of iso-butane and attempts were made to associate particular surface characteristics with combustion efficiency. In particular, the effects of Ce addition to Pt/Al<sub>2</sub>O<sub>3</sub> systems were studied. A number of other metal oxide (Mn, Cr, Zr) additives were investigated and the use of CeO<sub>2</sub> and ZrO<sub>2</sub> as alternative supports to Al<sub>2</sub>O<sub>3</sub> was also studied. The effect of high temperature (800°C) aging and reduction (500°C) on the activity of calcined catalysts was determined.

The use of Ce, Cr or Mn additives was found to be potentially beneficial for the iso-butane oxidation activity of Pt/Al<sub>2</sub>O<sub>3</sub>. TPR experiments showed that the addition of Ce, Cr, Mn or Zr to Pt/Al<sub>2</sub>O<sub>3</sub> resulted in a bimetallic surface interaction which affected surface reducibility. XPS indicated that the nature of Pt-Ce interaction varied depending on the loading of Ce. After impregnation and calcination at 630°C, the presence of Ce, at Ce : Pt  $\geq$  8 : 1 atomic ratio, generally resulted in poorer oxidation activity relative to Pt/Al<sub>2</sub>O<sub>3</sub> with higher temperatures required to achieve the same level of i-C<sub>4</sub>H<sub>10</sub> conversion. However, at lower Ce loadings (Ce : Pt  $\leq$  1 : 1 atomic ratio), oxidation activity was not so adversely affected and one sample, containing 0.29 wt.% Ce, was found to be noticeably more active than monometallic Pt/Al<sub>2</sub>O<sub>3</sub>. Reduction of a 0.5 wt.% Pt/Al<sub>2</sub>O<sub>3</sub> catalyst resulted in considerable loss of activity. The addition of Ce, Mn, or Cr appeared to help prevent this deactivation. Temperature Programmed Reduction (TPR) profiles indicated that the existence of an interaction between Pt and Ce in Pt-Ce/Al<sub>2</sub>O<sub>3</sub> samples was associated with improved activity following reduction.

In general, the activity of the Pt catalysts increased after initial testing in the reactant mixture. The most active 0.5 wt.% Pt/Al<sub>2</sub>O<sub>3</sub> catalysts were obtained after aging in the stoichiometric air : i-C<sub>4</sub>H<sub>10</sub> reaction mixture or in a static air atmosphere. H<sub>2</sub> chemisorption measurements indicated the main effect of aging was to increase Pt particle size. The reaction was concluded to be structure sensitive on Pt/Al<sub>2</sub>O<sub>3</sub> with sintered Pt crystallites being more active than highly dispersed smaller Pt particles. The presence of Ce, Mn, Cr or Zr additives had an adverse effect on the activity of Pt/Al<sub>2</sub>O<sub>3</sub> after aging in an O<sub>2</sub>-containing atmosphere.

After impregnation and calcination at 630°C, a 0.5 wt.% Pt/ZrO<sub>2</sub> catalyst was considerably more active than a 0.5 wt.% Pt/Al<sub>2</sub>O<sub>3</sub>. Addition of 2.3 wt.% Zr to a 0.5 wt.% Pt/Al<sub>2</sub>O<sub>3</sub> catalyst had, however, a detrimental effect on catalyst activity. It was concluded that the higher activity of Pt/ZrO<sub>2</sub> relative to Pt/Al<sub>2</sub>O<sub>3</sub> was due to the presence of larger Pt particles on the former support due to its considerably lower surface area.

## **ACKNOWLEDGEMENTS**

I wish to thank my supervisor, Dr. Odilla Finlayson, for her support and guidance throughout my years in Dublin City University. I would also like to thank my fellow postgraduate students and the academic and technical staff in the School of Chemical Sciences.

I am grateful to Mr. Sandy Monteith and all at the ETC in Brunel University for their hospitality during my visit. Thanks also to all those who helped in the preparation of this thesis especially Rhona, Spencer and Ted.

I must thank the many members of AG20 during my postgraduate years, particularly Dominic Delicato, Mick o Brien and Mick Giles. I wish to also express my gratitude to all in the 38 household for many good times during these years, particularly Ted, Shane, Data, Brian, Joe and Spencer.

A special word of gratitude to friends and family. In particular to my parents for their encouragement, guidance and help. Thanks.

## GENERAL INTRODUCTION

Heterogeneous catalytic combustion is widely used in domestic, industrial and environmental appliances (1). The main areas of application involve energy generation (catalytic heaters, catalytic boilers, catalytic gas turbines) and pollution control (car exhaust clean-up, odour abatement). Mixtures of fuel and air are passed over a catalyst maintained at a temperature high enough to favour total oxidation. Reaction occurs with the liberation of energy and oxidised products. Total oxidation is achieved in most cases, yielding carbon dioxide and water which may be safely discharged into the atmosphere.

When compared to conventional thermal combustion processes, catalytic combustion offers several advantages (2). The presence of a catalyst provides better control of oxidation over wider fuel:air ratios. In conventional processes too high a concentration of fuel may result in the feed mixture going outside explosion limits while with very low fuel:air ratios combustion may become unstable. Catalytic activation of the reactants also means it is possible to obtain complete combustion at lower operating temperatures. These low temperatures result in the minimisation of nitrogen oxide emissions. Nitrogen and oxygen react together at temperatures higher than approximately 1650°C. In thermal and flame combustion, thermal initiation of gas-phase radicals means such temperatures may be easily achieved. Catalytic combustion can be controlled to produce lower temperatures, and as a result, to produce significantly lower amounts of unwanted oxides. Energy recovery can also be improved by careful catalyst design, enabling a more efficient use of fuel. The main disadvantages are that the catalyst materials are often expensive (precious metals such as Pt are commonly used) and have a finite lifetime. High operating temperatures can cause thermal degradation of the active phase and/or the support material resulting in a gradual decline in performance. The catalyst can also be poisoned by strong adsorption of reactants, products or impurities on sites which would otherwise be available for catalysis.

The main requirements for an efficient combustion catalyst include high catalytic activity, high thermal stability and good resistance to poisoning (1). Depending on the application, the relative importance of these criteria can vary. For high temperature operation, such as in gas turbines, thermal resistance is very important. In such applications operating temperatures may be in the range 1100-1400°C (1). At these temperatures resistance to poisoning is not so important since many common poisons, such as sulphur and lead compounds, show little tendency to form stable compounds with the catalyst surface due to their high volatility. In addition, high activity may not play a major role in the choice of catalyst since differences in specific activity of different materials tend to be negligible at such high temperatures. In other areas, such as

exhaust gas treatment, operating temperatures and reactant concentrations can be much lower (3). Hence, a highly active catalyst is required to allow ignition of the fuel:air mixture at as low a temperature as possible and to maintain complete combustion at the lowest inlet temperatures and the highest values of mass throughput. The main focus of this thesis is on the development of efficient low temperature active catalysts for the combustion of iso-butane. A variety of supported (0.5wt.%) Pt catalysts are investigated and attempts are made to associate particular surface characteristics with combustion efficiency. In particular, the effect of Ce addition to Pt/Al<sub>2</sub>O<sub>3</sub> systems is investigated.

The structure of this thesis consists of four chapters. Chapter one involves a review of the relevant literature on combustion catalysts. In particular it details studies of the total oxidation activity of supported noble metal catalysts and their characterisation. The use of cerium as a non-noble metal additive is also reviewed.

Chapter two outlines the preparation and initial characterisation of the catalysts. In chapter three the activity of Pt/Al<sub>2</sub>O<sub>3</sub>, Pt-Ce/Al<sub>2</sub>O<sub>3</sub> and Pt/CeO<sub>2</sub> catalysts is investigated. The reducibility and activity of the various catalyst surfaces is examined and X-ray Photoelectron Spectroscopy analysis of the catalyst surfaces is discussed. The effects of high temperature aging in different environments (air, argon and the air : i-butane reaction mixture) on the combustion activity and surface properties of the catalysts are also investigated. Finally, the use of Pt/ZrO<sub>2</sub> is examined and compared to Pt/Al<sub>2</sub>O<sub>3</sub>.

Chapter four details a similar study of Al<sub>2</sub>O<sub>3</sub> supported Pt-Mn, Pt-Cr and Pt-Zr catalysts and all catalysts are compared with monometallic Pt/Al<sub>2</sub>O<sub>3</sub>.

## **CHAPTER 1**

### **Catalytic Combustion**

## **1.1 Introduction**

Metals (e.g. Pt, Ag), metal oxide-semiconductors (e.g.  $V_2O_5$ ,  $MoO_3$ ,  $CuO$ ) and complex semiconductors-spinels (e.g.  $CoAl_2O_4$ ,  $NiAl_2O_4$ ,  $CuAl_2O_4$ ) are the catalysts most widely used for the oxidation of hydrocarbons (1). The oxidation may be partial or total, both of which are industrially important processes. Selective partial oxidation is used for the production of numerous basic chemicals e.g. conversion of n-butane to maleic anhydride using vanadium pentoxide or the production of ethylene oxide from ethylene using silver catalysts (4). Complete combustion of hydrocarbons to  $CO_2$  and  $H_2O$  is widely used in pollution control and for the production of energy. Applications include the removal of volatile organic contaminants (VOCs) from industrial emissions (3), car-exhaust catalysts (5, 6, 7), fume abatement devices (8), and catalytic heaters, boilers and gas turbines (1, 9). This review will focus on studies involving complete oxidation catalysts.

Trimm (2) has reviewed the literature up to 1983 on kinetic studies of total oxidation involving catalysis. In general, the catalysts used can be classified as either metal oxides or noble metals.

In comparing the combustion activity of Pt and Pd with base metal oxides, several advantages associated with the noble metals have been found (1, 7):

- higher specific activity for hydrocarbon oxidation,
- greater resistance to the loss of low temperature activity,
- less deactivation by sulphur at temperatures below  $500^\circ C$ , and
- relative ease of preparation in a highly dispersed form on several different support materials .

The main advantages associated with the use of metal oxides are the lower cost of the raw material and the higher thermal stability at selected compositions (1). The latter fact makes the use of metal oxide systems in high temperature combustion applications particularly promising. Metal oxides also show greater resistance to certain poisons, especially halogens, As, Pb and P (3). However, in general, Zwinkels et al. (1) stated that because of their higher specific activity, which results in lower ignition temperatures, the use of noble metals as combustion catalysts has always been favoured. Although the main emphasis of this thesis is on the use of noble metal catalysts, a short review of the use of metal oxides as total oxidation catalysts will be detailed first. According to Spivey (3), the literature on catalytic oxidation over metal oxides is more

extensive than is that on noble metals. A fully comprehensive review is beyond the scope of this thesis, therefore only selected reviews and studies will be briefly discussed.

## **1.2 Catalytic Combustion on Metal Oxides.**

Golodets (10) classified metal oxide catalysts by the stability of the oxide. The most stable oxides ( $\Delta H_{298^\circ} > 270$  kJ/g-atom O) are the alkali and alkali earth metals, metals such as Sc, Ti, V, Cr, Mn, the rare earth metals and the actinides, Ge, In, Sn, Zn, Al. Oxides with intermediate stability ( $\Delta H_{298^\circ} = 166$ -270 kJ/g-atom O) include Fe, Co, Ni, Cd, Sb, Pb. Finally, oxides that are unstable ( $\Delta H_{298^\circ} < 166$  kJ/g-atom O) include the noble metals Ru, Rh, Pd, Pt, Ir, Au, and Ag. This classification presumes that the noble metals remain reduced during oxidation at moderate temperatures and that, even when supported on refractory oxides such as  $\text{Al}_2\text{O}_3$ , the mechanism of oxidation on these metals may involve only molecular oxygen in the incoming gas stream (3, 10). For some of the stable and intermediately stable metal oxides, lattice oxygen is known to be involved in the oxidation of hydrocarbons and other reactants in  $\text{O}_2$ -containing gas streams (3). A consequence of this classification of oxides is that there exists some level of optimum metal-oxygen interaction, above which the oxygen is adsorbed too strongly and effectively poisons the active sites and below which chemisorption is too weak, only a small fraction of the surface is covered and catalytic activity is low. This behaviour agrees with the commonly used "volcano" plot, shown in Fig 1.1, which describes the relationship between catalytic activity and strength of adsorption of reactants for many catalytic reactions (11). Some parameters which have been used to measure strength of oxygen adsorption are: the heat of formation of the oxide from the elemental metal (per oxygen atom), the heat of chemisorption of oxygen on evaporated metal films, the heat of dissociation of the first oxygen atom from the oxide and the heat of reaction for reoxidation of the catalyst (3).

Metal oxides have been classified on the basis of electrical conductivity into three groups by Spivey (3). These are n-type semiconductors, p-type semiconductors and insulators. On heating in air n-type oxides lose oxygen while p-type oxides gain oxygen. Oxygen adsorption occurs far more readily on p-type oxides because electrons can be easily removed from the metal cations to form active species such as  $\text{O}^{-2}$  or  $\text{O}^-$ . When electrons migrate in one direction, positive holes move in the opposite way; hence the term p-type semiconductors. These adsorbed oxygen species are highly reactive e.g.  $\text{O}^-$  is known to oxidise CO and  $\text{H}_2$  even at  $-196^\circ\text{C}$  (3). On n-type oxides oxidation occurs via lattice oxygen with oxide regeneration by gaseous  $\text{O}_2$ . No adsorbed oxygen species such as  $\text{O}^-$  are formed. Because adsorbed oxygen species are more reactive than lattice oxide

ions, p-type oxides are generally more active, especially for deep oxidation. Lattice oxygen is thought to be more important for the selective formation of partially oxidised products while both lattice and adsorbed species are thought to be involved in total oxidation. Insulators have very low electrical conductivity's because of the strictly stoichiometric metal-oxygen ratio in the lattice and very low electron mobility and are generally not active oxidation catalysts (3).

Highly active catalysts were thought to generally involve p-type oxides which adsorb oxygen at an optimum level producing very mobile chemisorbed surface oxygen (3). This is in agreement with the "volcano" plot shown in Fig. 1.1. The most active metal oxides were thought to be those of V, Cr, Mn, Fe, Co, Ni and Cu, based on these criteria and confirmed by experiment (3).

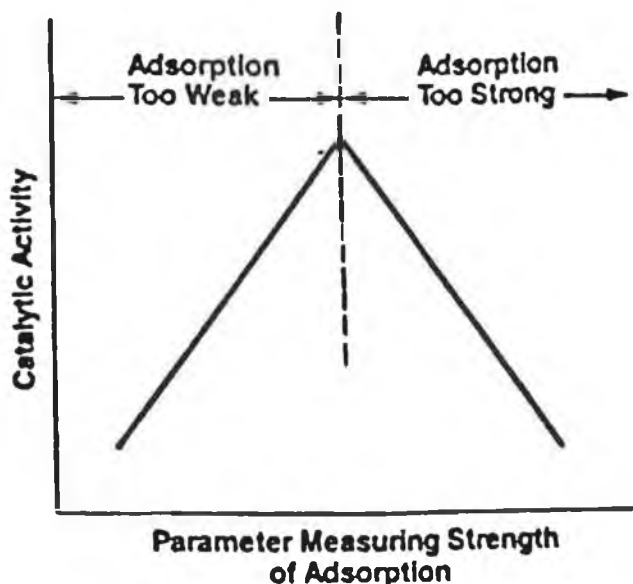
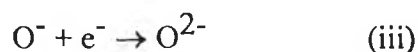
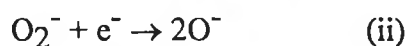
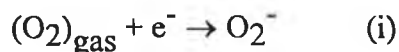


**Figure 1.1 : Catalytic Activity versus Strength of Chemisorption of Reactants (11).**

In 1990, Sokolovskii (12) reviewed the principles of oxidative catalysis on metal oxides and noted that the most active complete oxidation catalysts are those which bind oxygen at a high rate despite a low heat of oxygen adsorption. On interaction of oxygen with oxide catalysts, the  $O_2$  molecule undergoes primary activation to produce reactive radical ion forms,  $O^-$  and  $O_2^-$ . These species can then undergo further transition to become incorporated into the oxide lattice as  $O^{2-}$ . The steps involved can be shown as follows (3, 12);



where  $O^{2-}$  produced in step (iii) becomes incorporated into the oxide lattice. Active catalysts were thought to be ones which bind oxygen at a high rate to generate active states (steps (i) and (ii)) but slowly transform these states into oxide lattice ions (step (iii)), thereby providing a high concentration of reactive species on the catalyst surface. One of the most active oxide catalysts, namely cobalt oxide, was found to satisfy these criteria (12).

In a review of combustion catalysts for high temperature applications, Zwinkels et al. (1) stated that highly reactive adsorbed oxygen species were usually considered to be the important active sites for complete oxidation on metal oxides. On reviewing some studies of metal oxide systems, it was concluded that oxides containing Co, Cr, Mn, Fe, Cu and Ni were potentially interesting for catalytic combustion. The use of complex mixed oxides such as perovskites and spinels was also reviewed (1). At low temperatures, when the activity of lattice oxygen was negligibly low, complete oxidation of methane over perovskites was thought to proceed by reaction of weakly adsorbed surface oxygen with gaseous methane in an Rideal-Eley type mechanism. At higher temperatures, lattice oxygen became reactive after thermal desorption of adsorbed oxygen (1, 13). Zwinkels et al. (1) noted that although the temperatures for 50% conversion on the most active perovskite catalysts were similar to those obtained for Pt catalysts, the noble metal catalysts reached 100% conversion at approximately 100°C lower than the perovskites. This was explained by differences in the nature of surface oxygen species on the different catalysts. Lower surface coverage of the perovskites due to the weakly bound nature of the active surface oxygen species resulted in suppressed activity at higher temperatures. On Pt, dissociatively adsorbed oxygen was thought to be the active species which does not desorb as quickly at high temperatures (1).

In a review of the use of automotive exhaust catalysts in 1980, Kummer (7) found that catalysts composed only of base metal oxides were not used, because of the more desirable properties of noble metals. However it was stated that, on the basis of activity, the preferred metal oxides would be  $Co_3O_4$ , CuO, and  $MnO_2$  for CO oxidation while for hydrocarbon reactions  $Cr_2O_3$  was also recommended. For hydrocarbon oxidation, the activity ranking of these oxides was reported to depend on the structure of the molecules to be oxidised and in particular whether hydrocarbon adsorption was via the double bond (for olefins) or the cleavage of a C-H bond (for paraffins). For olefin oxidation, CuO and  $MnO_2$  had high catalytic activity per unit surface area. For paraffins or larger molecular weight olefins, where chemisorption requires, or can be via, breakage of a C-H bond,  $Cr_2O_3$  was similar in activity per unit surface area to CuO and  $MnO_2$ , but not to  $Co_3O_4$ , which possessed the highest activity. In general, olefins were more

easily oxidised than paraffins probably because of more facile chemisorption via the double bond (7).

In a study of hydrocarbon combustion over  $\text{CuO}/\text{Al}_2\text{O}_3$  catalysts in the temperature range 140 to 510°C (14), variation in catalytic activity with hydrocarbon structure was again noted. The following conclusions were reached:

- methane is the most difficult hydrocarbon to oxidise, while acetylene is the least difficult;
- in general, the ease of oxidation increases with carbon number;
- for a given carbon number, the ease of oxidation increases with decreasing degree of saturation.

Anderson et al. (15) examined the catalytic oxidation of methane. A wide variety of supported and unsupported oxides and supported Pt and Pd samples were screened using a microcatalytic reactor. Catalysts were tested at different temperatures using a constant ratio of feed rate of  $\text{CH}_4$  to bulk volume of catalyst sample. Excess  $\text{O}_2$  was used in the feedstream (0.66 $\text{cm}^3$  pulses of  $\text{CH}_4$  in a stream of  $\text{O}_2$  flowing at 40 $\text{cm}^3\text{min}^{-1}$ ).  $\text{Co}_3\text{O}_4$  was found to be the most active single component catalyst tested, in agreement with a previous study by Yant and Hawk (16). However its' activity was decreased when impregnated on alumina, possibly because of the formation of  $\text{CoAl}_2\text{O}_4$  (15). For  $\text{Al}_2\text{O}_3$  supported samples the activity of the metals and metal oxides per gram of active metal decreased in the following order:

$\text{Pt} > \text{Pd} > \text{Cr} > \text{Mn} > \text{Cu} > \text{Ce} > \text{Co} > \text{Fe} > \text{Ni} > \text{Ag}$ .

The activation energies for the more active supported catalysts were between 87 and 104 kJ per mole using the Arrhenius equation. Catalysts with low activity had higher activation energies. No account was taken of surface areas in this study (15) so specific activities could not be compared.

The catalytic oxidation of a number of  $\text{C}_5$  and  $\text{C}_6$  hydrocarbons was studied by Stein et al (17). The catalysts were evaluated using a pulse microcatalytic technique and activities were compared on the basis of the temperature required to obtain 80% conversion. The most active oxides were those of Co, Ni, Mn, Cr, and Fe. In particular,  $\text{Co}_3\text{O}_4$  showed good activity performance. No direct relationship between activity and surface area was found but the more active catalysts had at least a moderate surface area (17).

The relationship between  $\Delta H_o$  and catalytic combustion activity of metal oxides has been studied (18, 19), where  $\Delta H_o$  represents the heat of formation of the catalyst oxides divided by the number of oxygen atoms in the oxide molecule. For samples tested, the catalytic activity increased with decreasing strength of the metal-oxygen bond e.g. Fig. 1.2. The authors noted that the left side of the typical "volcano" plot (see Fig 1.1) was absent but would be expected to appear if metals of lower  $\Delta H_o$  than Pt were tested as had been found in a separate study of propylene oxidation over the same catalysts but also including Ag (18). For the oxidation of isobutene and acetylene, the catalyst surface was thought to be increasingly covered by oxygen and decreasingly covered by hydrocarbon as the  $\Delta H_o$  value increased (19). For stable and intermediately stable metal oxides, the rate-determining step for these compounds was concluded to be the surface reaction between adsorbed oxygen and adsorbed hydrocarbon involving the breaking of a metal-oxygen bond. For Pt and Pd, the surface was thought to be fully covered by hydrocarbon with the slow reaction step being the chemisorption of oxygen. For the oxidation of propane, the reaction kinetics were virtually first order in hydrocarbon and independent of oxygen irrespective of the catalyst. This was attributed to the weak nature of propane adsorption on all catalysts (19).

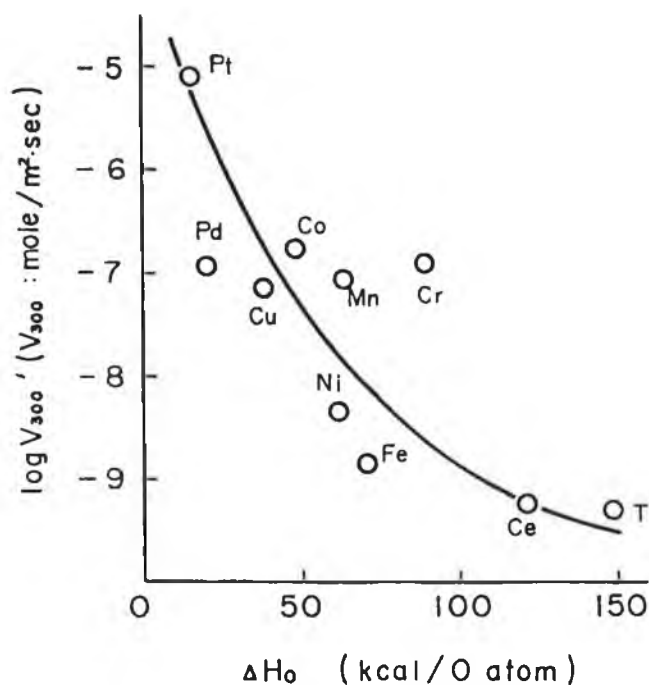


**Figure 1.2 : Correlation of the Catalytic Activity and  $\Delta H_o$  in the oxidation of  $C_3H_8$  (19).** Reactant gas composition consisted of 50 vol.%  $O_2$ , 48 vol.%  $N_2$  and 2 vol.% hydrocarbon.

### 1.3 Catalytic Combustion on Noble Metals.

A brief discussion on the use of noble metals as complete oxidation catalysts will now be presented. A more in-depth analysis of some of the key literature on hydrocarbon oxidation over supported catalysts will then be given in sections 1.3.1 to 1.3.3.

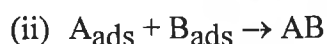
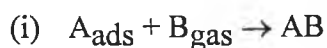
The higher combustion activity of noble metals, relative to metal oxides, is well documented (1, 3, 7, 18), and Zwinkels et al. (1) state that their application as complete oxidation catalysts has always been favoured. The high activity of noble metals for complete oxidation is associated with their inherent ability to activate O-H, O-O, C-H and H-H bonds (20). The most common noble metals used are Pt and Pd, either on their own, or alloyed with closely related metals such as Ru, Rh, Os, and Ir (3). In principle any of the noble metals could be used as oxidation catalysts but problems with sintering, volatility and irreversible oxidation have meant that most practical systems employ Pt and Pd (3, 7). Limited supply and the resulting high cost of the other metals also restricts their use (3).

The activity of noble metals varies depending on the reactant molecule. For example, Pd is preferred to Pt for the complete oxidation of CO, olefins and CH<sub>4</sub>, while the opposite is true for the oxidation of paraffinic hydrocarbons (C<sub>3</sub> and higher) and both have similar activity for the oxidation of aromatic compounds (7). As previously mentioned (14), hydrocarbons vary widely in their ease of oxidation. In his review, Dwyer (6) gave a set of guidelines for the ease of oxidation of hydrocarbons but the rules can only be treated in a qualitative sense as they do not account for differences in oxidation mechanisms on different catalysts. The general trends reported, in order of ease of oxidation, are:

- branched chain>straight chain;
- acetylenes>olefins>saturated;
- C<sub>n</sub>>.....C<sub>3</sub>>C<sub>2</sub>>C<sub>1</sub>;
- aliphatic>alicyclic>aromatic.

In 1989, Spivey (3) found little research that dealt with the mechanism of complete oxidation on noble metals but that most reported information was concerned primarily with overall performance. In his review, it was concluded that the mechanism on noble metal catalysts followed either a Langmuir-Hinshelwood type of mechanism or an Eley-Rideal mechanism. The latter would involve reaction between adsorbed oxygen

and a gas phase reactant [mechanism (i)], while in the former, reaction between adsorbed oxygen and adsorbed reactant would occur [mechanism (ii)].



It was noted that the existence of a Langmuir-Hinshelwood mechanism i.e. type (ii), may be particularly important for the oxidation of mixtures of different compounds, where competitive adsorption would presumably be important e.g. see reference (19). For nucleophilic reactants such as olefins, which are more strongly adsorbed on metal surfaces than paraffinic hydrocarbons (19), a Langmuir-Hinshelwood mechanism was expected (3).

Wei (5) noted that the kinetics of oxidation over noble metals are much more complex than for metal oxides, with every chemical species having an inhibiting effect on the rate of oxidation of another species and CO being a particularly strong self-poison especially when present in high concentrations at lower reaction temperatures (3, 5). It has been reported that self-inhibition by CO decreases at higher temperatures and lower concentrations of CO because the concentration of CO adsorbed on the metal surface decreases while that of oxygen increases with a possible change in the dominant mechanism from one of Langmuir-Hinshelwood to one of Eley-Rideal (3, 5).

Under the O<sub>2</sub>-rich conditions of many hydrocarbon oxidation studies, the metal surface is often covered with oxygen due to dissociative adsorption of O<sub>2</sub> from the reactant mixture (1, 3, 13, 21). Therefore, generally no (or a small negative) influence of the oxygen pressure on the reaction rate is commonly found (1, 21). In agreement with this theory, Morooka et al. (19) found the oxidation of propane on Pt to be approximately first order in propane and zero order in oxygen suggesting the slow step to involve either the chemisorption or reaction of propane on the oxygen covered surface. However, for more strongly adsorbed hydrocarbons, acetylene and isobutene, the oxidation was approximately first order in oxygen and negative order in hydrocarbon suggesting the rate-determining step is the chemisorption of oxygen on the surface covered by hydrocarbon (19) and that the oxidation of unsaturated reactants is self-inhibited when present at high concentrations (7). According to Margolis (22) the mechanism of hydrocarbon oxidation on metals and their oxides can have much in common. When the oxide film is fairly thick (about several tens of atomic layers) the chemical and electronic properties of the catalyst surface will be determined by the oxide film properties and the metal will exert no considerable effect on catalysis, whereas with a thin layer (of several atomic layers) the catalytic properties will depend on the nature of the metal support (22). In her survey on the "high" conversion of hydrocarbons to carbon dioxide, Margolis

reported the kinetics over Pt to vary from zero to first order in oxygen and -1 to second order with respect to hydrocarbon concentrations. The change in the order of the kinetic equation as a function of molecular structure of the hydrocarbon was thought to provide evidence for a rate-determining step which seemed to be related to the nature of hydrocarbon species formed in adsorption. In certain cases the rate-determining step was the chemisorption of oxygen (22).

Thus, the mechanism or kinetics of oxidation can vary depending on the catalyst used (3), the reactant to be oxidised (19, 22), and the reaction conditions e.g. temperature and reactant concentration (3, 5).

There are three main types of metal surface whose catalytic activity and adsorptive properties have been investigated (23). The first is a bulk sample, usually in the form of a single crystal or a fine wire. The second type of surface is an evaporated metal film. The third consists of small particles of metal supported on a finely divided oxide powder such as  $\text{Al}_2\text{O}_3$ ,  $\text{SiO}_2$  or  $\text{MgO}$ . The support is not necessarily inert (although it often is) and when it participates in the catalytic process the catalyst is said to be bifunctional (23). The purpose of the support is not only to increase surface strength but also to increase the available surface area (24).

Investigations of supported Pt catalysts have shown that carbon dioxide and water are formed as products in a highly selective manner over a wide range of experimental conditions such as temperature and reactant composition (22). However the activity of such catalysts has been shown to vary considerably with:

- type of support used e.g. (25);
- method of sample preparation and pretreatment conditions. The latter may involve exposure to oxidising or reducing environments at particular temperatures e.g. (26);
- conditions of reaction such as temperature and reactant composition (21);
- use of promoters such as base metal oxides e.g. (21);

Variations in these parameters cause changes in the structure and chemical properties of the metal component in supported catalysts and hence result in different catalytic properties. Many researchers believe that complete oxidation on supported noble metal catalysts is a structure sensitive reaction with larger metal crystallites showing higher activity than very well dispersed small metal particles (1). One possible

explanation given is that adsorbed oxygen is less tightly bound on the larger particles and hence is more reactive (27, 28, 29). Other studies, however, have found no evidence to support structure sensitivity (30, 31). Moreover it has been proposed that some catalysts are actually "reaction-sensitive" structures, as described in (32), and that adsorption of reactants can cause changes in the morphology of the noble metals. This was thought to result in activation of the samples on exposure to the reaction mixture (30, 31) and may have been responsible for the apparent structure sensitivity, found in other studies, in which larger metal particles were produced by artificial aging in the reaction mixture e.g. (27).

The remainder of this section of the review will focus on a more in-depth discussion of the literature involving catalytic oxidation using supported noble metal catalysts. For convenience, studies will be divided into three sections. In the first section, the catalytic oxidation of methane will be discussed, while the next section will deal with studies of higher hydrocarbons. Section three will give a short overview on the application of noble metal catalysts in automotive exhaust catalysts.

Most studies are concerned with short chain alkanes, and in particular CH<sub>4</sub>, because they are relatively difficult to oxidise compared to other hydrocarbons such as alkenes or higher molecular weight species (7, 29, 33). Methane is also of interest because of its' abundance and the direct applicability to the catalytic combustion of natural gas (29).

### 1.3.1 Oxidation of Methane

As previously discussed, Anderson et al. (15) found alumina-supported noble metals to show superior performance to metal oxide catalysts for the combustion of methane. In another early study, Mezaki and Watson (34) investigated the kinetics of CH<sub>4</sub> oxidation on a 0.5% Pd/Al<sub>2</sub>O<sub>3</sub> catalyst. A flow-type integral reactor was used to study CH<sub>4</sub> conversion in the temperature range 320 to 380°C. A number of possible reaction models were linearised and fitted to the experimental rate data. A reaction mechanism was proposed in which a surface reaction between gaseous methane and adsorbed oxygen was the rate-controlling step, producing adsorbed carbon dioxide and adsorbed water. The catalytic activity of the Pd catalyst was found to initially decrease during operation, possibly due to the adsorption of water vapour which was contained in the gas stream and produced by the oxidation reaction (34).

Firth and Holland (35) studied CH<sub>4</sub> oxidation on Pd, Pt, Rh and Ir supported on Al<sub>2</sub>O<sub>3</sub>, in an attempt to gain information on the effect of the electronic structure on the reaction. Before use, all catalysts were heated at 900°C in a 12% methane and air

mixture to reduce any oxide to the metal. At a partial pressure of 0.02 atm CH<sub>4</sub> and 0.215 atm O<sub>2</sub>, the apparent activation energies ( $E_a$ ) of Pt, Rh and Ir were determined as 200, 113 and 71 kJ.mole<sup>-1</sup> respectively. For Pd the activation energy was 139 kJ.mole<sup>-1</sup> below 290°C and 52 kJ.mole<sup>-1</sup> at higher temperatures. The change in activation energy (87 kJ.mole<sup>-1</sup>) for Pd at 290°C was noted as being similar to the heat of formation of PdO (85 kJ.mole<sup>-1</sup> (19)), and this was thought to indicate that adsorbed oxygen at higher temperatures was similar to the oxygen in PdO (35).

The reaction mechanism was thought to involve adsorption of both reactants (35). The kinetic results obtained indicated that once the metal surface was completely covered with oxygen, CH<sub>4</sub> could adsorb without competing with oxygen. However at lower temperatures or pressures of oxygen, some oxygen adsorption sites were still empty and hence competitive adsorption of methane and oxygen became important. Thus there were two types of sites for CH<sub>4</sub> adsorption, one which could also adsorb oxygen and one which could not. A direct correlation between the strength of the metal-oxygen bonds and the apparent activation energies (below 290°C) for the different metals, was found. As the metal-oxygen single-bond strength increased the apparent activation energy decreased, implying the formation of a metal-oxygen bond in the reaction sequence. For all samples, only CO<sub>2</sub> and H<sub>2</sub>O were detected as products using infra-red and mass spectroscopy indicating they formed more than 98% of the reaction products (35).

The kinetics of CH<sub>4</sub> oxidation on supported Pt and Pd catalysts was studied by Cullis and Willatt (36). A pulse-flow microreactor technique was used to investigate the reaction at temperatures between 227-527°C with CH<sub>4</sub>:O<sub>2</sub> ratios varying from 1:10 to 10:1. Under the conditions used the rate of reaction was thought to depend only on the chemical processes occurring on the catalyst surface. Effects, such as homogeneous oxidation and interparticle diffusion, appeared to be absent. The supports examined were TiO<sub>2</sub>, ThO<sub>2</sub>,  $\gamma$ -Al<sub>2</sub>O<sub>3</sub>, SnO<sub>2</sub> and SiO<sub>2</sub>. Precious metal loadings varied from 1 to 40% on the powdered refractory metal oxides. Catalyst characterisation was achieved using N<sub>2</sub> physisorption, H<sub>2</sub> chemisorption, Transmission Electron Microscopy (TEM), Scanning Electron Microscopy (SEM), and X-ray Photoelectron Spectroscopy (XPS). The activity of both metals improved when supported on oxides of large surface area, such as  $\gamma$ -Al<sub>2</sub>O<sub>3</sub>, even though the supports themselves did not appreciably catalyse the reaction. SnO<sub>2</sub> was the only oxide to show high activity at 600°C (36).

Experiment showed that the rate of oxidation over supported catalysts, was usually about first order in CH<sub>4</sub> and tended to be independent of oxygen concentration (36). A mechanism was proposed involving the reaction of adsorbed methane with

strongly adsorbed oxygen. At the temperatures of oxidation, CH<sub>4</sub> adsorption was expected to be dissociative. This was supported by the fact that hydrogen was formed during pyrolysis of CH<sub>4</sub> and that carbon left on the surface could be reconverted to CH<sub>4</sub> when hydrogen was passed through the catalyst bed (36).

In general, slightly lower rates of methane combustion were achieved with Pt and this was attributed to the different abilities of the two metals to adsorb oxygen (36). The adsorption of oxygen onto the catalyst surface was deemed to be an essential step. The amount of oxygen adsorbed depended on the precious metal, its loading and the support material used. For example, Pd on TiO<sub>2</sub> and ThO<sub>2</sub> supports adsorbed less oxygen than Pd on  $\gamma$ -Al<sub>2</sub>O<sub>3</sub>. Pd adsorbed roughly 100 times more oxygen when supported on Al<sub>2</sub>O<sub>3</sub> than a corresponding Pt catalyst. A clear correlation between oxygen uptake and catalytic activity of supported Pd catalysts was found as shown in Fig 1.3 (36).

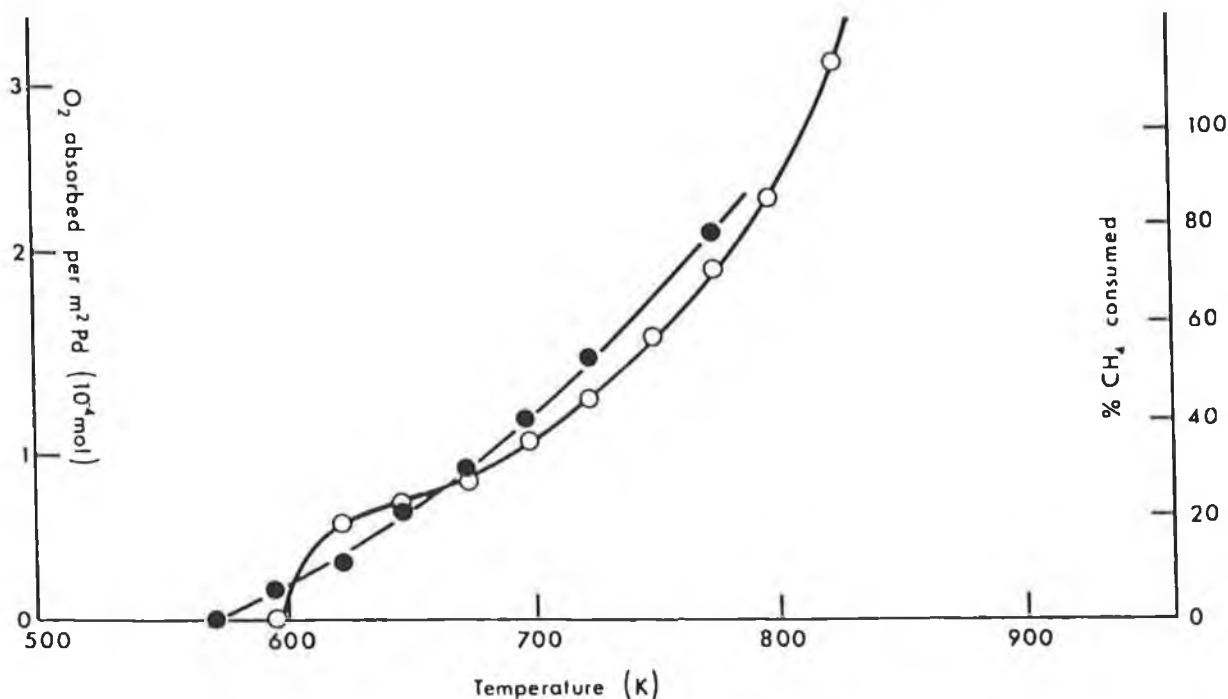


**Figure 1.3 : O<sub>2</sub> Uptake and CH<sub>4</sub> Combustion Activity of a 2.7% Pd/TiO<sub>2</sub> catalyst as a function of Temperature (36). (○), Oxygen adsorption (O<sub>2</sub> pulse volume, 0.25 cm<sup>3</sup>): (●), CH<sub>4</sub> conversion (pulse volume, 5 cm<sup>3</sup> (contained 2.2 × 10<sup>-6</sup> mol. CH<sub>4</sub> and 5.9 × 10<sup>-6</sup> mol. O<sub>2</sub>).**

Optimum activity was achieved only when sufficient oxygen was adsorbed from the gaseous reaction mixture onto a previously reduced palladium surface (36). However, oxygen adsorption at high temperatures was found to be detrimental to oxidation activity as it resulted in tightly bound surface oxygen, similar to palladium oxide, which was less reactive. It was believed that this non-reactive oxygen species may represent an intermediate stage in the formation of Pd(II) oxide and that it could explain the lack of activity observed when Pd was exposed to O<sub>2</sub> above 450°C. Oxygen penetration into the bulk of polycrystalline Pd foil was demonstrated by Campbell et al. (37) who proposed that oxidative catalysis over Pd could be referred to as being over Pd containing a significant amount of oxygen in solid solution near the surface. Cullis and Willatt (36) proposed that because Pd can adsorb oxygen into its' bulk an oxygen reservoir is provided which prevented methane pyrolysis from occurring when it was adsorbed.

Rates of CH<sub>4</sub> oxidation were measured as a function of temperature (36). Plots of the logarithm of reaction rate versus reciprocal temperature showed a sudden change in slope at a temperature referred to as the transition temperature, as shown in Fig. 1.4. Pt catalysts exhibited a sudden increase in activity at this temperature while Pd samples underwent a more gradual transition. At temperatures below the transition temperature, the activation energies of Pt catalysts for CH<sub>4</sub> oxidation were generally higher than those for Pd. At higher temperatures, the reverse was true. At low temperatures, E<sub>a</sub> values were in the range 83 to 95 kJ.mol<sup>-1</sup> for Pd and 108 to 116 kJ.mol<sup>-1</sup> for Pt. In the high temperature region values ranged from 23 to 45 kJ.mol<sup>-1</sup> for Pd and 19 to 24 kJ.mol<sup>-1</sup> for Pt. In general, changes in the reactant composition did not affect the activation energy, however the transition temperature was dependent on reactant composition as well as the catalyst and support used (36).

With supported Pd, a change in the activation energy of CH<sub>4</sub> oxidation at higher temperatures was also found by Firth and Holland (35) who proposed that Pd was present in a similar form to PdO above the transition temperature. In apparent agreement with this theory, Cullis and Willatt (36) proposed that the overall activation energy at lower temperatures for supported Pd catalysts may have been the sum of the activation energies for the oxidation of Pd and for CH<sub>4</sub> oxidation by the resulting palladium oxide. However, above the transition temperature, oxidation of the precious metal may no longer have been an important step in the mechanism. At these higher temperatures, the activation energies for CH<sub>4</sub> on supported Pt or Pd were correlated with those obtained for preoxidised samples. It was noted that transition from chemical control to diffusion limitation could also have been responsible for the sudden changes in activation energy observed at the transition temperature (36).

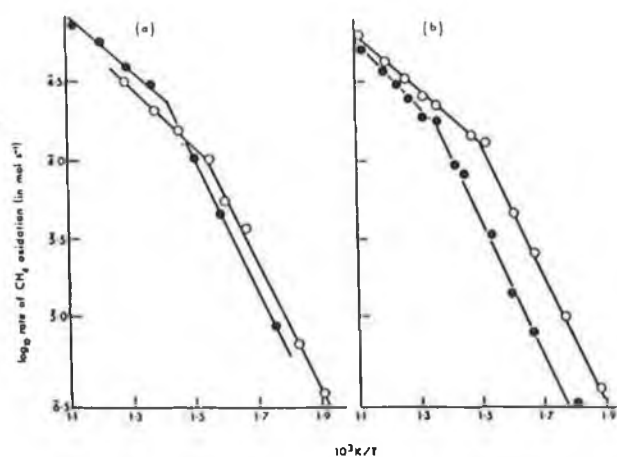


**Figure 1.4 :** Rate of CH<sub>4</sub> Oxidation versus Temperature for some supported catalysts(36). Pulse volume 5 cm<sup>3</sup> (contained 4.2 × 10<sup>-5</sup> mol. CH<sub>4</sub> and 1.9 × 10<sup>-5</sup> mol. O<sub>2</sub>). (a)-(O), 2.7 wt.% Pd/TiO<sub>2</sub>; (●), 2.7 wt.% Pd/γ-Al<sub>2</sub>O<sub>3</sub>; (b)-(O), 20 wt.% Pd/ThO<sub>2</sub>; (●), 2.7 wt.% Pd/α-Al<sub>2</sub>O<sub>3</sub>.

Activity measurements on preoxidised PtO<sub>2</sub> and PdO samples revealed that the former oxide was more active, requiring a lower temperature for the CH<sub>4</sub> oxidation reaction to occur (36). Using a 0.5 cm<sup>3</sup> pulse volume, containing 1.04 × 10<sup>-6</sup> moles of CH<sub>4</sub>, 29% conversion of CH<sub>4</sub> was achieved with a 2.7% PdO/ThO<sub>2</sub> catalyst at ca.380°C, while the same conversion was achieved on 2.7% PtO<sub>2</sub>/ThO<sub>2</sub> at ca.280°C (36).

The effect of varying the metal particle size was examined (36). Larger metal particles were found in samples with higher metal loadings (depending on preparation procedure), and samples which had been pretreated at high temperatures. For increased metal loadings on a given support, the overall rate of CH<sub>4</sub> oxidation increased for both CH<sub>4</sub>-rich and O<sub>2</sub>-rich mixtures but the activity per unit mass of Pd and, to a lesser extent, the activity per unit area of palladium decreased. For example, the rates of CH<sub>4</sub> oxidation, at 410°C and a CH<sub>4</sub>:O<sub>2</sub> ratio of 1:0.45, are compared in Table 1.1 for Pd/TiO<sub>2</sub> and Pd/γ-Al<sub>2</sub>O<sub>3</sub> samples of different loadings. Similar results were found for Pt although no values per unit area of Pt were given for higher loadings.

**Table 1.1 :** Effect of catalyst loading on the rate of methane oxidation (36)

Catalyst	Reaction Rate
	10 <sup>-2</sup> mol.s <sup>-1</sup> .g <sup>-1</sup> of precious metal (10 <sup>-2</sup> mol.s <sup>-1</sup> .m <sup>-2</sup> of precious metal)
2.7 wt.% Pd/TiO <sub>2</sub>	16.57 (3.64)
20 wt.% Pd/TiO <sub>2</sub>	3.05 (1.05)
2.7 wt.% Pd/γ-Al <sub>2</sub> O <sub>3</sub>	21.56 (5.60)
11 wt.% Pd/γ-Al <sub>2</sub> O <sub>3</sub>	6.42 (3.34)

On exposure of a 2.7% Pd/ $\gamma$ -Al<sub>2</sub>O<sub>3</sub> catalyst to prolonged high temperature pretreatment in flowing air the average metal particle diameter increased from 14 to 80 nm, while the catalytic activity per gram of metal, under CH<sub>4</sub>-rich conditions, remained almost unaffected (36). This may indicate the specific activity per unit area of metal increased but the authors concluded that the rate of CH<sub>4</sub> oxidation was independent of particle size. As the metal:support ratio increased, the oxygen uptake was reduced and XPS analysis showed greater metallic character for higher metal loadings. This was thought to indicate a diminished ability of larger particles to adsorb oxygen (36).

Oh et al. (21) found the activity of  $\gamma$ -Al<sub>2</sub>O<sub>3</sub>-supported catalysts to decrease in the order Pd > Rh > Pt for the oxidation of CH<sub>4</sub>, under both oxidising and reducing conditions. Catalysts were prepared by incipient wetness impregnation with aqueous metal salts and calcined at 500°C in flowing air. Noble metal loadings were between 0.1-0.2 wt.%. Activity was monitored using an integral flow reactor system with a feedstream composition of 0.2 vol.% CH<sub>4</sub>, 0.1 vol.% CO (if present) and variable levels of O<sub>2</sub> in a He background. CH<sub>4</sub> oxidation was monitored using temperature run-up experiments with fixed feed composition, and variable composition experiments at a fixed temperature. In run-up experiments, the temperature required for onset of CH<sub>4</sub> oxidation was approximately the same for each particular metal, in reducing and oxidising feedstreams. However, once reaction began the CH<sub>4</sub> conversion increased much more sharply with temperature in the reducing feedstream. CH<sub>4</sub> conversions as a function of temperature in oxidising and reducing feed streams are shown, in Fig 1.5.

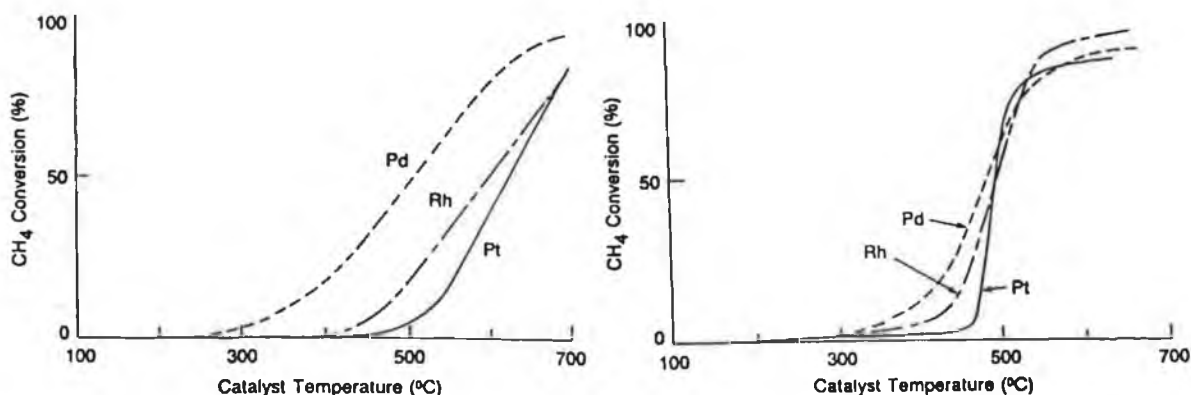
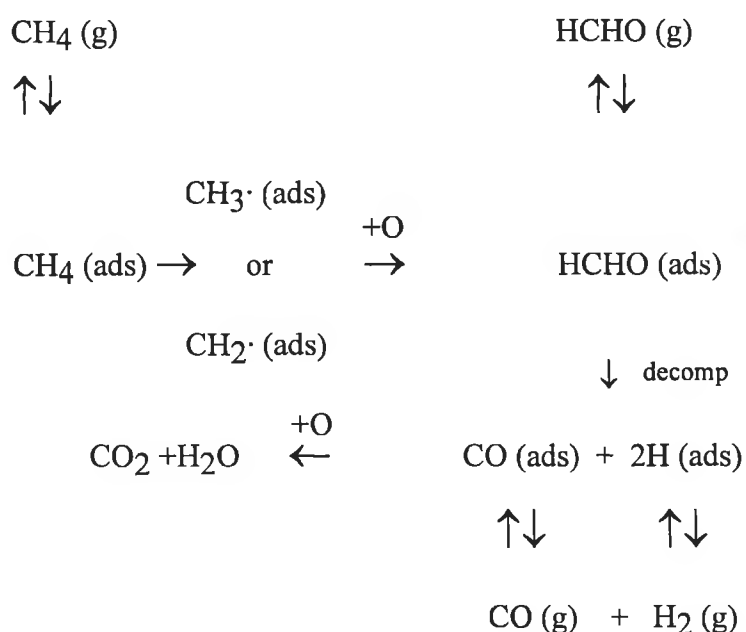
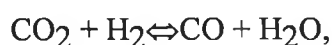


**Figure 1.5 : Conversion of CH<sub>4</sub> versus Temperature over Al<sub>2</sub>O<sub>3</sub>-supported noble metals (21). (A)-oxidising feedstream (0.2 vol.% CH<sub>4</sub>, 0.1 vol.% CO and 1 vol.% O<sub>2</sub>); (B)-reducing feedstream (0.2 vol.% CH<sub>4</sub>, 0.1 vol.% CO, 0.33 vol.% O<sub>2</sub>).**

The CH<sub>4</sub> conversion in temperature run-up experiments was virtually unaffected by the presence of CO in the feed which was expected as CO oxidation occurs well below the temperature required for CH<sub>4</sub> oxidation (21). However, a correlation between oxygen coverage of the metal surface and activity was found, by monitoring oxidation of 0.2% CH<sub>4</sub> (in He carrier gas) as a function of oxygen inlet concentration at ~550°C. At low oxygen levels, there was insufficient adsorbed oxygen to allow reaction and at high levels oxidation was retarded due to inhibition of the adsorption of CH<sub>4</sub> by the preferentially adsorbed oxygen. Slightly to the fuel-rich side of stoichiometry of the reactants, it was found that both could compete successfully with each other for chemisorption and an optimum activity was attained. Although it was acknowledged that a detailed mechanism was not understood, a mechanism was proposed involving reaction of dissociatively adsorbed methane (methyl or methylene radicals) with adsorbed oxygen. This was proposed to result in CO<sub>2</sub> and H<sub>2</sub>O as the main reaction products. The proposed mechanism was summarised as



Under the reaction conditions studied, it was thought that an adsorbed formaldehyde intermediate, once formed would rapidly decompose to form adsorbed CO and adsorbed H rather than desorb into the gas phase as formaldehyde (HCHO) molecules. The water-gas shift reaction,



was found to play an important role in determining product selectivity over Rh/Al<sub>2</sub>O<sub>3</sub> but not over Pt/Al<sub>2</sub>O<sub>3</sub> or Pd/Al<sub>2</sub>O<sub>3</sub>. No partial oxidation products, other than CO and H<sub>2</sub> were formed in significant quantities (21).

Seimanides and Stoukides (38) studied CH<sub>4</sub> oxidation on porous polycrystalline Pd supported on yttria-stabilised zirconia in a continuous-stirred tank reactor (CSTR) between 450 and 600°C at atmospheric total pressure. Products were analysed by gas chromatography with the concentration of CO<sub>2</sub> produced being monitored additionally by an infrared CO<sub>2</sub> analyser. Kinetic measurements were made using CH<sub>4</sub> partial pressures between  $1.23 \times 10^{-2}$  and  $7.85 \times 10^{-2}$  bar and O<sub>2</sub> partial pressures between  $0.24 \times 10^{-2}$  and  $6.83 \times 10^{-2}$  bar with N<sub>2</sub> as diluent. Homogeneous gas phase oxidation as well as internal and external diffusional effects were all absent under reaction conditions studied. CO<sub>2</sub> and H<sub>2</sub>O were the only products observed in measurable quantities. After an initial induction period of approximately 48 hours, catalyst activity remained constant for at least eight weeks and all data reported were taken after the termination of the induction period (38).

The rate of reaction was found to be proportional to O<sub>2</sub> partial pressure at low O<sub>2</sub> partial pressures, while at higher pO<sub>2</sub> the rate became almost independent of O<sub>2</sub> partial pressure. The rate was first order in CH<sub>4</sub> at all temperatures and pressures examined (38). This indicated an Eley-Rideal mechanism in which gaseous CH<sub>4</sub> reacted with adsorbed atomic oxygen. A kinetic model was proposed in which chemisorbed oxygen (rather than PdO) was the active species for CH<sub>4</sub> oxidation to CO<sub>2</sub> and H<sub>2</sub>O (38).

The thermal chemistry of Pd in air, with relation to CH<sub>4</sub> oxidation activity, was studied using Thermogravimetric Analysis (TGA) by Farrauto et al (39). Depending on pre-treatment conditions two different types of oxygen/palladium species were observed for Pd/ $\gamma$ -Al<sub>2</sub>O<sub>3</sub>. These were designated as PdO/Al<sub>2</sub>O<sub>3</sub> and PdO<sub>x</sub>-Pd/Al<sub>2</sub>O<sub>3</sub>. The former species was assigned to well dispersed Pd particles and decomposed between 800 and 850°C similar to unsupported crystalline PdO. The latter form was associated with chemisorbed oxygen dispersed on larger bulk Pd metal particles and decomposed at temperatures between 750 and 800°C. To reform PdO species, the temperature must firstly be decreased well below 650°C indicating the existence of a significant hysteresis between decomposition to Pd and re-formation of the oxide. For supported Pd, both PdO<sub>x</sub> and PdO species could be reformed after cooling and reheating. On reheating unsupported Pd in air, only the PdO<sub>x</sub>-Pd species could be formed. No crystalline PdO, which was the only species initially present before decomposition, was reformed on this sample (39).

On reheating metallic Pd/Al<sub>2</sub>O<sub>3</sub> in air, chemisorption of oxygen occurred at low temperatures to produce some oxygen/palladium species which promoted chemisorption of oxygen as the temperature was increased (39). Once a skin of this

PdO<sub>x</sub>/Pd species was formed, subsequent heating above 570°C resulted in dissolution and/or reaction of oxygen into the underlying Pd metal to form a solid solution of oxygen in the bulk of the metal, as proposed by other authors for the oxidation of Pd at high temperatures (36, 37). Oxygen uptakes were found to far exceed monolayer coverage based on chemisorption studies (39). It was proposed that pitting and cavity formation, caused by oxidation of underlying Pd layers, may explain restructuring phenomena of PdO crystallites postulated by other authors to explain increases in activity for aged samples relative to fresh samples (30, 31).

CH<sub>4</sub> oxidation on 4% Pd/Al<sub>2</sub>O<sub>3</sub> was studied as a function of temperature for a reaction feedstream of 1% CH<sub>4</sub> in air (39). Catalyst preparation was by incipient wetness method, followed by reduction with hydrazine, drying overnight at 120°C and calcination at 500°C for two hours. For a fresh sample, CH<sub>4</sub> conversion began at ~340°C, rising to 30% by 430°C and nearing completion at 650°C. Cyclic heating and cooling experiments indicated that above 500°C, CH<sub>4</sub> oxidation occurs only when the catalyst contains PdO. The inability of Pd metal to adsorb oxygen at high temperatures was thought to result in complete inactivity towards CH<sub>4</sub> oxidation above 650°C. Thus it was concluded that for high temperature CH<sub>4</sub> oxidation, the presence of PdO phases in supported Pd catalysts is essential to allow oxygen chemisorption and reaction to occur (39).

Niwa et al. (40) monitored the catalytic activity of Pt catalysts for CH<sub>4</sub> oxidation using a continuous flow method, in the temperature range 300-500°C, with a feed gas of CH<sub>4</sub>, O<sub>2</sub> and N<sub>2</sub> (composition 1 : 2 : 7) at a flow rate of 100 ml.min<sup>-1</sup>. Catalysts were prepared by impregnation with chloroplatinic acid, followed by oxidation at 400°C for 3 hours in flowing air and finally reduction in flowing H<sub>2</sub> at 300°C for 3 hours. On comparing Al<sub>2</sub>O<sub>3</sub>, SiO<sub>2</sub>, and SiO<sub>2</sub>-Al<sub>2</sub>O<sub>3</sub> supports, the turn-over frequency decreased in the order, Pt/SiO<sub>2</sub>-Al<sub>2</sub>O<sub>3</sub> > Pt/Al<sub>2</sub>O<sub>3</sub> > Pt/SiO<sub>2</sub>. For 0.2% Pt catalysts the activation energy increased in the same order with E<sub>a</sub> values of 54, 87 and 139 kJ.mol<sup>-1</sup> respectively. The rate of combustion was found to be almost first order in CH<sub>4</sub> and independent of oxygen partial pressure for a 2.0% Pt/Al<sub>2</sub>O<sub>3</sub> catalyst under the experimental conditions used. The activity of Pt was found to be affected by the support used due to metal-support interaction (40).

Temperature Programmed Reduction (TPR) was used to assess the reducibility of the catalysts and catalytic activity was related to the ease of reduction of the Pt sites present (40). Prior to TPR experiments, catalysts were reduced in H<sub>2</sub>-Ar and then reoxidised in O<sub>2</sub>-N<sub>2</sub> at 500°C for 1 hour. TPR was then achieved in the H<sub>2</sub>-Ar mixture (H<sub>2</sub>, 6.2 vol.%), with a linear rate of temperature increase from room temperature to 600°

C. Sites reduced at lower temperatures were deemed to possess weaker Pt-O bonds and thus were considered the active component for CH<sub>4</sub> oxidation. For these lower temperature reduction sites a clear correlation between peak temperature and catalytic activity was found. As the peak temperature decreased, the turn-over frequency increased and the activation energy decreased. The concentration of these active sites, associated with low temperature reduction, was in the order, Pt/SiO<sub>2</sub> > Pt/Al<sub>2</sub>O<sub>3</sub> > Pt/SiO<sub>2</sub>-Al<sub>2</sub>O<sub>3</sub>. This is the inverse order to that of catalytic activity which led to the conclusion that although Pt/SiO<sub>2</sub>-Al<sub>2</sub>O<sub>3</sub> had the most active site, its' concentration was only a small portion of the reducible platinum oxides present on this support. No simple relationship between reducibility and metal dispersion, measured by CO chemisorption, could be found. Except for lower loading Pt/Al<sub>2</sub>O<sub>3</sub> samples, the oxidation state of Pt was calculated to be in the vicinity of PtO<sub>2</sub>. For 0.1 and 0.2% Pt/Al<sub>2</sub>O<sub>3</sub> samples, hydrogen spillover, may have been the cause of higher than expected hydrogen consumption's. The authors noted that because of the low loading of Pt and the high remaining Al<sub>2</sub>O<sub>3</sub> surface area, the spillover of dissociatively adsorbed hydrogen atoms from metal sites onto the support surface, where they could be stabilised as hydroxide groups, might have occurred during TPR (40).

CH<sub>4</sub> oxidation rates over Pt were measured by Otto (41) using a recirculation batch reactor and a mass spectrometer. Pt/ $\gamma$ -Al<sub>2</sub>O<sub>3</sub> samples in the range from 0.03 to 30% Pt were prepared by multiple impregnation procedures with chloroplatinic acid. Standard sample preparation included exposure to oxygen at 500°C for 20 hours before testing. Pt dispersion was evaluated using chemisorption measurements with CO and O<sub>2</sub> adsorbates. Oxidation activity was measured under highly oxidising conditions and less than 2% of the carbon in CH<sub>4</sub> was converted to products other than CO and CO<sub>2</sub>. In the range investigated ( $2.5 < O_2/CH_4 < 60$ ) the reaction rate was first order in CH<sub>4</sub> and zero order in O<sub>2</sub>. Reaction rates and activation energies varied depending on the Pt loading. Below 1.4 wt.% Pt, the turnover frequency was constant. However further increases in Pt loading led to higher turnover rates with a maximum at 5 wt.%. Above this loading, reaction rates decreased again. It was concluded that reaction was favoured on larger Pt particles, but that above 5 wt.% loss of surface atoms by growth of crystal size was not compensated by additional gain in site activity. For lower Pt concentrations, in which samples the metal was very well dispersed with essentially each Pt atom being a surface atom, the apparent activation energy was  $\sim 146 \text{ kJ.mol}^{-1}$ . For higher loadings (5-30 wt.%), the activation energy was  $\sim 112.3 \text{ kJ.mol}^{-1}$ . At these higher concentrations larger Pt particles were formed with a larger fraction of subsurface atoms (41).

Sample pretreatment was also found to affect the oxidation activity (41). Hydrogen had a tendency to increase the reaction rate while oxygen decreased it..

Changes in catalyst activity with pretreatments were thought to be too slow to be attributable to differences in the activity of reduced and oxidised surfaces. Instead, activity changes were attributed to Pt sintering in a hydrogen environment and redispersion in oxygen. These effects were found to be slow and barely noticeable at 450 °C but became more apparent at 500°C and pretreatment procedures were performed at 500°C. At this temperature, sintering and redispersion phenomena were noticed for Pt loadings as low as 0.03 wt.%. Sintering was thought to increase Pt particle size with a concurrent increase in activity in spite of the loss in exposed surface Pt (41).

It was concluded that CH<sub>4</sub> oxidation over Pt/γ-Al<sub>2</sub>O<sub>3</sub> is a structure sensitive reaction (41). The kinetics observed were consistent with the existence of at least two different Pt entities, assigned as dispersed and particulate platinum oxide, which were thought to differ in particle size and oxidation state. Unique Pt clusters of extraordinary activity may also have been indicated, by the fact that an optimum metal loading was found to exist in the transition zone between dispersed and particulate Pt, but this could not be ascertained with the data available. Larger particles, produced at higher concentrations, were found to show the kinetics of unsupported Pt black. Reaction kinetics depended strongly on sample pretreatment and were not found to be consistent with an Eley-Rideal mechanism but may have indicated the controlling step to be the dissociation of CH<sub>4</sub> (41).

Briot et al. (27) found that artificial aging of 1.95 wt.% Pt/Al<sub>2</sub>O<sub>3</sub> in a methane/oxygen/nitrogen mixture (O<sub>2</sub> : CH<sub>4</sub> : N<sub>2</sub> = 4 : 1 : 95) for 14 hours at 600°C resulted in an increase in Pt particle size from 2 nm to 12 nm. This resulted in a slight increase in the activity, expressed per mole of metal, for reaction temperatures below 427 °C. Hence the turnover number, i.e. activity expressed per surface Pt atom, was much higher on the larger Pt particles as the fraction of Pt atoms exposed to the surface had decreased. A decrease in the Pt-O surface bond strength which leads to increased reactivity of the adsorbed oxygen was proposed as the reason for this increase in specific reaction rate. Microcalorimetric measurements showed a decrease in the heat of oxygen chemisorption with increased Pt particle size. Larger particles also chemisorbed less oxygen. Titration of chemisorbed oxygen with gaseous hydrogen showed the reactivity of the chemisorbed species increased with particle size. For Pt particle diameters of ~2 nm, titration of adsorbed oxygen did not occur at -78°C. However for diameters of ~12 nm almost all chemisorbed oxygen was titrated by hydrogen at this temperature. The authors noted that the interaction of the CH<sub>4</sub> molecule with the Pt particles could also have been affected by the size of the crystallites and that this may have contributed to the increased activity observed for larger particles (27).

Catalyst was prepared by impregnation of  $\text{Al}_2\text{O}_3$  with hexachloroplatinic acid in aqueous solution (27). Calcination was at  $500^\circ\text{C}$  in a flow of nitrogen followed by reduction in flowing hydrogen overnight at the same temperature. Activity measurements were made using a flow-reactor with gas chromatographic analysis of products. At a given temperature, a slight decrease in activity was noted as a function of time and activity measurements were extrapolated to zero time of reaction. The reactants were diluted in  $\text{N}_2$  to prevent overheating effects and the reaction was thought to be under kinetic control. A comparison of the activities of the freshly reduced and aged samples, as a function of temperature, is shown in Fig. 1.6.

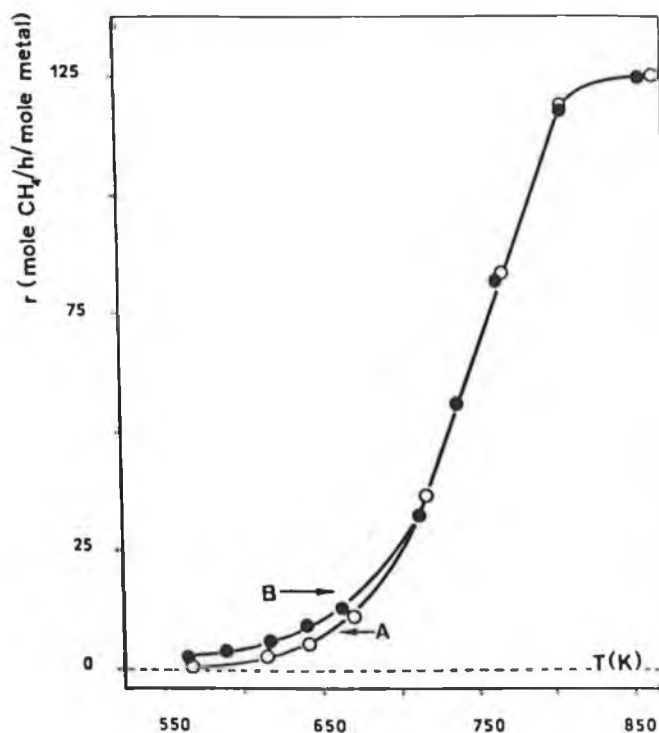


**Figure 1.6 : Rate of  $\text{CH}_4$  Oxidation versus Temperature for fresh (A) and aged (B)  $\text{Pt}/\text{Al}_2\text{O}_3$  samples (27). Rate is expressed as moles of  $\text{CH}_4$  converted per hour per mole of introduced metal.**

The apparent activation energy decreased on aging in the reaction mixture from  $100 \text{ kJ}\cdot\text{mol}^{-1}$  to  $70 \text{ kJ}\cdot\text{mol}^{-1}$  (27). Pt particle size was examined using chemisorption measurements and TEM. TEM analysis showed that larger Pt particles were not spherical and many were faceted indicating that a change in particle morphology may also have explained the greater specific activity after aging (27).

In a later study of  $\text{CH}_4$  oxidation, on 1.95 wt.%  $\text{Pd}/\text{Al}_2\text{O}_3$  under approximately the same conditions to those described above, the reaction was again thought to be structure sensitive (28). After aging the catalyst in the reaction mixture at  $600^\circ\text{C}$ , the turnover number was strongly enhanced (by a factor of 20 at  $400^\circ\text{C}$ ) and the

Pd particle size increased from 7 nm to 16 nm. As for Pt/Al<sub>2</sub>O<sub>3</sub> (27), the reactivity of adsorbed oxygen was again shown to increase on larger particles, using hydrogen titration measurements at low temperatures (28). The activities of the freshly reduced and aged Pd samples are shown in Fig. 1.7.

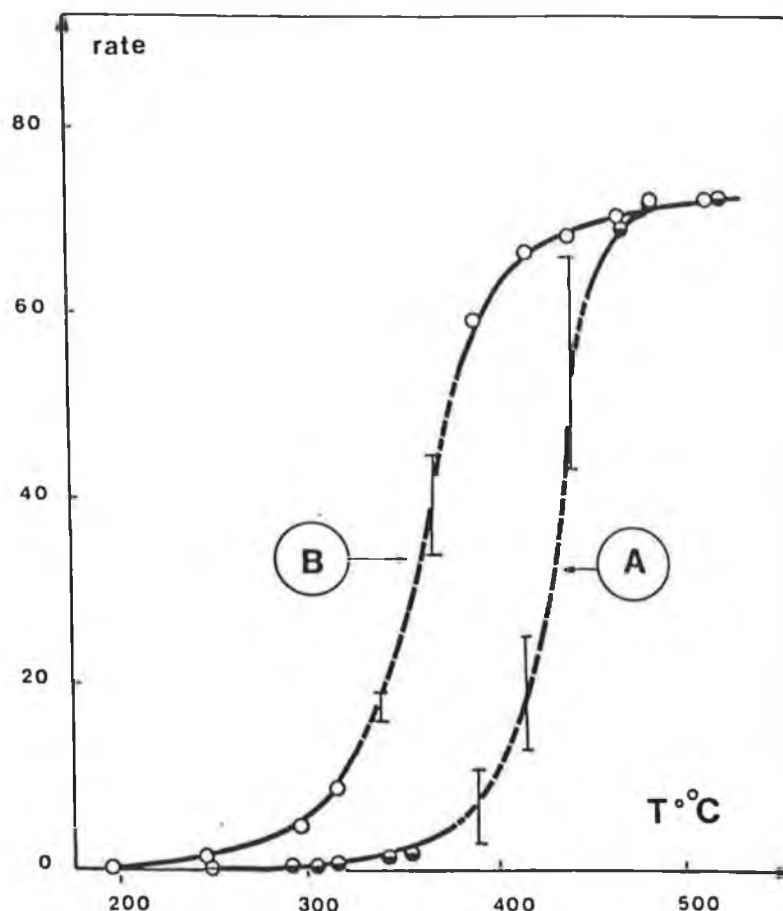


**Figure 1.7 : Rate of CH<sub>4</sub> Oxidation versus Temperature for fresh (A) and aged (B) Pd/Al<sub>2</sub>O<sub>3</sub> (28). Rate is expressed as moles of CH<sub>4</sub> converted per hour per mole of introduced metal.**

The apparent activation energy was 104 kJ.mol<sup>-1</sup> for the fresh sample, and 74 kJ.mol<sup>-1</sup> for the aged sample (28). Activation energies were deduced from Arrhenius plots at conversions below 5%. The increase in specific activity on aging, was thought to be very large to be explained solely by the increase in particle size. Other hypotheses proposed included deposition of carbon resulting in a modification of the active sites. Surface reconstruction of the Pd crystallites on exposure to the reactants was also considered and these theories were supported by the fact that aging in 4 vol.% O<sub>2</sub> in N<sub>2</sub> at 600°C for 14 hours produced no increase in activity. Thus, it appeared that both reactants were necessary for activity enhancement, which may have been due to preferential exposure of active Pd planes in the aged sample. The authors noted that for

both Pt and Pd catalysts, hydrogen reduction of the aged samples did not modify catalyst behaviour i.e. the rate of reaction was still higher than for freshly reduced samples (27,28).

The formation of bulk PdO in Pd/Al<sub>2</sub>O<sub>3</sub> samples on exposure to the O<sub>2</sub>-CH<sub>4</sub>-N<sub>2</sub> reaction mixture was reported (28). In Temperature Programmed Oxidation (TPO) experiments, PdO formation was found to occur at 340 and 390°C for aged and fresh samples respectively i.e. bulk Pd oxidation occurred faster on larger particles. The reaction rate was found to increase with time on-stream at certain temperatures and this was correlated with PdO formation at these temperatures. For fresh samples, activity increased with time between 390 and 480°C. For aged samples, the corresponding temperature range was 340 to 420°C. At temperatures above and below these values activity remained constant with time. It was concluded that CH<sub>4</sub> oxidation over supported Pd occurs on a palladium oxide phase in an oxygen-rich reactant mixture, even if the catalyst is initially present in a reduced form (28).

Hicks et al. (29) found CH<sub>4</sub> oxidation on a series of supported Pd and Pt catalysts to be structure sensitive. Structure sensitivity was thought to be explained by differences in the reactivity of adsorbed oxygen on the metal surfaces. Pd catalysts exhibited greater turnover numbers than Pt. Turnover frequencies were expressed in moles of CO<sub>2</sub> produced per second per mole of surface metal atoms present initially before testing (29).

Catalysts were prepared by ion-exchange or incipient wetness impregnation on  $\gamma$ -Al<sub>2</sub>O<sub>3</sub>, ZrO<sub>2</sub>,  $\alpha$ -AlOOH, and Y<sub>2</sub>O<sub>3</sub>/ZrO<sub>2</sub> supports (29). Calcination was achieved at either 500 or 700°C for 2 hours. Metal loadings were in the range 0.5 - 2.3 wt.%. Catalytic rates were measured, in the temperature range 260 to 370°C, in a fixed-bed microreactor on samples which were reduced in flowing hydrogen for 1 hour before testing. Conversions were kept below 2% and CO<sub>2</sub> was the only product observed by gas chromatography under the oxidising conditions used (29).

For supported Pt, two distinct Pt phases were present (29). These were referred to as dispersed Pt and crystalline Pt and were distinguishable by the infrared spectra of adsorbed CO. Using 5% excess oxygen, methane conversion was found to be 10 to 100 times higher on platinum crystallites than on dispersed Pt. This was attributed to the fact that the latter was converted to PtO<sub>2</sub> while the crystallites became covered with more reactive chemisorbed oxygen during reaction. The ratio of PtO<sub>2</sub> to Pt crystallites (covered with more reactive oxygen) was thought to increase as the dispersion of Pt increased. However, no conclusive correlation of Pt dispersion with turnover frequency was found. Whether or not, the dispersed or crystalline phases were formed depended

more on the support composition and the method of preparation, than on the degree to which Pt is dispersed over the support. Al<sub>2</sub>O<sub>3</sub> was capable of stabilising Pt in a highly dispersed state. Supports, such as ZrO<sub>2</sub> or relatively inert Al<sub>2</sub>O<sub>3</sub> ( $\alpha$ -ALOOH calcined at 1050°C for 2 hours), did not stabilise Pt dispersion and Pt crystallites were formed. The main differences found between the dispersed and crystalline Pt phases are summarised in Table 1.2.

**Table 1.2:** Properties of Pt phases present in supported methane oxidation catalysts (29)

Pt phase	IR frequency of adsorbed CO (cm <sup>-1</sup> )	Turnover frequency (s <sup>-1</sup> ) at 335°C	Activation Energy (kJ.mol <sup>-1</sup> )
Dispersed	2068 (broad band)	0.001-0.01	137-162
Crystalline	2080 (narrow band)	0.05-0.11	116

Over Pd, the turnover frequency was found to depend on particle size (29). Samples which consisted of low concentrations of Pd highly dispersed on Al<sub>2</sub>O<sub>3</sub> had low activity. By contrast three samples which consisted of larger Pd particles exhibited high activity. In an accompanying paper (42), it was found that the extent of Pd oxidation depended on particle size. Small crystallites were completely oxidised at 300°C and 110 Torr of oxygen, while large crystallites were partially oxidised. The completely oxidised Pd was reported to disperse over Al<sub>2</sub>O<sub>3</sub> support as PdO while the partially oxidised Pd was broken into smaller crystallites which were covered with a layer of oxygen (42). It was found that CH<sub>4</sub> oxidation activity was 10 to 100 times higher on the latter phase (29). At 335°C, turnover rates were between 0.02 to 0.06 s<sup>-1</sup> and 1.2 to 5.6 s<sup>-1</sup> for dispersed PdO and Pd crystallites respectively. These turnover frequencies were based on initial dispersion and thus were thought not to be completely accurate, as bulk oxidation of Pd was found to occur under the reaction conditions which causes metal crystallites to break apart (42). This results in all the oxide which is formed being exposed and available to participate in catalysis. Recalculated average turnover values were estimated as 0.02 s<sup>-1</sup> for dispersed PdO and 1.3 s<sup>-1</sup> for Pd crystallites on the assumption that the dispersion was 1.0 for small particles and 0.5 for large particles (29).

The dependence of catalytic activity on time in the reaction mixture varied from sample to sample for both Pt and Pd (29). Morphological changes were indicated, by changes in the IR band of adsorbed CO with time in the reaction mixture, which could be correlated with changes in oxidation activity. It was noted that residual chlorine poisoning of some samples prepared by ion-exchange of the metal chloride with  $\gamma$ -Al<sub>2</sub>O<sub>3</sub>

may have been present. These samples exhibited reaction rates which increased steadily throughout the run, as if a poison was slowly being removed from the metal particles (29).

In support of these studies (27, 28, 29, 41), which have found changes in catalytic properties of Pt and Pd with changes in particle size, other studies have found variations in the oxidation state of the metals with particle size e.g. (39, 43, 44, 45). As previously discussed, Farrauto (39) found the existence of two types of oxygen species on supported Pd catalysts. One of these was associated with smaller well dispersed Pd particles which existed as PdO, with properties similar to crystalline palladium oxide. The other phase consisted of a palladium-oxide species dispersed on the surface of larger Pd particles (PdO<sub>x</sub>/Pd). Chou and Vannice (43) found variations in the Pd-O bond strength on supported Pd in a microcalorimetric study of oxygen adsorption. They found that the heat of oxygen adsorption strongly increases when the metal particle size decreases and concluded that changes in the electronic properties of small Pd crystallites were mainly responsible for the changes in metal-oxygen bond strength. It was thought that such electronic changes might therefore be responsible for changes in catalytic properties, rather than geometric reasons such as a requirement for multiple bonding of the reactant with the metal surface. This latter phenomenon might result in certain site ensembles with a specific arrangement of surface atoms having higher activity (43). The existence of two distinct phases of supported Pt catalysts, namely dispersed PtO<sub>2</sub> and crystalline Pt, has been shown (44). In a separate study, variation in the reducibility of the two phases following preoxidation has been shown using XPS (45). Following reduction at 150°C, particulate Pt was present as the reduced metal, but dispersed Pt required a higher temperature for reduction and thus was still oxidised. In this study (45), dispersed Pt was thought to exist as PtO rather than PtO<sub>2</sub>. Mc Cabe et al. (46) found the oxidation of Pt particles to have a passive nature. In other words, oxidation is essentially limited to the surface layer of Pt atoms and thus smaller Pt particles were more completely oxidised than larger crystallites (46).

Baldwin and Burch (30, 31) investigated a variety of supported Pd samples for CH<sub>4</sub> oxidation and could find no sensible correlation between Pd particle size and catalytic activity. In the initial study (30), Pd/Al<sub>2</sub>O<sub>3</sub> catalysts (1 and 5 wt.% Pd) were prepared by wet impregnation from palladium chloride solutions acidified with hydrochloric acid. Before testing, the samples were calcined using a variety of calcination temperatures (500-850°C) and times. Hydrogen chemisorption was used to determine Pd surface areas and dispersions. Average Pd particle diameters were in the range 2 to 70 nm. Results indicated that catalysts with higher metal loadings and those which were calcined at high temperatures had larger Pd particles. Catalyst testing was

performed under continuous-flow conditions in an oxygen-rich atmosphere (1% CH<sub>4</sub>/air). Problems such as external or internal diffusion limitations and severe temperature gradients within the catalyst bed were deemed to be absent under the conditions used to test the samples (30).

On initial testing of the calcined samples, area specific rate constants (at 350° C) were much larger for samples prepared with  $\delta$ -Al<sub>2</sub>O<sub>3</sub> than for those prepared with  $\gamma$ -Al<sub>2</sub>O<sub>3</sub> (30). However for both supports no correlation between the area specific rate constant and Pd particle size was found. For example two catalysts, 5 wt.% Pd/ $\gamma$ -Al<sub>2</sub>O<sub>3</sub> and 5 wt.% Pd/ $\delta$ -Al<sub>2</sub>O<sub>3</sub>, which were calcined under identical conditions had similar particle sizes (70 and 61 nm respectively) but had area specific rate constants differing by almost a factor of 100. Catalyst activity was found to increase with time during the course of the reaction for many samples. For some samples this activation occurred within a few minutes of introducing the reaction mixture while for others activation continued for up to five days or more. Fig. 1.8 illustrates an example of this phenomenon.

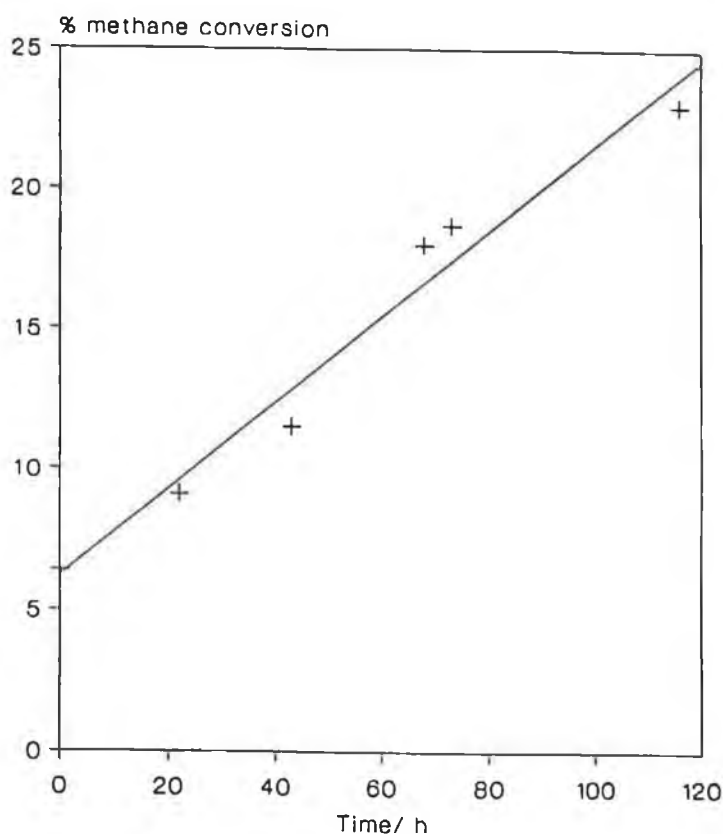


**Figure 1.8 : In-Situ activation of 1 wt.% Pd/Al<sub>2</sub>O<sub>3</sub> in a 1% CH<sub>4</sub> in air reaction mixture. Plot of CH<sub>4</sub> conversion versus time at 375° C (30).**

Hydrogen chemisorption results showed that the effect of the activation was to increase the Pd particle size, while at the same time increasing the activity with CH<sub>4</sub> conversion occurring at lower temperatures, as shown in Fig 1.9 (30). Sintering of the Pd particles on activation was not, however, thought to be the reason for the increased activity. On comparing two 5 wt.% Pd/ $\gamma$ -Al<sub>2</sub>O<sub>3</sub> samples, one of which was activated (at 405°C for 60 hours following calcination at 500°C for 16 hours) and one freshly calcined (at 600°C for 16 hours), the activated sample was 94 times more active despite containing the same average Pd particle size (8.8 nm) as the calcined catalyst. As both samples used the same support, a simple support effect could not be used to explain the activity enhancement. Heat retention was ruled out as a possible cause of apparent activation as activated samples were found to be active 100°C below the unactivated samples (see Fig 1.9) and had been stored at room temperature prior to retesting. Pulse experiments, in which a significant build-up of heat was not possible, confirmed activity enhancement after heating the samples in the reaction mixture. Thus, the activity enhancement was concluded as being a real and permanent effect caused by exposure to the reaction mixture (30).

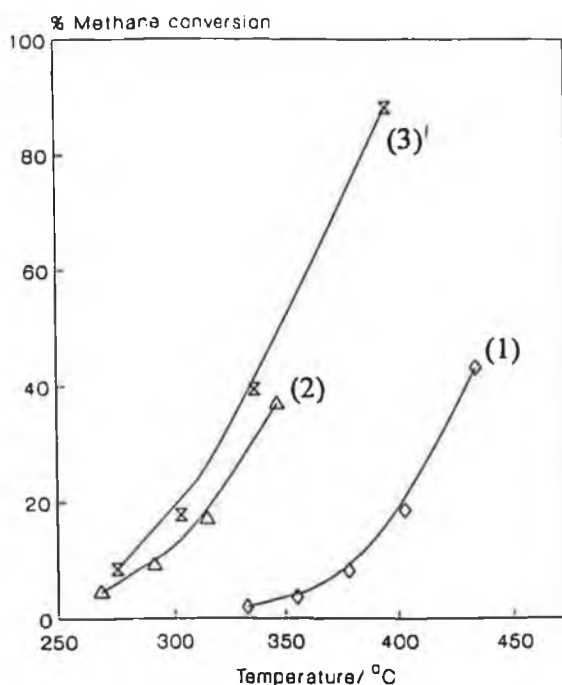


**Figure 1.9 : CH<sub>4</sub> Conversion versus Temperature over 5 wt.% Pd/Al<sub>2</sub>O<sub>3</sub> (30).** (1) - fresh sample. (2) - sample activated in 1% CH<sub>4</sub> in air for 144 hours at 373°C. (3) - sample activated in 1% CH<sub>4</sub> in air for 60 hours at 405°C.

Separate experiments demonstrated that activation could not be achieved on heating in air or in methane and could not be attributed to the effects of water vapour produced in the CH<sub>4</sub> combustion reaction (30). It was only when the reaction between air and CH<sub>4</sub> was actually taking place that activation was observed. In-situ modification of the nature of the Pd particles was proposed as one possible explanation, with activated metal particles exposing crystal faces which are more favourable for reaction. This might also explain why catalysts on  $\delta$ -Al<sub>2</sub>O<sub>3</sub> were more active than those supported on  $\gamma$ -Al<sub>2</sub>O<sub>3</sub>, due to differences in the morphology of the Pd particles on the different supports (30).

Further tests were performed to try and elucidate the reason for the activity enhancement on exposure to the reactants (31). Reconstruction of the palladium oxide crystallites was proposed as a possible cause with only a small fraction of the Pd surface being active for CH<sub>4</sub> combustion. Samples were examined with Al<sub>2</sub>O<sub>3</sub> and SiO<sub>2</sub> supports using palladium nitrate and palladium chloride. Samples were calcined at temperatures between 400-600°C for 16 hours. Both the support material and precursor salt were found to affect catalyst behaviour but were not the primary cause of increased activity of the catalysts. Pre-reduction of the samples was found not to affect activation i.e. very significant changes in the activity of the samples could occur for precursors which were calcined, or calcined and then reduced prior to testing (31).

The possibility that increased activity with time on stream was due to the removal of chlorinated species has been previously proposed (29). This possibility was thought to be unimportant in the above study (31), as passing wet air over the catalysts did not noticeably affect the activity. Heating in wet air should remove HCl and thus accelerate activation but this was not found to be the case (31). The activity of some samples prepared from the nitrate precursor also improved on exposure to the reaction mixture, which further discounts the possibility of chlorine removal as the cause of activation. Carbon deposition was shown to occur under reaction conditions, even in the strongly oxidising environment, but the authors were unsure as to the role this might play in the activation process (31).

Reconstruction of the Pd catalysts under reaction conditions was proposed as the primary reason for activation (31). Silica-supported samples were found to show very strong changes in their TPR profiles after heating in the reaction mixture while the changes for alumina-supported samples were less dramatic. At the same time, silica-supported catalysts showed very quick, dramatic increases in activity during continuous-flow testing while alumina-supported samples were activated over much longer periods with similar large improvements in area specific rate constants. It was proposed that

reconstruction occurred more easily on  $\text{SiO}_2$  than on  $\text{Al}_2\text{O}_3$ , thus causing activation to occur over shorter periods of time on the former support (31).

Surface science studies were reported as having previously shown that the morphology of supported noble metals can be significantly altered by different gas treatments (31). It was thought that small molecules, such as  $\text{CH}_4$ , impinging on the catalyst surface with high kinetic energy could transfer some of this energy to surface atoms, thus facilitating restructuring of the surface. This in turn would facilitate bond breaking in the incident molecule. An alternative explanation was that, rather than this type of temporary reconstruction involving metal crystallites, the reconstruction involved palladium oxide particles with a slower more permanent reconstruction, driven by the energy evolved upon oxidation. It was noted that these mechanisms were only speculative but may explain the dramatic activity increases observed during  $\text{CH}_4$  combustion on supported Pd catalysts (30, 31).

Ribeiro et al. (47) studied the complete oxidation of  $\text{CH}_4$  in a reaction mixture of 2%  $\text{CH}_4$  in air at  $277^\circ\text{C}$ , and atmospheric pressure. Catalysts were prepared by incipient wetness impregnation of  $\text{Al}_2\text{O}_3$  and  $\text{ZrO}_2$  supports with  $\text{PdCl}_2$  or  $\text{Pd}(\text{NH}_3)_2(\text{NO}_2)_2$  precursors. Final calcination temperatures varied from  $500^\circ\text{C}$  to  $850^\circ\text{C}$ . Heat and mass transfer limitations were thought to be absent in their rate measurements (47).

The reaction products were found to strongly inhibit the oxidation reaction (47). The reaction order for  $\text{H}_2\text{O}$  was found to be -1. Inhibition was thought to be due to the ability of  $\text{H}_2\text{O}$  to compete effectively with  $\text{CH}_4$  for adsorption sites. It was proposed that  $\text{H}_2\text{O}$  may react with the active PdO sites to reversibly form  $\text{Pd}(\text{OH})_2$  at the PdO surface, effectively blocking access of  $\text{CH}_4$  to the active PdO phase. The inhibitory effect of  $\text{CO}_2$  was found to be more complex. At low levels, the reaction order was independent of  $\text{CO}_2$  concentration. However, above 0.5 vol.%  $\text{CO}_2$ , the observed reaction order was -2. The surface chemistry of this strong inhibition was unknown. It was noted that activity comparisons between different catalysts would be complicated by product inhibition and this might explain variations in reaction rates reported in the literature (47).

Sample activation on exposure to the reaction mixture was reported by Ribeiro et al. (47) for all samples tested. Most of the rate increase occurred during the first 3 hours of reaction and for the next 21 hours, the rate per gram of catalyst stayed constant or decreased slightly. The steady state rate was about 2.5 times the initial value. The only exception found to this general trend was a 0.77% Pd/Si- $\text{Al}_2\text{O}_3$  sample. Pretreatment of the catalysts in air was found to make activation more difficult. Reduction in  $\text{H}_2$  or

pretreatment in 100% C<sub>2</sub>H<sub>4</sub> or 100% CH<sub>4</sub>, before reaction, had no effect on the activation. It was concluded that samples were only activated on heating in the reaction mixture, and a surface reconstruction or change in morphology of the PdO phase under reaction conditions was proposed as a possible explanation. Sample activation was not due to gross redispersion of Pd during reaction as the number of active sites, measured by H<sub>2</sub> titration of adsorbed oxygen at 100°C, remained constant (47).

The dependence of reaction rate on Pd particle size and support material was determined, once steady state had been reached in the reaction mixture (47). The steady state turnover rate was found to vary from  $2 \times 10^{-2} \text{ s}^{-1}$  to  $8 \times 10^{-2} \text{ s}^{-1}$  when the particle size varied from 2 to 110 nm. It was concluded that CH<sub>4</sub> oxidation, under steady state conditions in excess oxygen, was a structure insensitive reaction. Particle size, support material, and Pd precursor salt were thought to have a minimal effect on the turnover rate. The large differences in turnover rates in other studies, e.g. (29), were attributed to the use of incompletely activated samples and the authors reported that their turnover rates were close to the maximum values reported in other studies (47). The small variation in turnover rate may have been due to non-structure-sensitive effects, such as the removal of chlorine (47). Treatment of the catalysts in air at temperatures below 727°C resulted in the formation of a stable PdO phase, which spread across the oxide support surface as a monolayer and had low activity. A bulk PdO phase formed on metallic Pd, produced by calcination at 850°C, had the highest per site activity (47).

Marti et al. (48) recently investigated CH<sub>4</sub> oxidation on novel Pd/ZrO<sub>2</sub> catalysts, prepared by oxidation of Pd<sub>1</sub>Zr<sub>3</sub> metal alloy under different conditions. Kinetic studies were carried out in a continuous fixed-bed microreactor at temperatures of 127-527°C and atmospheric pressure, using a reactant mixture ratio of CH<sub>4</sub>:O<sub>2</sub> = 1:4. Analysis of the reaction mixture was achieved with an on-line quadrupole mass spectrometer. Turnover frequencies were calculated on the basis of moles of CO<sub>2</sub> produced at 247°C per second per mole of surface Pd initially present. Catalysts prepared from the metal alloy were activated by heating, either in air at a temperature between 300 and 450°C for 2 hours, or by in-situ activation in the reaction mixture at these temperatures for 2 hours. Two reference catalysts, 5 wt.% Pd/ZrO<sub>2</sub> and 25.6 wt.% Pd/ZrO<sub>2</sub>, were prepared by incipient wetness impregnation and co-precipitation, respectively. These samples were calcined in air at 500°C for two hours and then reduced in H<sub>2</sub> for 2 hours at 300°C. For both conventionally prepared samples, activity was found to improve on exposure to the reaction mixture. Because of this, both reference samples were treated in the reaction gas mix at 450°C for 2 hours prior to kinetic measurements. The turnover values of the catalysts prepared from Pd<sub>1</sub>Zr<sub>3</sub> were more than twice as high as those of the conventionally prepared catalysts. The overall activities

of the catalysts prepared from Pd<sub>1</sub>Zr<sub>3</sub> were dependent on the conditions of activation. Turnover rates varied from  $2.0 \times 10^{-3}$  to  $3.3 \times 10^{-3} \text{ s}^{-1}$  for these samples, with the most active sample being one which was prepared from the amorphous alloy by in-situ activation at 425°C. Apparent activation energies varied from 88 to 97 kJ.mol<sup>-1</sup> for the alloy samples. The 5 wt.% Pd/ZrO<sub>2</sub> and 25.6 wt.% Pd/ZrO<sub>2</sub> had apparent activation energies of 94 and 76 kJ.mol<sup>-1</sup> respectively. The high turnover rates for the samples prepared from Pd<sub>1</sub>Zr<sub>3</sub> alloy were attributed to an extremely large interfacial area between palladium phases (Pd and PdO) and the zirconia support in these samples. This was thought to help stabilise the active PdO phase against reduction to the pure metal due to an enhanced supply of oxygen through the ion-conducting zirconia to the active Pd phases (48, 49). The superior catalytic performance of similar catalysts, prepared from amorphous PdZr<sub>2</sub> alloys, for CO oxidation was also explained in this manner (49). XPS analysis showed that zirconia existed as non-stoichiometric ZrO<sub>2-x</sub>, in the surface and subsurface region (49).

### 1.3.2 Oxidation of Higher Hydrocarbons

Hiam et al (50) studied the catalytic oxidation of C<sub>2</sub> to C<sub>4</sub> alkanes on a Pt filament. The ignition temperature for each hydrocarbon was measured, as a function of hydrocarbon concentration for various hydrocarbon-O<sub>2</sub> mixtures, with O<sub>2</sub> concentrations well in excess of the stoichiometric requirements. The temperature of the filament was gradually increased, in a constant flow of the reactant gases, until exothermic reaction began. Reaction caused a change in filament resistance which was measured with the Wheatstone bridge apparatus. For n-C<sub>4</sub>H<sub>10</sub>, the ignition temperature varied from 180°C at an O<sub>2</sub>:C<sub>4</sub>H<sub>10</sub> ratio of 53:1 to 227°C at an O<sub>2</sub>:C<sub>4</sub>H<sub>10</sub> ratio of 238:1. For C<sub>3</sub>H<sub>8</sub> the ignition temperature varied from 220°C at an O<sub>2</sub>:C<sub>3</sub>H<sub>8</sub> ratio of 43:1 to 285°C at an O<sub>2</sub>:C<sub>3</sub>H<sub>8</sub> ratio of 192:1. Kinetic data were examined for C<sub>2</sub>H<sub>6</sub> and i-C<sub>4</sub>H<sub>10</sub> and the alkanes mentioned above. It was found that catalytic activity was related to the C-H bond strength of the hydrocarbon molecule, suggesting that hydrogen abstraction was involved in the adsorption process onto the metal surface. Oxidation of C<sub>3</sub>H<sub>8</sub> and n-C<sub>4</sub>H<sub>10</sub> was easier than that of C<sub>2</sub>H<sub>6</sub> and the introduction of a side-chain, such as in iso-butane, further decreased the activation energy required. The activation energies were found to be 113.6, 70.7, 70.7, and 42.4 kJ.mol<sup>-1</sup> for C<sub>2</sub>H<sub>6</sub>, C<sub>3</sub>H<sub>8</sub>, n-C<sub>4</sub>H<sub>10</sub>, and i-C<sub>4</sub>H<sub>10</sub> respectively. This suggested that both C<sub>3</sub>H<sub>8</sub> and n-C<sub>4</sub>H<sub>10</sub> involved an identical step,

such as hydrogen abstraction from  $\text{CH}_2$  rather than from the primary carbon atom, as in the case of  $\text{C}_2\text{H}_6$ . For  $i\text{-C}_4\text{H}_{10}$ , the introduction of a tertiary carbon atom further facilitated hydrogen abstraction in the catalytic process. Mass spectrometer analysis of the effluent stream from the reaction vessel indicated the formation of  $\text{CO}_2$  as the only carbon-containing product and this was thought to indicate the absence of gas-phase reactions under the conditions used (50).

In a further study of platinum- and palladium-catalysed oxidation of several organic compounds, Schwartz et al. (51) found platinum to be the more effective catalyst. The compounds investigated included aliphatic alkanes, alkenes, alcohols, and ketones. Catalytic oxidation was studied using a similar procedure to that described above (50) with hydrocarbon concentration kept at less than 2 vol.% of the total gas mixture (51). For alkanes, the oxidation rate was found to be first order in hydrocarbon over both Pt and Pd. Olefins exhibited first order kinetics over Pd but inverse fractional order for Pt (51).

$n\text{-C}_8\text{H}_{18}$  was found to have the same activation energy over Pt, as  $n\text{-C}_4\text{H}_{10}$  and  $\text{C}_3\text{H}_8$  in the previous study (50), i.e.  $\sim 70 \text{ kJ}\cdot\text{mol}^{-1}$ , indicating hydrogen abstraction from a secondary carbon atom was involved in the adsorption process for all three compounds (51). The catalytic properties for complete oxidation were suggested to be more favourable when the metal surface had the ability to chemisorb hydrocarbon and oxygen on neighbouring sites. Such a condition appeared to be more easily achieved with Pt rather than with Pd. The stronger tendency of Pd to be oxidised to a stable palladium oxide under the reaction conditions used, resulted in the exhibition of properties more similar to those of a metal oxide semiconductor than a metal, and this was thought to inhibit hydrocarbon adsorption onto the catalyst surface. This was thought to be particularly true in the case of alkanes while it had no deleterious effects with olefins or alcohols. Thus the process of alkane oxidation seemed to involve "balanced" chemisorption of both oxygen and hydrocarbon with the latter occurring by dissociative chemisorption in which the weakest C-H bond is broken (50, 51).

Cant and Hall (52) examined the catalytic oxidation of  $\text{C}_2\text{H}_4$  and  $\text{C}_3\text{H}_6$  over  $\text{SiO}_2$ -supported Pt, Pd, Ir, Ru, and Rh. Kinetic studies were performed in a single-pass flow reactor with a reactant stream of olefin,  $\text{O}_2$  and helium (to a total pressure of 1 atm). Because of the extreme exothermic nature of the reactions, low olefin conversions were maintained to keep the apparent rise in catalyst temperature due to heat of reaction below  $3^\circ\text{C}$ . Products were analysed by gas chromatography after pre-concentration by accumulation in a sampling loop at  $-78$  or  $-196^\circ\text{C}$  for a fixed time interval. Partial oxidation products were identified by comparison of retention times with those of

authentic samples and by mass spectroscopic analysis of samples eluting from the chromatography columns. Catalysts were prepared by impregnation of SiO<sub>2</sub> with aqueous solutions of Pd(NO<sub>3</sub>)<sub>2</sub>, Ru(NO<sub>3</sub>)<sub>3</sub>, Pt(NH<sub>3</sub>)<sub>2</sub>(NO<sub>2</sub>)<sub>2</sub>, Rh(NO<sub>3</sub>)<sub>3</sub> and H<sub>2</sub>IrCl<sub>6</sub> to produce noble metal loadings of ~ 5%. All samples were prereduced at 300°C for 3-6 hours before analysis (52).

CO<sub>2</sub> and H<sub>2</sub>O were the main reaction products (52). The main partial oxidation products were acetic acid and acetaldehyde from C<sub>2</sub>H<sub>4</sub>. For C<sub>3</sub>H<sub>6</sub>, acrolein, acetone and small quantities of acrylic acid or propionic acid were also formed. Of these products, only acrolein was considered to fulfil the requirements for consideration as a possible intermediate in the total oxidation reaction to CO<sub>2</sub> and H<sub>2</sub>O. No C<sub>2</sub>H<sub>6</sub> or C<sub>3</sub>H<sub>8</sub> was produced during the oxidation of C<sub>2</sub>H<sub>4</sub> or C<sub>3</sub>H<sub>6</sub>, even though these noble metals were noted to readily effect self-hydrogenation of olefins under non-oxidising conditions (52).

The effect of changes in O<sub>2</sub> partial pressure (10-150 Torr) on the rates of olefin oxidation to CO<sub>2</sub> and H<sub>2</sub>O were examined at a constant olefin pressure of 20 Torr. Similarly, the dependence of reaction rates on olefin partial pressures (3-80 Torr) were determined at a constant O<sub>2</sub> pressure of 65 Torr. Three different types of pressure dependencies were found. For Pt and Pd, the rate of total oxidation decreased with olefin pressure and increased with oxygen pressure; for Rh and Ir, the rate increased with olefin pressure and was inhibited by oxygen; for Ru the rate increased with oxygen pressure and was nearly independent of olefin pressure. It was thought that the catalytic process might involve the adsorption of both reactants which must compete for surface sites, as rate dependencies tended to be negative order in one reactant or the other. Thus, for Pt and Pd, olefin adsorption might be expected to be stronger than O<sub>2</sub> adsorption, while for Ir and Rh, the reverse would be true. For each metal, the behaviour was similar for both olefins (52).

Activation energies were in the range 65 to 120 kJ.mol<sup>-1</sup> and tended to correlate inversely with the catalytic activity of the metals (52). The approximate order of activity for the oxidation of both olefins was Pt ≥ Pd > Ir > Ru ≥ Rh. Activity comparisons were made on the basis of the temperature at which each catalyst oxidised the olefins to CO<sub>2</sub> and H<sub>2</sub>O at a specific rate of 10<sup>12</sup> molecules.cm<sup>-2</sup>.sec<sup>-1</sup> under standard conditions of 20 Torr olefin and 65 Torr O<sub>2</sub>. This temperature varied from 91 to 198°C and 98 to 188°C for C<sub>2</sub>H<sub>4</sub> and C<sub>3</sub>H<sub>6</sub>, respectively. Activities were also compared on the basis of specific rates at 130°C for C<sub>2</sub>H<sub>4</sub> and at 150°C for C<sub>3</sub>H<sub>6</sub>. It was found that the specific activity increased as the %d character of the metals decreased. The %d character refers to the percentage participation of the metal atom d-orbitals in metal

bonding e.g. the number of *vacancies* in the d-orbital is greater for Pd (46% d character) than for Rh (50% d-character). The fact that the order of activity was the exact reverse of that for reactions involving hydrogen led the authors to conclude that the reason for the differing catalytic activity of the metals was due to differing abilities to activate oxygen, rather than olefin (52).

Yu-Yao (53) investigated the oxidation of CO, C<sub>3</sub>H<sub>6</sub>, 1-hexene, and toluene under excess oxygen over Pt, Pd, and Rh. The noble metal catalysts were either, supported on  $\gamma$ -Al<sub>2</sub>O<sub>3</sub> powder (0.023% to 0.22% noble metal loading) by conventional impregnation, or used in the form of unsupported metal wires. Supported catalysts were calcined in air at 600, 700, 800 or 900°C for 4 hours before testing. A flow reactor apparatus was used at reaction temperatures between 150 and 500°C.

The rate measurements were conducted in three modes (53). The first type of measurements were used for the evaluation of kinetic parameters, for which the reactor was operated isothermally with conversion levels below 20%. The second type was used to study the existence of partial oxidation reactions and higher conversions were utilised. Finally, the % conversion to CO<sub>2</sub> was measured as a function of temperature to give activity indicator curves for the practical application of the catalysts. Noble metal dispersions were estimated using CO chemisorption for the supported samples (53).

On comparing alumina-supported precious metals with unsupported wires, two different types of kinetics were exhibited for the oxidation of hydrocarbons and carbon monoxide (53).

Oxidation of the unsaturated hydrocarbons over the unsupported wires was found to be positive order with respect to O<sub>2</sub> and inhibited by olefin for Pt and Pd, while for Rh the reverse was true (53). This is in agreement with the kinetic parameters determined by Cant and Hall for SiO<sub>2</sub> supported samples (52) and was again rationalised on the basis of a Langmuir-Hinshelwood mechanism involving competitive adsorption of both hydrocarbon and O<sub>2</sub> on the metal surface (53). In such a case, the lower ionisation potential of Rh, which should lead to stronger O<sub>2</sub> adsorption, would explain self-poisoning by O<sub>2</sub>. For Pt and Pd, strong adsorption of the unsaturated hydrocarbons through the  $\pi$ -bonds was proposed to explain the apparent negative order in olefin. The kinetics of oxidation of C<sub>3</sub>H<sub>6</sub> and 1-hexene were similar but showed a sharp contrast to those found for alkanes in a separate study (54). This suggested that adsorption of olefins on the surface through the double bond was a common step which played a primary role in the oxidation reaction with a minor effect of the chain length (53).

Supported noble metal catalysts showed two types of kinetics, referred to as type 1 and type 2 (53). Type 1 kinetics was used to describe catalysts whose kinetics resembled those of the unsupported wires. For type 2 kinetics, the olefin oxidation was less self-inhibited by hydrocarbon (for Pt and Pd) and by O<sub>2</sub> (for Rh) than for samples exhibiting Type 1 kinetics. Type two kinetics was generally associated with lower precious metal concentrations and higher dispersions. On such surfaces, the activation energy for olefin oxidation was generally found to be lower with metal surfaces of higher oxidation state involved. The conversion curves differed for the two types of kinetic behaviour. Type 1 samples were found to exhibit more dramatic light-off phenomena with a sharp rise in conversion from 20 to 100% in a very narrow range of temperature. In-situ reduction of samples exhibiting type 2 kinetics often lead to conversion curves approaching those typical of type 1 for CO oxidation. It was thought that type 2 sites were in a more oxidised state during reaction and thus were more characteristic of Rh and Pd than Pt (53).

Activity comparisons were only made for samples with similar kinetic parameters (53). While the specific rate of CO oxidation was found to be similar for both supported and unsupported samples showing Type 1 kinetics, that of C<sub>3</sub>H<sub>6</sub> was at least one order of magnitude lower on supported catalysts. This was rationalised based on a size effect with the larger hydrocarbon molecule requiring several adjacent metal sites for adsorption (53).

Partial oxidation products were observed in the oxidation of C<sub>3</sub>H<sub>6</sub>, C<sub>6</sub>H<sub>12</sub> and toluene e.g. CO, aldehydes (53). The amount of partial oxidation products formed depended on the reaction conditions, the hydrocarbon and the metal involved. Partial products increased with decreasing O<sub>2</sub>:hydrocarbon ratio and decreasing reaction temperature. Pt gave the lowest degree of complete combustion and Rh the highest. The tendency of the olefins to result in partial oxidation products was greatest for C<sub>6</sub>H<sub>12</sub> and smallest for C<sub>3</sub>H<sub>6</sub> (53).

In a similar study of C<sub>1</sub> to C<sub>4</sub> n-alkanes under oxidising conditions, by the same author, complete conversion of the hydrocarbon to CO<sub>2</sub> was reported to occur in all cases (54). Although no reason was given to explain the greater tendency of the unsaturated hydrocarbons to form partial oxidation products (53, 54), the trends shown may suggest that partial oxidation is favoured under reaction conditions which result in lower O<sub>2</sub> and greater hydrocarbon surface coverage of the noble metal. Schwartz et al. (51) also reported that partial oxidation of olefins (C<sub>2</sub>H<sub>4</sub>) was favoured at lower O<sub>2</sub> concentrations.

For the alkane oxidation study (54), noble metal catalysts on  $\gamma$ - $\text{Al}_2\text{O}_3$  were prepared and calcined, in the same manner as that described above (53), in the range 0.022-1.0%. Most of the kinetic parameters reported were obtained with  $\text{O}_2$ /alkane ratios ranging from 0.7 to 5 times the stoichiometric ratio for the alkane. Kinetic parameters were found to be quite similar for  $\text{Al}_2\text{O}_3$ -supported catalysts and unsupported wires for each precious metal/alkane couple. Reaction rate was fractional order with respect to alkane and zero order with respect to  $\text{O}_2$  for Pd and Rh catalysts. Over Pt catalysts, the partial reaction orders varied from 0.6 to 3 for the alkanes and from -1 to -3 for  $\text{O}_2$  depending on the hydrocarbon chain length. Kinetic parameters were found to be more difficult to measure for Pt as they varied with reaction conditions. For Pt, reaction rate increased with increasing chain length of the alkanes while for the other metals this increase was not as pronounced. A mechanism was proposed involving dissociative chemisorption of the alkane as the rate-determining step, followed by its' reaction with  $\text{O}_2$  adsorbed on an adjacent site. Adsorption of the reactants was thought to be competitive and hence surface coverage of each was interdependent. Both Pd and Rh were expected to be covered with oxygen under  $\text{O}_2$  rich conditions. However Pt, because of its' higher ionisation potential, was expected to have decreased  $\text{O}_2$  surface coverage and thus reaction rate was predicted to vary more with hydrocarbon/ $\text{O}_2$  ratio and ease of chemisorption of the alkane. Under reducing conditions, a reversal of the sign of the reaction orders on Pt was noted. Activation energies for Pd and Rh wires varied from 70 to 108  $\text{kJ}\cdot\text{mol}^{-1}$ . For Pt wire values ranged from 87 to 108  $\text{kJ}\cdot\text{mol}^{-1}$ . Because of large differences in the kinetics, a general comparison of the activity of the three metals was thought to be unwarranted. However, it was noted that the activity of Pd wire for the oxidation of  $\text{CH}_4$  and  $\text{C}_2\text{H}_6$  was greater than that of Pt, while for  $\text{C}_3\text{H}_8$  and  $\text{C}_4\text{H}_{10}$ , Pt was more active (54).

Although the kinetic parameters were found to be unchanged for supported and unsupported samples, the reaction rate per surface precious metal atom i.e. the specific reaction rate, over each  $\text{Al}_2\text{O}_3$  supported sample was less than that over the corresponding wire (54). Specific reaction rates were measured for a reaction mixture of 1%  $\text{O}_2$  and 0.1% alkane and generally decreased with increasing dispersion of the supported noble metal. For example, an increase in the calcination temperature of a 0.22% Pt/ $\text{Al}_2\text{O}_3$  sample from 600 to 900°C caused a decrease in Pt dispersion from 0.19 to 0.06 moles of CO chemisorbed per mole of Pt. At the same time the total oxidation activity towards n- $\text{C}_4\text{H}_{10}$ , expressed as the total number of moles of  $\text{CO}_2$  produced per second per mole of Pt at 225°C, only decreased from 0.42 to 0.31 (54).

At a given dispersion, the deactivation by the  $\text{Al}_2\text{O}_3$  support for each metal was less for  $\text{CH}_4$  than for the larger molecules (54). This was consistent with an idea that

more adjacent sites were needed for the adsorption of the larger alkanes. Highly dispersed metal was thought to oxidise more easily which may also have contributed to the lower activity, in line with results for samples containing CeO<sub>2</sub> [see section 1.4] (54).

The specific reaction rate over Rh/Al<sub>2</sub>O<sub>3</sub> was less dependent on dispersion than it was for Pt and Pd (54). The total oxidation activity, expressed per mole of Rh, decreased sharply with increasing calcination temperature. It was thought that aging of Rh/Al<sub>2</sub>O<sub>3</sub> may have been different from that of Pt/Al<sub>2</sub>O<sub>3</sub>, even though both showed large decreases in dispersion, as Rh can be incorporated into the sublayer of Al<sub>2</sub>O<sub>3</sub> upon heating above 700°C (55). In a previous study (56), the oxidation of n-C<sub>4</sub>H<sub>10</sub> on 0.34-12.40 wt.% Rh/Al<sub>2</sub>O<sub>3</sub> (pretreated at 500°C) was found to be structure insensitive under highly oxidising conditions. On catalysts of low Rh loading, the oxidation rate increased until the saturation concentration of Rh on the Al<sub>2</sub>O<sub>3</sub> surface was reached beyond which the rate levelled off. The turnover number per surface Rh atom was found to remain fairly constant over the complete concentration range. The activation energy also remained constant at ~100 kJ.mol<sup>-1</sup> and the reaction orders with respect to n-C<sub>4</sub>H<sub>10</sub> and O<sub>2</sub> were 0.2 and 0.1 respectively (56).

The possibility of structure sensitivity in the oxidation of CH<sub>4</sub> has already been discussed e.g. (27, 28, 29). Investigations of particle size effects in the oxidation of higher hydrocarbons on supported metal catalysts have also been reported e.g. (26, 57, 58).

Carballo and Wolf (57) studied kinetics and crystallite size effects in the oxidation of propylene on 1% Pt/γ-Al<sub>2</sub>O<sub>3</sub>. The experiments were carried out in a dual reactor-chemisorption apparatus which allowed for in-situ determination of Pt particle size by H<sub>2</sub> chemisorption. Analysis was achieved by gas chromatography. Catalyst preparation was by impregnation of γ-Al<sub>2</sub>O<sub>3</sub> powder with chloroplatinic acid and the sample was then prerduced at 500°C for 12 hours. This resulted in a Pt particle size of 11Å. Samples with Pt particle sizes of 60 and 144Å were prepared by sintering of the 11Å catalyst at 700°C in O<sub>2</sub> for 10 hours and 30 hours, respectively. Both of these samples were then reduced again at 500°C for 12 hours (57).

Kinetic experiments were performed at C<sub>3</sub>H<sub>6</sub> conversions lower than 20%, using C<sub>3</sub>H<sub>6</sub> concentrations in the range 0.1 to 2% (v/v) with a constant O<sub>2</sub> concentration of 20% (v/v) (57). In one run, O<sub>2</sub> concentration was varied to establish the effect on reaction. Reaction rate generally decreased during reaction. Oxygen pretreatment restored the catalytic activity suggesting a form of self-poisoning due to carbon residues from the hydrocarbon-oxygen mixture. Surface rearrangements under the reaction mixture were mentioned as being possible. It was found necessary to pretreat all catalysts

at 360°C in O<sub>2</sub> for 2 hours prior to testing in order to attain maximum reaction rate, minimum deactivation and improved reproducibility (57).

Reaction rate was determined for all three catalysts at 100, 110, 120 and 130°C (57). At low C<sub>3</sub>H<sub>6</sub> concentrations, the rate increased with C<sub>3</sub>H<sub>6</sub> concentration until it reached a maximum and then decreased. At high C<sub>3</sub>H<sub>6</sub> concentrations the rate became concentration independent (see Fig 1.10). The order with respect to O<sub>2</sub> concentration was 0.5. The data obtained did not fit a simple reaction mechanism, such as Langmuir-Hinshelwood kinetics, and were thought to suggest a complex reaction network. An apparent activation energy of ~42 kJ.mol<sup>-1</sup> was found for the 11Å sample which was noted as being somewhat lower than previously reported values e.g. (51, 52). This was ascribed to the different pretreatment procedure used in this study (57).

Comparison of the reaction rate per gram of catalyst for the samples, with crystallite sizes of 11, 60, and 144Å, revealed only a slight decrease with increasing Pt particle size (57). Thus, the specific reaction rate per square meter of surface Pt increased considerably for the larger crystallite size (144Å) e.g. Fig 1.10 below.

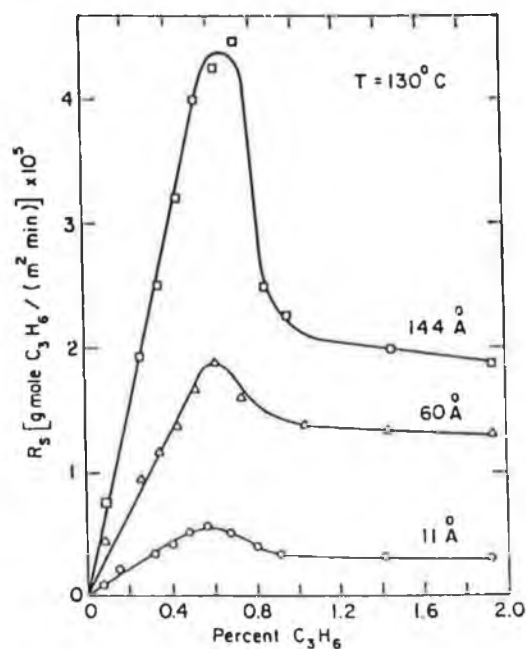


**Figure 1.10 : Specific Reaction Rate ( $R_s$ ) versus C<sub>3</sub>H<sub>6</sub> Concentration at 130°C for three different Pt particle sizes (57).**

It was envisaged that the increase in crystallite size decreased the fraction of Pt atoms in edges and kinks and increased the fraction of atoms in terraces (57). It was suggested that propylene is oxidised more readily on the latter because the bonds between the metal and reactants are weaker in these terrace sites leading to higher specific reaction rates. The authors assumed that the reduction in surface metal area, as

shown by chemisorption results for the sintered samples, was mainly due to crystallite growth rather than metal encapsulation by the support. This assumption was based on electron microscopy studies in the literature which demonstrated that in the temperature range investigated, the major result of heating the catalyst in air was crystallite growth. In support of this argument, Harris (59) found, using TEM, that heating of Pt/Al<sub>2</sub>O<sub>3</sub> in air at 700°C produced rapid sintering, with particle sizes increasing from 50 to 300 Å after 8 hours. Furthermore, Carballo and Wolf (57) believed that metal encapsulation would prevent reaction from occurring as well as H<sub>2</sub> chemisorption.

Völter et al. (26) investigated the effect of platinum oxidation state on the combustion of n-heptane by using different pre-treatments and reaction conditions for Pt/Al<sub>2</sub>O<sub>3</sub> samples. In a previous study, it was found that in highly dispersed systems the Pt exists in an oxidised form as Pt<sup>4+</sup>, whereas treatment at high temperatures causes a decomposition of the highly dispersed phase into poorly dispersed metallic Pt i.e. crystalline Pt (44). Combustion was found to occur on both phases, but the latter was more active (26).

Two types of Pt/Al<sub>2</sub>O<sub>3</sub> catalyst were prepared, one containing 0.5 wt.% Pt prepared by impregnation of  $\gamma$ -Al<sub>2</sub>O<sub>3</sub> with H<sub>2</sub>PtCl<sub>6</sub> referred to as (PtCl), and one containing 0.1 or 0.5 wt.% Pt with no chlorine present referred to as (Pt) (26). Total oxidation of n-C<sub>7</sub>H<sub>16</sub> was monitored using a continuous flow system with 0.1g of catalyst. A flow of O<sub>2</sub> or air saturated with 10 Torr n-C<sub>7</sub>H<sub>16</sub> was used and conversion was determined by gas chromatography. The testing procedure used involved initially heating the sample in O<sub>2</sub> or air to 350°C and then adding n-C<sub>7</sub>H<sub>16</sub>. The temperature was then decreased in steps of 10°C with conversion determined at each step after 20 minutes. Once the lowest temperature at which reaction occurred was reached the sample was heated up, step by step, again. Calination of the samples was performed between 500 and 900°C, to produce a range of Pt dispersions for both types of catalyst. Pt dispersions were measured using H<sub>2</sub> chemisorption at 0°C. The only reaction product reported was CO<sub>2</sub> (26).

As the amount of crystalline Pt increased with increasing calcination temperature for the chlorine-containing (PtCl) sample, so did the conversion of n-C<sub>7</sub>H<sub>16</sub> (26). For example, at 195°C, conversion was less than 10% for a sample calcined at 500°C, while for a sample calcined at 900°C conversion was greater than 40%. This increase in activity with increasing calcination temperature was ascribed to increased metallic character of the Pt. Treatment of a (PtCl) sample in argon at 900°C, which produced even more metallic Pt, caused an even greater increase in activity with conversion increasing to greater than 80% at 195°C. Pre-reduction of the (PtCl) sample in H<sub>2</sub> at 500°C, also

produced a highly active species for n-heptane oxidation. This was attributed to the formation of some large Pt crystals during reduction as dispersed Pt would be expected to reoxidise during heating up, before starting the reaction. For the non-chloride containing (Pt) sample, calcination temperature was found to have very little effect on conversion which remained at a constant level between 40 to 60% at a reaction temperature of 230°C. The initial dispersion was relatively low which hinted to the existence of larger amounts of active crystalline Pt, even after low temperature calcination at 500°C, for non-chloride containing samples. It was noted that the independence of activity on thermal treatments for (Pt) samples could also have been indicative of a heterogeneous-homogeneous reaction mechanism with only a small amount of crystalline Pt necessary to initiate combustion. Treatment of the (Pt) samples with HCl, heavily poisoned samples which were calcined at lower temperatures but had little effect on less dispersed (Pt) samples. Chlorine was thought to poison the reaction, by enabling Pt redispersion to occur as found in a previous study (44). It was thought that the redispersion process would be more facile with a dispersed rather than a sintered sample. Hence the greater susceptibility of the (Pt) samples calcined at lower temperatures to chloride poisoning (26).

The study also found that combustion in pure oxygen, as opposed to air, was detrimental to oxidation activity for chloride-containing samples (26). This was thought to further indicate the greater activity of zero-valent Pt relative to oxidised Pt, as during the combustion in air a reducing effect of heptane in the mixture would become more dominant and the oxidised Pt will be more likely to be reduced. As with chloride poisoning, dispersed Pt was again more susceptible to O<sub>2</sub> poisoning than sintered Pt. The observed increase in activity with reduced dispersion only applied to oxidising reaction conditions as oxidation of dispersed surface Pt is less likely to occur under reducing atmospheres. Hence for the hydrogenation of CO under reducing conditions a decrease in activity with decreased dispersion was observed, and it was noted that this is also the case in other systems such as reforming reactions on Pt samples (26).

Völter et al. (26) also reported that under certain critical conditions very pronounced periodic oscillations of combustion occurred. This oscillatory behaviour was again explained in terms of the dual-site model proposed i.e. active metallic Pt competing in the combustion process with less active oxidic surface Pt. On maintaining a furnace temperature of 178°C, the catalyst temperature was found to vary between 140 and 190°C and the n-C<sub>7</sub>H<sub>16</sub> conversion between 10 and 95%. The frequency of this oscillation was about 0.8 h<sup>-1</sup> and it was only found for one particular sample. Basically, it was explained in terms of alternating formation and reduction of oxidic Pt. During the period of increasing conversion, exothermic reaction occurred on metallic Pt until almost all the

$\eta$ -C<sub>7</sub>H<sub>16</sub> was removed, after which time conversion began to decrease as there was an excess of O<sub>2</sub> in the mixture and the metallic Pt was transformed into less active oxidic Pt with a consequent drop in activity and hence temperature. Once conversion reached a minimum, the reducing effect of  $\eta$ -C<sub>7</sub>H<sub>16</sub> was restored along with activity (26).

Otto et al (58) found that the specific activity of Pt/ $\gamma$ -Al<sub>2</sub>O<sub>3</sub> catalysts, for C<sub>3</sub>H<sub>8</sub> oxidation, increased with increasing Pt particle size. Pt/Al<sub>2</sub>O<sub>3</sub> catalysts in the concentration range 0.03 to 30 wt.% were prepared by multiple impregnation of the support with chloroplatinic acid. Sample pretreatment involved calcination at 600°C, followed by reduction at 400°C in H<sub>2</sub> for 2 hours and then heating in O<sub>2</sub> at 500°C for 20 hours. This procedure was thought to maximise Pt dispersion on the support. Catalysts were tested in a recirculation batch reactor using an initial oxygen-rich mixture of 1.5 mol.% C<sub>3</sub>H<sub>8</sub> and 15 mol.% O<sub>2</sub> with Ar as the carrier gas. In most cases the initial pressures were 10 and 100 Torr for C<sub>3</sub>H<sub>8</sub> and O<sub>2</sub> respectively. Product analysis was achieved using mass spectroscopy and more than 97% of the carbon in C<sub>3</sub>H<sub>8</sub> was converted to CO<sub>2</sub>. The reaction was found to be first order with respect to C<sub>3</sub>H<sub>8</sub> and independent of O<sub>2</sub> concentration under the oxygen-rich conditions used (58).

To study the variation in oxidation activity as a function of Pt concentration, each reactor charge was fixed at 4 mg Pt (58). The rate constant for C<sub>3</sub>H<sub>8</sub> oxidation at 275°C was found to increase from  $1.25 \times 10^{-3} \text{ min}^{-1}$  at 0.03 wt.% to  $8.04 \times 10^{-3} \text{ min}^{-1}$  at 30 wt.% Pt. Pt dispersion was estimated using CO chemisorption at room temperature. It was found that Pt particle size increased with Pt loading, as the dispersion decreased. When the dispersion values were used to convert the reaction rates to rates per surface Pt atom, i.e. turnover frequencies, the activity increase with particle size was even more pronounced. The recalculated rate constants were  $1.15 \times 10^{-3}$  and  $9.20 \times 10^{-2} \text{ min}^{-1}$  for the 0.03 wt.% and 30 wt.% samples, respectively. Within experimental error, the apparent activation energy for the reaction remained constant within the particle size range investigated at  $\sim 92 \text{ kJ.mol}^{-1}$ . This indicated that the change in reaction rate with particle size was not due to a change in the rate determining step. The increased reaction rate on larger Pt particles was therefore thought to reflect a change in the reaction-site density rather than a change in Pt-O bond strength (58).

Sintering of highly dispersed Pt samples by heating in H<sub>2</sub> at high temperature was also found to increase the reaction rate (58). Sintering of a 0.12 wt.% Pt sample at 500°C in H<sub>2</sub> for 63 hours, resulted in an increase in the reaction rate constant at 275°C (per 4 mg Pt) from  $1.5 \times 10^{-3}$  to  $4.6 \times 10^{-3} \text{ min}^{-1}$ . It was found that excessive sintering ultimately defeated the benefits of an increased turnover frequency, achieved on the larger particles, because the fraction of surface Pt lost became too large. As the sintering

temperature was increased to 800°C, a maximum rate constant of  $10.3 \times 10^{-3} \text{ min}^{-1}$  was found which was thought to be comparable to the maximum achieved in the concentration experiments. A further increase in temperature to 900°C resulted in a lower rate. It was not possible to measure turnover frequencies for the sintered samples as chemisorption measurements could not be performed in-situ. On use of the sintered catalysts for propane oxidation, the activity slowly decreased to the initial rate. This effect was attributed to redispersion of the Pt in the presence of propane, as the decrease in activity was too slow to be attributed to O<sub>2</sub> poisoning. Pt particle size in the sintered samples was not measured but the increased rate was assumed to be due to Pt sintering as a previous TEM study (60) had showed that heating in H<sub>2</sub> above 500°C caused an increase in Pt particle size.

In comparing the catalytic oxidation of methane (41) with that of propane (58), it was found that the maximum turnover frequency exists at a smaller Pt concentration, and thus smaller Pt particle size, for methane oxidation (5 wt.% vs. 30 wt.% Pt). Propane oxidation was, therefore, more structure sensitive. The authors were less inclined to associate the increase in rate with the presence of more reactive oxygen on the larger particles as the activation energy remained constant with changes in Pt dispersion. As the reduction temperature of oxidised Pt is known to decrease with increasing particle size e.g. (45), the results suggested that either the removal of oxygen from Pt does not affect the activation energy or the reaction cannot take place on highly dispersed Pt (58). This latter supposition would imply that there are some larger Pt particles present, even in the most highly dispersed samples. A speculative explanation of the observed structure sensitivity was given involving a Langmuir-Hinshelwood reaction mechanism, in which propane was sparsely adsorbed on suitable sites or site ensembles which predominated on larger crystallites. It was suggested that surface oxygen facilitated the dissociation of C<sub>3</sub>H<sub>8</sub> molecules with the rate determining step involving surface reaction of an alkane-oxygen complex. The surface-complex concentration was thought to increase rapidly with particle size in the oxidation of C<sub>3</sub>H<sub>8</sub> (58).

The oxidation of C<sub>3</sub>H<sub>8</sub> over Pt has been found to depend on the support used as well as the particle size. Hubbard et al. (33) investigated C<sub>3</sub>H<sub>8</sub> oxidation on ZrO<sub>2</sub> and compared the results to those for Al<sub>2</sub>O<sub>3</sub>-supported samples in the above study (58). Pt/ZrO<sub>2</sub> samples in the concentration range 0.02 to 1.5 wt.% were prepared, pretreated and tested in the same manner as for the Pt/Al<sub>2</sub>O<sub>3</sub> samples. An O<sub>2</sub>:C<sub>3</sub>H<sub>8</sub> ratio of 12:1 was used for activity measurements, with each sample containing 4 mg Pt (33). Because of the large amounts of sample required for 0.02-0.04 wt.% Pt/ZrO<sub>2</sub> samples, mass transfer problems developed. To overcome this a constant amount of sample (1g) was used for these catalysts and the data was normalised to represent 4 mg. A ZrO<sub>2</sub> support

was chosen for comparison with  $\text{Al}_2\text{O}_3$  because of the distinctly different properties of the two supports. The zirconia used was a highly crystalline material with a relatively low BET surface area of  $5.5 \text{ m}^2/\text{g}$ , while the  $\text{Al}_2\text{O}_3$  was poorly crystalline with a much higher surface area of  $85 \text{ m}^2/\text{g}$  (33).

Under the excess  $\text{O}_2$  conditions used, the reaction on  $\text{Pt}/\text{ZrO}_2$  was found to be first order in  $\text{C}_3\text{H}_8$  and independent of  $\text{O}_2$  concentration (33). The apparent activation energy remained constant at  $\sim 74 \text{ kJ}\cdot\text{mol}^{-1}$  over the entire Pt concentration range studied. Hence changes in reaction rate for the different samples were attributed to changes in the density of active sites. Within experimental error, the difference in activation energy for  $\text{C}_3\text{H}_8$  over  $\text{Pt}/\text{Al}_2\text{O}_3$  (58) and  $\text{Pt}/\text{ZrO}_2$  (33) was thought to be insignificant. At a fixed amount of Pt (4 mg), the oxidation rate constant decreased from  $152 \times 10^{-3}$  to  $6.55 \times 10^{-3} \text{ min}^{-1}$  on increasing the metal concentration from 0.02 to 1.5 wt.%  $\text{Pt}/\text{ZrO}_2$ (33). Assuming a maximum dispersion of unity, the specific rate constant, per surface Pt atom, was greatest at the lowest concentrations and decreased by a factor of two to a constant value of  $72.9 \times 10^{-3} \text{ min}^{-1}$  above 0.10 wt.%. Thus, for  $\text{Pt}/\text{ZrO}_2$ , highly dispersed samples were more active; this was attributed to greater surface roughness and the presence of kink and step sites. Such surface sites were deemed to favour catalysis to a greater extent than the planar or terrace sites which predominate on larger particles. The specific rate constants as a function of metal concentration for  $\text{Al}_2\text{O}_3$  and  $\text{ZrO}_2$  supports are shown in Fig. 1.11 (33).

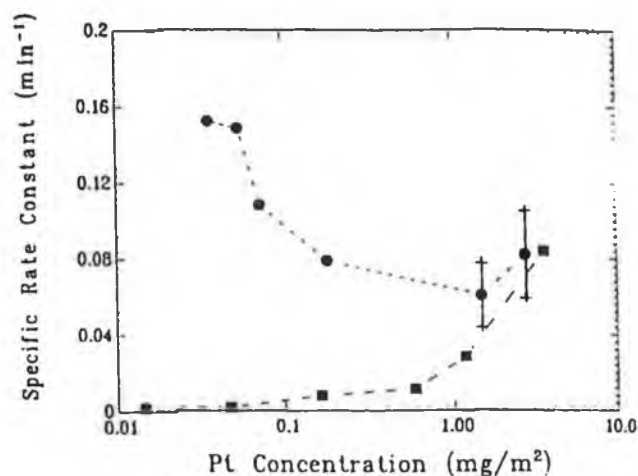


**Figure 1.11 : Specific Rate Constant for  $\text{C}_3\text{H}_8$  Oxidation (per Pt surface atom at  $275^\circ\text{C}$ ) versus Pt Concentration (33). (●)- $\text{Pt}/\text{ZrO}_2$  ; (■)- $\text{Pt}/\gamma\text{-Al}_2\text{O}_3$ .**

To account for the difference in support surface area the abscissa unit used in Fig 1.11 was a metal concentration term defined as the amount of Pt per BET surface area (33). The greater activity of  $\text{Pt}/\text{ZrO}_2$  compared to  $\text{Pt}/\text{Al}_2\text{O}_3$  at low Pt concentrations

was attributed to deactivation of small Pt particles by the  $\gamma$ -Al<sub>2</sub>O<sub>3</sub> support. At higher concentrations, the larger Pt particles were not in as close contact with the support material and hence the specific oxidation rate was not affected by the support material and is approximately the same for both supports. Studies have shown that small Pt particles supported on Al<sub>2</sub>O<sub>3</sub> require a higher reduction temperature (45, 55). This observation was concluded as being evidence of a metal-support interaction (33). ZrO<sub>2</sub> has been shown to be a less reactive support towards Pt by infrared data of CO adsorption (29). Dispersed Pt on  $\gamma$ -Al<sub>2</sub>O<sub>3</sub> had a CO adsorption band at 2068 cm<sup>-1</sup> and could be distinguished from crystalline Pt which had an adsorption band at 2080 cm<sup>-1</sup>. For Pt/ZrO<sub>2</sub> only one CO adsorption band at 2080 cm<sup>-1</sup> was observed over the entire concentration range. This was used as evidence that ZrO<sub>2</sub> does not interact strongly with Pt (33). Thus, it was speculated that highly dispersed Pt is very active provided the metal is supported on an inert material. An alternative explanation involving promotion of dispersed Pt by the ZrO<sub>2</sub> support could not be ruled out (33).

Treatment of a 0.10 wt.% Pt/ZrO<sub>2</sub> sample in H<sub>2</sub> at 500°C for 40 hours, resulted in significantly enhanced activity which was postulated as being due to removal of residual chlorine, not effected by standard pretreatment conditions (33). H<sub>2</sub> treatment of Pt/Al<sub>2</sub>O<sub>3</sub> samples also resulted in an increase in activity (41, 58). However for Pt/Al<sub>2</sub>O<sub>3</sub>, subsequent exposure of the catalyst to an oxidising environment, was found to reverse the effect of the H<sub>2</sub> treatment (41, 58) and this was attributed to redispersion of the Pt (44). Exposure to O<sub>2</sub> at 500°C was found to have no such effect on Pt/ZrO<sub>2</sub> which was explained in terms of a lack of metal-support interaction which prevents redispersion from occurring on Pt/ZrO<sub>2</sub> (33).

In a subsequent study (25), the C<sub>3</sub>H<sub>8</sub> oxidation activity of Pt supported on Al<sub>2</sub>O<sub>3</sub>, ZrO<sub>2</sub> and SiO<sub>2</sub> was investigated using two different types of reactors, a batch recirculation reactor and an integral flow reactor. Each sample contained 1 mg of Pt and the activity data for batch recirculation studies were recalculated to represent 4 mg of Pt, to allow comparison with earlier studies (33, 58). A flow mixture of 5 cm<sup>3</sup>/min C<sub>3</sub>H<sub>8</sub>, 70 cm<sup>3</sup>/min O<sub>2</sub> and 1300 cm<sup>3</sup>/min argon (C<sub>3</sub>H<sub>8</sub>:O<sub>2</sub> = 1:14) was used for integral flow studies, to measure C<sub>3</sub>H<sub>8</sub> conversion as a function of temperature in the range 150 to 500°C (25). Pt/SiO<sub>2</sub> samples were prepared in the concentration range 0.10-4.76 wt.% Pt. For metal loadings below 0.50 wt.%, samples were prepared using an ion-exchange method with tetraammine platinum chloride. Higher metal loadings were prepared by multiple impregnation of SiO<sub>2</sub> with chloroplatinic acid. The SiO<sub>2</sub> used had a surface area of 223.6 m<sup>2</sup>/g. A first order dependence in C<sub>3</sub>H<sub>8</sub> and zero order in O<sub>2</sub> was found for Pt/SiO<sub>2</sub> samples. The apparent activation energy was 69 kJ.mol<sup>-1</sup>. Within

experimental error, this value agreed with those for Al<sub>2</sub>O<sub>3</sub> (58) and ZrO<sub>2</sub> (33), and remained constant with variations in particle size (25).

For Pt/SiO<sub>2</sub>, the batch reactor data indicated a slight increase in activity with increasing particle size (25). However light-off curves obtained from flow-reactor experiments yielded a more substantial increase in activity with particle size. This was indicated by a decrease in the temperature of 50% conversion, T<sub>50</sub>, by about 50°C on increasing Pt concentration from 0.10 to 4.76 wt.%. For γ-Al<sub>2</sub>O<sub>3</sub> and ZrO<sub>2</sub> supports, the results of flow experiments agreed with those found in the batch recirculation studies discussed above (33). The activity of Pt/Al<sub>2</sub>O<sub>3</sub> was found to increase with metal concentration. T<sub>50</sub> decreased from ~390°C to ~350°C, on changing Pt loading from 0.05 wt.% to 9.17 wt.% (25). This indicated the 9.17 wt.% Pt/Al<sub>2</sub>O<sub>3</sub> sample to be about 50 times more active when Pt dispersions were taken into account. For Pt/ZrO<sub>2</sub>, lower metal loadings appeared to be more active. Over a 0.04 wt.% Pt/ZrO<sub>2</sub> sample, T<sub>50</sub> was 283°C compared to 315°C on a 0.81 wt.% Pt sample. When Pt surface areas were taken into account the activity was found to remain constant, within experimental error. For highly dispersed samples, the activity ranking was found to be,



using data from both reactors (25). For larger metal particles the effect of the support material was less pronounced. This was attributed to decreased metal-support interaction as the Pt concentration increased. Recirculation-batch reactor studies yielded the same turnover rates on all three supports at higher loadings. In disagreement, flow-reactor experiments showed an apparent activity decrease in the order silica > zirconia > alumina. The differences were difficult to explain but limitations of the light-off curves, and in particular of the parameter T<sub>50</sub>, in describing variations in catalytic activity were noted as possible contributing factors. Changes in catalytic activity with different supports were attributed to changes in reaction-site density, as changes in apparent activation energy, beyond experimental error, were not found (25).

Kooh et al. (61) investigated the effect of catalyst structure and carbon deposition, on n-C<sub>7</sub>H<sub>16</sub> oxidation over supported Pt and Pd catalysts with initial dispersions ranging from 3 to 81%. The catalysts were prepared from Pt(NH<sub>3</sub>)<sub>4</sub>Cl<sub>2</sub>, H<sub>2</sub>PtCl<sub>6</sub>, and H<sub>2</sub>PdCl<sub>6</sub> on ZrO<sub>2</sub> and Al<sub>2</sub>O<sub>3</sub> with BET surface areas of 83 and 40 m<sup>2</sup>/g respectively. Catalysts were prepared by either ion-exchange or incipient wetness impregnation and were calcined in air at temperatures between 500 and 900°C for 2 hours. n-C<sub>7</sub>H<sub>16</sub> conversions were monitored in a fixed-bed microreactor with 0.1-0.7g of catalyst and product analysis achieved using on-line gas chromatography. Reaction temperature was in the range 75 to 200°C with 20 Torr n-C<sub>7</sub>H<sub>16</sub>, 245 Torr O<sub>2</sub>, and 795

Torr helium. Conversions were maintained below 1% to prevent heat and mass transfer influences and CO<sub>2</sub> was the only product observed. Catalysts were characterised by in-situ gas titration, temperature programmed oxidation and infrared spectroscopy of adsorbed CO (61).

The turnover frequencies for both Pt and Pd samples were determined (61). Plots of the logarithm of turnover frequency versus time showed a decrease in slope after a certain period of time, for some catalysts, which indicated the existence of two sites of high and low intrinsic activity. These sites were labelled A and B respectively. The apparent activation energies for a 0.3 wt.% Pt/ZrO<sub>2</sub> sample and a 5.0 wt.% Pt/Al<sub>2</sub>O<sub>3</sub> sample, were found to be the same, within experimental error, at 79 kJ.mol<sup>-1</sup>. The activities of all the catalysts tested were compared by extrapolating the rate measurements to 140°C using an apparent activation energy of 79 kJ.mol<sup>-1</sup>. The turnover frequencies of the A sites were thereby determined as; 0.02 s<sup>-1</sup> for Pt particle diameters less than 20Å, 0.45 s<sup>-1</sup> for Pt crystallites greater than 50Å, 0.002 s<sup>-1</sup> for Pd crystallites less than 20Å, and 0.07 s<sup>-1</sup> for Pd particles greater than 50Å. For B sites, Pt was 10 times more active than Pd and large Pt crystallites were 4 times more active than small ones. The difference in turnover frequencies for different samples was attributed to changes in the density of active sites present (61).

Temperature programmed oxidation (TPO) experiments showed that a large quantity of carbon deposited on the catalysts during n-C<sub>7</sub>H<sub>16</sub> oxidation and this was found to result in deactivation of the samples during oxidation (61). The amount of carbon deposited during n-C<sub>7</sub>H<sub>16</sub> oxidation at low temperatures was found to exceed that deposited when the catalyst was exposed to heptane alone at the same temperatures. Measurement of the number of accessible metal sites by gas adsorption techniques, using H<sub>2</sub>, O<sub>2</sub>, and CO, also indicated carbon deposition after reaction. Most of the carbon could be displaced from the metal surface by regeneration, involving oxidation at 500°C for 20 minutes followed by reduction at 300°C for 20 minutes. It was thought that, during reaction, most of the metal surface was initially covered with carbon. TPO experiments showed that the amount of carbon deposition and the deactivation rate, depended on the support, the metal and the amount of metal deposited. Small Pt crystallites of less than 20Å in diameter deposited much less carbon and deactivated much more slowly than crystallites greater than 50Å in diameter. Switching from ZrO<sub>2</sub> (40 m<sup>2</sup>/g) to Al<sub>2</sub>O<sub>3</sub> (83 m<sup>2</sup>/g) for a 5 wt.% Pt sample increased the coke formation per surface metal atom 5 times, and decreased the deactivation rate 5.5 times. It was concluded that carbon formed on the metal sites could be removed either by oxidation to CO<sub>2</sub> or migration to the support. Increasing the support surface area or decreasing the metal particle size was thought to facilitate the latter phenomenon and it was concluded

that the faster the carbon migrates to the support, the slower the carbon fouls the metal surface and the slower the deactivation rate. The rates of n-C<sub>7</sub>H<sub>16</sub> oxidation and deactivation both followed zero-order dependencies on the n-C<sub>7</sub>H<sub>16</sub> and the O<sub>2</sub> partial pressures. These kinetics were thought to indicate fast adsorption of heptane and oxygen followed by slow surface reaction. The deactivation rate was first order in active sites with catalysts that were active for coke formation also being active for n-C<sub>7</sub>H<sub>16</sub> oxidation. Larger particles were thought to exhibit higher turnover frequencies for oxidation, higher rates of carbon accumulation and, if carbon migration to the support is slow, higher rates of deactivation (61).

Structure sensitivity in the oxidation of CO by Pt catalysts has also been investigated e.g. (62, 63). McCarthy et al. (62) studied CO oxidation on supported Pt as a function of sintering severity. It was found that at low CO concentrations the reaction was demanding with smaller Pt crystallites being less active. This was explained in terms of the small particles having a stronger tenacity for O<sub>2</sub> to yield PtO, from which entity O was extracted by CO with difficulty. As the crystallite size increased, O extraction was less difficult and the specific rate increased. At high CO concentrations the reaction was no longer structure sensitive and the rate was thought to depend solely upon the chemisorption of O<sub>2</sub> on a surface partially covered with CO (62). Akubuiro et al. (63) found the reaction to be structure sensitive in the entire CO concentration range studied. The decreased reaction rate on small Pt crystallites was attributed to stronger chemisorption of reactant molecules. The support used was found to affect the oxidation activity with Al<sub>2</sub>O<sub>3</sub>-supported samples having relatively low activity compared to other supports such as TiO<sub>2</sub> or SiO<sub>2</sub>. Infrared studies of CO adsorption indicated that the bond between Pt and CO was strongest for Pt/Al<sub>2</sub>O<sub>3</sub>. This was attributed to some form of metal-support interaction and resulted in lower activity towards CO oxidation in terms of both activation energy and turnover frequency (63).

### 1.3.3 Automotive Exhaust Catalysts

Automotive pollution control is a major application for precious metal catalysts. The three metals involved are Pt, Pd and Rh and several reviews of their use in automotive exhaust catalysts have appeared in the literature (5, 6, 7, 64, 65).

In 1989, 42% of the western worlds' demand for platinum was for the manufacture of autocatalysts, for palladium the corresponding figure was 8%, while for rhodium it was a massive 81% (66). The requirement for Pt, Pd and Rh in autocatalysts is determined by the reactions to be catalysed, which are

- Hydrocarbon  $\rightarrow$  H<sub>2</sub>O + CO<sub>2</sub> (oxidation)
- CO  $\rightarrow$  CO<sub>2</sub> (oxidation)
- NO<sub>x</sub>  $\rightarrow$  N<sub>2</sub> + H<sub>2</sub>O (reduction)

The principal requirement of the early autocatalysts was to oxidise unburnt hydrocarbons and carbon monoxide (66). To do this, catalysts of Pt, Pd or a mixture of these two elements were employed. In his review, Kummer (7) reported that the specific activity of Pd is greater than that of Pt for the oxidation of CO, olefins and CH<sub>4</sub>, while the opposite is true for the oxidation of paraffinic hydrocarbons (C<sub>3</sub> and higher). Silver et al. (67) found that, while Pt exhibited better performance than Pd under fuel-lean conditions the opposite was found under fuel-rich conditions. Pt was proposed to be more efficient in abstracting hydrogen from hydrocarbons than Pd (51), while Pd has been reported to be more efficient in adsorbing oxygen (36). Hence it was thought that in an oxygen rich environment when hydrogen abstraction is rate limiting, Pt should perform well, while under oxygen-lean conditions the greater affinity of Pd for oxygen would be preferred (67). When the fuel:oxidant ratio varies with time, as in automotive exhausts, the presence of both metals might, therefore, be expected to be beneficial. Pt is thought to be more resistant to poisoning while Pd is less susceptible to sintering (7, 68). Silver et al. (67) reported that because of greater resistance to sintering, Pd performed well after aging relative to Pt in an automotive exhaust environment.

More recently legislation has required the reduction of nitrogen oxides to nitrogen and water and rhodium has been introduced into autocatalysts (66). Kummer (7) stated that Rh is very active for NO reduction, is much less inhibited by CO and sulphur compounds in the fuel-rich region than Pt, produces less NH<sub>3</sub> than Pd and is therefore used as the principal ingredient for NO removal. In the early nineteen-eighties, dual bed systems were used containing a reduction catalyst (usually Pt/Rh) followed by an oxidation catalyst (usually Pt/Pd) (66). However modern technology employs sophisticated electronic control of air-fuel ratios to enable the use of a single catalyst to remove all three pollutants in one unit. Such "three-way" catalysts (TWCs) have been reported to almost invariably contain platinum and rhodium in a ratio of 5:1 as the active metals (66). Figure 1.12 illustrates the conversion efficiency of this type of Pt-Rh "three-way" catalyst for simultaneous CO, NO<sub>x</sub> and hydrocarbon removal as a function of the air-fuel ratio.

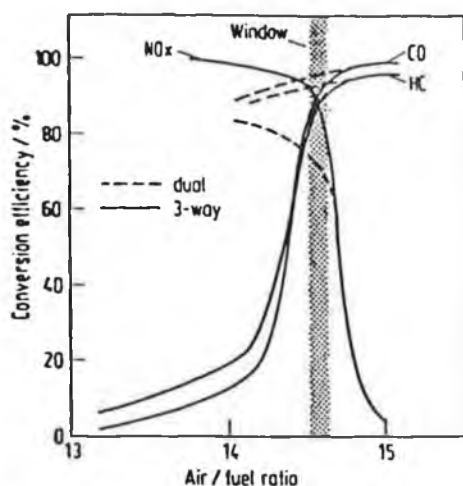


**Figure 1.12 : Typical Efficiency Scan for a Three-Way Catalyst as a function of Air:Fuel Ratio (69).**

From Fig. 1.12, it is evident that the "three-way" catalyst is capable of achieving efficient conversion of all three pollutants only when the air:fuel ratio is close to the stoichiometrically balanced composition of 14.6. Under conditions more reducing than the 14.6 air:fuel ratio, the conversion efficiency of the catalyst for reducing nitrogen oxides is high but the conversion efficiency for oxidising hydrocarbons and carbon monoxide declines rapidly. Under conditions more oxidising than 14.6, the efficiency of the catalyst for oxidising carbon monoxide and hydrocarbons is high and conversion of nitrogen oxides declines. In order to provide the stoichiometrically balanced exhaust gas composition required for efficient three-way catalyst operation, an air:fuel ratio control system has been developed for use in automobile exhaust systems. This involves a so-called closed-loop electronic control system which utilises an exhaust oxygen sensor and on-board microprocessor to control the engine's air:fuel ratio and provide exhaust gas compositions that help to maintain optimal conversions (69).

It has been reported that beneficial and detrimental effects of bimetallic synergism and alloying can further complicate these systems (67, 68). In 1995, Maire et al. (70) presented X-ray absorption spectroscopic evidence to support the existence Pt-Rh alloy phases in three-way catalysts. The presence of bimetallic particles was thought to be beneficial for practical catalyst performance but the authors were unsure as to the nature of these beneficial effects (70).

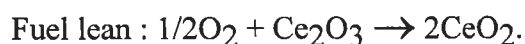
Progressive widening and tightening of automotive pollution control has led to more and more demand for precious metals in this application (66). Using larger catalyst volumes or increased noble metal contents is one way to improve performance. However factors such as high Pt and Rh prices, noble metal scarcity, low recycling recovery rates for Rh and increased global usage of noble metals make this an unfavourable option (67).

The use of alternative non-noble metal containing catalysts such as Cu-Cr systems (71) and perovskites (72) has been investigated and the use of Pd as an alternative metal to Pt has also received attention in the recent literature (67, 73). Engler et al. (73) reported that the growing interest in Pd systems is driven by its lower cost relative to Pt and also by potential scarcity problems with Pt due to its extensive use. It was noted that improvements in fuel quality with significantly lower lead and sulphur contents, poisons to which Pd is more sensitive than Pt, have led to greater interest in Pd in more recent years (73).

A more commonly applied route towards significant performance improvements involves the incorporation of base metal promoters into TWC formulations (67). The most common of these promoters is cerium which has been reported to enhance, in particular, the removal of  $\text{NO}_x$  and CO at near stoichiometric air-fuel ratios with only slight improvements in hydrocarbon oxidation activity (67).

The addition of base metal additives, such as  $\text{CeO}_2$  or  $\text{MoO}_3$ , to  $\text{Al}_2\text{O}_3$ -supported noble metals has been found to result in increased noble metal dispersion and to prevent agglomeration of the noble metals (7, 55, 74, 75). This was thought to allow for maximum utilisation of the noble metal surface (55). However, highly dispersed noble metals have been reported to exhibit lower specific activity per surface noble metal atom than larger metal particles particularly for the oxidation of paraffinic hydrocarbons (7, 75).

In automotive exhausts, the air/fuel ratio varies in a cyclic manner and catalyst performance can be improved by the use of a component that readily undergoes a redox reaction (7).  $\text{CeO}_2$  is often added because of its' redox properties which can allow for a relatively rapid change in its' oxidation state with a change in the redox potential of the exhaust gas. This change in oxidation state involves the reversible removal and addition of oxygen and hence is termed " oxygen storage ". This would involve a redox reaction such as (75),



Thus,  $\text{CeO}_2$  is capable of storing oxygen under fuel-lean conditions and subsequently releasing it under fuel-rich conditions. When the exhaust gas has a fuel-rich (net-reducing, air:fuel ratio < 14.6) composition,  $\text{CeO}_2$  is thought to readily undergo reduction to provide oxygen for the oxidation of  $\text{H}_2$ , CO and hydrocarbons, while in the fuel-lean region (net-oxidising, air:fuel > 14.6) the reduced state removes excess oxygen

from the exhaust gas. Alternatively, in the fuel lean region, the reduced component may interact with NO. In either case, the reduced component aids NO removal either by direct reaction or indirectly by reducing the O<sub>2</sub> concentration during a fuel-lean cycle. If the exhaust stoichiometry then changes back to fuel-rich conditions, the oxidised component can again be used to oxidise CO and hydrocarbons (7).

Other benefits of the use of CeO<sub>2</sub> as an additive in supported metal catalysts, which have been proposed include:

- stabilisation of the alumina support (76);
- promotion of water gas shift activity i.e.  $\text{CO} + \text{H}_2\text{O} \rightarrow \text{CO}_2 + \text{H}_2$  (75);
- provision of lattice oxygen for reaction with adsorbed reactants (21);

Many studies have been made on the use of Ce in precious metal catalysts and the remainder of this survey will involve discussion of some of the findings (section 1.4).

## 1.4 Use of Ceria in Supported Noble Metal Combustion Catalysts

This section of the literature review will focus on the use of CeO<sub>2</sub> in noble metal catalysts, both as a support and as an additive in Al<sub>2</sub>O<sub>3</sub>-supported catalysts. Studies of the use of CeO<sub>2</sub> in such samples will be discussed under three separate headings. In the first section, some selected studies concerning the possible benefits of CeO<sub>2</sub> for the dynamic performance of automotive exhaust catalysts, where the fuel:air ratio of the feed gas varies with time, will be reviewed. The next section will concentrate on studies of the conversion of CO to CO<sub>2</sub> using CeO<sub>2</sub> containing catalysts under steady-state conditions. Finally, studies which detail the effects of CeO<sub>2</sub> on the hydrocarbon oxidation activity of noble metals under steady-state conditions, which are of particular interest in this thesis, will be discussed. Some of these latter studies also involve simultaneous study of CO oxidation. As the main focus of this thesis is on the effects of CeO<sub>2</sub> under steady-state conditions, such studies will receive greater attention.

### 1.4.1 Oxygen Storage Capacity (OSC) and Water Gas Shift (WGS) Activity.

Three-way automotive catalysts operate only momentarily in stoichiometric exhaust conditions, even when used in vehicles with closed-loop control of the air:fuel ratio. This is because of the step-like response of the exhaust oxygen sensor and the rapidly changing operating conditions of an automobile which leads to rapid oscillation of the air-fuel ratio. Because of continuous air-fuel ratio adjustments, the exhaust gas stoichiometry undergoes small 0.5-4 Hz variations with an amplitude of approximately  $\pm 0.5$  air-fuel ratio units (69). The exhaust stoichiometry varies between fuel-rich (net-reducing) and fuel-lean (net oxidising) conditions. Under fuel-rich conditions, catalyst performance for CO and hydrocarbon removal is expected to deteriorate. Conversely, NO emissions are expected to increase during fuel-lean excursions (see Fig. 1.12). However, it is thought that catalyst performance under these oscillating conditions is, in general, better than that predicted from steady-state efficiency. This improved performance has been related to several characteristic processes occurring under dynamic operating conditions including oxygen storage and water-gas shift reaction (7). The effects of CeO<sub>2</sub> on these transient processes have been investigated in numerous studies e.g. (68, 77, 78, 79, 80).

Hegedus et al. (68) found that the addition of CeO<sub>2</sub> improved the initial performance of poison-resistant three-way catalysts in transient operation. The performances of four catalysts, containing Pt/Rh, Pt/Rh/Ce, Pt/Rh/Pd and Pt/Rh/Pd/Ce, were evaluated and compared using steady-state and cycled engine dynamometer tests as

well as cycled tests in a laboratory reactor. The pelleted support used had a surface area of  $129 \text{ m}^2/\text{g}$  and a total pore volume of  $0.887 \text{ cm}^3/\text{g}$ . The noble metals were deposited by spraying with aqueous solutions of their chlorine complexes, while Ce was deposited using an aqueous nitrate solution. After impregnation the catalysts were dried and then fired in air at  $550^\circ\text{C}$  for 4 to 5 hours. Average metal loadings were approximately 0.048, 0.0027, 0.018, and 1.0 wt.% for Pt, Rh, Pd, and Ce, respectively in the different catalysts (68).

In each static dynamometer test the air:fuel ratio was held constant and the effect of cerium was minimal (68). In contrast, cycled dynamometer tests, in which the air:fuel ratio oscillated  $\pm 0.5$  units around its' midpoint setting at a frequency of 1 Hz, showed significant improvements in NO and CO conversions at certain air:fuel settings using freshly prepared Ce-containing samples compared to samples without Ce. The authors noted that it was particularly relevant that the presence of Ce resulted in improved CO and NO conversions near the stoichiometric air:fuel ratio typically employed in automotive applications. This was thought to be due to some sort of surface storage effect in the cycled tests but the authors were unsure as to which feedstream component(s) were being stored and slowly released during the air:fuel transients. The catalysts were also tested in a cycled feedstream in a laboratory reactor and Ce improved CO and NO conversions at all cycling frequencies (0.1-6 Hz) while propylene conversions over the fresh catalysts were too high to distinguish the effect of Ce. However, after aging of the catalysts in the static dynamometer, the only significant benefit of Ce presence was in improved CO performance (68).

Yao and Yu-Yao (77) noted that, below  $1000^\circ\text{C}$ ,  $\text{CeO}_2$  can be reduced by  $\text{H}_2$  only to  $\text{Ce}_2\text{O}_3$ . It was found that the total oxygen storage capacity (OSC) of  $\text{CeO}_2$ -containing catalysts depended on several factors including ceria loading and the presence of a precious metal.  $\text{CeO}_2/\text{Al}_2\text{O}_3$  samples were prepared by wetting the  $\text{Al}_2\text{O}_3$  support with the desired concentration of  $\text{Ce}(\text{NO}_3)_3$ , and, after drying, were calcined at  $500\text{-}800^\circ\text{C}$  for 16 hours. Precious metals were added to the supports by conventional impregnation using  $\text{PdCl}_2$ ,  $\text{H}_2\text{PtCl}_6$ , and  $\text{Rh}(\text{NO}_3)_3$  followed by calcination between  $600\text{-}900^\circ\text{C}$ . OSC was investigated using  $\text{O}_2$  chemisorption, TPR and pulse injection measurements. Pulse injection measurements were performed in two modes, one of which involved measuring the total amount of CO oxidised in a series of CO pulses after an  $\text{O}_2$  pulse until no more CO oxidation was observed, and the other involved measuring the amount of CO oxidised in only one pulse following an  $\text{O}_2$  pulse. The latter measurement was expected to represent most closely the Oxygen Storage Capacity of the catalysts in actual operation and was referred to as OSC, while the former result represented the Oxygen Storage Capacity Complete or OSCC (77).

On comparing the OSC of CeO<sub>2</sub>, CeO<sub>2</sub>/Al<sub>2</sub>O<sub>3</sub>, PM/CeO<sub>2</sub>/Al<sub>2</sub>O<sub>3</sub> and PM/CeO<sub>2</sub> [ where PM = Pt / Pd / Rh] samples, it was found that a PM-CeO<sub>2</sub> interaction occurred which lowered the reduction temperature of surface CeO<sub>2</sub>, as shown by TPR, and also seemed to increase the dispersion of CeO<sub>2</sub> on the alumina support thereby resulting in highest OSC when all three components were present (77). Under the same conditions, OSC values for CeO<sub>2</sub>, 20% CeO<sub>2</sub>/Al<sub>2</sub>O<sub>3</sub>, 0.23% Pt/CeO<sub>2</sub> and 0.3% Pt/23% CeO<sub>2</sub>/Al<sub>2</sub>O<sub>3</sub> samples, were  $0.14 \times 10^2$ ,  $0.17 \times 10^2$ ,  $0.26 \times 10^2$ , and  $1.49 \times 10^2$   $\mu\text{mol O}_2/\mu\text{mol CeO}_2$ , respectively, as measured by pulse injection technique at 500°C. OSC was found to decrease with increasing precalcination temperature up to 800°C. However catalyst comparisons were made after pretreatment at 800°C, as this was thought to be more representative of the type of conditions encountered in automotive applications (77).

Su et al. (78) investigated the effects of catalyst formulation and aging history on the effective OSC of three-way catalysts. It was found that addition of ceria to precious metal catalysts significantly enhanced the catalysts' OSC after aging in an oxidising environment at high temperatures (78).

Catalysts consisting of various combinations of Rh, Pt, and the base metals, NiO or CeO<sub>2</sub>, on  $\gamma$ -Al<sub>2</sub>O<sub>3</sub>, were prepared (78) in a similar manner to that in (77). All samples studied were based on a monolith substrate (78). Rh loadings were in the range 0.01-0.025 wt.% and Pt concentrations varied from 0.033-0.18 wt.%. Catalysts with CeO<sub>2</sub> had Ce levels between 1.1 and 3.1 wt.%. The samples were subjected to different types of aging treatments. The first type involved thermal aging for eight hours at 700, 800 or 900°C under an oxidising atmosphere containing 5% O<sub>2</sub>, 6% CO<sub>2</sub>, and 12% H<sub>2</sub>O in N<sub>2</sub>. Catalysts were also subjected to simulated durability testing, to determine the effects of Pb, P and SO<sub>2</sub> poisons. The dynamic OSC of each sample at 500 and 600°C was determined, by exposing the catalyst to oxidising and reducing pulses in a continuous cyclic manner. The oxidising pulse consisted of 1% O<sub>2</sub> while the reducing pulse contained 2% CO. Ultra-high purity He was used as the carrier gas and concentration profiles of each pulse were monitored using a residual gas analyser. OSC was evidenced by a CO<sub>2</sub> peak accompanying the CO pulse (78).

The OSC of the each catalyst containing both CeO<sub>2</sub> and noble metal was significantly greater than the sum of the OSCs for the samples containing noble metal and CeO<sub>2</sub> separately, after similar thermal treatments (78). This enhancement was assigned to a beneficial synergistic effect as a result of promoted redox reaction of the CeO<sub>2</sub> by the noble metal and a stabilised precious metal dispersion by the ceria. After aging at 900°C, ceria-containing Rh catalysts showed an OSC of about 1.3 moles of O<sub>2</sub>

per 100 moles of (Rh + Ce), at 500°C. The corresponding OSCs for similarly aged Rh and CeO<sub>2</sub> samples were, respectively, 0.3 and 0.1 moles of O<sub>2</sub> per 100 moles of Rh or Ce. Significantly decreased OSC of noble metal-only catalysts was reported after aging for 8 hours at 900°C and this was attributed to severe sintering during the thermal pretreatment. In contrast, CeO<sub>2</sub>-containing Rh and Pt catalysts showed an appreciable OSC even after 72 hours aging at 900°C. The fact that the noble metals in catalysts with higher ceria contents appeared to be more effective in promoting the CeO<sub>2</sub> redox reaction, than those in samples with lower CeO<sub>2</sub> loadings, was thought to provide inferential evidence for improved noble metal dispersion with increasing Ce:PM ratio. The PM dispersions in these samples were not assessed. It was thought that adsorption on partially reduced ceria (as a result of promoted redox reaction in the presence of PM), would complicate conventional adsorption techniques. The authors noted that complete reduction of CeO<sub>2</sub> to Ce<sub>2</sub>O<sub>3</sub> would result in OSC of 25 moles of O<sub>2</sub> per mole of Ce and that only 1-2% of the ceria present was active for the redox reaction, even in the presence of PM. The addition of NiO was found to be less useful in improving catalyst OSC than CeO<sub>2</sub> and only resulted in enhanced OSC after mild pretreatments. Evidence was suggested that the OSC of a vehicle-aged three-way catalyst containing CeO<sub>2</sub>, would be adversely affected by exposure to SO<sub>2</sub> as well as sintering. In the absence of CeO<sub>2</sub> or NiO, the presence of SO<sub>2</sub> in the aging atmosphere was found to have no effect on the OSC of the PM (78).

Herz and Sell (79) investigated the dynamic performance of automotive catalysts. Both oxygen storage and water-gas shift processes were thought to contribute to CO removal under dynamic conditions in engine exhaust. Pt/Rh/Ce/Al<sub>2</sub>O<sub>3</sub>, Pt/Ce/Al<sub>2</sub>O<sub>3</sub> and Pt/Rh/Al<sub>2</sub>O<sub>3</sub> catalysts were prepared by incipient wetness impregnation of Al<sub>2</sub>O<sub>3</sub> beads with aqueous solutions of H<sub>2</sub>PtCl<sub>6</sub>, RhCl<sub>3</sub>.3H<sub>2</sub>O, and Ce(NO<sub>3</sub>)<sub>3</sub>. Samples were calcined in air at 500°C for 4 hours and exposed to engine exhaust for several hours before mounting in a converter in the exhaust system of a gasoline engine. Metal loadings of 2.6, 0.5, and 143 μmol. g<sup>-1</sup> for Pt, Rh, and Ce, respectively, were used on the transitional Al<sub>2</sub>O<sub>3</sub> (surface area = 105 m<sup>2</sup>/g) (79).

Catalysts were evaluated using an experimental procedure which involved stabilisation of the catalyst under fuel-rich exhaust conditions, followed by a 1-second exposure to fuel-lean conditions (79). The catalyst was subsequently switched to fuel-rich conditions and CO conversion was monitored using infrared diode laser spectroscopy. On transition from fuel-lean to fuel-rich conditions the expected drop in CO conversion did not happen instantaneously. For the Pt/Ce catalyst, this transient enhancement could be accounted for by reaction of CO with oxygen stored in the catalyst and CO adsorption and accumulation over the noble metals in the catalyst. For Rh-containing samples the improvements in CO conversions were too large to be explained

solely by these processes and were consistent with a transient enhancement of water-gas shift reaction over Rh. Improvements in the water-gas shift activity of Rh following exposure to fuel-lean feedstreams have been associated with the formation of more active surface Rh-oxide under oxidising conditions (80). Participation of the water-gas shift reaction in CO removal following the lean to rich transition could not be ruled out for the Pt/Ce catalyst (79). It was noted that no significant enhancement of water-gas shift activity by Ce was apparent.

The autocatalysts were also assessed using a Federal Test Procedure (79). In this test, CO conversions decreased in the order Pt/Rh/Ce > Pt/Ce > Pt/Rh. This was thought to indicate that oxygen accumulation and reaction over Ce contributed more to CO conversion during driving than water-gas shift over Rh (79).

Weibel et al. (80) also found that oxygen storage and water gas shift activity were important processes affecting CO conversions in experiments where the air:fuel ratio was varied in a cyclic manner. Rh/Al<sub>2</sub>O<sub>3</sub> and Rh-Ce/Al<sub>2</sub>O<sub>3</sub> catalysts were examined in the absence and presence of H<sub>2</sub>O. Metal loadings of 0.003 and 1.02 wt.% for Rh and Ce, respectively, were used. Catalysts were prepared by wet impregnation of Al<sub>2</sub>O<sub>3</sub> powder (100 m<sup>2</sup>/g) with aqueous solutions of RhCl<sub>3</sub> and Ce(NO<sub>3</sub>)<sub>3</sub>. The catalysts were calcined in air at 450°C for 2 hours and then reduced in H<sub>2</sub> under the same temperature conditions. In all tests, the samples were stabilised under reducing conditions for 30 minutes at 450°C before testing. Catalysts were firstly tested under a feedstream of CO, NO, O<sub>2</sub>, N<sub>2</sub> and hydrocarbon, in which the air:fuel ratio was varied at a cycling frequency of either 0.075 Hz or 1 Hz and an oscillation amplitude of +/- 0.25 units of the mean air:fuel ratio. CO and NO conversions were reported as a function of the mean air:fuel ratio at 450°C. On addition of ceria to Rh/Al<sub>2</sub>O<sub>3</sub>, CO conversions were enhanced on the fuel-rich side of stoichiometry, and this was attributed to oxygen storage effects of the CeO<sub>2</sub> component. At a mean air:fuel setting of 14.6 typically employed in closed-loop engine control applications (69), the conversion of CO was improved slightly in the presence of Ce. In the presence of water vapour, CO conversions on Rh-Ce/Al<sub>2</sub>O<sub>3</sub> were further improved which was attributed to water gas shift reaction (80).

To try and confirm these observations, step-change experiments were performed, at 450°C, in feedstreams containing only CO, N<sub>2</sub>, O<sub>2</sub> and water vapour (if necessary) (80). In these experiments the catalysts were firstly exposed to 1% CO (rich step) for 2 minutes, after which the feedstream was switched to 1% O<sub>2</sub> (lean-step) for a specific length of time between 1s and 11 hours. The feedstream was then switched back to 1% CO. CO<sub>2</sub> formation was monitored each 3s. For experiments in the absence of H<sub>2</sub>O, a CO<sub>2</sub> peak was formed instantaneously on the lean to rich step transition and the

difference in the amount of CO<sub>2</sub> formed over Rh-Ce/Al<sub>2</sub>O<sub>3</sub> and Rh/Al<sub>2</sub>O<sub>3</sub> was attributed to the storage of O<sub>2</sub> by ceria. During the initial rich step all the Ce was converted to Ce<sup>3+</sup>. After the rich to lean step transition, the oxidation of Ce<sup>3+</sup> to Ce<sup>4+</sup> occurred at a very fast rate initially with 51% of the Ce reoxidised after only 20 seconds. This was attributed to oxidation of Ce at the Rh-Ce interface with dissociation of O<sub>2</sub> on Rh sites and oxygen spillover to the neighbouring cerium. The rate of ceria oxidation then decreased with time in the lean exposure. Subsequent switching to the rich environment resulted in CO<sub>2</sub> production which could be attributed to reduction of the ceria by CO i.e. oxygen storage (80).

Similar step experiments were performed using 1%CO/10%H<sub>2</sub>O as the reducing feedstream for the rich steps (80). In the initial rich step, negligible WGS activity was found. However after the lean step in 1% O<sub>2</sub>, oxidised Rh/Al<sub>2</sub>O<sub>3</sub> and Rh-Ce/Al<sub>2</sub>O<sub>3</sub> had significant WGS activity with CO<sub>2</sub> production being found after only 1 second exposure to the oxidising step. There was no correlation between oxidation time and WGS activity. Rh-Ce/Al<sub>2</sub>O<sub>3</sub> had higher activity following lean to rich transition compared to Rh/Al<sub>2</sub>O<sub>3</sub>, but the activity decreased more rapidly when ceria was present which was attributed to decreased stability of the Rh-oxide (80).

Other studies have also reported improved 3-way conversions for supported noble metals under oscillating conditions in the presence of CeO<sub>2</sub>. For example, Löff et al. (81) found that addition of 30 wt.% CeO<sub>2</sub> enhanced the conversions of CO, C<sub>3</sub>H<sub>6</sub>, and NO over Pt/Al<sub>2</sub>O<sub>3</sub> at the fuel-rich side of stoichiometry, under dynamic air:fuel conditions in a flow reactor in the absence of SO<sub>2</sub>. Kim (82) found CeO<sub>2</sub> to be an effective promoter of three-way catalyst performance for CO removal under O<sub>2</sub>-deficient conditions. The beneficial effects of CeO<sub>2</sub> addition to Pt-Pd-Rh/Al<sub>2</sub>O<sub>3</sub> samples was associated with enhancement of the water-gas shift reaction. Additional oxygen storage may also have contributed to making CeO<sub>2</sub> the most effective of the non-noble metal additives tested for the removal of CO under the conditions used (82).

Murrell et al. (83) found evidence for strong noble metal-ceria interaction in CeO<sub>2</sub>-supported Pt, Rh, Pd, and Ir samples. The nature of this interaction was examined using X-ray photoelectron spectroscopy (XPS) and Laser Raman spectroscopy (LRS) techniques. Samples were prepared on high purity CeO<sub>2</sub> (130 m<sup>2</sup>/g) using Rh(NO<sub>3</sub>)<sub>2</sub>, H<sub>2</sub>IrCl<sub>6</sub>, Pd(NO<sub>3</sub>)<sub>2</sub>, and Pt amine complex and were then calcined at a variety of different temperatures in the range 350-1000°C. It was reported that CeO<sub>2</sub> had the capacity to form isolated surface oxide M-O groups with all the noble metals (M), in the form of a Strong Oxide Support Interaction (SOSI). For Pt-CeO<sub>2</sub>, an interaction of this type was found to result in surface Pt existing in the form of a Pt-O complex formed at

the Pt-CeO<sub>2</sub> interface. This was found to stabilise both Pt and CeO<sub>2</sub> surface areas on exposure to high temperature calcination in an oxidising environment. Even after calcination at 1000°C, the Pt-O surface structure was still retained in high concentration on the CeO<sub>2</sub> surface in spite of considerable loss of CeO<sub>2</sub> surface area. It was proposed that certain ceria surface sites strongly bond to the M-O complex, and only these strongly bound surface M-O groups are retained at very high temperatures. Addition of Pt beyond the capacity of CeO<sub>2</sub> to form the Pt<sup>+2</sup>-complex resulted in Pt sintering to form large metal particles. The M-O phase could be recovered as a highly dispersed metal phase upon reduction at 500°C in H<sub>2</sub>. Although CeO<sub>2</sub> appeared to have superb ability to stabilise Pt under oxidising conditions, exposure to cyclic redox aging conditions at 850°C for 8 hours was found to result in severe Pt sintering with complete loss of the Raman band associated with surface Pt-O. This was thought to be due to loss of the M-O complex during the reducing swing of the aging cycle, and to indicate that, under dynamic conditions in automotive catalysts, the role of CeO<sub>2</sub> was probably more one of a poison scavenger (e.g. SO<sub>2</sub>) and/or as an oxygen storage component rather than a stabiliser of precious metal dispersion (83).

#### 1.4.2 Oxidation of Carbon Monoxide (CO)

In addition to enhancing the transient performance of three-way catalysts as discussed above, Ce has been found to be capable of altering the kinetic behaviour of such catalysts as a result of interaction with supported noble metals. Studies concerning the nature of this interaction and its' effects on the steady-state CO oxidation activity of supported noble metals will now be discussed.

As previously discussed, Hegedus et al. (68) studied three-way conversions on Pt/Rh, Pt/Rh/Ce, Pt/Rh/Pd, and Pt/Rh/Pd/Ce catalysts. The light-off performance of these samples for CO oxidation was also evaluated using a laboratory reactor under oxidising conditions. The feedstream consisted of 1.5% O<sub>2</sub>, 0.3% CO, 0.025% C<sub>3</sub>H<sub>6</sub>, 10% CO<sub>2</sub>, 10% H<sub>2</sub>O, and N<sub>2</sub> to 100% (all by vol.) and the temperature was gradually increased at 10°C/min. On comparison of the temperature for 50% CO conversion over the different samples tested, the presence of Ce was found to result in improved light-off performance for fresh catalysts. This was thought to be due to increased noble metal dispersions as indicated by separate experiments. After catalyst sintering at 900°C for 2 hours in air, improved CO removal was found for catalysts containing Pd. However, Ce addition resulted in poorer performance for both Pt/Rh and Pt/Rh/Pd samples after aging. This was thought to indicate that Ce degrades the thermal stability of Pt (68).

Summers and Ausen (84) found that cerium oxide interacts with Al<sub>2</sub>O<sub>3</sub>-supported Pt, Pd and Rh in a manner which affected both metal dispersions and catalytic

activity. 0.05 wt.% Pt and 0.02 wt.% Pd/ $\gamma$ -Al<sub>2</sub>O<sub>3</sub> samples were prepared with Ce concentrations in the range 0 to 13.0 wt.%. The catalysts were prepared by initial impregnation of Al<sub>2</sub>O<sub>3</sub> with Ce(NO<sub>3</sub>)<sub>3</sub> in HCl solution. After calcination, the noble metals were deposited by impregnation with HCl solutions of H<sub>2</sub>PtCl<sub>6</sub> and PdCl<sub>2</sub>, and samples were calcined again. Calcination steps were performed at 500°C for 4 hours. Aging experiments on these catalysts involved heating at 700-900°C in either ambient air, N<sub>2</sub> or 5 vol.% H<sub>2</sub> for 6 hours. The  $\gamma$ -Al<sub>2</sub>O<sub>3</sub> spheres used had a surface area of 120 m<sup>2</sup>/g. Surface areas decreased on addition of CeO<sub>2</sub> which was attributed to plugging of the Al<sub>2</sub>O<sub>3</sub> pores by the CeO<sub>2</sub> (84).

For fresh Pt-Ce catalysts, the apparent Pt dispersion, measured by CO chemisorption, decreased with increasing Ce content (84). The authors were unsure as to whether this was due to agglomeration of the Pt particles during preparation or an interaction between Pt and Ce which inhibited CO chemisorption. As the effect of increasing CeO<sub>2</sub> content on the Al<sub>2</sub>O<sub>3</sub> surface was not known, it was not possible to determine how the Ce loading would affect interaction between the noble metal and the support and the resulting Pt dispersions. After thermal aging in air at 900°C, the average apparent Pt particle size for the non-ceria containing sample increased from 11Å to 89Å. At low ceria levels the particle size increase was even more dramatic i.e. even greater apparent loss of Pt dispersion. However with higher CeO<sub>2</sub> levels the apparent Pt dispersion after aging in air increased with CeO<sub>2</sub> loading, and for the sample with 13.0 wt.% Ce the apparent particle size remained constant at ~28Å, before and after aging. Pd dispersions were unaffected by CeO<sub>2</sub> loading in fresh samples but decreased with increasing loading for air-aged (900°C) samples. For H<sub>2</sub>-aged samples, Pt dispersions again decreased relative to fresh samples, but were considerably improved in the presence of CeO<sub>2</sub>, and were significantly larger than Pt dispersions for the air-aged samples except at the highest CeO<sub>2</sub> loading sample. Further investigation revealed that a Pt<sub>5</sub>Ce alloy was formed on heating of Pt black and CeO<sub>2</sub> together in H<sub>2</sub> at 900°C, and it was thought likely this should occur on the supported samples being investigated as well. Thus, the improved dispersions after H<sub>2</sub> aging at 900°C in the presence of CeO<sub>2</sub> may have been related to alloy formation. Infrared CO adsorption studies on fresh samples (1 wt.% metal/Al<sub>2</sub>O<sub>3</sub>, 1 wt.% metal/13.0 wt.% Ce/Al<sub>2</sub>O<sub>3</sub>) showed that CO chemisorption on Pd was unaffected by CeO<sub>2</sub>. However, these studies indicated an increased oxidation of some surface platinum sites in ceria-containing samples, which was attributed to a Pt-CeO<sub>2</sub> interaction with CeO<sub>2</sub> noted as being a powerful oxidising agent (84).

CO oxidation was monitored as a function of temperature under strongly oxidising conditions in a feedstream of 0.3 vol.% CO, 0.025 vol.% C<sub>3</sub>H<sub>6</sub>, 1.5 vol.% O<sub>2</sub>,

10 vol.% CO<sub>2</sub> and 10 vol.% H<sub>2</sub>O in N<sub>2</sub> (84). Fig. 1.13 compares the temperature required for 30% CO conversion over the different catalysts.

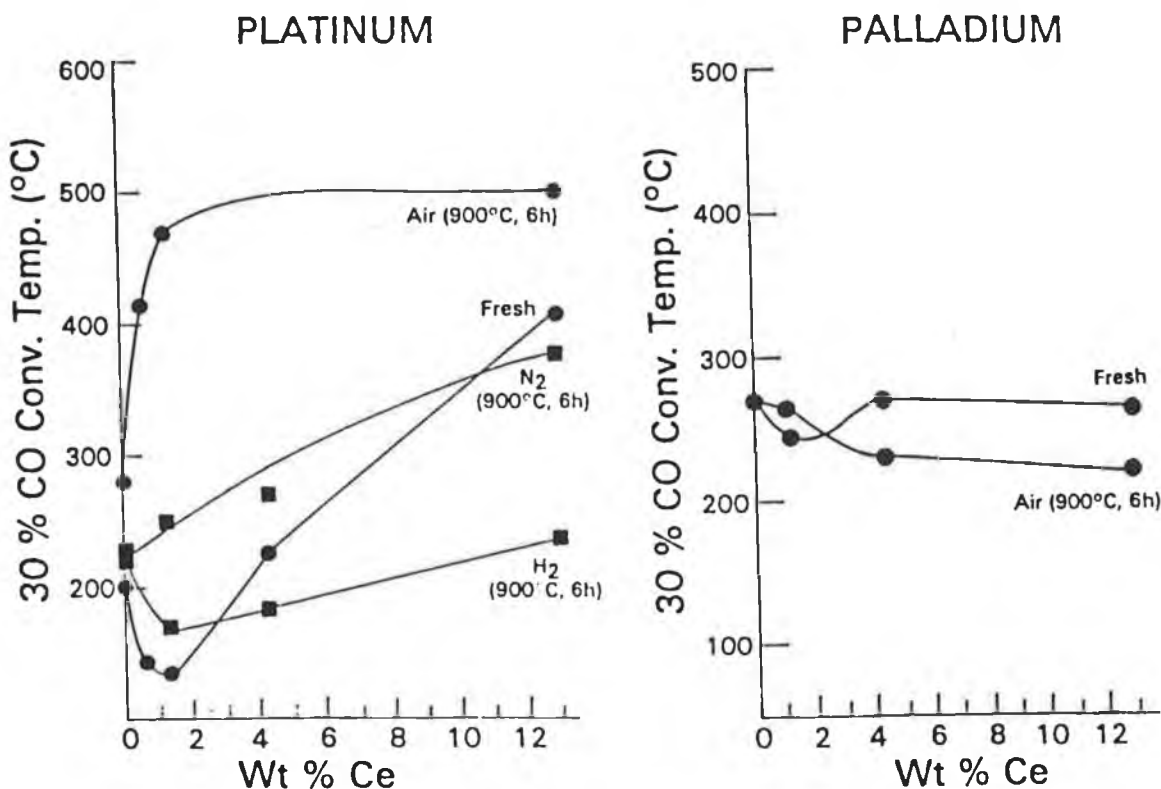


**Figure 1.13 : Effects of Ce Loading on the CO Oxidation Activity of fresh and thermally aged Pt and Pd catalysts (84).**

Improvements in CO oxidation activity are seen to have occurred on addition of small amounts of CeO<sub>2</sub> (0.6 - 1.3 wt.%) to Al<sub>2</sub>O<sub>3</sub>-supported Pt and Pd samples (84). However with increasing Ce content ( $\geq 4.4$  wt.%) the CO conversion activity of the fresh catalysts greatly deteriorated for Pt but not for Pd samples. For Pt, both of these changes were concluded as due to a PM-Ce interaction as Ce/Al<sub>2</sub>O<sub>3</sub> does not appreciably catalyse CO oxidation under the conditions used. Both the enhancement of CO conversions at low loadings and the deterioration of CO conversions at high loadings, were diminished by treatment of fresh Pt-Ce/Al<sub>2</sub>O<sub>3</sub> catalysts with SO<sub>2</sub>. This was explained in terms of SO<sub>2</sub> as a strong reducing agent reacting with CeO<sub>2</sub> (a strong oxidising agent) to destroy the interaction of CeO<sub>2</sub> with Pt (84).

The activity of Pd for CO oxidation was much less sensitive to CeO<sub>2</sub> presence and pretreatment conditions than Pt, as shown in Fig 1.13 (84). Aging in air at 900°C

was found to result in significant activity loss for the higher CeO<sub>2</sub>-loaded Pt samples which was attributed to extensive Pt-Ce interaction. At lower aging temperatures, the decline in activity upon aging was not as pronounced. Both Pt/Al<sub>2</sub>O<sub>3</sub> and Pt/1.3 wt.% Ce/Al<sub>2</sub>O<sub>3</sub> showed a gradual decline in activity with increasing aging temperature up to 800°C in air. After aging in H<sub>2</sub> at 900°C the activity of Pt at higher Ce loadings ( $\geq$  4.4 wt.% Ce) was improved relative to the activity of the corresponding fresh samples (84).

A series of 0.05 wt.% Pt and 0.002 wt.% Rh catalysts with either 0 or 1.3 wt.% Ce were prepared and pretreated in a similar manner to that described above for Pt and Pd samples (84). The only difference in preparation procedure was that the noble metal impregnating solutions were not acidified with HCl. Freshly prepared and aged samples were then tested for three-way conversion activity under steady state conditions. Three-way conversions over Rh were less sensitive to CeO<sub>2</sub> than those over Pt. CeO<sub>2</sub> was found to severely inhibit CO oxidation over both fresh and air-aged Pt samples (84).

In general, both Pd and Rh appeared less sensitive to ceria addition than Pt samples (84). The authors found that the complexity of Pt-Ce chemistry (e.g. cerias' ability to oxidise Pt and to form alloys with Pt of the type Pt<sub>5</sub>Ce on high temperature reduction at  $\sim$ 900°C) made it difficult to explain the effects of the promoter on the activity and dispersion of the noble metal. It was concluded that the activity of Pt was a function of several parameters including Ce loading, gaseous aging environment and aging temperature (84).

As previously discussed, Yu-Yao (53) found Al<sub>2</sub>O<sub>3</sub>-supported noble metal catalysts to exhibit two different types of kinetic behaviour for the oxidation of CO and olefins. Type 1 kinetics was used to describe kinetics which resembled those found for unsupported noble metal wires. Type 1 kinetics were first order with respect to O<sub>2</sub>, and negative first order with respect to CO over Pt, Pd, and Rh. Type 2 kinetics were remarkably different to Type 1, and were characteristic of highly dispersed noble metals which were thought to be in a higher oxidation state. Type 2 kinetics were positive order with respect to CO, almost independent of O<sub>2</sub> partial pressure, and generally involved lower activation energies. The presence of CeO<sub>2</sub> was found to promote Type 2 kinetics. Catalyst preparation involved coating the  $\gamma$ -Al<sub>2</sub>O<sub>3</sub> powder with CeO<sub>2</sub> by impregnation with Ce(NO<sub>3</sub>)<sub>3</sub>, and calcination of the resultant solid at 800°C. The noble metals were then deposited by impregnation and the catalysts were calcined at a temperature in the range 600-900°C for 4 hours or more. Rate measurements were made mostly under O<sub>2</sub>-rich conditions in a flow reactor. Promotion of Type 2 kinetics by CeO<sub>2</sub> was associated with charge transfer between Ce and neighbouring precious metal particles resulting in a higher oxidation state in the precious metal. As discussed previously, Yao and Yu-Yao

(77) reported that noble metals can promote the reduction of  $Ce^{4+}$  to  $Ce^{3+}$ . Hence, charge transfer between the neighbouring metals on the catalyst surface may be expected (53). Summers and Ausen (84) reported increased oxidation of some surface Pt sites in the presence of  $CeO_2$ , with the latter component acting as an oxidising agent.

Yu-Yao (53) noted that promotion of Type 2 kinetics by  $CeO_2$  may also have involved increased dispersion of the noble metal. However, this was not measured as it was thought that the determination of dispersions by conventional adsorption techniques would be complicated for  $CeO_2$ -containing samples due to precious metal-ceria interactions. Both Pd and Rh were found to have a higher tendency to exhibit Type 2 kinetics due to their lower ionisation potentials relative to Pt (53). On comparing  $PM/Al_2O_3$  and  $PM/CeO_2/Al_2O_3$  ( $PM = Pd$  or  $Rh$ ) samples which exhibited Type 2 kinetics, it was found that for Pd the presence of ceria did not significantly alter the specific CO oxidation rate per mg of Pd. On the other hand, the addition of  $CeO_2$  enhanced CO oxidation on Rh samples by an order of magnitude.  $CeO_2$  was thought to stabilise surface Rh by preventing its' diffusion into the  $Al_2O_3$  support when heated above  $700^\circ C$ . Reduction of  $CeO_2$ -containing Pt and Pd samples, resulted in kinetics approaching Type 1, and also resulted in considerably increased reaction rates (per mg of Pt) which were higher than those reported for non-ceria containing samples. For example, a 0.23% Pt, 20%  $CeO_2/Al_2O_3$  catalyst calcined at  $700^\circ C$  produced 0.8 moles of  $CO_2$ /min-mg of Pt, at  $300^\circ C$  in a reaction mixture containing 0.5%  $O_2$  and 0.5% CO in He. The corresponding reaction rate for a 0.22% Pt/ $Al_2O_3$  catalyst was 1.9 moles of  $CO_2$ /min-mg of Pt. Reduction of the  $CeO_2$  containing sample led to a dramatic increase in reaction rate to 14 moles of  $CO_2$ /min-mg of Pt. However, reduction of non-ceria containing samples was not investigated (53).

Yu-Yao and Kummer (85) examined the oxidation of CO by low-loaded noble metal/ $Al_2O_3$  catalysts in which the noble metal was highly dispersed. A novel method of catalyst preparation was used involving thermal transport of the noble metals from a metal sheet to the  $Al_2O_3$  support surface by heating the two components together in air. The effect of different preparation temperatures and the presence of  $CeO_2$  on CO oxidation activity was determined, and catalytic activities were compared with those of catalysts with similar compositions prepared by conventional impregnation. For all  $CeO_2$ -containing samples, the  $Al_2O_3$  was firstly coated with  $CeO_2$  as in (53). For impregnated catalysts, the noble metal was then added to the support by incipient wetness impregnation with  $H_2PtCl_6$ ,  $PdCl_2$ , or  $Rh(NO_3)_3$  (85). The catalysts were dried and calcined at  $800^\circ C$ . With the thermal transport technique, noble metal sheets were placed over the support powder in a  $\alpha$ - $Al_2O_3$  dish. The dish was covered with a  $\alpha$ - $Al_2O_3$  top and heated in a muffle furnace at the desired temperature for a specified time.

The Pt concentration in these samples was determined by neutron activation analysis. As the Pd and Rh concentrations were not determined, direct comparisons of activity for these catalysts was not possible. CO oxidation activity was monitored using a stoichiometric mix of 0.67% CO and 0.33% O<sub>2</sub> in He at atmospheric pressure. Reaction rates for these highly dispersed samples, were 0 to positive fractional order with respect to CO and O<sub>2</sub> (85), and were noted as being in agreement with the Type 2 kinetics discussed above in (53).

For all CeO<sub>2</sub>-containing samples, a strong Pt-CeO<sub>2</sub> and Rh-CeO<sub>2</sub> interaction was observed as characterised by deactivation in an oxidising atmosphere and a sharp increase in activity after reduction (85). After reduction at 450°C with 1% CO, 50% CO oxidation was achieved at 325°C for an impregnated catalyst with a Pt concentration of 125 ppm in the absence of CeO<sub>2</sub>. For a similar 135 ppm Pt catalyst containing 8.7 wt.% CeO<sub>2</sub>, the corresponding temperature was 166°C. The effects of CeO<sub>2</sub> on Pd catalysts were not as pronounced (85).

The activities of samples prepared by impregnation and thermal transport were found to be comparable (85). For catalysts prepared by the latter method, the presence of CeO<sub>2</sub> was found to enhance Pt uptake on the Al<sub>2</sub>O<sub>3</sub> support as well as enhancing catalyst activity, after pre-reduction, as shown in Fig 1.14. It is also evident in Fig. 1.14 that the catalytic activity of Pt/Al<sub>2</sub>O<sub>3</sub> increased sharply at low CeO<sub>2</sub> contents even though the Pt uptake was only slightly increased. On further increasing the CeO<sub>2</sub> level, the Pt content increased considerably, but the activity remained almost constant under the reaction conditions used. For Rh catalysts prepared by thermal transfer, a significant enhancement of CO oxidation activity was also found with the addition of CeO<sub>2</sub>. This was assumed to indicate improved Rh uptake by the support and was particularly pronounced for Rh/CeO<sub>2</sub>/Al<sub>2</sub>O<sub>3</sub> samples prepared at 900°C. The transfer of Pd, as inferred by the activity results, was not affected by the presence of CeO<sub>2</sub>. This was noted as being in agreement with weak Pd-CeO<sub>2</sub> interactions found for the impregnated catalysts, as also indicated by the studies discussed above (53, 84).

Thermal transport from the bulk noble metals to the supports was only found to be possible on preparation in air and not in vacuo or under reducing conditions (85). Metal transport was, therefore, thought to involve gaseous volatile oxides of the metals and was enhanced by the presence of CeO<sub>2</sub> for Pt and Rh. It was concluded that CeO<sub>2</sub> interacts strongly with Pt and Rh to enhance CO oxidation, relative to noble metal-only catalysts, after pre-reduction. The authors were unsure as to whether or not redox reactions of Ce contributed to overall CO oxidation activity (85).

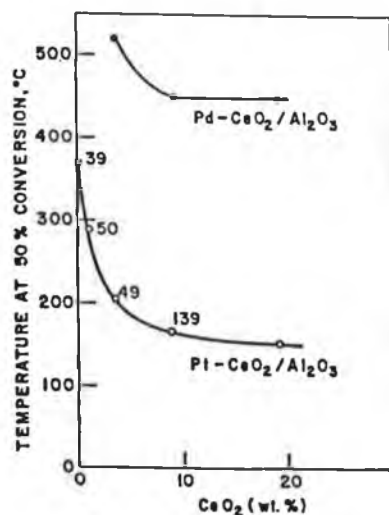


Figure 1.14 : CO Oxidation Activity(○) and Pt Uptake (in ppm) as a Function of CeO<sub>2</sub> Content (85). Catalysts prepared by a thermal transport technique (at 800°C for 6 hours.) and reduced at 450°C prior to testing.

Migration of Pt from one support to another was found to be possible based on experiments in which the Pt was deposited on one support with the resulting catalyst then heated in the presence of the other support (85). Migration from CeO<sub>2</sub> to Al<sub>2</sub>O<sub>3</sub> was found to be possible as well as migration from Al<sub>2</sub>O<sub>3</sub> to CeO<sub>2</sub>, even though the affinity of CeO<sub>2</sub> was greater than that of Al<sub>2</sub>O<sub>3</sub> for Pt. It was noted that this may cause dynamic redistribution to take place between different supports when catalysts are used under oxidising conditions (85).

A series of Rh/Ce/Al<sub>2</sub>O<sub>3</sub> catalysts of fixed Rh loading (0.014 wt.% Rh) and variable Ce loadings (0 to 15 wt.%) were examined by Oh and Eickel (86) for CO oxidation using an internal-recycle mixed-flow reactor with CO-O<sub>2</sub> in N<sub>2</sub> feedstreams. Catalyst activity was characterised in two ways, using temperature run-up experiments with fixed reactant composition and isothermal experiments (196°C) with variable composition (86).

Catalysts were prepared by incipient wetness impregnation in a stepwise manner with aqueous solutions of Ce(NO<sub>3</sub>)<sub>3</sub> and RhCl<sub>3</sub> (86). In most cases Ce was deposited first followed by calcination at 500°C for 4 hours. The Rh was then deposited and the calcination step repeated. The Al<sub>2</sub>O<sub>3</sub> spheres used had a BET surface area of 112 m<sup>2</sup>/g which was decreased on addition of CeO<sub>2</sub>. This latter fact was presumed to be due to plugging of some of the Al<sub>2</sub>O<sub>3</sub> micropores. Catalysts were characterised by a number of techniques including X-ray diffraction, H<sub>2</sub> chemisorption, and temperature programmed desorption (TPD) of adsorbed CO. The reducible nature of CeO<sub>2</sub> was

thought not to interfere with Rh dispersions, measured by H<sub>2</sub> chemisorption, which indicated little change in Rh particle size on addition of 2 wt.% Ce. CeO<sub>2</sub> particle diameters, measured by XRD, were 28, 53 and 65 Å for Ce loadings of 2, 9, and 15 wt.% Ce respectively. All catalysts were reduced at 450°C prior to CO oxidation tests (86).

The effects of Ce addition on CO oxidation kinetics, at 196°C, over Rh/Al<sub>2</sub>O<sub>3</sub> were found to depend strongly on the stoichiometry of the reactant mixture (86). In strongly oxidising environments (i.e. pO<sub>2</sub> >> pCO), the reaction kinetics were not particularly altered by the presence of Ce. On the other hand, the kinetics were appreciably altered by the addition of sufficient amounts of CeO<sub>2</sub> (≥ 2 wt.% Ce), when the oxidation was studied under moderately oxidising or net-reducing conditions. These Ce induced changes involved a suppression of the CO inhibition effect and decreased apparent activation energy which are in agreement with the Type 2 kinetics reported by Yu Yao (53). In a 1 vol.% CO and 1 vol.% O<sub>2</sub> feedstream, the activation energy decreased from 117.3 to 84.4 kJ.mol<sup>-1</sup> on increasing the Ce loading from 0 to 15 wt.% (86). Although the apparent activation energy for 0.014 wt.% Rh/Al<sub>2</sub>O<sub>3</sub> remained relatively constant at 108.2-116.5 kJ.mol<sup>-1</sup> on varying the O<sub>2</sub> concentration in the range 0.5 to 5 vol.% at a CO concentration of 1 vol.%, that of a 0.014 wt.% Rh sample containing 9 wt.% Ce increased from 87.4 kJ.mol<sup>-1</sup> to 110.2 kJ.mol<sup>-1</sup> in the same range. The reaction rate was found to exhibit decreased sensitivity to gas-phase O<sub>2</sub> concentration in the presence of CeO<sub>2</sub>, again in agreement with Yu Yao (53). The dependence on O<sub>2</sub> concentration changed from first order to 0.37th order on addition of 9 wt.% Ce (86).

These kinetic changes led to enhanced CO oxidation activity of a 0.014% Rh/Al<sub>2</sub>O<sub>3</sub> catalyst under moderately oxidising or net reducing conditions (86). The enhanced CO oxidation activity at high CO concentrations, was concluded as being due to a synergistic Rh-Ce interaction and was not due to the additional activity derived from Ce. This was shown by the fact that a Rh/Ce/Al<sub>2</sub>O<sub>3</sub> catalyst was significantly more active than a physical mix of Rh/Al<sub>2</sub>O<sub>3</sub> and Ce/Al<sub>2</sub>O<sub>3</sub> catalysts containing the same absolute levels of Ce and Rh. The effects of CeO<sub>2</sub> addition were found to be independent of whether the Ce was deposited on the Al<sub>2</sub>O<sub>3</sub> support before or after the Rh (86).

Oh and Eickel (86) rationalised the different kinetics for Rh/CeO<sub>2</sub>/Al<sub>2</sub>O<sub>3</sub> samples under different environments on the basis of two different types of reaction mechanism. In an O<sub>2</sub>-rich reactant mixture, it was thought that the oxidation of CO would proceed by a Langmuir-Hinshelwood mechanism over both Rh/Al<sub>2</sub>O<sub>3</sub> and Rh/CeO<sub>2</sub>/Al<sub>2</sub>O<sub>3</sub> with reaction between adsorbed CO and adsorbed oxygen. Under moderately oxidising or net-reducing conditions, it was proposed that as the CO

concentration increased, the adsorption of oxygen onto the catalyst surface would become limited due to increasing saturation of surface sites with adsorbed CO. Therefore the oxidation rate was adversely affected over Rh/Al<sub>2</sub>O<sub>3</sub>. This CO inhibition effect was not found in the presence of CeO<sub>2</sub> and it was postulated that CO oxidation over Rh/CeO<sub>2</sub>/Al<sub>2</sub>O<sub>3</sub> under these conditions was occurring via a different pathway involving a surface reaction between CO adsorbed on Rh and oxygen derived from CeO<sub>2</sub>. This additional oxygen from CeO<sub>2</sub> would therefore effectively increase the surface oxygen concentration and thereby suppress the CO inhibition effect (86).

Rh/CeO<sub>2</sub> exhibited the same type of kinetic dependence as Rh/CeO<sub>2</sub>/Al<sub>2</sub>O<sub>3</sub> (86). This was thought to provide indirect evidence for the participation of lattice oxygen in the reaction mechanism because lattice oxygen at the Pt-ceria interface in Pt/CeO<sub>2</sub> samples had been previously reported to be involved in CO<sub>2</sub> formation during CO TPD (87). The fact that higher CeO<sub>2</sub> loadings were required for kinetic behaviour to be altered, lead to the conclusion that larger three-dimensional particles were more effective in donating oxygen than highly dispersed ceria at lower concentrations (86). As shown in Fig. 1.15, in a strongly reducing feedstream where the proposed mechanism would be expected to dominate, addition of 2 wt.% or more Ce resulted in considerably enhanced CO oxidation. It was thought that as the CeO<sub>2</sub> loading was increased the number of CeO<sub>2</sub> particles in the vicinity of the Rh particles increased, thereby increasing the availability of surface oxygen for CO oxidation. The circumference of the Rh particles was thought to be the limiting factor at higher concentrations ( $\geq 15$  wt.% Ce in Fig. 1.15) (86).

Results of IR and TPD studies of CO adsorption, suggested against charge transfer between the Rh and Ce (and the resulting changes in the adsorptive properties of the Rh) as the reasons for the modification of CO kinetics by ceria (86). Both techniques showed no appreciable change in the interaction of CO with Rh in the presence of ceria. The authors noted that another possible mode of Rh-Ce interaction was a strong metal-support interaction (i.e. SMSI) involving decoration of Rh particles by CeO<sub>2</sub> moieties but this was thought to be unlikely even acknowledging the fact that the catalysts were pre-reduced at 450°C prior to each experiment (86).

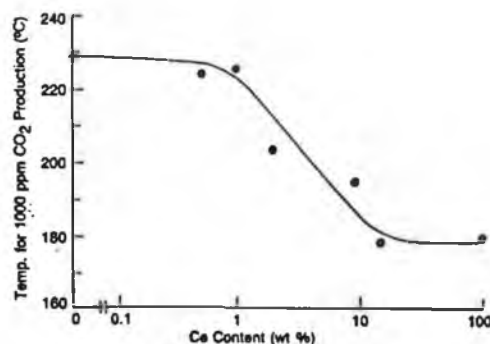


**Figure 1.15 : CO Oxidation Activity versus Ce Content in a 0.014 wt.% Rh/Al<sub>2</sub>O<sub>3</sub> Catalyst (86). Feedstream contained 5 Vol.% CO and 0.5 Vol.% O<sub>2</sub>.**

In disagreement with Oh and Eickel (86), Löff et al. (81) found significant changes in the CO and NO TPD spectra of supported Pt and Rh catalysts in the presence of CeO<sub>2</sub>. Catalytic activity for CO oxidation was also enhanced with addition of CeO<sub>2</sub> to Al<sub>2</sub>O<sub>3</sub>-supported samples under the conditions used (81). A noble metal-ceria interaction, possibly associated with oxygen vacancies in ceria adjacent to the noble metal particles, was proposed to explain these results. Pt, Rh, and Pt + Rh samples supported on Al<sub>2</sub>O<sub>3</sub>, CeO<sub>2</sub> and 20 wt.% CeO<sub>2</sub>/Al<sub>2</sub>O<sub>3</sub> were prepared by impregnation of the supports with aqueous solutions of H<sub>2</sub>PtCl<sub>6</sub> and/or RhCl<sub>3</sub>. Calcination was achieved at 500°C in air for two hours. The support surface areas were 140 m<sup>2</sup>/g, 107 m<sup>2</sup>/g and 120 m<sup>2</sup>/g for Al<sub>2</sub>O<sub>3</sub>, CeO<sub>2</sub> and CeO<sub>2</sub>/Al<sub>2</sub>O<sub>3</sub>, respectively. Both monolithic and powder samples were studied. For the former samples, noble metal loadings were 1.5 wt.% Pt and/or 0.3 wt.% Rh based on the weight of the washcoat support. For the CeO<sub>2</sub> and Al<sub>2</sub>O<sub>3</sub> powders, loadings of 1 or 3 wt.% Pt or 1 wt.% Rh were used (81).

TPD experiments were performed in a quartz flow reactor cell (81). Samples were oxidised in 2% O<sub>2</sub> in Ar for 5 minutes at 600°C and then reduced in 4% H<sub>2</sub> in Ar under the same conditions before analysis. Noble metal-ceria interaction was found to occur for both CeO<sub>2</sub> and CeO<sub>2</sub>/Al<sub>2</sub>O<sub>3</sub>-supported samples as shown by the appearance of a high temperature CO desorption peak at ~ 470°C, not present for Al<sub>2</sub>O<sub>3</sub>-supported samples. TPD of NO was also modified in the presence of CeO<sub>2</sub>. TPD spectra for Pt samples indicated that Pt was predominantly deposited on CeO<sub>2</sub> in the Pt/CeO<sub>2</sub>/Al<sub>2</sub>O<sub>3</sub> sample which is in agreement with other studies that have shown Pt to have greater affinity for CeO<sub>2</sub> relative to Al<sub>2</sub>O<sub>3</sub> (85, 88). XPS analysis of reduced 1 wt.% Pt/CeO<sub>2</sub> and 3 wt.% Pt/Al<sub>2</sub>O<sub>3</sub> samples, showed no difference in the chemical state of Pt with essentially metallic Pt present on both supports (81). Thus, the noble metal-ceria interaction was not thought to involve a simple electronic perturbation of the noble metal. The CeO<sub>2</sub>-induced shift in the TPD spectra of CO towards higher temperatures

was attributed to an increase in the number of atomically isolated Pt and Rh atoms which are associated with stronger dicarbonyl CO adsorption and/or to the creation of a new type of sites where the CO molecules are bonded through the carbon atoms to the Pt or Rh particles and the oxygen atoms to the reduced CeO<sub>2</sub>. The fact that the total amount of desorbed CO was almost unchanged on addition of ceria was thought to support the latter explanation. One possible explanation given for the differences in CO TPD spectra compared with those obtained by Oh and Eickel (86), was that different experimental conditions were employed (81). Activity measurements performed in the TPD cell showed that the activity of reduced Pt, Rh, and Pt + Rh samples was increased upon addition of CeO<sub>2</sub> for both  $\text{CO} + \frac{1}{2}\text{O}_2 \rightarrow \text{CO}_2$  and  $\text{CO} + \text{NO} \rightarrow \text{CO}_2 + \frac{1}{2}\text{N}_2$  reactions with stoichiometric gas mixtures (81).

Catalysts containing 0.7-0.8 wt.% Pt on either Al<sub>2</sub>O<sub>3</sub> or 30% CeO<sub>2</sub>/Al<sub>2</sub>O<sub>3</sub> were also tested under steady state conditions in a flow reactor for both CO oxidation and water-gas shift (WGS) activity (81). The catalyst activity was monitored as a function of inlet reactor temperature between 150 and 400°C in a feedstream of 1.8% CO, 10% H<sub>2</sub>O, 10.9% CO<sub>2</sub>, and 0.24% O<sub>2</sub>. After the first run, the catalyst sample was then conditioned in-situ at 450°C for 30 minutes before being cooled to 150°C and retested. In-situ conditioning in this manner was found to result in increased low-temperature activity for CeO<sub>2</sub>-containing samples during Run 2. The authors noted that Oh and Eickel (86) attributed enhanced CO oxidation in the presence of CeO<sub>2</sub> to the donation of lattice oxygen under fuel-rich conditions. In this study (81), it was found that addition of 20 ppm SO<sub>2</sub> to the reaction mixture poisoned the promotion of steady-state CO oxidation at low temperatures by CeO<sub>2</sub>. SO<sub>2</sub> had no effect on the low temperature activity of Pt/Al<sub>2</sub>O<sub>3</sub>. The effects of SO<sub>2</sub> exposure on the TPD spectra of CO were also monitored and showed that the ceria-induced shift in the CO TPD completely vanished, indicating poisoning of the noble metal-ceria interaction. It was proposed that it was the more strongly adsorbed CO species which reacted with lattice oxygen from ceria to form CO<sub>2</sub>, especially at low temperatures. SO<sub>2</sub> poisoned the enhancement of low temperature CO oxidation activity by CeO<sub>2</sub> due to the formation of Ce(III)-sulphate, which prevented the formation of these double bonded and/or dicarbonyl CO surface species. A slight increase in WGS activity by CeO<sub>2</sub> was also found under the steady state conditions used. SO<sub>2</sub> poisoning at high temperatures was attributed to a detrimental effect on WGS reaction (81).

The addition of CeO<sub>2</sub> to Pt/Al<sub>2</sub>O<sub>3</sub> catalysts has been studied by Serre et al. (89), particularly with relation to its' effect on CO oxidation by oxygen. Lattice oxygen from ceria was reported to be capable of enhancing catalyst activity following prereduction. 2% Pt/Al<sub>2</sub>O<sub>3</sub>, 14.5% CeO<sub>2</sub>/Al<sub>2</sub>O<sub>3</sub>, and 2% Pt-14.5% CeO<sub>2</sub>/Al<sub>2</sub>O<sub>3</sub>

catalysts were prepared by impregnation of  $\gamma$ -Al<sub>2</sub>O<sub>3</sub> (pellets or powdered) with aqueous solutions of Ce(NO<sub>3</sub>)<sub>3</sub> and H<sub>2</sub>PtCl<sub>6</sub>. For the sample with both metals, CeO<sub>2</sub> impregnation preceded that of Pt and calcination was at 400°C for 2 hours in air after each impregnation step. Catalysts were examined using two different types of light-off tests with different space velocities (89).

For the low space velocity test, 4.72g of pelleted catalyst was used with a constant flowrate of 100 cm<sup>3</sup>/min and a heating rate of 10°C/min from room temperature to 700°C (89). For these tests, the feedstream consisted of 1.5% CO and 1.5% O<sub>2</sub> in He. Catalysts were either prereduced or preoxidised for 1 hour at 700°C in 1.5% CO/He or 5% O<sub>2</sub>/He, respectively. Under these low space velocity tests, adsorption-desorption phenomena could be studied as well as light-off activity. During equilibration of prereduced catalysts under the reactant feedstream at room temperature, reoxidation of ceria was found to occur as indicated by O<sub>2</sub> uptakes for the CeO<sub>2</sub>/Al<sub>2</sub>O<sub>3</sub> and Pt/CeO<sub>2</sub>/Al<sub>2</sub>O<sub>3</sub> samples. However, complete reoxidation of prereduced ceria at room temperature only occurred in the presence of noble metal. For Pt-containing samples, CO adsorption occurred at room temperature. For preoxidised samples, no significant change in catalyst activity was found on addition of CeO<sub>2</sub> to Pt/Al<sub>2</sub>O<sub>3</sub>. For prereduced samples, activity decreased in the order Pt/CeO<sub>2</sub>/Al<sub>2</sub>O<sub>3</sub> > Pt/Al<sub>2</sub>O<sub>3</sub> > CeO<sub>2</sub>/Al<sub>2</sub>O<sub>3</sub> as shown by the light-off curves in Fig 1.16 (89).

High space velocity tests were performed using 100 mg of catalyst powder and a flow rate of 250 cm<sup>3</sup>/min (89). Catalysts were exposed to either lean (0.5% CO and 0.5% O<sub>2</sub>/N<sub>2</sub> i.e. oxidising) or rich (1% CO and 0.25% O<sub>2</sub>/N<sub>2</sub> i.e. reducing) gas mixtures for 1 hour at 490°C before testing. The catalyst sample was then cooled to room temperature under the same gas composition. Purging of the sample in the test gas mixture at room temperature then preceded testing, which involved heating to 490°C at 4 °C/min in either the rich or lean mixture. For Pt/Al<sub>2</sub>O<sub>3</sub>, catalyst activity was independent of either the activation or test gas mixture composition, with CO oxidation occurring at approximately the same temperature in all cases examined. However, Pt/CeO<sub>2</sub>/Al<sub>2</sub>O<sub>3</sub> was considerably more active after activation in the rich-mixture. Also the activation energy for CO oxidation in a lean mixture following rich-gas activation for Pt/CeO<sub>2</sub>/Al<sub>2</sub>O<sub>3</sub> was much lower than that for Pt/Al<sub>2</sub>O<sub>3</sub> after lean-gas pretreatment, ~48 kJ.mol<sup>-1</sup> for Pt/CeO<sub>2</sub>/Al<sub>2</sub>O<sub>3</sub> and ~94 kJ.mol<sup>-1</sup> for Pt/Al<sub>2</sub>O<sub>3</sub>. This indicated a different reaction mechanism was occurring on very reactive sites produced in the presence of both CeO<sub>2</sub> and Pt (89).

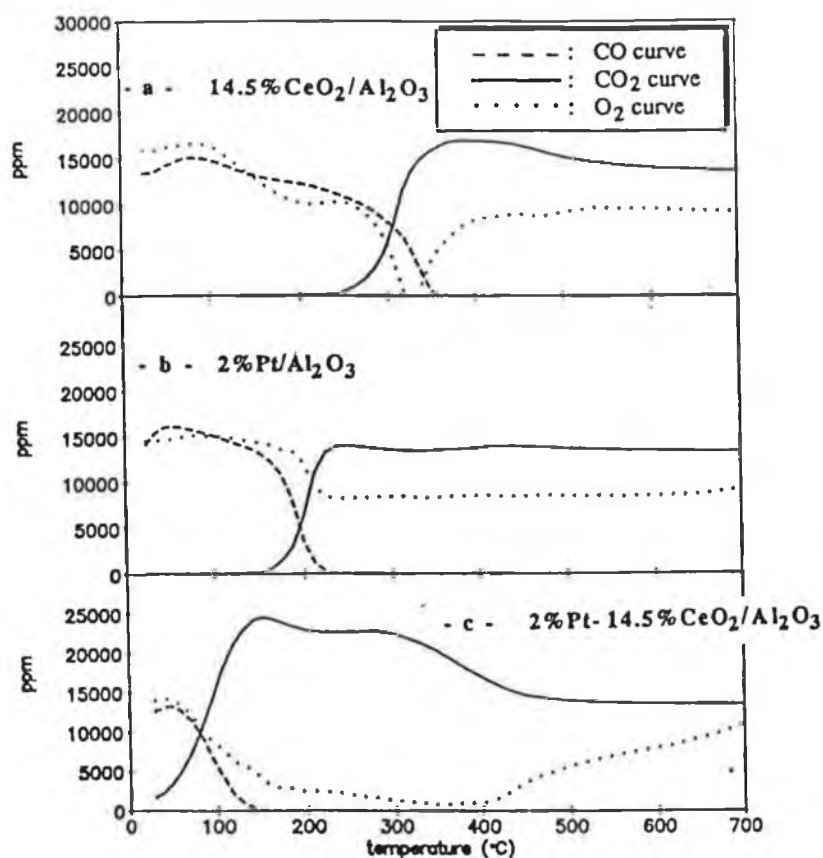


Figure 1.16 : Light-off tests performed at low space velocity on pre-reduced catalysts (89).

For both high and low space velocity light-off tests, it was found that a Pt-CeO<sub>2</sub> interaction in Pt/CeO<sub>2</sub>/Al<sub>2</sub>O<sub>3</sub> samples resulted in a large enhancement of catalytic activity after reductive pretreatment, but this phenomenon could be reversed by subsequent oxidative treatment (89). The very high activity on pre-reduction was tentatively assigned to Pt<sup>0</sup>-CeO<sub>2</sub> sites located at the metal-ceria interface, with the key factor in increasing low temperature activity being the initiation of the oxidation of CO adsorbed on the metallic Pt by "oxide" from the ceria. After pre-oxidation of Pt/CeO<sub>2</sub>/Al<sub>2</sub>O<sub>3</sub>, the performance was very similar to that of the Pt-only samples. Under these conditions the Pt<sup>0</sup>-CeO<sub>2</sub> sites were proposed to be converted to inactive PtO<sub>2</sub>-CeO<sub>2</sub> with the "bulk" Pt remaining in the metallic form. In this situation, the reaction was thought to proceed only on Pt<sup>0</sup> sites, exactly as for the Pt/Al<sub>2</sub>O<sub>3</sub> samples, via a Langmuir-Hinshelwood mechanism in which O<sub>2</sub> adsorption on Pt sites was inhibited at low temperatures due to saturation of the Pt surface with CO. In the absence of the CeO<sub>2</sub> promoting effect, O<sub>2</sub> adsorption and subsequent reaction with adsorbed CO to produce CO<sub>2</sub> was only initiated at higher temperatures. The availability of lattice oxygen from ceria for reaction at low temperatures with CO adsorbed on neighbouring Pt<sup>0</sup>, was proposed to enhance light-off activity following reduction of Pt/CeO<sub>2</sub>/Al<sub>2</sub>O<sub>3</sub>.

Stabilisation of Pt in an oxidised state, at the Pt-CeO<sub>2</sub> interface, was thought to result in this "interfacial" Pt being oxidised after preoxidation at a high temperature (700°C). Al<sub>2</sub>O<sub>3</sub>-supported PtO<sub>2</sub> was not expected to be stable under the high temperature preoxidation conditions used and hence "bulk" Pt was expected to be in the reduced state after both reductive and oxidative pre-treatments. This was thought to also hold true for the samples in the high space velocity test, even though pre-oxidation was performed at 490°C, because the reducing effect of CO was expected to predominate on cooling in the O<sub>2</sub>/CO mixture before testing. This was in agreement with the fact that the activity of Pt/Al<sub>2</sub>O<sub>3</sub> was found to be independent of pretreatment conditions used, in both high and low space velocity testing (89).

In 1995, Bunluesin et al. (90) found evidence to support the existence of a second, ceria-mediated reaction mechanism when Rh was supported on CeO<sub>2</sub>. This mechanism was thought to involve oxygen from the CeO<sub>2</sub> reacting with CO adsorbed on the Rh and prevailed under certain reaction conditions as had been found in a previous study (91). Support for this theory came from TPD studies which showed that oxygen from ceria could migrate onto Rh and react with adsorbates on the Rh (92). Reaction conditions which favoured the ceria-mediated mechanism were low temperatures, high P<sub>CO</sub> and low P<sub>O<sub>2</sub></sub> (90).

In preparing the catalysts, a ceria film, ~10 μm thick, was deposited onto an alumina foil by spray pyrolysis of an aqueous solution of Ce(NO<sub>3</sub>)<sub>3</sub>, while holding the foil between 327 and 397°C in air (90). Two different Rh catalysts, with different Rh particle sizes, were prepared by vapor deposition of Rh onto the ceria film in ultrahigh vacuum. CO oxidation kinetics, at differential conversions, were monitored over a wide pressure and temperature range. Catalysts were pretreated under CO oxidation conditions at 377°C before rate measurement. It was thought that reaction rates on the CeO<sub>2</sub> support itself could be ignored as samples without Rh exhibited rates that were at least an order of magnitude less than those measured with Rh under all conditions investigated. The dependence of the reaction rate on CO pressure is shown, in Fig.1.17, for both Rh/CeO<sub>2</sub> and Rh/Al<sub>2</sub>O<sub>3</sub> samples,

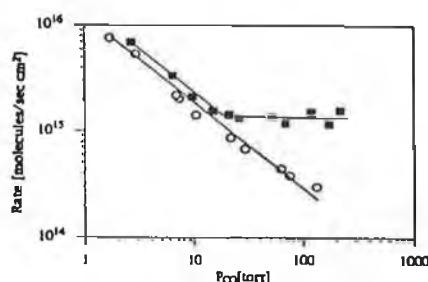


Figure 1.17 : CO Oxidation Rate versus P<sub>CO</sub> on model Rh/ceria (■) and Rh/alumina (○) catalysts (90). pO<sub>2</sub> = 0.3 Torr at 300°C.

On Rh/Al<sub>2</sub>O<sub>3</sub>, the rate was found to be negative first order in CO over the entire range investigated, which was thought to indicate saturation of the Rh surface with adsorbed CO which inhibits the reaction by preventing oxygen adsorption (90). However for Rh/CeO<sub>2</sub> at high CO pressures, the reaction is no longer poisoned by CO. This suggested the onset of a new mechanism which does not require oxygen to adsorb on the CO-saturated Rh. This was supported by the O<sub>2</sub> pressure dependencies which showed a decreased dependency on O<sub>2</sub> concentration at higher CO pressures for Rh/CeO<sub>2</sub>. The tendency of CeO<sub>2</sub> to alter the kinetics of CO oxidation was found to increase at lower temperatures e.g. the ceria-mediated reaction mechanism was observed at lower CO pressures at 190°C than at 300°C. The ceria-mediated reaction mechanism had an activation energy of between 49.9 and 62.4 kJ.mol<sup>-1</sup> compared to a value of between 104 and 112.3 kJ.mol<sup>-1</sup> for Rh/CeO<sub>2</sub> at lower CO pressures. Thus the proposed ability of the lattice oxygen from ceria to react with CO adsorbed on Rh, at high CO pressures, was expected to improve catalyst light-off since reaction could occur at lower temperatures. This ceria-related mechanism was found to be more important for smaller Rh particle sizes. One possible explanation for this was the existence of a greater Rh-CeO<sub>2</sub> interfacial area. The authors noted that their suggested mechanism was in agreement with that proposed by Oh and Eickel (86) on addition of CeO<sub>2</sub> to Rh/Al<sub>2</sub>O<sub>3</sub>. This suggested that bulk CeO<sub>2</sub> was not required for observation of the ceria-mediated reaction mechanism, but that it could also occur for Al<sub>2</sub>O<sub>3</sub>-supported samples containing CeO<sub>2</sub> as an additive (90). It was not known whether or not the proposed benefits of CeO<sub>2</sub> would be of advantage in typical high-temperature applications such as automotive exhaust catalysts. It was thought that it may find significance in other applications (90).

As mentioned above, Zafiridis and Gorte (92), studied TPD of CO from Rh/CeO<sub>2</sub>. Evidence was found for the formation of CO<sub>2</sub> by oxidation of adsorbed CO by oxygen from the ceria migrating onto the Rh particles, at temperatures as low as 127°C. Catalysts were prepared by deposition of Rh onto an amorphous ceria film in ultrahigh vacuum, and TPD measurements were made in an ultrahigh vacuum chamber between room temperature and 327°C. The authors noted that in a previous study (93) involving model Pt/CeO<sub>2</sub> catalysts, no evidence was found for oxygen migration onto Pt (92).

Jin et al (87) studied the temperature programmed desorption of CO and CO<sub>2</sub> from Pt/CeO<sub>2</sub> and found that lattice oxygen from ceria could play an important role in the oxidation of CO on Pt catalysts. This is in disagreement with the findings of Zafiridis

and Gorte (93). Zafiridis and Gorte (92) thought that the conflict between the two studies (87, 93) could have been due to the use of higher surface area  $\text{CeO}_2$  by Jin et al (87). This was expected to shift desorption to higher temperatures and indicated that oxygen can migrate from ceria to Pt but at lower rates than for Rh catalysts (92).

Jin et al. (87) proposed that lattice oxygen at the Pt- $\text{CeO}_2$  interface was involved in the formation of significant amounts of  $\text{CO}_2$  from CO adsorbed on Pt, at temperatures above  $127^\circ\text{C}$ . The formation of CO during the TPD of  $\text{CO}_2$  was proposed to involve the reverse process i.e. oxygen donation from  $\text{CO}_2$  to a lattice vacancy at the interface to produce CO adsorbed on Pt. These processes are illustrated in Fig. 1.18.

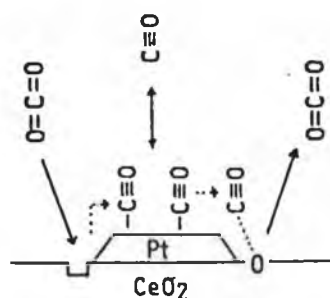


**Figure 1.18 : Involvement of Lattice Oxygen in the Conversion of CO to  $\text{CO}_2$  and  $\text{CO}_2$  to CO during TPD experiments on Pt/ $\text{CeO}_2$  (87).**

Samples were prepared with 2 wt.% Pt on  $\text{CeO}_2$  ( $5 \text{ m}^2/\text{g}$ ) by impregnation with  $\text{H}_2\text{PtCl}_6$  in aqueous solution (87). Calcination was at either  $200$  or  $400^\circ\text{C}$  in air to produce average Pt crystal sizes of  $370$  and  $130 \text{ \AA}$ , respectively. Before measurement, samples were heated under vacuum at  $527^\circ\text{C}$  for 1 hour. Samples could be preoxidised or prerduced in the TPD chamber as required. TPD experiments were performed from  $-73$  to  $527^\circ\text{C}$  at a heating rate of  $2^\circ\text{C}/\text{sec}$  set with a temperature programmer (87).

A number of mechanisms were considered to explain the formation of  $\text{CO}_2$  during CO TPD (87). These included disproportionation of CO into  $\text{CO}_2$  and C, and oxidation of CO by chemisorbed oxygen on Pt or by preadsorbed water or hydroxyl species. However these were all rejected in favour of the mechanism in Fig. 1.18. Isotopic exchange experiments using  $^{18}\text{O}$  and  $\text{C}^{18}\text{O}$  helped confirm this hypothesis.  $\text{H}_2$  treatment at  $500^\circ\text{C}$  completely suppressed  $\text{CO}_2$  formation from CO while preoxidation

increased the conversion of CO to CO<sub>2</sub> to almost 80%. Conversion of CO<sub>2</sub> to CO during TPD of CO<sub>2</sub> was enhanced on prerduced samples and was completely suppressed by O<sub>2</sub> pretreatment at 100°C for 5 minutes (87).

The dependence of TPD characteristics on pretreatment conditions was thought to indicate that the abundance of lattice oxygen and lattice oxygen vacancies at the Pt/CeO<sub>2</sub> interface determined the CO/CO<sub>2</sub> TPD profiles (87). This mechanism was supported by the fact that the amount of interconversion of CO and CO<sub>2</sub> was related to the size of the Pt particles. Samples calcined at 400°C had smaller Pt crystal sizes and greater CO/CO<sub>2</sub> interconversions. This was ascribed to a greater Pt-CeO<sub>2</sub> interfacial area in these samples. IR studies showed the presence of small amounts of adsorbed CO on Pt following CO<sub>2</sub> adsorption which was explained in terms of a limited number of oxygen vacancies at the Pt-CeO<sub>2</sub> interface (87).

Leclercq et al. (94) studied CO + NO and CO + NO + O<sub>2</sub> reactions on Pt/Al<sub>2</sub>O<sub>3</sub>, Pt/Rh/Al<sub>2</sub>O<sub>3</sub>, Pt/CeO<sub>2</sub>/Al<sub>2</sub>O<sub>3</sub>, and Pt/Rh/CeO<sub>2</sub>/Al<sub>2</sub>O<sub>3</sub>. Catalysts were prepared by impregnation of the supports with H<sub>2</sub>PtCl<sub>6</sub> and RhCl<sub>3</sub> solutions. Pt, Rh and CeO<sub>2</sub> loadings of 1, 0.2, and 12 wt.%, respectively, were used. Dispersions were quoted as 0.55 for Pt/Al<sub>2</sub>O<sub>3</sub> and 1.00 for Pt/Rh/Al<sub>2</sub>O<sub>3</sub>. Addition of 12 wt.% CeO<sub>2</sub> to the  $\gamma$ -Al<sub>2</sub>O<sub>3</sub> support increased the surface area from 100 to 128 m<sup>2</sup>/g. Catalysts were tested in feedstreams of 0.5 mole% CO + 0.56 mole% NO in He, and 0.75 mole% CO + 0.28 mole% NO + 0.26 mole% O<sub>2</sub> in He. A plug flow reactor was used for temperature programmed experiments from 100 to 550°C. Before testing, catalysts were heated at 500°C in He and then activated in the CO + NO reactant mixture at the same temperature. In the absence of O<sub>2</sub>, CO and NO conversions were higher than those expected from the stoichiometry of CO + NO reactions. A complex reaction mechanism, involving various competitive steps, was proposed in which CO adsorbed on the metal sites could migrate towards the metal-support interface and be oxidised by oxygen atoms from the support. One possible route for NO dissociation could then involve interaction with the oxygen vacancies in the support. CeO<sub>2</sub> was found to be capable of improving catalyst activity and this was explained on the basis of better availability of oxygen atoms from CeO<sub>2</sub> due to better oxidation-reduction properties relative to Al<sub>2</sub>O<sub>3</sub>. The promoting effect of CeO<sub>2</sub> was particularly important for experiments in the presence of O<sub>2</sub> with light-off temperatures improved by 100°C for CO oxidation and 70°C for NO reduction (94).

Munuera et al. (95) investigated the interaction of H<sub>2</sub>, O<sub>2</sub>, CO, and CO/O<sub>2</sub> with Rh/CeO<sub>2</sub> and Rh/TiO<sub>2</sub> using XPS, TPD and Ar<sup>+</sup> sputtering experiments. Rh loadings in the range 2.5-3 wt.% were used. CeO<sub>2</sub>-supported samples were prepared by

incipient wetness impregnation with  $\text{Rh}(\text{NO}_3)_3$  and were calcined at  $400^\circ\text{C}$  in an  $\text{O}_2$  flow for 4 hours. TPD experiments were performed using a linear heating ramp of  $30^\circ\text{C}/\text{min}$  up to  $700^\circ\text{C}$ . CO oxidation to  $\text{CO}_2$  in TPD experiments was thought to occur on three different types of sites, namely, metallic Rh, the support and, in particular at the metal-support interface. These latter sites were thought to involve oxygen-vacancies in the  $\text{CeO}_2$  support. A cyclic catalytic process was proposed, involving the formation of a  $\text{Ce}^{4+} - \text{O}_2^{2-} - \text{Rh}^+$  species following oxygen incorporation into reduced ceria. CO oxidation could then occur, via the production of a  $\text{Rh}^{3+}$  species, to produce  $\text{CO}_2$  with the catalyst reverting to its initial reduced state involving metallic Rh and oxygen vacancies in the support with Ce present as  $\text{Ce}^{3+}$ .  $\text{Ar}^+$  sputtering experiments with  $\text{TiO}_2$ -supported samples, showed that the creation of oxygen vacancies in the support, resulting in the presence of  $\text{Ti}^{3+}$ , significantly enhanced the oxidation of Rh to  $\text{Rh}^{3+}$  particularly in the presence of CO. The authors concluded that there was clear evidence for an important role played by oxygen vacancies at the metal-support interface in the redox chemistry of Rh, and probably other noble metals, in these type of catalysts under CO oxidation conditions (95).

Hardacre et al. (96) studied model Pt(111)/ceria catalysts prepared by ultrahigh vacuum (UHV) deposition of ceria films onto a clean Pt surface. It was thought that these model catalyst studies might provide information about phenomena which underlie the behaviour of dispersed catalysts used in common applications. Reaction kinetic measurements indicated that, in some circumstances,  $\text{CeO}_2$  can behave as a very active CO oxidation catalyst with the noble metal acting as a promoter. Results suggested that fully encapsulated Pt was even more active than the clean Pt surface because of this phenomenon (96).

Reaction kinetics were studied in a small pressure cell, coupled to a UHV/XPS chamber (96). The cell was operated as a differential batch reactor with analysis of reaction products by a quadrupole mass spectrometer. A CO: $\text{O}_2$  ratio of 2:1 was used to study CO oxidation at temperatures between  $50$ - $157^\circ\text{C}$ . Conversions were maintained below 5% in order to obtain reliable kinetic parameters. Ce deposition was expected to result in uniform  $\text{CeO}_2$  films covering the Pt surface (96).

At low  $\text{CeO}_2$  coverage's ( $< \sim 0.5$  monolayers (ML)), the CO oxidation rate over Pt increased (96). This enhancement of Pt activity was thought to arise from oxygen spillover from  $\text{CeO}_2$  to react with CO adsorbed on Pt or from the formation of highly active interfacial sites at the metal/oxide boundary. As the  $\text{CeO}_2$  coverage was further increased the oxidation rate began to decrease significantly to an undetectably low level at between 0.8 and 1.3 ML of ceria. This was accompanied by a sharp increase in

activation energy and was associated with the predominance of a new reaction mechanism involving interfacial sites where CO<sub>2</sub> desorption was rate-limiting. At higher CeO<sub>2</sub> coverage's (> 1.3 ML) the CO oxidation rate began to increase, and the activation energy to decrease, as a function of CeO<sub>2</sub> coverage. At ~ 10ML coverage, the reaction rate reached a limiting value of about 6 times higher than that obtained on the clean Pt(111) surface. At this high coverage, no surface Pt sites were detectable by CO/TPD titration. Thus the high activity was associated with the CeO<sub>2</sub>. A mechanism was proposed involving promotion of an oxygen vacancy in CeO<sub>2</sub> by electron transfer from the encapsulated metal. Jin et al. (87) found that oxygen vacancy formation in CeO<sub>2</sub> can play a role in the oxidation of CO to CO<sub>2</sub>. This was proposed by Hardacre et al (96) to explain the high activity of the fully encapsulated metal with lattice vacancies being refilled by oxygen from the gas phase. The role of CeO<sub>2</sub> as an oxidation catalyst was further supported by the fact that changes in ceria morphology resulted in considerable changes in CO oxidation activity of the samples. The authors did note that there may still have been a very small number of undetectable but extremely active bare Pt surface sites at these high CeO<sub>2</sub> coverage's, which could have accounted for the phenomena observed. However the encapsulation model was deemed more likely (96).

A close contact between metal and CeO<sub>2</sub> was found to be very important in achieving enhancement of the CeO<sub>2</sub> oxidation activity by underlying Pt (96). Thus it was noted that, in more practical supported catalysts, a very high degree of metal dispersion might be desirable. It was proposed that in such practical materials, partial encapsulation of the metal rather than complete encapsulation by CeO<sub>2</sub> might be more desirable to allow a contribution of Pt towards the overall oxidation rate and also to possibly facilitate O<sub>2</sub> spillover from the Pt to promote regeneration of the active sites in the oxide phase (96).

### 1.4.3 Oxidation of Hydrocarbons

In this section, studies which examine the effects of Ce on hydrocarbon oxidation activity of noble metals, in the presence or absence of CO and other feedstream components, will be discussed.

Yu-Yao (54) examined the total oxidation of C<sub>1</sub>-C<sub>4</sub> alkanes over Pt, Pd, and Rh catalysts. The kinetic properties of unsupported wire catalysts and catalysts supported on Al<sub>2</sub>O<sub>3</sub> and CeO<sub>2</sub>/Al<sub>2</sub>O<sub>3</sub> were compared. Supported samples were prepared by incipient wetness impregnation of  $\gamma$ -Al<sub>2</sub>O<sub>3</sub> or CeO<sub>2</sub> precoated Al<sub>2</sub>O<sub>3</sub> powders with the precious metal salt solution, followed by calcination between 600-900°C for 4 hours or

more. Oxidation activity was monitored in a quartz flow reactor following preheating of the sample to 500°C in 1% O<sub>2</sub> in He to remove combustible surface contaminants. Metal dispersions were determined by CO chemisorption at 25°C after pre-reduction in H<sub>2</sub> at 500°C. The dispersions of the CeO<sub>2</sub>-containing samples could not be determined because CeO<sub>2</sub> was thought to be reducible by H<sub>2</sub> at the conditions used, and could also adsorb CO (54).

Alkane conversion, from zero to 100%, was monitored as a function of temperature over the supported samples (54). An inlet O<sub>2</sub>:alkane ratio of twice the stoichiometric ratio was used. Under these reaction conditions, each CeO<sub>2</sub>/Al<sub>2</sub>O<sub>3</sub> supported Pt and Pd catalyst tested was less active than its counterpart without CeO<sub>2</sub>. On the contrary, Rh activity was slightly improved in the presence of CeO<sub>2</sub>. This was attributed to stabilisation of the Rh on the surface by CeO<sub>2</sub> inhibiting its' dissolution into the Al<sub>2</sub>O<sub>3</sub> support. Ceria was also found to affect the kinetics of oxidation over both Pt and Pd. For a Pt/CeO<sub>2</sub>/Al<sub>2</sub>O<sub>3</sub> catalyst of 0.05% Pt, it was thought that Pt was in a more oxidised state following interaction with the CeO<sub>2</sub> and that the oxidised state was less active. On addition of 23% CeO<sub>2</sub>, the reaction became zero order with respect to O<sub>2</sub> rather than O<sub>2</sub> inhibition and the reaction was less dependent on hydrocarbon concentration compared with Pt/Al<sub>2</sub>O<sub>3</sub> or Pt metal. After a brief reduction of the Pt/CeO<sub>2</sub>/Al<sub>2</sub>O<sub>3</sub> sample, its kinetic behaviour was similar to that of Pt/Al<sub>2</sub>O<sub>3</sub> and Pt wire samples. The effects of reduction were slowly reversed upon exposure to O<sub>2</sub>-rich conditions. For Pd/CeO<sub>2</sub>/Al<sub>2</sub>O<sub>3</sub>, a transient high activity was noticed immediately after reduction but the reduced state was less stable than for Pt. It was proposed that the lower activity of Pd/CeO<sub>2</sub>/Al<sub>2</sub>O<sub>3</sub> compared to Pd/Al<sub>2</sub>O<sub>3</sub>, under the standard conditions used, was due to the dispersed Pd having a greater tendency to be oxidised in the presence of CeO<sub>2</sub>. The lower activity was not thought to be due to a decrease in Pd dispersion. For Rh, kinetic parameters were not altered by addition of CeO<sub>2</sub> and it was thought that Rh would be expected to be oxidised in the presence or absence of CeO<sub>2</sub> (54).

Gandhi and Shelef (74) discussed the effects of oxide additives, such as CeO<sub>2</sub> or MoO<sub>3</sub>, on Al<sub>2</sub>O<sub>3</sub> -supported noble metals. The oxygen ions of such oxides are more reactive than those in Al<sub>2</sub>O<sub>3</sub>, and interaction with the noble metal was reported to result in a higher dispersion of the noble metals on the Al<sub>2</sub>O<sub>3</sub>. It was reported that the addition of 3.7% Ce to a 0.07% Pt/ $\gamma$ -Al<sub>2</sub>O<sub>3</sub> catalyst strongly inhibited the oxidation of C<sub>3</sub>H<sub>8</sub> in an oxidising environment, as illustrated in Fig. 1.19. This was attributed to the improved dispersion of the Pt particles. The addition of cerium was thought to prevent the agglomeration of Pt into larger metallic particles necessary for hydrocarbon oxidation. The authors noted that structure insensitive reactions, such as the oxidation of

unsaturated hydrocarbons or carbon monoxide, were expected to be enhanced by this improved dispersion (74).

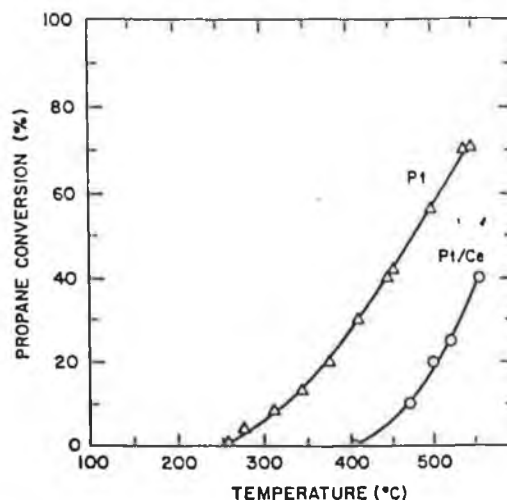


**Figure 1.19 :** Effect of 3.7%  $\text{CeO}_2$  on  $\text{C}_3\text{H}_8$  Oxidation on a 0.07% Pt/ $\gamma$ - $\text{Al}_2\text{O}_3$  catalyst (74). Feedstream contained 1000 ppm  $\text{C}_3\text{H}_8$  and 2%  $\text{O}_2$ .

Shyu et al. (97) studied interaction between Pd and  $\text{CeO}_2$ , in catalysts prepared by impregnation of  $\text{CeO}_2$ ,  $\text{CeO}_2/\text{Al}_2\text{O}_3$  and  $\text{CeAlO}_3/\text{Al}_2\text{O}_3$  with aqueous solutions of  $\text{Pd}(\text{NO}_3)_2$ . A flow reactor system was used to monitor  $\text{C}_3\text{H}_8$  oxidation activity with a reactant mixture of 1000 ppm  $\text{C}_3\text{H}_8$  and varying amounts of  $\text{O}_2$ . All samples were reduced in 3%  $\text{H}_2$  (in  $\text{N}_2$ ) at 500°C for 3 hours and then cooled to room temperature before testing. Decreased  $\text{C}_3\text{H}_8$  oxidation activity in an oxidising environment in the presence of  $\text{CeO}_2$  was attributed to ceria promotion of the oxidation of Pd to  $\text{PdO}$ , in the presence or absence of  $\text{Al}_2\text{O}_3$  (97).

$\text{C}_3\text{H}_8$  oxidation activity was monitored using a 10 wt.% Pd/ $\gamma$ - $\text{Al}_2\text{O}_3$  sample. For a reaction mixture of 1000 ppm  $\text{C}_3\text{H}_8$  and 2%  $\text{O}_2$  in  $\text{N}_2$ , addition of 10 wt.%  $\text{CeO}_2$  was found to increase the temperature required for 50% conversion,  $T_{50}$ , from 288 to 343°C (97). On reducing the  $\text{O}_2$  concentration to the stoichiometric ratio, i.e.  $\text{C}_3\text{H}_8:\text{O}_2 = 1:5$ , the deactivation by  $\text{CeO}_2$  was not as pronounced, with  $T_{50}$  values of 304 and 329°C for Pd/ $\text{Al}_2\text{O}_3$  and Pd/ $\text{CeO}_2/\text{Al}_2\text{O}_3$ , respectively.  $\text{C}_3\text{H}_8$  conversion as a function of  $\text{O}_2$  concentration in the feedgas is shown in Fig. 1.20.

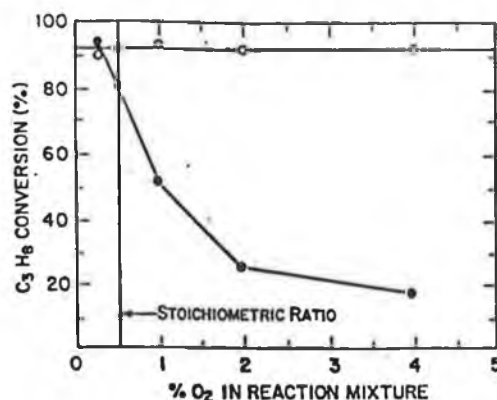


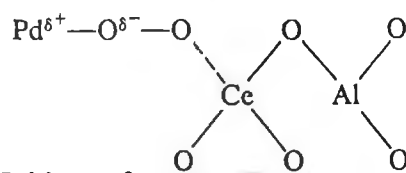
**Figure 1.20 : C<sub>3</sub>H<sub>8</sub> Oxidation, as a function of O<sub>2</sub> Concentration in the feed gas, on 10 wt.% Pd/ $\gamma$ -Al<sub>2</sub>O<sub>3</sub> with (●) and without (○) 10 wt.% CeO<sub>2</sub> (97). C<sub>3</sub>H<sub>8</sub> = 1000 ppm, 350°C.**

It was concluded that CeO<sub>2</sub> only caused deactivation of Pd when the O<sub>2</sub> concentration exceeded that of the stoichiometric ratio. Thus it was thought that for practical applications, the air/fuel ratio should be adjusted to near the stoichiometric ratio when both Pd and CeO<sub>2</sub> were present. This would allow for more efficient use of Pd without losing the other important functions of CeO<sub>2</sub> (97). These later functions were reported by Harrison et al. (76) to include oxygen storage, washcoat stabilisation and enhancement of water-gas shift activity.

Shyu et al. (97) also reported the existence of a complex interaction among CeO<sub>2</sub>, Pd and Al<sub>2</sub>O<sub>3</sub> as indicated by XPS and XRD results. Both CeO<sub>2</sub> and CeO<sub>2</sub>/Al<sub>2</sub>O<sub>3</sub> were found to be capable of promoting reoxidation of Pd, in ambient air, following reduction in H<sub>2</sub> at 920°C. No reoxidation was found to occur in ambient air for Pd/Al<sub>2</sub>O<sub>3</sub>. This was noted as being in agreement with other studies in the literature which have proposed increased oxidation of noble metals when in contact with CeO<sub>2</sub> e.g. (53, 54). In addition Pd was found to have an affect on the reduction and oxidation properties of CeO<sub>2</sub> on Al<sub>2</sub>O<sub>3</sub> according to the reversible reaction,



with the forward reaction proceeding in the presence of H<sub>2</sub> at 920°C and the reaction in the presence of O<sub>2</sub> at 500°C (97). Both reactions were found to be promoted by the presence of Pd. A tentative model was proposed to explain observations involving oxygen adsorption from air by coordination of Pd to CeAlO<sub>3</sub> to form an O<sub>2</sub><sup>-</sup> species, which was stabilised by coordination of Pd, based on the structure,



Oxidation of this surface complex resulted in splitting of the  $\text{O}_2^-$  species to form bulk PdO and  $\text{CeO}_2$ , while reduction at mild temperatures produced metallic Pd and  $\text{CeAlO}_3$ . Thus,  $\text{CeO}_2$  was found to promote oxidation of Pd, and Pd could catalyse interconversions between  $\text{CeO}_2/\text{Al}_2\text{O}_3$  and  $\text{CeAlO}_3$  under appropriate conditions (97).

Oh et al. (21) studied  $\text{CH}_4$  oxidation on two sets of Pt, Pd, and Rh catalysts. For one set the metals were supported individually on spheres of  $\gamma\text{-Al}_2\text{O}_3$ , while for the other, spheres of Ce-modified  $\text{Al}_2\text{O}_3$  were used. A 6 wt.% Ce loading was used with noble metal loadings between 0.1-0.2 wt.%. The procedures used for catalyst preparation, and for testing in an integral flow reactor have already been described in section 1.3.1 (21).

Ce was found to have a detrimental effect on  $\text{CH}_4$  oxidation activity, in an oxidising environment, for Pt and in particular for Pd (21). During temperature run-up experiments, the temperature required for 50% conversion was found to increase by almost  $200^\circ\text{C}$  following addition of Ce to Pd/ $\text{Al}_2\text{O}_3$ . This was attributed to a noble metal-cerium interaction which was proposed to promote the formation of inactive bulk Pd oxide. It has been reported that bulk PdO is considerably less active for  $\text{CH}_4$  oxidation than surface oxygen adsorbed on Pd crystallites (29, 36). The effect on Pt was similarly explained due to Pt being converted to a less active, oxidised state in the presence of Ce. It was thought that the oxidation state of Rh under reaction conditions was likely to be more affected by the stoichiometry of the reactant gas mixture than by the presence of Ce (21).

Under reducing conditions, the main influence of Ce was in reducing the amount of CO produced by the Pt and Pd systems at high temperatures (21). The promotion of CO oxidation by Ce was tentatively ascribed to oxidation of CO adsorbed on the noble metal by surface oxygen derived from neighbouring ceria particles to produce  $\text{CO}_2$ . This resulted in the availability of less  $\text{O}_2$  for oxidation of  $\text{CH}_4$ . Hence, although the low temperature activity of Pt and Pd for  $\text{CH}_4$  oxidation in a reducing feedstream was unaffected by Ce, the net result was lower high temperature  $\text{CH}_4$  conversions due to more complete oxidation to  $\text{CO}_2$  rather than partial oxidation to CO. For Rh/ $\text{Al}_2\text{O}_3$ , the CO conversions remained almost unchanged by addition of Ce. This was thought to imply that the nature of the metal-ceria interaction was different for Rh or that CO conversions over Rh were related more to the extent of water gas shift reaction. Experiments performed at  $550^\circ\text{C}$  with a fixed level of  $\text{CH}_4$  and variable levels of  $\text{O}_2$ ,

showed similar behaviour to samples without Ce i.e. a maximum in CH<sub>4</sub> conversion at an O<sub>2</sub> concentration at which both reactants could successfully compete for adsorption onto the noble metal surface. These experiments also revealed a widening of the air:fuel ratio over which maximum activity could be maintained for Pt/Ce/Al<sub>2</sub>O<sub>3</sub>, relative to Pt/Al<sub>2</sub>O<sub>3</sub> (21).

Engler et al. (98) studied Pt and Rh catalysts on CeO<sub>2</sub>/Al<sub>2</sub>O<sub>3</sub> supports with varying CeO<sub>2</sub>:Al<sub>2</sub>O<sub>3</sub> ratios of 0:100, 30:70, 70:30, and 100:0. Sample preparation involved deposition of Pt, Rh and CeO<sub>2</sub> components onto a  $\gamma$ -Al<sub>2</sub>O<sub>3</sub> washcoat on a cordierite monolith. Catalysts were prepared by impregnation with aqueous Ce(NO<sub>3</sub>)<sub>3</sub>, H<sub>2</sub>PtCl<sub>6</sub>, and RhCl<sub>3</sub>. Noble metal samples were calcined at 700°C for 2 hours and then reduced in H<sub>2</sub> at 550°C to produce the fresh catalysts. Aging of the samples was achieved in air at 950°C for 24 hours. Surface analysis and activity measurements (engine tests, integral model gas tests, differential reactor tests) led the authors to conclude the existence of a strong metal-CeO<sub>2</sub> interaction which affected both the oxidation state and the catalytic activity of the noble metal. For example, XPS analysis provided evidence that the noble metals existed in a more oxidised state when supported on CeO<sub>2</sub> relative to Al<sub>2</sub>O<sub>3</sub>. The catalytic effect was reported to be more pronounced for Pt and involved a strongly positive effect on CO + 1/2O<sub>2</sub> and CO + NO reactions with a slightly negative effect regarding hydrocarbon oxidation (98).

The light-off activity of the samples was examined in an integral test apparatus using a gas composition of N<sub>2</sub>, O<sub>2</sub>, CO<sub>2</sub>, CO, H<sub>2</sub>, C<sub>3</sub>H<sub>8</sub>, NO, and H<sub>2</sub>O (98). The catalyst was heated under a constant flow of the model gas from 75 to 450°C at a heating rate of 15°C/min and the conversions were monitored, simultaneously. Before testing, the catalysts were preconditioned by heating to 450°C in the gas mixture. Under reducing conditions, catalyst activity was compared on the basis of the temperature of 50% conversion (T<sub>50</sub>). CeO<sub>2</sub> was found to have a more considerable effect on Pt samples than on Rh samples. T<sub>50</sub> for CO and NO on fresh Pt catalysts was improved in the presence of CeO<sub>2</sub>. However, for hydrocarbon removal the Pt/Al<sub>2</sub>O<sub>3</sub> sample showed the highest conversions. For aged samples, CeO<sub>2</sub> still exerted a promoting effect on CO and NO removal. Hydrocarbon performance on the aged samples was very poor with T<sub>50</sub> values of >450°C, for Pt samples with CeO<sub>2</sub>:Al<sub>2</sub>O<sub>3</sub> mass ratios of 0:100, 30:70 and 100:0, being reported (98).

Nunan et al. (99) examined the effects of Ce on the physico-chemical properties and catalytic activity of three-way catalysts. Pt/Rh/Al<sub>2</sub>O<sub>3</sub>, Pt/Rh/Ce/Al<sub>2</sub>O<sub>3</sub> and Pt/Rh/CeO<sub>2</sub> samples were studied in a full complement synthetic exhaust gas mixture consisting of H<sub>2</sub>, CO, C<sub>3</sub>H<sub>6</sub>, C<sub>3</sub>H<sub>8</sub>, NO, O<sub>2</sub>, N<sub>2</sub>, CO<sub>2</sub>, and H<sub>2</sub>O in the presence

and absence of SO<sub>2</sub>. CeO<sub>2</sub> presence was found to be potentially beneficial for hydrocarbon, as well as CO conversions, after activation in the reaction mixture. Sixteen different samples were tested with nominal CeO<sub>2</sub> loadings of 0, 6, and 25 wt.% Ce on  $\gamma$ -Al<sub>2</sub>O<sub>3</sub>. Various CeO<sub>2</sub> crystallite sizes in the range 60 to ~1000Å were obtained by using different methods of preparation on the Al<sub>2</sub>O<sub>3</sub> support with laboratory aging at 900°C in 10% H<sub>2</sub>O/90% air used to produce the very large crystallites. Following CeO<sub>2</sub> introduction, supports were sized to 425-850µm with wire screens. Pt and Rh were then introduced by impregnation with aqueous solutions of H<sub>2</sub>PtCl<sub>6</sub> and RhCl<sub>3</sub>. Calcination was achieved in air at 600°C for 6 hours. Noble metals were added to the pure CeO<sub>2</sub> support in the same manner. Catalytic activity tests were performed on samples with Pt and Rh loadings in the ranges of 0.34-0.83 wt.% and 0.033-0.066 wt.%, respectively. The catalysts were tested in a tubular reactor using a catalyst mass of 1g and a flow rate of 5l/min. Different testing cycles were used. In the absence of SO<sub>2</sub>, catalysts were heated at 5°C/min in a stoichiometric mixture to 450°C (Rise-1), held at 450°C for 0.5 hours, cooled to 50°C, and then reheated to 450°C in the stoichiometric mixture (Rise-2). Catalytic activity was monitored during Rise-1 and Rise-2. During the hold and drop between Rise-1 and Rise-2, catalysts could be exposed to either fuel-rich, fuel-lean, or stoichiometric exhaust mixtures (99).

Testing of the catalysts in this manner showed that large activity changes occurred following exposure to the exhaust gas mixture (99). The stoichiometric nature of the gas(es) to which the catalysts were exposed between Rise-1 and Rise-2 was found to be critical in determining Rise-2 activity. Considerable catalyst activation was found to occur following exposure to fuel-rich or stoichiometric exhaust gas and this was associated with in-situ reduction of the catalysts by the low levels of H<sub>2</sub> (0.26 vol.%) present. Removal of H<sub>2</sub> from the exhaust gas led to complete loss of activation. Ce was found to be an important catalyst component in the activation process with the main benefits being in improved CO oxidation. However hydrocarbon conversions were also improved in the presence of Ce following activation, especially for smaller CeO<sub>2</sub> crystallite sizes. For example, exposure of a 0.77%Pt, 0.04%Rh, 6%Ce/Al<sub>2</sub>O<sub>3</sub> catalyst to a stoichiometric mixture between Rise-1 and Rise-2 resulted in a considerable enhancement in CO, NO and hydrocarbon (HC) conversions. During Rise-2, the temperature of 25% conversion, T<sub>25</sub>, was lowered by ~150°C for CO and ~100°C for both NO and HC. For a similar catalyst, without CeO<sub>2</sub>, Rise-2 activity was considerably lower. In the presence of SO<sub>2</sub>, catalyst activation was still achieved in the presence of CeO<sub>2</sub>. Activation of the samples in stoichiometric or rich gas mixtures was found to be reversible upon exposure to lean gas and this could result in net deactivation. A correlation between CeO<sub>2</sub> crystallite size and catalytic activity during Rise-2 was found with greater activation achieved using smaller crystallite sizes. The Rise-1 and Rise-2

activities of a Pt, Rh, 6 wt.% Ce/  $\gamma$ -Al<sub>2</sub>O<sub>3</sub> catalyst as a function of CeO<sub>2</sub> crystallite size are shown in Figures 1.21(a) and 1.21(b), for catalysts which were exposed to a stoichiometric mixture after Run 1 (99).

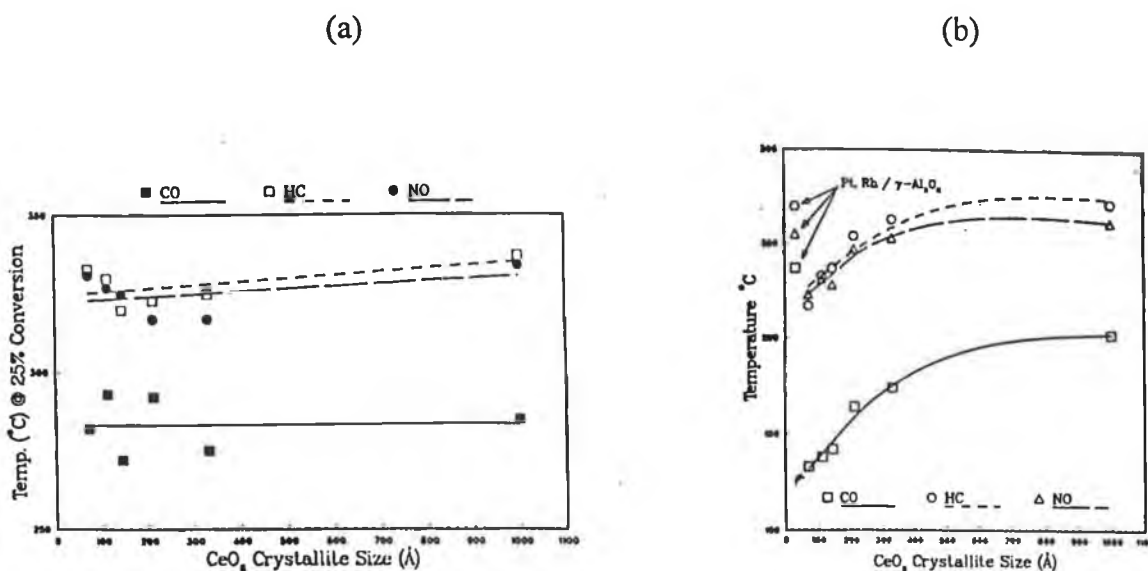


Figure 1.21 : Rise 1 (a) and Rise 2 (b) activity as a function of CeO<sub>2</sub> crystallite size for a 0.77wt.%Pt, 0.04 wt.%Rh, 6wt.%Ce/  $\gamma$ -Al<sub>2</sub>O<sub>3</sub> catalyst (99). Catalysts were tested and activated in a stoichiometric SO<sub>2</sub>-free exhaust gas mixture.

Catalyst characterisation, by scanning transmission electron microscopy (STEM), temperature programmed reduction (TPR) and X-ray photoelectron spectroscopy (XPS), was used to further investigate the processes involved in activation (99). STEM analysis showed that a larger fraction of Pt was associated with CeO<sub>2</sub> than expected based on the relative surface areas of CeO<sub>2</sub> and Al<sub>2</sub>O<sub>3</sub>. Increased Pt-CeO<sub>2</sub> interaction was found with decreasing crystallite size. This led to the suggestion that interaction between Pt and CeO<sub>2</sub> was important in the activation process. This was supported by results for 0.6 wt.%Pt/ $\gamma$ -Al<sub>2</sub>O<sub>3</sub> and 0.6 wt.% Pt/CeO<sub>2</sub> catalysts, shown in Table 1.3. Following activation in a fuel-rich mixture, T<sub>25</sub> was lowered by 37, 23, and 20°C for CO, HC, and NO, respectively, with the Pt/Al<sub>2</sub>O<sub>3</sub> sample during Rise-2. For the CeO<sub>2</sub>-supported Pt, activity enhancement was considerably greater with corresponding T<sub>25</sub> improvements of 250, 145, and >135°C for CO, HC, and NO, respectively, relative to Rise-1. The performance features of Pt/CeO<sub>2</sub> were noted as being most similar to the Pt/Rh/Ce/Al<sub>2</sub>O<sub>3</sub> samples having the smallest CeO<sub>2</sub> crystallite size (99).

**Table 1.3 : Temperature for 25% conversion of CO, NO and hydrocarbon (HC) exhaust components over 0.6wt.%Pt/  $\gamma$ -Al<sub>2</sub>O<sub>3</sub> and 0.6wt.%Pt/CeO<sub>2</sub> catalysts (99).** Testing was done in a stoichiometric exhaust gas mixture with activation between Rise 1 and Rise 2 in a fuel-rich mixture.

Catalyst	Temperature of 25% Conversion (°C)					
	Rise-1			Rise-2		
	CO	HC	NO	CO	HC	NO
Pt/ $\gamma$ -Al <sub>2</sub> O <sub>3</sub>	282	365	360	245	342	340
Pt/CeO <sub>2</sub>	355	450	>	105	305	315
		450				

TPR profiles also suggested the existence of a direct noble metal-CeO<sub>2</sub> interaction with synergistic reduction of Pt, Rh and surface Ce being proposed (99). This proposal was based on the appearance of a low temperature reduction peak when all three components were present which was associated with their combined reduction. The appearance of this peak and its increased size for smaller CeO<sub>2</sub> crystallites appeared to correlate with improved light-off performance after activation. TPR profiles also showed that exposure to fuel-rich mixtures, associated with activation, resulted in extensive reduction of the surface components. XPS results also indicated that fully reduced noble metal was involved in the active state of the catalyst. Reoxidation of CeO<sub>2</sub> during handling was thought to occur before XPS analysis of the reduced samples, and determination of the Ce oxidation state in activated samples was complicated. XPS analysis of a Pt/Rh/CeO<sub>2</sub> sample showed evidence for Rh coverage by CeO<sub>2</sub> indicating a SMSI effect. Indications of Pt sintering after exposure to exhaust gas was found in both TPR and XPS analyses (99).

The authors (99) concluded that Pt migrated selectively to CeO<sub>2</sub> during preparation and that direct interaction between Pt and CeO<sub>2</sub> led to dramatic improvements in catalyst light-off activity following in-situ reduction. Reduction of the noble metal and surface ceria components was thought to be combined and this resulted in highly active sites which were thought to involve reduced surface Ce in contact with reduced noble metal. Catalyst performance was measured under stoichiometric, non-oscillating conditions. Under the mild conditions used, the impact of CeO<sub>2</sub> could not be attributed to oxygen storage, promotion of water gas shift activity, promotion of noble metal dispersion or stabilisation of the support. It was thought that the main benefit of CeO<sub>2</sub> was improved CO light-off activity after activation. The removal of CO at lower

temperatures was proposed to prevent CO inhibition and thereby allow for more effective hydrocarbon and NO conversion (99).

Diwell et al. (75) also reported activation of ceria-containing Pt catalysts following mild pre-reduction in H<sub>2</sub>. Dramatic improvements in low temperature conversions of CO, NO and C<sub>3</sub>H<sub>6</sub> were observed. However, alkane (C<sub>3</sub>H<sub>8</sub> and CH<sub>4</sub>) oxidation activity was adversely affected (75).

Catalysts were prepared by impregnation of  $\gamma$ -Al<sub>2</sub>O<sub>3</sub>, CeO<sub>2</sub>, and 75 wt.% Al<sub>2</sub>O<sub>3</sub>-25 wt.% CeO<sub>2</sub> supports with Pt and Rh precursors (75). Activity measurements were performed using a simulated exhaust gas mixture containing CO<sub>2</sub>, H<sub>2</sub>O, NO, SO<sub>2</sub>, CH<sub>4</sub>, C<sub>3</sub>H<sub>8</sub>, C<sub>3</sub>H<sub>6</sub>, H<sub>2</sub>, O<sub>2</sub>, and CO. Catalysts were heated at 5°C/min from 150 to 600°C at a constant flow rate of the model gas mixture. Conversion efficiencies for the various mixture components were measured by continuously monitoring the outlet gases after the catalyst (75).

A study of 0.9 wt.% Pt/Al<sub>2</sub>O<sub>3</sub> and 0.9% Pt/CeO<sub>2</sub>-Al<sub>2</sub>O<sub>3</sub> samples, revealed that the presence of CeO<sub>2</sub> resulted in stabilisation of Pt dispersions (75). On heating the samples in air for 2 hours, substantial sintering of the Pt on the Al<sub>2</sub>O<sub>3</sub> support occurred at temperatures higher than 600°C. Addition of ceria resulted in a reasonable stabilisation of Pt dispersions up to temperatures of 700-800°C. This was ascribed to a Pt-CeO<sub>2</sub> interaction involving the formation of a surface complex of Pt<sup>2+</sup> - O<sub>2</sub><sup>-</sup> - Ce<sup>4+</sup>. TPR studies provided further evidence for the existence of a Pt-CeO<sub>2</sub> interaction. Combined reduction of both species was found which resulted in more facile Pt reduction. Under oxidising fuel-lean conditions, this Pt-CeO<sub>2</sub> interaction was found to have a detrimental effect on the oxidation activity of Pt for both CO and C<sub>3</sub>H<sub>8</sub>, as shown in Fig. 1.22.

The reduced activity, in the presence of CeO<sub>2</sub>, was attributed to the existence of Pt in a more oxidised state (75). Although this would be expected to have a positive effect on Pt dispersion, the increased Pt-O bond strength was expected to be detrimental to oxidation activity. CeO<sub>2</sub> was reported to increase the low temperature conversions of both CO and NO<sub>x</sub> on a 0.18 wt.% Rh/Al<sub>2</sub>O<sub>3</sub> catalyst, following calcination in air at 800°C. This was attributed to stabilisation of surface Rh by prevention of a Rh/Al<sub>2</sub>O<sub>3</sub> interaction during the high temperature pre-treatment (75).

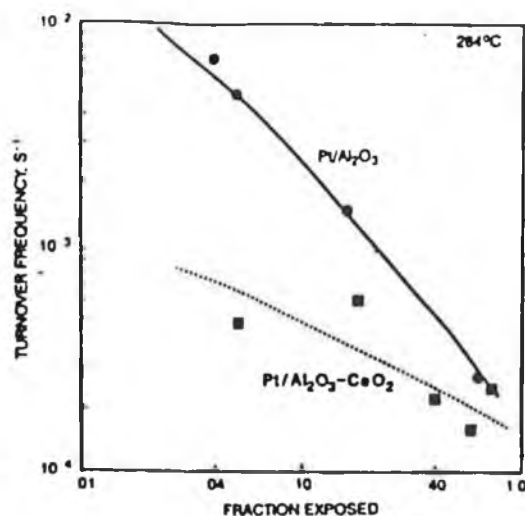


**Figure 1.22 : Turnover Frequency versus Fraction of Pt Exposed for C<sub>3</sub>H<sub>8</sub> Oxidation on 0.9 wt.% Pt catalysts (75).**

Pre-reduction of a 0.9 wt.% Pt/CeO<sub>2</sub> catalyst was found to result in an enhanced Pt-CeO<sub>2</sub> interaction with increased low temperature conversion of all feedstream components, except methane and propane, in a slightly fuel-rich gas mixture (75). The catalyst was calcined at 500°C in air, and activity was measured both before and after reduction in 1% H<sub>2</sub> at 600 or 900°C. Activity enhancement was greater at the lower reduction temperature and was reversible on aging in air at >500°C. The effects of the different catalyst pretreatment conditions were investigated by TPR, XPS, CO Chemisorption and BET surface area measurement. The authors proposed that reduction of the Pt/CeO<sub>2</sub> catalyst resulted in a strong Pt-CeO<sub>2</sub> interaction involving encapsulation of the Pt by the partially reduced oxide. Increased CO and NO removal was associated with the formation of ionised vacancies in the ceria support. Oxidation of these vacancies was thought to occur by NO (or H<sub>2</sub>O or O<sub>2</sub>), with subsequent reduction of the oxidised vacancies by CO. Neighbouring Pt particles were thought to play a role by acting as an electron donor or sink. More recently, Hardacre et al. (96) proposed a similar mechanism for the oxidation of CO by model CeO<sub>2</sub>-encapsulated Pt catalysts. The lower alkane activity was attributed to encapsulation of the metal particles (75). It was noted that this model could not explain increases in low temperature alkene activity after reduction. The activity enhancement, following reduction of the calcined sample at 600°C, is shown in Figures 1.23(a) and 1.23(b). It was thought that the low temperature activity changes that occurred on reduction, could not be explained by a simple reduction of Pt to a more metallic state as proposed by Yu-Yao (53), and indicated an induced Pt-CeO<sub>2</sub> interaction that greatly affected the nature and activity of the catalytic sites. The reduction conditions used by Yu-Yao (53) were not as stringent as those in this study (75). The model

proposed represented only a working hypothesis and further work was deemed necessary to assess its validity (75).

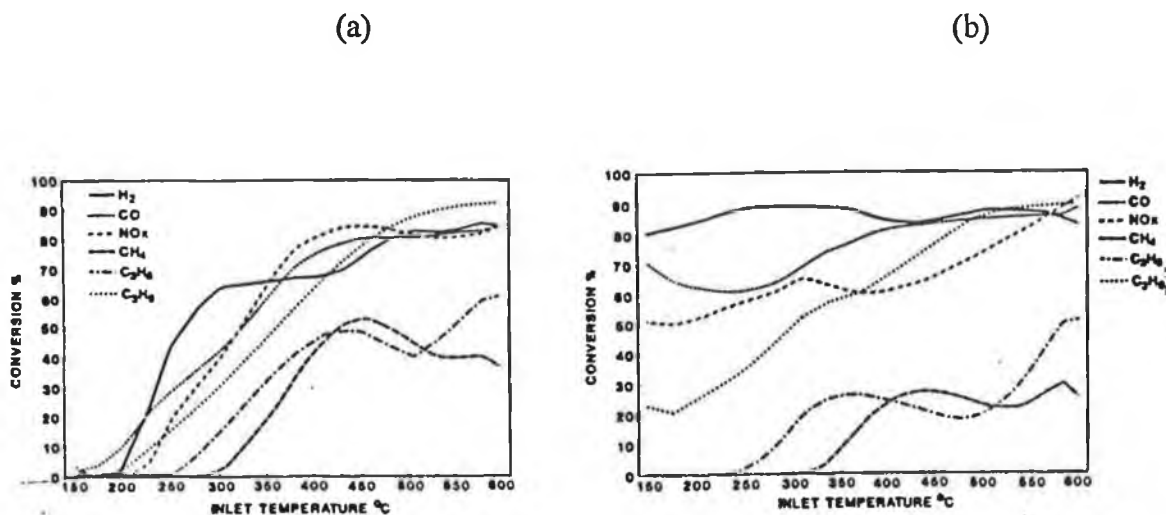


**Figure 1.23 : Light-off Curves for 0.9 wt.% Pt/CeO<sub>2</sub>. (a) After calcination at 500°C and (b) after calcination followed by reduction at 600°C (75).**

Silver et al. (67) investigated the effects of washcoat composition and aging conditions on the three-way activity of single noble metal catalysts. Addition of Ce to Pt and Pd-only catalysts was found to be potentially beneficial. Catalysts were prepared by adding the noble metals to washcoats containing varying amounts of alumina and cerium, and impregnating on monolithic cordierite substrates. Catalysts were exposed to two different types of engine aging cycles before being evaluated in conventional automotive emission test methods with three-way conversions monitored at 450°C. The less severe aging cycle involved an inlet temperature of 760°C and the more severe one was operated at an inlet temperature of 850°C. Both aging cycles were operated under fuel-lean conditions. After aging, the performance of Pt-only catalysts improved with increasing amounts of Ce in the washcoat. The addition of Ce to the Al<sub>2</sub>O<sub>3</sub> washcoat resulted in improved hydrocarbon, CO and NO conversions, especially at stoichiometric conditions (A/F = 14.56). The three-way conversions of Pt samples at various Ce loadings as a function of air:fuel (A/F) ratio, are shown in Fig. 1.24, after aging under the milder conditions for 100 hours.

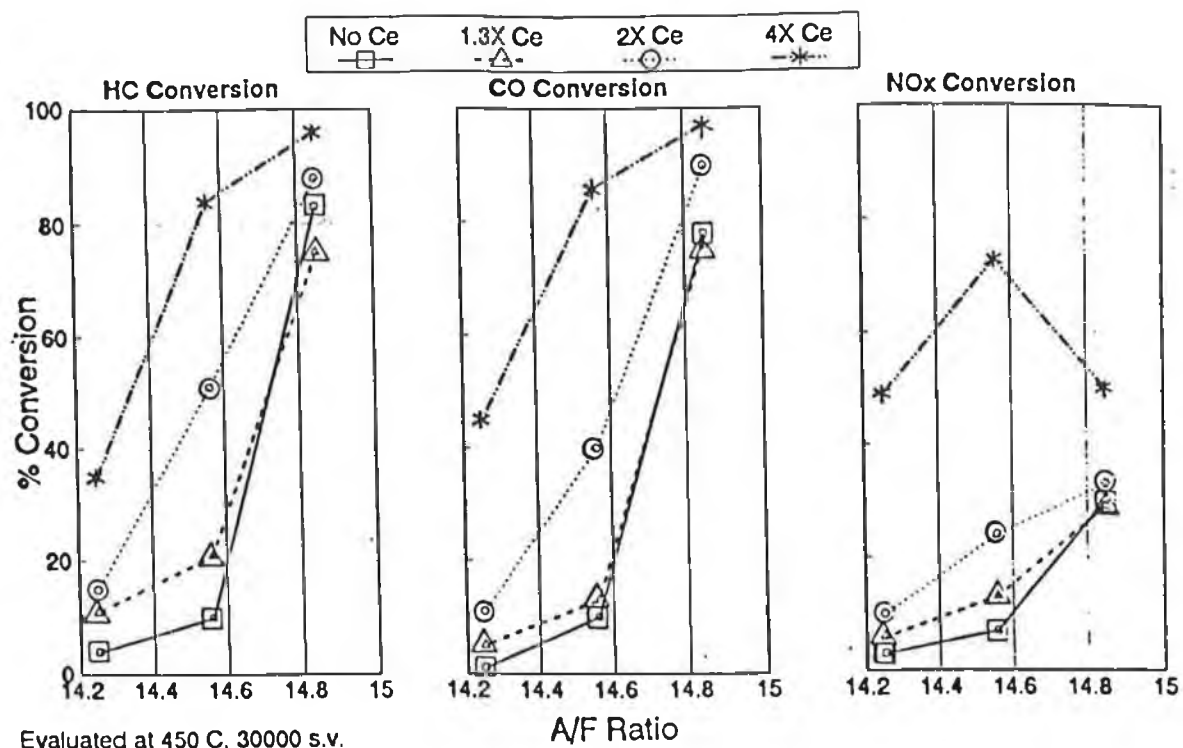


**Figure 1.24 : Effects of Ce on the performance of a Pt-only catalyst as a function of air:fuel ratio at 450°C (67). Catalysts aged at 760° C in a fuel-lean engine cycle prior to testing.**

From Fig. 1.24, it is seen that increasing the Ce loading resulted in improved conversions over the entire Ce range studied (67). The loading of Ce in these samples was not quoted but increasing values of X were used to indicate increased levels of Ce. After the more severe aging cycle, Ce addition was much less beneficial but still maintained higher stoichiometric conversions than the Al<sub>2</sub>O<sub>3</sub>-only washcoat. The effects of Ce were attributed to stabilisation of Pt dispersion, under the aging conditions used, by keeping some of the Pt in a partially oxidised state which was harder to sinter. It was thought that as the Ce content increased, the amount of partially oxidised Pt also increased. In addition, it was proposed that ceria may also improve the performance of Pt by acting as an oxygen source for CO conversion. A similar effect of Ce on Pd-only catalysts was reported. For Rh-only catalysts, the conversion performance was not as sensitive to cerium content. The Rh catalysts were reported to perform best over blank Al<sub>2</sub>O<sub>3</sub> or Al<sub>2</sub>O<sub>3</sub> stabilised by Zr. The latter additive was thought to improve the high temperature durability of Rh on Al<sub>2</sub>O<sub>3</sub>, by preventing strong metal-support interaction (67).

Pirault et al. (100) examined the activity of Pt or Pt-Rh on  $\text{Al}_2\text{O}_3$  and 12 wt.%  $\text{CeO}_2/\text{Al}_2\text{O}_3$  supports for the oxidation of  $\text{C}_3\text{H}_6$  and  $\text{C}_3\text{H}_8$ . Hydrocarbon oxidation was performed in a flow reactor system with a flame ionisation detector (FID). The  $\text{O}_2$ :hydrocarbon ratio in the reactant mixture was 10:1 with  $\text{N}_2$  used as the diluent. Catalysts were evaluated by studying their light-off behaviour with a constant flow of the gas mixture from  $100^\circ\text{C}$  to  $500^\circ\text{C}$  at a heating rate of  $3^\circ\text{C}\cdot\text{min}^{-1}$ . Catalysts were prepared using two different methods, the first of which involved co-impregnation of Pt and Rh onto the support material in one step. This preparation procedure was designated C.I.. The second method of preparation involved a two-step procedure, with impregnation of Pt followed by impregnation of Rh, and was designated S.I. (100).

The presence of  $\text{CeO}_2$  was reported to inhibit the oxidation of both hydrocarbons after an initial calcination step at  $500^\circ\text{C}$ . This inhibiting effect of  $\text{CeO}_2$  was attributed to a charge transfer from the precious metals to surface cerium which resulted in a higher oxidation state of the noble metal and therefore lower activity. The inhibiting effect was found to occur for Pt and Pt-Rh samples, irrespective of whether the latter were prepared by the C.I. or S.I. procedure. The inhibiting effect on catalyst activity by  $\text{CeO}_2$  for  $\text{C}_3\text{H}_6$  oxidation disappeared after sample reduction at  $500^\circ\text{C}$  before the catalytic run. However,  $\text{C}_3\text{H}_8$  oxidation activity was still adversely affected by  $\text{CeO}_2$  even after pre-reduction (100).

The oxidation of ethylene by  $\text{O}_2$  over a Pt/ $\text{CeO}_2$  catalyst has been studied by Mendelovici and Steinberg (101) who proposed a role for lattice oxygen from  $\text{CeO}_2$  in the oxidation mechanism. A 2 wt.% Pt/ $\text{CeO}_2$  sample was prepared by impregnation of pure  $\text{CeO}_2$  with  $\text{H}_2\text{PtCl}_6$  followed by reduction in a stream of  $\text{H}_2$  for 3 hours at  $250^\circ\text{C}$ . The BET surface area of the support was  $50 \text{ m}^2/\text{g}$ , and the H/Pt ratio of the resultant catalyst was determined as 0.35 by  $\text{H}_2$  adsorption. The reactions between  $\text{O}_2$  and  $\text{C}_2\text{H}_4$  were carried out in both static and pulse reactors in the temperature range  $100\text{--}400^\circ\text{C}$ . Pressures were between 150 and 500 Torr and the partial pressure of  $\text{O}_2$  and  $\text{C}_2\text{H}_4$  was less than 40%. The diluent used was He. In the static reactor experiments, samples were activated by evacuation at  $\sim 10^{-6}$  Torr at  $500^\circ\text{C}$  for 3 hours. In the pulse reactor, samples were activated by pre-evacuation or by exposure to a preceding pulse of  $\text{O}_2$  or  $\text{C}_2\text{H}_4$  (101).

In addition to  $\text{CO}$ ,  $\text{CO}_2$ , and  $\text{H}_2\text{O}$ , other products obtained were  $\text{CH}_4$  and  $\text{C}_2\text{H}_6$  at temperatures higher than  $300^\circ\text{C}$  (101). The formation of  $\text{C}_2\text{H}_6$  and  $\text{CH}_4$  was thought to be the result of the reaction of  $\text{C}_2\text{H}_4$  or  $\text{CO}$ , respectively, with  $\text{H}_2$  produced by the water gas shift reaction. Oxidation on pure  $\text{CeO}_2$  resulted in  $\text{CO}_2$  and  $\text{H}_2\text{O}$ , with no partial oxidation products observed. It was reported that reaction of  $\text{CO}$  and  $\text{H}_2\text{O}$ , and

of CO and H<sub>2</sub>, could only occur in the presence of Pt. Thus, the production of partial oxidation products, such as CH<sub>4</sub>, was associated with Pt presence (101).

In the static reactor, at temperatures higher than 300°C, the oxidation of C<sub>2</sub>H<sub>4</sub> was found to proceed in the presence or absence of O<sub>2</sub> (101). Results from the pulse reactor confirmed the formation of reaction products (CO<sub>2</sub>, CO, CH<sub>4</sub> and C<sub>2</sub>H<sub>6</sub>) at these higher temperatures, when pulses of C<sub>2</sub>H<sub>4</sub> were injected without O<sub>2</sub>. In these experiments, the activity of the catalyst decreased continuously with increasing pulse number, in the absence of O<sub>2</sub>. A reaction mechanism was proposed in which lattice oxygen from the support was involved in the oxidation of C<sub>2</sub>H<sub>4</sub> to CO or CO<sub>2</sub> at higher temperatures. In the presence of gaseous oxygen, there was a continuous supply of oxygen to refill oxide vacancies and activity was more stable with increasing pulse number. Electron Spin Resonance experiments were used to show the role performed by lattice oxygen from the CeO<sub>2</sub> support in the oxidation of C<sub>2</sub>H<sub>4</sub> at temperatures higher than 300°C on the 2 wt.% Pt/CeO<sub>2</sub> catalyst used. At temperatures below 300°C, complete oxidation was thought to occur with no participation from lattice oxygen (101).

## **1.5 Summary**

Some of the more relevant sections of the preceding literature review to the current study will now be summarised.

### **CH<sub>4</sub> Oxidation on Noble Metal Catalysts**

Some of the main findings of the review on CH<sub>4</sub> oxidation on noble metal catalysts are summarised in Table 1.4.

From the table, it is clear that different reaction mechanisms have been proposed for particular catalysts. Baldwin and Burch (30) noted that one possible reason why different reaction mechanisms have been proposed for Pd catalysts is that the nature and oxidation state of the metal surface is largely unknown and probably varied from study to study. For example, it was unknown whether oxidation was occurring on Pd metal, PdO or a Pd surface partially covered with oxygen, or even on a mixture of all three types of sites simultaneously. This latter case was thought most likely to occur in supported catalysts with a wide range of crystallite sizes since smaller Pd particles have been reported to have a greater tendency to exist in an oxidised form than larger crystallites (36, 42).

The oxidation of CH<sub>4</sub> on supported Pt (27, 29, 41) and Pd (28, 29) catalysts has been proposed to be a structure-sensitive reaction. Briot et al. (27) studied the effects of aging a Pt/Al<sub>2</sub>O<sub>3</sub> catalyst in the CH<sub>4</sub> oxidation mixture. It was reported that larger Pt particles present after aging were more active than smaller particles present in the fresh catalyst. A decreased Pt-O bond strength which led to increased reactivity of adsorbed oxygen on the larger particles was proposed to explain increased reaction rates. Other possible explanations included more favourable CH<sub>4</sub> adsorption on the larger particles or a change in Pt particle morphology upon aging (27). This latter theory was postulated in a later study of Pd/Al<sub>2</sub>O<sub>3</sub> (28). For Pd, the increase in activity upon aging was thought to be too large to be explained solely by increased particle size (28). Hicks et al. (29) reported higher turnover rates for a crystalline Pt phase when compared to a dispersed phase, while for Pd turnover frequencies increased with increasing particle size. Changes in particle morphology of Pt and Pd on exposure to the oxidation mixture could be correlated with changes in activity (29). Baldwin and Burch (30) found no sensible correlation between Pd particle size in Pd/Al<sub>2</sub>O<sub>3</sub> samples and CH<sub>4</sub> oxidation activity. Supported Pd catalysts were reported to be activated upon exposure to the reaction mixture. Activation only occurred when reaction between CH<sub>4</sub> and O<sub>2</sub> was occurring and was associated with a change in particle morphology which resulted in the exposure

**Table 1.4 : Summary of methane oxidation studies**

Catalyst(s)	CH <sub>4</sub> : O <sub>2</sub>	Type of Reactor*	Order in CH <sub>4</sub> O <sub>2</sub>	Mechanism <sup>b</sup>	Active Species	Activity Comparisons	Ref.
Pd on Al <sub>2</sub> O <sub>3</sub>	-----	CF	1 0	ER	---	---	(34)
Pd/Pt/Rh/Ir on Al <sub>2</sub> O <sub>3</sub>	variable	SM	-- --	LH	---	---	(35)
Pt/Pd on various supports	1:10-10:1	PF	1 0	LH	Surface oxygen on Pd more active than bulk PdO	Pd>Pt PtO <sub>2</sub> >PdO	(36)
Pt on various supports	1:2	CF	1 0	---	Related to reducibility of surface Pt oxides	Pt/SiO <sub>2</sub> -Al <sub>2</sub> O <sub>3</sub> > Pt/Al <sub>2</sub> O <sub>3</sub> > Pt/SiO <sub>2</sub>	(40)
Pt/Al <sub>2</sub> O <sub>3</sub>	1:2.5-1:60	RB	1 0	not ER	Larger Pt particles (SS). Possibly unique clusters of very high activity	---	(41)
Pt/Pd/Rh on Al <sub>2</sub> O <sub>3</sub>	variable	CF	-- --	LH	Surface oxygen on Pd more active than bulk PdO	Pd > Rh > Pt	(21)
Pd/ZrO <sub>2</sub>	variable	CSTR	1 V <sup>#</sup>	ER	Weakly chemisorbed oxygen rather than PdO	---	(38)
Pt/Pd on various supports	1:2.2	CF	-- --	---	Crystalline Pt phase (SS, RS) Larger Pd particles (SS, RS)	Pd > Pt	(29)
Pd/Al <sub>2</sub> O <sub>3</sub>	1:20**	CF	-- --	---	PdO phase necessary at high temperatures	---	(39)
Pd/Al <sub>2</sub> O <sub>3</sub>	1:4	CF	-- --	---	PdO phase in O <sub>2</sub> -rich mixture Larger Pd particles (SS, RS)	---	(28)
Pt/Al <sub>2</sub> O <sub>3</sub>	1:4	CF	-- --	---	Larger Pt particles (SS, RS)	---	(27)
Pd on various supports	1:20**	CF and PF	-- --	---	RS (Not SS)	---	(30, 31)
Pd on various supports	1:10**	CF	-- --	---	RS (Not SS)	---	(47)

\*-CF = Continuous Flow; SM = Static Microcalorimetric; PF = Pulsed Flow; CSTR = continuous stirred tank reactor.

\*\*-assuming 20% O<sub>2</sub> in air.      \$-ER = Eley-Rideal; LH = Langmuir-Hinshelwood.      #-V = variable.

SS = proposed structure sensitivity i.e. catalyst activity depends on metal particle size or the presence of crystalline or dispersed metal phases.

RS = proposed reaction sensitivity i.e. catalyst activity altered during reaction due to changes in metal particle morphology.

of crystal faces which were more favourable for reaction (30, 31). Ribeiro et al. (47) also found that the activity of supported Pd increased with time in the CH<sub>4</sub> oxidation mixture. Again, this was tentatively associated with a change in morphology of surface Pd under reaction conditions. Ribeiro et al. (47) also reported that CH<sub>4</sub> oxidation rates were unaffected by changes in Pd particle size, but in apparent contradiction, reported that calcination at higher temperatures produced a more metallic Pd phase which had higher per site activity while calcination at lower temperatures resulted in low activity (47).

### **Oxidation of C<sub>2</sub>-C<sub>8</sub> Hydrocarbons on Noble Metal Catalysts**

Some of the main findings of the review on hydrocarbon oxidation on noble metal catalysts are summarised in Table 1.5.

The proposed Langmuir-Hinshelwood mechanism was supported by kinetic measurements which suggested that the order of reaction in each reactant depended on their relative ease of adsorption on the noble metal in question (52-54). The kinetics of complete oxidation have been reported to vary depending on the nature of the hydrocarbon (saturated/unsaturated) and the noble metal (Pt/Pd/Rh) used (51-54).

Structure-sensitive effects were observed in several studies (26, 53, 54, 57, 61). The oxidation of C<sub>3</sub>H<sub>8</sub> over Pt was found to depend on the support used as well as the particle size (25, 33). Changes in reaction rate for Pt on the different supports, namely Al<sub>2</sub>O<sub>3</sub>, SiO<sub>2</sub> and ZrO<sub>2</sub>, were attributed to changes in the density of active sites since the activation energy remained constant. The effect of the support on reaction rate was greatest for highly dispersed samples. For less dispersed Pt phases, metal-support interactions were thought to be reduced with the support having less of an effect on catalytic activity (25). For low-loaded dispersed samples, Pt/ZrO<sub>2</sub> was more active than Pt/Al<sub>2</sub>O<sub>3</sub> which was attributed to deactivation of Pt by metal-support interactions in the latter catalysts (33). For Pt/ZrO<sub>2</sub>, oxidation activity decreased with decreasing metal dispersion. This was thought to indicate that dispersed Pt may be more active than larger Pt crystallites when detrimental metal-support interactions are absent (33).

**Table 1.5 : Summary of hydrocarbon oxidation studies**

Catalyst(s)	Hydrocarbon (HC) Studied	O <sub>2</sub> :HC	Type of Reactor*	Mechanism <sup>§</sup>	Activity Comparisons	Ref.
Pt filament	C <sub>2</sub> -C <sub>4</sub> alkanes	variable, excess O <sub>2</sub>	CF	LH	---	(50)
Pt/Pd filament	various organic compounds	variable, excess O <sub>2</sub>	CF	LH	Pt > Pd	(51)
Pt/Pd/Ir/Ru/Rh on SiO <sub>2</sub>	C <sub>2</sub> H <sub>4</sub> , C <sub>3</sub> H <sub>6</sub>	3.25:1	CF	LH	Pt ≥ Pd > Ir > Ru ≥ Rh	(52)
Pt/Pd/Rh wire Pt/Pd/Rh on Al <sub>2</sub> O <sub>3</sub>	C <sub>3</sub> H <sub>6</sub> , 1-hexene, toluene	10:1 or 20:1	CF	LH	Wire > Supported (SS)	(53)
Pt/Pd/Rh wire Pt/Pd/Rh on Al <sub>2</sub> O <sub>3</sub>	C <sub>1</sub> -C <sub>4</sub> alkanes	10:1	CF	LH	Wire > Supported, Larger Pt and Pd particles more active (SS)	(54)
Pt on Al <sub>2</sub> O <sub>3</sub>	C <sub>3</sub> H <sub>6</sub>	200:1-10:1	CF	complex (not LH)	Larger Pt particles more active (SS)	(57)
Pt on Al <sub>2</sub> O <sub>3</sub>	n-C <sub>7</sub> H <sub>16</sub>	75:1 or 15:1	CF	---	Crystalline Pt <sup>0</sup> > Dispersed Pt <sup>4+</sup> (SS)	(26)
Pt on Al <sub>2</sub> O <sub>3</sub>	C <sub>3</sub> H <sub>8</sub>	10:1	RB	LH	Larger Pt particles more active (SS)	(58)
Pt on ZrO <sub>2</sub> /Al <sub>2</sub> O <sub>3</sub>	C <sub>3</sub> H <sub>8</sub>	12:1	RB	---	Depended on support Material	(33)
Pt on ZrO <sub>2</sub> /Al <sub>2</sub> O <sub>3</sub> /SiO <sub>2</sub>	C <sub>3</sub> H <sub>8</sub>	12:1 or 14:1	RB and CF	---	Depended on support Material	(25)
Pt/Pd on Al <sub>2</sub> O <sub>3</sub> /ZrO <sub>2</sub>	n-C <sub>7</sub> H <sub>16</sub>	12.25:1	CF	LH	Pt > Pd Larger Pt and Pd crystallites more active (SS)	(61)

\*-CF = Continuous Flow; PF = Pulsed Flow.

§-LH = Langmuir-Hinshelwood.

SS = proposed structure sensitivity i.e. catalyst activity depends on metal particle size or the presence of crystalline or dispersed metal phases.

## **Use of CeO<sub>2</sub> in Supported Noble Metal Oxidation Catalysts**

### **Oxidation of Carbon Monoxide**

Some of the main findings of the review on CO oxidation on Ce-containing noble metal catalysts are summarised in Table 1.6.

### **Hydrocarbon Oxidation**

A brief summary of the effects of Ce on the hydrocarbon oxidation activity of noble metals, as detailed in section 1.4.3, will be given in section 3.1 as an introduction to work carried out in the present study.

**Table 1.6 : Summary of CO oxidation studies on Ce-containing noble metal catalysts**

Catalyst(s)*	Effect of Ce on Activity	Proposed Phenomena	Ref
NM/Al <sub>2</sub> O <sub>3</sub> , 0-13 wt.% Ce.	Depended on pretreatment conditions and Ce loading. Effects greater on Pt than Pd/Rh.	CeO <sub>2</sub> acted as a strong oxidising agent to cause increased oxidation of surface Pt sites.	(84)
NM/Al <sub>2</sub> O <sub>3</sub> or CeO <sub>2</sub> -Al <sub>2</sub> O <sub>3</sub>	Caused a change in the kinetics of oxidation. Reduction ⇒ ↑ activity of Pt-CeO <sub>2</sub> /Al <sub>2</sub> O <sub>3</sub> .	Kinetics affected by increased oxidation of metal sites in the presence of CeO <sub>2</sub> .	(53)
NM/Al <sub>2</sub> O <sub>3</sub> or CeO <sub>2</sub> -Al <sub>2</sub> O <sub>3</sub>	For Rh and Pt, ↑ Activity after reduction and ↓ Activity in an oxidising environment.	-----	(85)
Rh/Al <sub>2</sub> O <sub>3</sub> , 0-15 wt.% Ce; Rh/CeO <sub>2</sub>	↑ Activity under moderately oxidising or net reducing conditions.	Involvement of lattice oxygen from CeO <sub>2</sub>	(86)
Pt/Al <sub>2</sub> O <sub>3</sub> or CeO <sub>2</sub> -Al <sub>2</sub> O <sub>3</sub>	↑ Activity at low temperatures after activation in the test gas under reducing conditions.	Involvement of lattice oxygen from CeO <sub>2</sub> .	(81)
Pt/Al <sub>2</sub> O <sub>3</sub> or CeO <sub>2</sub> -Al <sub>2</sub> O <sub>3</sub>	↑ Activity after pre-reduction.	Involvement of lattice oxygen from CeO <sub>2</sub> .	(89)
Rh/CeO <sub>2</sub> or Rh/Al <sub>2</sub> O <sub>3</sub>	Suppression of CO inhibition effect.	Involvement of lattice oxygen from CeO <sub>2</sub> .	(90)
Pt/CeO <sub>2</sub>	Fully encapsulated Pt highly active.	CeO <sub>2</sub> -catalysed oxidation of CO to CO <sub>2</sub> , with role of underlying Pt as a promoter.	(96)

\*-NM = Pt, Pd or Rh.

## REFERENCES

- (1) Zwinkels, M. F. M, Järås, S. G. and Menon, P. G., *Catal. Rev. Sci. Eng.* **35**, 319 (1993).
- (2) Trimm, D. L., *Appl. Catal.* **7**, 249 (1983).
- (3) Spivey, J. J., in "Catalysis" (Bond, G. C. and Webb, G., eds.), The Royal Society of Chemistry, Cambridge, UK, 1989.
- (4) Campbell, I. M., "Catalysis at Surfaces", University Press, Cambridge, 1988.
- (5) Wei, J., *Advan. Catal.* **24**, 57 (1975).
- (6) Dwyer, F. G., *Catal. Rev.* **6**, 261 (1972).
- (7) Kummer, J. T., *Prog. Energy Combust. Sci.* **6**, 177 (1980).
- (8) Acres, G. J. K., *Plat. Met. Rev.* **14**, 2 (1970).
- (9) Pfefferle, L. D. and Pfefferle, W. C., *Catal. Rev. Sci. Eng.* **29**, 219 (1987).
- (10) Golodets, G. I., "Heterogeneous Catalytic Reactions Involving Molecular Oxygen", Elsevier, Amsterdam, 1983.
- (11) Bond, G. C., "Heterogeneous Catalysis", Clarendon Press, Oxford, 1987.
- (12) Sokolovskii, V. D., *Catal. Rev. Sci. Eng.* **32**, 1 (1990).
- (13) Arai, H., Yamada, T., Eguchi, K. and Seiyama, T., *Appl. Catal.* **26**, 265 (1986).
- (14) Accomazzo, M. A. and Nobe, K., *Ind. Eng. Chem. Prod. Res. Dev.* **4**, 425 (1965).
- (15) Anderson, R. B., Stein, K. C., Feenan, J. J. and Hofer, L. J. E., *Ind. Eng. Chem.* **53**, 809 (1961).
- (16) Yant, W. P. and Hawk, C.O., *J. Am. Chem. Soc.* **49**, 1454 (1927).
- (17) Stein, K. C., Feenan, J. J., Thompson, G. P., Shultz, J. F., Hofer, L. J. E. and Anderson, R. B., *Ind. Eng. Chem.* **52**, 671 (1960).
- (18) Morooka, Y. and Ozaki, A., *J. Catal.* **5**, 116 (1966).
- (19) Morooka, Y., Morikawa, Y. and Ozaki, A., *J. Catal.* **7**, 23 (1967).
- (20) Nieuwenhuys, B. E., Ponec, V., van Koten, G., van Leeuwen, P. W. N. M. and Santen, R.A., in "Catalysis" (Moulijn, J. A., van Leeuwen, P. W. N. M. and van Santen, R. A., eds.), Studies in Surface Science and Catalysis, Vol. 79, 89-158, Elsevier, Amsterdam, 1993.
- (21) Oh, S. H., Mitchell, P. J. and Siewert, R. M., *J. Catal.* **132**, 287 (1991).
- (22) Margolis, L. Ya., *Advan. Catal.* **14**, 429 (1963).
- (23) Gasser, R. P. H., "An Introduction to Chemisorption and Catalysis", Clarendon Press, Oxford, 1985.
- (24) Atkins, P.W. and Clugston, M. J., "Principles of Physical Chemistry", Pitman Press, Bath, 1982.
- (25) Hubbard, C. P., Otto, K., Gandhi, H. S. and Ng, K. Y. S., *J. Catal.* **144**, 484 (1993).
- (26) Völter, J., Lietz, G., Spindler, H. and Lieske, H., *J. Catal.* **104**, 375 (1987).
- (27) Briot, P., Auroux, A., Jones, D. and Primet, M., *Appl. Catal.* **59**, 141 (1990).
- (28) Briot, P. and Primet, M., *Appl. Catal.* **68**, 301 (1991).
- (29) Hicks, R. F., Qi, H., Young, M. L. and Lee, R. G., *J. Catal.* **122**, 280 (1990).
- (30) Baldwin, T.R. and Burch, R., *Appl. Catal.* **66**, 337 (1990).
- (31) Baldwin, T. R. and Burch, R., *Appl. Catal.* **66**, 359 (1990).
- (32) Burch, R., in "Catalysis" (Bond, G. C. and Webb, G., eds.), Vol. 7, 149-196, The Royal Society of Chemistry, London, 1985.
- (33) Hubbard, C. P., Otto, K., Gandhi, H. S. and Ng, K. Y. S., *J. Catal.* **139**, 268 (1993).

- (34) Mezaki, R. and Watson, C. C., *Ind. Eng. Chem. Process Des. Dev.* **5**, 62 (1966).
- (35) Firth, J. G. and Holland, H. B., *J. Chem. Soc. Faraday Trans.* **65**, 1121 (1969).
- (36) Cullis, C. F. and Willatt, B. M., *J. Catal.* **83**, 267 (1983).
- (37) Campbell, C. T., Foyt, D. C. and White, J. M., *J. Phys. Chem.* **81**, 491 (1977).
- (38) Seimanides, S. and Stoukides, M., *J. Catal.* **98**, 540 (1986).
- (39) Farrauto, R. J., Hobson, M. C., Kennelly, T. and Waterman, E. M., *Appl. Catal.* **81**, 227 (1992).
- (40) Niwa, M., Awano, K. and Murakami, Y., *Appl. Catal.* **7**, 317 (1983).
- (41) Otto, K., *Langmuir* **5**, 1364 (1989).
- (42) Hicks, R. F., Young, M. L., Lee, R. G. and Qi, H., *J. Catal.* **122**, 294 (1990).
- (43) Chou, P. and Vannice, M. A., *J. Catal.* **105**, 342 (1987).
- (44) Lieske, H., Lietz, G., Spindler, H. and Völter, J., *J. Catal.* **81**, 8 (1983).
- (45) Shyu, J. Z. and Otto, K., *Appl. Surface Sci.* **32**, 246 (1988).
- (46) Mc. Cabe, R. W., Wong, C. and Woo, H. S., *J. Catal.* **114**, 354 (1988).
- (47) Ribeiro, F. H., Chow, M. and Dalla Betta, R. A., *J. Catal.* **146**, 537 (1994).
- (48) Marti, P. E., Maciejewski, M. and Baiker, A., *J. Catal.* **139**, 494 (1993).
- (49) Schlögl, R., Loose, G., Wesemann, M. and Baiker, A., *J. Catal.* **137**, 139 (1992).
- (50) Hiam, L., Wise, H. and Chaikin, S., *J. Catal.* **9**, **10**, 272 (1968).
- (51) Schwartz, A., Holbrook, L. L. and Wise, H., *J. Catal.* **21**, 199 (1971).
- (52) Cant, N. W. and Hall, W. K., *J. Catal.* **16**, 220 (1970).
- (53) Yu-Yao, Y. F., *J. Catal.* **87**, 152 (1984).
- (54) Yu-Yao, Y. F., *Ind. Eng. Chem. Prod. Res. Dev.* **19**, 293 (1980).
- (55) Yao, H. C., Gandhi, H. S. and Shelef, M., in "Metal-Support and Metal-Additive Effects in Catalysis" (Imelik, B., Naccache, C., Coudurier, G., Praliaud, H., Meriaudeau, P., Gallezot, P., Martin, G. A. and Vadrine, J. C., eds.), Studies in Surface Science and Catalysis, Vol. 11, 159-169, Elsevier, Amsterdam, 1982.
- (56) Yao, H. C., Yu-Yao, Y. F. and Otto, K., *J. Catal.* **56**, 21 (1979).
- (57) Carballo, L. M. and Wolf, E. E., *J. Catal.* **53**, 366 (1978).
- (58) Otto, K., Andino, J. M. and Parks, C. L., *J. Catal.* **131**, 243 (1991).
- (59) Harris, P. J. F., *J. Catal.* **97**, 527 (1986).
- (60) Yao, H. C., Sieg, M. and Plummer Jr., H. K., *J. Catal.* **59**, 365 (1979).
- (61) Kooh, A. B., Han, W. J., Lee, R. G. and Hicks, R. F., *J. Catal.* **130**, 374 (1991).
- (62) McCarthy, E., Zahradnik, J., Kuczynski, G. C. and Carberry, J. J., *J. Catal.* **39**, 29 (1975).
- (63) Akubuiro, E. C., Verykios, X. E. and Lesnick, L., *Appl. Catal.* **14**, 215 (1985).
- (64) Crucq, A. and Frennet, A. (eds.), "Catalysis and Automotive Pollution Control", Elsevier, Amsterdam, 1987.
- (65) Crucq, A. (ed.), "Catalysis and Automotive Pollution Control II", Elsevier, Amsterdam, 1991.
- (66) Steel, M. C. F., in "Catalysis and Automotive Pollution Control II" (Crucq, A., ed.), Studies in Surface Science and Catalysis, Vol. 71, 105-114, Elsevier, Amsterdam, 1991.
- (67) Silver, R. G., Summers, J. C. and Williamson, W. B., in "Catalysis and Automotive Pollution Control II" (Crucq, A., ed.), Studies in Surface Science and Catalysis, Vol. 71, 167-180, Elsevier, Amsterdam, 1991.
- (68) Hegedus, L. L., Summers, J. C., Schlatter, J. C. and Baron, K., *J. Catal.* **56**, 321 (1979).

- (69) Taylor, K. C., in “*Catalysis and Automotive Pollution Control*” (Crucq, A. and Frennet, A., eds.), Studies in Surface Science and Catalysis, Vol. 30, 97-116, Elsevier, Amsterdam, 1987.
- (70) Maire, F., Capelle, M., Meunier, G., Beziau, J. F., Bazin, D., Dexpert, H., Garin, F., Schmitt, J. L. and Maire, G., in “*Catalysis and Automotive Pollution Control III*” (Frennet, A. and Bastin, J.-M., eds.), Studies in Surface Science and Catalysis, Vol. 96, 749-762, Elsevier, Amsterdam, 1995.
- (71) Stegenga, S., Dekker, N., Bijsterbosch, J., Kapteijn, F., Moulijn, J., Belot, G. and Roche, R., in “*Catalysis and Automotive Pollution Control II*” (Crucq, A., ed.), Studies in Surface Science and Catalysis, Vol. 71, 353-369, Elsevier, Amsterdam, 1991.
- (72) Simonot, L., Garin, F. and Maire, G., in “*Catalysis and Automotive Pollution Control III*” (Frennet, A. and Bastin, J.-M., eds.), Studies in Surface Science and Catalysis, Vol. 96, 203-213, Elsevier, Amsterdam, 1995.
- (73) Engler, B. H., Lindner, D., Lox, E. S., Schäfer-Sindlinger, A. and Ostgathe, K., in “*Catalysis and Automotive Pollution Control III*” (Frennet, A. and Bastin, J.-M., eds.), Studies in Surface Science and Catalysis, Vol. 96, 441-460, Elsevier, Amsterdam, 1995.
- (74) Gandhi, H. S. and Shelef, M., in “*Catalysis and Automotive Pollution Control*” (Crucq, A. and Frennet, A., eds.), Studies in Surface Science and Catalysis, Vol. 30, 199-214, Elsevier, Amsterdam, 1987.
- (75) Diwell, A. F., Rajaram, R. R., Shaw, H. A. and Truex, T. J., in “*Catalysis and Automotive Pollution Control II*” (Crucq, A., ed.), Studies in Surface Science and Catalysis, Vol. 71, 139-152, Elsevier, Amsterdam, 1991.
- (76) Harrison, B., Diwell, A. F. and Hallett, C., *Plat. Met. Rev.* **32**, 73 (1988).
- (77) Yao, H. C. and Yu-Yao, Y. F., *J. Catal.* **86**, 254 (1984).
- (78) Su, E. C., Montreuil, C. N. and Rothschild, W. G., *Appl. Catal.* **17**, 75 (1985).
- (79) Herz, R. K. and Sell, J. A., *J. Catal.* **94**, 166 (1985).
- (80) Weibel, M., Garin, F., Bernhardt, P., Maire, G. and Prigent, M., in “*Catalysis and Automotive Pollution Control II*” (Crucq, A., ed.), Studies in Surface Science and Catalysis, Vol. 71, 195-206, Elsevier, Amsterdam, 1991.
- (81) Lööf, P., Kasemo, B., Björnkvist, L., Andersson, S. and Frestad, A., in “*Catalysis and Automotive Pollution Control II*” (Crucq, A., ed.), Studies in Surface Science and Catalysis, Vol. 71, 253-274, Elsevier, Amsterdam, 1991.
- (82) Kim, G., *Ind. Eng. Chem. Prod. Res. Dev.* **21**, 267 (1982).
- (83) Murrell, L. L., Tauster, S. J. and Anderson, D. R., in “*Catalysis and Automotive Pollution Control II*” (Crucq, A., ed.), Studies in Surface Science and Catalysis, Vol. 71, 275-289, Elsevier, Amsterdam, 1991.
- (84) Summers, J. C. and Ausen, S. A., *J. Catal.* **58**, 131 (1979).
- (85) Yu-Yao, Y. F. and Kummer, J. T., *J. Catal.* **106**, 307 (1987).
- (86) Oh, S. H. and Eickel, C. C., *J. Catal.* **112**, 543 (1988).
- (87) Jin, T., Okuhara, T., Mains, G. J. and White, J. M., *J. Phys. Chem* **91**, 3310 (1987).
- (88) Shyu, J. Z. and Otto, K., *J. Catal.* **115**, 16 (1989).
- (89) Serre, C., Garin, F., Belot, G. and Maire, G., *J. Catal.* **141**, 9 (1993).
- (90) Bunluesin, T., Cordatos, H. and Gorte, R. J., *J. Catal.* **157**, 222 (1995).
- (91) Zafiris, G. S. and Gorte, R. J., *J. Catal.* **143**, 86 (1993).
- (92) Zafiris, G. S. and Gorte, R. J., *J. Catal.* **139**, 561 (1993).
- (93) Zafiris, G. S. and Gorte, R. J., *Surf. Sci.* **276**, 86 (1992).

- (94) Leclerq, G., Dathy, C., Mabilon, G. and Leclerq, L., in "*Catalysis and Automotive Pollution Control II*" (Crucq, A., ed.), Studies in Surface Science and Catalysis, Vol. 71, 181-194, Elsevier, Amsterdam, 1991.
- (95) Munuera, G., Fernandez, A. and Gonzalez-Elipe, A. R., in "*Catalysis and Automotive Pollution Control II*" (Crucq, A., ed.), Studies in Surface Science and Catalysis, Vol. 71, 207-220, Elsevier, Amsterdam, 1991.
- (96) Hardacre, C., Ormerod, R. M. and Lambert, R. M., *J. Phys. Chem.* **98**, 10901 (1994).
- (97) Shyu, J. Z., Otto, K., Watkins, W. L. H., Graham, G. W., Belitz, R. K. and Gandhi, H. S., *J. Catal.* **114**, 23 (1988).
- (98) Engler, B., Koberstein, E. and Schubert, P., *Appl. Catal.* **48**, 71 (1989).
- (99) Nunan, J. G., Robota, H. J., Cohn, M. J. and Bradley, S. A., *J. Catal.* **133**, 309 (1992).
- (100) Pirault, L., El Azami El Idrissi, D., Marécot, P., Dominguez, J. M., Mabilon, G., Prigent, M. and Barbier, J., in "*Catalysis and Automotive Pollution Control III*" (Frennet, A. and Bastin, J.-M., eds.), Studies in Surface Science and Catalysis, Vol. 96, 193-202, Elsevier, Amsterdam, 1995.
- (101) Mendelovici, L. and Steinberg, M., *J. Catal.* **93**, 353 (1985).

## **CHAPTER 2**

### **Catalyst Preparation and Characterisation**

## 2.1 Introduction

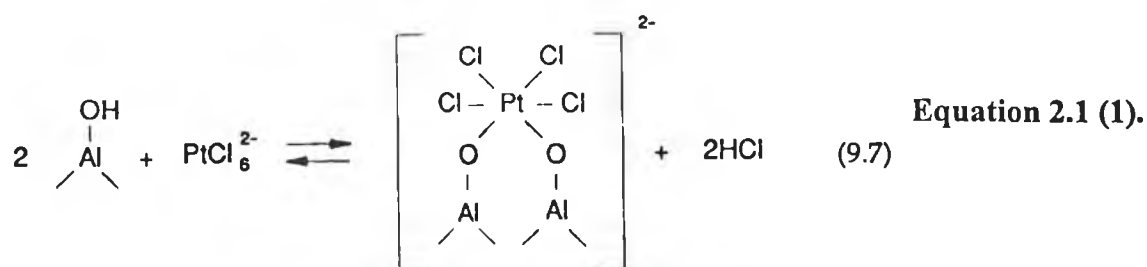
In this chapter, the preparation of supported Pt and bimetallic catalysts by a "wet" impregnation procedure is described. The concentration and dispersion of Pt in the prepared catalysts was determined using Atomic Absorption Spectroscopy (AAS) and H<sub>2</sub> chemisorption techniques, respectively. The specific surface area of each of the support materials used, i.e.  $\gamma$ -Al<sub>2</sub>O<sub>3</sub>, CeO<sub>2</sub> and ZrO<sub>2</sub>, was also determined using a BET technique.

### 2.1.1 Catalyst Preparation

Pt/Al<sub>2</sub>O<sub>3</sub> catalysts are conventionally prepared by impregnation of  $\gamma$ -Al<sub>2</sub>O<sub>3</sub> with an aqueous solution of chloroplatinic acid, H<sub>2</sub>PtCl<sub>6</sub> (1). In its basic form, the impregnation procedure involves contacting the support with the impregnating solution for a certain period of time and then drying the support. Following impregnation, catalyst activation is achieved by calcination and/or reduction (1).

There are two main impregnation techniques generally used, referred to as "incipient wetness" and "wet" impregnation. "Incipient wetness" (also called "dry" or "pore volume") is generally used with preshaped support materials, and involves the use of an amount of solution which is just sufficient to fill the pore volume, or slightly less. For powdered supports, "wet" impregnation, in which the volume of impregnating solution is substantially larger than the pore volume, is often applied (1).

Impregnation of  $\gamma$ -Al<sub>2</sub>O<sub>3</sub> with aqueous H<sub>2</sub>PtCl<sub>6</sub> is thought to proceed via adsorption of the acid onto the Al<sub>2</sub>O<sub>3</sub> surface, according to Eq. 2.1.



The Pt adsorption capacity of typical  $\gamma$ -Al<sub>2</sub>O<sub>3</sub> is reported to be of the order of 1.5  $\mu\text{mol.m}^{-2}$ . However, it is usual to use a Pt loading considerably lower than that corresponding to saturation. Typically, 1 wt.% or less is applied. For a typical surface area of  $\gamma$ -Al<sub>2</sub>O<sub>3</sub> of around 250  $\text{m}^2\text{g}^{-1}$ , this corresponds to a Pt concentration of 0.2  $\mu\text{mol.m}^{-2}$  of Al<sub>2</sub>O<sub>3</sub> or less (1).

One of the most important properties of a supported metal, affecting catalytic activity, is the degree to which the metal is spread over the surface of the support material and available for participation in surface reactions. This is commonly referred to as the metal dispersion. As well as metal loading, a number of preparation variables can have a major effect on the dispersion of the supported metal. These include the metal precursor salt, and the conditions used for activation of the catalyst (2, 3).

### 2.1.2 Catalyst Characterisation

#### **BET Surface Area Measurement**

Measurement of the total surface area of a sample can be achieved by non-specific physical adsorption of a suitable adsorbate (4). Physical adsorption (physisorption) describes the interaction between solids and gases (or liquids and gases) which is due to Van der Waals forces i.e. no chemical bonding takes place. Both the interacting surface atom and the gas molecules more or less retain their identities. On the other hand, if the gas molecule splits into atoms, radicals or ions which are separately adsorbed or if electron transfer or sharing occurs then the adsorption process is referred to as chemisorption (5).

Typical adsorbates used in physisorption measurements are simple non-polar molecules such as the rare gases or nitrogen (4). Physical adsorption is non-selective; for example, N<sub>2</sub> can adsorb on any surface at sufficiently low temperatures. Although multilayer adsorption can occur, a value for only monolayer coverage of the entire surface can be derived using the BET (Brunauer-Emmett-Teller) equation which describes multilayer physical adsorption data (4, 5).

In this study, the total surface areas of the catalyst support materials are determined, using the BET gas adsorption technique, by the non-selective physical adsorption of N<sub>2</sub> at liquid N<sub>2</sub> temperatures (77K). At these temperatures, the N<sub>2</sub> gas condenses onto the surface of the solid sample. From the total amount of N<sub>2</sub> adsorbed, the volume required for monolayer coverage can be determined. Multiplication of the number of molecules in the monolayer, by the cross sectional area of the assumed cubic volume occupied by each molecule of N<sub>2</sub> ( $1.62 \times 10^{-19} \text{ m}^2$ ), yields the surface area of the solid (6).

#### **Total Metal Content**

Atomic Absorption Spectroscopy (AAS) can be used for the selective determination of the total content of a particular metallic element in a sample (7). Flame AAS involves the use of a combustion flame to convert the analyte in solution into atoms

in the vapour phase freed from their chemical surroundings. The sample solution is introduced into the flame as an aerosol. Once the analyte ions have been converted to free atoms (i.e. removed from their chemical environment, but not ionised), the flame then becomes a sample cell. The free atoms produced adsorb radiation focused on the flame from an external source. The wavelength of the incident radiation used is specific to the metal in question in that its absorption results in transition of the ground state atoms to an excited electronic state. Usually the transition between the ground state and the first excited state, known as the first resonance line, is used as it has the strongest absorptivity and hence gives maximum sensitivity. Transitions from the ground state to the first excited state occur when the frequency of the incident radiation is exactly equal to the frequency of the first resonance line. The absorptivity for a given element decreases as the energy difference between the ground state and the excited state increases. Hence sensitivity is lost if radiation wavelengths other than that of the first resonance line are employed. Unabsorbed radiation passes through the flame into a monochromator, that isolates the resonance line, and then into a photodetector that measures the power of the transmitted radiation. The amount of incident radiation absorbed by the sample, i.e. the absorbance, is measured based on the difference in radiant power of the resonance line in the presence and absence of analyte atoms in the flame. Absorbance,  $A$ , can be related to the concentration of the analyte in solution by the Beer-Lambert law, which can be written as:

$$A = \log (P_0/P) = abC.$$

where  $P_0$  = radiant power transmitted in the absence of analyte;

$P$  = radiant power transmitted in the presence of analyte;

$a$  = absorptivity constant ( $\text{liter grams}^{-1} \text{ cm}^{-1}$ );

$b$  = horizontal path length of radiation through the flame (cm);

$C$  = concentration of adsorbing material ( $\text{grams liter}^{-1}$ ).

A plot of absorbance versus metal concentration in standard solutions should, therefore, be a straight line from which the concentration of an unknown solution can be determined (7). The Pt content of the prepared catalysts was determined in this manner.

## Metal Surface Area

Selective chemisorption of a relatively specific gaseous adsorbate, can be used to determine the surface area of the catalytically active metal component of supported catalysts such as Pt/Al<sub>2</sub>O<sub>3</sub> (4). This is as opposed to the total surface area measurement achieved by non-selective physisorption. The major differences between physisorption (physical adsorption) and chemisorption (chemical adsorption) processes are listed in Table 2.1.

The use of chemisorption for specific surface area measurement requires that the measurement of gaseous adsorption be made under conditions where gas uptake occurs exclusively or predominantly on the metal surface. The chemisorption stoichiometry, i.e. the average number of surface metal atoms associated with the adsorption of each adsorbate atom or molecule, must be known to allow the number of surface metal atoms and thus the metal surface area, to be estimated. The total metal surface area is given by:

$$A = n_m^s \cdot X_m \cdot n_s^{-1}$$

where,  $n_m^s$  is the number of adsorbate molecules required for monolayer coverage of the metal surface,  $X_m$  is the chemisorption stoichiometry with reference to the adsorbate molecule, and  $n_s$  is the number of metal atoms per unit area of surface (4).

Once the number of surface metal sites available for adsorption of reactants has been determined, catalyst performance can be expressed in terms of the activity per surface metal atom. This is commonly referred to as the Turnover Frequency or Turnover Number (TOF, TON) and the oxidation activity of different catalysts is often compared on this basis e.g. (8, 9).

The degree of dispersion of the metal on the support material is often expressed as the ratio of the total number of surface metal atoms (determined by chemisorption) to the total number of metal atoms present in the catalyst (determined by AAS) (4). Metal dispersions in supported catalysts are of considerable importance as they indicate how much of the total amount of metal present is potentially available for adsorption of reactants and participation in the catalytic process (5).

The determination of free metal surface area using chemisorption methods can also be used to estimate the average diameter of the metal particles present (4), and can help in determining the extent of typical catalyst deactivation processes such as sintering

Table 2.1 : Major differences between Physical Adsorption and Chemisorption (5).

<u>Physical Adsorption</u>	<u>Chemisorption</u>
1. Caused by van der Waals forces (no electron transfer).	1. Caused by covalent/electrostatic forces (electron transfer / sharing occurs).
2. Heat of adsorption 8 to 25 kJ/mol.	2. Heat of adsorption 40 to 830 kJ/mol.
3. A general phenomenon, such as the condensation of a gas.	3. Specific and selective.
4. Physisorbed layer removed by evacuation.	4. Removed only by evacuation and heating.
5. Multimolecular adsorption below the critical temperature of the gas.	5. Never exceeds a unimolecular layer.
6. Appreciable only below the critical temperature.	6. Often at high temperature also.
7. Rate: instantaneous.	7. May be fast or slow; sometimes involves an energy of activation.
8. Molecules adsorbed intact.	8. Dissociates into atoms, ions or radicals.
9. Adsorbent not strongly affected.	9. Strongly affected (surface compound formation).
10. There are many borderline cases.	

e.g. (10, 11), decoration of the metal by the support material e.g. (12), or poisoning of the metal crystallites by processes such as coking e.g. (13). Distinction between sintering, decoration, and poisoning processes often requires the use of complimentary characterisation techniques. For example, by combining chemisorption measurements with the determination of mean particle size using X-ray Diffraction (XRD) measurements, poisoning and/or decoration effects can be distinguished from sintering effects (14). The other major techniques used in the estimation of metal particle size and dispersion in supported metal catalysts are Transmission Electron Microscopy (TEM) and X-ray Photoelectron Spectroscopy (XPS) (5).

Lemaitre et al. (5) reported that, even though the accuracy of chemisorption methods often requires comparison with complimentary measurements made using other independent techniques, chemisorption is the most used technique for measurement of catalyst dispersions and, insofar as correlation with catalytic activity is concerned, chemisorption measurements are probably the most relevant as they involve specific measurement of surface atoms available to gaseous molecules. Other advantages of chemisorption techniques include their convenience for routine analysis and that they involve less expensive equipment than either XRD, TEM, or XPS methods, with the possibility that activity measurements can sometimes be made within the same experimental set-up (5).

In this study, a pulse flow chemisorption technique using  $H_2$  as the adsorbate gas, will be used to investigate the Pt surface area, dispersion, and particle size in the catalysts under investigation. An introduction to the use of chemisorption as a quantitative probe for the investigation of metal surfaces in supported catalysts will now be given and some selected studies of supported Pt catalysts will be discussed.

In dealing with the measurement of surface area, dispersion, and average particle size of supported metal catalysts by selective chemisorption techniques, there are several factors to be noted (4, 15). Firstly, it is important to know the extent to which adsorption on the support material is occurring. This may involve intrinsic adsorption properties of the support i.e. adsorption which would have occurred even in the absence of the metallic component. Spillover of the adsorbate from the metal to the support material may also occur. Supported catalysts typically consist of a metallic component which can dissociatively adsorb a diatomic molecule, such as  $O_2$  or  $H_2$ , and a support material which cannot dissociate the molecule at the temperature of observation. It has been found that dissociative adsorption on the metal can act as a source of atoms which can migrate to the non-metal and participate there in various processes such as oxidation, reduction or adsorption (16, 17). Such a transport of atoms from the dissociating to the non-dissociating surface is called spillover. If spillover occurs in a chemisorption

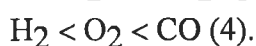
measurement, then the amount of adsorbate uptake by the catalyst will be greater than that expected based on the amount of exposed metal atoms. Spillover problems have been found to occur to a dramatic extent for H<sub>2</sub> chemisorption measurements on Pt/carbon catalysts (15, 17) where the net number of H<sub>2</sub> atoms adsorbed can exceed the number of Pt atoms present by a factor of 3 to 10, even after correction for an intrinsic amount adsorbed on the support alone (17). Anderson (4) stated that for well reduced impurity-free supported metal catalysts using stable (i.e. non-reducible) supports, the magnitude of spillover contribution to the total H<sub>2</sub> uptake under the conditions used for hydrogen adsorption measurement is generally very small or negligible. However it was thought that for catalysts used in hydrocarbon reactions where carbonaceous deposits might be expected, the possible occurrence of spillover must be recognised (4).

Another factor which must be considered in chemisorption measurements is the possibility of solution or incorporation of the adsorbate gas into the bulk of the metal. For example, the use of H<sub>2</sub> chemisorption for the estimation of Pd surface area is reported to be influenced by the need to avoid conditions where H<sub>2</sub> absorption into the metal occurs to an undesirable extent (4). In order to obtain the adsorption due to the metal-only, it is important to choose measurement conditions under which absorption of the gas into the metal and adsorption/spillover of the gas onto the support material are minimised. Any required corrections for possible contributions should be made (4, 15). In order to minimise physisorption contributions, Gruber (18) recommended use of the highest possible temperature and the lowest possible pressure with a low boiling adsorbate which is chemisorbed readily by the metal but not by the support.

The determination of metal particle size from dispersion measurements can also be complicated by the degree of interaction between the metal particles and the support material (15). Supported noble metals are often strongly bonded to the support surface meaning that only part of the metal surface is available for gas adsorption. In extreme cases, this can involve strong encapsulation of the metal particles in the support surface and is referred to as Strong Metal-Support Interaction (SMSI). This type of effect has been used to explain loss of chemisorption capacity, following high temperature reduction of Pt on Al<sub>2</sub>O<sub>3</sub> (19) and CeO<sub>2</sub> (12) supports, in cases where TEM studies showed that no significant agglomeration of Pt particles had occurred. In such cases, a large error is introduced into the determination of mean particle size from free surface area measurement (14, 15). A similar error can be introduced if the metal crystallites being measured are partly poisoned. In both these cases, large differences may occur between the mean particle size estimated from chemisorption and from X-ray line broadening or electron micrographs, due to inaccessibility of part of the metal surface to the adsorbate molecules (14).

The conditions used for catalyst preparation prior to testing must be given due consideration (4, 15). Catalyst pretreatment is assumed to generate a clean impurity-free metal surface to allow for accurate surface area estimation. Generally, this involves pre-reduction of the catalyst followed by removal of any residual H<sub>2</sub> before testing. Appropriate conditions are chosen to ensure complete catalyst reduction to the metal. Care must also be taken to ensure that the catalyst pretreatment does not affect the dispersion of the metal e.g. by causing sintering of the metal particles or reaction of the metal particles with the carrier. In judging the free metal surface area and dispersion values obtained by chemisorption techniques, it should always be noted that the condition of the metal surface during catalytic action can deviate considerably from that arrived at after the pretreatment procedure which always precedes chemisorption. During catalytic action the metallic part of the catalyst surface is often covered by strongly adsorbed atoms, molecules or carbonaceous deposits, and only a small fraction of the metal surface may be catalytically active. This is thought to be one reason why a direct correlation between free metal surface area and catalyst activity is often absent (15).

The choice of adsorbate can also affect the determination of specific metal surface area by selective chemisorption. The most common gaseous adsorbates, used in the determination of metal dispersions, are H<sub>2</sub>, CO, O<sub>2</sub> and N<sub>2</sub>O (4, 15). H<sub>2</sub> is generally the preferred choice because monolayer formation and the chemisorption stoichiometry can be more easily controlled. The extent of adsorption of H<sub>2</sub>, O<sub>2</sub>, and CO on high surface area SiO<sub>2</sub> and Al<sub>2</sub>O<sub>3</sub> stand in increasing order



Thus, intrinsic support adsorption is also minimised by the choice of H<sub>2</sub> as adsorbate. N<sub>2</sub>O is the least commonly used of these adsorbates for platinum group metals. However, it is the preferred adsorbate for examination of supported copper and silver catalysts (4).

The use of O<sub>2</sub> chemisorption for estimation of Pt surface area is thought to be less reliable than that of H<sub>2</sub>, because the chemisorption stoichiometry of O<sub>2</sub> is thought to be more variable and irreproducible by comparison with that of H<sub>2</sub> e.g. (4, 18, 20). Wilson and Hall (20) studied chemisorption on Pt/Al<sub>2</sub>O<sub>3</sub> samples and found O<sub>2</sub> chemisorption to be less useful than that of H<sub>2</sub> in reflecting changes in the metal surface area when comparisons were made with electron micrograph particle size distributions. It was found that the stoichiometry of O<sub>2</sub> adsorption was variable and depended on Pt particle size, with the number of O<sub>2</sub> atoms held per surface Pt atom increasing as the catalyst was sintered (20). Gruber (18) reported that O<sub>2</sub> uptake exceeded that of H<sub>2</sub> for large Pt particles on Al<sub>2</sub>O<sub>3</sub>, particularly if the adsorption measurement was carried out

above room temperature. This phenomenon has been ascribed to O<sub>2</sub> incorporation into the bulk of the metal particles (4, 18).

CO does not behave as O<sub>2</sub> in terms of incorporation into the bulk of metal particles (4). However, there are other problems associated with the translation of the amount of CO adsorbed into free metal surface area. CO chemisorption on metals, such as Pt, can occur in two forms, i.e. linear and bridged (see Fig. 2.1). The former results in a chemisorption stoichiometry of one and the latter in a Pt/CO ratio of 2. These two forms have different adsorption energies and the relative proportions of both can vary with temperature and pressure as well as particle size (4).



**Figure 2.1 : Linear and Bridged forms of CO adsorption on Metals (4).**

Thus, the number of surface metal sites associated with the adsorption of one CO molecule can vary. For example, Gruber (18) found that the mechanism of CO adsorption on supported Pt depended on the nature of the support and on the degree of metal dispersion. The fraction of CO adsorbed in the bridged structure was found to decrease with decreasing metal dispersion (18). Another potential problem with the use of CO as an adsorbate, is that it can form carbonyl compounds with some metallic species it adsorbs to, particularly when the metal is finely divided (4, 15). Despite these uncertainties, CO/Pt<sub>surface</sub> ratios of 0.70 (21) and 1.00 (12) have been used to estimate Pt dispersions in supported oxidation catalysts.

The use of H<sub>2</sub> as an adsorbate for the estimation of free metal surface areas and metallic dispersions has been recommended (4). Organisations which strive for standardisation e.g. the American Society for Testing Materials, and the Research Group on Catalysis, Council of Europe, in general also recommend H<sub>2</sub> (15). Hence, its use can help to facilitate inter-laboratory comparisons. Other advantages associated with the use of H<sub>2</sub> include the fact that H<sub>2</sub> uptake is mainly associated with the metallic part of the catalyst and that the uptake by the non-metallic part is relatively small in most cases (5,

15). Physical adsorption of  $H_2$ , on both metallic and non-metallic components, is thought to be negligible if measurements are carried out at ambient temperature and pressure (15). Disadvantages associated with the use of  $H_2$  include the possibility of dissolution and of misleading results being obtained due to residual hydrogen in the catalyst after pre-reduction at high temperatures (5). It is generally assumed that one hydrogen atom is adsorbed per surface metal atom (4, 15). As the main interest of this study is in the use of  $H_2$ , the remainder of this discussion will focus mainly on this adsorbate.

$H_2$  chemisorption measurements can be made using either static or flow methods (4).

In static volumetric or gravimetric techniques, sample preparation is achieved by  $H_2$  reduction followed by vacuum outgassing at an elevated temperature (4). After cooling of the sample to the measurement temperature,  $H_2$  adsorption is measured as a function of pressure to produce an adsorption isotherm. Classical volumetric techniques, in which  $H_2$  uptake is determined from the variation of the gas pressure in a known volume, are still the most commonly used chemisorption methods (22). The general principle involves knowing the amount of gas initially present in a calibrated volume and subtracting from it the amount remaining after equilibrium with the catalyst sample, to determine the extent of adsorption. The pressure changes caused by adsorption can be related to the amount of gas adsorbed using the ideal gas laws. In gravimetric methods, the extent of adsorption is measured directly via the mass increment. A typical chemisorption isotherm is shown in Fig. 2.2.

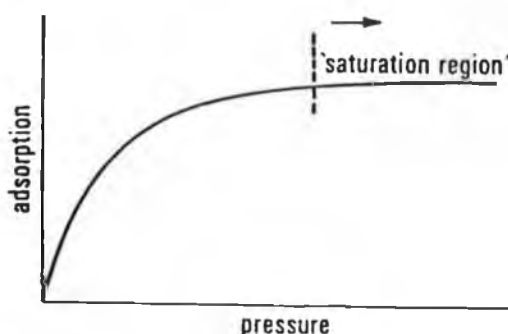


**Figure 2.2 : General features of a chemisorption isotherm (4).**

The 'saturation' region of the chemisorption isotherm (see Fig 2.2) is the part most relevant for estimation of the monolayer uptake. As well as  $H_2$  solution into the metal and intrinsic/spillover adsorption onto the support material,  $H_2$  uptake beyond that required for monolayer coverage of the metal surface can also occur due to formation of

weakly chemisorbed H<sub>2</sub> on the metal surface resulting in a higher than expected chemisorption stoichiometry i.e. H/metal<sub>surface</sub> > 1 (4,15). The nature of this weakly bound hydrogen is in doubt but it has been reported to involve chemisorption rather than physical adsorption (15). This weakly chemisorbed hydrogen has been defined as "hydrogen in excess of the strongly held monolayer" (15).

For metal particle sizes of greater than 1nm in diameter, H<sub>2</sub> adsorption exceeding that expected for monolayer coverage can be corrected for by back-extrapolation of the saturation region of the isotherm to zero pressure (4, 22). Anderson (4) recommended the use of the back-extrapolation method, as it not only corrects for intrinsic adsorption on the support material (assuming this adsorption varies linearly with pressure in the saturation region) but will also help to correct for any effects due to spillover, solution, or weak adsorption beyond monolayer coverage, assuming they do not occur to a large extent. However, for metal particle sizes less than 1nm in diameter, it was thought that the amount of H<sub>2</sub> adsorbed can considerably exceed the expected ratio of one hydrogen atom per surface metal atom i.e. X<sub>m</sub> < 2 (4). Correction for this by the back-extrapolation technique was thought to be inadequate and it was suggested that the monolayer H<sub>2</sub> uptake be obtained based on the amount of irreversibly adsorbed hydrogen. This latter value can be obtained, in static techniques, by firstly measuring the total adsorption of H<sub>2</sub> and then evacuating the sample at room temperature. Measurement of the adsorption isotherm is then repeated to determine the amount of reversibly adsorbed hydrogen which was removed on evacuation. The isotherm for irreversible adsorption is then obtained by subtraction. One potential problem with this technique is that it is thought that, for particle sizes greater than 1nm, monolayer coverage includes some contribution from weak reversible chemisorption on the metal. If this holds true for the smaller metal particles (<1nm), then use of the irreversible isotherm will result in underestimation of the value for monolayer uptake (4).

For dispersed Pt, Anderson (4) recommended that, in cases where an unreasonably large contribution from intrinsic adsorption on the support is absent, the H<sub>2</sub> chemisorption measurement be done between 0 to 27°C and at pressures of up to about 3 kPa, rather than at higher temperatures, to allow greater confidence in the chemisorption stoichiometry and reduce spillover effects. Chemisorption of H<sub>2</sub> on Pt is instantaneous at ambient temperature and is thought to readily achieve a complete monolayer coverage on the exposed Pt surface (5) The use of higher temperatures can, however, be more convenient due to a reduced slow H<sub>2</sub> uptake component and Anderson (4) suggested that optimum conditions should be determined experimentally in each situation. For example, Gruber (18) used a temperature of 200°C for H<sub>2</sub> chemisorption measurements on Pt/Al<sub>2</sub>O<sub>3</sub> reforming catalysts and determined net adsorption isotherms for the Pt

component by subtraction of the adsorption isotherm for the support material on its own under identical conditions. The elevated temperature used by Gruber (18) was chosen to minimise adsorption on the  $\text{Al}_2\text{O}_3$  support. A minima in the support adsorption at this temperature was found experimentally by determining intrinsic adsorption as a function of temperature in the range 140-500°C at various  $\text{H}_2$  pressures.  $\text{H}_2$  was thought to be a particularly suitable adsorbate for volumetric adsorption measurements due to its lower tendency for physisorption on the support than CO. Absorption of  $\text{H}_2$  into the Pt was thought to be negligible at the temperature used (18).

Flow chemisorption methods allow for faster determination of monolayer uptakes without the need for high vacuum equipment. The major advantage is the speed at which routine measurements can be made compared to the classical techniques (23, 24). Sample preparation involves reduction followed by outgassing in a flow of inert gas. In earlier continuous flow applications, sample analysis involved contacting the catalyst with a flow of inert gas containing a small amount of adsorbate and the volume chemisorbed was estimated from the time required for breakthrough of the adsorbate, relative to a blank (24).

In this study, a pulse flow adsorption method, first reported by Gruber (23), is used for the determination of Pt surface areas by  $\text{H}_2$  chemisorption. In this method, which is derived from the continuous flow technique, a pulse of  $\text{H}_2$  is injected into the flow of an inert gas passing over the catalyst sample. The volume of  $\text{H}_2$  present in the pulse is monitored using a Thermal Conductivity Detector (TCD), before and after contact with the catalyst. The volume adsorbed on the catalyst sample is determined by the difference in the two measurements. A minor modification of this technique involves the use of several pulses, each individually smaller than the expected uptake, until the monolayer uptake is complete (24). This method requires several fully eluted pulses to be recorded at the end of the measurement, against which any partly adsorbed pulses can be calibrated. Argon is recommended as the carrier gas to be used when  $\text{H}_2$  is the adsorbate gas, to ensure a sufficient difference in thermal conductivity for adequate sensitivity (4).

The use of the pulse flow technique is thought to minimise reversible adsorption effects relative to static techniques (4). In the latter, time is allowed for adsorption equilibrium to be achieved and the final adsorbate pressure can be quite high. By contrast, in the pulse technique, the concentration or partial pressure of the test gas over the catalyst drops to zero since all of the test gas not chemisorbed is carried away in the gas flow. Therefore, physisorption is expected to be only possible in the form of some retardation and tailing of the test gas pulse (23). Because of this, Gruber (18, 23) was more inclined to use CO (rather than  $\text{H}_2$ ) as the adsorbate because it is easier to

detect using conventional thermal conductivity techniques, and problems with physisorption on the support (which resulted in the choice of H<sub>2</sub> for volumetric measurements) were not as important. In spite of the differences in the conditions of measurement, Lemaitre et al. (5) reported that the results obtained by pulse flow methods have, in general, been found to be in good agreement with those from volumetric or gravimetric methods.

Anderson (4) thought that the dynamic pulse method should only measure chemisorption which occurs rapidly and irreversibly since the final adsorbate pressure is extremely low. However, in using a pulse H<sub>2</sub> chemisorption method to investigate Pt/SiO<sub>2</sub> and Pt/Al<sub>2</sub>O<sub>3</sub> samples, Freel (24) found that part of the H<sub>2</sub> pulse had a substantial residence time on the Pt due to a weak reversible form of H<sub>2</sub> adsorption on Pt even at room temperature. This was indicated by considerable tailing of the pulse peak after passage across a Pt/SiO<sub>2</sub> sample which was not seen when using a SiO<sub>2</sub>-only sample. The volume of unwanted reversibly adsorbed H<sub>2</sub> was found to increase, and the amount of irreversibly adsorbed H<sub>2</sub> to decrease, with increasing adsorption temperature above 25°C. For example, a 0.7 wt.% Pt/Al<sub>2</sub>O<sub>3</sub> sample, which took up  $1.22 \times 10^{19}$  hydrogen atoms per gram at 25°C, took up only  $0.31 \times 10^{19}$  atoms per gram at 300°C. On cooling the sample to 25°C immediately after the latter determination, the sample took up a further  $0.94 \times 10^{19}$  hydrogen atoms per gram. Although it was thought that flow uptakes at elevated temperatures were probably related to Pt dispersion, measurements were made at room temperature to try and determine Pt dispersions and particle sizes as accurately as possible. H<sub>2</sub> chemisorption data at room temperature was found to be in accord with that determined in separate experiments using a static chemisorption measurement method and the stoichiometry assumed in conventional static methods was therefore also applied to calculate Pt dispersions from the pulse results i.e.  $X_m = 2$ . At elevated temperatures (200-300°C), H<sub>2</sub> uptakes could not be treated in the same manner due to the substantial amount of H<sub>2</sub> which was reversibly chemisorbed at this temperature. Comparison of measurements made at 25°C with electron micrographs led to the conclusion that the pulse adsorption data provided an acceptable estimate of Pt dispersion for 2 wt.% Pt samples. For a 0.5 wt.% Pt/Al<sub>2</sub>O<sub>3</sub> sample, however, comparison of adsorption data with the corresponding electron micrograph was reported to be less encouraging (24). In a separate study using the same technique (25), H<sub>2</sub> was found to be a more suitable adsorbate than either CO or O<sub>2</sub>, because the stoichiometry of adsorption was relatively constant over a wider range of crystallite sizes.

For Pt a stoichiometry of one hydrogen atom adsorbed per surface Pt atom (i.e.  $X_m = 2$ ) is generally assumed, with the assumption being regarded as tentative for Pt

particle sizes less than 1 nm in diameter (4, 15). This stoichiometry assumes that small Pt crystallites have surface properties identical to those of bulk Pt metal where each surface atom also adsorbs approximately one hydrogen atom (26). Uncertainties in this stoichiometry of H<sub>2</sub> chemisorption have, however, been found, particularly for highly dispersed Pt, with H/Pt<sub>total</sub> values of greater than unity being reported for both Al<sub>2</sub>O<sub>3</sub> and SiO<sub>2</sub> supported samples (27, 28, 29, 30, 31). For example, Lieske et al. (27) used a dynamic pulse apparatus to determine Pt dispersions in Pt/Al<sub>2</sub>O<sub>3</sub> samples, and found that for highly dispersed samples with a Pt loading of 0.5 wt.%, H/Pt values of  $\approx 1.1$  existed, which was not thought to be unusual for extremely dispersed Pt. Duivenvoorden et al. (28) used a volumetric apparatus to determine H<sub>2</sub> uptakes at 25°C on SiO<sub>2</sub> and Al<sub>2</sub>O<sub>3</sub> supported Pt, Rh and Ir. The total amount of chemisorbed H atoms was determined by back-extrapolation of the linear high pressure part (20 kPa < P < 80 kPa) of the isotherm to zero pressure. H/metal values of greater than unity were found which meant that chemisorption measurements could not be used directly to measure average metal particle size due to uncertainty in the stoichiometry of adsorption at the surface. The high H<sub>2</sub> chemisorption values were explained in terms of multiple adsorption on exposed metal atoms at edge and corner positions i.e. surface stoichiometry exceeding unity, rather than in terms of spillover or subsurface H<sub>2</sub> absorption. The latter phenomenon was ruled out due to the non-existence of subsurface metal atoms. Spillover was ruled out due to the fact that variation of H<sub>2</sub> uptakes was associated more with the different metals used rather than with variation of the support used (28). Mc Cabe et al. (29) determined H/Pt values of as high as 1.5 for highly dispersed Pt/SiO<sub>2</sub> which was attributed to multiple H adsorption per Pt atom or spillover of H atoms onto the support. Multiple adsorption of H atoms on 0.1-0.8% Pt/Al<sub>2</sub>O<sub>3</sub> reforming catalysts was proposed by Alder and Keavney (30), who found that dispersed Pt was considerably more efficient in H<sub>2</sub> adsorption than bulk Pt. H<sub>2</sub> adsorption was believed to occur in the spaces between dispersed Pt atoms rather than on top of each atom. It was thought that for at least some of the exposed faces, two such 'interstices' sites existed per Pt atom. This was used to explain the fact that some catalysts adsorbed a greater number of H atoms than the number of Pt atoms present (30).

Frennet and Wells (31) also reported H/Pt<sub>total</sub> ratios exceeding unity for SiO<sub>2</sub>-supported Pt, when volumetric techniques in different laboratories were compared using the same sample. Temperature Programmed Desorption (TPD) experiments showed that H<sub>2</sub> was adsorbed in various different forms on the catalyst surface. These included spillover H<sub>2</sub>, a weakly adsorbed state of H<sub>2</sub> on Pt, and a strongly adsorbed state with a H/Pt value of unity. Dispersions calculated from the amount of surface Pt associated with the strongly adsorbed H<sub>2</sub> state in room temperature experiments, yielded Pt dispersions which were in good agreement with those estimated by TEM. It was

concluded that unless conditions were found under which the only states of adsorbed H<sub>2</sub> were strongly adsorbed hydrogen (associated with H:Pt = 1:1) and spillover hydrogen, the dispersion of Pt in the 6.3 wt.% Pt/SiO<sub>2</sub> sample studied could not be determined in a straightforward manner from chemisorption experiments (31). Application of a combined pulse adsorption-H<sub>2</sub> TPD technique has been recommended to give information on the different forms of H<sub>2</sub> adsorption such as weakly adsorbed hydrogen and spillover hydrogen (14).

In spite of the inherent uncertainties, H<sub>2</sub> adsorption techniques have been widely used in the study of supported Pt oxidation catalysts as discussed in Chapter 1 e.g. (9, 11, 32, 33). Comparisons with Electron Microscopy have indicated that a reasonable estimation of Pt dispersion and particle size is obtained from the chemisorption results (9, 32). One exception to this is in cases where strong metal support interactions existed (12, 19).

The use of chemisorption methods for determination of noble metal surface areas in samples containing CeO<sub>2</sub> has been reported by some authors to be inadvisable due to possible complications associated with spillover/adsorption onto the CeO<sub>2</sub> component as the reducibility of CeO<sub>2</sub> is known to be increased in the presence of noble metals such as Pt, Pd and Rh e.g. (34, 35). However, several authors have studied noble metal dispersions in CeO<sub>2</sub>-containing samples using CO and H<sub>2</sub> chemisorption e.g. (12, 36, 37, 38). Such studies assumed that gas uptake on reduced CeO<sub>2</sub> was unaffected by the presence of the noble metal (12, 36) and a similar assumption is made in the present study. In support of this assumption, Oh and Eickel (36) reported that the reducible nature of the ceria additive was not expected to interfere with the determination of Rh dispersions on Rh/Al<sub>2</sub>O<sub>3</sub> and Rh/CeO<sub>2</sub>/Al<sub>2</sub>O<sub>3</sub> by H<sub>2</sub> chemisorption measurements. Separate results, from the same laboratory, had shown that CeO<sub>2</sub> reducibility as measured by H<sub>2</sub> uptake experiments, was virtually unaffected by the presence of small amounts of noble metals in the sample (36).

## 2.2 Experimental

### 2.2.1 Preparation of Catalysts

The powdered catalyst support materials used in this study were  $\gamma$ -Al<sub>2</sub>O<sub>3</sub> (supplied by Condea), CeO<sub>2</sub> (supplied by Sigma), and ZrO<sub>2</sub> (supplied by Aldrich). A series of supported Pt catalysts were prepared. The sample compositions and alpha numeric codes are outlined in Table 2.2.

**Table 2.2 : Preparation Details for Samples Used in Study.**

Sample Code	Impregnation Method*	Pt wt.%	Ce wt.%	Mn wt.%	Cr wt.%	Zr wt.%	Support
PA	---	0.5	---	---	---	---	Al <sub>2</sub> O <sub>3</sub>
PA1	---	1.0	---	---	---	---	Al <sub>2</sub> O <sub>3</sub>
PA3	---	3.0	---	---	---	---	Al <sub>2</sub> O <sub>3</sub>
PA5	---	5.0	---	---	---	---	Al <sub>2</sub> O <sub>3</sub>
PC	---	0.5	---	---	---	---	CeO <sub>2</sub>
PZ	---	0.5	---	---	---	---	ZrO <sub>2</sub>
PC0.5A	C	0.5	0.15	---	---	---	Al <sub>2</sub> O <sub>3</sub>
PC1A	C	0.5	0.29	---	---	---	Al <sub>2</sub> O <sub>3</sub>
PC8A	C	0.5	2.90	---	---	---	Al <sub>2</sub> O <sub>3</sub>
**SPC8A	S	0.5	2.90	---	---	---	Al <sub>2</sub> O <sub>3</sub>
**SCP8A	S	0.5	2.90	---	---	---	Al <sub>2</sub> O <sub>3</sub>
PC10A	C	0.5	3.60	---	---	---	Al <sub>2</sub> O <sub>3</sub>
PC17A	C	0.5	6.00	---	---	---	Al <sub>2</sub> O <sub>3</sub>
PMn1A	C	0.5	---	0.11	---	---	Al <sub>2</sub> O <sub>3</sub>
PMn10A	C	0.5	---	1.40	---	---	Al <sub>2</sub> O <sub>3</sub>
PCr1A	C	0.5	---	---	0.11	---	Al <sub>2</sub> O <sub>3</sub>
PCr10A	C	0.5	---	---	1.33	---	Al <sub>2</sub> O <sub>3</sub>
PZr10A	C	0.5	---	---	---	2.30	Al <sub>2</sub> O <sub>3</sub>

\*Note : impregnation method for bimetallic samples. C = co-impregnation, S = step impregnation.

\*\*SPC8A  $\Rightarrow$  Pt impregnation preceded Ce impregnation.

SCP8A  $\Rightarrow$  Ce impregnation preceded Pt impregnation.

For the Pt-only catalysts - Pt/Al<sub>2</sub>O<sub>3</sub>, Pt/CeO<sub>2</sub>, and Pt/ZrO<sub>2</sub> - the letter 'P' in the sample code indicates the presence of Pt, while the letters 'A', 'C', and 'Z' are used to represent the Al<sub>2</sub>O<sub>3</sub>, CeO<sub>2</sub> and ZrO<sub>2</sub> supports, respectively. For samples which do not contain 0.5 wt.% Pt, a numerical value is added to the sample code which represents the nominal wt.% Pt present. For example, PA5 denotes a nominal 5 wt.% Pt/Al<sub>2</sub>O<sub>3</sub> catalyst. Samples were prepared by impregnation of the support material with excess solution (approximately 3 cm<sup>3</sup>g<sup>-1</sup> Al<sub>2</sub>O<sub>3</sub>) of H<sub>2</sub>PtCl<sub>6</sub>.6H<sub>2</sub>O (Johnson Matthey) in ethanol i.e. 'wet' impregnation. The appropriate amount of chloroplatinic acid was dissolved in ethanol in a round bottomed flask. The support material was added to the Pt solution. After mixing for 0.5h at room temperature, the ethanol was removed by rotary evaporation at 70°C. The sample was dried at 45°C overnight and calcined at 630°C for 15 minutes. Drying and calcination steps were achieved in a static air atmosphere in a muffle furnace.

A series of bi-metallic samples, Pt-Ce, Pt-Mn, Pt-Cr, and Pt-Zr supported on Al<sub>2</sub>O<sub>3</sub>, were prepared with a nominal Pt content of 0.5 wt.%. The letters 'P' and 'A' in the sample code are again used to represent Pt and Al<sub>2</sub>O<sub>3</sub>, respectively. The presence of cerium is indicated by the letter 'C', while 'Mn' indicates manganese, 'Cr' indicates chromium, and 'Zr' denotes zirconium. The numerical value in the sample code indicates the atomic ratio of the two metals present. For example, the code PC10A, is used to represent a Pt-Ce/Al<sub>2</sub>O<sub>3</sub> sample with an approximate Pt:Ce atomic ratio of 1:10. All but two of the samples, were prepared by co-impregnation of the Al<sub>2</sub>O<sub>3</sub> support with excess solution of H<sub>2</sub>PtCl<sub>6</sub>.6H<sub>2</sub>O (Johnson Matthey) and either Ce(NO<sub>3</sub>)<sub>3</sub>.6H<sub>2</sub>O (Aldrich), Cr(NO<sub>3</sub>)<sub>3</sub>.9H<sub>2</sub>O (Riedel de Haën), Mn(NO<sub>3</sub>)<sub>2</sub>.4H<sub>2</sub>O (Riedel de Haën), or ZrOCl<sub>2</sub>.8H<sub>2</sub>O (Aldrich). Co-impregnation was achieved by dissolving the appropriate amounts of the two metal salts in ethanol (3 cm<sup>3</sup>g<sup>-1</sup> Al<sub>2</sub>O<sub>3</sub>) in a round bottomed flask. The Al<sub>2</sub>O<sub>3</sub> support was then added. After mixing for 0.5h at room temperature, the solvent was removed by rotary evaporation and the sample dried and calcined, using the standard conditions described above. For samples containing Zr, problems with solubility of the ZrOCl<sub>2</sub>.8H<sub>2</sub>O salt resulted in the use of approximately 7 cm<sup>3</sup> of solvent per gram of Al<sub>2</sub>O<sub>3</sub>. Two Pt-Ce/Al<sub>2</sub>O<sub>3</sub> samples were prepared by step-impregnation. This is denoted by the letter 'S' in the sample codes for these samples. For one of the samples, the Al<sub>2</sub>O<sub>3</sub> was firstly impregnated with a solution of H<sub>2</sub>PtCl<sub>6</sub> in ethanol, using the standard procedure described above. After calcination, the resulting Pt/Al<sub>2</sub>O<sub>3</sub> sample was impregnated with Ce(NO<sub>3</sub>)<sub>3</sub>.6H<sub>2</sub>O in the same manner and the calcination step was repeated (SPC8A). For the other sample, the impregnation sequence was reversed with Ce deposition preceding that of Pt (SCP8A).

Ce/Al<sub>2</sub>O<sub>3</sub>, Mn/Al<sub>2</sub>O<sub>3</sub>, Cr/Al<sub>2</sub>O<sub>3</sub>, and Zr/Al<sub>2</sub>O<sub>3</sub> samples were also prepared, in the absence of Pt. Impregnation of the Al<sub>2</sub>O<sub>3</sub> support with the appropriate metal salt was achieved using the same procedure as for Pt/Al<sub>2</sub>O<sub>3</sub>. The alpha numeric codes for these samples are C10A, Mn10A, Cr10A, and Zr10A, as the amount of metal present would correspond to a Pt:metal atomic ratio of 1:10 for samples containing 0.5 wt.% Pt.

### 2.2.2 BET Surface Areas

A Micromeritics Pulse Chemisorb 2700 was used to determine the surface areas of the powdered support materials. A schematic diagram of the instrument is given in Fig. 2.3. The instrument consisted of a prep. line for sample pretreatment prior to analysis and a test line connected to a TCD. Specific surface areas were determined using a single point BET method, based on the amount of N<sub>2</sub> adsorbed at liquid N<sub>2</sub> temperatures from a 30% N<sub>2</sub>/70% He mixture (supplied by Air Products Ltd., Special Gases Group).

Prior to each analysis, instrument calibration was performed by injecting 1 cm<sup>3</sup> of N<sub>2</sub> at room temperature and calibrating the instrument to display the appropriate surface area occupied by 1 cm<sup>3</sup> of N<sub>2</sub>. This procedure was repeated until the surface area displayed was reproducible as the calibrated value. The surface area occupied by 1 cm<sup>3</sup> of N<sub>2</sub>, under the conditions used, was calculated using the BET equation as outlined in Appendix A.

For analysis, the sample was weighed out accurately into a clean dry sample tube which had been pre-weighed. The tube was then attached to the Pulse Chemisorb 2700 on the prep. line. The sample was pretreated by outgassing in the N<sub>2</sub>/He mixture at room temperature for 5 minutes, purging at 100°C for 30 minutes, and finally at 250°C for 90 minutes. The gas flow rate used was 15 cm<sup>3</sup>/min.. The sample was then cooled to room temperature and switched to the test line by means of a 4-port valve (see Fig. 2.3).

To test, the sample tube was immersed in a dewar of liquid N<sub>2</sub> and adsorption of N<sub>2</sub> from the N<sub>2</sub>/He mixture was monitored using the TCD. Desorption was then achieved on heating the sample to room temperature, by replacing the dewar with a beaker of H<sub>2</sub>O at room temperature. The precalibrated instrument displayed the adsorption/desorption surface areas in m<sup>2</sup>. The adsorption peak was not as sharp as the desorption one and was therefore expected to be integrated with less precision. Hence, the desorption peak area value was used for the calculation of sample surface area. The adsorption-desorption cycle was repeated at least once for each sample. The sample was then switched to the prep. line before removing from the instrument and reweighing. The final sample weight was then used to calculate the sample surface area in m<sup>2</sup>g<sup>-1</sup>.

Differences of less than 10% were observed between adsorption and desorption peaks and successive desorption peaks agreed within 2%. Analysis of different samples of the same material resulted in surface areas which were in agreement within 6%.

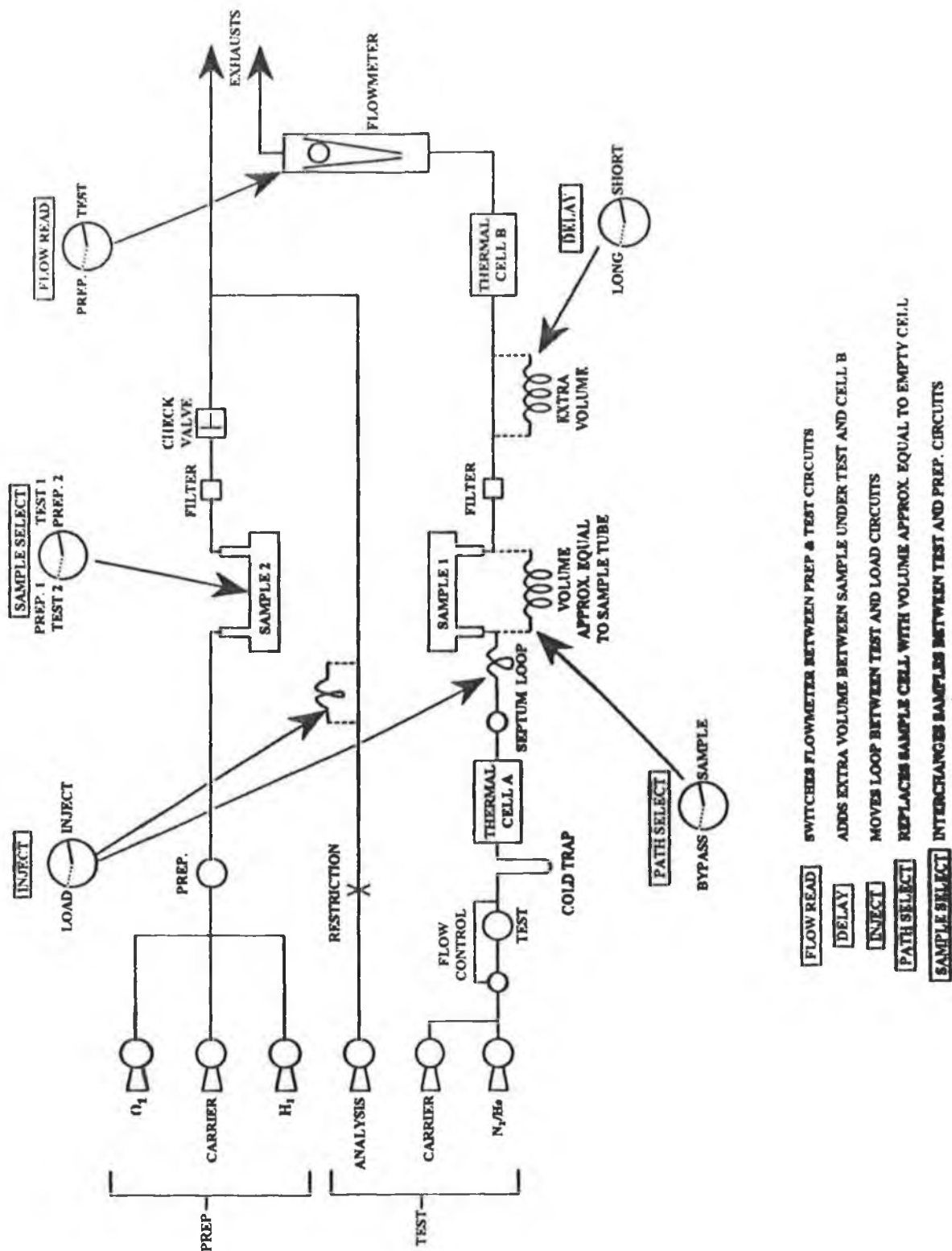


Figure 2.3 : Schematic Diagram of Pulse Chemisorb 2700.

### 2.2.3 Total Metal Content

The Pt content of the prepared catalysts was determined, after acid digestion, by Flame AAS. Comparison of sample digests with standard solutions of known Pt content was achieved using a Perkin Elmer Atomic Absorption Spectrometer 3100.

For the preparation of standard solutions, a 100 ppm Pt solution was initially prepared by dilution of 10 cm<sup>3</sup> of a 1000 ppm standard stock solution (BDH, SpectrosoL) in a 100 cm<sup>3</sup> volumetric flask. This solution was then used to prepare a series of standard solutions in the concentration range of 0 to 50 ppm Pt. Each standard was prepared by dilution to a final volume of 50 cm<sup>3</sup> in a volumetric flask, with 0.5 cm<sup>3</sup> of concentrated HCl and 1 cm<sup>3</sup> of 1000 ppm LaCl<sub>3</sub> (BDH, SpectrosoL) solution. Distilled H<sub>2</sub>O was used in the preparation of all samples and standards.

For sample digestion, a known weight of sample (typically 0.25g for 0.5 wt.% Pt samples) was used which gave a Pt concentration of approximately 25 ppm following digestion. The minimum amount of HF (Riedel de Haën, GPR grade) required to break up the support material, approximately 1 cm<sup>3</sup>, was added to the sample. After 0.5h with intermittent swirling, 7.5 cm<sup>3</sup> of freshly prepared aqua regia was added and the sample was heated to near dryness. 0.5 cm<sup>3</sup> of concentrated HCl was then added and the sample was reconstituted to 50 cm<sup>3</sup> in a volumetric flask, with 1 cm<sup>3</sup> of 1000 ppm LaCl<sub>3</sub> solution.

Atomic absorption measurements were then carried out in triplicate for both samples and standard solutions, under the following conditions;

**Table 2.3 : Instrumental Parameters for Atomic Absorption Spectroscopy**

Light Source	Pt hollow cathode lamp
Lamp Current	10 mA
Wavelength	265.9 nm
Slit Width	0.7 nm
Burner Head	single slot
Flame Description	Air-Acetylene, oxidising, fuel lean, blue.

A standard curve of absorbance versus Pt concentration was prepared and used to determine the Pt concentration in each sample digest, from which the Pt content of the sample was determined. For each catalyst prepared, two different samples were digested

and analysed, and the average Pt content was found. The difference in the value for Pt content between duplicate samples of the nominal 0.50 wt.% Pt catalysts, was determined to be  $\pm 0.05$  wt.%.

#### 2.2.4. Metal Surface Area

##### **Apparatus**

Chemisorption measurements were performed using the excess pulse technique as pioneered by Gruber (23). A schematic diagram of the apparatus used is shown in Fig. 2.4.

H<sub>2</sub> and Ar gases were purified before use. H<sub>2</sub> purification was achieved, using a Johnson Matthey EP1 purifier unit, by passage through a Pd-Ag alloy membrane heated to 250°C. Argon was purified, using a B.O.C. rare gas purifier, by passage over:

- (i) titanium granules at 700°C to remove N<sub>2</sub> and O<sub>2</sub> by chemical reaction,
- (ii) a copper oxide furnace at 450°C for the removal of hydrocarbons, H<sub>2</sub> and CO by chemical reaction, and finally
- (iii) a molecular sieve at ambient temperature to remove moisture and CO<sub>2</sub> by physical adsorption.

This treatment procedure is claimed to reduce total impurities in the Ar down to a level of < 1 volume per million.

After purification, either Ar or H<sub>2</sub> could be passed over the catalyst sample contained in a u-tube (17 in Fig. 2.4), for sample preparation. For analysis, pulses of H<sub>2</sub> were injected into the Ar carrier stream from a loop (13) located upstream of the thermal conductivity detector (16). The H<sub>2</sub> pulse then passed through one limb of the detector, through the catalyst bed, and then through the other limb of the detector. Two peaks, the areas of which corresponded to the amount of H<sub>2</sub> present before and after chemisorption, were thereby recorded and integrated (see Fig. 2.5). The difference in the peak areas measured, served directly as a measure of the amount of H<sub>2</sub> chemisorbed on the sample.

The detector and two temperature equilibration coils (14, 15) were immersed in ambient temperature water baths to protect the detector and gas stream from temperature fluctuations.

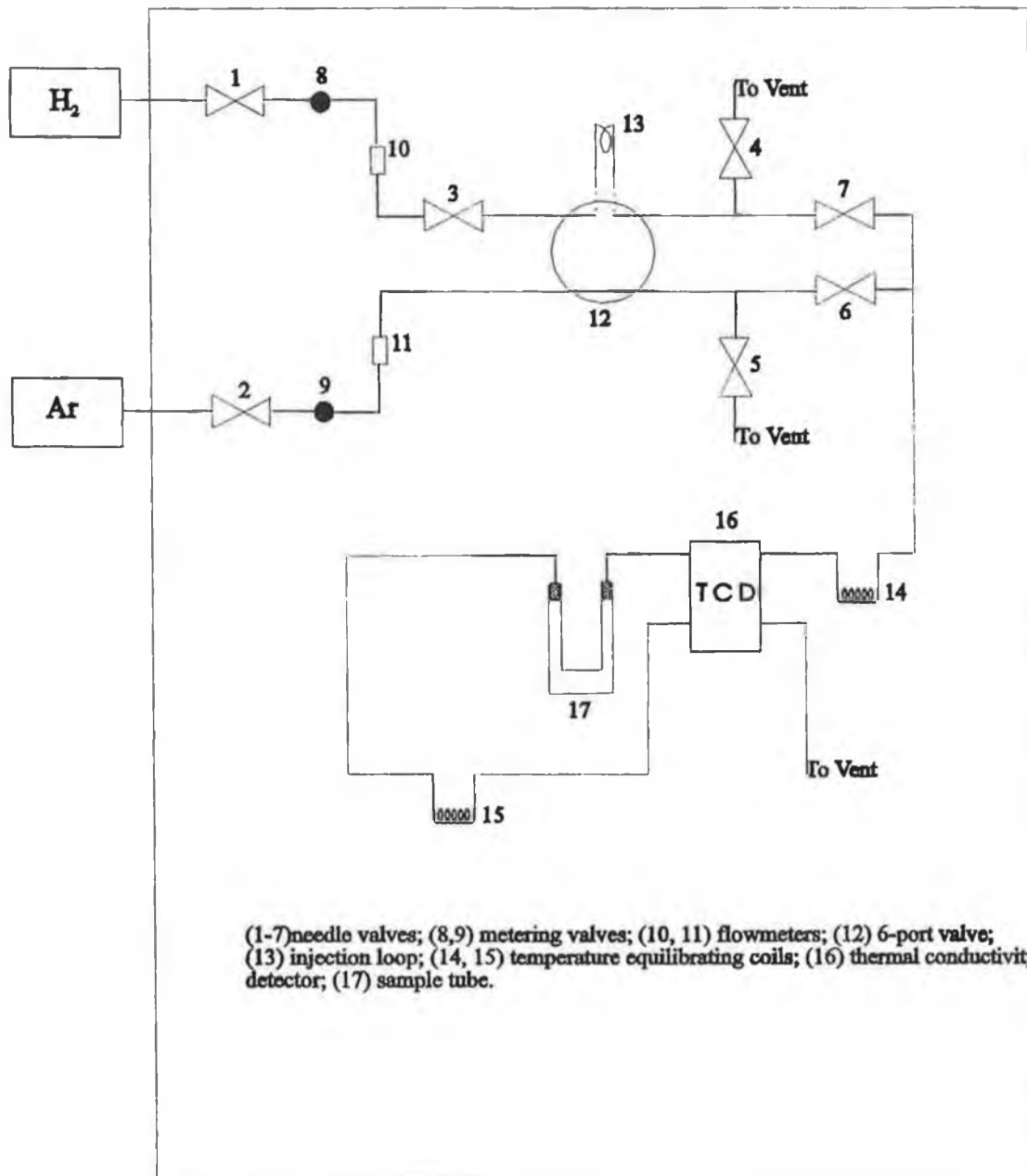
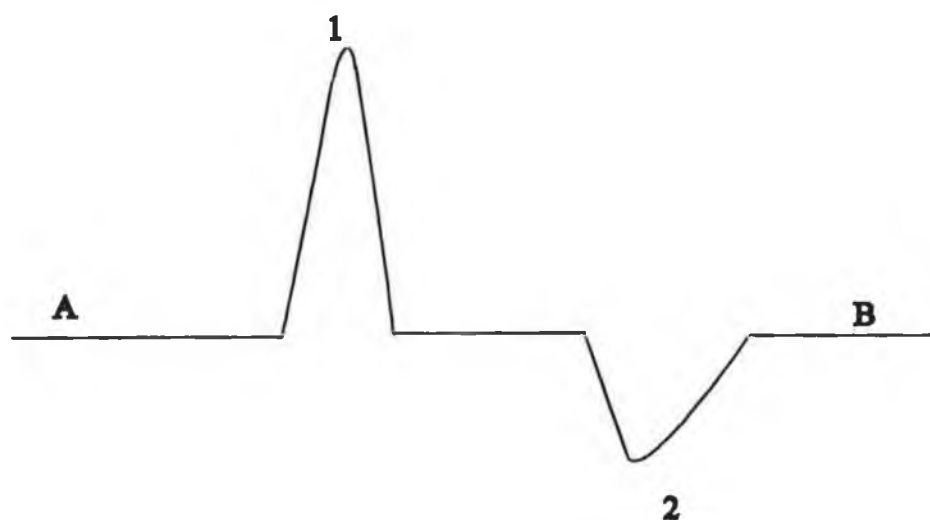


Figure 2.4 : Schematic Diagram of the Pulse Flow Chemisorption Unit.

- A - Injection Point.  
B - End of Run.  
1 - Entrance Peak i.e peak before chemisorption.  
2 - Exit Peak i.e peak after chemisorption.



**Figure 2.5 : Typical Concentration Profile of a H<sub>2</sub> Chemisorption Pulse.**

### **Calibration Procedures and Choice of Experimental Conditions**

This form of chemisorption had not been used in the laboratory prior to this study. As such it was necessary to calibrate the detector response with respect to flow rate and loop volume and to decide on the various instrumental conditions to be used, before any surface area measurements could be made.

A detector current of 20 mA on the Gow Mac power supply unit was used. This was found to be sufficiently sensitive to give an adequate response to the H<sub>2</sub> pulse.

#### Variation in Peak Area with Flow Rate of Argon.

The response of the detector to a given amount of H<sub>2</sub> varied depending on the Ar flow rate used. The variation of peak area with carrier flow rate is shown in Fig. 2.6 for a 0.05 cm<sup>3</sup> loop volume, and in Fig. 2.7 for a 0.025 cm<sup>3</sup> loop volume. At lower flow rates, peaks were bigger due to longer interaction of the H<sub>2</sub> pulse with the detector but

were also broader due to slower passage across the detector. Peak tailing was particularly evident at lower flow rates due to diffusion of the H<sub>2</sub> pulse into the carrier stream and hence lower flow rates were expected to lead to less accurate integration of peak area.

As the TCD response was obviously flow rate dependent, it was important to do all measurements at a constant flow rate. The flow rate chosen had to meet two requirements,

(i) it had to be slow enough to provide sufficient contact between the sample and the adsorbate gas and to give a reasonably sensitive detector response.

(ii) it had to be fast enough to avoid excessive diffusion of the gas pulse into the carrier stream. Such diffusion might broaden the concentration profile to such an extent that it cannot be reliably measured by a conventional TCD.

Although the peak area versus flow rate curves are non-linear, one can easily predict the peak area at a given flow rate. A flow rate of 40 cm<sup>3</sup>/min. was chosen.

#### Linearity of Detector Response with Loop Volume

The linearity of detector response with loop volume was determined using three different loops with volumes of 25, 50, and 100 μl. The results are shown in Fig. 2.8 and Fig. 2.9.

For the 100 μl loop, it was necessary to use a very low flow rate of 14 cm<sup>3</sup>/min. to keep the integrator peaks on scale. At this flow rate, the plot of peak area versus loop volume is seen to be linear (see Fig. 2.8). Thus, although detector response was non-linear with flow rate, at a given flow rate the response varied linearly with the amount of H<sub>2</sub> present. Figure 2.8 was fitted using a linear regression computer package which showed the intercept on the x-axis to be negative at '-3 μl'. The 'dead space' volume of the system was thereby determined to be 3 μl (0.003 cm<sup>3</sup>) and this was added to the loop volume in all calculations. As shown in Fig. 2.9, the peak area varied linearly with loop volume at higher flow rates as well.

In these blank reactor tests it was noticed that, due to elution time through the detector, the second peak was shorter and broader than the entrance peak and usually the integrated peak area was consequently larger for the exit peak. In order to account for this, it was thought necessary to calibrate the two peaks with respect to each other under the experimental conditions chosen for analysis. To do this, a series of injections were

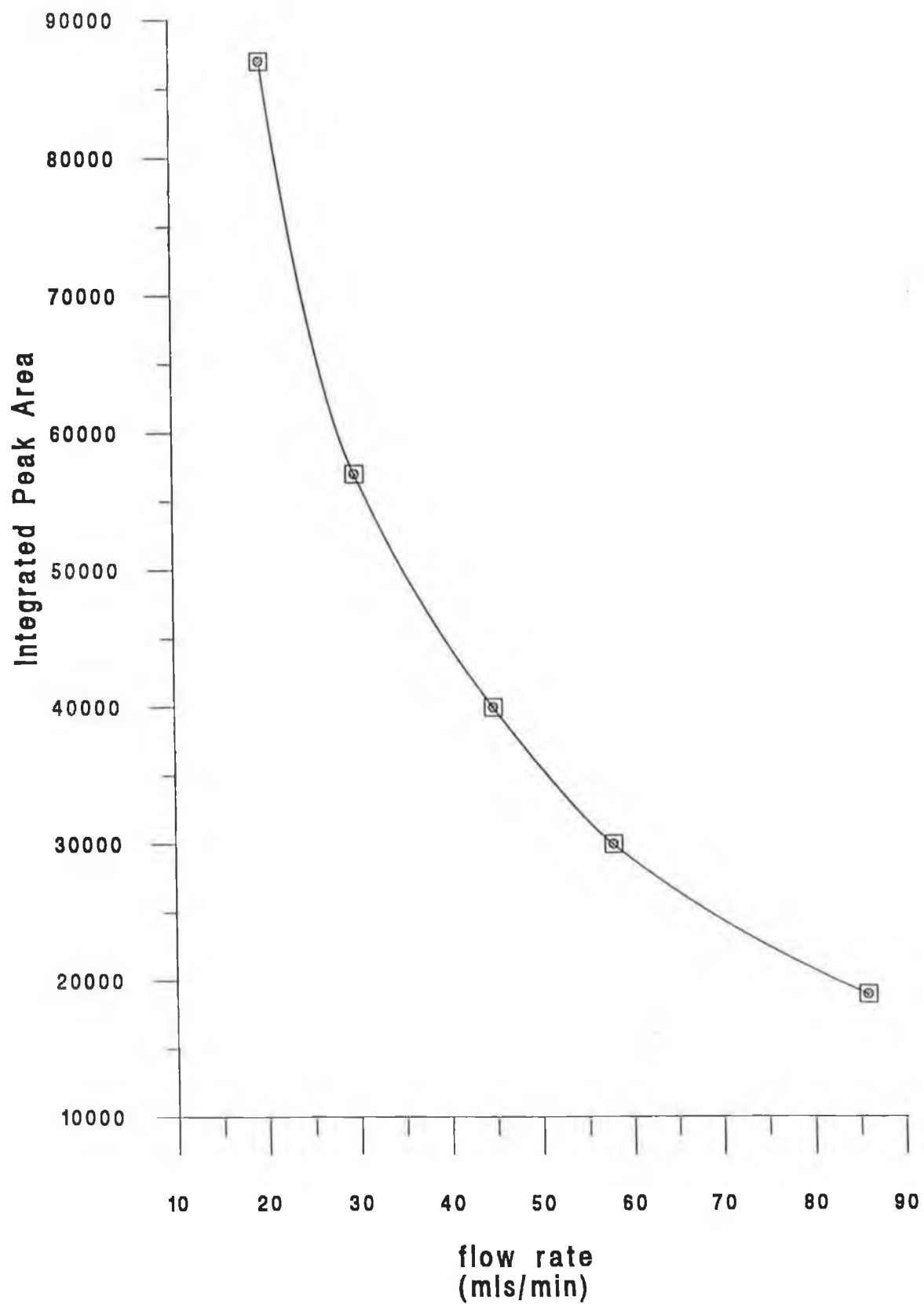


**Figure 2.6 : Peak Area versus Argon Flow Rate for a 0.05 cm<sup>3</sup> loop volume.**

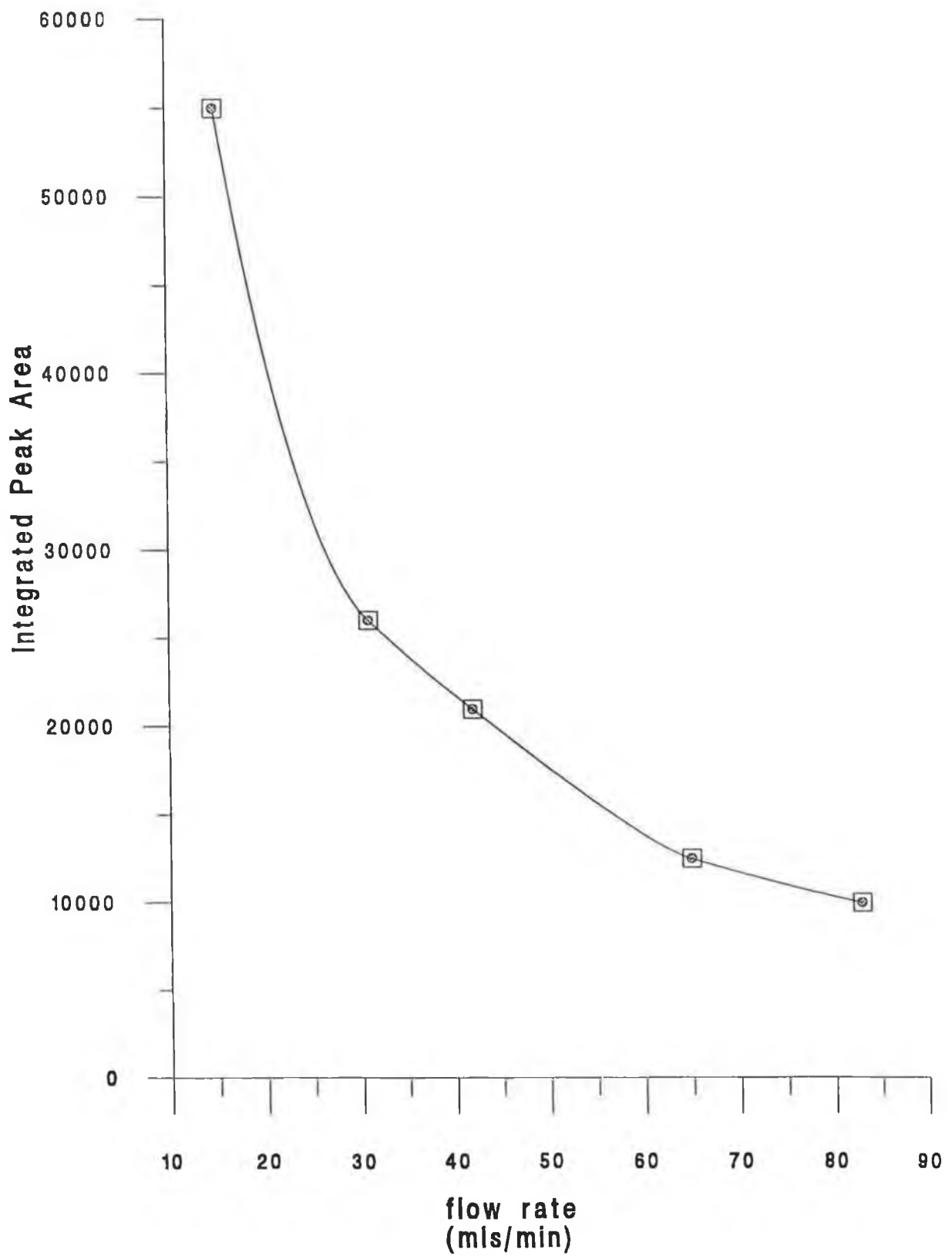


**Figure 2.7 : Peak Area versus Argon Flow Rate for a 0.025 cm<sup>3</sup> loop volume.**

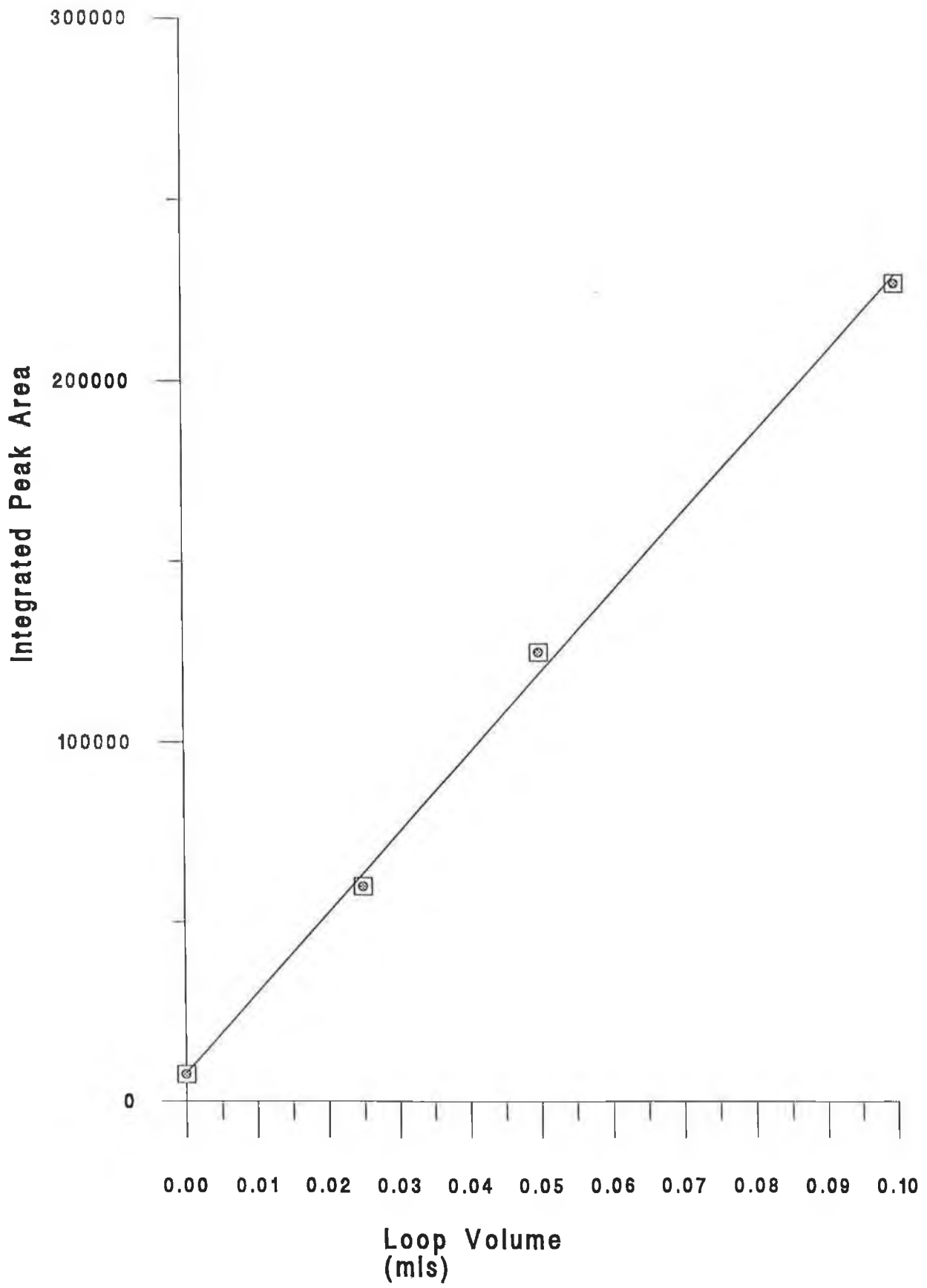


Figure 2.8 : Peak Area versus Loop Volume at a flow rate of 14 cm<sup>3</sup>/min.

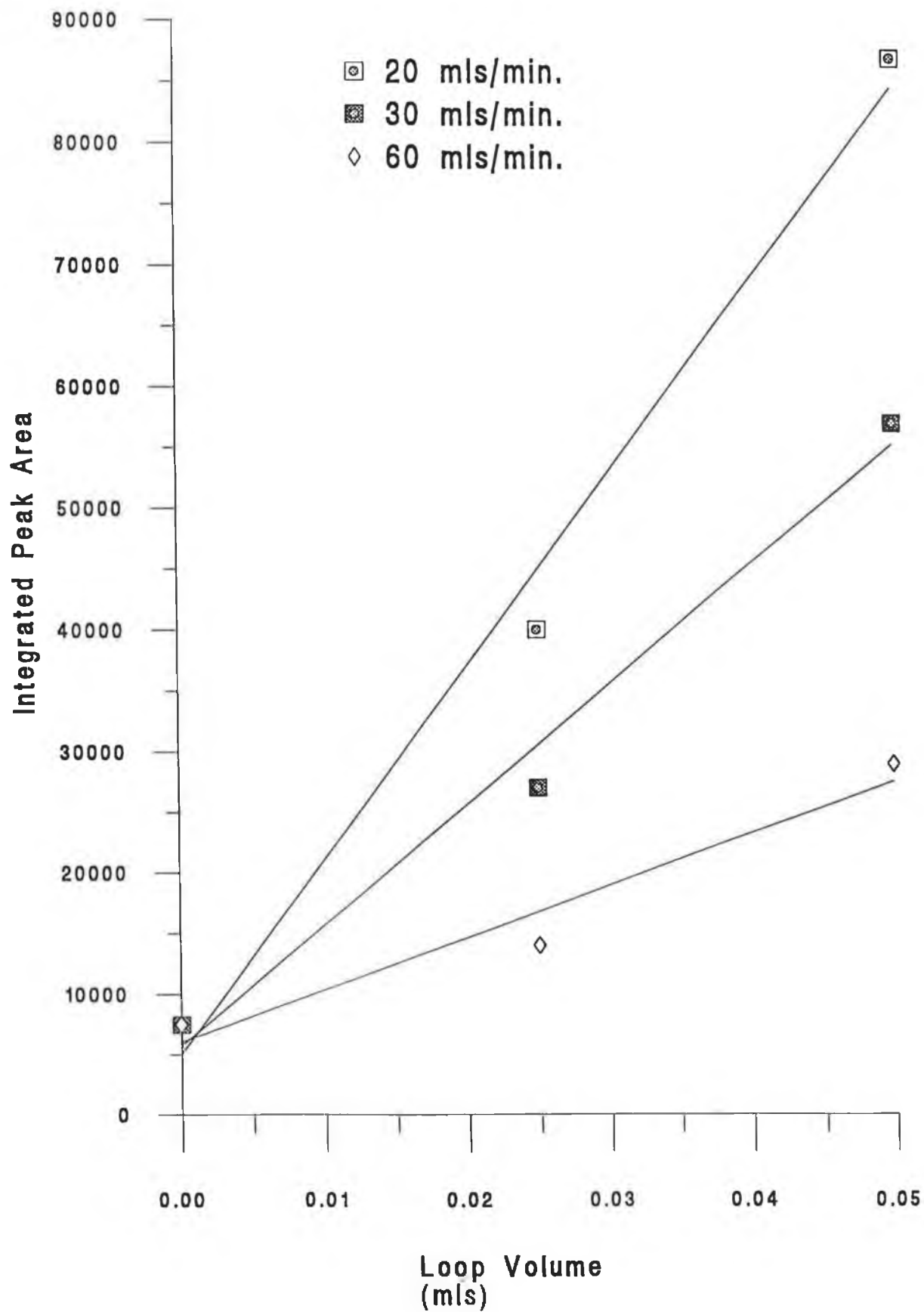


Figure 2.9 : Peak Area versus Loop Volume at various flow rates.

made through a blank sample tube and the average ratio of the two peak areas was calculated in terms of the exit peak area as a % of the entrance peak area. Under the instrumental parameters chosen, this figure was typically  $101.0 \pm 2.0$  %. It was found necessary to standardise integrator run time in order to minimise variations in exit peak area.

The standard measurement conditions chosen were:-

- (i)  $40 \text{ cm}^3/\text{min}$ . Ar flow;
- (ii)  $0.053 \text{ cm}^3$  loop volume (including the dead space volume);
- (iii) 20 mA detector supply; and
- (iv) Integrator run time of 3.2 minutes.

In order to ensure that these conditions resulted in reliable chemisorption measurements, a EuroPt-1 (6.3% Pt/SiO<sub>2</sub>) catalyst was tested at regular intervals during the analysis of catalyst samples. EuroPt-1 was prepared by Johnson Matthey for the Council of Europe Research Group on Catalysis with the intention of being used as a standard reference catalyst in the scientific community. Frennet and Wells (31) compared H<sub>2</sub> chemisorption results for this sample from several laboratories and reported that higher than expected H<sub>2</sub> uptakes for the amount of surface Pt present can occur due to adsorption of H<sub>2</sub> on the sample in forms other than that associated with strong chemisorption on the Pt surface. The amount of H<sub>2</sub> uptake associated with strong chemisorption and a H/Pt ratio of unity was calculated to be  $105 \mu\text{moles}$  of H<sub>2</sub> per gram of catalyst, based on comparison with TEM and TPD studies. However, the total H<sub>2</sub> chemisorption capacity of EuroPt-1 was found to be  $200 \mu\text{mol.g}^{-1}$  (31).

In this study, the average H<sub>2</sub> uptake was found to be  $149 \mu\text{mol.g}^{-1}$  which compares with results of between  $160$  and  $190 \mu\text{mol.g}^{-1}$  found in previous studies (39). However, it should be noted that these latter results were obtained using conventional static volumetric techniques (39).

### **Sample Analysis**

The standard procedure used for sample analysis was as follows. A plug of chemically clean glass wool (soaked in 2M nitric acid solution and rinsed with 5-10 litres of distilled water) was placed in the outlet arm of a clean, dry sample tube. The tube was then preweighed and a known weight of sample was added. The tube was attached to the chemisorption unit (item 17 in Fig 2.4). The glass wool plug served to prevent small amounts of the catalyst sample being carried into the gas lines.

Treatment of the catalyst prior to analysis was as follows. The sample was purged in Ar ( $40 \text{ cm}^3/\text{min.}$ ) at room temperature for 0.25h, at  $125^\circ\text{C}$  for 1h, and at a temperature between  $250\text{-}400^\circ\text{C}$  for 0.5h. The latter temperature depended on the subsequent temperature to be used for reduction. These conditions were used to ensure removal of moisture from the sample. The sample was then reduced in  $\text{H}_2$  ( $40 \text{ cm}^3/\text{min.}$ ) at an elevated temperature and finally purged in Ar at the same temperature to remove any residual  $\text{H}_2$  and leave a clean reduced surface for testing. A number of different reducing and purging conditions were used:-

- (a)  $200^\circ\text{C}$  for 20 min. in  $\text{H}_2$ ,  
 $200^\circ\text{C}$  for 20 min. in Ar.
- (b)  $250/350/400^\circ\text{C}$  for 20 min. in  $\text{H}_2$ ,  
 $250/350/400^\circ\text{C}$  for 40 min. in Ar.

From now on, the temperature of reduction will be used to distinguish which of the above conditions was used for sample preparation. Reduction at  $400^\circ\text{C}$  was found to result in the highest  $\text{H}_2$  chemisorption uptake. The effect of increasing the reduction time at  $400^\circ\text{C}$  to 45 min. was investigated for a 0.5 wt.% Pt sample and was found to have no effect on  $\text{H}_2$  uptake. It was concluded that 20 min. was sufficient to fully reduce the surface Pt present in the 0.5 wt.% samples being tested.

Chemisorption measurements were made at room temperature and pressure. A  $\text{H}_2$  pulse was injected into the Ar carrier stream and the amount of  $\text{H}_2$  chemisorbed by the sample was calculated from the difference in TCD response before and after passage across the catalyst. Adsorbed  $\text{H}_2$  was then removed by heating in Ar for 20 min. at the temperature of pre-reduction. The sample was re-cooled to room temperature and the chemisorption measurement repeated. For each sample, at least two adsorption-desorption cycles were performed until two successive adsorption results agreed within  $\pm 7\%$ . For samples which had undergone further pretreatments other than the preparation procedure outlined in section 2.2.1,  $\text{H}_2$  uptakes were sometimes quite low and reproducibility was not as good. After testing, the sample tube was reweighed to determine the final weight of sample.

$\text{H}_2$  uptakes were determined for the samples prepared in section 2.2.1 and also for sample PA after it had been artificially aged in air at  $800^\circ\text{C}$  for 8h. From the amount of  $\text{H}_2$  adsorbed, the Pt surface area, Pt dispersion, and average Pt particle diameter in each sample was calculated as outlined in Appendix B.

## **2.3 Results and Discussion**

### **2.3.1 BET Surface Area**

The BET surface areas of the support materials (shown in Table 2.4) decreased in the order  $\gamma\text{-Al}_2\text{O}_3 > \text{CeO}_2 > \text{ZrO}_2$ . The surface area of sample, PC10A, was also determined and found to be  $197\text{m}^2\text{g}^{-1}$ . This is a decrease of 11% compared to an average value of  $221\text{m}^2\text{g}^{-1}$  measured for the  $\text{Al}_2\text{O}_3$  support material itself. This reduction in surface area may have been due to plugging of some of the  $\text{Al}_2\text{O}_3$  micropores by either Pt or Ce. Addition of Ce to  $\text{Al}_2\text{O}_3$  support materials has been previously shown to result in a decrease in support surface area (36, 38, 40). Summers and Ausen (38) showed that the effect of Ce addition was to plug some of the pores of the  $\text{Al}_2\text{O}_3$  support and thereby cause a decrease in pore volume with a concomitant loss of BET surface area.

**Table 2.4 : Surface Areas of the Support Materials**

Sample	Surface Area ( $\text{m}^2\text{g}^{-1}$ )
$\gamma\text{-Al}_2\text{O}_3$	221
$\text{CeO}_2$	36
$\text{ZrO}_2$	5
PC10A	197

### **2.3.2 Total Metal Content**

The results of the atomic absorption analysis are shown in Table 2.5. The Pt contents of the nominal 0.5, 1 and 3 wt.% Pt samples, as determined by AAS, are within  $\pm 0.10$  wt.% of the theoretical value for all the samples prepared. For the higher theoretical loading of 5 wt.% on  $\text{Al}_2\text{O}_3$ , Pt content was determined as 5.6 wt.%. It is noted that Cr was listed as one of the interferents for Pt analysis in the AAS instrument manual. However this was not expected to affect the results obtained in this study because addition of  $\text{LaCl}_3$  and HCl to samples and standards is thought to counteract any such interference effects. The Pt contents of the Pt/ $\text{ZrO}_2$  [PZ] and Pt/ $\text{CeO}_2$  [PC] catalysts were not determined due to difficulties with sample digestion.

**Table 2.5 : Pt Contents as Determined by AAS**

Sample Code	Pt Content Theoretical (wt.%)	Pt Content Determined (wt.%)
PA	0.50	0.53
PA1	1.00	1.10
PA3	3.00	2.90
PA5	5.00	5.60
PC0.5A	0.50	0.54
PC1A	0.50	0.53
PC8A	0.50	0.60
SPC8A	0.50	0.53
SCP8A	0.50	0.46
PC10A	0.50	0.58
PC17A	0.50	0.59
PC	0.50	ND
PMn1A	0.50	0.42
PMn10A	0.50	0.41
PCr1A	0.50	0.43
PCr10A	0.50	0.41
PZr10A	0.50	0.40
PZ	0.50	ND

ND = not determined.

### 2.3.3 Metal Surface Area

The results from H<sub>2</sub> chemisorption analysis for samples which were pre-reduced at between 200-250°C are shown in Table 2.6.

As the Pt loading increased from 0.53 to 5.60 wt.% on  $\gamma$ -Al<sub>2</sub>O<sub>3</sub> for samples PA, PA1, PA3, and PA5, the measured Pt surface area also increased from 0.76 to 1.55 m<sup>2</sup>g<sup>-1</sup>. A concurrent decrease in the amount of Pt available on the surface relative to the total amount of Pt present (i.e. % dispersion) is seen to have occurred from 58.0 to 11.2% indicating that less of the total Pt present was available for surface reactions. Otto et al (3) also found that the Pt dispersion, as measured by CO chemisorption, decreased as the Pt loading on  $\gamma$ -Al<sub>2</sub>O<sub>3</sub> (85m<sup>2</sup>g<sup>-1</sup>) was increased above 0.40 wt.%. This was attributed to the formation of larger particles with a greater fraction of subsurface atoms (3). Although it may appear reasonable to assume that Pt surface area and dispersion should follow the

indicated patterns, the results in Table 2.6 should be treated with some reservation as accurate measurements of the actual Pt surface areas of these samples because of the low pre-reduction temperature used i.e. 200°C. Increasing the pre-reduction temperature was thought to result in a more accurate measurement of Pt surface area, as discussed below.

**Table 2.6 : H<sub>2</sub> Chemisorption Measurements (for samples pre-reduced at 200-250°C)**

Sample Code	Reduction Temp. (°C)	H <sub>2</sub> Adsorbed (cm <sup>3</sup> g <sup>-1</sup> )	Pt Surface Area (m <sup>2</sup> g <sup>-1</sup> sample)	Dispersion (%)
PA	200	0.176	0.76	58.0
PA1	200	0.204	0.88	32.3
PA3	200	0.284	1.22	17.1
PA5	200	0.360	1.55	11.2
PC0.5A	200	0.094	0.40	30.4
PC1A	200	0.049	0.21	16.3
PC8A	200	0.105	0.46	30.6
PC10A	200	0.126	0.55	37.9
PC17A	200	0.091	0.39	26.8
PA	250	0.160	0.69	52.4
PC10A	250	0.187	0.80	55.9

In order to try and gain more efficient use of Pt by maximising dispersion it was decided to use a nominal loading of 0.5 wt.% Pt for the remainder of this study.

When using a pre-reduction temperature of 200°C for 0.5 wt.% Pt/Al<sub>2</sub>O<sub>3</sub> samples, the chemisorption results (in Table 2.6) indicate that the presence of Ce caused a decrease in the available Pt surface area and in the apparent dispersion. The extent of this decrease did not appear to be in any way proportional to the Ce loading used. However, uncertainties in achieving total Pt reduction to the zerovalent metal prior to measurement are expected to have affected the accuracy of these results. The importance of the preparation procedure used is illustrated by the fact that pre-reduction at 250°C resulted in a greater H<sub>2</sub> uptake for sample PC10A than for sample PA while the opposite was true when the samples were pre-reduced at 200°C.

The chemisorption data for samples after reduction at 400°C are shown in Table 2.7.

**Table 2.7 : H<sub>2</sub> Chemisorption Measurements (for samples pre-reduced at 400°C)**

Sample Code	H <sub>2</sub> Adsorbed (cm <sup>3</sup> g <sup>-1</sup> )	Pt Surface Area (m <sup>2</sup> g <sup>-1</sup> sample)	Dispersion (%)
PA	0.331	1.43	108.7
PA	0.341	1.47	111.9
PA(aged)	0.026	0.11	8.5
PC0.5A	0.306	1.32	98.6
PC10A	0.330	1.42	99.1
PC10A	0.324	1.39	97.1
PC17A	0.172	0.75	51.4
PC17A	0.171	0.74	50.6
SPC8A	0.243	1.04	79.8
SCP8A	0.231	1.00	87.4
PCr1A	0.252	1.09	101.9
PCr10A	0.259*	1.11	110.1
PZr10A	0.251**	1.08	109.2
PC	0.055	0.24	19.2***
PZ	0.009	0.04	3.0***
C10A	nd	-----	-----
Cr10A	0.020	-----	-----
Zr10A	0.019	-----	-----

\*After correction for H<sub>2</sub> adsorbed on sample Cr10A.

\*\*After correction for H<sub>2</sub> adsorbed on sample Zr10A.

\*\*\*Calculated assuming a nominal Pt loading of 0.5 wt.%.

nd = none detected.

From comparison of Tables 2.6 and 2.7, it is apparent that increasing the pre-reduction temperature to 400°C caused a considerable increase in the amount of H<sub>2</sub> uptake. For example, sample PA had a H<sub>2</sub> uptake of 0.176 cm<sup>3</sup>g<sup>-1</sup> after reduction at 200 °C and this increased to an average uptake of 0.336 cm<sup>3</sup>g<sup>-1</sup> after reduction at 400°C. Similarly, for sample PC10A H<sub>2</sub> uptake increased from 0.126 to 0.327 cm<sup>3</sup>g<sup>-1</sup>. This increase may have been due to more complete reduction of surface Pt, as indicated by Temperature Programmed Reduction profiles of the samples that were obtained after reduction at the various pretreatment temperatures, and was therefore expected to give a more accurate representation of the total Pt surface area. Previous TPR studies of highly

dispersed Pt/Al<sub>2</sub>O<sub>3</sub>, have reported Pt reduction to occur at temperatures as high as 420°C (41) and 500°C (42). Therefore, it is quite probable that reduction below 400°C was insufficient to completely reduce all of the surface Pt. Anderson (4) recommended the use of a temperature of as high as 350-400°C at a H<sub>2</sub> pressure of 101 kPa for reduction of supported Pt in order to ensure complete removal of adsorbed oxygen.

If it is assumed that pre-reduction at 400°C resulted in measurement of the true complete surface area then the dispersion of Pt in the Al<sub>2</sub>O<sub>3</sub>-supported samples was very high. Indeed, for several samples values of greater than 100% were found. This is, of course, impossible and may be explained by one or more reasons.

One possible explanation is experimental error, either in the chemisorption measurement or in the determination of total metal content by atomic absorption spectroscopy. However, the reproducibility of the dispersion measurement when repeated for catalysts PA, PC10A, and PC17A, would tend to argue against this suggestion. The difference in dispersion values between duplicate tests was at maximum ±3.2% which would not account for the dispersion values of 111.9%, 110.1%, and 109.2%, determined for samples PA, PCr10A, PZr10A respectively.

Overestimation of Pt surface area and dispersion could have occurred due to physical adsorption or weak reversible chemisorption of H<sub>2</sub> on the catalyst surface. As discussed in section 2.1.2, the use of a pulse technique should minimise contributions from these phenomena (4, 23). Freel (24) found that even with pulse measurements there was a component of unwanted reversible H<sub>2</sub> adsorption on Pt. However, the use of room temperature measurements, as employed in this study, was thought to minimise reversible chemisorption (24).

Spillover of adsorbed H<sub>2</sub> from metal sites onto the support material could also have resulted in over estimation of the amount of H<sub>2</sub> required for monolayer coverage. In particular for CeO<sub>2</sub>-containing samples, H<sub>2</sub> spillover must be considered as a possible interferent in the chemisorption measurement, since the reduction of CeO<sub>2</sub> by H<sub>2</sub> has been reported to be promoted in the presence of Pt (43). Although Rh has been reported to be even more effective than Pt in promoting the reduction of CeO<sub>2</sub> by H<sub>2</sub> (44), Oh and Eickel (36) reported that the reducible nature of CeO<sub>2</sub> did not interfere with the determination of Rh dispersions in Al<sub>2</sub>O<sub>3</sub>-supported samples but they did not cite the conditions used for sample preparation or for H<sub>2</sub> uptake measurement. From Table 2.7, it can be seen that sample C10A did not adsorb any detectable amount of H<sub>2</sub> under the conditions used.

Dispersion values of greater than 100% could also be explained by the existence of a H:Pt stoichiometry of greater than unity i.e. that more than one hydrogen atom was adsorbed per surface Pt atom. Anderson (4) noted that for metal particle sizes of less than 10Å in diameter, the assumption of a stoichiometry of unity should be regarded as tentative. The average Pt particle sizes measured here for the more highly dispersed catalysts are around this value (see Table 2.8). A H:Pt value of  $\approx 1.1$  was reported by Lieske et al. (27) for a highly dispersed 0.5 wt.% Pt/Al<sub>2</sub>O<sub>3</sub> catalyst. The catalyst was prepared by impregnation of Al<sub>2</sub>O<sub>3</sub> with a solution of H<sub>2</sub>PtCl<sub>6</sub> in dilute HCl. Chemisorption measurements were made at 0°C using a dynamic pulse apparatus following prerduction of the sample at 500°C in H<sub>2</sub> for 1h and subsequent purging in Ar for 1h. A similar stoichiometry may have been exhibited by some of the dispersed samples investigated in this study.

**Table 2.8 : Average Pt Particle Diameters for Catalyst Samples (as calculated from chemisorption data)**

Sample Code	Pt Surface Area (m <sup>2</sup> g <sup>-1</sup> Pt)	Pt Particle Size (Å)
PA	274	10
PA(aged)	21	133
PC0.5A	244	11
PC10A	243	11
PC17A	127	22
SPC8A	198	14
SCP8A	217	13
PCr1A	253	11
PCr10A	271	10
PZr10A	270	10
PC	48	58
PZ	8	349

Due to the uncertainties in the exact form(s) of H<sub>2</sub> adsorption involved in H<sub>2</sub> uptake, and in the state of the catalyst surface after the pretreatment procedure, the use of a second complimentary technique such as TEM would be helpful in assessing the accuracy of the chemisorption results. TEM analysis was not available to this study.

However, Briot et al. (9) made comparisons with TEM micrographs and found that H<sub>2</sub> chemisorption provided an acceptable measurement of Pt dispersion and particle size in a 2 wt.% Pt/Al<sub>2</sub>O<sub>3</sub> catalyst, when a H:Pt stoichiometry of unity was assumed. A similar conclusion was reached by Freel (24) when using a pulse technique to investigate supported Pt catalysts. Speandel and Boudart (45) found that Pt particle sizes, determined by H<sub>2</sub> chemisorption assuming a H:Pt ratio of unity for 0.6 wt.% Pt/Al<sub>2</sub>O<sub>3</sub> catalysts, were in close agreement with values determined by X-ray Diffraction line broadening experiments when the crystallite size was in the range 50-1000Å where the latter technique was capable of accurate measurement.

Taking the foregoing provisos into account, comparison of H<sub>2</sub> chemisorption measurements for samples which underwent the same pretreatment procedure at 400°C seems a reasonable basis for discussion.

From Table 2.7, it is seen that after calcination at 630°C, sample PA consisted of highly dispersed Pt particles with the average Pt surface area measured as 1.45m<sup>2</sup>g<sup>-1</sup> corresponding to a Pt dispersion of 110.3%. For samples with a Pt:Ce ratio of 1:0.5 and 1:10, a very high dispersion of Pt was maintained with values of 98.6% and 98.1% measured for samples PC0.5A and PC10A, respectively. On increasing the level of Ce for sample PC17A, the H<sub>2</sub> chemisorption capacity of the Pt present was lowered considerably to give an apparent dispersion of 51.0% and a Pt surface area of 0.75m<sup>2</sup>g<sup>-1</sup>. Stepwise impregnation of the two metals, either with Pt deposition preceding that of Ce or vice versa for samples SPC8A and SCP8A, also resulted in loss of surface Pt. SPC8A had a free metal surface area of 1.04m<sup>2</sup>g<sup>-1</sup> and a dispersion of 79.8%, while for SCP8A values of 1.00m<sup>2</sup>g<sup>-1</sup> and 87.4% were measured. The presence of Cr or Zr at ten times the atomic level of Pt did not appear to have any effect on Pt dispersion, with values of 110.1% and 109.2% found for samples PCr10A and PZr10A, respectively. For both of these samples, correction was made for intrinsic adsorption on the support material i.e. samples Cr10A and Zr10A. For all the other samples adsorption on the support material was found to be negligible i.e. if any H<sub>2</sub> uptake was measured, it was below the experimental error expected. The average Pt particle sizes for the above samples, as calculated from chemisorption data, varied from 10 to 22Å with the largest value being exhibited by the less well dispersed sample, PC17A (see Table 2.8).

For samples PC and PZ, a considerably lower active metal surface area was found, when compared to the Al<sub>2</sub>O<sub>3</sub>-supported samples, indicating poorer Pt dispersion on the lower surface area support materials. For PC, Pt surface area, dispersion, and average particle diameter, were calculated to be 0.24m<sup>2</sup>g<sup>-1</sup>, 19.2%, and 58Å,

respectively. The corresponding values for PZ were  $0.04\text{m}^2\text{g}^{-1}$ , 3.0%, and  $349\text{\AA}$ , which indicated the presence of very large particles on the  $\text{ZrO}_2$  support.

The chemisorption data for sample PA after it had been aged in air at  $800^\circ\text{C}$  for 8h are also shown in Tables 2.7 and 2.8. The results reflect a severe loss of Pt surface area for the aged sample which was expected to occur due to agglomeration of the Pt particles during the high temperature treatment in the oxidising environment via a process known as sintering (11, 46, 47). After aging, the available Pt surface area decreased from  $1.45\text{m}^2\text{g}^{-1}$  to  $0.11\text{m}^2\text{g}^{-1}$  which indicated an increase in the average Pt particle diameter from 10 to  $133\text{\AA}$ .

Carballo and Wolf (11) studied the catalytic oxidation of  $\text{C}_3\text{H}_6$  on Pt/ $\gamma$ - $\text{Al}_2\text{O}_3$ . Similar to this study, it was found that aging of 1% Pt/ $\gamma$ - $\text{Al}_2\text{O}_3$  in  $\text{O}_2$  at  $700^\circ\text{C}$  lead to a reduction in  $\text{H}_2$  chemisorption capability (11). The average apparent Pt particle size was found to increase from  $11\text{\AA}$  to  $60\text{\AA}$  and  $144\text{\AA}$  after aging for 10h and 30h, respectively. The assumption that Pt particle growth was the reason for loss of  $\text{H}_2$  uptake was justified on the basis that the aged samples were considerably more active than the fresh sample. It was thought that if encapsulation of the metal by the support material was the cause of decreased  $\text{H}_2$  chemisorption, then the specific reaction rate would be expected to decrease (11, 12). Likewise, in this study, sample PA was found to be considerably more active after aging (see section 3.3.3). Thus, it would appear that loss of Pt surface area was attributable to particle growth rather than support surface area loss due to thermal transformations. The latter phenomenon has been reported to result in catalyst deactivation due to encapsulation of the active metal (12, 48).

In support of this argument, Harris (46) found that heating of a 6.3 wt.% Pt/ $\text{Al}_2\text{O}_3$  sample in air at  $700^\circ\text{C}$  caused very rapid sintering to occur. TEM analysis showed that the mean particle diameter had increased from 50 to  $300\text{\AA}$  after 8h (46). Dautzenberg and Wolters (47) studied the effects of various heat treatments on the state of dispersion of Pt in  $\text{Al}_2\text{O}_3$ -supported catalysts using  $\text{H}_2$  chemisorption, X-ray diffraction and electron microscopy as analytical techniques. Exposure to an oxygen-containing atmosphere above  $500^\circ\text{C}$  was found to result in agglomeration of Pt particles which caused a decrease in  $\text{H}_2$  chemisorption capacity (47).

Thus it can be concluded that sintering of the well dispersed Pt particles was the most probable cause of the significant loss of Pt surface area found for sample PA after high temperature aging in air. On the same basis, it is concluded that although there may be uncertainties in the accuracy of surface area measurements by  $\text{H}_2$  chemisorption, the technique does appear to reflect changes in available Pt surface area in a simple, straightforward manner.

The use of base metal oxide additives such as CeO<sub>2</sub> or MoO<sub>3</sub> has been proposed to increase the extent to which a noble metal such as Pt can be deposited in a dispersed manner on  $\gamma$ -Al<sub>2</sub>O<sub>3</sub> (42, 49, 50), and also to prevent the agglomeration of dispersed Pt into discrete particles (12, 51, 52). This latter phenomenon has been attributed to a Pt-CeO<sub>2</sub> interaction which helps to maintain Pt in an oxidised state which is more difficult to sinter than metallic Pt (12, 51, 53).

Diwell et al. (12) studied samples of 0.9 wt.% Pt on  $\gamma$ -Al<sub>2</sub>O<sub>3</sub>, and 75 wt.% Al<sub>2</sub>O<sub>3</sub>-25 wt.% CeO<sub>2</sub>, support materials using CO chemisorption and reported improved Pt dispersion in the presence of CeO<sub>2</sub> for samples which were aged in air at temperatures between 600-800°C for 2h. Silver et al. (51) proposed that improved performance for 'aged' automotive exhaust catalysts with increasing amounts of CeO<sub>2</sub> in the Al<sub>2</sub>O<sub>3</sub> washcoat, was due to stabilisation of Pt dispersion but they did not report Pt dispersions. Hegedus et al. (54) also found improved noble metal dispersion in automotive exhaust catalysts on addition of Ce, but, in disagreement with Silver et al. (51), thought that Ce degraded the thermal stability of Pt and therefore resulted in loss of performance after sintering in air at 900°C for 2h (54). Su et al. (34) studied the OSC of samples containing noble metals supported on  $\gamma$ -Al<sub>2</sub>O<sub>3</sub> and CeO<sub>2</sub>- $\gamma$ -Al<sub>2</sub>O<sub>3</sub> washcoats on a monolith substrate, and found inferential evidence which suggested that noble metal dispersion was improved as the Ce:precious metal ratio was increased. However, precious metal dispersions were not assessed because it was thought that adsorption on partially reduced ceria (as a result of promoted redox reaction in the presence of noble metal) would complicate conventional adsorption measurements (34).

Shyu and Otto (41) found that addition of CeO<sub>2</sub> to Pt/Al<sub>2</sub>O<sub>3</sub> samples facilitated Pt dispersion as indicated by TPR, XPS, and XRD studies. This was attributed to a Pt:CeO<sub>2</sub> interaction which prevented the formation of particulate Pt. Pt was found to interact preferentially with CeO<sub>2</sub> even in the presence of a much larger Al<sub>2</sub>O<sub>3</sub> surface. Calcination of Pt/CeO<sub>2</sub> or Pt/CeO<sub>2</sub>-Al<sub>2</sub>O<sub>3</sub> at 800°C in air was found to result in a platinum-ceria interactive species with an oxidation state of Pt<sup>+2</sup>, attributable to PtO. For Pt/Al<sub>2</sub>O<sub>3</sub>, exposure to the same conditions was thought to result in the formation of a PtO<sub>2</sub>-Al<sub>2</sub>O<sub>3</sub> surface complex i.e. Pt<sup>+4</sup> (41). Murrell et al. (53) investigated Pt/CeO<sub>2</sub> samples using XPS and Laser Raman Spectroscopy (LRS) techniques and also reported the existence of a Pt-CeO<sub>2</sub> interaction which resulted in surface Pt existing in the form of a Pt-O complex formed at the Pt-CeO<sub>2</sub> interface. This was found to stabilise Pt surface area on exposure to an oxidising environment at high temperatures. Addition of Pt beyond the capacity of CeO<sub>2</sub> to form the Pt<sup>+2</sup>-complex resulted in Pt sintering to form large particles, while exposure to cyclic redox aging conditions also resulted in severe Pt

sintering attributed to loss of the Pt-O complex during the reducing swing of the aging cycle (53).

Le Normand et al. (40) attributed increased Pd dispersion on Al<sub>2</sub>O<sub>3</sub> in the presence of CeO<sub>2</sub> as being due to an electronic interaction between the transition metal and the rare earth in a low oxidation state. This was thought to inhibit noble metal mobility on the surface as proposed by Yermakov et al. (49, 50) who found that transition metals such as Pt and Pd can be maintained in a dispersed state by interaction with low valent ions anchored to the support surface. For Pt-Mo samples, such an interaction was found to result in electron transfer from Pt to Mo ions (49). Similar interactions have been proposed for noble metals in contact with CeO<sub>2</sub>, where electron transfer resulting in a partial reduction of the CeO<sub>2</sub> has been predicted based on electrochemical potentials (40) and supported by experimental evidence showing increased oxidation of surface Pt (37, 38).

In this study, the addition of Ce, particularly at higher levels (Pt:Ce  $\leq$  1:8), was found to result in decreased Pt dispersion for 0.5 wt.% Pt/Al<sub>2</sub>O<sub>3</sub> catalysts after calcination at 630°C. This contrasts with the studies discussed above which reported that Ce, in general, promoted noble metal dispersion on Al<sub>2</sub>O<sub>3</sub>.

The results of this study find closer agreement with the findings of Summers and Ausen (38) who studied the effect of varying Ce levels on the dispersion of Pt in 0.05 wt.% Pt/Al<sub>2</sub>O<sub>3</sub> catalysts. Samples were prepared by stepwise impregnation of  $\gamma$ -Al<sub>2</sub>O<sub>3</sub> spheres (120m<sup>2</sup>g<sup>-1</sup>) with Ce(NO<sub>3</sub>)<sub>3</sub> solution followed by impregnation with acidified H<sub>2</sub>PtCl<sub>6</sub> solution (38). Calcination was achieved at 500°C in air for 4h after both impregnation steps. Pt dispersions were evaluated using a flow CO chemisorption method. Based on the Ce loadings quoted (0-13 wt.% Ce), the atomic ratios of Pt:Ce in the samples studied were 1:0, 1:17, 1:36, 1:122, and 1:362. As the level of Ce increased in this range, the apparent dispersion of the fresh un-aged samples was found to decrease while the average Pt particle diameter increased from 11 to 28Å. The authors were unsure as to whether the loss of Pt dispersion with increasing Ce loading was due to agglomeration of the Pt during catalyst preparation or due to an interaction between Pt and Ce which inhibited CO chemisorption. The latter theory was suggested because Ce was found to interact with Pt in a manner that affected the Infra-Red stretching frequency of adsorbed CO on a Pt-13.0 wt.% Ce/Al<sub>2</sub>O<sub>3</sub> catalyst and also affected CO oxidation activity. As such, the authors were unsure as to whether the dispersion data was an accurate reflection of Pt particle size. It was noted that the intensity of the CO adsorption band in IR spectra was significantly greater for a Pt/Al<sub>2</sub>O<sub>3</sub> sample than the corresponding band for a sample containing 13.0 wt.% Ce, and this was thought to agree

with the chemisorption results i.e. Ce oxide apparently destabilised Pt with respect to sintering. The effect of increasing Ce loading on the Al<sub>2</sub>O<sub>3</sub> surface structure was unknown. Therefore it was not possible to speculate on how the Ce loading might affect interaction between the noble metal and the support material. The nature of metal-support interaction was deemed to be one of the factors controlling surface diffusional processes which were expected to be responsible for any agglomeration of Pt that might have occurred at the relatively low temperature used for calcination (38).

One possible explanation for loss of surface Pt at increased Ce loadings, as indicated by the results in Table 2.7, is loss of support surface area. Alder and Keavney (30) thought it unlikely that adsorption of chloroplatinic acid at low concentrations (0.1-0.8% Pt) on high surface area Al<sub>2</sub>O<sub>3</sub> (250m<sup>2</sup>g<sup>-1</sup>) could result in anything other than a discontinuous monolayer of chloroplatinate ions. Yao et al. (42, 55) reported that Pt which was deposited on  $\gamma$ -Al<sub>2</sub>O<sub>3</sub> was maintained in a dispersed phase at concentrations below 2.2 $\mu$ mol Pt/m<sup>2</sup> (BET), for samples which were heated in O<sub>2</sub> at temperatures up to 500°C after calcination at 400°C in air. At higher concentrations, Pt dispersion began to decrease due to inability of the support material to maintain Pt dispersion with excess Pt aggregating to form larger particles (55). The concentration of Pt in the 0.5% Pt catalysts investigated in this study was approximately 0.12 $\mu$ mol/m<sup>2</sup> of Al<sub>2</sub>O<sub>3</sub> which is considerably below this limiting value. As previously mentioned, addition of Ce to an Al<sub>2</sub>O<sub>3</sub> support has been found to result in a decrease of support surface area due to plugging of the Al<sub>2</sub>O<sub>3</sub> micropores (36, 38). In an investigation of 0.014 wt.% Rh/Ce/Al<sub>2</sub>O<sub>3</sub> catalysts, Oh and Eickel (36) found that the surface area of the Al<sub>2</sub>O<sub>3</sub> support (112m<sup>2</sup>g<sup>-1</sup>) decreased appreciably with increasing Ce loading in the range 0-15 wt.% for samples which were calcined at 500°C in air. However, this was thought to have a minimal effect on catalytic activity as the surface area was still high enough to maintain the noble metal reasonably well dispersed (36). Similarly, in this study, it seems unlikely that a simple decrease in support surface area could have been the only contributing factor to the loss of Pt dispersion, particularly for the higher level of Ce in sample PC17A for which dispersion decreased by ~50%. Even when taking into account the decrease in surface area of ~9% which was found after addition of 0.5% Pt and 3.6% Ce to the  $\gamma$ -Al<sub>2</sub>O<sub>3</sub> support for sample PC10A, the Pt concentration is still only 0.13 $\mu$ mol Pt/m<sup>2</sup> of sample. This is less than 6% of the saturation concentration of Pt in the dispersed phase as reported by Yao et al. (55). It should be noted that different calcination and pretreatment conditions were used in this study compared with those employed by Yao et al. (55). Thus, comparison may not be strictly valid as different heat treatments have been found to have different effects on Pt dispersion (47, 55). In particular, Yao et al. (55) reported that heat treatment in air or O<sub>2</sub> at  $\geq$ 600°C resulted in reduction or decomposition of dispersed Pt oxide to form metallic Pt which then

aggregated to form larger particles. As a calcination temperature of 630°C was used in this study, the concentration of Pt at which the Al<sub>2</sub>O<sub>3</sub> surface became saturated with dispersed metal was probably lower than that reported by Yao and co-workers (55).

As discussed previously, most authors (12, 41, 51, 53) attribute the dispersive effects of CeO<sub>2</sub> on supported Pt to the existence of a direct Pt-CeO<sub>2</sub> interaction which has been reported to maintain surface Pt in an oxidised state and thereby increase Pt stability against sintering. TPR profiles (see section 3.3.1) revealed the existence of a Pt-Ce surface interaction in the Pt-Ce/Al<sub>2</sub>O<sub>3</sub> samples used in this study which affected the reducibility of both of the metals. However, the chemisorption results indicate that, at higher levels of CeO<sub>2</sub>, this interaction caused a destabilisation of Pt dispersion in freshly calcined samples.

At lower temperatures (56) and smaller particle sizes (57), growth of Al<sub>2</sub>O<sub>3</sub>-supported Pt via sintering processes has been reported to be controlled by the mobility of Pt species along the substrate surface. Therefore, increased mobility of Pt is another factor which may have contributed to the formation of larger Pt crystallites, as indicated by H<sub>2</sub> uptake, for sample PC17A. One possibility is that the interaction of surface Pt and Ce could have resulted in greater diffusion of surface Pt, and thereby promoted sintering, during calcination at 630°C.

Loss of H<sub>2</sub> uptake might alternatively be explained if the nature of the Pt-CeO<sub>2</sub> interaction resulted in some form of coverage or encapsulation of surface Pt by Ce species. However, sample SPC8A had only a slightly lower Pt dispersion than sample SCP8A (79.8% vs. 87.4%), indicating that the sequence of impregnation did not have any great effect on the dispersion obtained which argues against the latter theory. If Pt was rendered inaccessible to H<sub>2</sub> adsorption due to a 'coverage' effect by the added CeO<sub>2</sub>, then one might expect sample SPC8A, in which Ce deposition followed that of Pt, to have a considerably lower Pt dispersion than sample SCP8A in which the reverse impregnation sequence was used. As discussed below, Ce was found to be in strong contact with the Al<sub>2</sub>O<sub>3</sub> surface. Thus, it may be improbable that Ce species would have been sufficiently mobile to migrate to the surface during calcination and cover the Pt. The slightly lower H<sub>2</sub> uptake for sample SPC8A relative to sample SCP8A may have been due to increased sintering of Pt in the former sample which might be expected as it had been exposed to two calcination steps at 630°C while Pt in the latter sample was only exposed to the standard 15 minutes calcination procedure.

Pt dispersion may also have been affected indirectly due to an interaction between CeO<sub>2</sub> and Al<sub>2</sub>O<sub>3</sub>. As discussed above, Summers and Ausen (38) postulated that deposition of CeO<sub>2</sub> on an Al<sub>2</sub>O<sub>3</sub> substrate might change the surface structure in such a

manner that could affect surface diffusional processes and hence the agglomeration of dispersed Pt during calcination. The formation of a cerium-alumina surface compound has been reported in the literature (40,41,58). XPS analysis, the results of which are presented in section 3.3.1 of this study, indicated the existence of a  $\text{CeO}_2\text{-Al}_2\text{O}_3$  interaction in Pt-Ce/ $\text{Al}_2\text{O}_3$  samples, which resulted in a  $\text{CeAlO}_3$ -like spectrum for Ce in the 3d region. This has been reported by Shyu et al. (58) to be due to the existence of a strong interaction between dispersed Ce and the  $\text{Al}_2\text{O}_3$  support which also affected the reducibility of supported ceria as shown by TPR studies. Similarly, in this study, a considerably different TPR profile was exhibited by sample C10A than that for unsupported  $\text{CeO}_2$  (see section 3.3.1). Therefore, the possibility that decreased Pt dispersion, on addition of Ce, was due to a Ce- $\text{Al}_2\text{O}_3$  interaction which affected the interaction of Pt with the support material and, thereby, Pt mobility on the support surface must be considered. In a similar manner, it has been reported (59) that addition of 1 atomic% Zr to high purity Ni affected the wetting and adhesion of the liquid Ni drops on  $\alpha\text{-Al}_2\text{O}_3$ . It was found, using electron photomicrographs, that Zr was concentrated in the vicinity of the Ni-substrate interface and chemically reduced the  $\text{Al}_2\text{O}_3$  support thereby weakening its structure. This was found to result in decreased adhesion of the Ni drop to the support with an increase in wetting angle of the drop to the support surface (59). If the wetting angle between supported metal crystallites and the support increases, then surface mobility should also increase (56).

Another possibility is that Ce interaction with  $\text{Al}_2\text{O}_3$  resulted in some form of extreme blocking of the surface sites associated with Pt adsorption, in which case Pt dispersion might have decreased even in the absence of increased surface mobility if the number of sites available for adsorption of chloroplatinate species was decreased dramatically.

As seen in Table 2.7, addition of Zr to 0.5% Pt/ $\text{Al}_2\text{O}_3$  at an atomic ratio of 1:10-Pt:Zr was found to have no discernible effect on Pt dispersion as measured by  $\text{H}_2$  chemisorption. A similar result was reported by Summers and Ausen (38) for a 0.05% Pt-0.2% Zr/ $\text{Al}_2\text{O}_3$  sample containing approximately the same atomic ratio of the two metals. However, at higher loadings (0.7-8.5 wt.%), Zr did result in a slight decrease in Pt dispersion. For catalysts containing Pt:Zr atomic ratios of approximately 1:30, 1:120, and 1:356, Pt dispersions of 0.96, 0.91, and 0.83, respectively, were reported compared to a value of 1.05 for a Pt-only sample (38)

Summers and Ausen (38) concluded that while Ce oxide interacted strongly with  $\text{Al}_2\text{O}_3$ -supported Pt to affect noble metal dispersion,  $\text{ZrO}_2$  did not. A similar conclusion could be reached for the dispersion data obtained in this study using lower

levels of Ce and Zr. However, any such conclusion would be tentative due to the fact that the effect of varying the Zr content of the catalysts was not determined.

The most important findings were that Pt was highly dispersed in the prepared samples, and that the presence of Ce appeared to cause a decrease of available Pt surface area, particularly, when the Pt:Ce atomic ratio was greater than or equal to 8:1. Considering the low concentration of Pt used, the decrease in H<sub>2</sub> uptake with increasing Ce content is most likely attributed to the existence of Pt-Ce and/or Ce-Al<sub>2</sub>O<sub>3</sub> interactions which affected either the degree of Pt sintering during calcination or the ability of dispersed Pt to adsorb hydrogen.

## **2.4 Summary**

A series of Al<sub>2</sub>O<sub>3</sub>-supported, Pt and bimetallic (Pt-Ce, Pt-Mn, Pt-Zr), catalysts were prepared by 'wet' impregnation of the support with ethanolic metal salt solutions. 0.5 wt.% Pt/CeO<sub>2</sub> and 0.5 wt.% Pt/ZrO<sub>2</sub> catalysts were prepared in the same manner.

The BET surface areas of the powdered support materials were determined to be 221m<sup>2</sup>g<sup>-1</sup>, 36m<sup>2</sup>g<sup>-1</sup>, and 5m<sup>2</sup>g<sup>-1</sup>, for  $\gamma$ -Al<sub>2</sub>O<sub>3</sub>, CeO<sub>2</sub>, and ZrO<sub>2</sub>, respectively.

Atomic Absorption Spectroscopy was employed to determine the metal content of the Al<sub>2</sub>O<sub>3</sub>-supported samples. The results showed that the Pt concentrations were in close agreement ( $\pm 0.10$  wt.% for all but one sample) with the nominal loadings expected based on the amount of H<sub>2</sub>PtCl<sub>6</sub> used for impregnation.

H<sub>2</sub> chemisorption results indicated that, on increasing the concentration of Pt from 0.5-5.6 wt.% on  $\gamma$ -Al<sub>2</sub>O<sub>3</sub>, the Pt surface area increased with a concomitant decrease in Pt dispersion.

For 0.5 wt.% Pt/ $\gamma$ -Al<sub>2</sub>O<sub>3</sub> catalysts, H<sub>2</sub> uptakes at room temperature showed that, in general, a very high dispersion of Pt was achieved by the preparation procedure employed for both Pt-only and bimetallic samples. The average apparent Pt particle diameter varied from 11 to 28Å. For bimetallic samples, it was found that the presence of Cr and Zr, at ten times the atomic concentration of Pt, had no discernible effect on Pt dispersion. However, the presence of Ce, particularly at higher levels ( $\geq 8:1$ -Ce:Pt atomic ratio), resulted in a decrease in Pt surface area and apparent Pt dispersion. Uncertainties in the nature of surface interactions made interpretation of the results for Pt-Ce samples difficult.

For nominal 0.5 wt.% Pt/CeO<sub>2</sub> and 0.5 wt.% Pt/ZrO<sub>2</sub> samples, Pt dispersion was significantly lower, than in the Al<sub>2</sub>O<sub>3</sub>-supported catalysts, presumably due to the lower support surface area. Average apparent Pt particle diameters were determined as 58 and 349Å for Pt/CeO<sub>2</sub> and Pt/ZrO<sub>2</sub>, respectively.

Aging of a 0.5 wt.% Pt/Al<sub>2</sub>O<sub>3</sub> sample in air at 800°C resulted in a considerable loss of H<sub>2</sub> chemisorption capacity. This was attributed to sintering of dispersed Pt to produce larger Pt crystallites. The average apparent Pt particle diameter in the aged sample was 133Å.

## REFERENCES

- (1) Geus, J. W. and van Veen, J. A. R., in "Catalysis" (Moulijn, J. A., van Leeuwen, P. W. N. M. and van Santen, R. A., eds.), Studies in Surface Science and Catalysis, Vol. 79, 335-360, Elsevier, Amsterdam, 1993.
- (2) Völter, J., Lietz, G., Spindler, H. and Lieske, H., *J. Catal.* **104**, 375 (1987).
- (3) Otto, K., Andino, J. M. and Parks, C. L., *J. Catal.* **131**, 243 (1991).
- (4) Anderson, J. R. and Pratt, K. C., "Introduction to Characterization and Testing of Catalysts", Academic Press, Australia, 1985.
- (5) Lemaitre, J. L., Menon, P. G. and Delannay, F., in "Characterisation of Heterogeneous Catalysts" (Delannay, F., ed.), 299-365, Dekker Press, New York, 1984.
- (6) Campbell, I. M., "Catalysis at Surfaces", University Press, Cambridge, 1988.
- (7) Willard, H. H., Merritt Jr., L. L., Dean, J. A. and Settle Jr., F. A., "Instrumental Methods of Analysis", Wadsworth Press, California, 1988.
- (8) Hicks, R. F., Qi, H., Young, M. L. and Lee, R. G., *J. Catal.* **122**, 280 (1990).
- (9) Briot, P., Auroux, A., Jones, D. and Primet, M., *Appl. Catal.* **59**, 141 (1990).
- (10) Baldwin, T.R. and Burch, R., *Appl. Catal.* **66**, 337 (1990).
- (11) Carballo, L. M. and Wolf, E. E., *J. Catal.* **53**, 366 (1978).
- (12) Diwell, A. F., Rajaram, R. R., Shaw, H. A. and Truex, T. J., in "Catalysis and Automotive Pollution Control II" (Crucq, A., ed.), Studies in Surface Science and Catalysis, Vol. 71, 139-152, Elsevier, Amsterdam, 1991.
- (13) Kooh, A. B., Han, W. J., Lee, R. G. and Hicks, R. F., *J. Catal.* **130**, 374 (1991).
- (14) Scholten, J. J. F., in "Preparation of Catalysts 2" (Delmon, B., Grange, P., Jacobs, P. and Poncelet, G., eds.), Studies in Surface Science and Catalysis, Vol. 3, 685-714, Elsevier, Amsterdam, 1979.
- (15) Scholten, J. J. F., Pijpers, A. P. and Hustings, A. M. L., *Catal. Rev. Sci. Eng.* **27**, 151 (1985).
- (16) Levy, R. B. and Boudart, M., *J. Catal.* **32**, 304 (1974).
- (17) Robell, A. J., Ballou, E. V. and Boudart, M., *J. Phys. Chem.* **68**, 2748 (1964).
- (18) Gruber, H. L., *J. Phys. Chem.* **66**, 48 (1962).
- (19) Den Otter, G. J. and Dautzenberg, F. M., *J. Catal.* **53**, 116 (1978).
- (20) Wilson, G. R. and Hall, W. K., *J. Catal.* **17**, 190 (1970).
- (21) Hubbard, C. P., Otto, K., Gandhi, H. S. and Ng, K. Y. S., *J. Catal.* **144**, 484 (1993).
- (22) Fierro, J. L. G. and Garcia De La Banda, J. F., *Catal. Rev. Sci. Eng.* **28**, 265 (1986).
- (23) Gruber, H. L., *Anal. Chem.* **134**, 1828 (1962).
- (24) Freel, J., *J. Catal.* **25**, 139 (1972).
- (25) Freel, J., *J. Catal.* **25**, 149 (1972).
- (26) Vannice, M. A., Benson, J. E. and Boudart, M., *J. Catal.* **16**, 348 (1970).
- (27) Lieske, H., Lietz, G., Spindler, H. and Völter, J., *J. Catal.* **81**, 8 (1983).
- (28) Duivenvoorden, F. B. M., Kip, B. J., Koningsberger, D. C. and Prins, R., *J. Phys. Colloq.* **C8**, 227 (1986).
- (29) Mc. Cabe, R. W., Wong, C. and Woo, H. S., *J. Catal.* **114**, 354 (1988).
- (30) Alder, S. F. and Keavney, J. J., *J. Phys. Chem.* **64**, 208 (1960).
- (31) Frennet, A. and Wells, P. B., *Appl. Catal.* **18**, 243 (1985).
- (32) Cullis, C. F. and Willatt, B. M., *J. Catal.* **83**, 267 (1983).
- (33) Akubuiro, E. C., Verykios, X. E. and Lesnick, L., *Appl. Catal.* **14**, 215 (1985).

- (34) Su, E. C., Montreuil, C. N. and Rothschild, W. G., *Appl. Catal.* **17**, 75 (1985).
- (35) Yu-Yao, Y. F., *J. Catal.* **87**, 152 (1984).
- (36) Oh, S. H. and Eickel, C. C., *J. Catal.* **112**, 543 (1988).
- (37) Engler, B., Koberstein, E. and Schubert, P., *Appl. Catal.* **48**, 71 (1989).
- (38) Summers, J. C. and Ausen, S. A., *J. Catal.* **58**, 131 (1979).
- (39) Bond, G. C. and Hui, L., *J. Catal.* **147**, 346 (1994).
- (40) Le Normand, F., Hilaire, L., Kili, K., Krill, G. and Maire, G., *J. Phys. Chem.* **92**, 2561 (1988).
- (41) Shyu, J. Z. and Otto, K., *J. Catal.* **115**, 16 (1989).
- (42) Yao, H. C., Gandhi, H. S. and Shelef, M., in "Metal-Support and Metal-Additive Effects in Catalysis" (Imelik, B., Naccache, C., Coudurier, G., Praliaud, H., Meriaudeau, P., Gallezot, P., Martin, G. A. and Vedrine, J. C., eds.), Studies in Surface Science and Catalysis, Vol. 11, 159-169, Elsevier, Amsterdam, 1982.
- (43) Yao, H. C. and Yu-Yao, Y. F., *J. Catal.* **86**, 254 (1984).
- (44) Harrison, B., Diwell, A. F. and Hallett, C., *Plat. Met. Rev.* **32**, 73 (1988).
- (45) Spenadel, L. and Boudart, M., *J. Phys. Chem.* **64**, 204 (1960).
- (46) Harris, P. J. F., *J. Catal.* **97**, 527 (1986).
- (47) Dautzenberg, F. M. and Wolters, H. B. M., *J. Catal.* **51**, 26 (1978).
- (48) Curley, J.W., Dreelan, M. J. and Finlayson, O. E., *Catal. Today* **10**, 401 (1991).
- (49) Yermakov, Y. I., *Catal. Rev. Sci. Eng.* **13**, 77 (1976).
- (50) Yermakov, Y. I. and Kuznetsov, B. N., *J. Mol. Catal.* **9**, 13 (1980).
- (51) Silver, R. G., Summers, J. C. and Williamson, W. B., in "Catalysis and Automotive Pollution Control II" (Crucq, A., ed.), Studies in Surface Science and Catalysis, Vol. 71, 167-180, Elsevier, Amsterdam, 1991.
- (52) Gandhi, H. S. and Shelef, M., in "Catalysis and Automotive Pollution Control" (Crucq, A. and Frennet, A., eds.), Studies in Surface Science and Catalysis, Vol. 30, 199-214, Elsevier, Amsterdam, 1987.
- (53) Murrell, L. L., Tauster, S. J. and Anderson, D. R., in "Catalysis and Automotive Pollution Control II" (Crucq, A., ed.), Studies in Surface Science and Catalysis, Vol. 71, Pg. 275-289, Elsevier, Amsterdam, 1991.
- (54) Hegedus, L. L., Summers, J. C., Schlatter, J. C. and Baron, K., *J. Catal.* **56**, 321 (1979).
- (55) Yao, H. C., Sieg, M. and Plummer Jr., H. K., *J. Catal.* **59**, 365 (1979).
- (56) Ruckenstein, E. and Pulvermacher, B., *J. Catal.* **29**, 224 (1973).
- (57) Wynblatt, P., in "Growth and Properties of Metal Clusters" (Bourdon, J, ed.), Studies in Surface Science and Catalysis, Vol. 4, 15-33, Elsevier, Amsterdam, 1980.
- (58) Shyu, J. Z., Weber, W. H. and Gandhi, H. S., *J. Phys. Chem.* **92**, 4964 (1988).
- (59) Reference (30) in (56.).

## **CHAPTER 3**

### **Study of Pt/Al<sub>2</sub>O<sub>3</sub>, Pt-Ce/Al<sub>2</sub>O<sub>3</sub> and Pt/CeO<sub>2</sub> Catalysts**

### **3.1 Introduction**

In this chapter, surface characterisation of the Pt/Al<sub>2</sub>O<sub>3</sub>, Pt-Ce/Al<sub>2</sub>O<sub>3</sub> and Pt/CeO<sub>2</sub> samples is discussed. The techniques used for characterisation were Temperature Programmed Reduction (TPR), X-ray Photoelectron Spectroscopy (XPS) and H<sub>2</sub> Chemisorption. An investigation of the activity of the samples for the oxidation of i-C<sub>4</sub>H<sub>10</sub>, both before and after TPR, is also discussed. In addition, the effects of different aging treatments on the activity and surface properties of the catalysts are examined. The activity and surface properties of a Pt/ZrO<sub>2</sub> catalyst, before and after aging, are also examined and compared with Pt/Al<sub>2</sub>O<sub>3</sub>.

Previous studies concerning the effects of Ce on the activity of supported noble metal catalysts for the complete oxidation of CO and hydrocarbons were reviewed in section 1.4.

For CO oxidation (see section 1.4.2), several studies found that the presence of CeO<sub>2</sub> can improve the activity of pre-reduced noble metal catalysts (1-7). Yu-Yao (8) reported that the activity of reduced Pt/CeO<sub>2</sub>/Al<sub>2</sub>O<sub>3</sub> catalysts was considerably greater than that of unreduced Pt/Al<sub>2</sub>O<sub>3</sub> or Pt/CeO<sub>2</sub>/Al<sub>2</sub>O<sub>3</sub> samples at equivalent Pt loadings under O<sub>2</sub>-rich conditions.

The effect of CeO<sub>2</sub> on the hydrocarbon oxidation activity of noble metals, and in particular Pt, is of greater relevance to this study. A brief summary of the main observations of some studies, previously discussed in section 1.4.3, will now be given.

Under oxidising conditions, Pt/CeO<sub>2</sub>/Al<sub>2</sub>O<sub>3</sub> catalysts were reported to be less active than corresponding Pt/Al<sub>2</sub>O<sub>3</sub> samples for the oxidation of alkanes (9-13). This was attributed by several authors to an increased oxidation of surface Pt sites in the presence of CeO<sub>2</sub> (9, 11, 12, 13), while Gandhi and Shelef (10) attributed lower activity to an improved dispersion of Pt particles. In this latter study, Ce was thought to prevent the agglomeration of dispersed Pt into larger metallic particles necessary for hydrocarbon oxidation (10). For Pd/Al<sub>2</sub>O<sub>3</sub> catalysts, CeO<sub>2</sub> addition was similarly reported to result in decreased alkane oxidation activity in an oxidising environment, which was attributed to the conversion of Pd to less active PdO (9, 11, 14). Under non-oxidising conditions, the effects of CeO<sub>2</sub> on noble metal oxidation activity were reported to be less dramatic. Shyu et al. (14) reported that CeO<sub>2</sub> only caused deactivation of Pd for C<sub>3</sub>H<sub>8</sub> oxidation when the O<sub>2</sub> concentration exceeded that of the stoichiometric ratio. Similarly, Oh et al. (11) found that under reducing conditions the main influence of Ce, on the oxidation of CH<sub>4</sub> over Pd/Al<sub>2</sub>O<sub>3</sub> or Pt/Al<sub>2</sub>O<sub>3</sub> catalysts, was in reducing the amount of CO produced at

higher temperatures. Low temperature CH<sub>4</sub> oxidation was not as adversely affected as it was under O<sub>2</sub>-rich conditions (11). The effect of reductive pretreatments on the alkane oxidation activity of Ce-containing noble metal catalysts has been investigated by several authors (6, 7, 9, 12, 13).

Engler et al. (6) investigated the activity of pre-reduced Pt/Al<sub>2</sub>O<sub>3</sub>, Pt/CeO<sub>2</sub> and Pt/CeO<sub>2</sub>/Al<sub>2</sub>O<sub>3</sub> samples for the conversion of CO and hydrocarbons in a simulated exhaust gas mixture. Under reducing conditions, the presence of CeO<sub>2</sub> had a strong positive effect on CO activity but hydrocarbon conversions were highest on the Pt/Al<sub>2</sub>O<sub>3</sub> sample (6)

Yu-Yao (9) reported that the activity of Pt/CeO<sub>2</sub>/Al<sub>2</sub>O<sub>3</sub> and Pd/CeO<sub>2</sub>/Al<sub>2</sub>O<sub>3</sub> catalysts for the oxidation of C<sub>1</sub>-C<sub>4</sub> alkanes, at an O<sub>2</sub>:alkane ratio of twice the stoichiometric ratio, was improved after pre-reduction. The effects of reduction were reported to be slowly reversed upon exposure to the O<sub>2</sub>-rich reaction conditions. The stability of the more active reduced state was greater for Pt than for Pd with only a transient high activity noticed immediately after reduction in the latter case (9).

Improvements in the activity of CeO<sub>2</sub>-containing three-way catalysts were reported to occur by Nunan et al (7) after in-situ activation in a synthetic exhaust gas mixture. Activation was associated with the reduction of Pt-CeO<sub>2</sub> interactive sites by low levels of H<sub>2</sub> in the test gas. This was thought to result in the production of highly active sites involving reduced noble metal in contact with reduced surface Ce. The main benefit of CeO<sub>2</sub>, present either as the support material or as an additive in Al<sub>2</sub>O<sub>3</sub>-supported catalysts, was in improved CO light-off activity after activation. The removal of CO at lower temperatures was proposed to prevent CO inhibition and thereby also allow for more effective hydrocarbon removal in the presence of Ce (7).

Diwell et al. (12) reported dramatic changes in the low temperature activity of Pt/CeO<sub>2</sub> catalysts after pre-reduction. Dramatic improvements in the low temperature conversions of CO, NO, and C<sub>3</sub>H<sub>6</sub> were observed while, at the same time, the oxidation of CH<sub>4</sub> and C<sub>3</sub>H<sub>8</sub> was adversely affected in a slightly fuel-rich gas mixture. These changes were attributed to the existence of a Pt-CeO<sub>2</sub> interaction during catalyst reduction (12).

Pirault et al. (13) reported that CeO<sub>2</sub> had an adverse effect on the activity of calcined Pt/Al<sub>2</sub>O<sub>3</sub> for the oxidation of C<sub>3</sub>H<sub>6</sub> and C<sub>3</sub>H<sub>8</sub>. Following reduction of the calcined samples, inhibition of alkane oxidation activity by CeO<sub>2</sub> was still exhibited, while alkene oxidation was no longer adversely affected (13).

In this chapter, the activity of Pt/Al<sub>2</sub>O<sub>3</sub>, Pt/CeO<sub>2</sub> and Pt-Ce/Al<sub>2</sub>O<sub>3</sub> catalysts for i-C<sub>4</sub>H<sub>10</sub> combustion, both before and after reduction, is examined.

The effects of catalyst aging in different environments on i-C<sub>4</sub>H<sub>10</sub> conversion is also investigated.

Silver et al. (15) examined the activity of Pt automotive catalysts after engine-aging under fuel-lean conditions. CO and hydrocarbon conversions over the aged samples were found to be improved, especially under stoichiometric conditions, by the addition of Ce to the Al<sub>2</sub>O<sub>3</sub> washcoat. The effects of Ce were attributed to a stabilisation of Pt dispersion during aging by maintaining some of the Pt in a partially oxidised state which was more difficult to sinter. It was noted that ceria may also have improved the activity of Pt by acting as an oxygen source for CO conversion (15). In apparent contradiction with Silver et al. (15), Gandhi and Shelef (10) reported that stabilisation of Pt dispersion by CeO<sub>2</sub> was expected to result in decreased activity for structure-sensitive reactions, such as the oxidation of hydrocarbons.

As discussed in section 1.3 of this thesis, the oxidation of alkanes on Pt/Al<sub>2</sub>O<sub>3</sub> has been reported by several authors to be a structure sensitive reaction which proceeds at a faster rate on larger Pt crystallites rather than highly dispersed particles (9, 16-20). Thus, it was of interest to investigate this theory in the catalysts being investigated in the present study. In order to do this, Pt/Al<sub>2</sub>O<sub>3</sub>, Pt/CeO<sub>2</sub> and Pt-Ce/Al<sub>2</sub>O<sub>3</sub> catalysts were aged under high temperature conditions expected to cause sintering of dispersed Pt into larger particles. The i-C<sub>4</sub>H<sub>10</sub> oxidation activity of the aged samples was then investigated and comparisons were made with the activity of the unaged samples and with the activity of a Pt/ZrO<sub>2</sub> catalyst. The effects of aging on the state of the catalyst surfaces were examined using H<sub>2</sub> chemisorption, TPR, and XPS techniques.

A brief introduction to the use of TPR and XPS techniques for catalyst characterisation will now be given and some relevant studies of supported catalysts will be discussed.

### 3.1.1 Temperature Programmed Reduction (TPR).

Reduction is often an important activation step in the preparation of supported metal catalysts (21). Hence, methods which follow the reduction process of catalyst surfaces can be of considerable value in surface characterisation. Temperature Programmed Reduction (TPR) is such a technique (21, 22).

In TPR, an inert gas containing a specified concentration of a reducing gas (typically H<sub>2</sub> or CO) is continuously passed over the catalyst sample while the

temperature is raised linearly with time. The difference between the inlet and outlet concentrations of the gas mixture is monitored as a function of temperature producing a reduction profile. The resulting TPR profile contains information on the nature of the reducible species present in the sample (22, 23). If, for example, chemisorbed oxygen was present on the surface in two different binding states with considerably different reactivities towards reduction, then one would expect the TPR profile to exhibit two distinct peaks. The peak temperatures would correspond to the temperatures at which each species was reduced. TPR has found applications in the study of Pt catalysts to investigate the nature of the Pt species present, and to determine changes in catalyst properties arising from different methods of preparation and/or activation e.g. see reference (24).

TPR profiles can also be used to show interactions between the catalyst components, which can affect the nature of the reducible sites present. This may involve an interaction between the metal and the support material e.g. Pt and Al<sub>2</sub>O<sub>3</sub> (25), or in the case of bimetallic catalysts, (e.g. Pt-Ce), interaction between the two supported metals (7). The latter is made possible by the fact that if the two metals are present as single component separate particles, then the TPR profile of the bimetallic system is expected to be a linear combination of the two single component profiles. However, if the components are closely associated, one may expect some degree of synergism between them in the reduction process, so that a linear combination of single component profiles no longer occurs. The origin of this synergism may, for example, lie in the catalytic effect an easily reducible metal can have on the subsequent reduction of the other catalyst component. In such a case, the reduction peaks for the two components would be brought closer to each other in the resulting profile (23).

Some of the literature on the study of Pt/Al<sub>2</sub>O<sub>3</sub>, Pt-Ce/Al<sub>2</sub>O<sub>3</sub>, and Pt/CeO<sub>2</sub> catalysts by TPR will now be reviewed. It is important to note that care must be taken when comparing TPR profiles obtained in different laboratories due to experimental effects (24). For example, variation in flow rates and mass of sample used can affect the reduction peak temperature and resolution, respectively.

### **TPR Studies of Pt/Al<sub>2</sub>O<sub>3</sub>**

For Pt/ $\gamma$ -Al<sub>2</sub>O<sub>3</sub> catalysts a considerable interaction between the Pt species and the support has been reported, which fixes Pt chemically to the support during calcination, so that upon subsequent reduction the Pt<sup>0</sup> species formed remains in intimate contact with the Al<sub>2</sub>O<sub>3</sub> (24, 26). This interaction has been postulated as important in helping to achieve a high degree of metal dispersion on the support material (24, 26). Several TPR studies have revealed that the existence of such a metal support interaction

can result in Al<sub>2</sub>O<sub>3</sub>-supported Pt requiring a higher reduction temperature than that required by unsupported Pt oxides and chlorides e.g. (24, 25, 27, 28, 29).

Mc Nicol and Short (30) examined the TPR of unsupported Adam's PtO<sub>2</sub>. A 95 vol.% N<sub>2</sub>: 5 vol.% H<sub>2</sub> gas stream was used as the reducing gas with a heating rate of 5-10°Cmin.<sup>-1</sup>. The resulting profile consisted of two peaks, one at room temperature and another at 80°C. The total H<sub>2</sub> uptake was found to correspond to that required for complete reduction of Pt<sup>4+</sup> to Pt<sup>0</sup> with the major fraction of the reduction process associated with the room temperature peak (30). The TPR profiles of Pt/Al<sub>2</sub>O<sub>3</sub> systems have been found in several investigations to exhibit reduction features at considerably higher temperatures. For example, Ebitani and Hattori (31) studied the TPR of a 0.6 wt.% Pt/Al<sub>2</sub>O<sub>3</sub> catalyst which was prepared by impregnation with H<sub>2</sub>PtCl<sub>6</sub> followed by drying at 110°C and calcination at 400°C. TPR experiments were performed in a 3% H<sub>2</sub>/Ar mixture after further calcination at 300°C and treatment in Ar flow in-situ at 300°C for 2h. On heating the catalyst sample to 450°C at 10°Cmin.<sup>-1</sup>, the profile obtained consisted of a single apparent H<sub>2</sub> consumption peak at 254°C which was thought to be attributable to the reduction of Pt oxides formed during calcination. A H<sub>2</sub>/Pt value of 1 was found indicating that Pt was present as PtO prior to TPR (31).

In a review of TPR studies of supported and unsupported Pt species, Hurst et al. (24) reported that the reduction profile of Pt/ $\gamma$ -Al<sub>2</sub>O<sub>3</sub> reforming catalysts had been typically reported to exhibit a single peak at ca.280°C with a H<sub>2</sub> consumption corresponding to a 4-electron process. It was noted that this temperature was considerably higher than that which had been reported for the reduction of unsupported tetravalent Pt chlorides or oxides. This indicated the existence of some form of chemical interaction between the Pt species and  $\gamma$ -Al<sub>2</sub>O<sub>3</sub> which stabilises surface Pt species against reduction. This interaction was thought most likely to occur during calcination of the reforming catalysts at ca.500°C (24).

Using TPR, Yao et al. (25) found that Pt oxide deposited on  $\gamma$ -Al<sub>2</sub>O<sub>3</sub> was present in two phases, namely, a particulate phase in which the Pt oxide was aggregated and had little interaction with the support, and a dispersed phase in which the Pt oxide had considerable interaction with the Al<sub>2</sub>O<sub>3</sub>. Samples with different Pt loading were prepared by impregnation of  $\gamma$ -Al<sub>2</sub>O<sub>3</sub> with aqueous H<sub>2</sub>PtCl<sub>6</sub> followed by drying at 120°C and calcining in air at 400°C for 2h. After further calcination in air at 500°C, TPR experiments were conducted using a flow of H<sub>2</sub>:Ar (15:85) gas mix as the sample temperature was increased at 8°Cmin.<sup>-1</sup>. The resulting profiles showed that unsupported PtO<sub>2</sub> was reduced below 25°C with a maximum rate at ca.5°C, while  $\gamma$ -Al<sub>2</sub>O<sub>3</sub> supported

samples showed varying reduction features in the temperature range -75 to 500°C. The profiles obtained are illustrated in Figure 3.1.

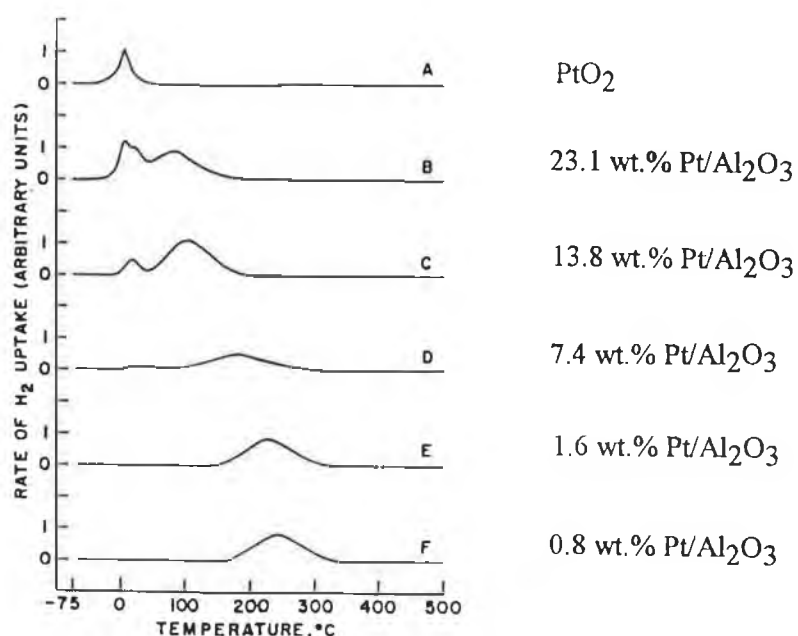
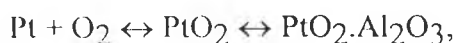


**Figure 3.1 : TPR profiles of PtO<sub>2</sub> and Pt/γ-Al<sub>2</sub>O<sub>3</sub> samples (25).**

From Fig. 3.1, it can be seen that higher Pt loadings on γ-Al<sub>2</sub>O<sub>3</sub> showed two reduction peaks, one of which corresponded approximately to the reduction temperature of unsupported PtO<sub>2</sub> and was assigned to a particulate PtO<sub>2</sub> phase. A higher temperature reduction peak was also apparent and was associated with the presence of more dispersed Pt oxide. At Pt loadings ≤1.6wt.%, only dispersed phase Pt oxide was found. H<sub>2</sub> uptake measurements during these reductions indicated that Pt oxide in the dispersed phase was PtO<sub>2</sub>, while Pt in the particulate phase was probably a mixture of PtO<sub>2</sub>, PtO, and metallic Pt. As the Pt content was lowered, the reduction temperature increased. This was thought to indicate that PtO<sub>2</sub> molecules experienced greater interaction with the support material due to improved dispersion and closer contact with the Al<sub>2</sub>O<sub>3</sub>. This interaction was suggested to involve either dissolution of the PtO<sub>2</sub> into the surface layer of Al<sub>2</sub>O<sub>3</sub>, or the formation of a PtO<sub>2</sub>-Al<sub>2</sub>O<sub>3</sub> complex (25, 27). Formation of this latter complex, according to the reaction,



was proposed by Johnson and Keith (26) to explain changes in the dispersion of Pt with oxidation conditions (different temperature and O<sub>2</sub> partial pressure) in a 0.6 wt.% Pt/Al<sub>2</sub>O<sub>3</sub> catalyst.

Huizinga et al. (21) also reported that there was a substantial interaction between  $\text{PtO}_2$  and  $\text{Al}_2\text{O}_3$  in a 5.2 wt.%  $\text{Pt}/\gamma\text{-Al}_2\text{O}_3$  catalyst which stabilised  $\text{PtO}_2$  particles on the  $\text{Al}_2\text{O}_3$  surface. The influence of drying, calcination, and passivation procedures on the TPR profile of Pt on  $\text{Al}_2\text{O}_3$  and  $\text{TiO}_2$  was investigated. Samples were prepared via a combined ion exchange and wet impregnation technique using  $\text{Pt}(\text{NH}_3)_4(\text{OH})_2$  as the precursor salt. TPR experiments were performed using a 5%  $\text{H}_2/\text{Ar}$  mix at a flow rate of  $300 \text{ cm}^3\text{h}^{-1}$  with a sample heating rate of  $5^\circ\text{Cmin}^{-1}$ . The reduction profiles obtained for 5%  $\text{Pt}/\text{Al}_2\text{O}_3$  after various pretreatments are shown in Fig. 3.2.

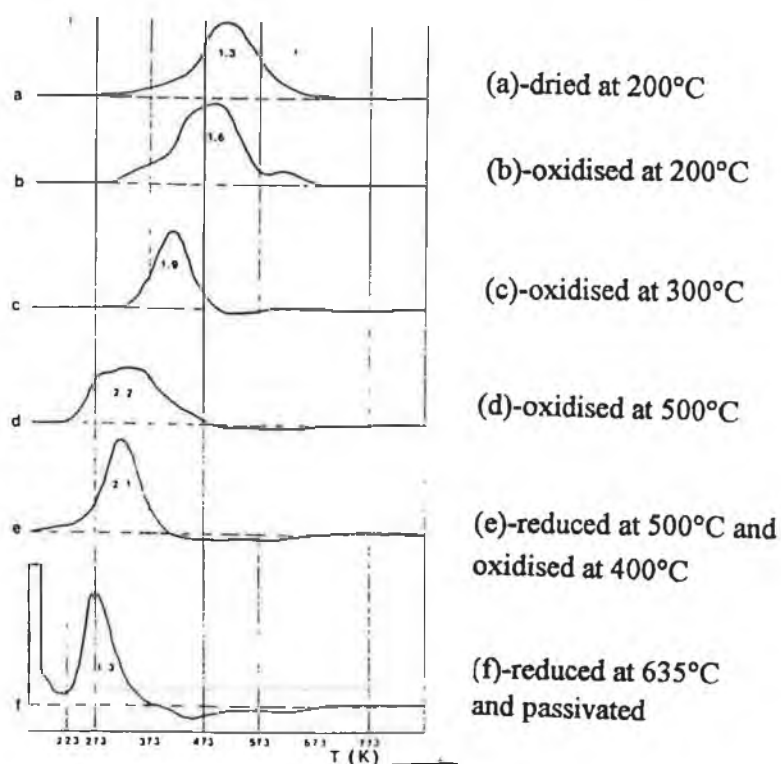


**Figure 3.2 : Reduction of  $\text{Pt}/\text{Al}_2\text{O}_3$  catalysts (21).** The values under the reduction peaks represent the total  $\text{H}_2$  consumption ( $\text{H}_2/\text{metal}$  value) for the entire TPR run.

The reduction peaks observed were asymmetric and broad indicating that several reducible Pt species were present (21). The profiles indicated that the reduction peak temperature of  $\text{Pt}/\text{Al}_2\text{O}_3$  was dependent on the temperature of oxidation after impregnation and drying. As the calcination temperature increased, the reduction peak shifted to lower temperatures and  $\text{H}_2$  consumption increased. This was ascribed to the formation of small  $\text{PtO}_2$  particles during oxidation which were reduced more easily than the original isolated  $\text{Pt}^{2+}$  ions present after drying of the impregnated sample (21).

These supported PtO<sub>2</sub> particles were found to be stabilised against decomposition during temperature programmed oxidation (TPO) by interaction with the Al<sub>2</sub>O<sub>3</sub> support (21). TPO experiments revealed that the decomposition of PtO<sub>2</sub> particles was shifted to higher temperatures for a pre-reduced Pt/Al<sub>2</sub>O<sub>3</sub> sample relative to bulk PtO<sub>2</sub>. The interaction of Pt with TiO<sub>2</sub> and SiO<sub>2</sub> supports was found to be considerably weaker, with PtO<sub>2</sub> decomposition occurring at lower temperatures than on Al<sub>2</sub>O<sub>3</sub> (21).

After passivation, the catalysts consisted of a metal core surrounded by a metal oxide skin (21). The passivation procedure involved firstly reducing the catalyst at 635° C, after which the passivation step involved slowly admitting O<sub>2</sub> to a stream of N<sub>2</sub> which was used to replace the H<sub>2</sub> from the reduction step. For passivated samples (see Fig. 3.2(f)), reduction of Pt/Al<sub>2</sub>O<sub>3</sub> was achieved even at -50°C. Due to the presence of the metallic core, H<sub>2</sub> could be dissociatively chemisorbed at low temperatures and induced reduction of the oxide surface layer (21).

McCabe et al. (32) reported that Pt oxidation by gaseous O<sub>2</sub> had a highly passivating nature. Oxidation was found to be essentially limited to the surface exposed layer of metal atoms for both bulk Pt and supported Pt particles with mean radii  $\geq 7.5\text{\AA}$ . This theory was postulated on the basis of TPR, chemisorption, x-ray scattering, and EXAFS data, which indicated that oxidation led to the formation of a surface film of oxide species on the Pt particles. The thickness of this film was less than or equal to one monolayer involvement of Pt atoms regardless of O<sub>2</sub> pressure (0.05-1.0 atm.), temperature (300-600°C), or length of O<sub>2</sub> exposure (2-250h). TPR experiments were performed in a 5% H<sub>2</sub>/Ar mixture at a flow rate of 10 cm<sup>3</sup>min<sup>-1</sup> and a heating rate of 7° C.min<sup>-1</sup>. Bulk PtO<sub>2</sub> samples were found to be reduced at various temperatures but always above 20°C. For supported samples (5.2% Pt/SiO<sub>2</sub> and 1% Pt/Al<sub>2</sub>O<sub>3</sub>), a standard sample preparation procedure was employed prior to TPR analysis. This involved reduction at 500°C, sintering in O<sub>2</sub>/He between 300 and 600°C, TPR up to 500°C, and finally, reoxidation in O<sub>2</sub>/He at 300°C. Subsequent reduction peak temperatures were always at or below those of bulk PtO<sub>2</sub> samples analysed and decreased with increasing sintering temperature. This was explained in terms of the passive nature of Pt oxidation rather than a support effect. This meant that larger particles had a core of metal atoms which increased the rate of reduction by promoting H<sub>2</sub> adsorption, dissociation, and reaction. Smaller Pt particles were concluded to have been more completely reoxidised in the pretreatment procedure employed and because of this showed reduction temperatures similar to large, chemically prepared, bulk PtO<sub>2</sub> particles. An alternative explanation involving a possible shift from an oxidic to a chemisorbed oxygen layer with increasing Pt particle size could also have explained the increased reactivity of the passivating oxygen layer with H<sub>2</sub>. H<sub>2</sub> uptakes in TPR profiles supported this latter theory (32).

TPR data argued against an effect of the support material on the oxidation characteristics of Pt crystallites (32). The absence of important support effects was suggested because of the similarity of TPR profiles for both SiO<sub>2</sub> and Al<sub>2</sub>O<sub>3</sub>-supported samples and also because the reduction peak temperatures for supported samples were always at or below those of bulk PtO<sub>2</sub> samples. No evidence was reported for the existence of a metal-support interaction which stabilised PtO<sub>2</sub> against reduction as was proposed by Yao et al. (25, 27). High temperature reduction peaks (above ca.227°C) were observed for samples which were not reduced prior to TPR (32). However, these were attributed to the presence of inorganic Pt compounds. The inclusion of a 500°C reduction step in the standard preparation procedure was thought to result in the decomposition of any inorganic Pt compounds, such as Pt oxychloride complexes on Al<sub>2</sub>O<sub>3</sub> (28, 29), which might have been present after impregnation and drying and were expected to be reduced at higher temperatures than PtO<sub>2</sub> species (32).

Niwa et al. (33) studied the TPR of Pt/Al<sub>2</sub>O<sub>3</sub>, Pt/SiO<sub>2</sub>, and Pt/SiO<sub>2</sub>-Al<sub>2</sub>O<sub>3</sub> samples, which were prepared by impregnation with H<sub>2</sub>PtCl<sub>6</sub> followed by drying at 110° C, oxidation in air at 400°C, and finally reduction in H<sub>2</sub> at 300°C. TPR analysis was carried out after further reduction and reoxidation steps. A 6.2 vol.% H<sub>2</sub>/Ar mix was used with samples containing about 0.5 mg of Pt. The TPR profiles obtained are illustrated in Fig. 3.3 and were found to depend on both the support and the metal loading (33).

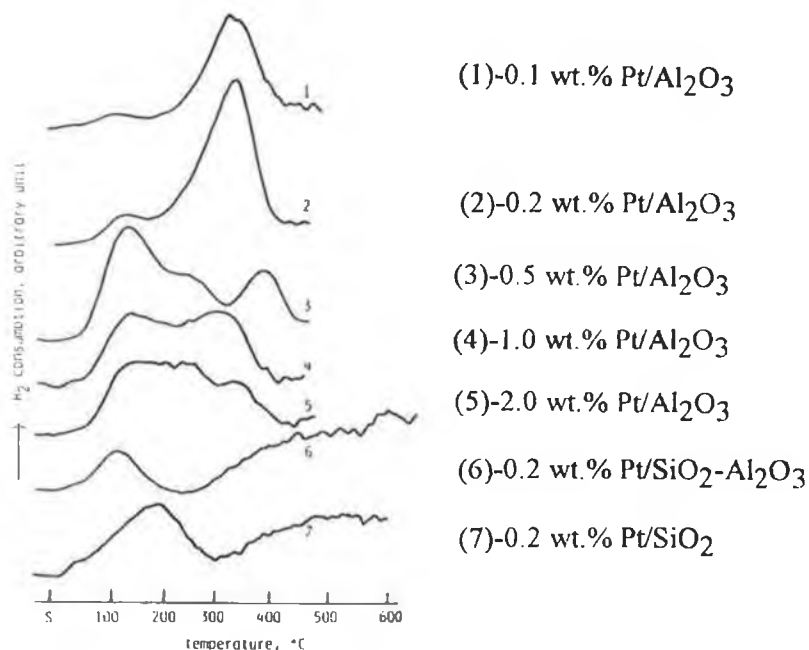


Figure 3.3 : TPR profiles of Pt/Al<sub>2</sub>O<sub>3</sub>, Pt/SiO<sub>2</sub>-Al<sub>2</sub>O<sub>3</sub> and Pt/SiO<sub>2</sub> (33).

The TPR profile of Pt/Al<sub>2</sub>O<sub>3</sub> samples always had two maxima at temperatures of below 200°C and above 300°C (33). H<sub>2</sub> uptakes indicated that the oxidation state of Pt, assumed to be PtO<sub>x</sub>, was in the vicinity of PtO<sub>2</sub>. For lower Pt loadings of 0.1 and 0.2 wt.% Pt on Al<sub>2</sub>O<sub>3</sub>, H<sub>2</sub> uptakes considerably exceeded that expected for PtO<sub>2</sub> reduction. This was possibly associated with spillover of adsorbed hydrogen onto the surface of alumina since such excessive H<sub>2</sub> uptakes could not be explained by the usual stoichiometry of platinum oxide (33).

Lieske et al. (28, 29) noted that considerable discrepancy existed in the literature as to the nature of oxidised Pt species on Al<sub>2</sub>O<sub>3</sub> with Pt:O ratios ranging from 1:1 to 1:2 and even up to 1:3.7 reported under different conditions. In light of this, the formation of oxidised Pt species on Al<sub>2</sub>O<sub>3</sub>-supported catalysts during treatments in O<sub>2</sub> at different temperatures was investigated using TPR, H<sub>2</sub> chemisorption, and uv-vis reflectance spectroscopy techniques (28, 29). TPR experiments were carried out on 0.5 and 1.0 wt.% Pt/Al<sub>2</sub>O<sub>3</sub> samples. A 5 vol.% H<sub>2</sub>/Ar mix was used as the reducing gas with a heating rate of 8°Cmin<sup>-1</sup>, a gas flow rate of 1500 cm<sup>3</sup>h<sup>-1</sup>, and ca. 1g of catalyst sample. Different procedures were employed to prepare both chloride-containing and chloride-free catalysts. Data obtained indicated that highly dispersed Pt was completely oxidised to Pt<sup>4+</sup> by O<sub>2</sub> treatment between 400 and 600°C, irrespective of whether the catalyst contained chloride or not. TPR spectra varied considerably with pretreatment conditions and the presence or absence of Cl. It was found that after impregnation with H<sub>2</sub>PtCl<sub>6</sub>, the platinate formed could be transformed into a [Pt<sup>4</sup>(OH)<sub>x</sub>Cl<sub>y</sub>]<sub>s</sub> species if treated in O<sub>2</sub> at 300°C, while calcination at higher temperatures of 450-600°C produced a [Pt<sup>4</sup>O<sub>x</sub>Cl<sub>y</sub>]<sub>s</sub> species. The former species showed a TPR peak at 260°C and the latter at 290°C. The subscript s was used for these species to symbolise a surface complex which was believed to be stabilised by some form of interaction with the alumina. Reduction of the [Pt<sup>4</sup>O<sub>x</sub>Cl<sub>y</sub>]<sub>s</sub> complex resulted in highly dispersed Pt metal on the support surface. The dispersed Pt thus formed was thought to form a molecular charge-transfer complex with oxidising sites of the Al<sub>2</sub>O<sub>3</sub> involving electron-deficient Pt and acidic Al<sub>2</sub>O<sub>3</sub> sites. Slight reoxidation of the dispersed metal between 200 and 400°C gave mainly a α-[PtO<sub>2</sub>]<sub>s</sub> species as well as a possible lower oxide species and/or residual Pt<sup>0</sup>. This α-[PtO<sub>2</sub>]<sub>s</sub> reduced at ca. 100°C in TPR. At higher temperatures of reoxidation (450 and 600°C), residual chloride on the Al<sub>2</sub>O<sub>3</sub> surface reacted to form [Pt<sup>4</sup>O<sub>x</sub>Cl<sub>y</sub>]<sub>s</sub> again. In O<sub>2</sub> treatments above 700°C crystalline Pt was formed with a significant decrease in H<sub>2</sub> uptake in TPR due to sintering. Reversion of this loss of dispersion was only possible in the presence of halogen and was connected with the formation of [Pt<sup>4</sup>O<sub>x</sub>Cl<sub>y</sub>]<sub>s</sub>. For non-chloride containing Pt/Al<sub>2</sub>O<sub>3</sub>, an additional PtO<sub>2</sub> surface species, termed β-[PtO<sub>2</sub>]<sub>s</sub>, could be formed by reoxidation of the reduced catalyst above 550°C. This species exhibited reduction over a wider temperature range with a less well defined TPR profile

than  $\alpha$ -[PtO<sub>2</sub>]<sub>s</sub>. The  $\alpha$ - and  $\beta$ -[PtO<sub>2</sub>]<sub>s</sub> species, formed on reoxidation of dispersed Pt, were thought to be stabilised by some form of interaction with Al<sub>2</sub>O<sub>3</sub> because the reduction temperatures observed were considerably higher than those reported for bulk PtO<sub>2</sub>. In addition, the uv-vis spectra obtained for these species were different to that obtained for a sample of bulk PtO<sub>2</sub> mixed with  $\gamma$ -Al<sub>2</sub>O<sub>3</sub> which supported the theory that PtO<sub>2</sub> existed as a surface complex in reoxidised Pt/Al<sub>2</sub>O<sub>3</sub> samples (28, 29).

### **TPR Studies of CeO<sub>2</sub>, Ce/Al<sub>2</sub>O<sub>3</sub>, Pt-Ce/Al<sub>2</sub>O<sub>3</sub> and Pt/CeO<sub>2</sub>**

Johnson and Mooi (34) investigated TPR of CeO<sub>2</sub> samples using a 5% H<sub>2</sub>/N<sub>2</sub> mix at a flow rate of 50 cm<sup>3</sup>min<sup>-1</sup> and a heating rate of 15°Cmin<sup>-1</sup> up to ca. 900°C. Three CeO<sub>2</sub> samples were examined with surface areas of 0.7, 13, and 27 m<sup>2</sup>g<sup>-1</sup>. Two reduction features were apparent on the profiles obtained. A low temperature reduction feature below ca. 700°C was ascribed to the reduction of "capping oxide" ions on the CeO<sub>2</sub> surface. The magnitude of this surface reduction feature was related to the BET surface area of the ceria sample and the associated H<sub>2</sub> uptake could be used as a measure of surface area. A second reduction feature was also observed at higher temperatures which was associated with bulk CeO<sub>2</sub> reduction (34).

The TPR of CeO<sub>2</sub>, as well as CeO<sub>2</sub>/Al<sub>2</sub>O<sub>3</sub> samples, was investigated by Shyu et al. (35). The supported samples were prepared by mixing an Al<sub>2</sub>O<sub>3</sub> slurry with the appropriate amount of an aqueous Ce(NO<sub>3</sub>)<sub>3</sub> solution followed by drying at 75°C and calcination at 800°C. TPR experiments were performed using a 10% H<sub>2</sub>/Ar mix at a flow rate of 30 cm<sup>3</sup>min<sup>-1</sup> as the reducing gas and a sample heating rate of 15°Cmin<sup>-1</sup>. Interpretation of the profiles obtained (see Fig. 3.4.) was made considering the thermodynamic favourability of the different reduction processes possible, as indicated by the equilibrium constants (K) for the reduction, by H<sub>2</sub>, of CeO<sub>2</sub> to CeO<sub>x</sub> (1.7 ≤ x ≤ 1.9), CeAlO<sub>3</sub>, or Ce<sub>2</sub>O<sub>3</sub>, at different temperatures. The TPR profile of CeO<sub>2</sub> (Fig. 3.4(a)) showed major peaks at ca. 580°C and above 800°C, along with a minor peak at about 450°C. The latter peak was assigned to the reduction of surface oxygen of the low surface area (~10m<sup>2</sup>g<sup>-1</sup>) CeO<sub>2</sub> sample. The higher temperature peaks were attributed to the formation of non-stoichiometric cerium oxides (CeO<sub>x</sub>, where x ranged from 1.7 to 1.9) and of bulk Ce<sub>2</sub>O<sub>3</sub>, respectively. Ce<sub>2</sub>O<sub>3</sub> is believed to be the final product in CeO<sub>2</sub> reduction at these temperatures (35, 36).

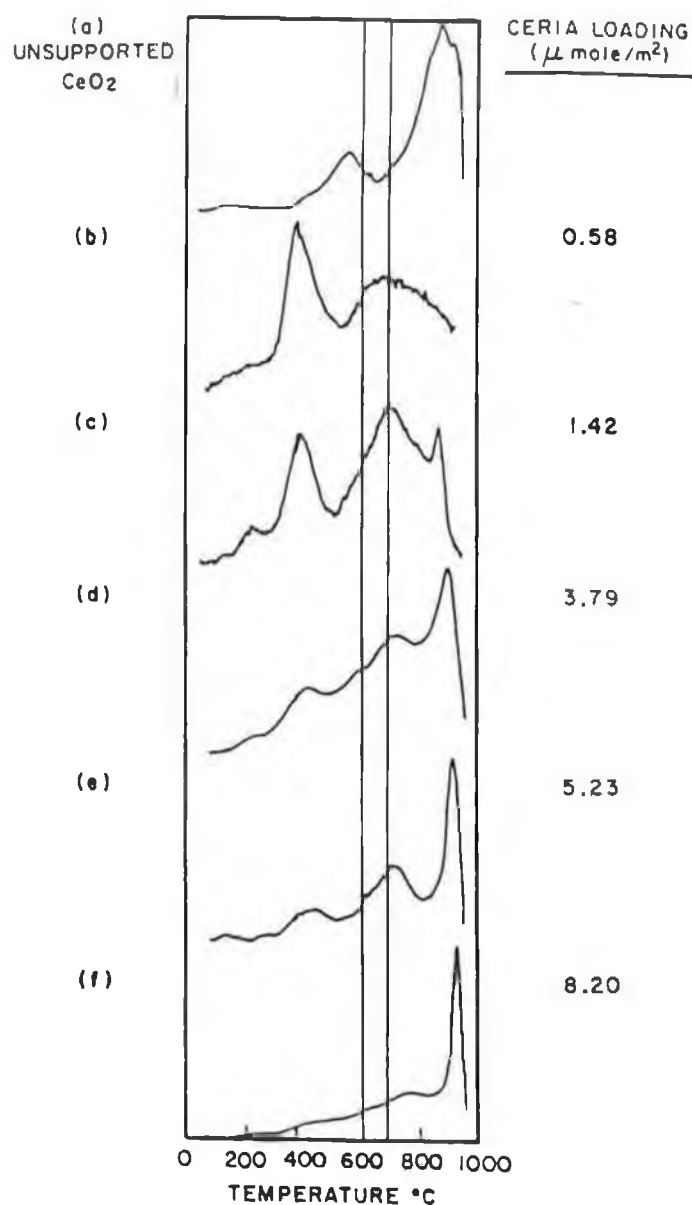


**Figure 3.4 : TPR profiles for CeO<sub>2</sub> and CeO<sub>2</sub>/Al<sub>2</sub>O<sub>3</sub> (35).**

For CeO<sub>2</sub>/Al<sub>2</sub>O<sub>3</sub> samples (35), XPS and raman spectroscopy data indicated the presence of three different Ce species, namely a 'CeAlO<sub>3</sub>-precursor' in the dispersed phase, small CeO<sub>2</sub> crystallites, and large CeO<sub>2</sub> particles (35). From Fig. 3.4(b), it is seen that the TPR profile for a 0.58  $\mu\text{molm}^{-2}$  CeO<sub>2</sub>/Al<sub>2</sub>O<sub>3</sub> sample (1.0 wt.% CeO<sub>2</sub>) consisted of two major peaks at ca.410°C and ca.720°C which were assigned to the reduction of surface oxygen of a 'CeAlO<sub>3</sub>-precursor' species and subsequent conversion of the partially reduced species to CeAlO<sub>3</sub>. At such low loadings, CeO<sub>2</sub> was shown by XPS

and raman spectroscopy to be predominately present in the form of this 'CeAlO<sub>3</sub>-precursor' species. Reduction experiments indicated that this species could be more easily reduced to CeAlO<sub>3</sub> than CeO<sub>2</sub> particles on Al<sub>2</sub>O<sub>3</sub>. As the CeO<sub>2</sub> loading was increased, two additional peaks were observed in the TPR traces (Fig. 3.4(c)-(f)) at ca.600°C and above 800°C. Below CeO<sub>2</sub> concentrations of 3.79 μmolm<sup>-2</sup>, the peaks at ca.410 and 720°C still represented the major reducible species. At 8.2 μmolm<sup>-2</sup> ceria loading, the peak above 800°C became the predominant species which was assigned to the characteristic reduction of bulk CeO<sub>2</sub>. The peak at 600°C was correlated with that at 580°C for the unsupported CeO<sub>2</sub> sample with the slight temperature shift attributed to a difference in ceria particle size. A peak below 300°C on the TPR profiles of CeO<sub>2</sub>/Al<sub>2</sub>O<sub>3</sub> was associated with the removal of adsorbed oxygen on Al<sub>2</sub>O<sub>3</sub> (35).

In a subsequent study, Shyu and Otto (37) investigated the TPR of CeO<sub>2</sub>- and Al<sub>2</sub>O<sub>3</sub>- supported Pt samples under the same experimental conditions as in (35). TPR profiles obtained are shown in Fig 3.5. Pt impregnation of the support materials was achieved with aqueous solutions of H<sub>2</sub>PtCl<sub>6</sub>.

The reduction profile of unsupported CeO<sub>2</sub> (Fig. 3.5(a)) showed the same features as found in the previous study (35). For 10 wt.% Pt/Al<sub>2</sub>O<sub>3</sub>, the major peak at ca.130°C was attributed to dispersed Pt on Al<sub>2</sub>O<sub>3</sub> coexisting, in the form of a PtO<sub>2</sub>-Al<sub>2</sub>O<sub>3</sub> complex, with bulk Pt<sup>0</sup> (37). It was predicted that this peak would move towards higher temperatures if the Pt concentration was decreased due to increased dispersion. The small peak at ca.400°C was associated with some residual dispersed phase Pt present in isolated patches even after calcination at 800°C (Fig 3.5(b)). For the 20 wt.% CeO<sub>2</sub>/Al<sub>2</sub>O<sub>3</sub> sample, the CeO<sub>2</sub> loading greatly exceeded monolayer coverage on Al<sub>2</sub>O<sub>3</sub>. Therefore both particulate and dispersed phases of CeO<sub>2</sub> were expected to be in co-existence on the surface. The TPR profile (Fig. 3.5(c)) showed four poorly resolved peaks which were associated with the removal of surface oxygen of ceria at ca.400°C, formation of non-stoichiometric CeO<sub>x</sub> species at ca.600°C, formation of CeAlO<sub>3</sub> from dispersed ceria on Al<sub>2</sub>O<sub>3</sub> at ca. 750°C, and the formation of Ce<sub>2</sub>O<sub>3</sub> above 800°C. The profile of a 5 wt.% Pt/CeO<sub>2</sub> sample (Fig. 3.5(d)) contained a peak at ca.200°C which was assigned to an interactive species of Pt and cerium. The main CeO<sub>2</sub> reduction peak was still apparent above 800°C. However, the absence of any peak associated with the formation of non-stoichiometric cerium oxides, normally present between 580 and 600° C, was tentatively attributed to an interaction between Pt and ceria which suppressed the formation of such oxide species. For the 10% Pt/Al<sub>2</sub>O<sub>3</sub> catalyst containing 20 wt.% CeO<sub>2</sub> (Fig. 3.5(e)), the peak at 240°C was deemed to be characteristic of a Pt-CeO<sub>2</sub> interaction and was thought to agree, within experimental error, with the peak at ca.200°

C in the Pt/CeO<sub>2</sub> sample. The peak at ca.400°C was thought to originate from a small amount of dispersed Pt associated with Al<sub>2</sub>O<sub>3</sub> (37).

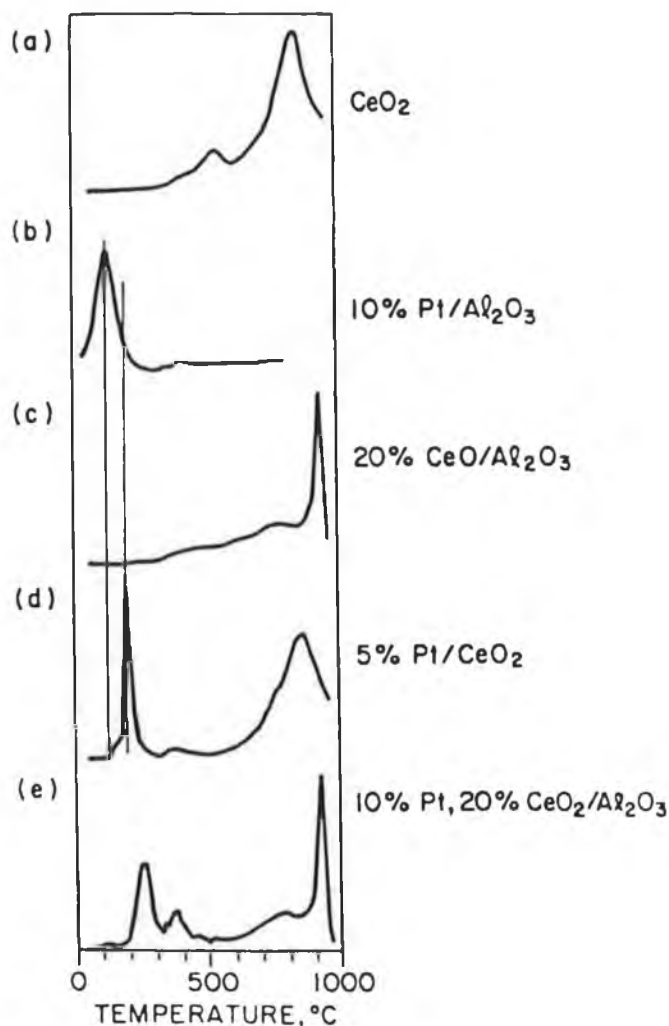


**Figure 3.5 : TPR profiles of a Pt/CeO<sub>2</sub>/γ-Al<sub>2</sub>O<sub>3</sub> system (37).**

Shyu and Otto (37) also studied the doping of a 3.6 wt.% CeO<sub>2</sub>/Al<sub>2</sub>O<sub>3</sub> sample with varying amounts of Pt and obtained the profiles illustrated in Figure 3.6. For the CeO<sub>2</sub>/Al<sub>2</sub>O<sub>3</sub> sample (Fig. 3.6(a)), the peak positions were consistent with those discussed above for 20 wt.% CeO<sub>2</sub>/Al<sub>2</sub>O<sub>3</sub> with an extra peak present at ca.100°C which was associated with adsorbed oxygen on Al<sub>2</sub>O<sub>3</sub>. Because of the relatively low concentration of particulate phase CeO<sub>2</sub>, the intensity of the peak assigned to the formation of Ce<sub>2</sub>O<sub>3</sub> (above 800°C) was relatively low compared with that associated with the formation of CeAlO<sub>3</sub> (at ca.760°C). On addition of 4 wt.% Pt (~ 1:1 Pt:CeO<sub>2</sub> atomic ratio) a peak emerged at ca.250°C in Fig 3.6(b) which corresponded to the reduction temperature of surface Pt in contact with CeO<sub>2</sub> in the 10% Pt/20% CeO<sub>2</sub>/Al<sub>2</sub>O<sub>3</sub> profile in Fig. 3.5(e). The interaction of Pt with 3.6% CeO<sub>2</sub> in the presence

of a much larger surface area of  $\text{Al}_2\text{O}_3$  led to the conclusion that Pt interacts preferentially with  $\text{CeO}_2$ . As the Pt concentration was increased to 8 and 10 wt.% (Fig. 3.6(c) and (d)), a new peak appeared at ca.420°C which was interpreted as being characteristic of dispersed Pt on  $\text{Al}_2\text{O}_3$  and became apparent only when the ceria surface had been saturated with Pt. The absence in Fig. 3.6(b)-(d), of any peak at ca.130°C associated with the presence of particulate phase Pt on  $\text{Al}_2\text{O}_3$  (see Fig. 3.5(b)) was thought to provide evidence that  $\text{CeO}_2$  facilitated Pt dispersion on  $\text{Al}_2\text{O}_3$ . This was supported by XRD results (37).

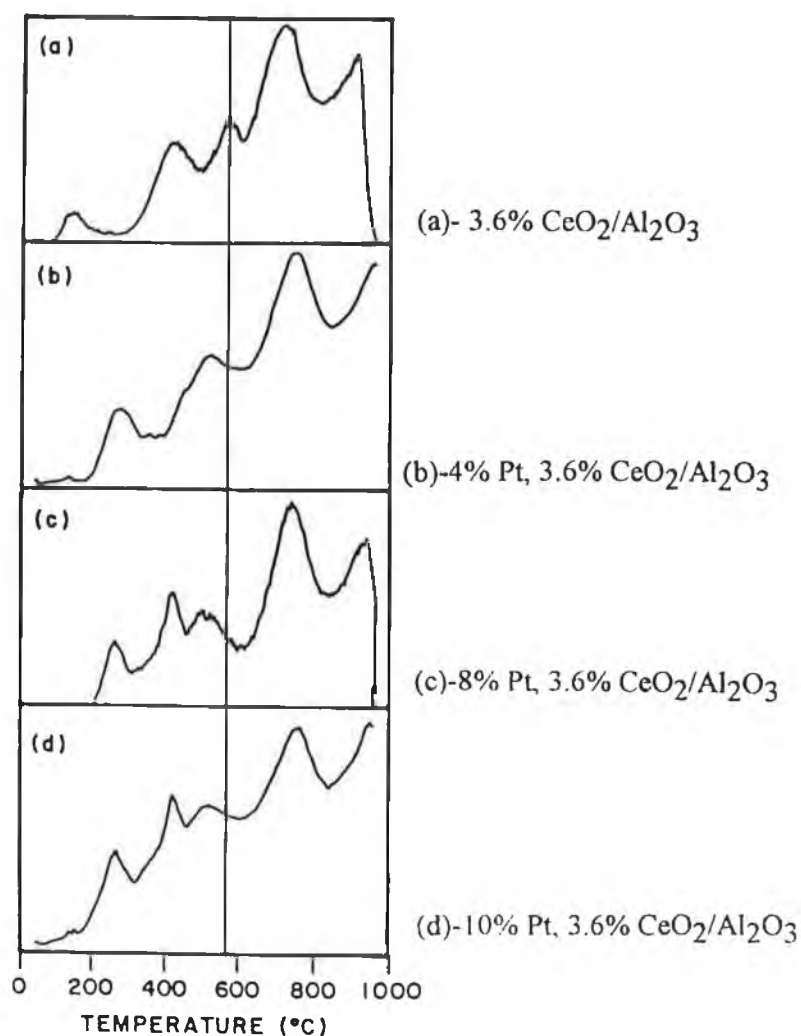


**Figure 3.6 : TPR profiles of 3.6 wt.%  $\text{CeO}_2/\text{Al}_2\text{O}_3$  containing Pt (37).**

Harrison et al. (38) reported that the TPR profile of  $\text{CeO}_2$  was substantially altered in the presence of platinum group metals. The TPR profile of ceria in  $\text{H}_2$  showed two reduction peaks. A peak at ca.500°C was assigned to the reduction of a surface

species and a higher temperature feature above 800°C was attributed to the reduction of bulk oxygen and the formation of lower oxides of cerium. Investigation of Rh/CeO<sub>2</sub>, Pd/CeO<sub>2</sub>, and Pt/CeO<sub>2</sub> samples showed that the presence of the noble metals promoted the reduction of surface oxygen of CeO<sub>2</sub> with Rh being particularly effective. For a 1 wt.% Rh/CeO<sub>2</sub> sample, the Rh itself reduced at ca.150°C while the surface reduction of CeO<sub>2</sub> was lowered to ca.350°C. Pt and Pd also promoted the reduction of surface oxygen of ceria, and the temperatures for the surface reduction were lowered. The promotion of ceria reduction by the noble metals was deemed to be important in possibly improving the oxygen storage capacity (OSC) of CeO<sub>2</sub> in automotive exhaust applications because reduction-reoxidation experiments on pure CeO<sub>2</sub> revealed that reduction under normal operating conditions may be difficult. Comparison of the reduction profiles for Rh/CeO<sub>2</sub> and Rh/Al<sub>2</sub>O<sub>3</sub> suggested that strong interaction between Rh and Al<sub>2</sub>O<sub>3</sub> may inhibit the redox capability of Rh under transient autocatalyst conditions. In contrast, interaction between Rh and CeO<sub>2</sub> maintained Rh in a reducible form (38).

Serre et al. (39) also reported that Pt had a promoting effect on the reduction of surface oxygen atoms of CeO<sub>2</sub>. The catalysts studied were prepared by impregnation of  $\gamma$ -Al<sub>2</sub>O<sub>3</sub> with aqueous solutions of Ce(NO<sub>3</sub>)<sub>3</sub> and/or H<sub>2</sub>PtCl<sub>6</sub>. Using CO as the reducing agent, the TPR profile of a 14.5% CeO<sub>2</sub>/Al<sub>2</sub>O<sub>3</sub> sample showed a wide reduction peak between 300 and 550°C accompanied by an unresolved peak on the high temperature side. Addition of 2% Pt caused a downscale shift in the temperature of the former peak associated with surface ceria reduction. Two possible explanations were given. A bimetallic interaction was proposed to occur on addition of Pt which may have caused a destabilisation of the surface Ce-O bond strength, and thereby promoted reduction by CO. This theory was noted as being in agreement with results previously reported by other studies which indicated charge transfer from metal to ceria, leading to partial reduction of the latter and a small increase in the oxidation state of the metal. An alternative interpretation of the TPR results was that CO adsorption on Pt could have caused a weakening of C-O bond strength and allowed easier insertion of an oxygen atom from ceria to produce CO<sub>2</sub>. The pretreatment procedure employed prior to TPR analysis involved an oxidation step at 700°C which was thought to cause decomposition of Pt oxide to metallic Pt. Therefore, no peaks associated with PtO<sub>2</sub> reduction were apparent in the TPR spectra obtained for Pt/Al<sub>2</sub>O<sub>3</sub> or Pt-CeO<sub>2</sub>/Al<sub>2</sub>O<sub>3</sub> samples (39).

Similarly, Yao and Yu-Yao (36) reported that precious metals lowered the reduction temperature and increased the OSC of CeO<sub>2</sub>. TPR profiles indicated the existence of two types of oxygen anions in CeO<sub>2</sub>, namely, a surface capping oxygen anion which attaches to a surface Ce<sup>4+</sup> ion in an octahedral co-ordination and was reduced at ca.500°C, and a bulk oxygen anion which is bonded to two Ce<sup>4+</sup> ions in the

bulk ceria and was reduced at 750°C. In agreement with the findings of Johnson and Mooi (34), the low temperature peak was found to increase in size with increasing ceria surface area (36). For Al<sub>2</sub>O<sub>3</sub>-supported ceria, the relative size of the two reduction features varied with ceria loading. At low loadings, the bulk ceria reduction peak was absent but at higher CeO<sub>2</sub> loadings, it became apparent at a slightly lower temperature than 750°C. The shift in bulk CeO<sub>2</sub> reduction temperature for supported samples was attributed to particle size effects. For the higher loading CeO<sub>2</sub>/Al<sub>2</sub>O<sub>3</sub> samples, a third reduction peak was present in the profiles at 850°C and was associated with the reduction of shared oxygen anions (shared between Ce<sup>4+</sup> and Al<sup>3+</sup> ions) in the interface between bulk CeO<sub>2</sub> and Al<sub>2</sub>O<sub>3</sub>. H<sub>2</sub> uptake indicated that complete reduction of Ce<sup>4+</sup> to Ce<sup>3+</sup> was achieved in the TPR experiments up to 900°C. TPR profiles indicated that CeO<sub>2</sub> was present in the dispersed phase on Al<sub>2</sub>O<sub>3</sub> at concentrations of up to 2.5 μmol of CeO<sub>2</sub> per m<sup>2</sup> (BET) of Al<sub>2</sub>O<sub>3</sub>, in agreement with chemisorption data (36).

On addition of precious metals (Pt or Rh) to CeO<sub>2</sub>, the TPR profiles exhibited peaks at temperatures below 150°C which were attributed to the reduction of the noble metals (36). The effects of the noble metals on the TPR profiles of CeO<sub>2</sub> and CeO<sub>2</sub>/Al<sub>2</sub>O<sub>3</sub> samples were similar. The presence of the noble metal caused an increase in the number of peaks between 150 and 500°C. This was proposed to result from the interaction of CeO<sub>2</sub> with precious metal in various states of aggregation during the reduction. Such interactions were thought to differentiate the bonding of the capping ceria oxygen anions in several ways while lowering the reduction temperature. The presence of the noble metals only promoted the reduction of the surface ceria component and did not appear to affect the two higher temperature CeO<sub>2</sub> reduction features. The TPR profiles of all samples were obtained using a 15% H<sub>2</sub>-85% Ar reducing gas mixture and a heating rate of 10°Cmin<sup>-1</sup> (36). CeO<sub>2</sub>/Al<sub>2</sub>O<sub>3</sub> samples, with and without noble metals, were prepared by conventional impregnation procedures (36) which have already been described in section 1.4.1 of the present study.

As discussed previously, Nunan et al. (7) found that the performance of Pt, Rh, Ce/γ-Al<sub>2</sub>O<sub>3</sub> catalysts, for the oxidation of CO and hydrocarbons in a synthetic gas mixture, improved considerably after catalyst activation in the presence of H<sub>2</sub>. This activation was thought to be associated with the combined reduction of noble metals and surface Ce. Some of the TPR profiles acquired for the catalysts investigated are shown in Figure 3.7. The γ-Al<sub>2</sub>O<sub>3</sub> substrate was found to take up H<sub>2</sub> at 700°C and this feature was also present in the profile of Pt, Rh/γ-Al<sub>2</sub>O<sub>3</sub> over a similar temperature range. A broad low temperature reduction peak, centred at 260°C, was assigned to Pt and Rh reduction in Pt, Rh/γ-Al<sub>2</sub>O<sub>3</sub>. For 6% Ce/γ-Al<sub>2</sub>O<sub>3</sub>, distinct peaks were noted at 360 and 490°C, and were assigned to surface Ce reduction. A further reduction feature above 600°C was

assigned to both H<sub>2</sub> uptake by the  $\gamma$ -Al<sub>2</sub>O<sub>3</sub> and some bulk Ce reduction. The TPR spectrum for Pt, Rh, Ce/ $\gamma$ -Al<sub>2</sub>O<sub>3</sub> was obviously not a superimposition of those for Pt, Rh/ $\gamma$ -Al<sub>2</sub>O<sub>3</sub> and Ce/ $\gamma$ -Al<sub>2</sub>O<sub>3</sub>. Instead completely new features were exhibited, consisting of a sharp low temperature peak centred at 175°C, a shoulder at 280°C, and a broad peak at 720°C. The shoulder at 280°C was attributed to the reduction of Pt and Rh on the  $\gamma$ -Al<sub>2</sub>O<sub>3</sub> component of the catalyst. The high temperature peak was associated with the reduction of bulk Ce and uptake by  $\gamma$ -Al<sub>2</sub>O<sub>3</sub>. The absence of any distinct surface Ce reduction features below 500°C, and the fact that the H<sub>2</sub> uptake for the peak at 175°C was greater than that expected for exclusively noble metal reduction, led to the conclusion that this peak was due to a synergistic reduction of Pt, Rh, and surface Ce. This conclusion was supported by the TPR profile of a Pt, Rh/CeO<sub>2</sub> sample which exhibited a sharp H<sub>2</sub> uptake at 180°C which was about 4.5 times that required for Pt and Rh reduction (7).

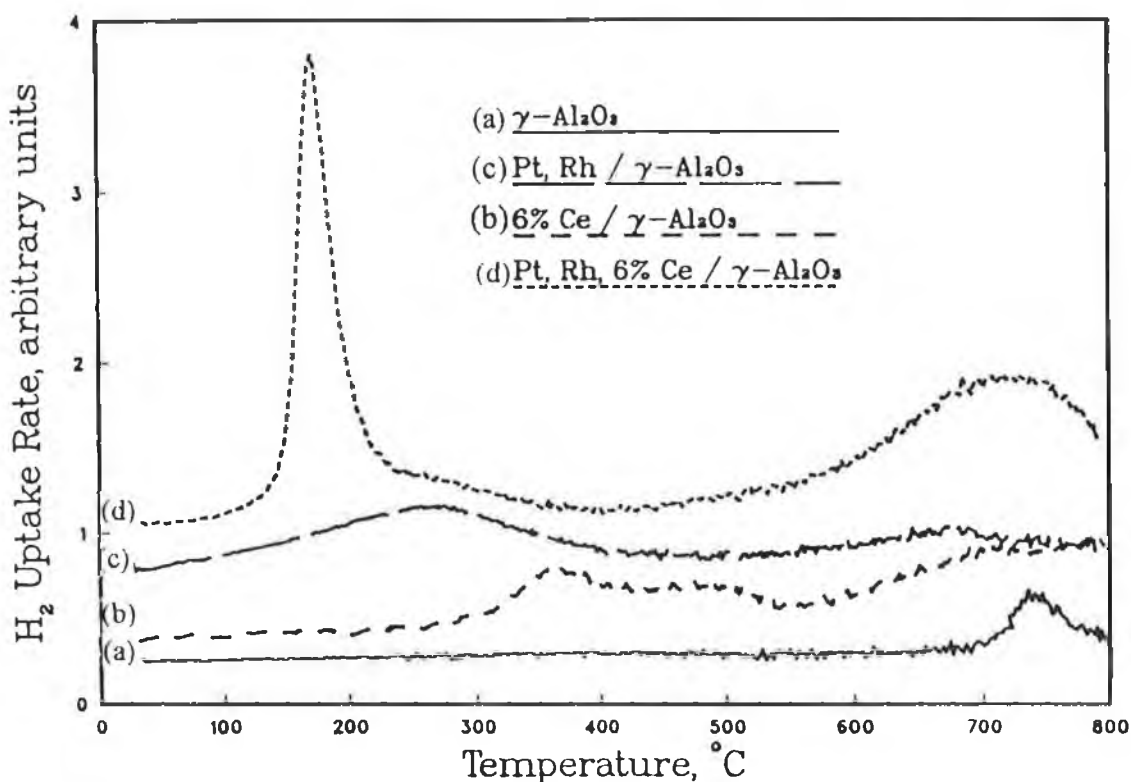


**Figure 3.7 :** Comparison of the TPR spectra for  $\gamma$ -Al<sub>2</sub>O<sub>3</sub> systems (7). Pt loading = 0.77 wt.% (nominal); Rh loading = 0.04 wt.% (nominal).

STEM analysis and catalytic activity data for a Pt/CeO<sub>2</sub> sample both indicated that catalyst activation in a reducing environment was associated mainly with direct Pt-Ce interaction, the degree of which increased with decreasing CeO<sub>2</sub> crystallite size (7). This was supported by TPR profiles of Pt, Rh, Ce/Al<sub>2</sub>O<sub>3</sub> which showed that the size of

the peak at ca.175°C, associated with synergistic noble metal-Ce reduction, increased with decreasing CeO<sub>2</sub> crystallite size while catalyst activation was enhanced. The increased activity was ascribed to an increased degree of noble metal interaction with smaller CeO<sub>2</sub> crystallites. Again, the fraction of ceria in interaction with the metal was deemed to solely involve the surface Ce component (7).

Diwell et al. (12) carried out TPR experiments using a 10% H<sub>2</sub>/N<sub>2</sub> reduction mixture at a flow rate of 40 cm<sup>3</sup>min<sup>-1</sup> and a sample heating rate of 10°Cmin<sup>-1</sup>. It was reported that the reduction of the Pt component of a Pt-CeO<sub>2</sub> interactive surface complex in a 0.9 wt.% Pt/CeO<sub>2</sub>-Al<sub>2</sub>O<sub>3</sub> sample, was more facile than that of platinum oxide dispersed on Al<sub>2</sub>O<sub>3</sub> in a 0.9 wt.% Pt/Al<sub>2</sub>O<sub>3</sub> sample. The TPR profiles of the samples, which were precalcined at 500°C, are shown in Fig 3.8. The broad reduction peak centred at 200°C for the Pt/Al<sub>2</sub>O<sub>3</sub>-CeO<sub>2</sub> sample was associated mostly with the surface reduction of Ce<sup>4+</sup> with a contribution from the Pt apparent as a shoulder at ca.100°C. The main Pt reduction peak for Pt/Al<sub>2</sub>O<sub>3</sub> had a maximum at 220°C (12).

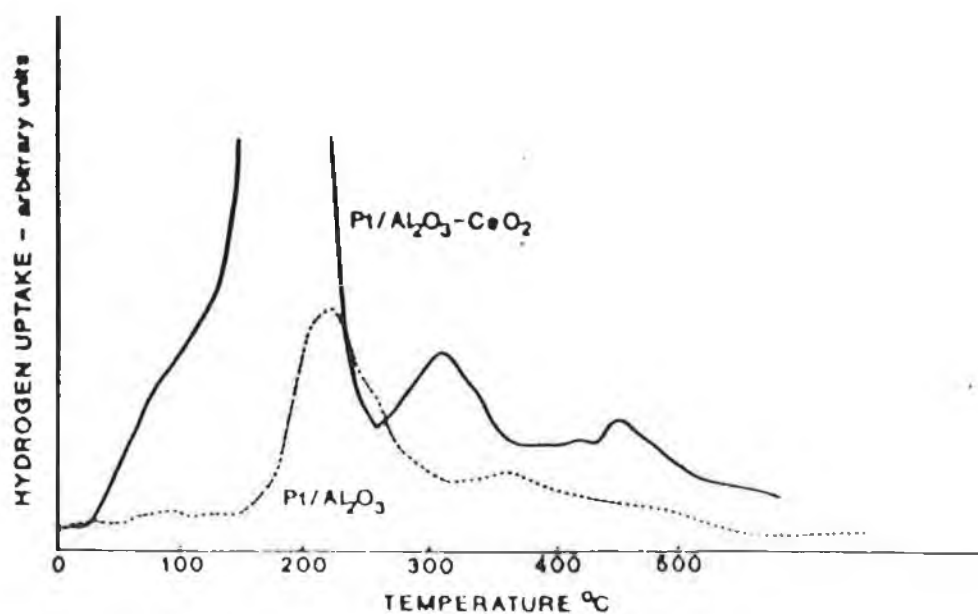


Figure 3.8 : TPR traces for 0.9 wt.% Pt/Al<sub>2</sub>O<sub>3</sub> and 0.9 wt.% Pt/Al<sub>2</sub>O<sub>3</sub>-CeO<sub>2</sub> catalysts (12).

The TPR traces acquired for a 0.9 wt.% Pt/CeO<sub>2</sub> sample are shown in Fig. 3.9 (12). The two samples which had been calcined in air prior to running the TPR showed similar features. These included a peak centred at ca.230°C which was assigned to the reduction of Pt and surface oxygen shared with Ce. A shoulder at ca.350°C was associated with CeO<sub>2</sub> which was not in close proximity to the Pt, and a peak at ca.800°C

was assigned to the reduction of bulk  $\text{CeO}_2$ . For the pre-reduced catalyst, the peak at ca.  $50^\circ\text{C}$  was suggested to have arisen from a strong Pt- $\text{CeO}_2$  interaction during reduction. No similar low temperature peaks were observed for either Pt/ $\text{Al}_2\text{O}_3$  or for ceria alone after the same pretreatment sequence.

(a)-calcined in air at  $500^\circ\text{C}$

(b)-calcined in air, then reduced in  $\text{H}_2$  at  $900^\circ\text{C}$

(c)-calcined in air, reduced in  $\text{H}_2$ , then recalcined in air.

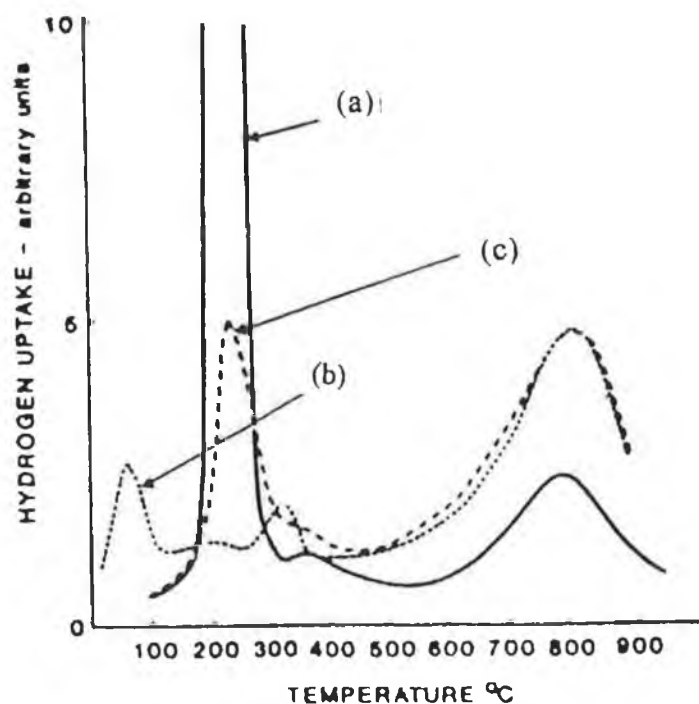


Figure 3.9 : TPR traces for 0.9 wt.% Pt/ $\text{CeO}_2$  catalysts (12).

A strong Pt/ $\text{CeO}_2$  interaction was proposed to occur during catalyst reduction at mild temperatures, involving encapsulation of the Pt by the partially reduced ceria. Such an interaction was presumed to be responsible for the dramatic changes observed in the activity of Pt/ $\text{CeO}_2$  catalysts after mild pre-reduction at  $600^\circ\text{C}$  in  $\text{H}_2$  (12).

### 3.1.2. X-ray Photoelectron Spectroscopy (XPS)

X-ray photoelectron spectroscopy (XPS) is a commonly used technique for the investigation of catalyst surfaces (40, 41). It provides information on the elemental composition of the surface region and can also distinguish between different chemical states of one element. The technique is based on the photoelectric effect, whereby adsorption of a photon of known energy,  $h\nu$ , by an atom results in the ejection of an electron of binding energy,  $E_b$ . The kinetic energy,  $E_k$ , of the emitted electron is given by,

$$E_k = h\nu - E_b.$$

In XPS, the intensity of photoelectrons,  $N(E)$ , is measured as a function of their kinetic energy. The spectrum can be a plot of  $N(E)$  versus  $E_k$ , or more commonly,  $N(E)$  versus  $E_b$  (40, 41).

Routinely used X-ray sources are Mg  $K\alpha$  ( $h\nu = 1253.6\text{eV}$ ) and Al  $K\alpha$  ( $h\nu = 1486.6\text{eV}$ ), both of which are of sufficient energy to result in the ejection of electrons from core, as well as valence, atomic levels. The core electron excitations give rise to sharp lines in the XPS spectrum. These lines are, more or less, specific for the chemical identity of the atoms from which excitation has occurred because each element has a characteristic set of core binding energies. The kinetic energies of the photoelectrons are typically in the range 0.2 to 1.5KeV. The mean free path of electrons with kinetic energies between 0 and 1500eV in a solid has been reported to be limited to between two and ten atomic layers (42). Hence, XPS probes mainly the outer layers of the catalyst. Surface sensitivity is increased as the binding energy increases (40, 42).

Binding energies are not only element specific but contain chemical information as well (40, 41). This is because the energy levels of core electrons depend to some extent on the chemical state of the atom. In general, the binding energy increases with increasing oxidation number of the emitting atom. The reason for this is that the attractive force which the electrons feel from the nucleus is increased in more positively charged ions relative to neutral atoms. Chemical shifts are typically in the range 0-3 eV for a given XPS line (40, 41).

Photoelectron peaks are labelled according to the quantum numbers of the level from which the electron originates (40). An electron coming from an orbital with main quantum number  $n$ , orbital momentum  $l$  (0, 1, 2, 3,...indicated as s, p, d, f,...) and spin momentum  $s$  (+1/2 or -1/2) is indicated as  $nl_{l+s}$ . Thus for electrons from the 4d level of a Pt atom, a doublet XPS peak would be seen with the photolines referred to as Pt 4d<sub>5/2</sub> and Pt 4d<sub>3/2</sub> depending on the value of  $s$ .

Although XPS is predominantly used for studying surface compositions and oxidation states, information can also be obtained on the dispersion of supported catalysts because of the surface sensitive nature of the technique (40).

As discussed in section 1.4, the presence of Ce next to noble metals has been proposed to result in electron transfer from the precious metal to the rare earth (8, 39, 43). Such an interaction has been proposed to explain suppression of noble metal oxidation activity on addition of CeO<sub>2</sub> to Al<sub>2</sub>O<sub>3</sub>-supported samples due to increased oxidation of the noble metal in an oxidising environment (9, 11-14). Charge transfer from Pt to Ce has also been proposed to explain Pt-promoted oxidation of CO by CeO<sub>2</sub>, due to a reduction in the enthalpy for lattice oxygen removal from the rare earth oxide (44).

Experimental evidence for the existence of an electronic interaction between supported noble metals and CeO<sub>2</sub> has been reported. For example, Le Normand et al. (43) reported XPS evidence which indicated increased oxidation of Pd when in contact with neighbouring Ce on an Al<sub>2</sub>O<sub>3</sub> support, and this was supported by thermodynamic considerations of the redox potentials of the two metals. Shyu et al. (14) reported that CeO<sub>2</sub> promoted the oxidation of Pd to PdO both in the presence and absence of Al<sub>2</sub>O<sub>3</sub>. This was based on the XPS spectra of Pd/Al<sub>2</sub>O<sub>3</sub>, Pd/CeO<sub>2</sub> and Pd-CeO<sub>2</sub>/Al<sub>2</sub>O<sub>3</sub> samples reduced at 920°C and subsequently exposed to ambient air. In the absence of CeO<sub>2</sub>, no reoxidation occurred on exposure to ambient air, whilst for Pd/CeO<sub>2</sub> complete reoxidation, and for Pd-CeO<sub>2</sub>/Al<sub>2</sub>O<sub>3</sub>, partial reoxidation occurred (14).

For Pt-CeO<sub>2</sub>/Al<sub>2</sub>O<sub>3</sub> catalysts, Summers and Ausen (1) and Yu-Yao (8, 9) presented IR and kinetic evidence to suggest that Ce promotes/stabilises an oxidised Pt surface species. XPS has also been used to show changes in the oxidation state of Pt in the presence of CeO<sub>2</sub>. Engler et al. (6) reported from XPS results that Pt was in a partly oxidised state when supported on CeO<sub>2</sub>, while only metallic Pt (Pt<sup>0</sup>) was found on  $\gamma$ -Al<sub>2</sub>O<sub>3</sub> under otherwise comparable conditions. Similarly, Rh was completely oxidised in Rh/CeO<sub>2</sub> and only partially oxidised in Rh/Al<sub>2</sub>O<sub>3</sub> (6). Shyu and Otto (37) reported that, after calcination at 800°C, Pt on CeO<sub>2</sub> existed as Pt<sup>2+</sup> ascribed to a PtO species. Under the same conditions, Pt on Al<sub>2</sub>O<sub>3</sub> existed as bulk metallic Pt with surface Pt showing the

characteristic XPS spectrum of  $\text{Pt}^{4+}$  which was associated with dispersed Pt existing in a  $\text{PtO}_2\text{-Al}_2\text{O}_3$  complex. For  $\text{Pt-CeO}_2/\text{Al}_2\text{O}_3$ , XPS spectra indicated that Pt existed as  $\text{Pt}^{2+}$  (PtO), which was thought to indicate preferential interaction of Pt with  $\text{CeO}_2$  and this theory was supported by TPR results. Following reduction at  $500^\circ\text{C}$ , Pt was reduced to  $\text{Pt}^0$  in all samples. However, after reduction at  $920^\circ\text{C}$ , Pt was present as PtO in  $\text{Pt-CeO}_2/\text{Al}_2\text{O}_3$  samples and remained in an oxidised state even after reduction at  $500^\circ\text{C}$ . This was tentatively attributed to the formation of a surface  $\text{Pt-CeO}_x/\text{Al}_2\text{O}_3$  complex, involving Pt in association with  $\text{Ce}^{3+}$ , formed during high temperature reduction (37).

In apparent contradiction with the above studies, Oh and Eickel (3) reported CO-TPD and IR studies which indicated the absence of any appreciable electronic effects on addition of Ce to a  $\text{Rh}/\text{Al}_2\text{O}_3$  catalyst. Results suggested that charge transfer between Rh and Ce was not the reason for modification of CO oxidation kinetics by ceria, since the adsorptive properties of Rh were apparently unaffected. Löff et al (4) found no evidence for a Pt-Ce electronic interaction from the XPS spectra of pre-reduced  $\text{Pt}/\text{Al}_2\text{O}_3$ ,  $\text{Pt}/\text{CeO}_2$ , and  $\text{Pt}/\text{CeO}_2\text{-Al}_2\text{O}_3$  samples. On all supports, the chemical state of Pt was close to that of Pt metal. The Pt 4f binding energy was apparently unaffected by  $\text{CeO}_2$ , indicating the absence of any large charge transfer between Pt and ceria. However, no comparison of the Pt oxidation state in pre-oxidised samples was made due to complications with the overlap of Pt 4f and Al 2p peaks (4).

XPS studies have also revealed changes in the chemical state of surface  $\text{CeO}_2$  in  $\text{CeO}_2/\text{Al}_2\text{O}_3$  and noble metal/ $\text{CeO}_2/\text{Al}_2\text{O}_3$  systems when compared with unsupported  $\text{CeO}_2$ . In particular, it has been reported that Ce, at low loadings on  $\text{Al}_2\text{O}_3$ , tends to form a ceria-alumina surface species which exhibits a  $\text{Ce}^{3+}$ -like XPS spectrum (i.e. oxygen deficient) as a result of its' strong interaction with the alumina surface (35, 43). Le Normand et al. (43) thought that partial reduction of ceria in oxidation catalysts might not be totally unexpected, in light of the well known oxygen storage properties of ceria in such catalysts (see section 1.4.1), even though  $\text{CeO}_2$  reduction by powerful reducing agents such as  $\text{H}_2$  or CO is known to be difficult (38).

Characteristic Ce 3d XPS spectra for  $\text{CeAlO}_3$  ( $\text{Ce}^{3+}$ ) and  $\text{CeO}_2$  ( $\text{Ce}^{4+}$ ) samples are shown in Fig. 3.10 (35). Compared with  $\text{CeO}_2$ ,  $\text{CeAlO}_3$  is seen to exhibit a considerably different spectrum in the Ce 3d region. In particular, for  $\text{CeAlO}_3$  the  $u'''$  peak is absent and the relative intensity of  $v'$  with respect to  $v$  (and  $u'$  with respect to  $u$ ) is increased substantially (see Fig 3.10). The percentage area of the  $u'''$  peak in the total Ce 3d region ( $\text{Ce } 3d_{5/2}(v)$  and  $\text{Ce } 3d_{3/2}(u)$ ) has been used to describe the relative amount of  $\text{Ce}^{4+}$  in a sample (14, 35, 37). This is based on the assumption that the Ce 3d spectrum of a partially oxidised Ce species can be approximated as a linear combination of spectra

recorded from the oxides and also assumes no preferential enrichment of  $\text{Ce}^{4+}$  over  $\text{Ce}^{3+}$  or vice versa.

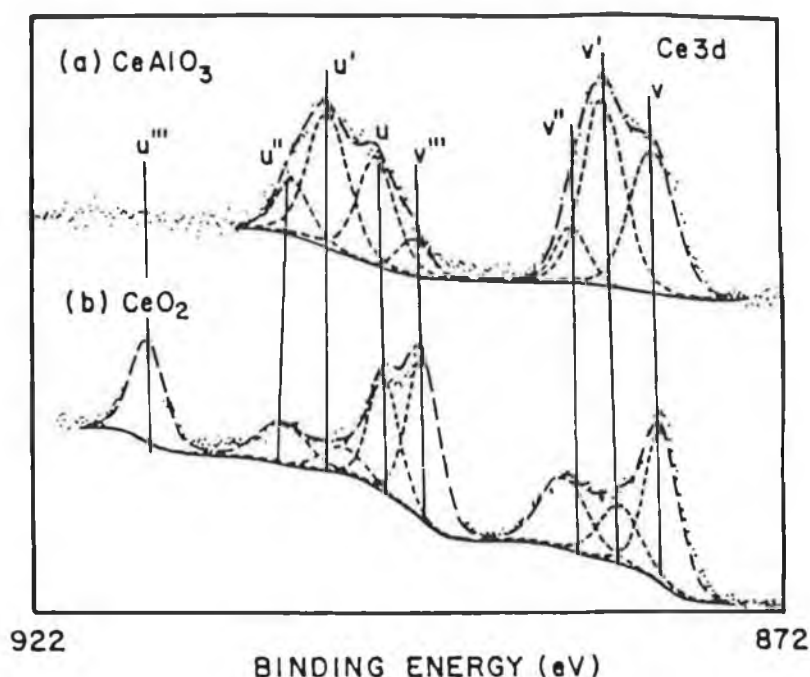


**Figure 3.10 : Ce 3d XPS spectra of  $\text{CeAlO}_3/\text{Al}_2\text{O}_3$ (a) and  $\text{CeO}_2$ (b) (35).**

Shyu et al. (35) found that for low  $\text{CeO}_2$  loadings, the Ce 3d XPS spectrum of  $\text{CeO}_2/\text{Al}_2\text{O}_3$  more closely resembled that of  $\text{Ce}^{3+}$  than  $\text{Ce}^{4+}$ . This was attributed to strong interaction between dispersed  $\text{CeO}_2$  and  $\text{Al}_2\text{O}_3$ . For low levels of  $\text{CeO}_2$  (below a dispersion limit of  $2.7 \mu\text{mol}$  of  $\text{CeO}_2$  per  $\text{m}^2$  of  $\text{Al}_2\text{O}_3$ ), two Ce species were thought to co-exist on the  $\text{Al}_2\text{O}_3$  surface, namely small  $\text{CeO}_2$  crystallites with properties resembling bulk  $\text{CeO}_2$  presumably due to weak interaction with the support and a dispersed Ce species which exhibited a  $\text{Ce}^{3+}$ -like spectrum in XPS and was referred to as a  $\text{CeAlO}_3$  precursor species. This latter species, which was found to dominate at very low loadings of  $\text{CeO}_2$  ( $<3.79 \mu\text{molm}^{-2}$ ), was presumed to be stabilised in the cation vacancies of the  $\text{Al}_2\text{O}_3$  and was not attributable to a  $\text{Ce}^{3+}$  compound because it was shown to be reducible in TPR experiments. As the  $\text{CeO}_2$  loading was increased, the % area of the  $u'''$  peak in the XPS spectra also increased, which suggested the growth of

dispersed CeO<sub>2</sub> species on the surface. Above the dispersion limit, growth of larger CeO<sub>2</sub> particles was found to occur. Reduction studies indicated that ceria in the form of the CeAlO<sub>3</sub> precursor and in small CeO<sub>2</sub> crystallite form, could be more easily reduced to CeAlO<sub>3</sub> than larger CeO<sub>2</sub> particles on Al<sub>2</sub>O<sub>3</sub>. Transformation to surface CeAlO<sub>3</sub> occurred on reduction above 600°C for dispersed Ce species, while even a partial conversion to CeAlO<sub>3</sub> from bulk CeO<sub>2</sub> required a temperature above 800°C. The fact that a higher temperature was required for the large CeO<sub>2</sub> particles was thought to be due to diffusional limitations of Ce to form the solid solution with Al<sub>2</sub>O<sub>3</sub>. Formation of CeAlO<sub>3</sub> was thought to involve some intermediate species in which ceria was at least partially reduced. CeAlO<sub>3</sub> was found to be thermally stable in air up to 600°C, unlike Ce<sub>2</sub>O<sub>3</sub> and other nonstoichiometric Ce oxides which tend to reoxidise in ambient air. Reduction of CeO<sub>2</sub> at 920°C followed by exposure to ambient air resulted in the same %u''' in the Ce 3d region of the XPS spectrum as for untreated CeO<sub>2</sub>, thereby indicating that complete surface reoxidation had occurred (35).

In a separate study, Shyu and Otto (37) reported the formation of CeAlO<sub>3</sub> from CeO<sub>2</sub>/Al<sub>2</sub>O<sub>3</sub> upon reduction at 920°C which was catalysed to completion by the presence of Pt. Without Pt, only partial reduction of Ce<sup>4+</sup> to Ce<sup>3+</sup> was achieved at 920°C. Similarly, Pd has been found to promote total conversion to bulk CeAlO<sub>3</sub> from CeO<sub>2</sub>/Al<sub>2</sub>O<sub>3</sub> (14). Both metals have been found to assist in the reverse reoxidation of bulk aluminate to CeO<sub>2</sub>/Al<sub>2</sub>O<sub>3</sub> (14, 37). XRD was used to confirm these observations. In support of the earlier study i.e. (35), the oxidation state of surface cerium in CeO<sub>2</sub>/Al<sub>2</sub>O<sub>3</sub>, Pd/CeO<sub>2</sub>/Al<sub>2</sub>O<sub>3</sub>, and Pt/CeO<sub>2</sub>/Al<sub>2</sub>O<sub>3</sub> samples, calcined at 800°C, was always found to be less than that in CeO<sub>2</sub> (i.e. <4+), based on the total %u''' in the Ce 3d spectra (14, 37). Again, this was assigned to a ceria-alumina interaction which resulted in highly stable dispersed ceria in a Ce<sup>3+</sup>-like state. The presence of the noble metals did not appear to have any effect on the chemical state of Ce following calcination, as similar %u''' values were found in both the presence and absence of the noble metals (14, 37).

Le Normand et al. (43) also found evidence to indicate partial reduction of ceria in Ce/γ-Al<sub>2</sub>O<sub>3</sub> and Pd-Ce/γ-Al<sub>2</sub>O<sub>3</sub> systems using XPS and X-ray absorption spectroscopy (XAS). The degree of reduction was found to be more pronounced on the surface and was influenced by various parameters including Ce loading, the presence of the transition metal, the nature of the transition metal precursor salt, and the experimental conditions employed for in-situ reduction (43).

In view of these previous studies, it was of interest to investigate the chemical state of both Pt and Ce in the Pt/Al<sub>2</sub>O<sub>3</sub>, Pt-Ce/Al<sub>2</sub>O<sub>3</sub> and Pt/CeO<sub>2</sub> samples under investigation in the present study, and to attempt to discern if there existed a relationship

between  $i\text{-C}_4\text{H}_{10}$  combustion activity and Pt oxidation state before and after different pretreatments. XPS analysis was of interest to investigate the surface elemental composition of the catalysts under study.

## **3.2 Experimental**

### **3.2.1 X-ray Photoelectron Spectroscopy (XPS)**

XPS measurements were carried out in the Experimental Techniques Centre (ETC) at Brunel University, Middlesex, using an Escalab 210 instrument. An Al  $K\alpha$  ( $h\nu = 1486.6\text{eV}$ ) anode was used as the excitation source with an analyser pass energy of  $50.0\text{eV}$ . Catalyst samples were presented as powders dusted onto double-sided adhesive tape mounted on stainless steel sample studs. For each sample examined, a survey scan from  $0\text{eV}$  to  $1350\text{eV}$  and expanded energy scans of the most important elemental peaks were obtained. For the survey scan a step size of  $1.00\text{eV}$  was employed, while for the expanded scans a step size of  $0.10\text{eV}$  was used.

### **3.2.2 $\text{H}_2$ Chemisorption Measurements**

The instrumental details and the procedure used for analysis by  $\text{H}_2$  chemisorption have already been described in Section 2.2.4. A pre-reduction temperature of  $400^\circ\text{C}$  was used for the preparation of all samples.

### **3.2.3 Temperature Programmed Reduction (TPR).**

A schematic diagram of the apparatus used for TPR experiments is illustrated in Fig. 3.11. TPR profiles were obtained using a  $5\% \text{H}_2/95\% \text{Ar}$  mixture supplied by Irish Industrial Gases (IIG). The gas was purified by passing it through a molecular sieve drying column and an oxygen trap at a flow rate of  $80 \text{cm}^3.\text{min}^{-1}$ . The gas then passed through the reference arm of the thermal conductivity cell, then through ca.  $0.3\text{g}$  of the catalyst sample held on a sintered disc in a quartz u-tube, and finally through the other arm of the TCD where any change in  $\text{H}_2$  concentration was monitored. The variation of  $\text{H}_2$  content with time was recorded while the sample was heated linearly from  $20^\circ\text{C}$  to  $500^\circ\text{C}$  at  $7^\circ\text{C}.\text{min}^{-1}$ . Since the gas flow was constant, the change in  $\text{H}_2$  concentration was proportional to the rate of reduction of the catalyst sample. The furnace used was supplied by Lenton Thermal Designs Systems Ltd. and had a programmable temperature controller. A cold trap at ca.  $-90^\circ\text{C}$  (liquid  $\text{N}_2/\text{ethanol}$  mix) was placed downstream of the sample to remove any  $\text{H}_2\text{O}$  or  $\text{HCl}$  from the gas before it reached the detector.

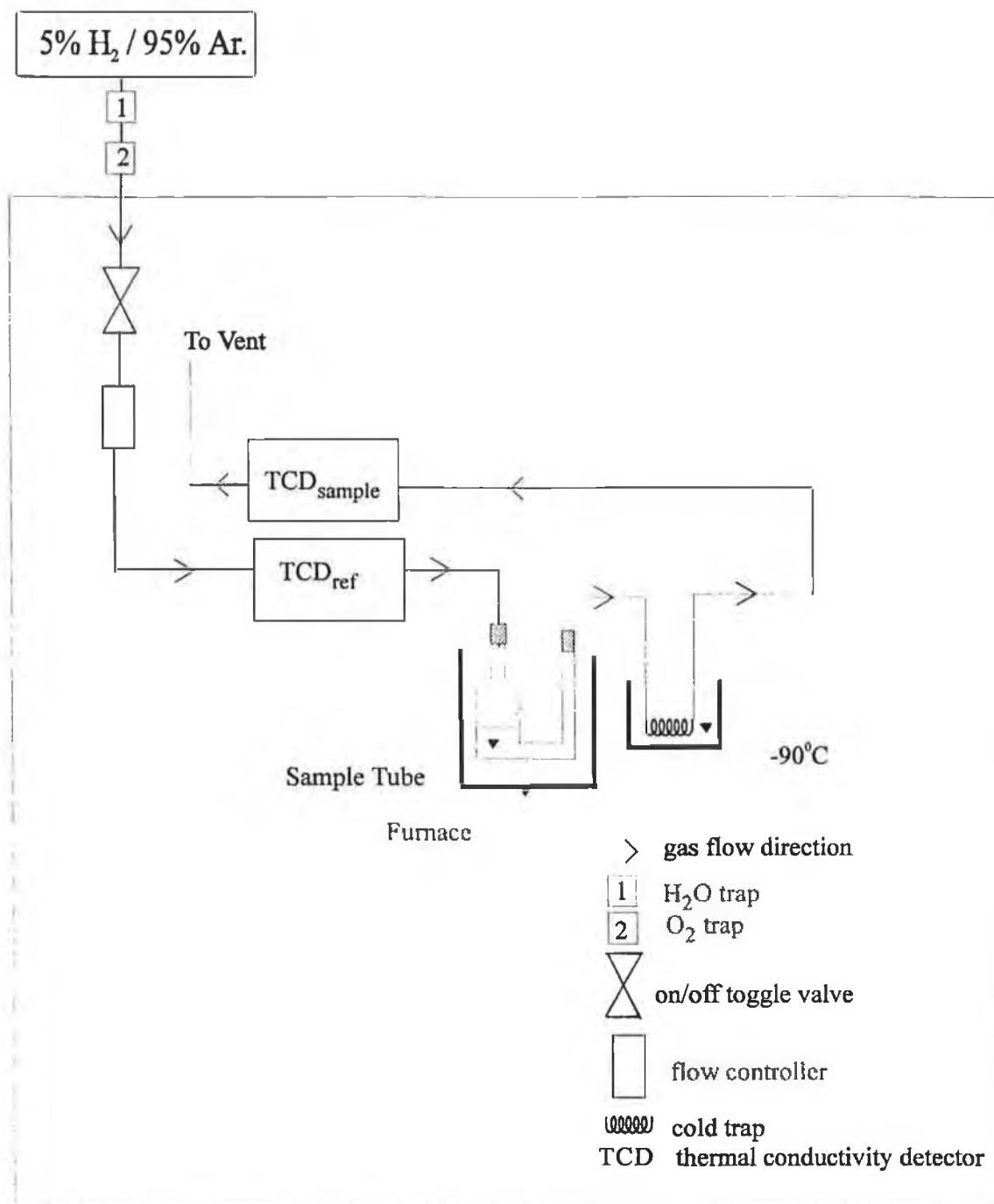


Figure 3.11 : Temperature Programmed Reduction Apparatus.

### 3.2.4. Activity Measurements

Catalytic activity of the different samples was compared by monitoring the combustion of  $i\text{-C}_4\text{H}_{10}$  as a function of temperature using a continuous flow apparatus. A schematic drawing of the activity unit used is shown in Fig. 3.12. The activity unit was designed to allow the controlled flow of an air :  $i\text{-C}_4\text{H}_{10}$  gas mixture over heated catalysts. The gases used were supplied by Air Products. Using a 4-port switching valve, the reaction mixture could be passed directly to the Gas Chromatograph (G.C.) (bypassing the sample) in order to check the "baseline" concentration of  $i\text{-C}_4\text{H}_{10}$  which was measured using a Flame Ionisation Detector (F.I.D). Flow rates of  $i\text{-C}_4\text{H}_{10}$  and air were measured using a bubble flow meter prior to each run, and were controlled using mass flow controllers with ranges of  $0\text{-}5\text{cm}^3\text{min}^{-1}$  and  $0\text{-}100\text{cm}^3\text{min}^{-1}$ , respectively. A cold trap at  $0^\circ\text{C}$  (ice) was placed downstream of the sample to remove any water produced before reaching the chromatograph. Gas samples were injected onto the chromatograph using a 1ml sampling valve. The instrumental conditions used for G.C. analysis are given in Table 3.1.

**Table 3.1** : Instrumental Conditions for G.C. Analysis.

Instrument	Pye Unicam 4550
Detector	Flame ionisation detector
Column	2m, 6mm i.d, Packed
Column Packing	Poropak Q
Carrier Gas	He (normal grade, Air Products) Flow rate : $40\text{ cm}^3\text{min}^{-1}$
Temperatures	Column : $200^\circ\text{C}$ Injector : $225^\circ\text{C}$ Detector : $225^\circ\text{C}$

For catalyst activity measurements, a stoichiometric mixture of iso-butane in air (ratio-ca.1:32) was used at a flow rate of  $16\text{cm}^3.\text{min}^{-1}$ . The reaction mixture was passed through 0.3g of the catalyst sample which was held on a sintered disc in a quartz u-tube. The sample was heated using a furnace supplied by Lenton Thermal Designs Systems Ltd. Unreacted  $i\text{-C}_4\text{H}_{10}$  was monitored at each temperature by in-situ G.C.. At each temperature, the effluent stream leaving the sample was monitored for at least 15 minutes until equilibrium was attained. After the first analysis run of a catalyst from  $20\text{-}350^\circ\text{C}$ , the sample was cooled to room temperature and the analysis was repeated i.e. each activity test performed on a given sample involved two runs from  $20\text{-}350^\circ\text{C}$ .

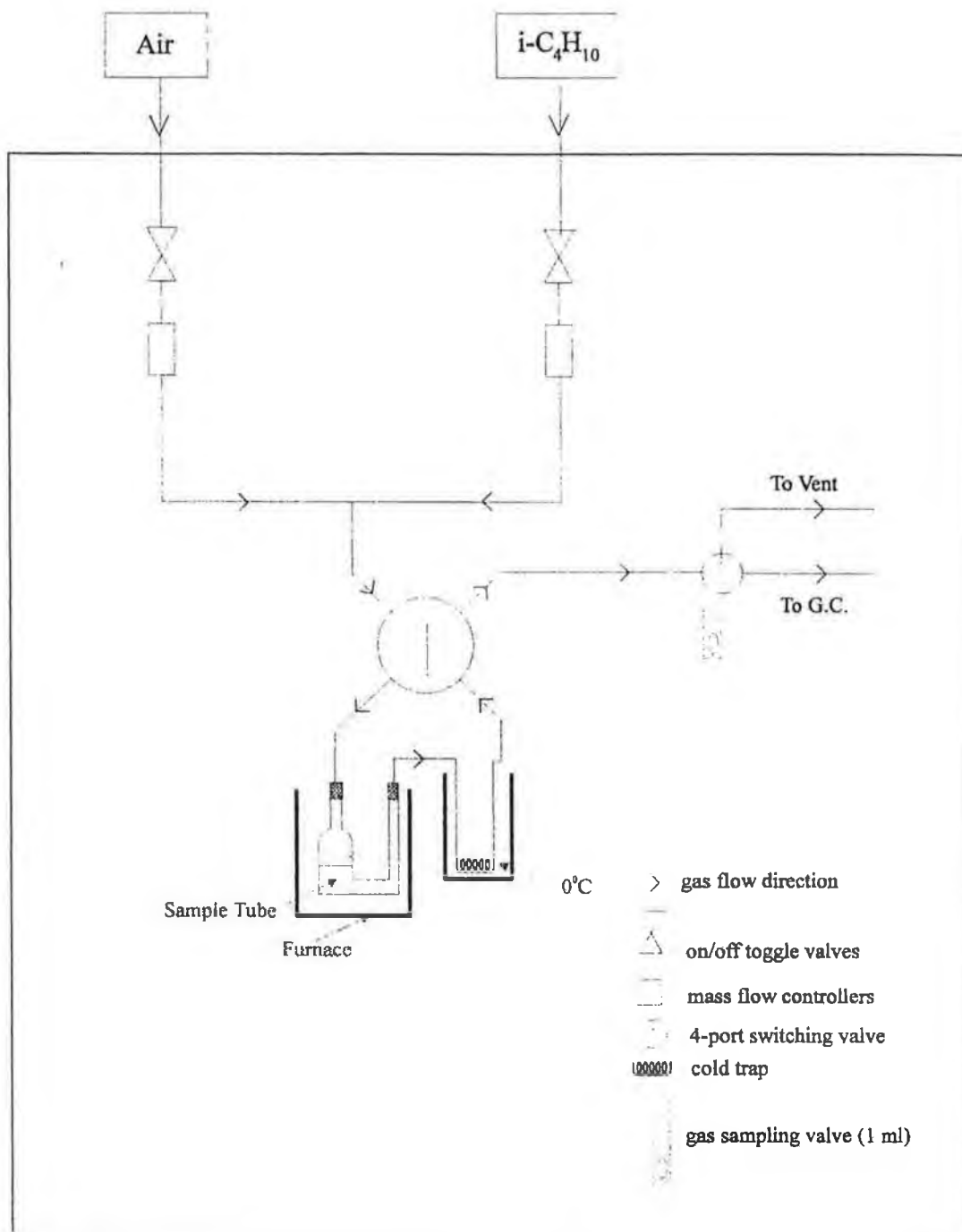


Figure 3.12 : Activity Unit for Catalyst Testing.



The TPR profiles and activity of the support materials, CeO<sub>2</sub>, γ-Al<sub>2</sub>O<sub>3</sub>, and 2.9% Ce/γ-Al<sub>2</sub>O<sub>3</sub> (sample C8A), were also assessed. TPR of uncalcined precursors of samples PA, PC1A, and PC8A, were also investigated.

### **[b] Aging Tests**

Samples of the catalysts PA, PC10A, PC, and PZ were artificially aged in different atmospheres at 800°C for 10 hours. Aging in static air was performed in a muffle furnace. Aging was also performed under continuous flow conditions in Ar at a flow rate of 40cm<sup>3</sup>min<sup>-1</sup>, and in the stoichiometric air : i-C<sub>4</sub>H<sub>10</sub> reaction mixture at a flow rate of 16cm<sup>3</sup>min<sup>-1</sup>.

Aged samples were investigated using H<sub>2</sub> chemisorption, TPR, and XPS techniques. The activity of the aged samples of PA, PC10A, and PC, and of catalyst PZ, both before and after aging, for the combustion of iso-butane in air was also examined.

### **3.3 Results and Discussion**

The results of sample analysis will be presented and discussed under three separate headings. In section 3.3.1, initial characterisation of the prepared catalysts using XPS and TPR is discussed. The oxidation activity of the catalysts is then discussed in section 3.3.2. The effects of activity testing on the catalyst surfaces is also examined using XPS, TPR and H<sub>2</sub> chemisorption measurements. Finally, in section 3.3.3, the effects of aging treatments on the catalyst surfaces is discussed.

#### **3.3.1 Characterisation of 'Fresh' Catalysts**

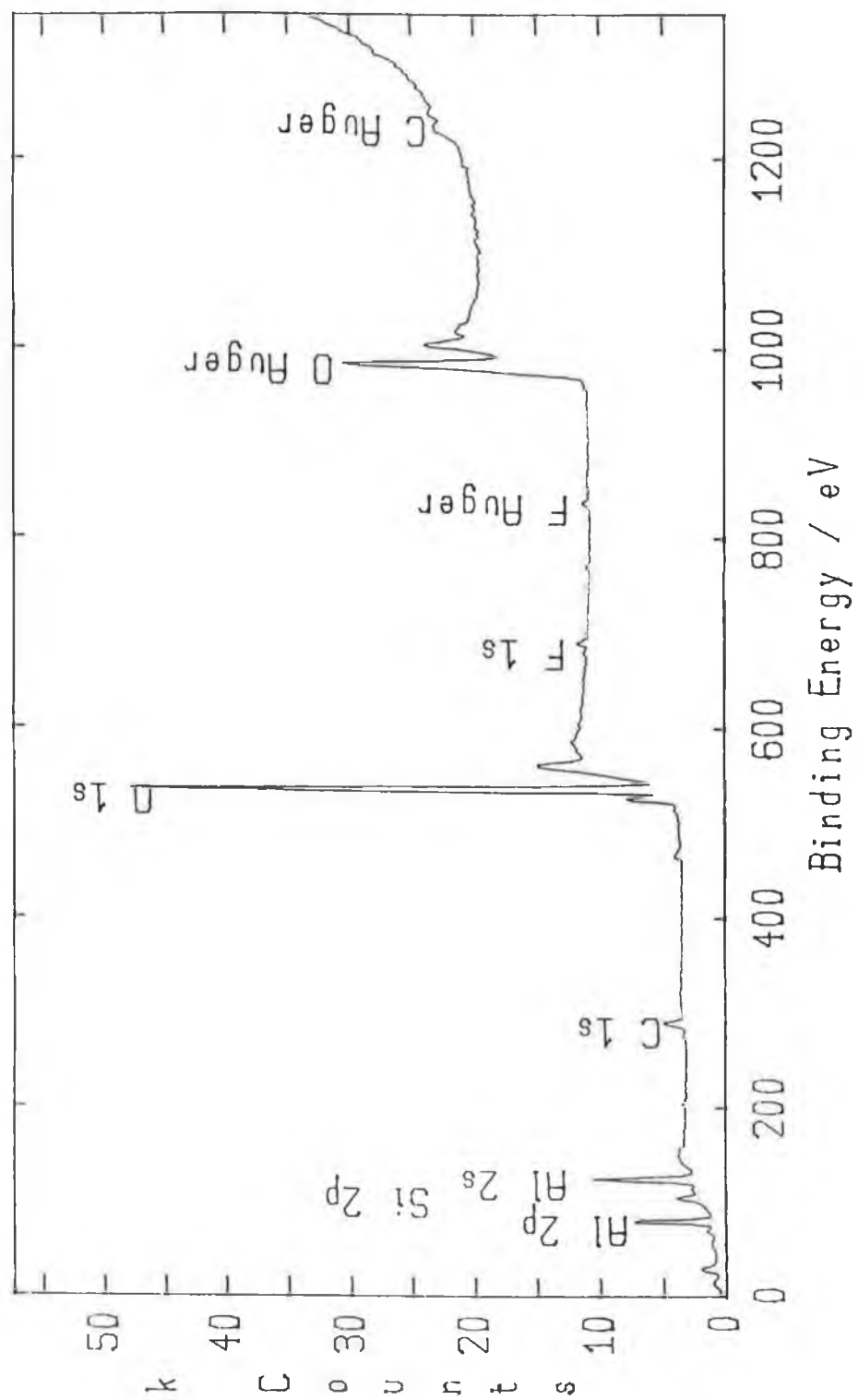
##### **X-ray Photoelectron Spectroscopy (XPS)**

XPS analysis was carried out on samples PA, PC, PC0.5A, and PC10A, after the standard preparation procedure described in section 2.2.1. The spectra obtained are illustrated in Fig. 3.13-3.16. Difficulty was encountered in analysing the data for the Al<sub>2</sub>O<sub>3</sub>-supported samples due to overlap of the Pt 4f and the Al 2p peaks in the region around 70.0eV to 80.0eV binding energy. Because of this the Pt 4d lines were analysed instead. Although these lines are less sensitive and relatively broad, the Pt 4d<sub>5/2</sub> line has been used in previous studies to investigate changes in the oxidation state of Al<sub>2</sub>O<sub>3</sub>-supported Pt (7, 45, 46). Due to the insulating nature of the samples, corrections for surface charging in the spectra illustrated was necessary. This was achieved by referencing the XPS binding energies to the adventitious C 1s line, which is done by finding the position in the spectra of the C 1s line and subtracting the difference, between this value and the accepted value for the C 1s peak at 284.6eV (46, 47), from the other peak positions. All peak positions discussed here are those obtained after this charge correction. Unless otherwise specified, standard peak positions for the different elements were obtained from references (47) and (48).

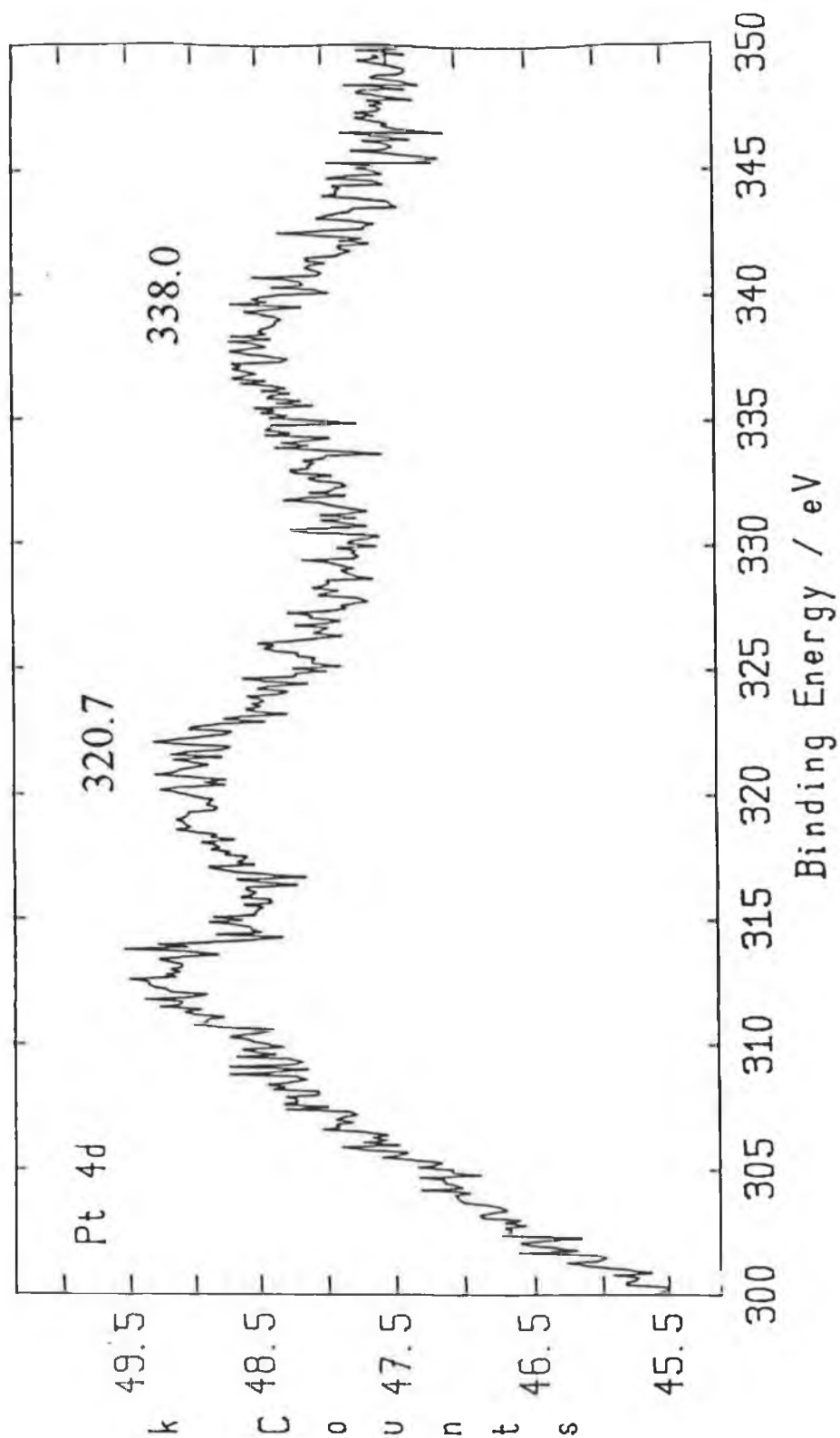
The XPS spectrum obtained for sample PA is illustrated in Fig. 3.13(a) and an expanded scan of the Pt 4d region is shown in Fig. 3.13(b). Main features of interest in the survey scan were the C 1s peak at 284.6eV, the Al 2p peak at 74.3eV, and the O 1s peak at 531.1eV. Both Si and F were also indicated to be present on the surface by the presence of Si 2p, F 1s, and F auger peaks at ca.100.0eV, ca.686.0eV and ca.832.0eV, respectively. Residual Cl from the H<sub>2</sub>PtCl<sub>6</sub> precursor salt may also have been present after calcination with the small peak at slightly higher than 200eV on the spectrum possibly attributable to the Cl 2p line expected at ca.199eV after charge correction. The expanded scan of the Pt 4d region contains peaks at 320.7eV and 338.0eV. After correction for sample charging, these peaks can be assigned to the Pt 4d<sub>5/2</sub> level at 315.6eV and the Pt 4d<sub>3/2</sub> level at 332.9eV, respectively. Shyu and Otto (45) reported Pt

4d<sub>5/2</sub> peak positions of 314.2 ± 0.3eV, 315.3 ± 0.3eV, and 317.0 ± 0.3eV for Pt foil, PtO, and PtO<sub>2</sub>, respectively. These positions were used to investigate the oxidation state of Pt in Pt/Al<sub>2</sub>O<sub>3</sub> samples with intermediate binding energies being assigned to mixtures of different oxidation states (45). Nunan et al. (7) also studied Al<sub>2</sub>O<sub>3</sub>-supported Pt by XPS and interpreted spectra in terms of Pt 4d<sub>5/2</sub> peaks in the binding energy region of 314.0-315.5eV for Pt<sup>0</sup>, and peaks above 315.5eV being attributable to oxidised Pt. A central peak position of 315.6eV, found in the present study, is therefore interpreted to indicate the presence of oxidised Pt in sample PA, with a Pt 4d<sub>5/2</sub> peak binding energy coinciding with that of PtO reported in the literature (45). Lieske et al. (28, 29) reported that oxidation of Pt/Al<sub>2</sub>O<sub>3</sub> between 400 and 600°C produced Pt<sup>4+</sup> species. Al<sub>2</sub>O<sub>3</sub>-supported Pt has been previously reported in other studies to exist as PtO<sub>2</sub> on the surface, with a Pt 4d<sub>5/2</sub> binding energy of 317.0eV found for samples which had been calcined at 800°C (37) and 525°C (46), but has also been found to show a Pt 4d<sub>5/2</sub> binding energy of 315.3eV corresponding to that of PtO after oxidation at 450°C (45).

The XPS spectra for sample PC are illustrated in Fig. 3.14(a)-(d). The main spectral features of interest in the survey scan (Fig. 3.14(a)) are the C 1s peak, the O 1s peak, and Ce 4d, Ce 4p, Ce 3d, and Ce auger peaks. Both Cl and Na are also indicated to be present on the surface by the apparent presence of Cl 2p, Cl auger, and Na 1s peaks at ca.200eV, ca.1304eV, and ca.1072eV, respectively. Expanded scans of the Pt 4d and Pt 4f regions are shown in Fig. 3.14(b) and (c), respectively. The peak positions for the Pt 4d<sub>5/2</sub> and Pt 4d<sub>3/2</sub> lines were 315.8eV and 332.5eV after correction for sample charging effects on the peaks at 322.5 and 339.2eV in Fig. 3.14(b). A Pt 4d<sub>5/2</sub> binding energy of 315.8eV indicates the presence of oxidised surface Pt (7, 45), with a very slight electropositive shift of 0.2eV relative to sample PA. Pt 4f<sub>7/2</sub> and Pt 4f<sub>5/2</sub> binding energies of 72.6eV and 75.7eV were found after correction for surface charging in Fig. 3.14 (c). Pt 4f<sub>7/2</sub> binding energies of 71.1 ± 0.2eV, 72.2 ± 0.2eV, and 74.2 ± 0.2eV have been reported for Pt<sup>0</sup>, PtO, and PtO<sub>2</sub> samples, respectively (45). Thus, both the Pt 4d<sub>5/2</sub> and Pt 4f<sub>7/2</sub> binding energies are slightly higher than those reported for PtO (45). Previous XPS studies of Pt/CeO<sub>2</sub> samples have reported surface Pt to exist as PtO (Pt<sup>2+</sup>) after oxidative treatment in air (12) or O<sub>2</sub> (4) at 500°C and after calcination at 800°C (37). In the present study, Pt also appears to exist as PtO in sample PC. An expanded energy scan of the Ce 3d region is illustrated in Fig. 3.14(d) which shows the typical features of CeO<sub>2</sub> (Ce<sup>4+</sup>) in this region (see Fig. 3.10). This is in agreement with the findings of Lööf et al. (4) who reported that the addition of Pt to a CeO<sub>2</sub> support does not affect the Ce 3d spectrum.

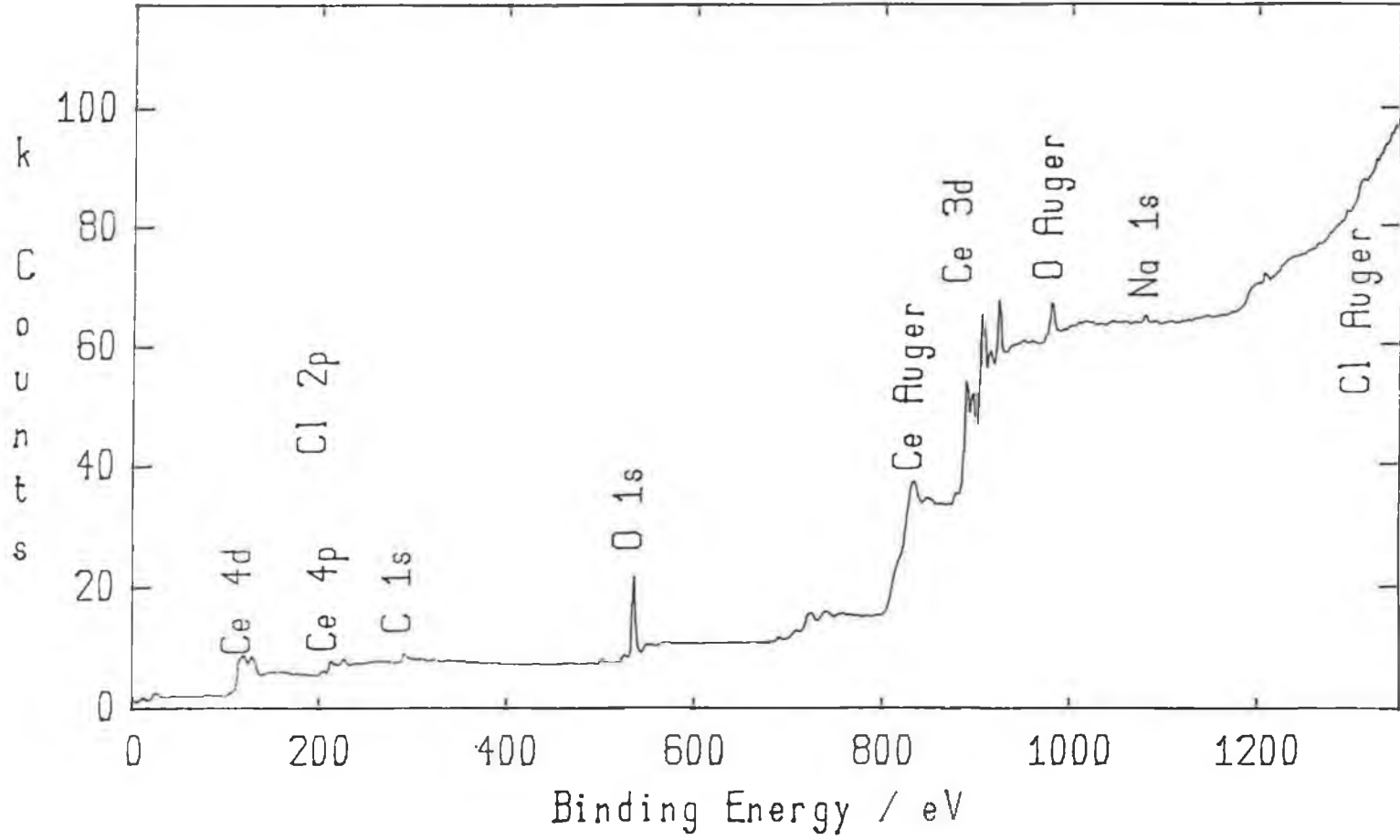


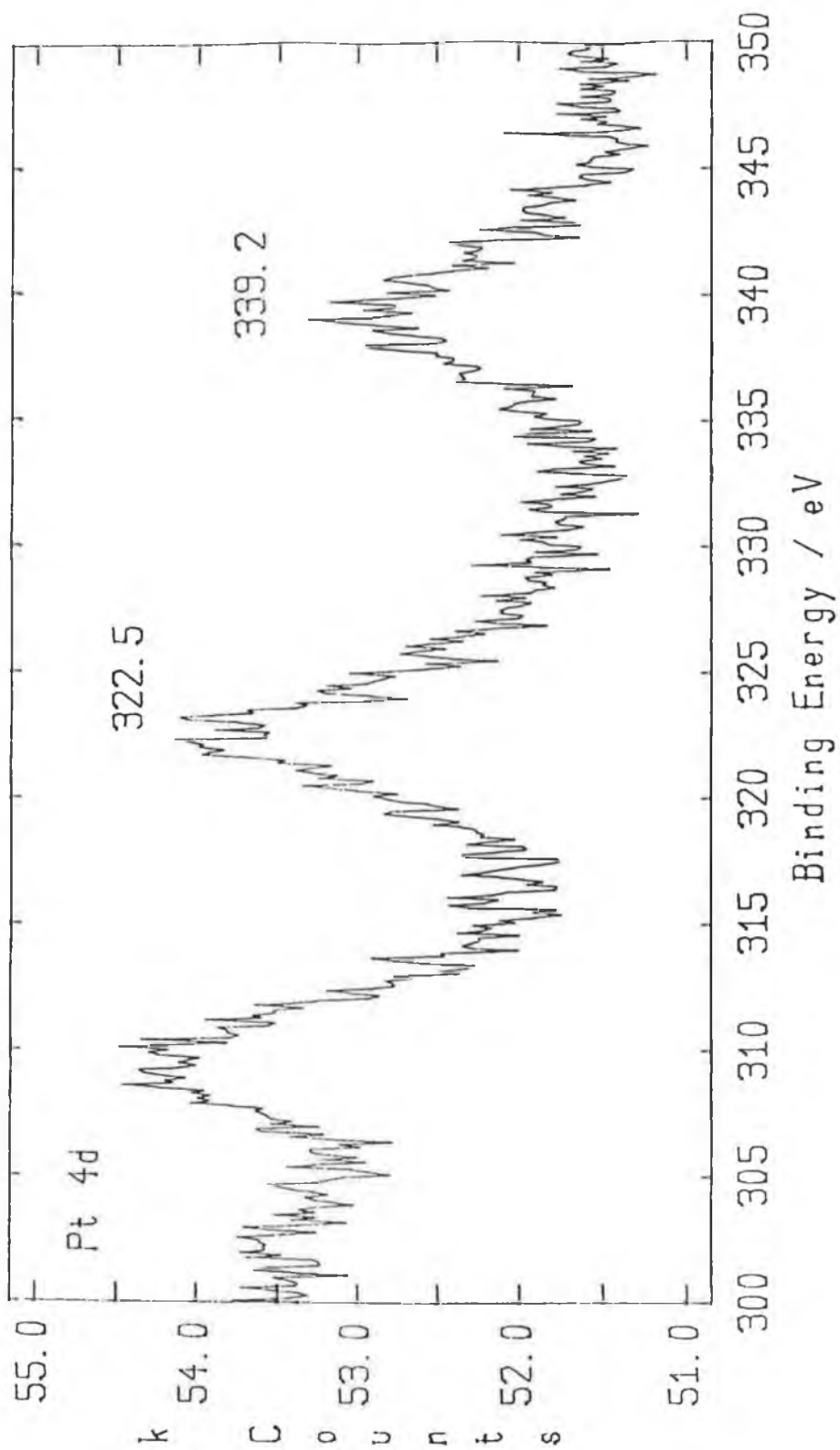
**Fig 3.13(a) : XPS spectrum of sample PA.**



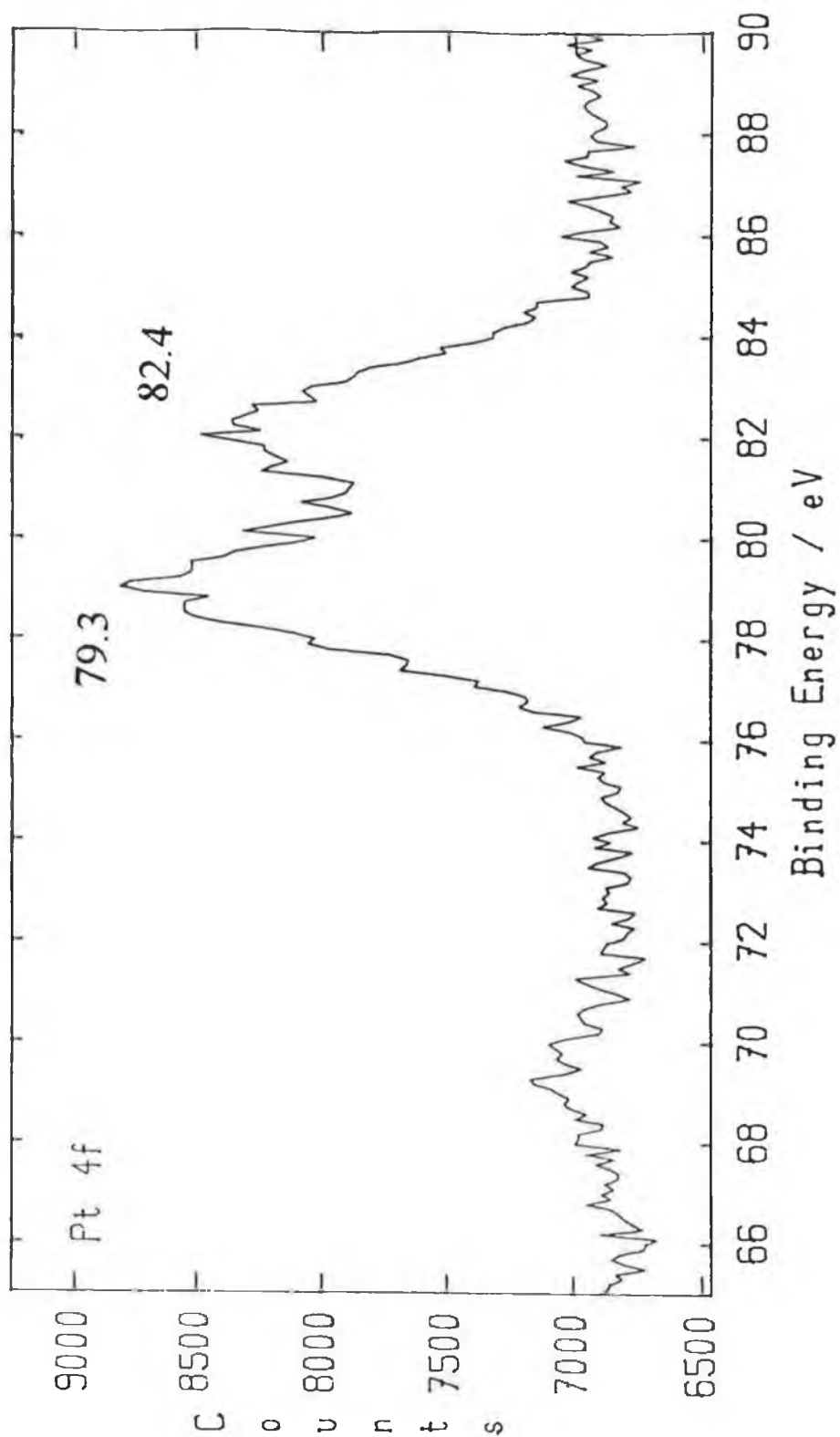
**Fig 3.13(b) :** XPS spectrum showing an expanded energy range scan in the Pt 4d region for sample PA. Charge Correction = 5.1 eV.

Fig. 3.14(a) : XPS spectrum of sample PC.





**Fig 3.14(b) : XPS spectrum showing an expanded energy range scan in the Pt 4d region for sample PC. Charge Correction = 6.7 eV.**



**Fig 3.14(c) : XPS spectrum showing an expanded energy range scan in the Pt 4f region for sample PC. Charge Correction = 6.7 eV.**

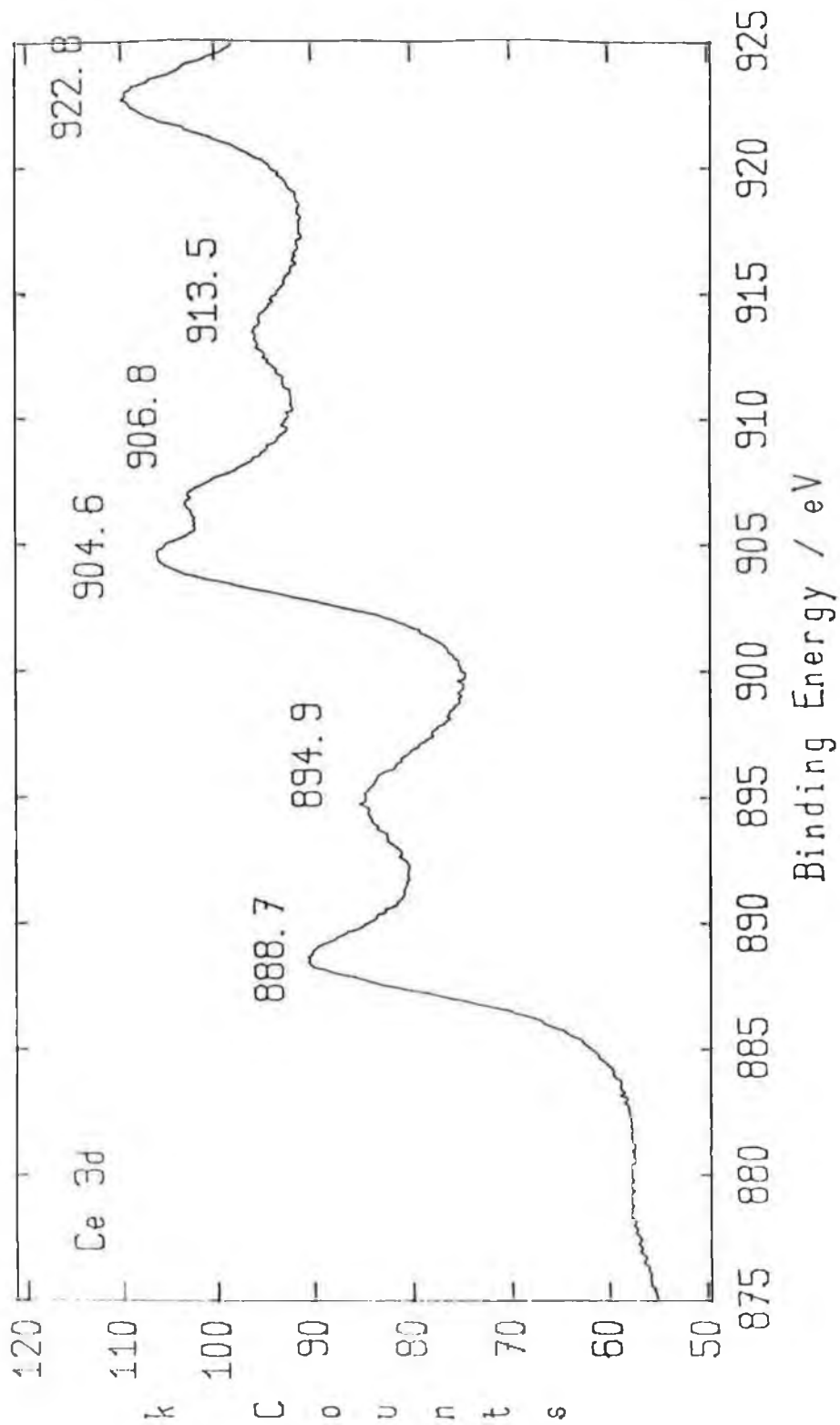
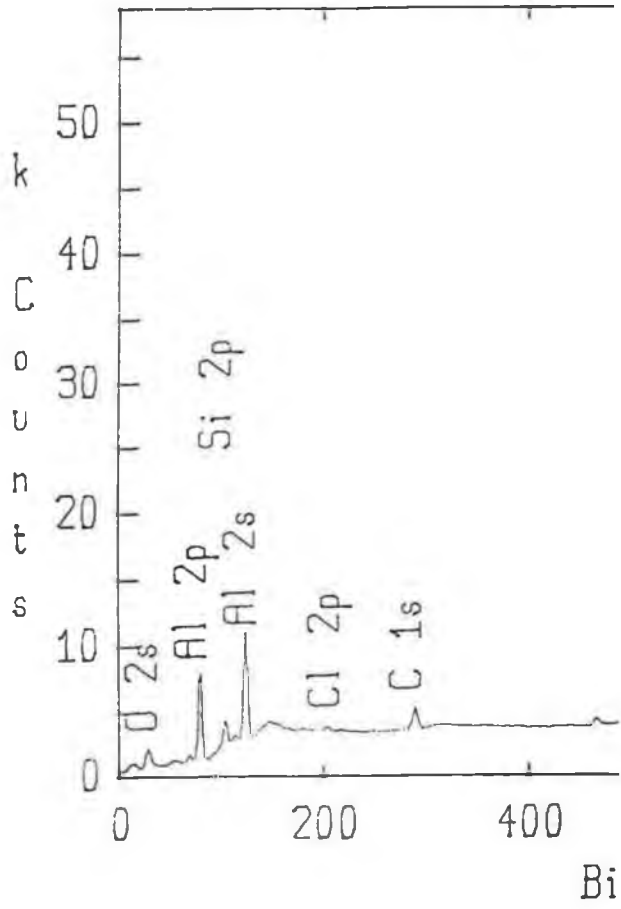


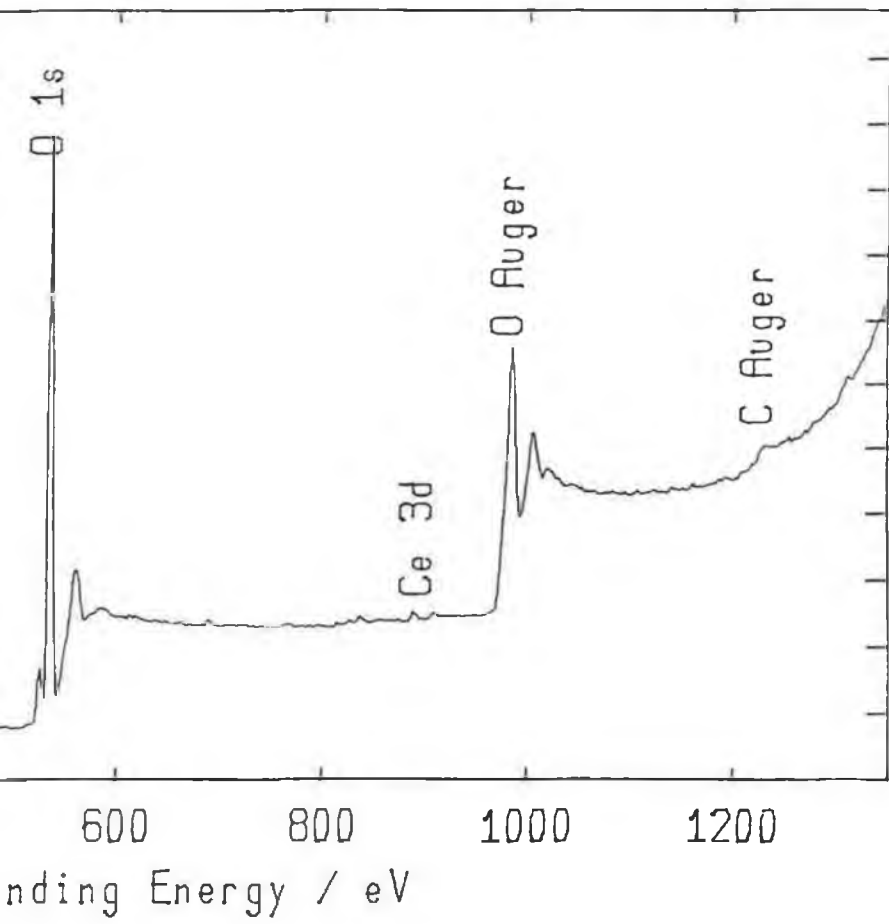
**Fig 3.14(d) : XPS spectrum showing an expanded energy range scan in the Ce 3d region for sample PC. Charge Correction = 6.7 eV.**

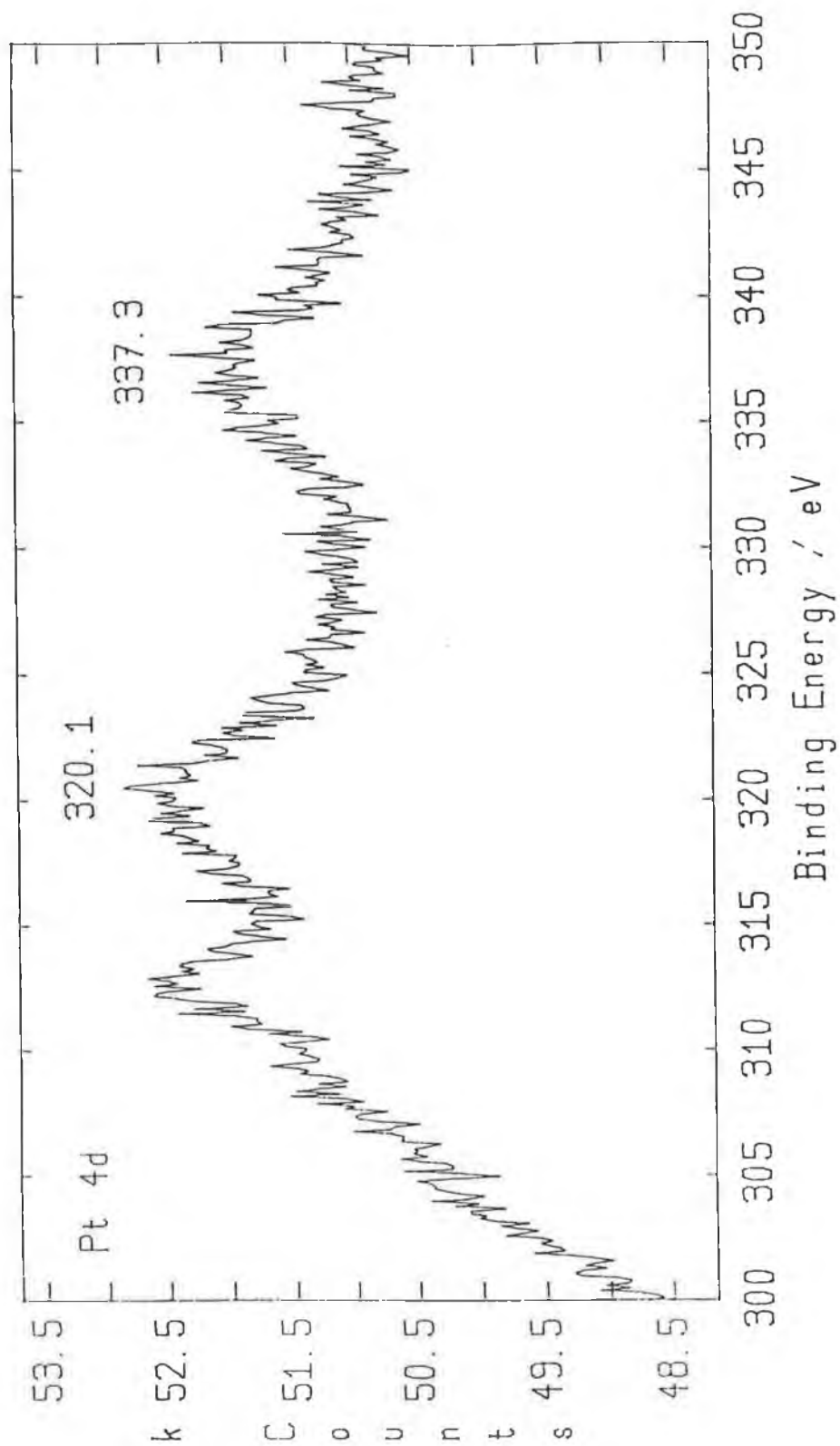
The XPS spectra for sample PC0.5A are illustrated in Fig. 3.15(a)-(c). The main features of the survey scan (Fig. 3.15(a)) include the C 1s peak, the O 1s peak, the Al 2p peak, and the Ce 3d feature. As for sample PA, both Cl and Si are also present. After charge correction, Pt 4d<sub>5/2</sub> and Pt 4d<sub>3/2</sub> peak positions were found to be 314.7eV and 331.9eV, respectively (Fig. 3.15(b)), indicating a decreased oxidation of surface Pt relative to samples PA and PC. The Pt 4d<sub>5/2</sub> binding energy was intermediate between that of Pt<sup>0</sup> and Pt<sup>2+</sup> (45). The Ce 3d spectrum (Fig. 3.15(c)) has a poorer signal-to-noise ratio than that obtained for sample PC due to the lower level of Ce present. However, it is evident that the Ce 3d spectrum is considerably different to that which was obtained for PC (see Fig. 3.14(d)). The spectrum obtained for sample PC0.5A resembles that of Ce<sup>3+</sup> more closely than that of Ce<sup>4+</sup> (see Fig. 3.10). In line with the conclusions of Shyu et al. (35), the Ce 3d spectral features are indicative of the presence of a ceria-alumina interactive species as the major surface Ce species at the low level present (0.15 wt.% Ce) and this interaction appeared to stabilise the Ce in a more reduced state than that in CeO<sub>2</sub>. This species was referred to by Shyu et al. (35) as a 'CeAlO<sub>3</sub>-precursor' because, even though its XPS spectrum resembled that of Ce<sup>3+</sup>, it was still reducible in TPR experiments. It has been reported that CeO<sub>2</sub> can be reduced only to Ce<sup>3+</sup> at temperatures below 900°C (36).

The survey scan for sample PC10A (fresh sample) is shown in Fig. 3.16(a) and is similar to that of PC0.5A (Fig. 3.15(a)) with a larger Ce 3d feature evident for PC10A due to the higher Ce content. Expanded scans of the C 1s, Pt 4d, and Ce 3d regions are illustrated in Fig. 3.16(b)-(d). After charge correction, Pt 4d<sub>5/2</sub> and Pt 4d<sub>3/2</sub> peaks (Fig. 3.16(c)) had central binding energy positions of 316.1 and 333.1eV, respectively. The increased binding energy for the Pt 4d<sub>5/2</sub> line relative to that for sample PA (316.1 vs. 315.6eV) may indicate increased oxidation of Al<sub>2</sub>O<sub>3</sub>-supported Pt surface species after addition of 3.6 wt.% Ce. An increase in the oxidation of Al<sub>2</sub>O<sub>3</sub>-supported Pt on addition of Ce has been previously proposed by several authors (1, 8, 9, 11, 12). Serre et al. (39) believed that a slight increase in Pt oxidation state may reflect charge transfer from metal to ceria, indicating that Ce is slightly reduced. This theory was supported by the fact that Pt promoted surface ceria reduction. As discussed below, TPR profiles indicated that Pt also promoted surface ceria reduction in the current study. As for sample PC0.5A, the Ce 3d spectrum for PC10A (Fig. 3.16(d)) bears a closer resemblance to that of Ce<sup>3+</sup> than that of Ce<sup>4+</sup> (see Fig. 3.10). Again, this is assumed to indicate the existence of a strong interaction between dispersed Ce and the Al<sub>2</sub>O<sub>3</sub> support, which stabilised Ce in a partially reduced state presumably due to the formation of a CeAlO<sub>3</sub>-like species (35). This is not unexpected since the concentration of CeO<sub>2</sub> in PC10A was

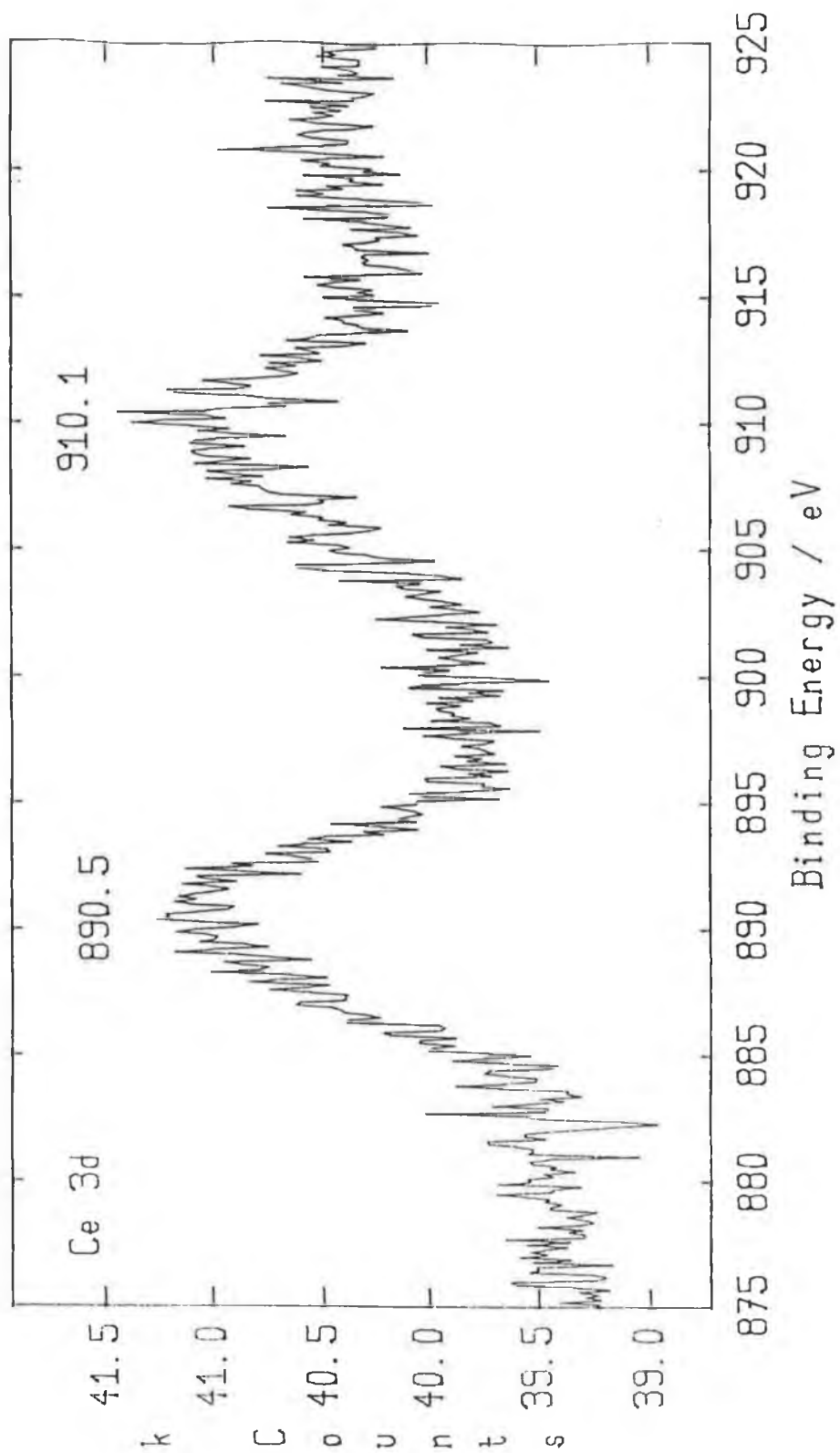
Fig 3.15(a) : XPS spectrum of sample PC0.5A.





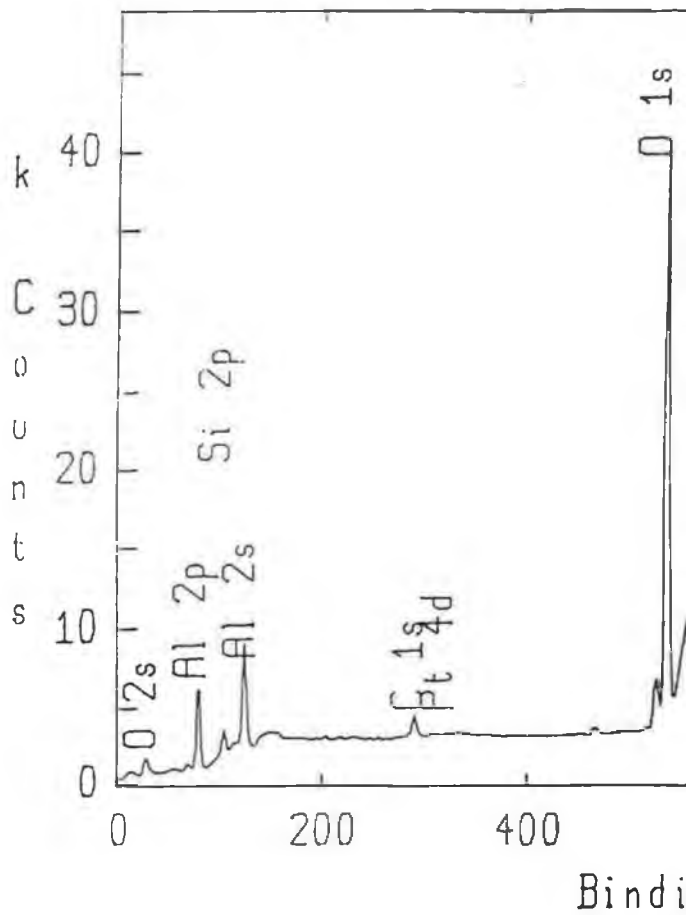


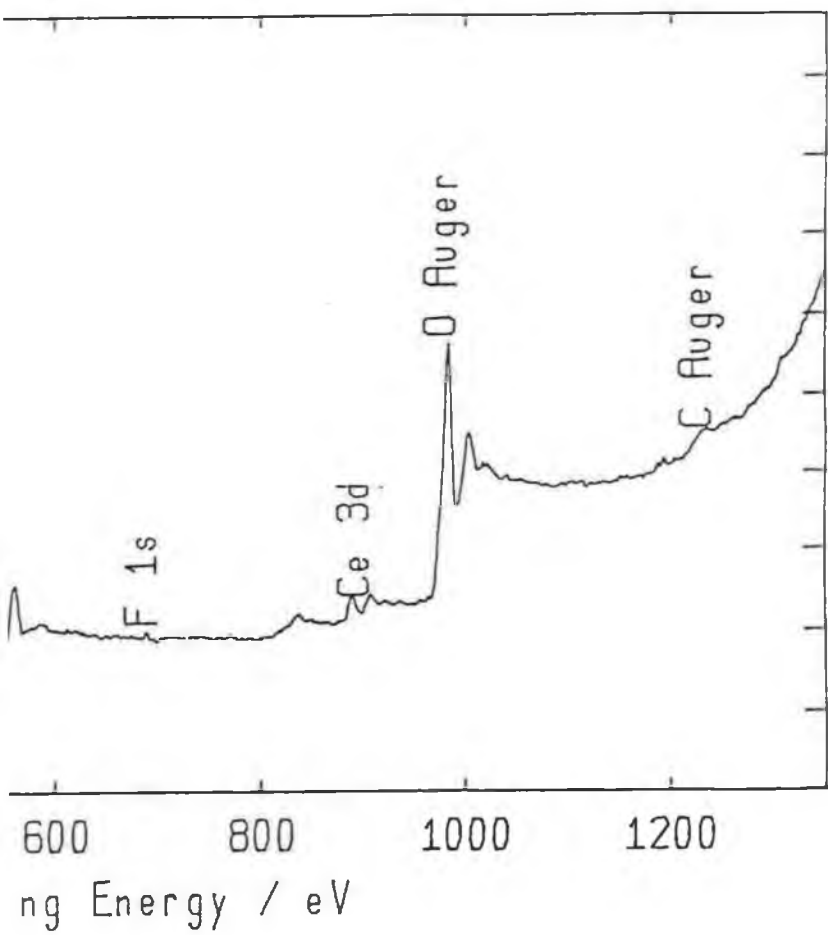
**Fig 3.15(b) : XPS spectrum showing an expanded energy range scan in the Pt 4d region for sample PC0.5A. Charge Correction = 5.4 eV.**



**Fig 3.15(c) : XPS spectrum showing an expanded energy range scan in the Ce 3d region for sample PC0.5A. Charge Correction = 5.4 eV.**

Fig 3.16(a) : XPS spectrum of sample PC10A.





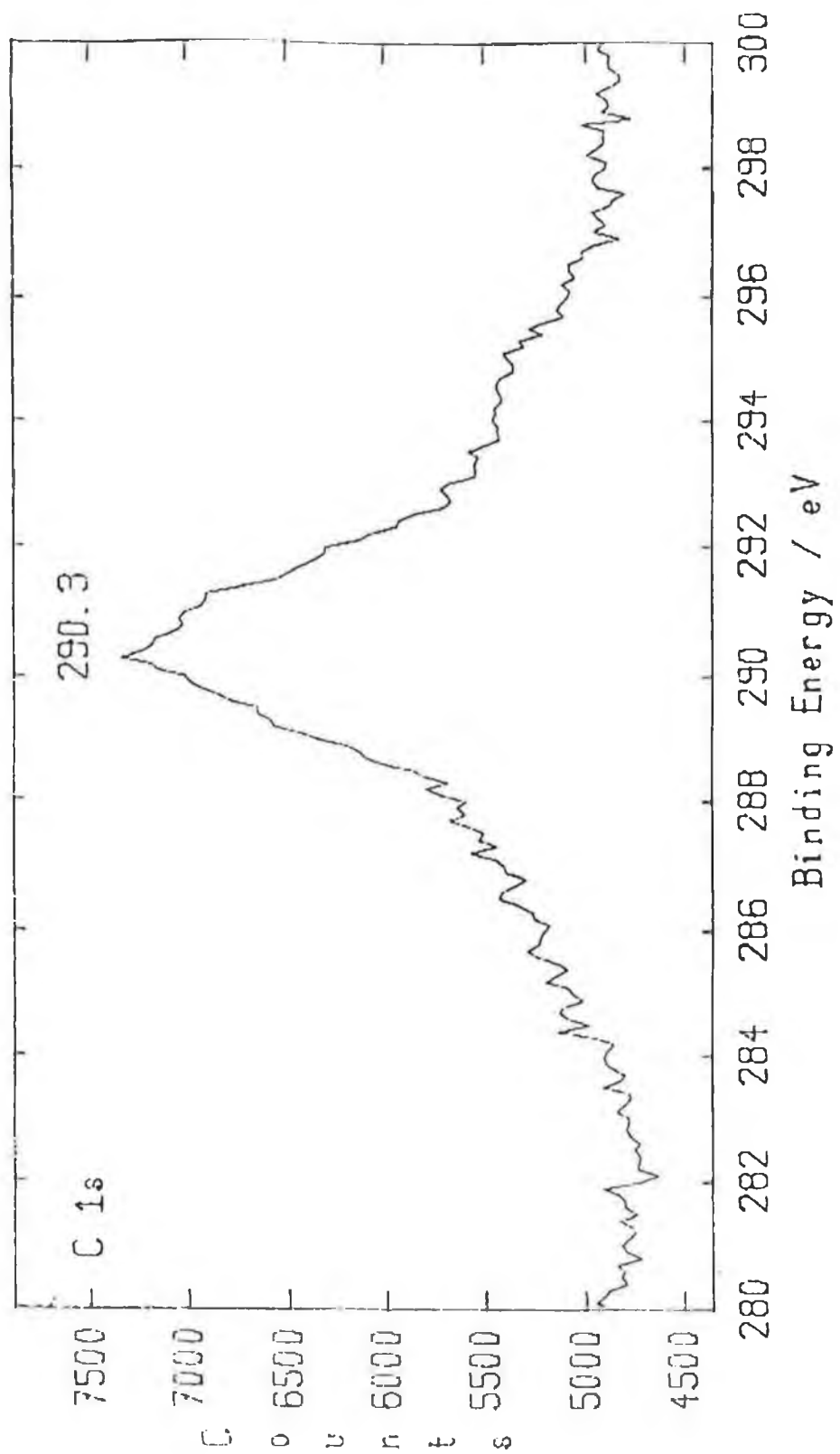


**Fig 3.16(b) : XPS spectrum showing an expanded energy range scan in the C 1s region for sample PC10A. Charge Correction = 5.7eV.**

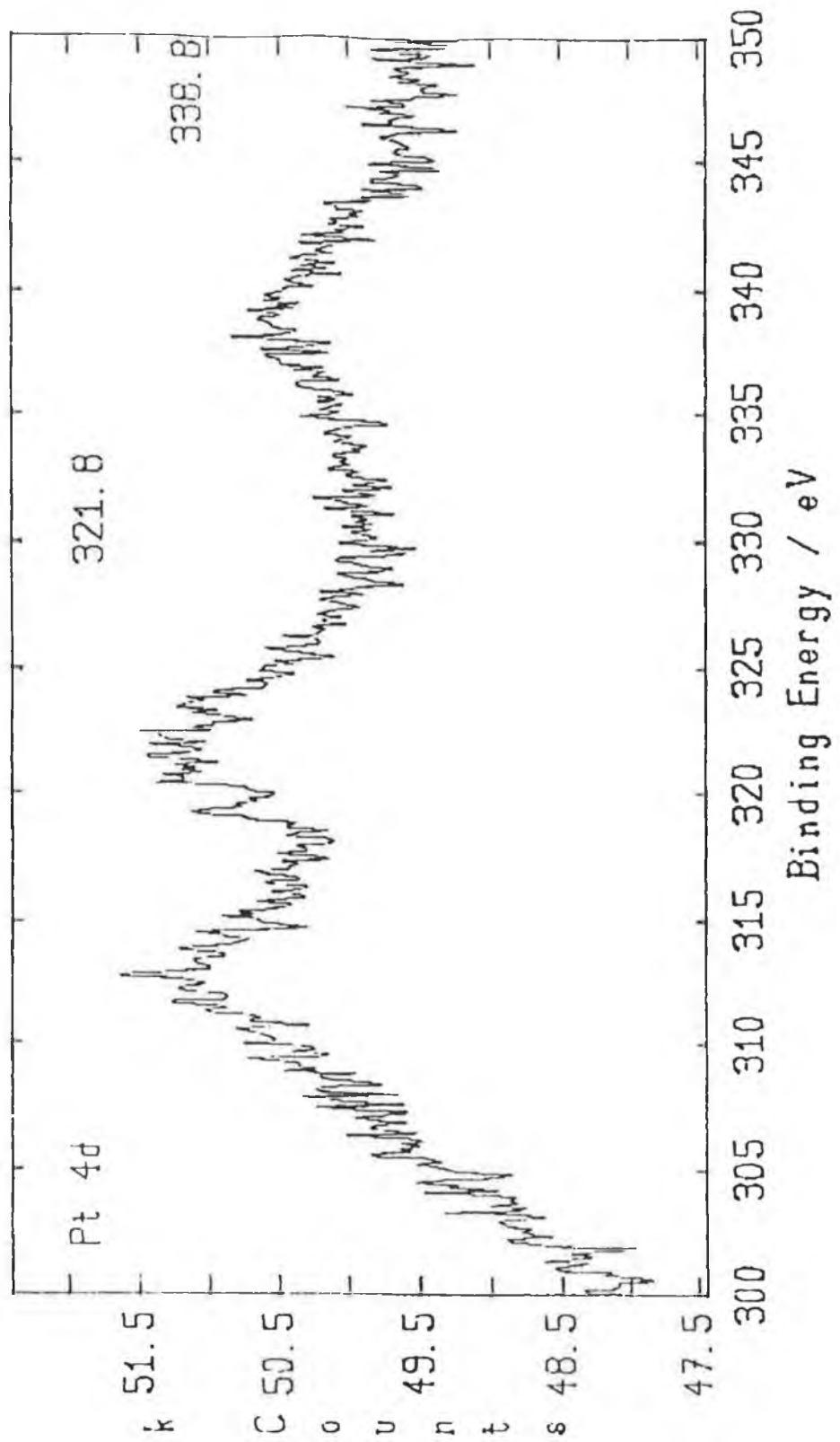


Fig 3.16(c) : XPS spectrum showing an expanded energy range scan in the Pt 4d region for sample PC10A. Charge Correction = 5.7eV.

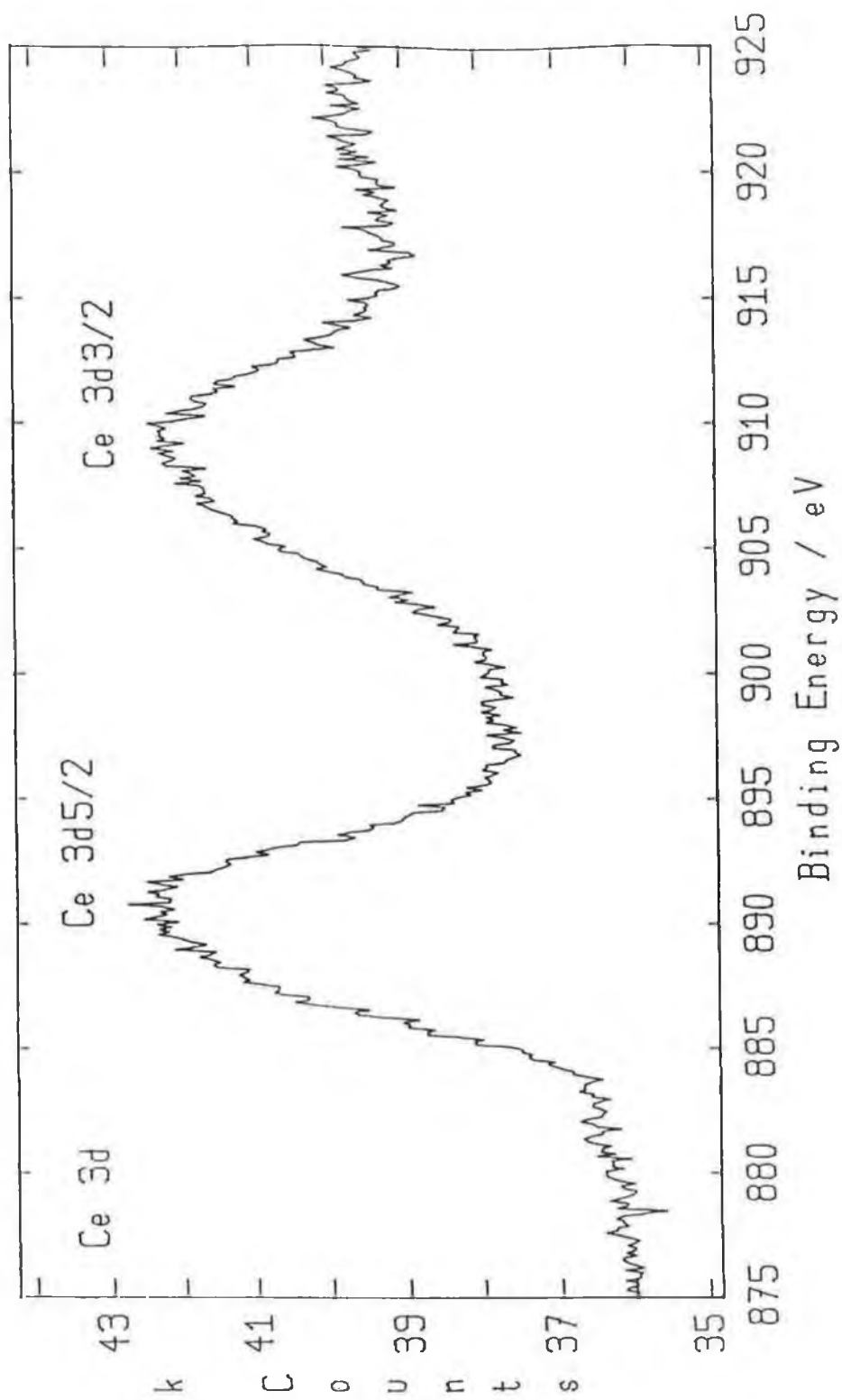


Fig 3.16(d) : XPS spectrum showing an expanded energy range scan in the Ce 3d region for sample PC10A. Charge Correction = 5.7eV.

only ca.1.1 $\mu$ moles per m<sup>2</sup> of Al<sub>2</sub>O<sub>3</sub>. CeO<sub>2</sub> has been reported to exist in the dispersed phase on Al<sub>2</sub>O<sub>3</sub> at concentrations below ca.2.5 $\mu$ molesm<sup>-2</sup> (35, 36). The maximum CeO<sub>2</sub> loading employed in the present study was ca.1.9 $\mu$ moles of CeO<sub>2</sub> per m<sup>2</sup> of Al<sub>2</sub>O<sub>3</sub> in sample PC17A which is below the reported dispersion limit. Therefore, Ce is expected to exist in a dispersed phase in all the samples analysed and the existence of strong ceria-Al<sub>2</sub>O<sub>3</sub> interaction, as indicated by the Ce 3d spectra obtained (Fig. 3.15(c) and 3.16(d)), is plausible.

Quantification of the data from the XPS spectra of the various samples analysed was carried out using sensitivity factors for the various elements which were obtained from reference (47). Table 3.2 shows the surface concentration (atomic %) of the major elements present in each sample. While these values may not be completely accurate they do allow comparison of elemental concentrations in the different samples since all values were obtained in the same manner.

**Table 3.2 : Atomic Concentration (%) of the Major Surface Elements Present in Each Sample as Determined from XPS Spectra.**

Sample	Pt 4d	Al 2p	Ce 3d	C 1s	O 1s
PA	0.061	30.121	---	8.821	60.997
PC	0.997	---	30.806	12.781	55.417
PC0.5A	0.061	31.154	0.327	8.109	60.349
PC10A	N.D.	N.D.	N.D.	N.D.	N.D.

N.D. = Not determined.

Table 3.3 summarises the measured binding energies for the Pt peaks in the calcined samples and also gives peak positions for Pt<sup>0</sup>, PtO and PtO<sub>2</sub> reported in previous studies.

**Table 3.3 : Summary of Pt Binding Energies in XPS**

Sample	Reference	Pt 4d <sub>5/2</sub> (eV)	Pt 4f <sub>7/2</sub> (eV)
PA	This work	315.6	---
PC	This work	315.8	72.6
PC0.5A	This work	314.7	---
PC10A	This work	316.1	---
Pt <sup>0</sup>	(45)	314.2	71.1
	(46)	314.1	---
"Pt <sup>0</sup> "/ $\gamma$ -Al <sub>2</sub> O <sub>3</sub>	(46)	313.5	---
PtO	(45)	315.3	72.2
PtO <sub>2</sub>	(45)	317.0	74.2
	(46)	318.0	---

To summarise, the XPS results would appear to suggest that Pt in samples PA and PC was oxidised and present as PtO. However, it must be noted that the low levels of Pt present in the samples, and the broad nature of the Pt 4d features analysed, introduced some considerable uncertainty into the determination of binding energies and also made it difficult to distinguish whether or not Pt was present on the surface in a number of different states (Pt<sup>0</sup>, PtO, PtO<sub>2</sub>). In spite of these problems, the Pt 4d<sub>5/2</sub> maxima binding energies measured for PA and PC were certainly considerably lower than those reported for PtO<sub>2</sub> (see Table 3.3). Pt in sample PC (Pt/CeO<sub>2</sub>) may have been slightly more electron-deficient than in sample PA (Pt/Al<sub>2</sub>O<sub>3</sub>) with a very small electropositive shift in the Pt 4d<sub>5/2</sub> peak binding energy measured for the former sample. For sample PC10A (Pt-3.6%Ce/Al<sub>2</sub>O<sub>3</sub>), Pt appeared to be more oxidised which might be attributed to the existence of a Pt-Ce interaction (1, 43). At lower levels of Ce (sample PC0.5A), Pt appeared to be less oxidised, relative to samples PA and PC, with a Pt 4d<sub>5/2</sub> binding energy intermediate between that reported for Pt metal and PtO (45). However, the binding energy measured was considerably higher than that reported for "Pt<sup>0</sup>"/ $\gamma$ -Al<sub>2</sub>O<sub>3</sub> by Bouwman and Biloen (46). Thus, it can be concluded that Pt was, at least, partially electron-deficient in sample PC0.5A after calcination.

For sample PC, the typical Ce 3d spectral features of CeO<sub>2</sub> (Ce<sup>4+</sup>) were exhibited. However, for Al<sub>2</sub>O<sub>3</sub>-supported samples, the Ce 3d spectra obtained more closely resembled that of Ce<sup>3+</sup> than Ce<sup>4+</sup> which could be concluded to show the existence of a strong interaction between Al<sub>2</sub>O<sub>3</sub> and dispersed Ce (35).

### Temperature Programmed Reduction (TPR)

The TPR profiles (TPR1) of the various samples investigated before testing for  $i\text{-C}_4\text{H}_{10}$  oxidation activity are illustrated in Fig. 3.17-3.22. Due to problems with detector stability and baseline drift, quantification of reduction peaks was not attempted and interpretation was restricted to qualitative purposes.

Fig. 3.17 shows the TPR profiles of the support materials used.  $\gamma\text{-Al}_2\text{O}_3$  (Fig. 3.17(a)) showed no reduction features in the temperature range investigated. This is in agreement with Nunan et al. (7) who reported  $\text{H}_2$  uptake associated with  $\gamma\text{-Al}_2\text{O}_3$  at ca.700°C but not below 500°C. The  $\text{CeO}_2$  profile (Fig. 3.17(b)) contains a major peak at ca.500°C with several shoulders apparent on the low temperature side. Other studies have reported two (34, 36, 38) or three (35) major reduction features for  $\text{CeO}_2$  in TPR profiles, as discussed in section 3.1.1. In the present study, the TPR peaks at slightly below 500°C were probably attributable to surface  $\text{CeO}_2$  reduction.

The profiles obtained for the  $\text{Ce}/\text{Al}_2\text{O}_3$  sample, C8A, are illustrated in Fig. 3.18. Both before and after calcination, a reduction peak is present at ca.370°C. The amount of  $\text{H}_2$  uptake decreased considerably after calcination. For  $\text{CeO}_2/\text{Al}_2\text{O}_3$  samples, several workers have reported a reduction feature around 400°C which was assigned to the reduction of a surface Ce species (7, 35, 37). In light of XPS analysis in the present study, the shoulder peak in the TPR profile of the calcined C8A sample might be assigned to surface reduction of a ceria-alumina interactive species. This is in agreement with the findings of Shyu et al. (35) who assigned a TPR peak at ca.400°C, for dispersed  $\text{CeO}_2/\text{Al}_2\text{O}_3$  samples, to the removal of surface oxygen of a 'CeAlO<sub>3</sub>-precursor' species which could then be converted to  $\text{CeAlO}_3$  at ca.720°C.

The TPR profiles of the uncalcined PA, PC1A, and PC8A catalyst precursors, which were dried at 45°C, are illustrated in Fig. 3.19. Adsorption of Pt as  $\text{H}_2\text{PtCl}_6$  onto  $\text{Al}_2\text{O}_3$  produces a  $(\text{PtCl}_6)^{2-}$  surface complex (29, 49). Lietz et al. (29) reported that this species remained after drying at 120°C. Hence, direct reduction of the uncalcined  $\text{Pt}/\text{Al}_2\text{O}_3$  precursor, PA, might be expected to have involved this unmodified surface species i.e.  $(\text{PtCl}_6)^{2-}$ . For the PA precursor sample, there are three main peaks apparent on the profile obtained (Fig. 3.19(a)) at ca.175°C, ca.240°C, and ca.470°C, with a shoulder peak at ca.320°C. These peaks may have been associated with the stepwise reduction of a  $(\text{PtCl}_6)^{2-}$  surface complex by  $\text{H}_2$ . For the PC1A profile (Fig 3.19(b)), major peaks are evident at ca.230°C and above 500°C. For sample PC8A, a very broad reduction peak is seen in Fig. 3.19(c) which is centred at ca.250°C with shoulders present at ca.150°C and ca.290°C and another small peak apparent at ca.350°C. The PC8A profile is obviously not a direct combination of the profiles obtained for the uncalcined

PA and C8A samples. Hence, some form of bimetallic (Pt-Ce) interaction is concluded to have occurred, even prior to calcination, which seemed to affect the reduction profiles of both metals (23). On calcination, changes occurred in the TPR profiles of all three samples, as expected, and will be discussed below.

Following calcination of the PA precursor at 630°C, the largest H<sub>2</sub> uptake peak is apparent at ca.420°C in Fig. 3.20(a). As discussed in section 3.1.1, several authors have reported the difficult nature of the reduction of surface Pt when highly dispersed on Al<sub>2</sub>O<sub>3</sub> (24, 25, 27, 37). The reason for this has been tentatively proposed to involve the existence of a PtO<sub>2</sub>-Al<sub>2</sub>O<sub>3</sub> surface complex which stabilises PtO<sub>2</sub> against reduction (25, 26, 27, 37). XPS analysis in the current study, indicated that oxidised Pt in sample PA after calcination was more likely to be present as PtO rather than PtO<sub>2</sub> based on the Pt 4d<sub>5/2</sub> peak binding energy. Shyu and Otto (45) also reported a Pt 4d<sub>5/2</sub> binding energy corresponding to that of PtO for Pt/Al<sub>2</sub>O<sub>3</sub> samples after oxidation. In agreement with other studies (21, 24, 25, 27, 37), Shyu and Otto (45) also reported that dispersed PtO was more difficult to reduce than particulate Pt phases with temperatures in excess of 300°C required for dispersed samples. In the present study, the high temperature (ca.420°C) reduction peak might be attributed to very well dispersed Pt oxide(s) which were more stabilised against reduction than either bulk PtO<sub>2</sub> (30) or larger supported Pt particles (25, 45), due to some form of strong interaction with the Al<sub>2</sub>O<sub>3</sub> support.

As can be observed from Fig. 3.20, sample PC (Fig. 3.20(b)) showed a considerably different TPR profile to sample PA (Fig. 3.20(a)). Following calcination, PC exhibited a major reduction peak at ca.265°C with a shoulder at ca.235°C, along with minor peaks at ca.200°C and between ca.420-450°C. In line with the conclusions of Shyu and Otto (37) and Diwell et al. (12), discussed previously in section 3.1.1., the main TPR feature in the region around 250°C is assigned to combined reduction of Pt and CeO<sub>2</sub> in an interactive surface species. Increased reducibility of surface CeO<sub>2</sub> in sample PC, relative to that in the absence of Pt (Fig 3.17(b)), is not unexpected as noble metals have been proposed to increase the redox properties of ceria, thereby, resulting in improvements in the Oxygen Storage Capacity (OSC) of automotive exhaust catalysts (36, 38).

The TPR profile of the prepared PC0.5A sample (Fig. 3.20(c)) is similar to that of PA (Fig 3.20(a)), with the most prominent peak appearing at a slightly lower temperature of ca.385°C. The apparent small increase in reducibility of Pt, relative to sample PA, was presumably due to interaction with the added Ce. A shoulder peak also

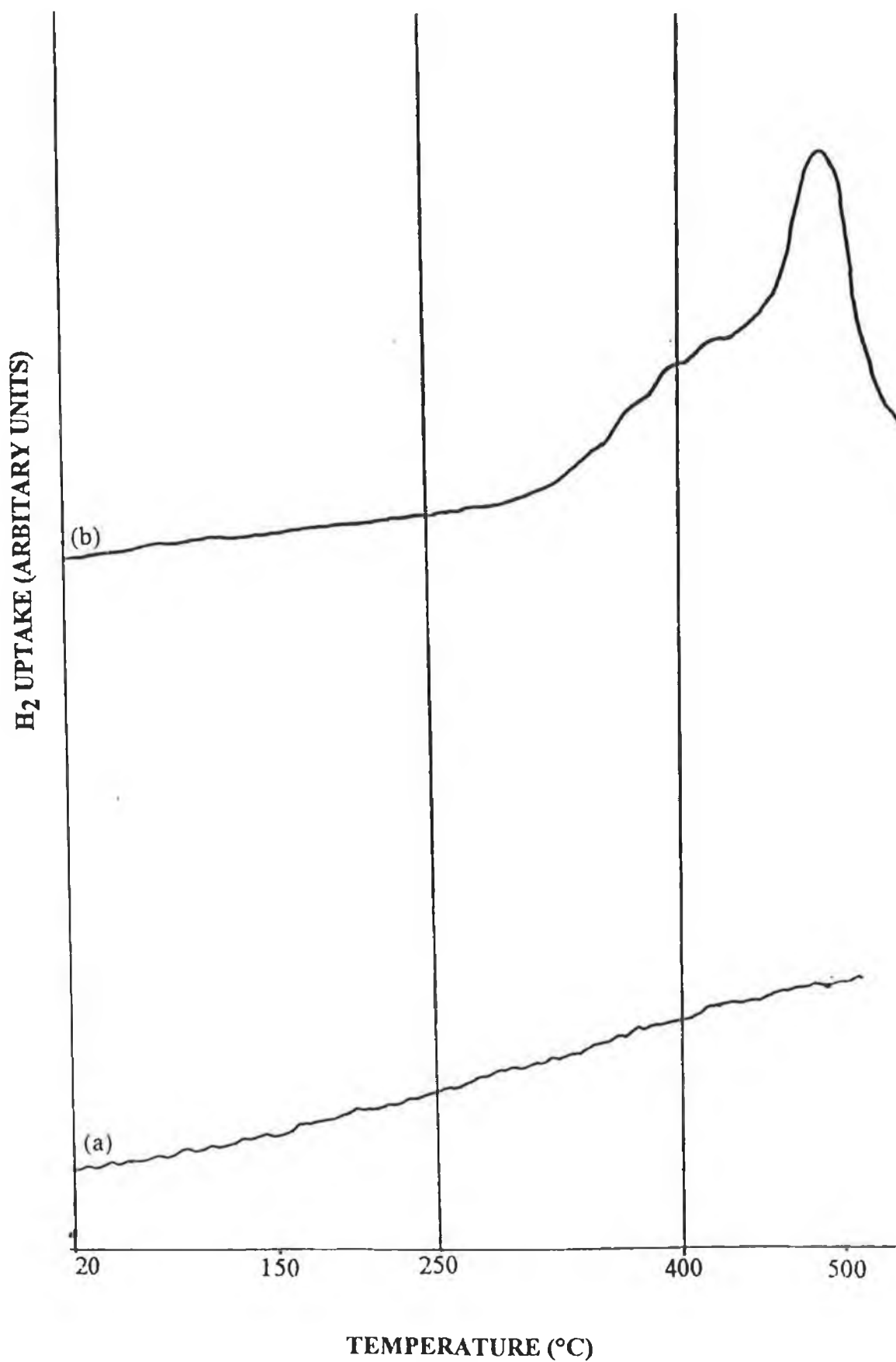


Fig 3.17 : TPR profiles of the support materials, (a)- $\gamma$ -Al<sub>2</sub>O<sub>3</sub>, (b)-CeO<sub>2</sub>.

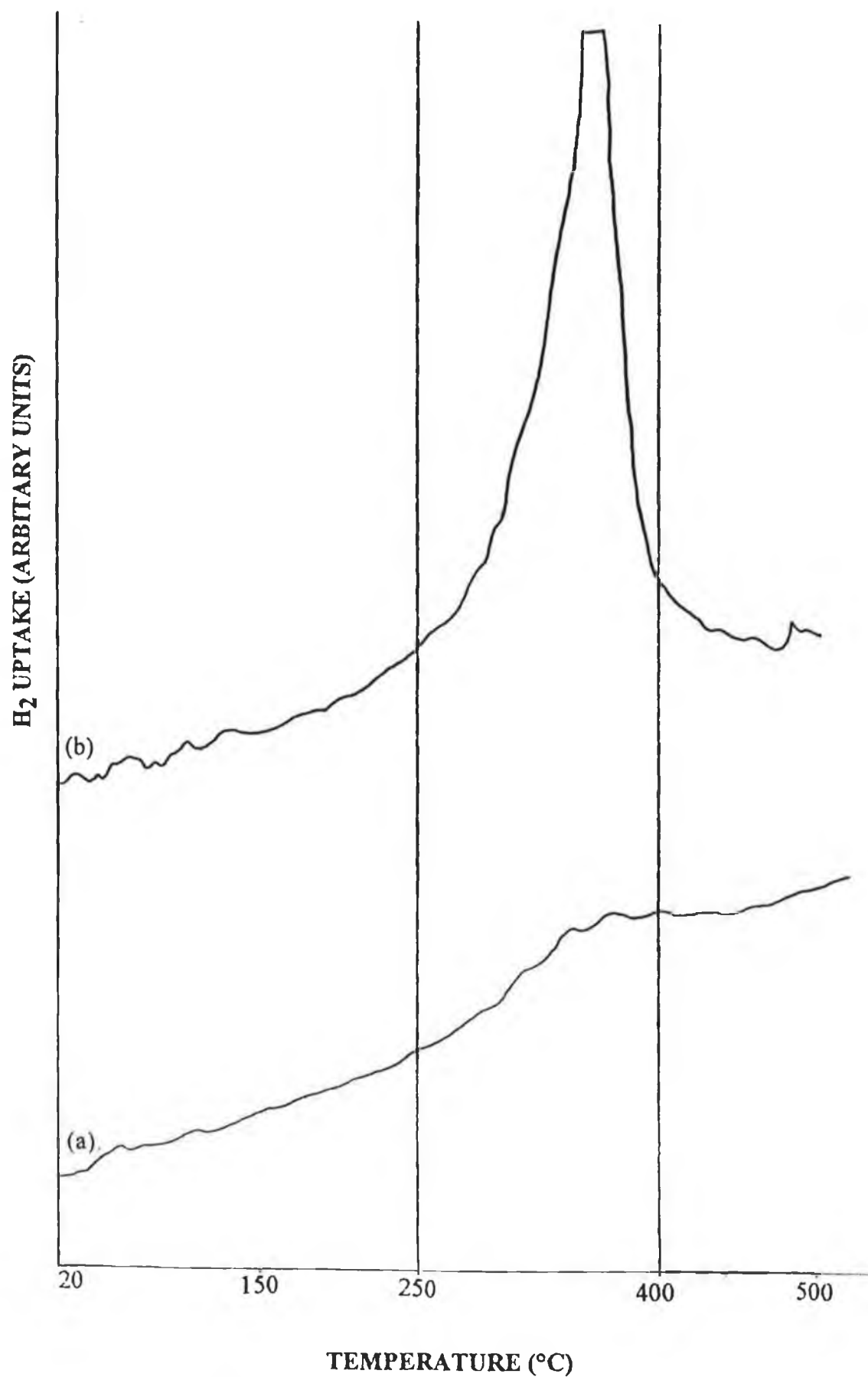
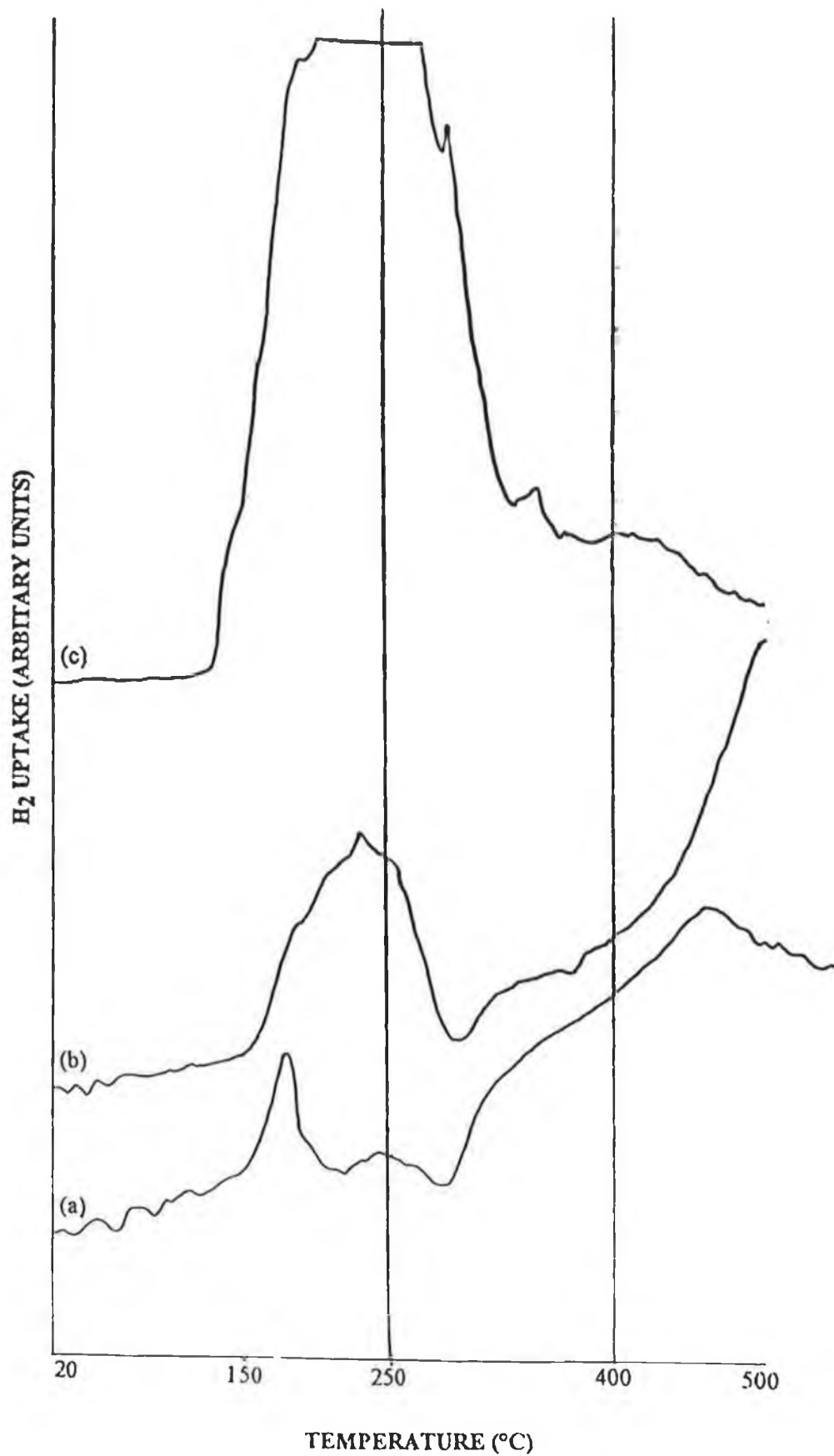


Fig 3.18 : TPR profiles of sample C8A, (a)-calcined, (b)-uncalcined.



**Fig 3.19 : TPR profiles of uncalcined precursors of samples (a)-PA, (b)-PC1A and (c)-PC8A.**

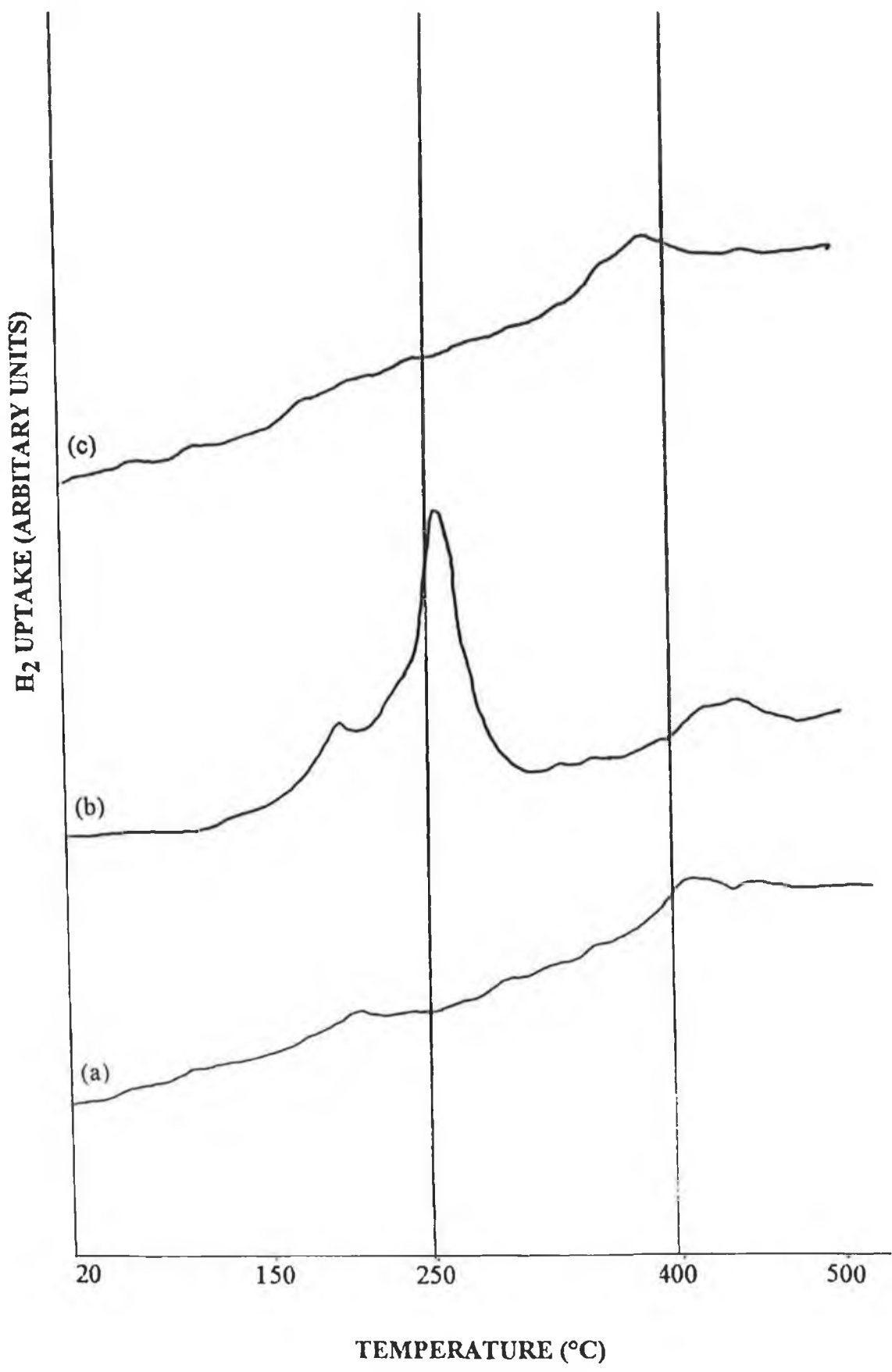


Fig 3.20 : TPR profiles of calcined samples, (a)-PA, (b)-PC, (c)-PC0.5A.

appears to be present on the reduction profile of PC0.5A at ca.360°C which might be associated with surface reduction of the small amount of dispersed Ce present. Some lower temperature reduction may also have occurred.

For sample PC1A, a downscale shift in the temperature of the major reduction peak of the calcined catalyst occurred from ca.400°C (in PA and PC0.5A) to ca.250°C (Fig. 3.21(a)). As discussed below, this is proposed to have been due to an interaction of Pt with the added Ce, since sample PC also showed a dominant reduction feature in the same temperature region. A small shoulder peak is also apparent in Fig. 3.21(a) at ca.375 °C, which corresponds well with the temperature of the shoulder peak in the profile of sample C8A (see Fig. 3.18(a)), and may have been associated with dispersed cerium whose reduction was not combined with that of Pt.

On increasing the Ce content to give a Ce:Pt atomic ratio of 8:1, the TPR profile of sample PC8A (Fig 3.21(b)) consists of a large peak at ca.250°C with a shoulder at ca.220°C. A small peak is also observed at ca.385°C. This latter feature can be assigned to the removal of surface oxygen of a Ce-Al<sub>2</sub>O<sub>3</sub> interactive species (35), as discussed previously for sample C8A. A similar profile was obtained for sample PC10A following calcination (Fig. 3.21(c)), however, the peak at ca.250°C was larger indicating a greater number of reducible sites on the catalyst surface. Both profiles bear a closer resemblance to that of PC (Fig. 3.20(b)) than that of PA (Fig. 3.20(a)). In light of the TPR studies of Shyu and Otto (37) and Diwell et al. (12), discussed in section 3.1.1, the peak at ca.250°C in the present study for Pt-Ce/Al<sub>2</sub>O<sub>3</sub> samples might be attributed to combined reduction of Pt and Ce surface species with the main contribution from the Ce component and the shoulder at ca.220°C possibly due to Pt reduction. Such a theory is supported by the similarity of the TPR feature to that obtained for Pt/CeO<sub>2</sub>, and the fact that the H<sub>2</sub> uptake increased when the amount of Ce present was increased. The difference in peak temperature for Pt-Ce/Al<sub>2</sub>O<sub>3</sub> samples (ca.250°C with the shoulder at ca.220°C) compared to Pt/CeO<sub>2</sub> (ca.265°C with the shoulder at ca.235°C), may have been due to a change in the nature of surface Ce species, as shown by XPS analysis which revealed that Ce was present in a more reduced state when supported on Al<sub>2</sub>O<sub>3</sub>. It could also have been due to a simple change in ceria particle size which has been previously reported to cause a shift in the reduction peak temperature of bulk ceria (35, 36).

The TPR profile obtained for sample SPC8A, after calcination is shown in Fig. 3.22(a), indicates the presence of both Pt-Ce and Pt-Al<sub>2</sub>O<sub>3</sub> interactive surface species, with the characteristic peaks at ca.250°C and ca.400°C present. This indicates

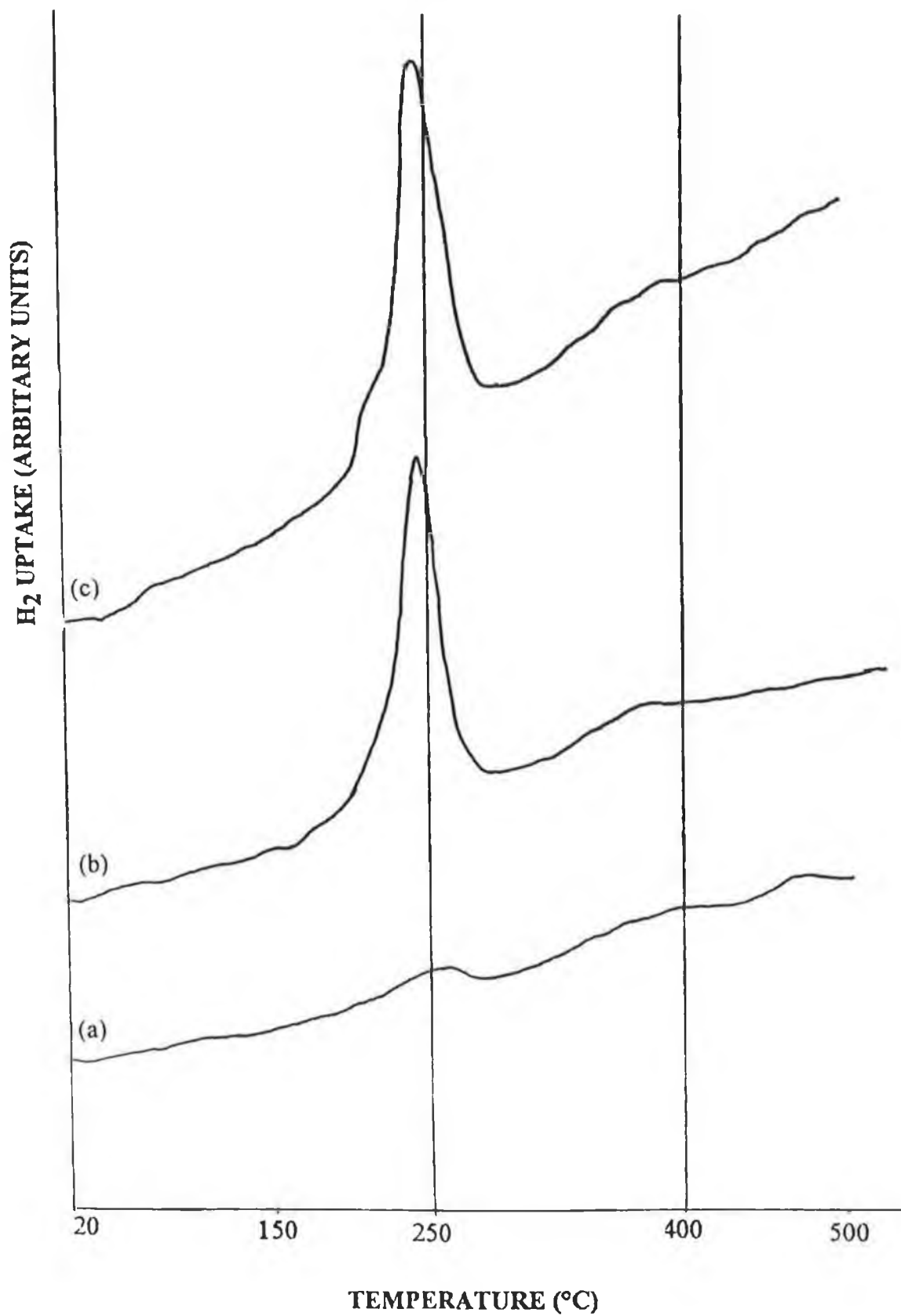


Fig 3.21 : TPR profiles of calcined samples, (a)-PC1A, (b)-PC8A, (c)-PC10A.

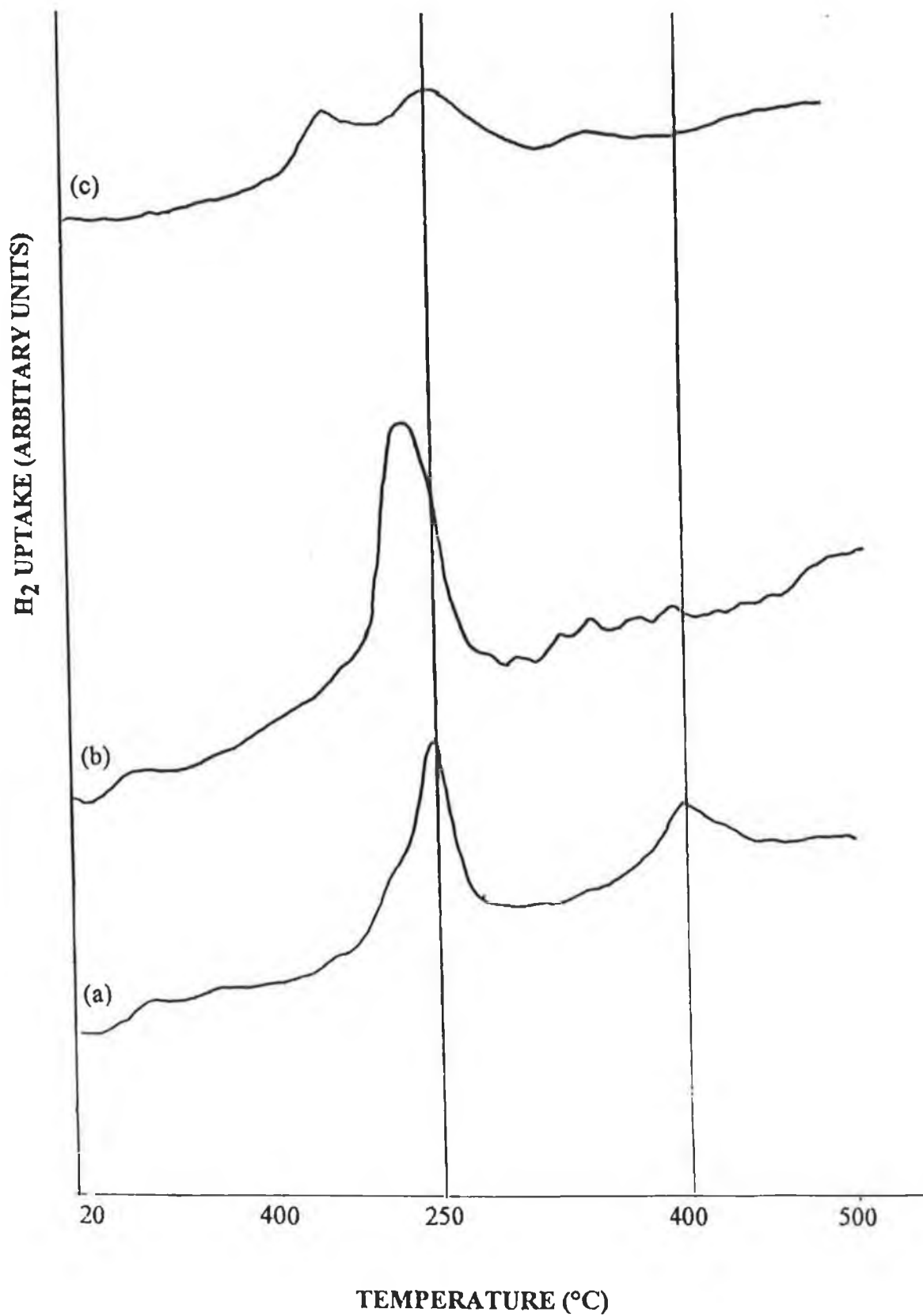


Fig 3.22 : TPR profiles of calcined samples, (a)-SPC8A, (b)-SCP8A, (c)-PC17A.

that impregnation of  $\gamma$ - $\text{Al}_2\text{O}_3$  with Pt prior to Ce addition gives rise to some Pt remaining in intimate contact with the  $\text{Al}_2\text{O}_3$  support. This did not occur when the metals were coimpregnated. For sample PC8A, all of the Pt seemed to interact preferentially with the Ce component and no Pt- $\text{Al}_2\text{O}_3$  surface species was apparent after calcination (Fig. 3.21(b)).

For sample SCP8A, Ce impregnation preceded that of Pt. The TPR profile obtained for the prepared sample is illustrated in Fig. 3.22(b). The profile bears a stronger resemblance to those of Pt/ $\text{CeO}_2$  and coimpregnated Pt-Ce/ $\text{Al}_2\text{O}_3$  samples than that of Pt/ $\text{Al}_2\text{O}_3$ . This indicates preferential interaction of Pt with the pre-deposited Ce.

For sample PC17A, the TPR profile obtained is illustrated in Fig. 3.22(c). It should be noted that an increased chart speed was used in obtaining the TPR profile of this sample. As for samples PC1A, PC8A, and PC10A, the main reduction peak occurs at a temperature of ca.250°C with the shoulder at ca.200°C now apparent as a distinct separate peak possibly because of the faster chart speed used.

To summarise, the main reduction features observed in the TPR profiles obtained for  $\text{Al}_2\text{O}_3$ -supported samples were;

- Feature (1) : A peak at ca.420°C which appeared to be associated with the reduction of dispersed  $\text{PtO}_x$  ( $x$ , most probably, = 1) on  $\text{Al}_2\text{O}_3$ . The apparent Pt reduction temperature was considerably higher than that reported for unsupported  $\text{PtO}_2$  (25, 30, 32). This was possibly due to the existence of a strong interaction between dispersed  $\text{PtO}_x$  species and the  $\text{Al}_2\text{O}_3$  support, which has been reported to stabilise surface Pt in an oxidised state (21, 24, 25, 27, 37, 45). An alternative explanation from Mc Cabe et al. (32) reported that reduction features at temperatures above 230°C for Pt/ $\text{Al}_2\text{O}_3$  samples might be associated with inorganic Pt complexes, possibly involving residual Cl from the  $\text{H}_2\text{PtCl}_6$  precursor salt or from the  $\text{Al}_2\text{O}_3$  surface to form Pt oxychloride species on  $\text{Al}_2\text{O}_3$  as reported by Lieske et al. (28, 29). The presence of such complexes in the catalysts used in the present study might be expected since XPS results indicated that Cl was present on the surface. Also the catalysts used were not subjected to any stringent reduction treatment prior to analysis which could have resulted in decomposition of any Cl species present (32). However, since XPS indicated that the average oxidation state of Pt was  $\text{Pt}^{2+}$  in the samples being investigated, it is unlikely that the  $\text{Pt}^{4+}$  complexes proposed by Lieske et al.(28, 29) could have been the major reducible surface species in the TPR profiles obtained. Alternatively, Park et al. (50) have proposed that high temperature TPR peaks arise from the interaction of isolated Pt atoms with strong acid sites. In any case, the reduction feature at ca.420°C can be concluded as being characteristic of some form of Pt- $\text{Al}_2\text{O}_3$  interactive species.

- Feature (2) : A peak at ca.250°C with a shoulder at ca.220°C. This feature is assigned to a Pt-Ce interactive species with the main contribution possibly from the Ce component and the shoulder on the low temperature side associated with Pt reduction (12, 37).

- Feature (3) : A shoulder peak at ca.370°C which is assigned to the removal of surface oxygen of a Ce-Al<sub>2</sub>O<sub>3</sub> interactive species (35).

In support of the above peak assignments, Shyu and Otto (37) also attributed TPR peaks for Pt/CeO<sub>2</sub>/Al<sub>2</sub>O<sub>3</sub> samples at ca.250°C and ca.420°C to Pt-CeO<sub>2</sub> and Pt-Al<sub>2</sub>O<sub>3</sub> interactive species, respectively.

On the TPR profile of Pt/CeO<sub>2</sub>, the predominant reduction peak occurred at ca.265°C with a shoulder apparent at ca.235°C. This feature was most probably associated with the combined reduction of PtO and CeO<sub>2</sub> (12, 37). Comparison of the TPR profiles for Pt/CeO<sub>2</sub> and CeO<sub>2</sub> samples, indicated that the presence of Pt resulted in more facile surface Ce reduction, in agreement with studies which have shown that the presence of noble metals can increase the oxygen storage capacity of CeO<sub>2</sub> due to noble metal-CeO<sub>2</sub> interaction (36, 38).

The TPR profiles obtained for calcined Pt-Ce/Al<sub>2</sub>O<sub>3</sub> samples were obviously not a direct superimposition of those for Pt/Al<sub>2</sub>O<sub>3</sub> and Ce/Al<sub>2</sub>O<sub>3</sub> samples. This indicates the existence of a bimetallic interaction on the surface (23). Differences in the profiles obtained for the catalyst precursors, PA, C8A, and PC8A, indicated that bimetallic interaction affected the reduction of both metals even before calcination.

For coimpregnated Pt-Ce/Al<sub>2</sub>O<sub>3</sub> samples, Pt appeared to interact preferentially with Ce rather than with Al<sub>2</sub>O<sub>3</sub>, even at very low Ce loadings (0.29% Ce), to give a TPR profile with the dominant feature at ca.250°C i.e. Feature (2). While co-impregnation of Pt and Ce onto  $\gamma$ -Al<sub>2</sub>O<sub>3</sub> led preferentially to a Pt-Ce surface interaction after calcination, stepwise impregnation of Pt prior to impregnation with Ce (SPC8A) appeared to result in both Pt-Ce and Pt-Al<sub>2</sub>O<sub>3</sub> interactive surface species with the typical features of both species on the TPR profile. For a sample SCP8A, prepared by impregnation of  $\gamma$ -Al<sub>2</sub>O<sub>3</sub> with Ce followed by Pt deposition, the TPR profile indicated preferential interaction of Pt with Ce rather than Al<sub>2</sub>O<sub>3</sub>, as for the coimpregnated samples. Löff et al. (4) and Shyu and Otto (37) also reported that Pt interacted preferentially with Ce even in the presence of a much larger Al<sub>2</sub>O<sub>3</sub> surface.

It should be noted that accurate interpretation of the TPR profiles was made difficult by the fact that the extent to which H<sub>2</sub> spillover onto the support had occurred

was always unknown (31, 33). Niwa et al. (33) reported that low loading of Pt and high remaining  $\text{Al}_2\text{O}_3$  surface may be enough to cause spillover problems. Another problem was that comparison of profiles with other studies will always be influenced, not only by catalyst loading and preparation conditions used, but also by experimental variables such as carrier flow rates and sample mass. Variation of the latter can affect resolution while changes in the flow rate will result in changes in reduction peak temperature (24).

### **H<sub>2</sub> Chemisorption**

Pt surface area, dispersion and particle size measurements in the calcined samples by H<sub>2</sub> chemisorption have already been discussed in section 2.3.3.

### 3.3.2 Oxidation Activity and its Effect on the Catalyst Surfaces

Figures 3.23-3.32 illustrate the conversion of  $i\text{-C}_4\text{H}_{10}$  as a function of temperature in Activity Tests A-C for the various catalysts investigated. The extent of butane conversion is given in terms of a percentage of the overall amount of butane present prior to reaction. None of the catalysts showed any activity at room temperature and, therefore, only measurements made between 100-350°C are illustrated. For most of the samples examined, the extent of conversion of  $i\text{-C}_4\text{H}_{10}$  increased as the temperature was raised. Total conversion (>99%) was achieved, in most cases, below 350°C.

From each curve, the light-off temperature (LOT) was measured as the temperature at which 2.5% conversion of  $i\text{-C}_4\text{H}_{10}$  was achieved. The LOT values for each sample, in the different activity test runs, are shown in Table 3.4. Similarly, the temperatures at which 10% conversion was achieved ( $T_{10}$  values) are shown in Table 3.5. The temperatures of 50%,  $T_{50}$ , and 90%,  $T_{90}$ , conversion are compared in Tables 3.6 and 3.7, respectively. For sample C8A, only LOT and  $T_{10}$  values were measured as 50% conversion was not achieved in the temperature range investigated.

On initial testing of the catalysts in Activity Test A, Run 1, the shape of the activity curve was similar for all samples with a rapid rise in activity evident from ca.20% to ca.90-100% conversion in a narrow temperature range (see Figures 3.23-3.32). However, it is evident, from Tables 3.4-3.7, that catalyst activity was affected by the presence of Ce, the loading of Ce, and the method of preparation used.

At the lowest level of Ce in sample PC0.5A oxidation activity was slightly improved in the low temperature region, relative to sample PA, with LOT and  $T_{10}$  values shifted to slightly lower temperatures for the former sample. However, the  $T_{90}$  value was slightly higher over PC0.5A relative to PA. On increasing the level of Ce for sample PC1A, catalyst activity was enhanced considerably with improvements in LOT,  $T_{10}$ ,  $T_{50}$ , and  $T_{90}$  values relative to those for PA. In contrast, for higher levels of Ce in samples PC8A, PC10A, PC17A, and in sample PC, the oxidation of  $i\text{-C}_4\text{H}_{10}$  was shifted to higher temperatures and all of these samples were less active than sample PA.

Comparison of LOT,  $T_{10}$ ,  $T_{50}$ , and  $T_{90}$  values for samples PC8A, SPC8A, and SCP8A, indicates that the method of impregnation of  $\text{Al}_2\text{O}_3$  with the metals affected catalyst activity. Sample SPC8A, in which Pt impregnation preceded that of Ce, was considerably more active than the other two samples which contained the same Ce loading. Sample SPC8A was also more active than sample PA.

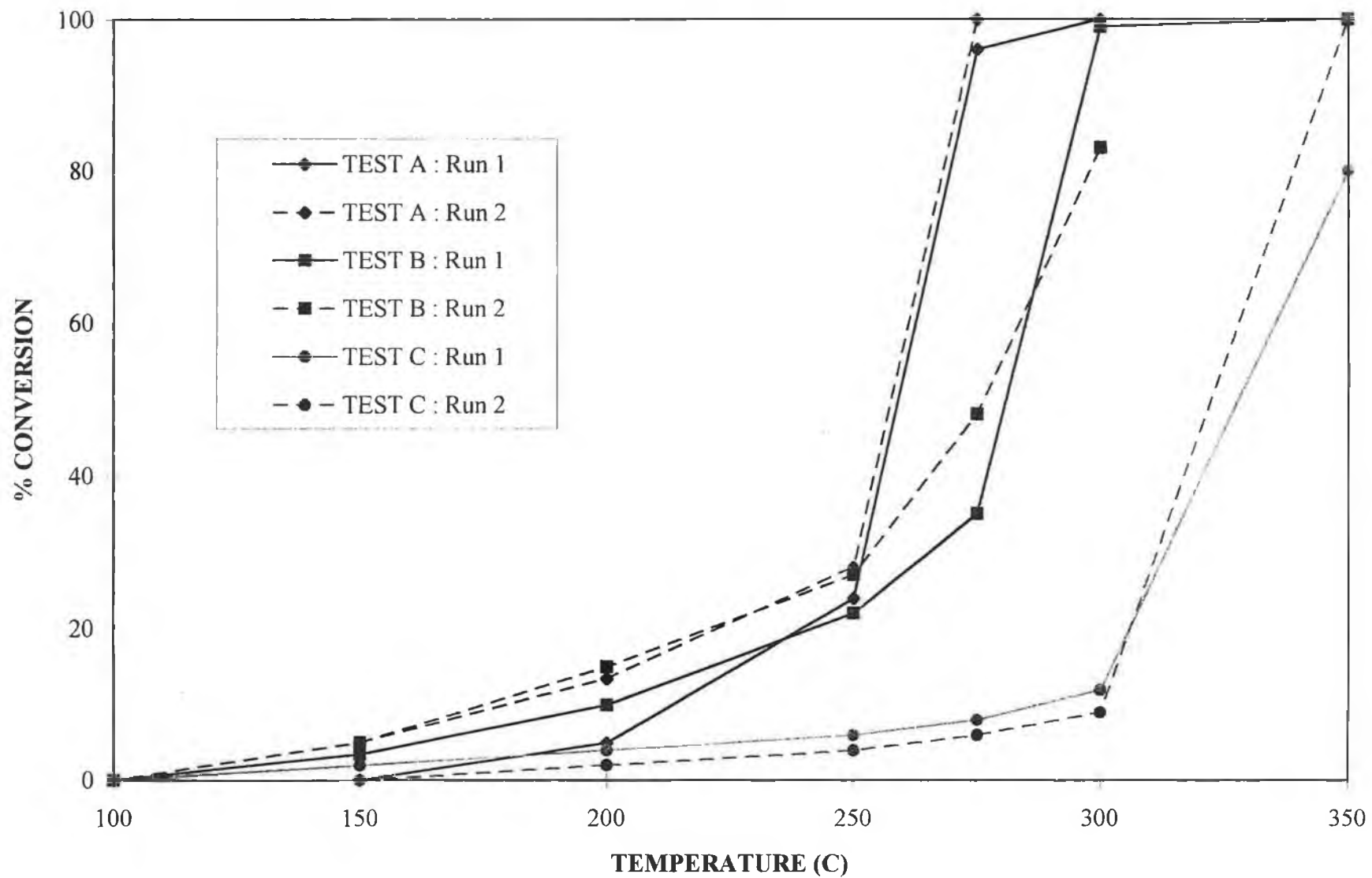


Fig. 3.23 : % iso-Butane Conversion versus Temperature for Sample PA.

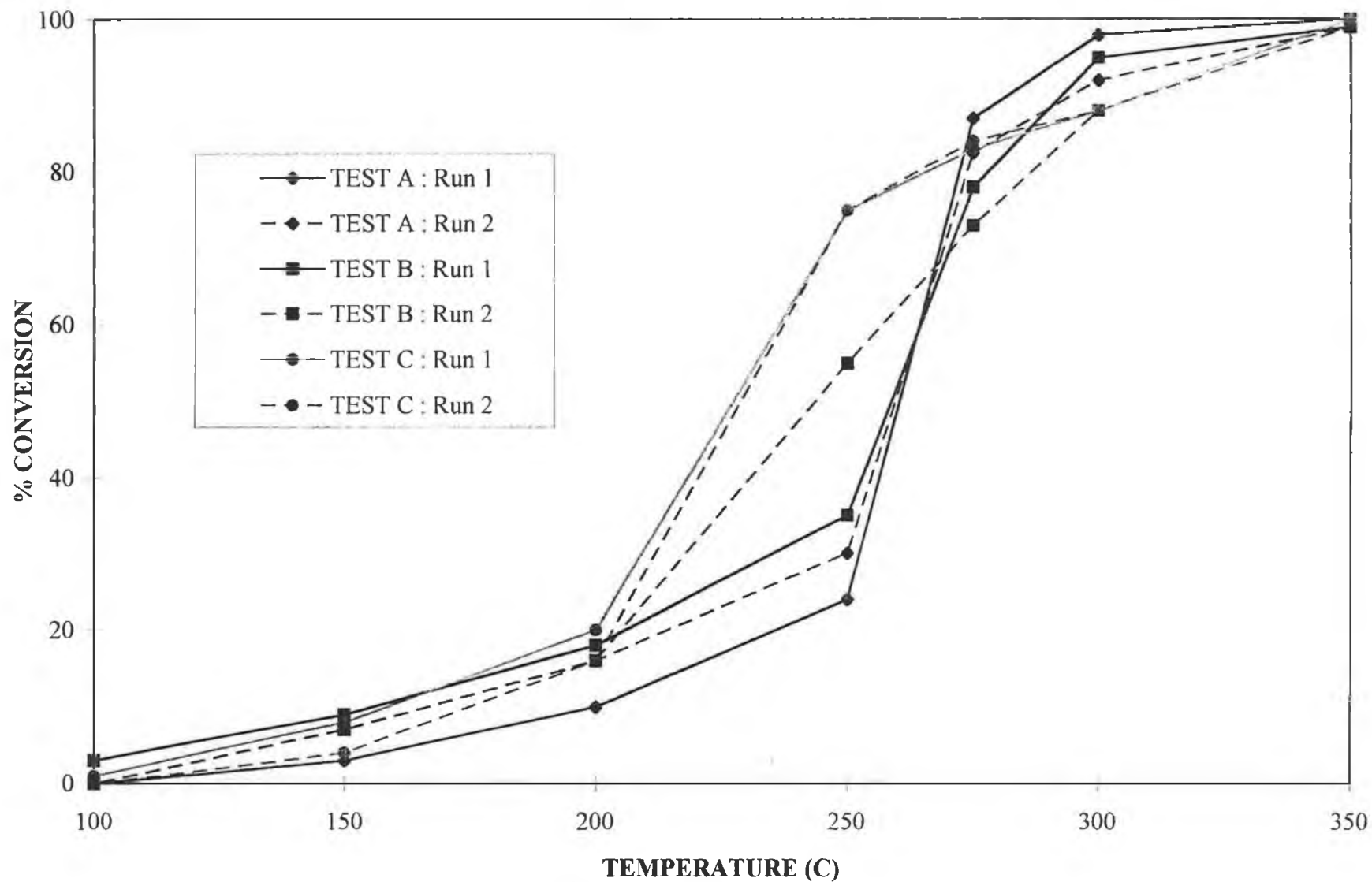


Fig. 3.24 : % iso-Butane Conversion versus Temperature for Sample PC0.5A.

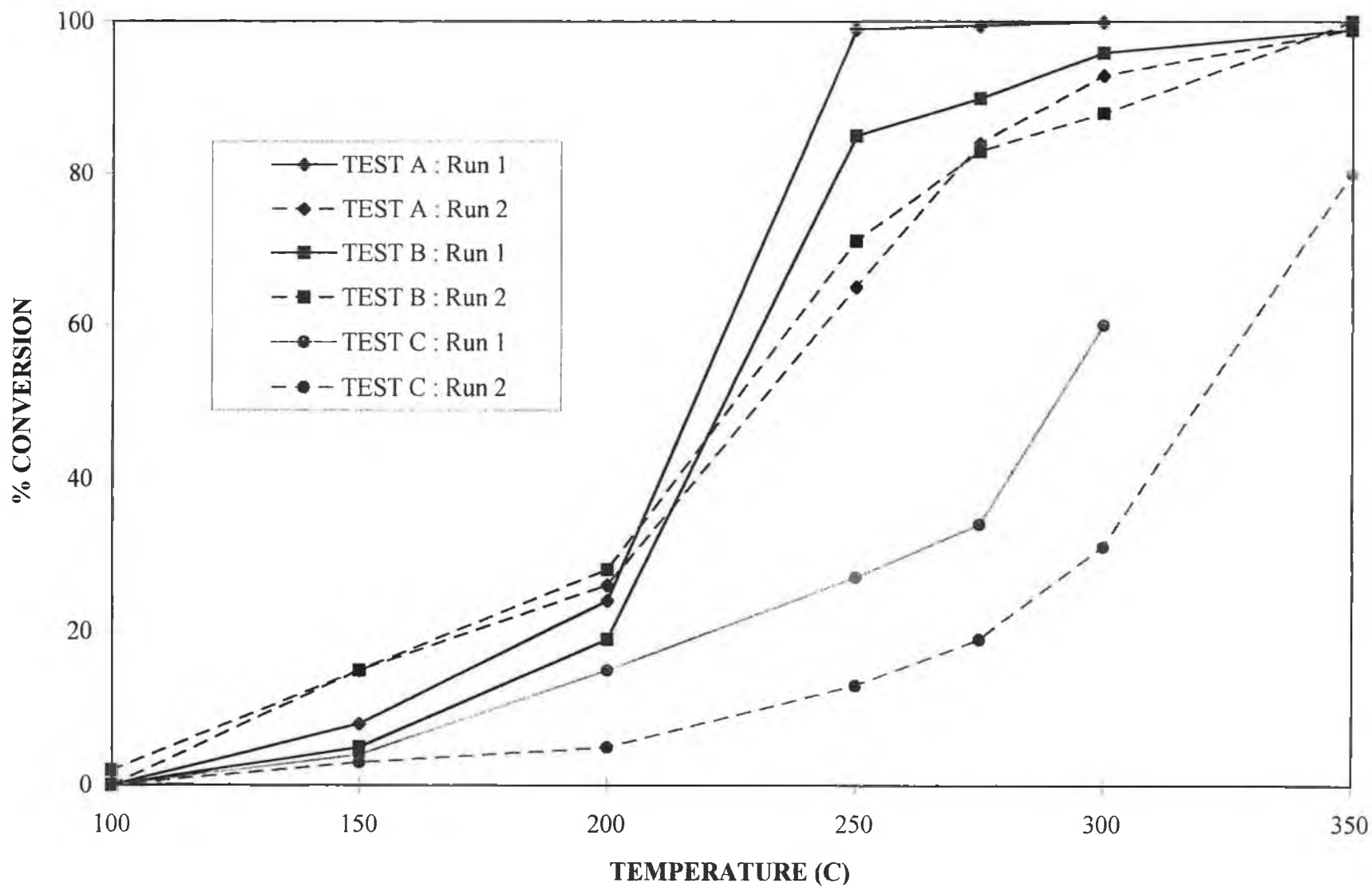


Fig. 3.25 : % iso-Butane Conversion versus Temperature for Sample PC1A.

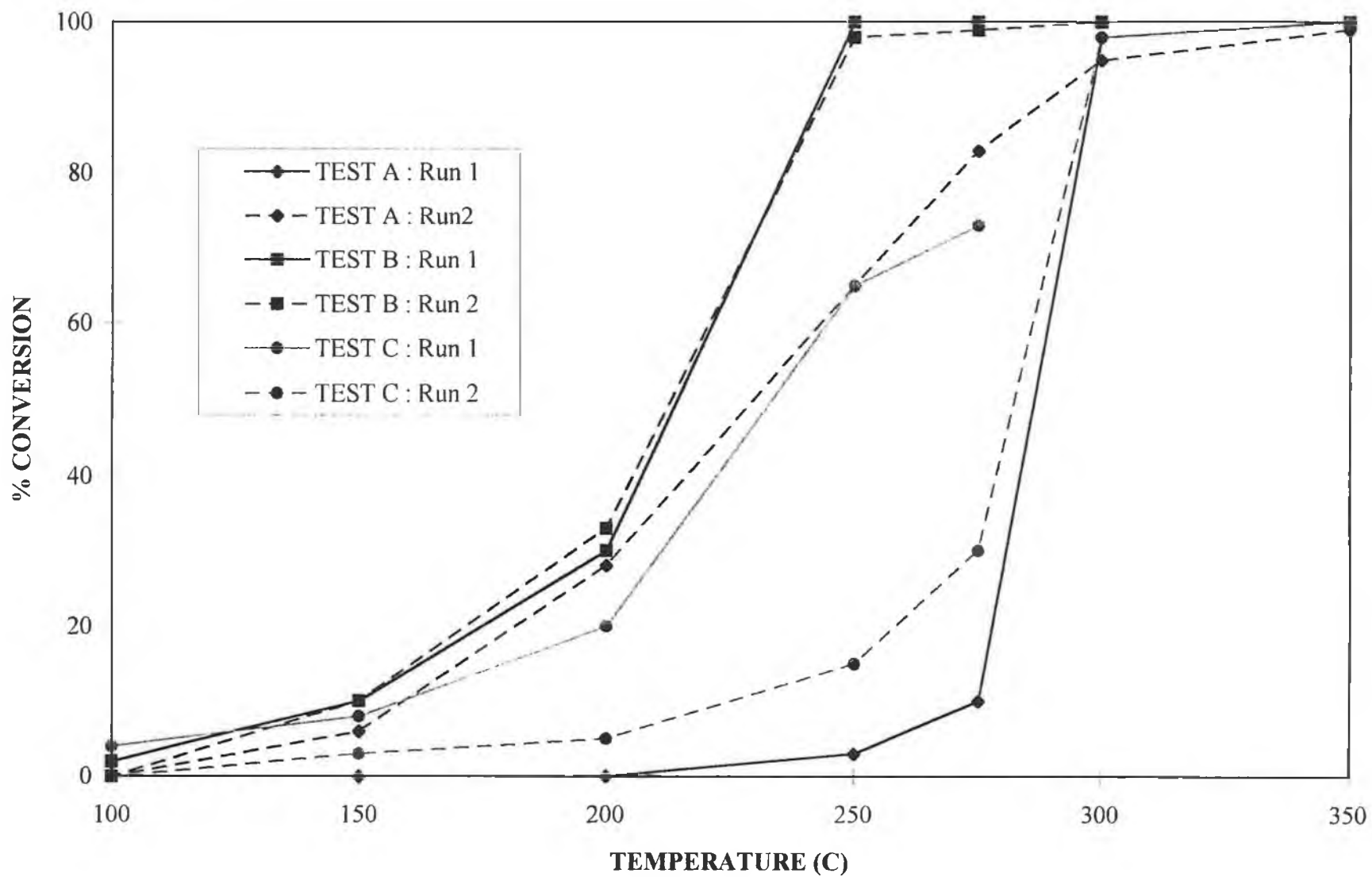


Fig. 3.26 : % iso-Butane Conversion versus Temperature for Sample PC8A.

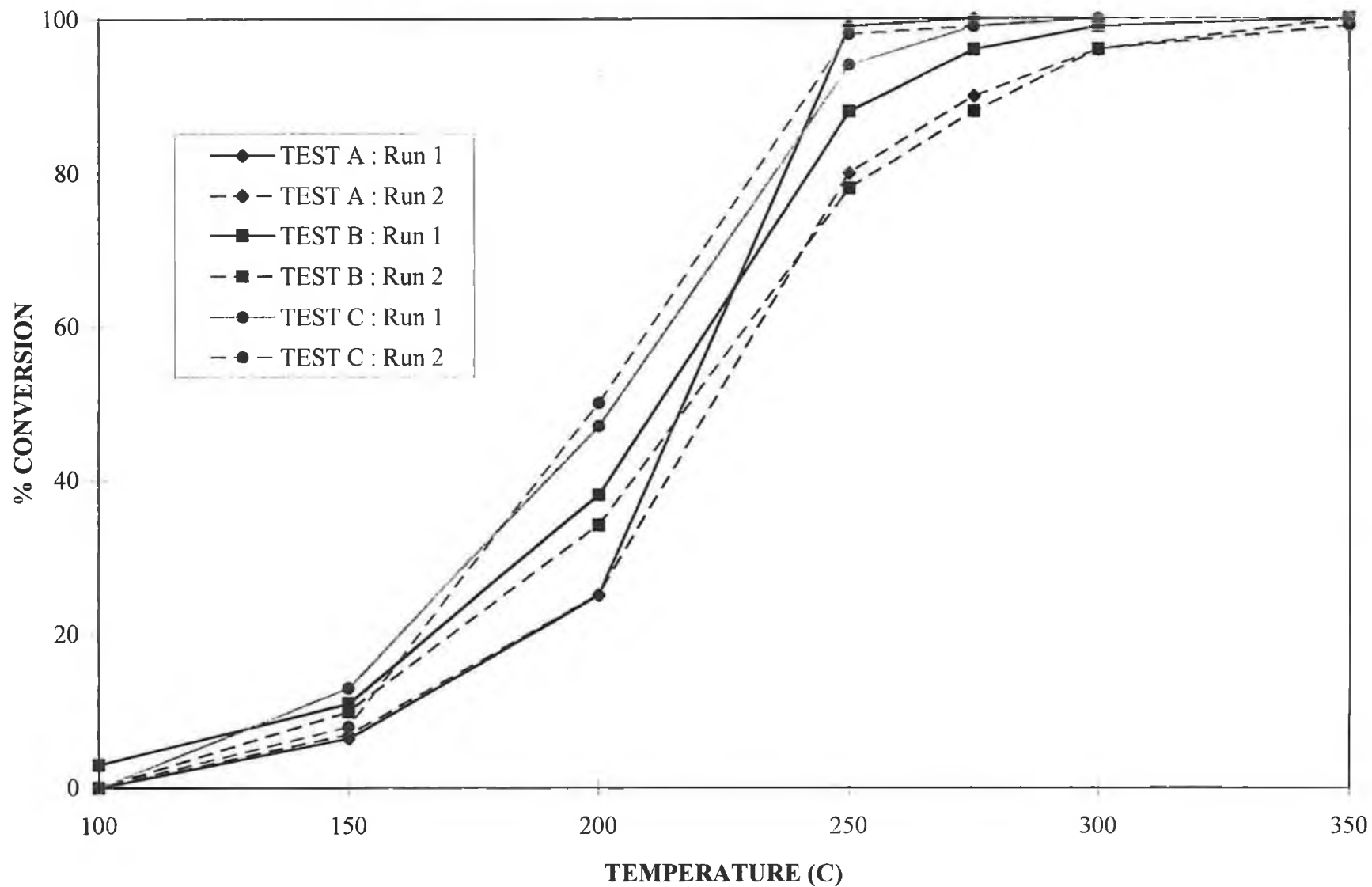


Fig. 3.27 : % iso-Butane Conversion versus Temperature for Sample SPC8A.

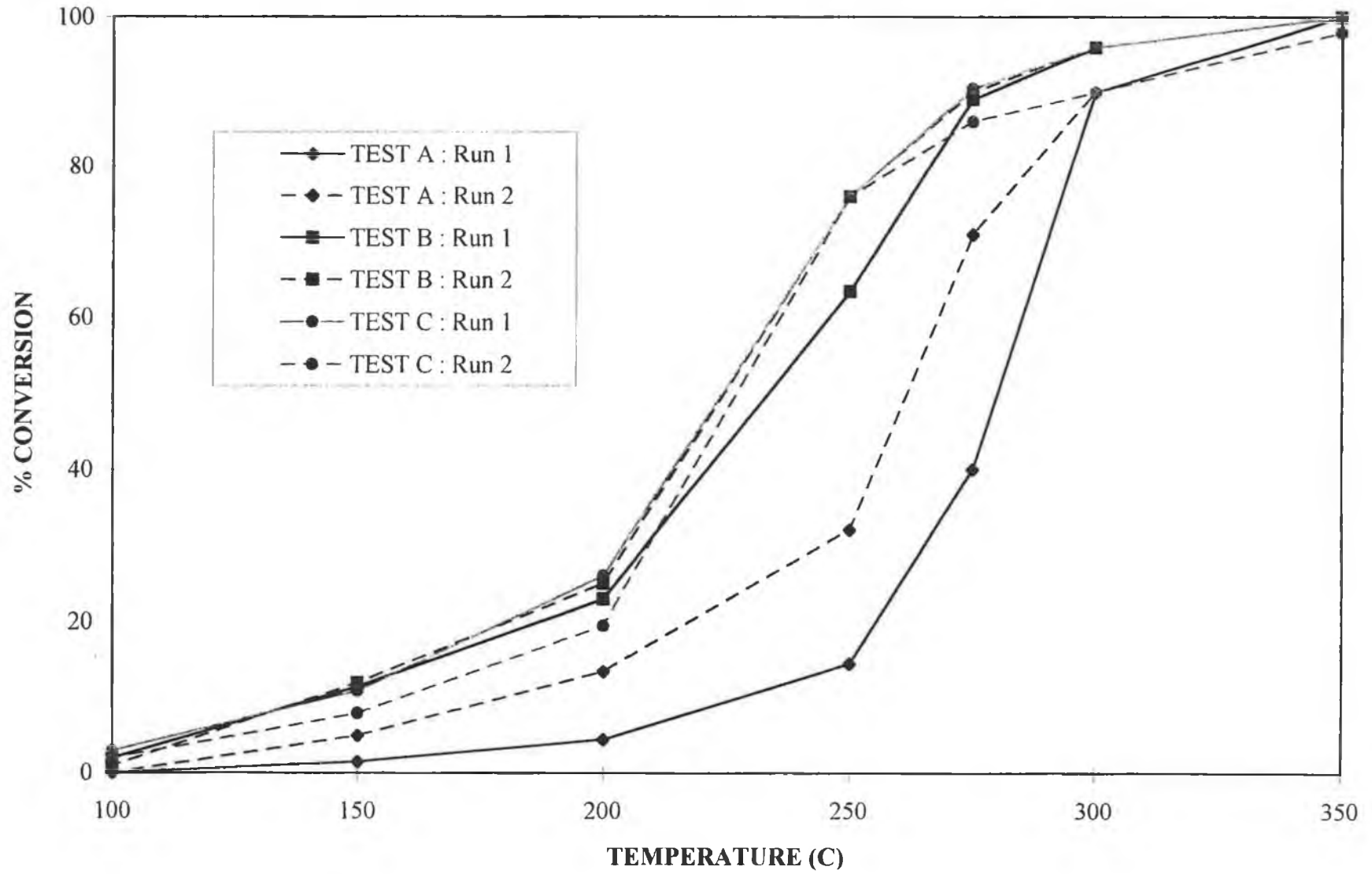


Fig. 3.28 : % iso-Butane Conversion versus Temperature for Sample SCP8A.

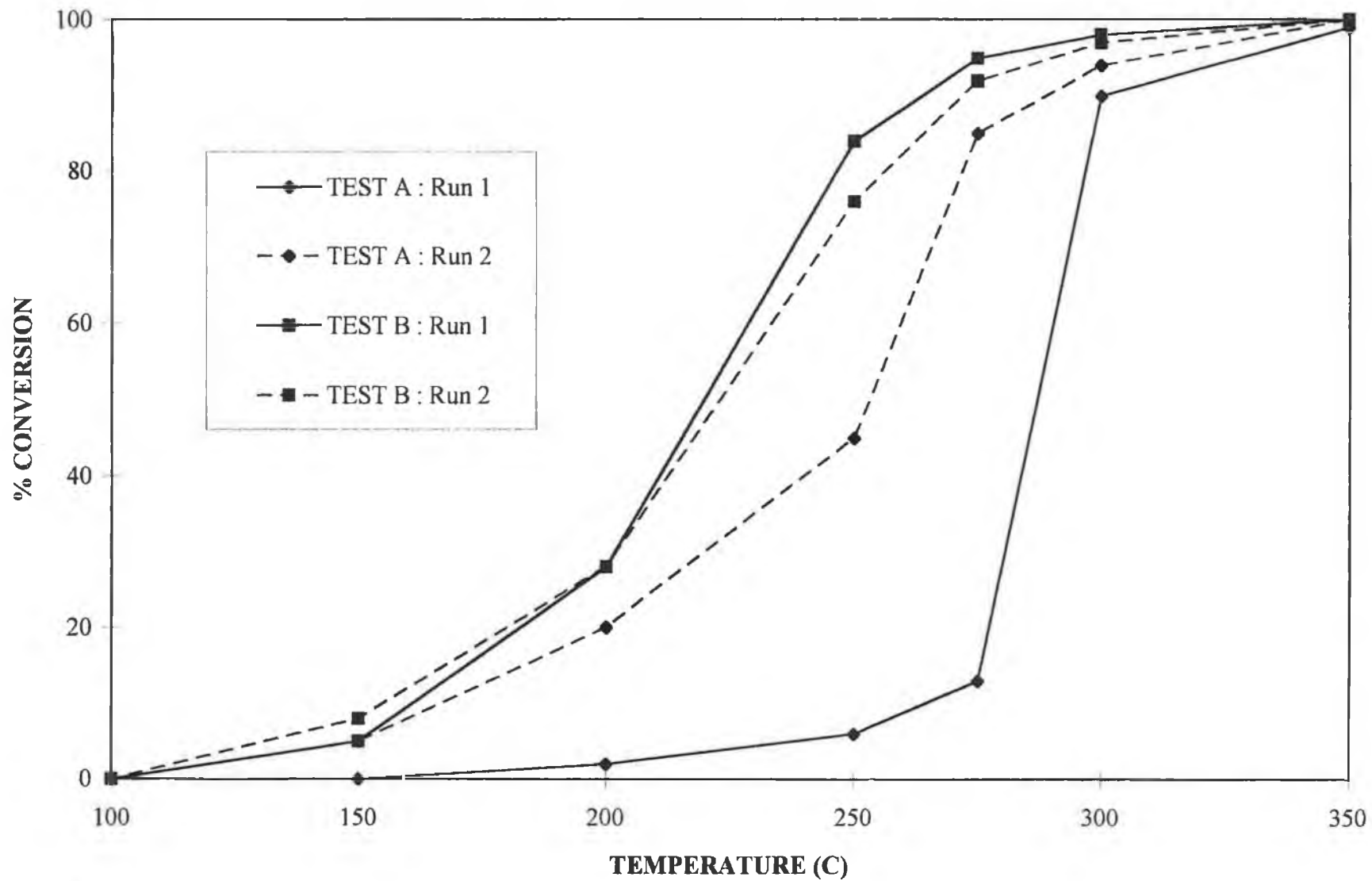


Fig. 3.29 : % iso-Butane Conversion versus Temperature for Sample PC10A.

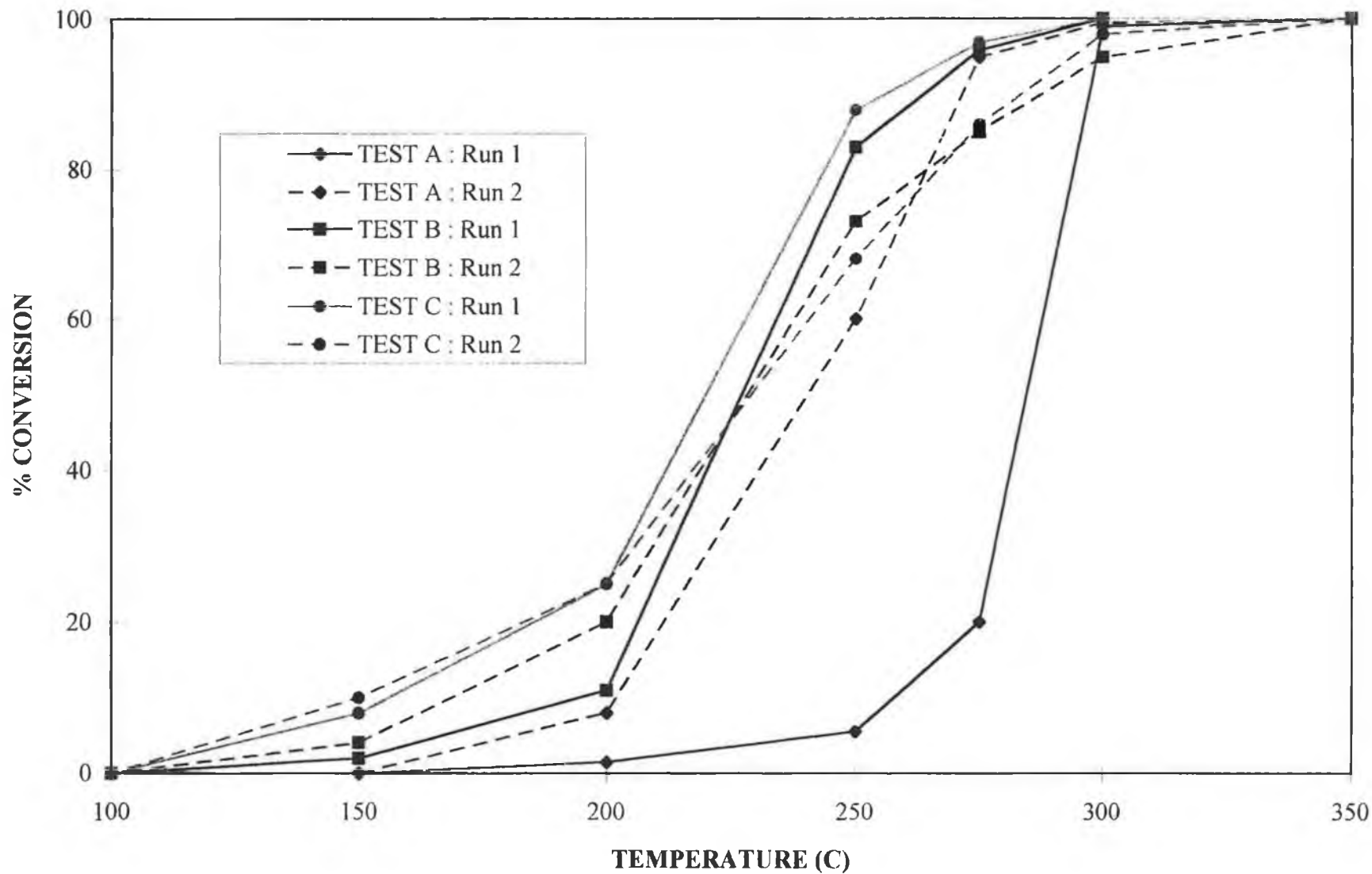


Fig. 3.30 : % iso-Butane Conversion versus Temperature for Sample PC17A.

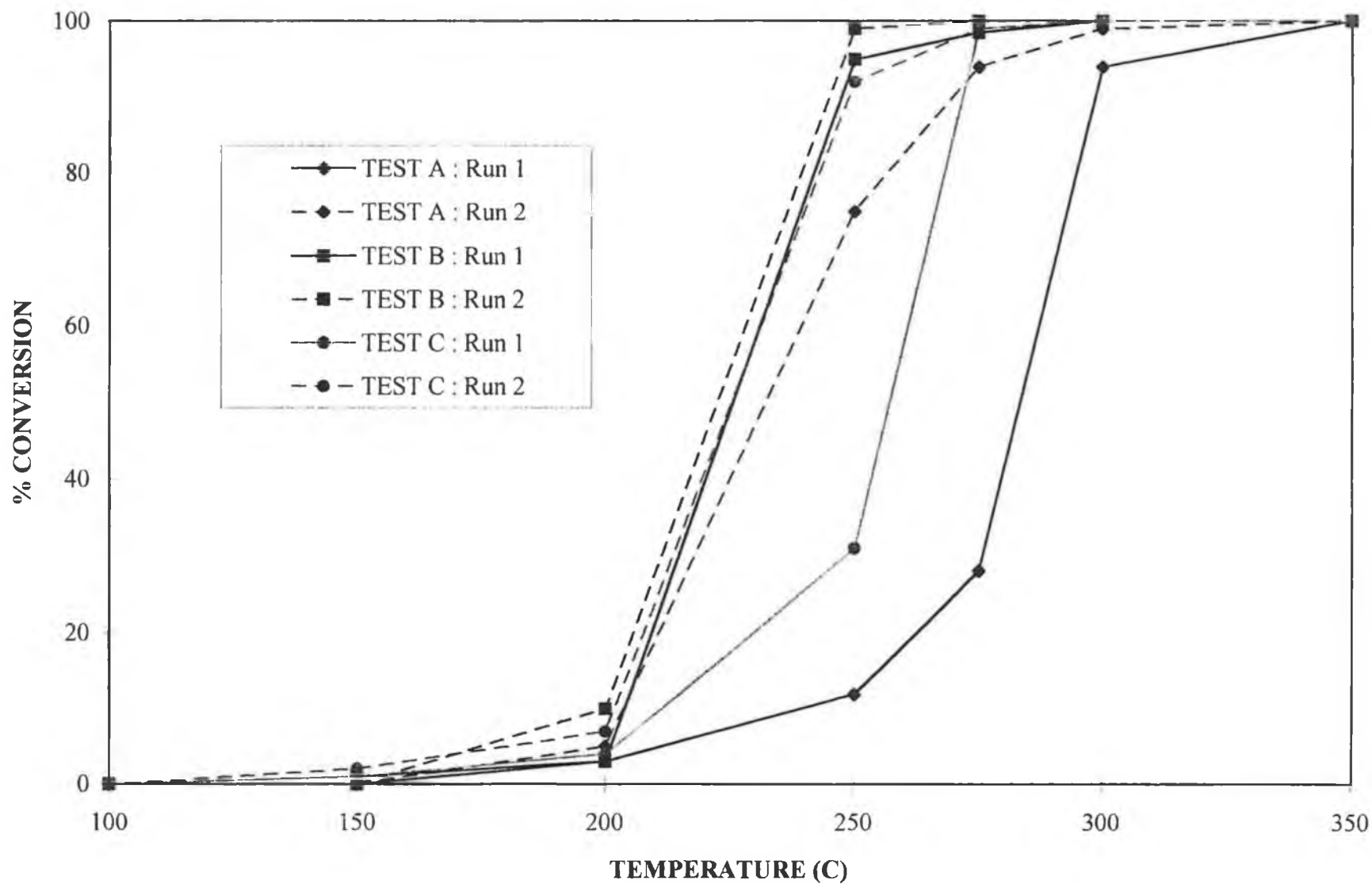


Fig. 3.31: % iso-Butane Conversion versus Temperature for Sample PC.

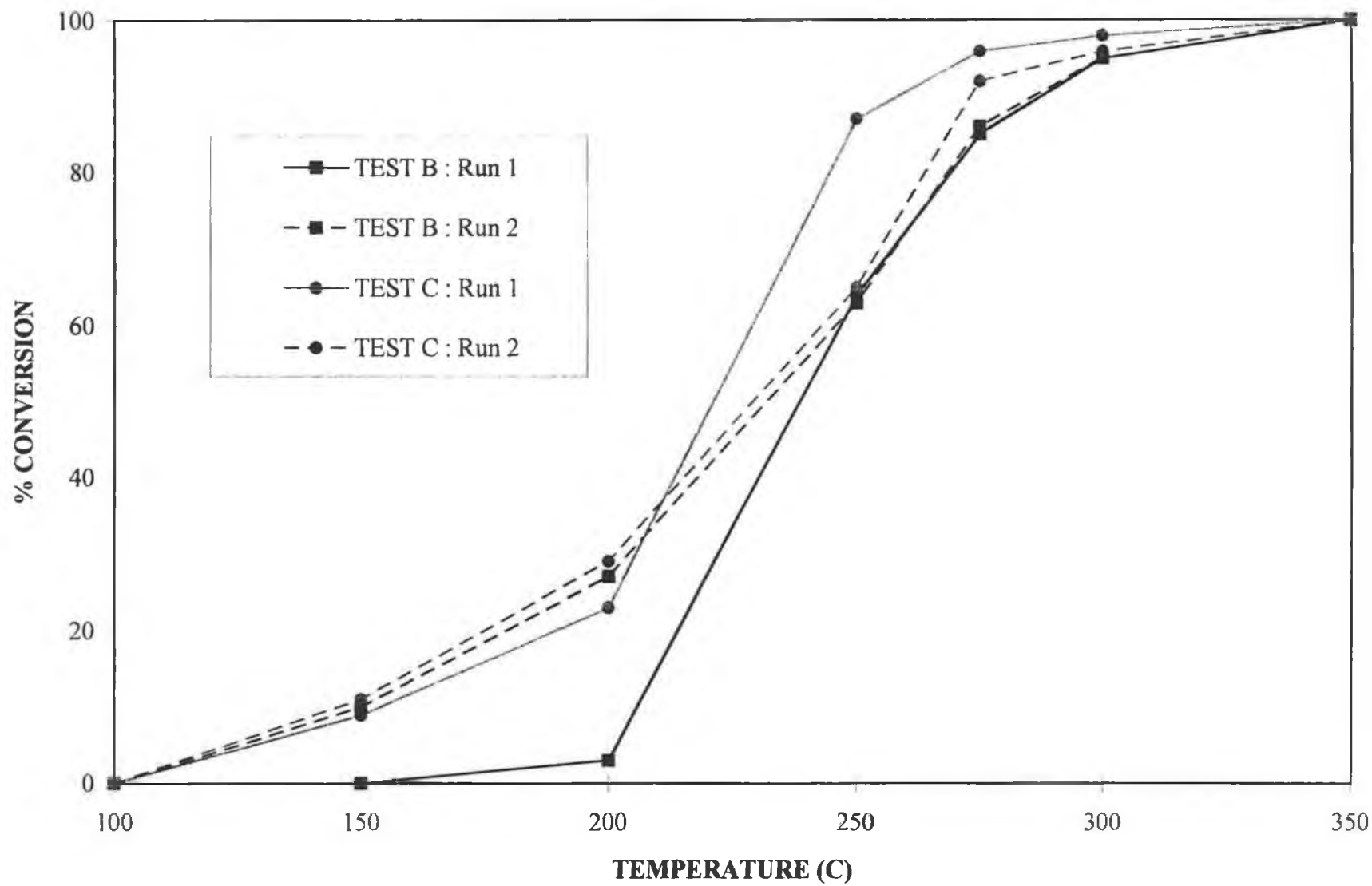


Fig. 3.32 : % iso-Butane Conversion versus Temperature for Sample PC8A\*\*.

**Table 3.4 : Light-off Temperatures (°C) for Iso-Butane Oxidation over Pt/Al<sub>2</sub>O<sub>3</sub>, Pt-Ce/Al<sub>2</sub>O<sub>3</sub>, and Pt/CeO<sub>2</sub> Catalysts.**

Sample	Activity Test A		Activity Test B		Activity Test C	
	Run 1	Run 2	Run 1	Run 2	Run 1	Run 2
PA	175	130	140	130	180	215
PC0.5A	150	130	100	115	110	130
PC1A	115	110	125	105	130	150
PC8A	240	120	100	110	100	145
PC8A**	----	----	200	115	115	115
SPC8A	125	120	100	115	110	115
SCP8A	165	125	100	105	100	105
PC10A	210	125	120	115	----	----
PC17A	220	170	155	135	115	110
PC	195	175	200	165	180	150
C8A	300	310	----	----	----	----

**Table 3.5 : Temperatures (°C) of 10% Iso-Butane Conversion (T<sub>10</sub> Values) over Pt/Al<sub>2</sub>O<sub>3</sub>, Pt-Ce/Al<sub>2</sub>O<sub>3</sub>, and Pt/CeO<sub>2</sub> Catalysts.**

Sample	Activity Test A		Activity Test B		Activity Test C	
	Run 1	Run 2	Run 1	Run 2	Run 1	Run 2
PA	215	185	200	180	295	300
PC0.5A	200	175	160	170	160	175
PC1A	155	135	170	135	180	240
PC8A	275	160	150	150	160	230
PC8A**	----	----	205	150	155	145
SPC8A	160	160	145	150	140	155
SCP8A	230	180	145	140	145	160
PC10A	265	165	160	155	----	----
PC17A	260	205	195	170	155	150
PC	240	205	205	200	215	200
C8A	355	355	----	----	----	----

**Table 3.6 :** Temperatures (°C) of 50% Iso-Butane Conversion ( $T_{50}$  Values) over  $Pt/Al_2O_3$ ,  $Pt-Ce/Al_2O_3$ , and  $Pt/CeO_2$  Catalysts.

Sample	Activity Test A		Activity Test B		Activity Test C	
	Run 1	Run 2	Run 1	Run 2	Run 1	Run 2
PA	260	255	280	275	330	320
PC0.5A	260	260	260	245	225	230
PC1A	215	230	220	225	290	320
PC8A	285	230	215	210	235	280
PC8A**	----	----	240	230	220	230
SPC8A	220	225	215	220	205	200
SCP8A	280	260	230	220	220	225
PC10A	285	250	220	220	----	----
PC17A	285	240	225	230	220	230
PC	285	230	225	220	260	225

**Table 3.7 :** Temperatures (°C) of 90% Iso-Butane Conversion ( $T_{90}$  Values) over  $Pt/Al_2O_3$ ,  $Pt-Ce/Al_2O_3$ , and  $Pt/CeO_2$  Catalysts.

Sample	Activity Test A		Activity Test B		Activity Test C	
	Run 1	Run 2	Run 1	Run 2	Run 1	Run 2
PA	270	270	290	>300	>350	340
PC0.5A	280	295	290	310	310	310
PC1A	240	290	275	310	>300	>350
PC8A	295	290	240	245	>300	295
PC8A**	----	----	290	285	255	270
SPC8A	240	275	255	280	245	240
SCP8A	300	300	280	275	275	300
PC10A	300	290	260	270	----	----
PC17A	295	270	265	290	260	285
PC	295	270	245	240	270	250

Comparison of light-off temperature for the various samples (Table 3.4) in Activity Test A, Run 1, showed the following order of activity:

PC1A> SPC8A> PC0.5A> SCP8A> **PA**> PC> PC10A> PC17A> PC8A.

Light-off temperatures were in the range 115-240°C. The order of activity in terms of T<sub>10</sub> (Table 3.5) was as follows:

PC1A> SPC8A> PC0.5A> **PA**> SCP8A> PC> PC17A> PC10A> PC8A.

T<sub>10</sub> values varied from 155-275°C. T<sub>50</sub> (Table 3.6) values were in the range 215-285°C and showed the following activity trend:

PC1A> SPC8A> **PA**≈ PC0.5A> SCP8A> PC10A≈ PC≈ PC17A≈ PC8A.

Finally, T<sub>90</sub> (Table 3.7) values were between 240-300°C and catalyst activity decreased in the order:

PC1A≈ SPC8A> **PA**> PC0.5A> PC17A≈ PC8A≈ PC> SCP8A≈ PC10A.

There was no apparent relationship between initial catalyst activity and the Pt surface area (see Table 2.7) of the calcined samples. From this table, it is seen that the order of Pt surface area of the various samples investigated by H<sub>2</sub> chemisorption was:

**PA**≥ PC10A> PC0.5A> SPC8A> SCP8A> PC17A > PC.

Turnover numbers (TON) for these samples at 250°C are compared in Table 3.8 in terms of the percentage iso-butane conversion per surface Pt atom. These values were calculated by dividing the percentage i-C<sub>4</sub>H<sub>10</sub> conversion per gram of catalyst sample, by the number of determined Pt surface sites per gram of sample. The number of Pt surface atoms per gram of catalyst was calculated from the volume of H<sub>2</sub> adsorbed in chemisorption measurements using equation (8) in Appendix B. Comparisons of site activity in the different samples on the basis of TONs calculated in this manner assumes that each Pt atom on the surface is an active site. Also, for the Ce-containing samples, there was some uncertainty as to the factors affecting H<sub>2</sub> chemisorption uptakes as discussed in section 2.3.3 and thus TON values for these samples in Table 3.8 may not be an accurate reflection of site activity.

From Table 3.8, the order of Pt site activity at 250°C in the calcined samples was:

SPC8A> PC> PC0.5A≥ **PA**> SCP8A> PC17A> PC10A.

**Table 3.8** : Turnover Numbers for Calcined Catalysts [(% conversion per surface Pt atom at 250°C) × 10<sup>-17</sup>]

Sample	TON* (% per Pt atom) × 10 <sup>-17</sup>
PA	0.47
PC0.5A	0.48
PC10A	0.11
PC17A	0.20
SPC8A	2.51
SCP8A	0.39
PC	1.35

ND = not determined.

\* Based on initial activity of the fresh samples.

On remeasuring the activity of the samples in Activity Test A, Run 2, initial activity (LOT) was achieved at a lower temperature with all samples compared to Run 1. Similarly, all but one catalyst exhibited lower T<sub>10</sub> values during Run 2. Thus, it appears that low temperature oxidation activity was improved for all the samples investigated following initial testing in the stoichiometric air : i-C<sub>4</sub>H<sub>10</sub> mixture. LOT and T<sub>10</sub> values were particularly enhanced for samples PC8A and PC10A. T<sub>50</sub> was also lowered for the higher Ce contents in samples PC8A, SCP8A, PC10A, PC17A, and in sample PC, during the second run. T<sub>50</sub> was almost unchanged for samples PA, PC0.5A, and SPC8A, but increased for sample PC1A. High temperature performance (T<sub>90</sub>) was enhanced for samples PC, PC17A, and PC10A, but disimproved for samples SPC8A, PC0.5A, and PC1A, and remained almost unaffected for PA, PC8A, and SCP8A.

The order of decreasing activity in terms of LOT, in the range 110-175°C, during Run 2 was:

PC1A > SPC8A ≈ PC8A > SCP8A ≈ PC10A > PA ≈ PC0.5A > PC17A > PC.

T<sub>10</sub> values were between 135-205°C and followed the activity trend:

PC1A > SPC8A ≈ PC8A > PC10A > PC0.5A > SCP8A > PA > PC17A ≈ PC.

T<sub>50</sub> values of between 225-260°C were found and catalyst activity decreased in the order:

SPC8A > PC1A ≈ PC8A ≈ PC > PC17A > PC10A > PA > PC0.5A ≈ SCP8A.

T<sub>90</sub> was achieved in the range 270-300°C and catalyst activity decreased according to:

PA ≈ PC17A ≈ PC > SPC8A > PC1A ≈ PC10A ≈ PC8A > PC0.5A > SCP8A.

During Run 2, the slope of the activity curves in the temperature region between initial activity (ca.20% conversion) and ca.100% conversion changed considerably for the bimetallic samples. A more gradual increase in activity as a function of temperature was noticeable for samples PC0.5A, PC1A, PC8A, SPC8A, SCP8A, PC10A, and PC17A. This may have indicated a change in reaction kinetics for these samples following initial testing (8).

XPS analysis was performed on sample PC0.5A after Activity Test A. The spectra obtained are shown in Fig. 3.33(a)-(e). From the survey scan (Fig. 3.33(a)), it is apparent that the major elements present on the surface were O, Al, Si, C, F, Cl, and Ce. Expanded scans of the O 1s and Al 2p regions are illustrated in Fig. 3.33(b) and (c). The Pt 4d region is shown in Fig 3.33(d) which has peaks at 320.1 and 337.6eV attributable to the Pt 4d<sub>5/2</sub> and Pt 4d<sub>3/2</sub> levels, respectively. After charge correction, the Pt 4d<sub>5/2</sub> peak binding energy was found to be 314.6eV which is the same as that in the fresh calcined sample (314.7eV) and indicates that there was no substantial change in the oxidation state of surface Pt after use for i-C<sub>4</sub>H<sub>10</sub> combustion at temperatures of up to 350°C. H<sub>2</sub> chemisorption results (see Table 3.10) indicated there was a considerable loss of available surface Pt (ca. 90% decrease in H<sub>2</sub> uptake) after use in the reaction mixture for Activity Test A. However the loss of surface Pt, as measured by XPS, was not as substantial with quantification of the elemental peaks showing a decrease in the measured Pt surface content from ca.0.06 atomic% to ca.0.04 atomic%. XPS analysis of a sintered (aged) PA sample (see section 3.3.3) revealed no decrease in Pt surface content. Thus, the loss of surface Pt after activity testing for sample PC0.5A might have involved some phenomenon other than an increase in Pt particle size. As discussed below, the TPR profile obtained after activity testing also indicated that no loss of Pt dispersion had occurred. Quantification of the C 1s peak revealed a small increase in surface C content with 9.6% C determined in sample PC0.5A after activity testing compared with 8.1% C in the fresh sample. Therefore, carbon deposition may have contributed to the decrease in surface Pt concentration. The Ce 3d spectrum illustrated in Fig. 3.33(e) indicates that surface Ce was still in intimate contact with the Al<sub>2</sub>O<sub>3</sub> surface following exposure to reaction conditions. The typical features of the Ce<sup>3+</sup> spectrum were still present indicating the existence of the 'CeAlO<sub>3</sub>-precursor' species (35). Ce 3d<sub>5/2</sub> peak positions were determined as 882.7eV(v) and 886.0eV(v'), and Ce 3d<sub>3/2</sub> features were discernible at 901.0eV(u) and 904.6eV(u').

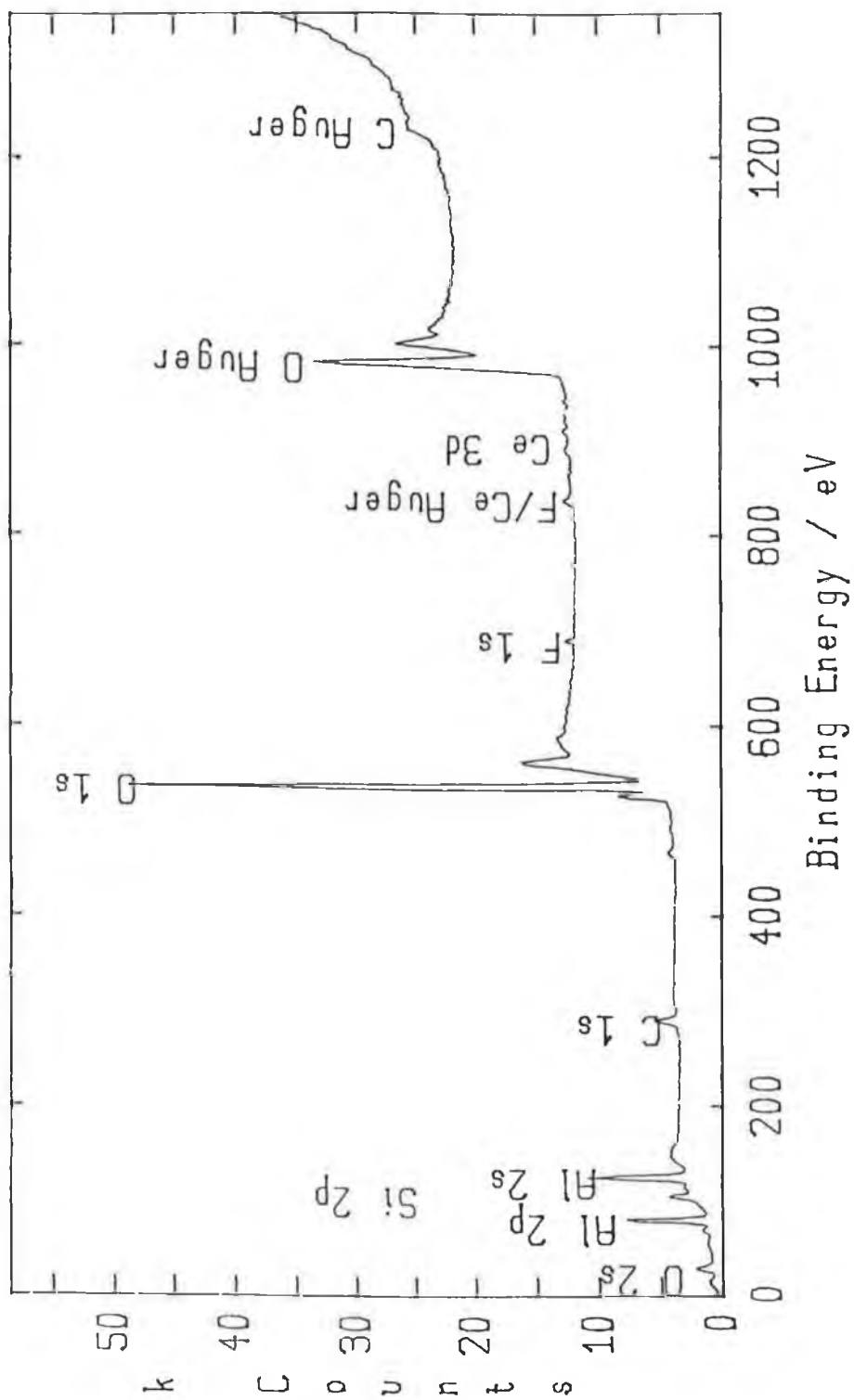
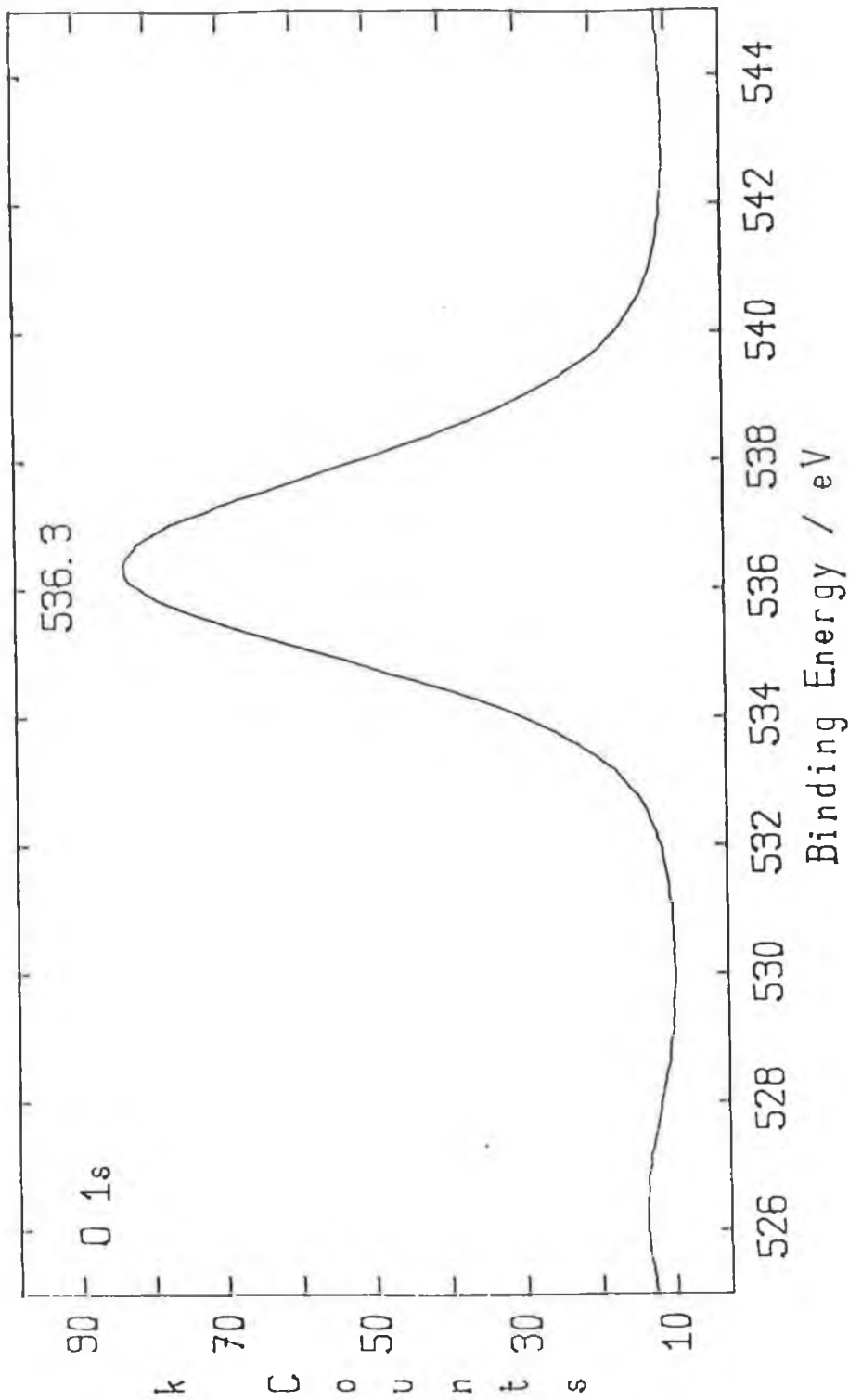
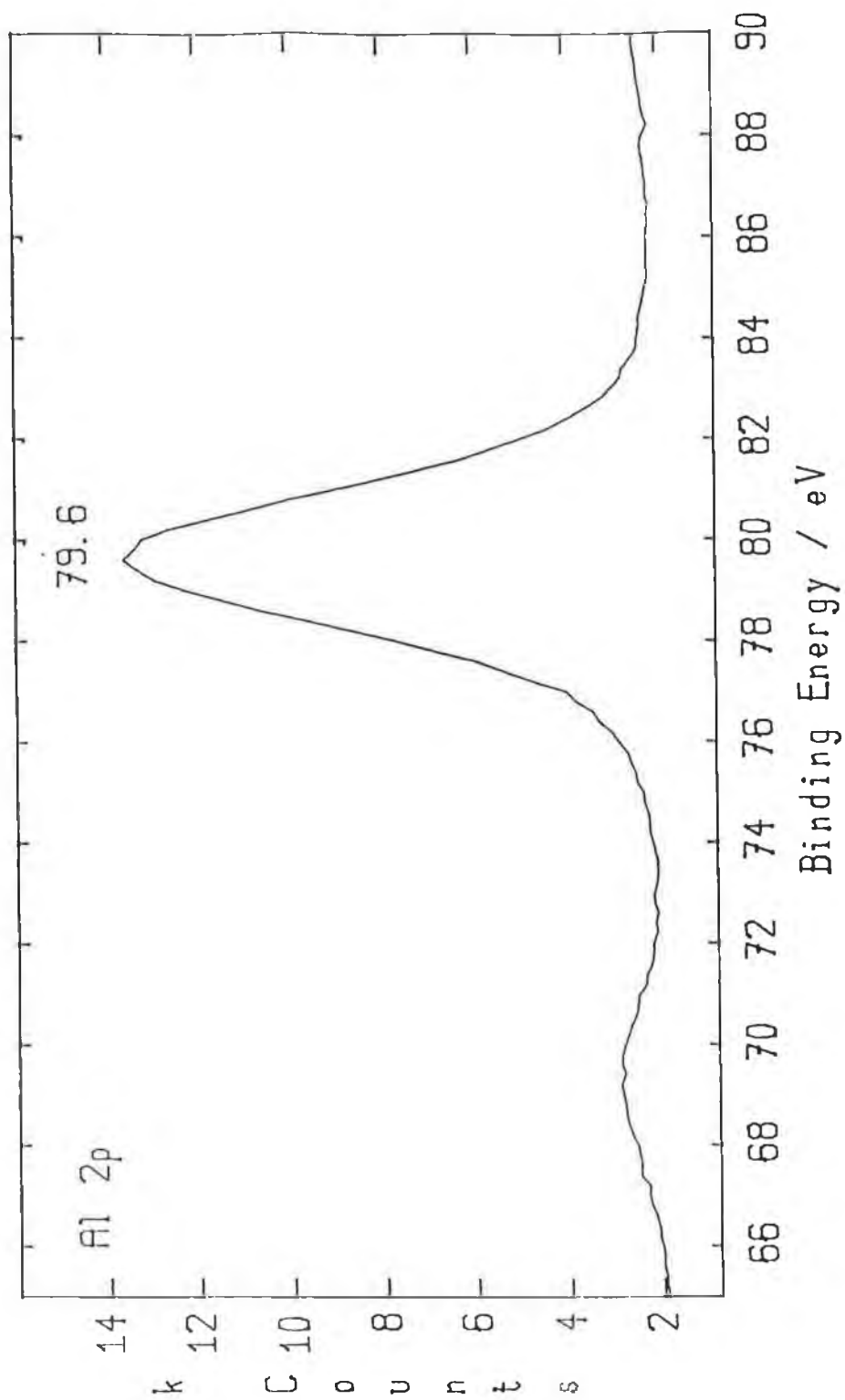


Fig 3.33(a) : XPS spectrum of sample PC0.5A after Activity Test A.



**Fig 3.33(b) :** XPS spectrum showing an expanded energy range scan in the O 1s region for sample PC0.5A after Activity Test A. Charge correction = 5.5 eV.



**Fig 3.33(c) : XPS spectrum showing an expanded energy range scan in the Al 2p region for sample PC0.5A after Activity Test A. Charge correction = 5.5 eV.**

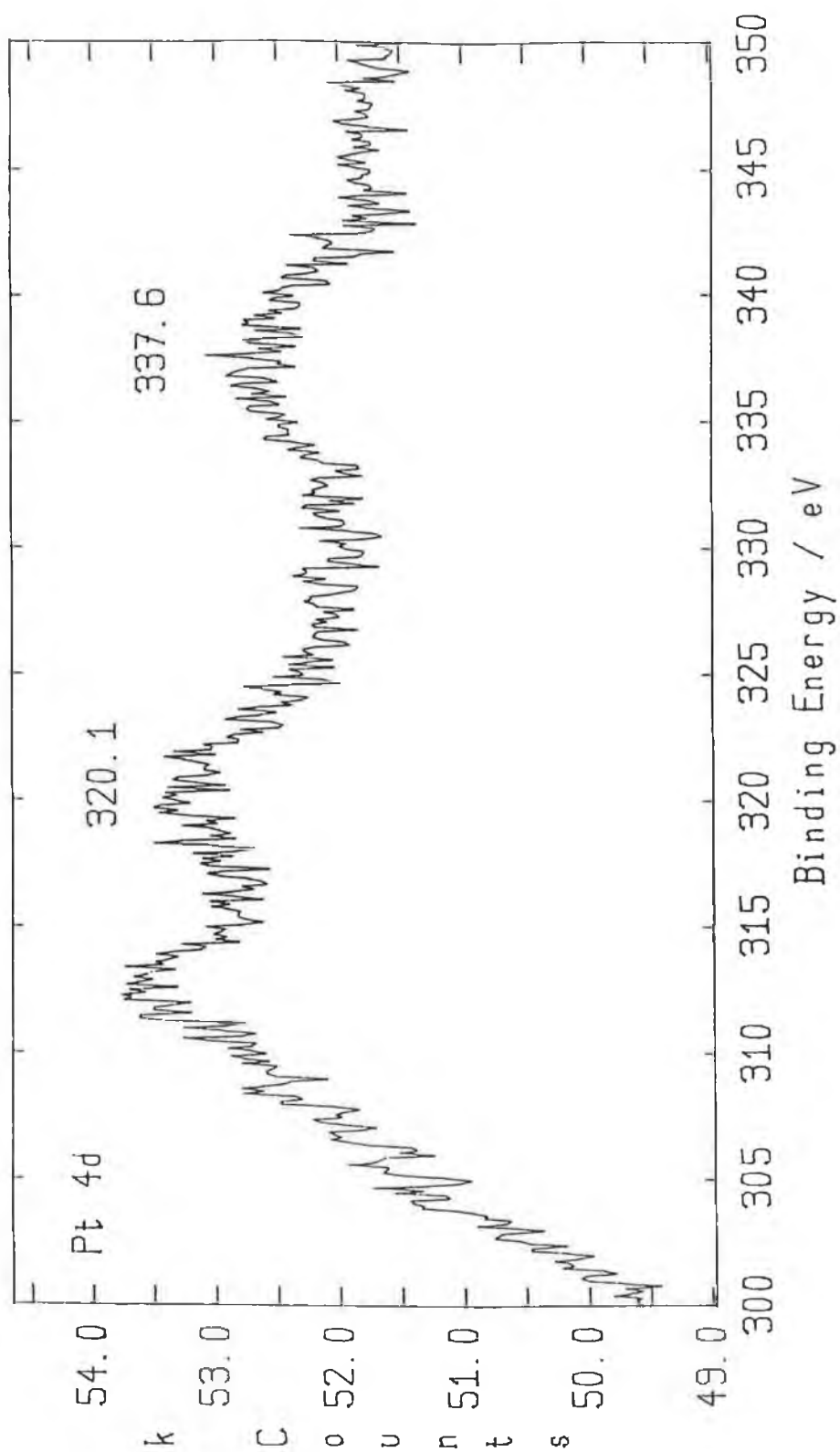


**Fig 3.33(d) : XPS spectrum showing an expanded energy range scan in the Pt 4d region for sample PC0.5A after Activity Test A. Charge correction = 5.5 eV.**

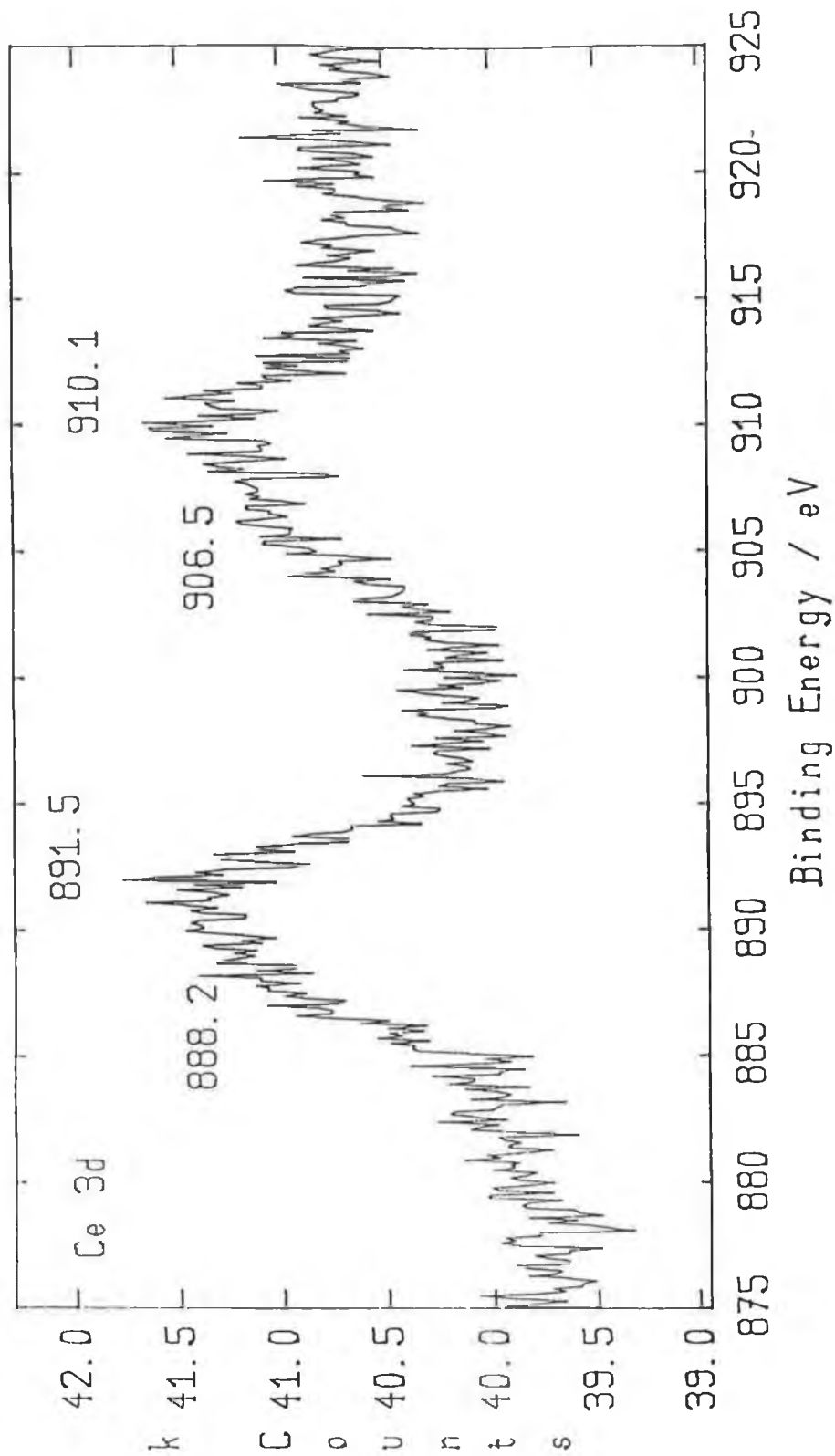


**Fig 3.33(e) :** XPS spectrum showing an expanded energy range scan in the Ce 3d region for sample PC0.5A after Activity Test A. Charge correction = 5.5 eV.

TPR profiles (TPR2) obtained for the various catalysts after Activity Test A are illustrated in Fig. 3.34-3.36.

For sample PA, the temperature of the main reduction feature was unchanged after exposure to the reaction mixture. However, a distinct increase in the size of the peak at ca.420°C occurred with a shoulder apparent at ca.395°C (compare Fig. 3.34(a) and Fig. 3.20(a)). As discussed previously, a peak at this temperature was probably associated with the reduction of Pt species in intimate contact with the Al<sub>2</sub>O<sub>3</sub> surface.

A small increase in the reducibility of Pt in sample PC0.5A relative to PA was apparent in the TPR profiles of the calcined samples (see Fig. 3.20(a) and (c)), presumably due to Pt-Ce interaction. The profile obtained for sample PC0.5A after Activity Test A (Fig. 3.34(b)) indicates that this interaction was lost on use in activity measurements. As for PA, a larger peak at ca.420°C (shoulder at ca. 395°C) is apparent after exposure to the reaction mixture. Again, this feature is attributable to the existence of some form of Pt-Al<sub>2</sub>O<sub>3</sub> interactive species. The fact that the reduction temperature remained very high, may indicate that no loss of Pt dispersion occurred during activity testing up to 350°C (37). The reason for the increase in H<sub>2</sub> uptake after reaction (Fig 3.34(b) versus Fig. 3.20(c)) is unknown. As discussed above, XPS analysis indicated that no increase in the surface oxidation state of Pt had occurred, and the intensity of the surface Pt 4d photoelectron peak actually decreased, after activity testing. Another possibility is that C-deposition onto the support surface during testing could have resulted in an increase in H<sub>2</sub> spillover onto the support in Fig. 3.34(b) (51).

The profile obtained for sample PC1A is shown in Fig. 3.34(c). Following use for i-C<sub>4</sub>H<sub>10</sub> oxidation, the main reduction peak was shifted from ca.250°C in the calcined sample (Fig. 3.21(a)) to ca.440°C and shows an increased H<sub>2</sub> uptake. This would appear to indicate that loss of Pt-Ce interaction had occurred during activity testing. As discussed previously, a reduction peak at ca.250°C in the calcined samples was attributable to the reduction of a Pt-CeO<sub>2</sub> surface interactive species. The TPR profile in Fig. 3.34(c) indicates that Pt was in greater contact with the Al<sub>2</sub>O<sub>3</sub> surface, rather than with CeO<sub>2</sub>, after testing. The profile resembles those of samples PA and PC0.5A after activity testing, although the peak temperature was higher by ca.20-25°C which would suggest that the Pt was slightly more difficult to reduce in sample PC1A.

The profiles obtained for samples PC8A, SCP8A and SPC8A after Activity Test A are shown in Fig. 3.35. For sample PC8A (Fig.3.35(a)) the main reduction peak is still seen to occur at ca.250°C indicating that Pt-Ce interaction on the catalyst surface was maintained after testing. However, the H<sub>2</sub> uptake was decreased following

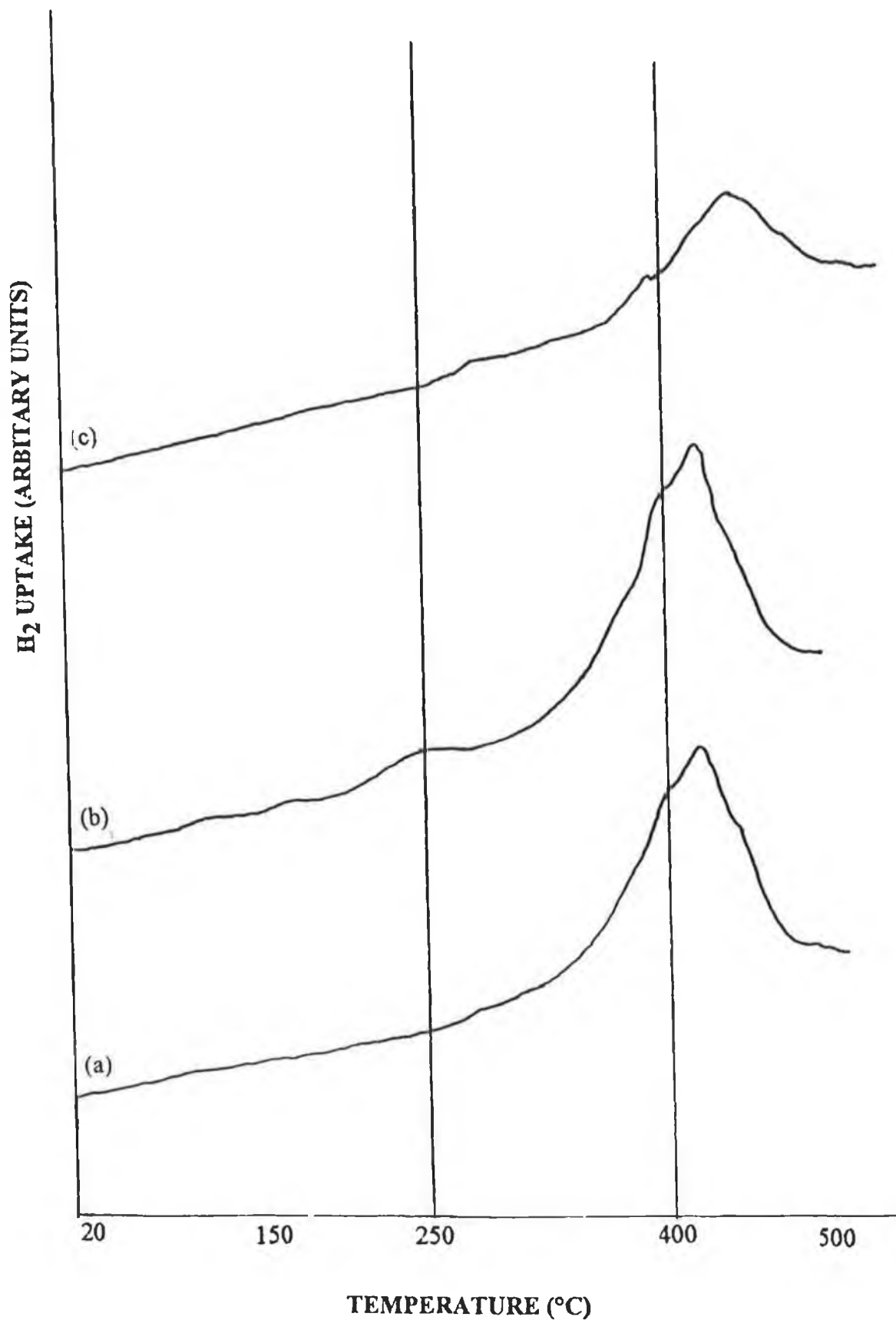


Fig 3.34 : TPR profiles of samples after Activity Test A, (a)-PA, (b)-PC0.5A, (c)-PC1A.

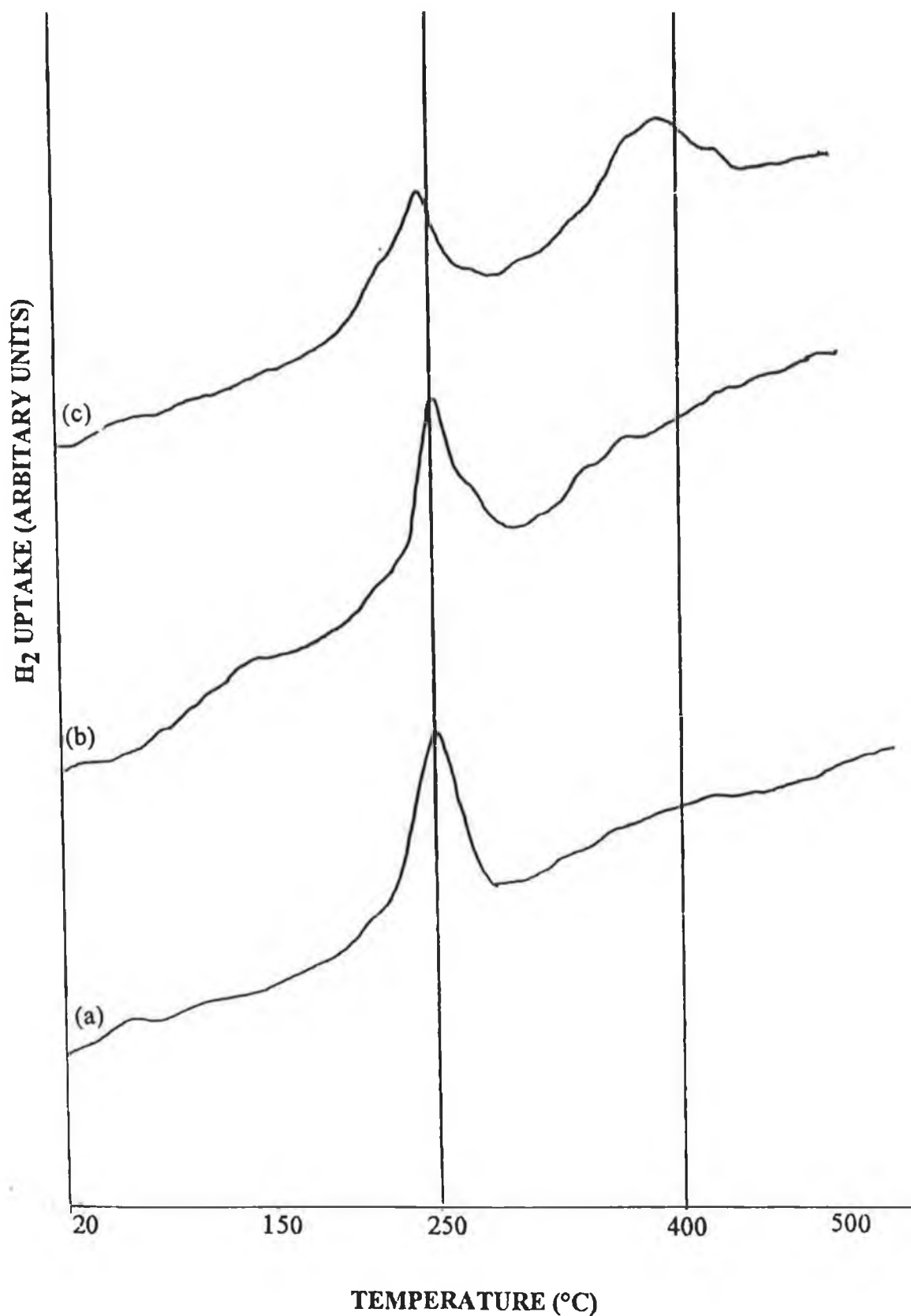


Fig 3.35 : TPR profiles of samples after Activity Test A, (a)-PC8A, (b)-SCP8A, (c)-SPC8A.

exposure to the reaction mixture and also the 'Ce-Al<sub>2</sub>O<sub>3</sub>' shoulder peak at ca.370°C was not as pronounced as for the fresh calcined sample (compare Fig. 3.21(b) and Fig. 3.35(a)). As for PC8A, the profile obtained for sample SCP8A after testing (Fig. 3.35(b)) also indicates that Pt was in more intimate contact with surface Ce rather than Al<sub>2</sub>O<sub>3</sub> after testing with the main reduction peak at ca.250°C. The profile obtained for sample SPC8A (Fig. 3.35(c)) indicates the presence of both Pt-Ce and Pt-Al<sub>2</sub>O<sub>3</sub> interactive surface species, with the characteristic peaks at ca.250°C and ca.400°C present. This was also the case for the calcined sample (Fig. 3.22(a)). However, the use of sample SPC8A for Activity Test A appeared to result in changes in the relative degree of interaction of the Pt with Ce and Al<sub>2</sub>O<sub>3</sub>. This indicates that Pt was mobile on the support surface during i-C<sub>4</sub>H<sub>10</sub> oxidation, in agreement with the TPR profiles for samples PC0.5A and PC1A. For SPC8A profiles both peaks were in co-existence, while for the co-impregnated samples activity testing appeared to result in the disappearance of Pt/Ce interaction and the simultaneous appearance of the Pt/Al<sub>2</sub>O<sub>3</sub> peak, presumably due to migration of Pt to surface sites where it experienced closer interaction with the Al<sub>2</sub>O<sub>3</sub> support rather than the Ce additive.

The TPR profile obtained for sample PC10A (Fig. 3.36(a)) indicates that Pt-Ce interaction on the catalyst surface was maintained after Activity Test A. As for PC8A, the size of the peak at ca.250°C was decreased following exposure to the reaction mixture and also the 'Ce-Al<sub>2</sub>O<sub>3</sub>' shoulder peak at ca.370°C was not as pronounced as for the fresh calcined sample (compare Fig. 3.21(c) and 3.36(a)). H<sub>2</sub> uptake was also decreased for samples PC17A and PC after Activity Test A as can be seen from comparisons of Fig. 3.36(b) with Fig. 3.22(c) and Fig. 3.36(c) with Fig. 3.20(b), respectively. For sample PC17A, a reduction feature at ca.250°C is still evident after testing which indicates that Pt-Ce surface interaction was maintained, while for PC the distinct loss of surface reducible species makes it difficult to interpret the profile obtained.

In general, the activity of Ce-containing samples increased after TPR, while sample PA became less active (Activity Test B, Run 1 versus Test A, Run 2). Following TPR, it can be seen from Tables 3.4-3.7 that samples containing Ce were generally more active than sample PA. During Activity Test B, Run 1, 50% and 90% conversion of i-C<sub>4</sub>H<sub>10</sub> was achieved at lower temperatures for sample PC and all Pt-Ce/Al<sub>2</sub>O<sub>3</sub> samples, except PC0.5A, compared to sample PA. LOT and T<sub>10</sub> values were also generally improved in the presence of Ce. Thus, it can be stated that, after TPR from 20-500°C, the presence of Ce, either as a support or as an additive in Pt/Al<sub>2</sub>O<sub>3</sub> catalysts, was potentially beneficial for the catalytic oxidation of i-C<sub>4</sub>H<sub>10</sub> under the conditions employed.

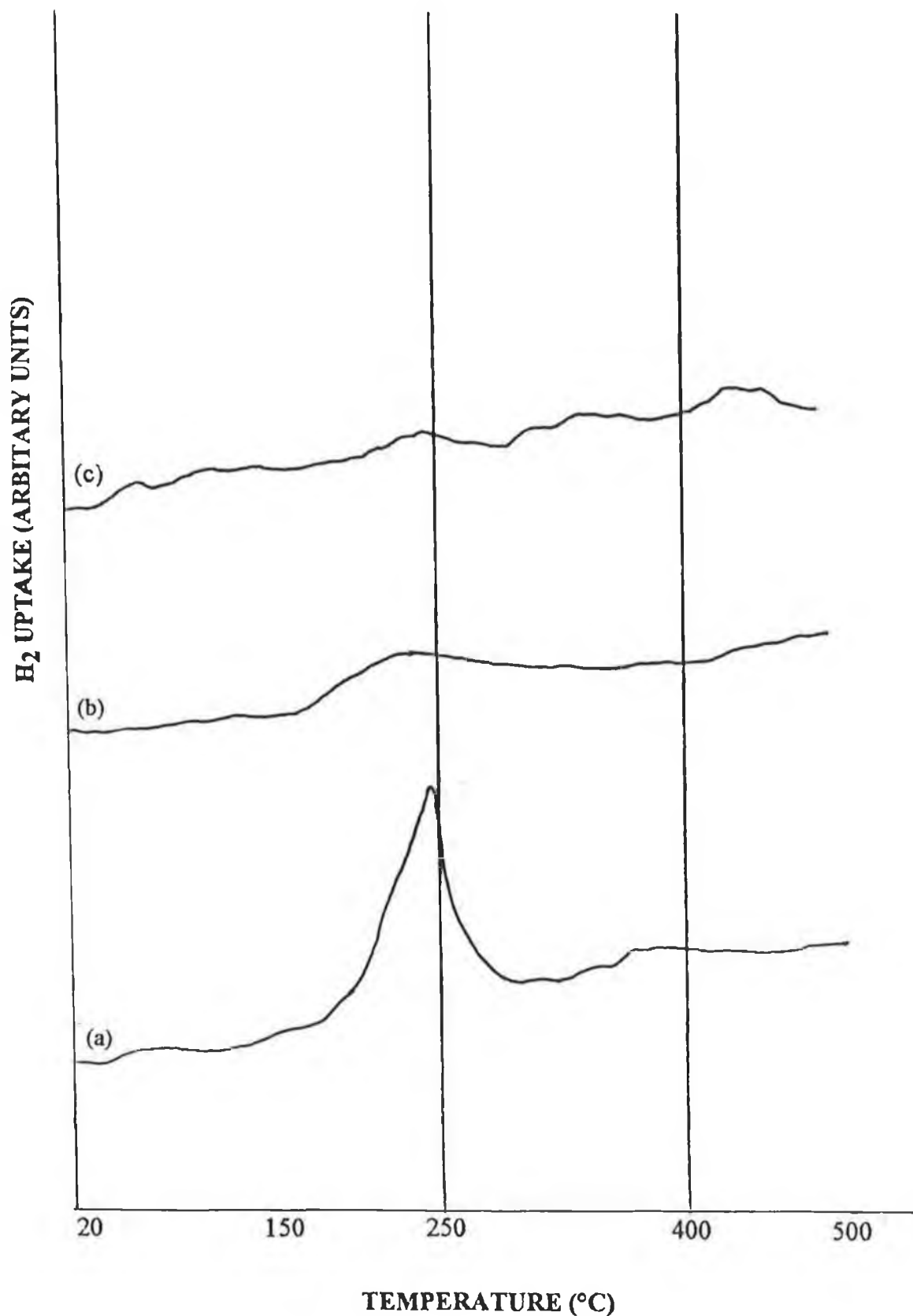


Fig 3.36 : TPR profiles of samples after Activity Test A, (a)-PC10A, (b)-PC17A, (c)-PC.

On comparison of LOT, T<sub>10</sub>, T<sub>50</sub>, and T<sub>90</sub> values in Activity Tests A and B, it can be seen that, following TPR, samples with Ce were, in general, more active than sample PA was prior to, as well as after, reduction. In terms of T<sub>50</sub>, all Ce-containing samples were more active in Test B than sample PA was in Tests A, B, or C.

The amount of Ce present affected activity after TPR, as well as before TPR. During Test B, Run 1, the order of activity in terms of LOT in the region 100-200°C was:

PC0.5A ≈ SPC8A ≈ SCP8A ≈ PC8A > PC10A > PC1A > PA > PC17A > PC8A\*\* ≈ PC.

The difference between samples PC8A and PC8A\*\* is that the latter was not used for Activity Test A prior to TPR. T<sub>10</sub> was reached between 145-205°C and catalytic activity decreased as follows:

SPC8A ≈ SCP8A > PC8A > PC0.5A ≈ PC10A > PC1A > PC17A > PA > PC ≈ PC8A\*\*.

In relation to T<sub>50</sub>, the activity trend was:

PC8A ≈ SPC8A > PC10A ≈ PC1A > PC ≈ PC17A > SCP8A > PC8A\*\* > PC0.5A > PA,

with T<sub>50</sub> values in the range 215-280°C. 90% conversion of i-C<sub>4</sub>H<sub>10</sub> required temperatures of between 240-290°C for the various catalysts, with the order of activity being:

PC8A ≈ PC > SPC8A > PC10A > PC17A > PC1A > SCP8A > PC8A\*\* ≈ PC0.5A ≈ PA.

It is evident that samples PC8A, SPC8A, and PC10A were among the most active catalysts at all temperatures investigated. Samples PA, PC, and PC17A required the highest temperatures for reaction to be initiated. However, sample PC17A and, in particular, sample PC showed a very rapid rise in conversion with temperature once T<sub>10</sub> had been reached. Comparison of samples PC8A and PC8A\*\* shows that the latter sample, which had not been used in the i-C<sub>4</sub>H<sub>10</sub> oxidation mixture prior to TPR, was considerably less active in Activity Test B, Run 1. This indicates that, as well as the level of Ce present, preliminary activation in the reaction mixture was also important in attaining higher activity following reduction.

On remeasuring the activity of the reduced samples in Activity Test B, Run 2, samples containing Ce were still generally more active than the Pt-only sample, PA. Once again, sample PC was slowest to reach LOT, but achieved 50 and 90% conversion of i-C<sub>4</sub>H<sub>10</sub> at considerably lower temperatures than sample PA due to a more rapid rise in activity following light-off.

The lower temperature activity of reduced PA was increased after use in the reaction mixture. However, at higher temperatures PA was less active in Run 2 compared to Run 1. For Pt-Ce/Al<sub>2</sub>O<sub>3</sub> samples, the effect of exposure to the reaction mixture in Test B, Run 1, on subsequent Run 2 activity varied for the different catalysts. It is noticeable, however, that the activity of sample PC8A\*\* was improved after initial testing with LOT and T<sub>10</sub> values being lowered considerably in Run 2, and slight improvements in T<sub>50</sub> and T<sub>90</sub> values also apparent.

During Test B, Run 2, LOT values varied from 105-165°C. In this temperature region, catalyst activity was in the order:

SCP8A ≈ PC1A > PC8A > PC0.5A ≈ PC8A\*\* ≈ SPC8A ≈ PC10A > PA > PC17A > PC.

In terms of T<sub>10</sub>, catalyst activity decreased in the order:

PC1A > SCP8A > PC8A ≈ SPC8A ≈ PC8A\*\* > PC10A > PC0.5A ≈ PC17A > PA > PC,

for values in the range 135-200°C. T<sub>50</sub> values varied from 210-275°C with catalytic activity decreasing as follows:

PC8A > PC ≈ SPC8A ≈ PC10A ≈ SCP8A > PC1A > PC17A ≈ PC8A\*\* > PC0.5A > PA.

For T<sub>90</sub>, which varied from 240°C to above 300°C, the order of activity was:

PC ≈ PC8A > PC10A > SCP8A > SPC8A > PC8A\*\* > PC17A > PC0.5A ≈ PC1A > PA.

One interesting fact is that the three samples which showed poorest activity in this higher temperature range were PC0.5A, PC1A and PA. For all of these samples, TPR<sub>2</sub> (Fig. 3.34) indicated that Pt was interacting strongly with Al<sub>2</sub>O<sub>3</sub>. For all the other Al<sub>2</sub>O<sub>3</sub>-supported samples, Pt appeared to be in greater contact with surface Ce rather than Al<sub>2</sub>O<sub>3</sub> during TPR.

TPR profiles (LTPR) obtained for the various catalysts after Activity Test B are illustrated in Fig. 3.37-3.39.

For samples PA, PC0.5A and PC1A (Fig. 3.37(a)-(c)) the dominant reduction feature occurs at ca. 420-450°C attributable to the reduction of a Pt-Al<sub>2</sub>O<sub>3</sub> interactive species. Similarly, for sample PC8A the main reduction feature after Activity Test B is seen at ca. 440-450°C in Fig. 3.38(a). The shift in reduction peak temperature from ca. 250°C in Fig. 3.35(a) is similar to that which occurred for sample PC1A in Test A, and

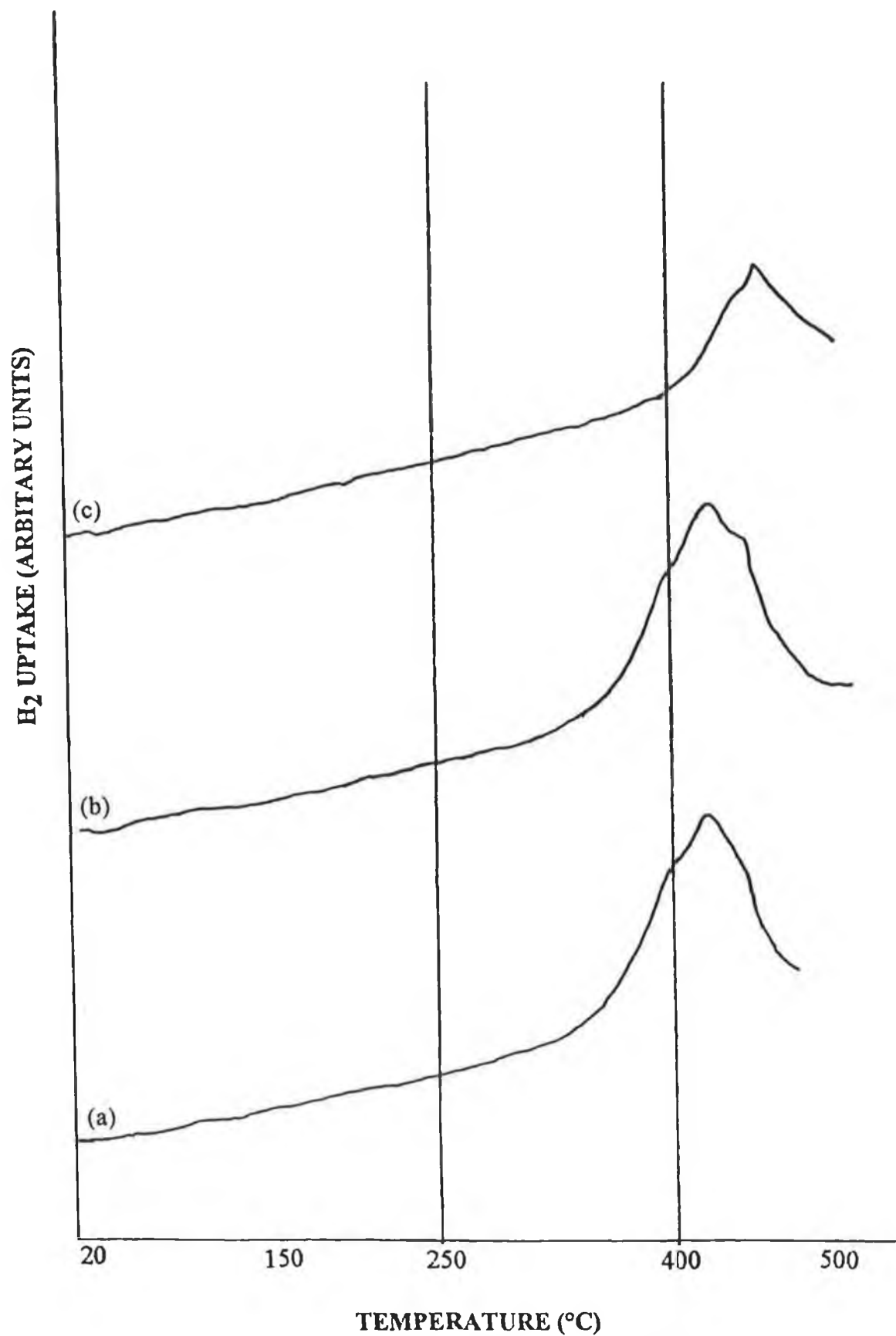


Fig 3.37 : TPR profiles of samples after Activity Test B, (a)-PA, (b)-PC0.5A, (c)-PC1A.

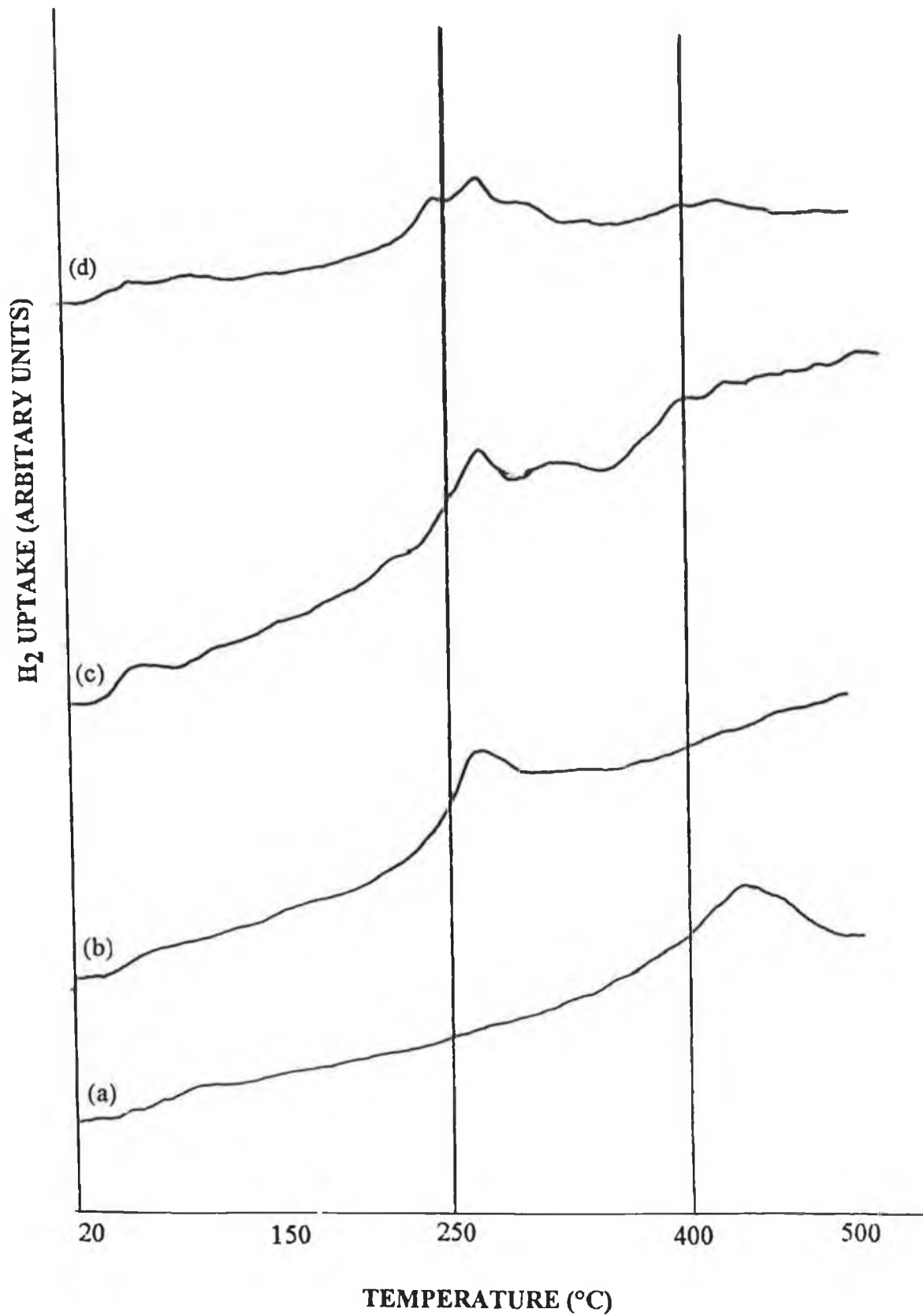


Fig 3.38 : TPR profiles of samples after Activity Test B, (a)-PC8A, (b)-PC8A\*\*, (c)-SCP8A, (d)-SPC8A.

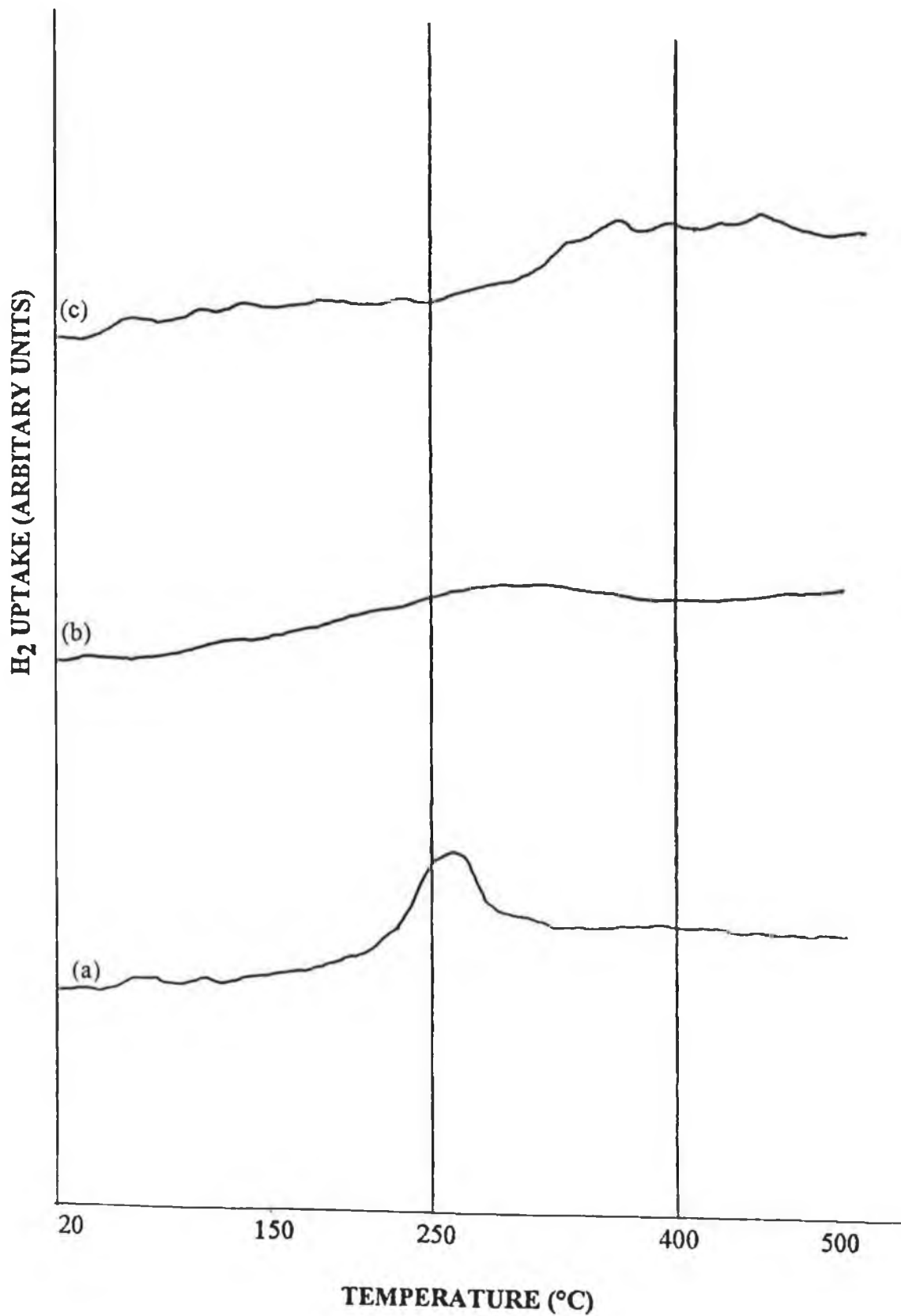


Fig 3.39 : TPR profiles of samples after Activity Test B, (a)-PC10A, (b)-PC17A, (c)-PC.

indicates that retesting of PC8A in Test B resulted in loss of Pt-Ce interaction and the formation of a Pt-Al<sub>2</sub>O<sub>3</sub> interactive species. The LTPR profile obtained for sample PC8A\*\* after Activity Test B is shown in Fig. 3.38(b) and indicates that Pt-Ce surface interaction was stable during initial testing with the main reduction peak evident at ca.270°C. The dominant reduction features for samples SCP8A (Fig. 3.38(c)) and SPC8A (Fig. 3.38(d)) are also evident at ca.270°C indicating the existence of a Pt-Ce surface interaction.

The LTPR profiles obtained for samples PC10A, PC17A and PC are shown in Fig. 3.39. For all of these samples, H<sub>2</sub> uptake decreased after Activity Test B as had been the case after Test A. For PC10A, the proposed Pt-Ce reduction feature at ca.250°C was still present in Fig. 3.39(a). For PC17A, Pt also appeared to be in greater contact with Ce rather than Al<sub>2</sub>O<sub>3</sub> with a broad reduction feature apparent in Fig. 3.39(b) at ca.300°C.

After prolonged reduction at 500°C for 2.5h in the LTPR step of the sample analysis procedure, catalytic activity during Test C appeared to be related to the nature of reducible surface species present in the LTPR profiles obtained.

Prolonged reduction at 500°C in the LTPR step resulted in a considerable loss of activity for samples PA, PC1A, and PC8A in Activity Test C. As discussed above, oxidised surface Pt appeared to be present in some form of interactive species with the Al<sub>2</sub>O<sub>3</sub> support in the LTPR profiles obtained for all of these samples. For sample PC0.5A, Pt also appeared to be more strongly interacting with the Al<sub>2</sub>O<sub>3</sub> rather than the Ce surface during LTPR. The activity of this sample did not, however, deteriorate significantly following reduction at 500°C.

In contrast to sample PC8A, sample PC8A\*\* did not show any major activity losses following LTPR. Both of these samples contained the same level of Ce, were prepared in the same manner, and had been previously activated in the reaction mixture. However, for sample PC8A\*\* the characteristic Pt-Ce reduction feature was still apparent in the LTPR profile obtained, while for sample PC8A, Pt-Ce interaction appeared to have been lost during prior activity tests (compare Figures 3.38(a) and (b)). Thus, it would appear that Pt-Ce interaction during reduction was somehow important in preventing the loss of activity which was apparent after reduction for most samples in which Pt-Al<sub>2</sub>O<sub>3</sub> interaction prevailed.

Similarly for samples SPC8A, SCP8A, PC17A, and PC, the profiles obtained prior to reduction at 500°C indicated the existence of some form of Pt-Ce interaction. None of these samples were deactivated to any great extent after LTPR and for some samples improvements in activity were evident in Test C.

After reduction at 500°C, Pt-Ce/Al<sub>2</sub>O<sub>3</sub> and Pt/CeO<sub>2</sub> samples were, in general, more active than sample PA. In Test C, Run 1, the order of decreasing activity with respect to LOT was:

PC8A≈ SCP8A> SPC8A≈ PC0.5A> PC17A≈ PC8A\*\*> PC1A> PA≈ PC.

Light-off occurred between 100 and 180°C. In terms of T<sub>10</sub>, catalyst activity decreased according to:

SPC8A> SCP8A> PC17A≈ PC8A\*\*> PC8A≈ PC0.5A> PC1A> PC> PA,

for values in the range 140-295°C. T<sub>50</sub> values were between 205-330°C and the activity trend was:

SPC8A> PC8A\*\*≈ SCP8A≈ PC17A> PC0.5A> PC8A> PC> PC1A> PA.

In terms of T<sub>90</sub>, catalyst activity decreased in the order:

SPC8A> PC8A\*\*> PC17A> PC> SCP8A> PC0.5A> PC8A> PC1A> PA,

in the temperature region from 245°C to above 350°C. The activity of samples PC1A and PC8A decreased with time during testing at temperatures above 250°C, while that of PA was found to increase with time in the reaction mixture at 350°C.

On retesting the catalysts in Test C, Run 2, the activity of samples PC1A and PC8A was found to have further decreased while sample PA did not show any significant further deactivation. LOT was between 105-215°C for the various catalysts with activity decreasing in the order:

SCP8A> PC17A> PC8A\*\*≈ SPC8A> PC0.5A> PC8A> PC1A≈ PC> PA.

10% conversion of i-C<sub>4</sub>H<sub>10</sub> was achieved between 145 and 300°C and the activity trend was:

PC8A\*\*> PC17A> SPC8A> SCP8A> PC0.5A> PC> PC8A> PC1A> PA.

With respect to T<sub>50</sub>, in the range 200-320°C, catalytic activity was in the order:

SPC8A> SCP8A≈ PC> PC8A\*\*≈ PC0.5A≈ PC17A> PC8A> PC1A≈ PA.

Finally,  $T_{90}$  values were in the region from 240°C to above 350°C and showed the activity trend:

SPC8A > PC > PC8A\*\* > PC17A > PC8A > SCP8A > PC0.5A > PA > PC1A.

XPS analysis was performed on sample PC8A after Activity Test C. The spectra obtained are shown in Fig. 3.40(a)-(c).

Once again, Ce appears to have been present in a reduced state on the catalyst surface with the Ce 3d spectrum resembling that of  $Ce^{3+}$  more so than that of  $Ce^{4+}$  (Fig. 3.40(b)). After charge correction, Ce 3d<sub>5/2</sub> peak positions of 882.3eV(v) and 885.6eV(v') were measured with Ce 3d<sub>3/2</sub> features at 901.6eV(u) and 904.5eV(u'). This indicates that dispersed Ce was still experiencing a strong interaction with the Al<sub>2</sub>O<sub>3</sub> support which stabilised the Ce in a partially reduced state (35).

Analysis of the Pt 4d region (Fig 3.40(c)) shows that a distinctive loss of surface Pt had occurred during activity and TPR tests. The loss of surface Pt was so great as to render the amount of Pt present too low to be quantified. Loss of Pt may have been due to metal sintering during activity testing or TPR experiments. However, this seems unlikely because the XPS spectrum of a sintered PA sample (Fig 3.44(b)) showed no decrease in the intensity of the Pt 4d features relative to a highly dispersed sample (Fig. 3.13(b)). Comparison of the catalyst activity for sintered samples (see section 3.3.3) and for samples in Activity Test C would also argue against sintering effects. Carbon deposition from the oxidation reaction mixture could also have made surface Pt inaccessible to surface sensitive techniques. However, this also seems an unlikely explanation for the loss in XPS signal as the C content on the surface was only 8.5% which is approximately the same as that found for fresh Al<sub>2</sub>O<sub>3</sub>-supported samples (see Table 3.2). Previous studies have reported that strong interaction between Pt and Al<sub>2</sub>O<sub>3</sub> (46, 52-54) or CeO<sub>2</sub> (12) supports can result in loss of surface Pt on reduction in H<sub>2</sub>. For example, Bouwman and Biloen (46) reported loss of Pt 4d photoline intensity for Pt/Al<sub>2</sub>O<sub>3</sub> after treatment in H<sub>2</sub> above 450°C. This was thought to be most likely attributable to migration of Pt to less exposed sites in the  $\gamma$ -Al<sub>2</sub>O<sub>3</sub> matrix because XRD work proved that no agglomeration had taken place (46). Dautzenberg and co-workers (52, 53) found that heat treatment in an O<sub>2</sub>-containing environment above 500°C caused agglomeration of Pt on Al<sub>2</sub>O<sub>3</sub>, while heat treatment in H<sub>2</sub> above 500°C did not. Although electron microscopy and x-ray diffraction analysis proved that excessive sintering did not occur in a reducing environment at the temperatures used, H<sub>2</sub> chemisorption measurements were considerably depleted. This was explained in terms of

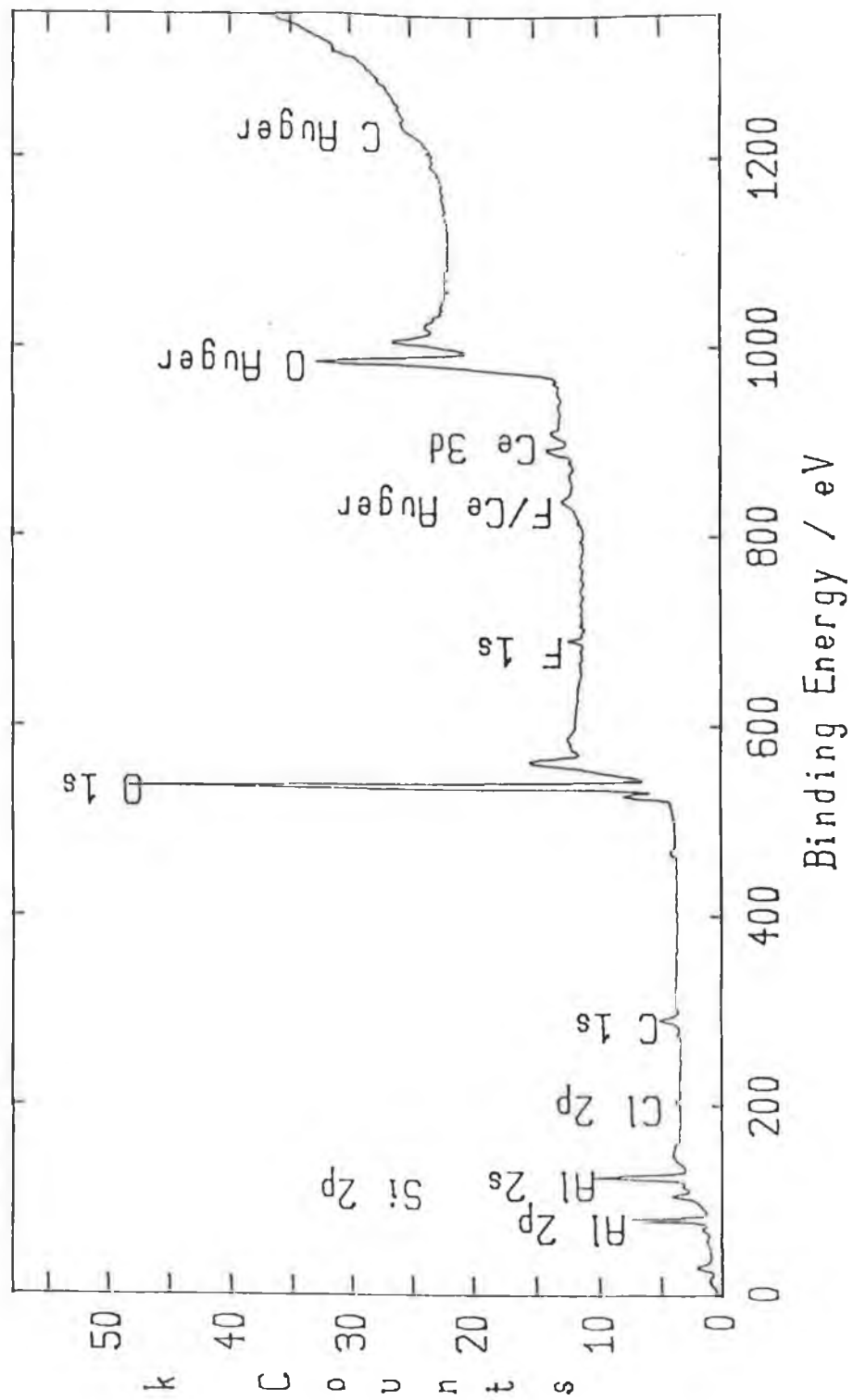


Fig 3.40 (a) : XPS spectrum of sample PC8A after Activity Test C.

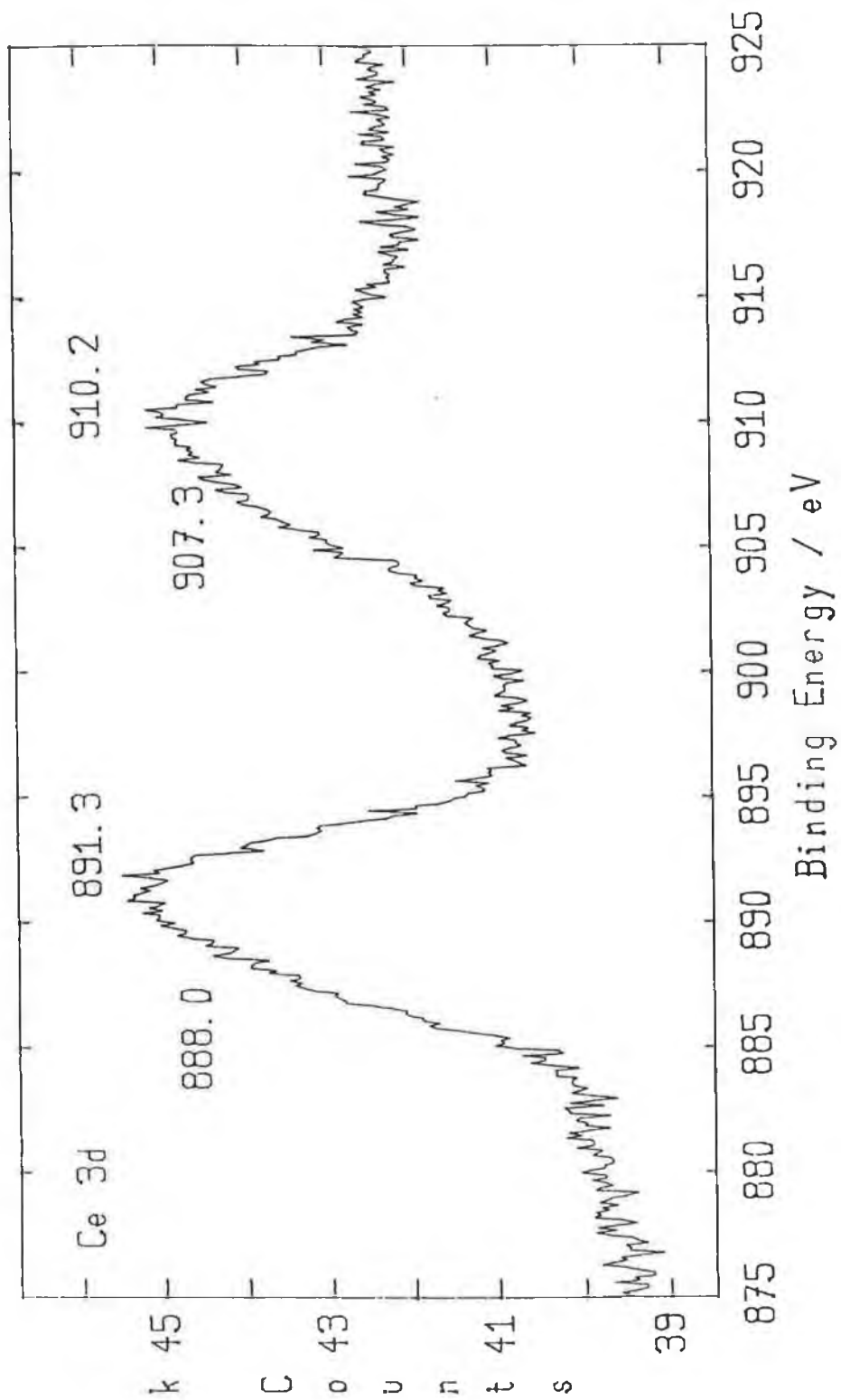
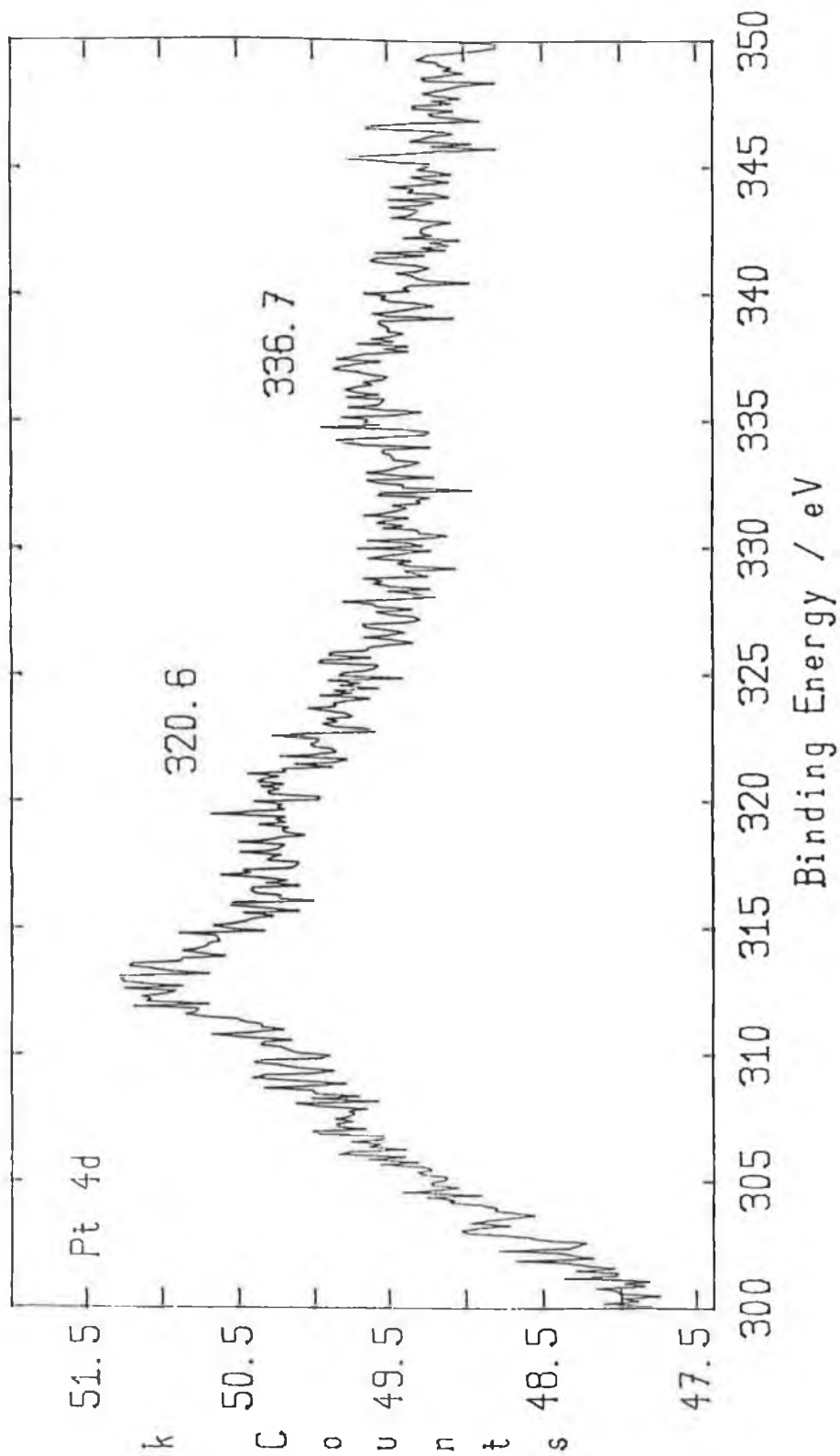


Fig 3.40(b) : XPS spectrum showing an expanded energy range scan in the Ce 3d region for sample PC8A after Activity Test C. Charge correction = 5.7eV.



**Fig 3.40(c) : XPS spectrum showing an expanded energy range scan in the Pt 4d region for sample PC8A after Activity Test C. Charge correction = 5.7eV.**

the formation of an alloy species between highly dispersed Pt particles and Al from the support (52, 53). Ren-Yuan et al. (54) also reported evidence for loss of surface Pt on reduction between 500-600°C due to combination with reduced Al atoms in the sublayers of the support. Similarly, for Pt/CeO<sub>2</sub> samples, Diwell et al. (12) reported loss of CO chemisorption capacity on reduction in H<sub>2</sub> at temperatures ≥600°C which was ascribed to induced metal-support interaction since TEM analyses indicated that the reduced samples still contained small Pt particles. A similar phenomenon may have occurred in the present study causing loss of Pt XPS intensity after testing of the samples and also a reduction in H<sub>2</sub> chemisorption uptake as discussed below. This would assume that reduction at 500°C, or exposure to the reaction mixture up to 350°C, could induce this type of strong metal-support interaction (SMSI behaviour (54)), even though reduction at 400°C prior to chemisorption measurements did not.

Comparison of the Pt 4d<sub>5/2</sub> binding energy of sample PC8A after testing with that of other samples is not considered appropriate because of considerable uncertainty in peak positions in Fig. 3.40(c). In any case, such comparison may have been invalidated because of the variety of pretreatment procedures to which the sample was exposed prior to measuring the XPS spectrum.

H<sub>2</sub> chemisorption measurements were carried out on various samples after Activity Test C and also indicated that a considerable loss of surface Pt sites had occurred during catalyst testing, in support of the XPS results for sample PC8A. The H<sub>2</sub> uptakes and apparent Pt surface areas determined are shown in Table 3.9.

**Table 3.9 : H<sub>2</sub> Chemisorption Results After Activity Test C**

Sample	H <sub>2</sub> Adsorbed (cm <sup>3</sup> g <sup>-1</sup> )	Pt surface Area (m <sup>2</sup> g <sup>-1</sup> )
PA	0.021	0.09
PC0.5A	0.015	0.06
PC1A	0.019	0.08
PC8A**	0.037	0.16
SPC8A	0.065	0.28
PC17A	0.031	0.13
PC	0.040	0.17

From comparison of Table 3.9 and Table 2.7, it can be seen that a considerable decrease in the available Pt surface area for H<sub>2</sub> chemisorption had occurred during catalyst testing. In order to investigate the reason for this apparent loss of Pt surface area,

the H<sub>2</sub> chemisorption capacity of sample PC0.5A was investigated after various stages of the experimental procedure. The H<sub>2</sub> uptakes after different experimental steps are shown in Table 3.10.

**Table 3.10 : H<sub>2</sub> Chemisorption Results for Sample PC0.5A (After Activity Tests and Reduction Steps).**

After Experimental Step	H <sub>2</sub> Adsorbed (cm <sup>3</sup> g <sup>-1</sup> )	Pt surface Area (m <sup>2</sup> g <sup>-1</sup> )
Fresh*	0.306	1.32
Activity Test A	0.025	0.11
Activity Test B	0.012	0.05
LTPR	0.025	0.11
Activity Test C	0.015	0.06

\* i.e. after impregnation and calcination.

From Table 3.10, it is apparent that the H<sub>2</sub> chemisorption capacity of sample PC0.5A was considerably depleted even after Activity Test A. One possible explanation for loss of surface Pt during activity testing is sintering of dispersed Pt to produce larger Pt particles in which only the outer Pt atoms are capable of H<sub>2</sub> chemisorption. Sintering of dispersed Pt on Al<sub>2</sub>O<sub>3</sub> has been reported to occur in an oxidising environment at temperatures above 500°C e.g. (16, 52, 55, 56). Völter et al. (17) reported that highly dispersed Pt on Al<sub>2</sub>O<sub>3</sub> is transformed into an oxidised Pt<sup>4+</sup> surface complex by treatment in air up to 500°C, while treatment at higher temperatures causes the decomposition of this complex to produce poorly dispersed metallic, crystalline Pt. In the present study, the temperatures used for catalyst testing in the air : iso-butane reactant stream were lower than those which are generally reported to cause metal sintering. However, exposure to the reaction mixture at temperatures of up to 350°C might have caused sintering of dispersed Pt to occur if the exothermic reaction occurring on the catalyst surface caused the temperature of the catalyst to rise considerably higher than that of the furnace used to heat the sample tube. Sintering of Al<sub>2</sub>O<sub>3</sub>-supported Pt samples at 800°C was found to cause a dramatic increase in oxidation activity (see section 3.3.3). The activity of the catalysts was also found to increase on exposure to the reaction mixture which might be explained if sintering was occurring during catalyst testing. However, catalyst activation on high temperature sintering was much larger than that produced by exposure to the reaction mixture. XPS and TPR spectra obtained after activity tests were considerably different to those obtained for sintered samples (section

3.3.3), which would also appear to argue against any dramatic sintering effects having occurred on exposure to the stoichiometric reaction mixture.

Fouling of the metal surface by carbon during reaction may also have contributed to loss of H<sub>2</sub> chemisorption capacity for the various samples. Kooch et al. (57) reported that carbon deposition on the surface of Pt/Al<sub>2</sub>O<sub>3</sub> and Pt/ZrO<sub>2</sub> samples during C<sub>7</sub>H<sub>16</sub> oxidation resulted in decreased H<sub>2</sub> and O<sub>2</sub> uptakes after reaction. Temperature programmed oxidation (TPO) experiments indicated that the amount of carbon deposited on a Pt/Al<sub>2</sub>O<sub>3</sub> sample from a reaction mixture which contained 11% stoichiometric excess of O<sub>2</sub>, exceeded that deposited when the catalyst was exposed to C<sub>7</sub>H<sub>16</sub> alone. However, it was found that oxidation at 500°C for 20min. caused the displacement of most of the carbon deposited on the catalyst during C<sub>7</sub>H<sub>16</sub> oxidation, and thereby resulted in the regeneration of catalyst chemisorption capacity (57). In light of this study (57), attempts were made to regenerate sample PC0.5A after exposure to the reaction mixture. For a sample of the catalyst which had been exposed to Activity Test B, subsequent exposure to air, at 450°C for 4h at a flow rate of 15cm<sup>3</sup>.min<sup>-1</sup>, caused an increase in H<sub>2</sub> chemisorption capacity from 0.012cm<sup>3</sup>g<sup>-1</sup> to 0.092cm<sup>3</sup>g<sup>-1</sup>. However, this was still considerably less than the original uptake of 0.306cm<sup>3</sup>g<sup>-1</sup> for the calcined sample. A subsequent regeneration attempt at 450°C for 4h did not cause any further increase in H<sub>2</sub> chemisorption capacity with a H<sub>2</sub> uptake of 0.093cm<sup>3</sup>g<sup>-1</sup> measured. Similarly, an attempt to regenerate sample PC17A, following Activity Test C of the analysis procedure, under the same conditions, led to an increase in H<sub>2</sub> uptake from 0.031cm<sup>3</sup>g<sup>-1</sup> to 0.115cm<sup>3</sup>g<sup>-1</sup>, compared with a value of 0.172cm<sup>3</sup>g<sup>-1</sup> for the fresh calcined sample. Otto (18) reported that redispersion of sintered Pt on Al<sub>2</sub>O<sub>3</sub> by O<sub>2</sub> exposure was very slow and barely noticeable at 450°C, and only became more apparent at 500°C. Lieske et al. (28) reported that redispersion was linked to the formation of a Pt oxychloride species on oxidation at temperatures between 500-600°C. Therefore, the increase in H<sub>2</sub> uptake after initial regeneration at 450°C can probably be attributed to carbon removal from the surface rather than redispersion of sintered Pt. Such a theory was supported by an unsuccessful attempt to redisperse a sintered PA sample under the same conditions (see section 3.3.3). XPS data revealed a slight increase in surface C-content for sample PC0.5A after Activity Test A. However, it does not appear that carbon, deposited from the reaction mixture, was the sole reason for the dramatic loss of available Pt since complete regeneration of chemisorption capacity was not achieved. The C-content of sample PC8A after Activity Test C was approximately the same as that in fresh calcined Al<sub>2</sub>O<sub>3</sub>-supported samples which supports the argument against carbon deposition as the only reason for loss of surface Pt during the analysis procedure. Even if coke had been removed from the surface during evacuation prior to XPS measurement,

carbon deposition could still not explain the loss of Pt 4d photoelectron intensity observed after testing of the catalysts.

As discussed previously, loss of surface Pt on reduction of Pt/Al<sub>2</sub>O<sub>3</sub> and Pt/CeO<sub>2</sub> samples has been reported to occur in XPS and chemisorption studies even though x-ray diffraction and electron microscopy analysis showed that agglomeration of Pt had not occurred to any great extent (12, 46, 52, 53, 54). Such phenomena were proposed to result from strong interaction between dispersed Pt and the support material during reduction. In order to ascertain if this type of effect could have explained the loss of H<sub>2</sub> uptake after sample analysis in the present study, calcined samples of the catalysts PA and PC10A were subjected to TPR up to 500°C and subsequent reduction at 500°C for 2.5h in the 5% H<sub>2</sub>/Ar mixture. For sample PA, the apparent Pt surface area decreased from 1.45m<sup>2</sup>g<sup>-1</sup> (0.335cm<sup>3</sup>g<sup>-1</sup> H<sub>2</sub> uptake) to 1.08m<sup>2</sup>g<sup>-1</sup> (0.251cm<sup>3</sup>g<sup>-1</sup> H<sub>2</sub> uptake) after this reduction procedure, while for sample PC10A the available Pt surface area was reduced by 0.25m<sup>2</sup>g<sup>-1</sup> (0.056cm<sup>3</sup>g<sup>-1</sup> decrease in H<sub>2</sub> chemisorption). This loss of H<sub>2</sub> uptake may have been due to sintering (18, 25) or metal-support interaction (46, 53, 54). However, the loss of surface Pt on reduction was considerably less than that observed after exposure to the air : i-C<sub>4</sub>H<sub>10</sub> reaction mixture in activity tests. Therefore, interaction of Pt with the support material during the reduction steps of the analysis procedure, may have been a contributing factor to the apparent loss of Pt surface area but did not appear to be the primary reason for decreased H<sub>2</sub> uptakes in samples after Activity Test C. H<sub>2</sub> chemisorption was depleted to a greater extent during activity testing than during reduction in H<sub>2</sub>/Ar under the experimental conditions employed for sample analysis.

To summarise the activity results, it appeared that the activity of Pt/Al<sub>2</sub>O<sub>3</sub> catalysts for i-C<sub>4</sub>H<sub>10</sub> oxidation varied depending on the presence/absence of Ce, the loading of Ce used, and the method of impregnation of the two metals. Catalyst activity for Pt/Al<sub>2</sub>O<sub>3</sub>, Pt-Ce/Al<sub>2</sub>O<sub>3</sub> and Pt/CeO<sub>2</sub> samples was also affected by the testing in the stoichiometric air : iso-butane mixture, and by reduction in a 5% H<sub>2</sub>/95% Ar mixture. The use of CeO<sub>2</sub>, either as a support or as an additive in Pt/Al<sub>2</sub>O<sub>3</sub> catalysts, was potentially beneficial depending on all of these variables.

In general, exposure of the catalysts to the stoichiometric air : iso-butane reaction mixture resulted in improved activity during subsequent testing. This was particularly true in terms of low temperature activity with 10% conversion of butane being achieved at lower temperatures on all but one catalyst following initial testing of the calcined samples. For some of the Pt-Ce/Al<sub>2</sub>O<sub>3</sub> catalysts which had Ce:Pt atomic ratios  $\geq$  8:1, and for Pt/CeO<sub>2</sub>, high temperature activity was also improved with 90%

conversion of  $i\text{-C}_4\text{H}_{10}$  being achieved at lower temperatures. It should be noted that some catalysts did show disimproved conversions at certain temperatures after initial exposure to the reaction mixture. However, in general, it can be stated that catalyst activity was enhanced after initial testing for  $i\text{-C}_4\text{H}_{10}$  oxidation activity. This was true both before and after pre-reduction, since sample PC8A\*\* also exhibited an increase in activity during Run 2 of the initial test.

There are a number of possible explanations for activation of the catalysts observed during activity tests including the removal of a deactivating chloride species (17, 19, 58, 59). In a study of  $\text{CH}_4$  oxidation over supported Pt and Pd catalysts, Hicks et al. (19) reported that some catalysts showed increased activity rates with increasing time in the reaction mixture. This was thought to possibly have been associated with the removal of residual chlorine in these samples which were prepared by ion-exchange of the metal chloride with  $\text{Al}_2\text{O}_3$  (19). Völter et al. (17) also reported that chloride acted as a poison for Pt/ $\text{Al}_2\text{O}_3$  catalysts in the oxidation of  $n\text{-C}_7\text{H}_{16}$ , due to promotion of Pt dispersion. In the current study, catalysts were prepared using  $\text{H}_2\text{PtCl}_6$  as the source of Pt. Therefore, the removal of Cl during activity tests could have contributed to the enhanced activity observed for some catalysts after exposure to the reaction mixture. The calcination procedure employed did not appear to be sufficient to remove all Cl from the catalyst surface. XPS analysis indicated the presence of Cl in calcined samples both before and after testing in the oxidation mixture. Unfortunately, quantification of Cl levels was not made.

In section 3.3.3, it can be seen that aging of catalysts in the reaction mixture at  $800^\circ\text{C}$  resulted in a dramatic enhancement of  $i\text{-C}_4\text{H}_{10}$  oxidation activity for Pt/ $\text{Al}_2\text{O}_3$  and Pt-Ce/ $\text{Al}_2\text{O}_3$  samples. This appeared to be associated with Pt sintering during aging to produce more active larger Pt crystallites, because aging in air at  $800^\circ\text{C}$ , in the absence of  $i\text{-C}_4\text{H}_{10}$ , caused a similar enhancement of catalyst activity. It is possible that some sintering of dispersed Pt may also have occurred during testing at lower temperatures causing the smaller increase in activity observed after initial testing. As discussed previously, sintering of Pt during the activity tests was indicated by  $\text{H}_2$  chemisorption results but XPS and TPR spectra indicated that sintering was not the sole reason for loss of surface Pt sites on exposure to the reaction mixture.

Baldwin and Burch (58, 59) reported that the activity of supported Pd catalysts for the oxidation of  $\text{CH}_4$  was enhanced considerably on exposure to the reactants. The possibility that this enhancement was due to the removal of a deactivating chloride species was discounted because passing wet air over the catalysts did not noticeably affect the activity. All the catalysts were prepared from acidified palladium chloride and

heating in wet air was expected to remove HCl from the catalyst surface and thus accelerate activation but this was not found to be the case. In addition, while sintering of Pd particles did occur during testing, this was also not believed to be the primary reason for catalyst activation. Improvements in CH<sub>4</sub> oxidation activity were only observed when reaction between CH<sub>4</sub> and air was taking place. Activation of the catalysts on exposure to the oxidation reaction was tentatively attributed to a change in Pd particle morphology during reaction, which led to the exposure of more active crystal faces (58, 59). A similar phenomenon may have been observed for some of the catalysts examined for *i*-C<sub>4</sub>H<sub>10</sub> oxidation in the present study.

A reducing effect of the *i*-C<sub>4</sub>H<sub>10</sub> in the reaction mixture may also have contributed to the activation of Ce-containing catalysts, since reduction has been reported to cause activation of Ce-containing noble metal catalysts (7, 9). However, the fact that sample PC8A\*\*, which had been pre-reduced prior to testing, was also activated on exposure to the reactants would seem to argue against a reducing effect of the stoichiometric oxidation mixture as being the primary cause of catalyst activation during activity tests.

Baldwin and Burch (58, 59) also noted that C-deposition during CH<sub>4</sub> oxidation may have affected changes in catalyst activity, but were unsure as to the role which this might play in the activation process observed. Carballo and Wolf (56) ascribed decreases in the activity of Pt/Al<sub>2</sub>O<sub>3</sub> on exposure to the reaction mixture, in C<sub>3</sub>H<sub>6</sub> oxidation, to a self-poisoning mechanism by C-residues. Thus, it may be unlikely that C-deposition was a contributory cause in catalyst activation observed in the present study.

Pre-reduction of the 0.5% Pt/Al<sub>2</sub>O<sub>3</sub> sample, PA, at 500°C in 5% H<sub>2</sub>-95% Ar, was found to cause a considerable loss of activity for *i*-C<sub>4</sub>H<sub>10</sub> oxidation. This is in direct disagreement with the findings of Völter et al. (17) and Otto and co-workers (18, 20). Völter et al. (17) reported that pre-reduction of a chloride-containing 0.5% Pt/Al<sub>2</sub>O<sub>3</sub> catalyst at 500°C in H<sub>2</sub> resulted in an increase in activity for *n*-C<sub>7</sub>H<sub>16</sub> oxidation. This was attributed to the formation of larger Pt particles during reduction (17). Similarly, Otto (18) found that reduction of Pt/γ-Al<sub>2</sub>O<sub>3</sub> catalysts in H<sub>2</sub> at 500°C caused an increase in CH<sub>4</sub> oxidation activity. Again, this was attributed to sintering of Pt particles during reduction, and, was observed for Pt loadings as low as 0.03wt.% (18). A similar phenomenon was reported in a study of C<sub>3</sub>H<sub>8</sub> oxidation on Pt/γ-Al<sub>2</sub>O<sub>3</sub> catalysts (20). In the present study, some loss of H<sub>2</sub> chemisorption capacity was observed for sample PA after reduction at 500°C. However it is uncertain as to whether this was due to metal sintering (25, 17, 18, 20) or interaction of Pt with the support material (46, 52, 53, 54).

The fact that oxidation activity was decreased after reduction supports the latter explanation, because sintering has been found to cause catalyst activation (see section 3.3.3).

Previous results from this laboratory (60), have also indicated that reduction of Pt/Al<sub>2</sub>O<sub>3</sub> catalysts can cause a decrease in i-C<sub>4</sub>H<sub>10</sub> oxidation activity. In the present study, loss of activity upon prolonged reduction at 500°C appeared to be associated with catalysts in which there was some form of interaction between Pt and the Al<sub>2</sub>O<sub>3</sub> support. This was suggested by TPR profiles obtained immediately prior to high temperature reduction, which indicated that Pt in these samples required a reduction temperature of above 400°C. This reduction feature was attributable to the reduction of oxidised surface Pt species in close interaction with Al<sub>2</sub>O<sub>3</sub>. For catalysts whose TPR profiles did not exhibit this reduction feature, reduction at 500°C did not cause any significant catalyst deactivation.

As mentioned previously, suppression of the activity of Pt/Al<sub>2</sub>O<sub>3</sub> catalysts for alkane oxidation in an oxidising environment, on addition of CeO<sub>2</sub>, has been attributed to the conversion of Pt into a less active, more oxidised state as a result of interaction with the Ce (9, 11, 12, 13). Similarly, Shyu et al. (14) attributed a negative effect of CeO<sub>2</sub>, on the C<sub>3</sub>H<sub>8</sub> oxidation activity of Pd/Al<sub>2</sub>O<sub>3</sub>, to the promotion of Pd oxidation, to less active PdO, by ceria. The possibility that decreased oxidation activity in the presence of Ce was related to improved dispersion of Pt on Al<sub>2</sub>O<sub>3</sub> has also been proposed (10, 12).

In the present study, examination of calcined catalysts for the oxidation of i-C<sub>4</sub>H<sub>10</sub> in a stoichiometric reaction mixture revealed that the presence of Ce, at Ce:Pt ≥ 8:1, resulted in poorer activity performance relative to Pt/Al<sub>2</sub>O<sub>3</sub> at a Pt loading of 0.5wt.%. The only exception to this general trend was sample SPC8A. A 0.5wt.% Pt/CeO<sub>2</sub> sample was also less active than Pt/Al<sub>2</sub>O<sub>3</sub> after calcination in air. However, for Pt-Ce/Al<sub>2</sub>O<sub>3</sub> catalysts with lower Ce loadings, i.e. samples PC0.5A and PC1A, oxidation activity was not as adversely affected by the presence of Ce. In fact, sample PC1A was found to be noticeably more active than the Pt-only sample, PA, after calcination.

The effects of Ce addition on the activity of Pt/Al<sub>2</sub>O<sub>3</sub> can be attributed to the existence of an interaction between Ce and Pt, which affected the activity of the noble metal, since Ce/Al<sub>2</sub>O<sub>3</sub> (sample C8A) did not appreciably catalyse the i-C<sub>4</sub>H<sub>10</sub> oxidation in the temperature range investigated. TPR profiles revealed the existence of an interaction between Pt and Ce in both Pt-Ce/Al<sub>2</sub>O<sub>3</sub> and Pt/CeO<sub>2</sub> catalysts. For calcined samples of catalysts PC10A and PC, XPS results (see section 3.3.1) tentatively indicated

that this interaction may have resulted in increased oxidation of surface Pt sites, with a slight increase in Pt 4d<sub>5/2</sub> binding energy relative to sample PA. Such a phenomenon would be in agreement with previous studies, which have reported increased oxidation of surface Pt in Pt-Ce/Al<sub>2</sub>O<sub>3</sub> (1, 8, 9) and Pt/CeO<sub>2</sub> (6) catalysts relative to Pt/Al<sub>2</sub>O<sub>3</sub>, and might explain the lower i-C<sub>4</sub>H<sub>10</sub> oxidation activity of these samples relative to PA after calcination in air (9, 11, 12). XPS spectra of sample PC0.5A, before and after testing in the reaction mixture, revealed that the nature of Pt-Ce interaction at lower Ce loadings may have been somewhat different to that at higher levels, since the Pt 4d<sub>5/2</sub> binding energy for this sample was lower than that of PA. This might have contributed to the different effects which Ce had on the activity of Pt/Al<sub>2</sub>O<sub>3</sub> at different Ce loadings.

Summers and Ausen (1) studied CO oxidation on Pt/Al<sub>2</sub>O<sub>3</sub> and Pt-Ce/Al<sub>2</sub>O<sub>3</sub> catalysts and also found that the effect of Ce on catalyst activity depended on the level used. Addition of small amounts of Ce to 0.05wt.% Pt/Al<sub>2</sub>O<sub>3</sub> was found to cause improvements in CO oxidation activity up to a Ce:Pt atomic ratio of 36:1. At higher Ce:Pt ratios, CO conversion over the catalysts, which were calcined at 500°C, was seriously deteriorated. These activity changes were thought to be attributable to Pt-Ce interactions because Ce-Al<sub>2</sub>O<sub>3</sub> did not appreciably catalyse CO oxidation under the conditions used. Both the enhancement of CO oxidation at lower Ce loadings and the deterioration at higher levels of Ce, were diminished by treatment of the fresh catalysts with SO<sub>2</sub>. This was interpreted in terms of SO<sub>2</sub> acting as a strong reducing agent and reacting with CeO<sub>2</sub> (a strong oxidising agent) to destroy the interaction of CeO<sub>2</sub> with Pt and thereby, prevent oxidation of surface Pt sites by CeO<sub>2</sub> (1). In view of this study (1) and other previous studies (6, 8, 9, 11, 12, 13, 14, 43), the most apparent explanation for the changes in Pt activity for i-C<sub>4</sub>H<sub>10</sub> oxidation in the presence of Ce, is the existence of an electronic interaction between the two metals which may have affected the degree of oxidation of surface Pt sites. Such an explanation is tentatively supported by limited XPS results and by the fact that the presence of Pt promoted surface CeO<sub>2</sub> reduction in TPR experiments. This latter phenomenon was reported by Yu-Yao (8) to support the possibility of charge transfer between precious metal and neighbouring CeO<sub>2</sub> particles in Al<sub>2</sub>O<sub>3</sub>-supported catalysts.

In disagreement with Diwell et al. (12) and Gandhi and Shelef (10), changes in catalyst activity on addition of Ce to Pt/Al<sub>2</sub>O<sub>3</sub> cannot be attributed to improvements in Pt dispersion in the present case. H<sub>2</sub> chemisorption results (see Table 2.7) indicated that the Pt-only sample, PA, had the highest degree of Pt dispersion after calcination. In any case, there was no sensible relationship apparent between Pt surface area and catalyst activity for the calcined samples.

In general, the activity of Pt-Ce/Al<sub>2</sub>O<sub>3</sub> and Pt/CeO<sub>2</sub> catalysts increased after TPR while Pt/Al<sub>2</sub>O<sub>3</sub> became less active. In addition, the existence of a Pt-Ce surface interaction during reduction appeared to be important in preventing loss of i-C<sub>4</sub>H<sub>10</sub> oxidation activity upon reduction at 500°C in the 5% H<sub>2</sub>-95% Ar reduction mixture.

As discussed previously, Nunan et al. (7) reported that the presence of Ce in Pt/Rh/Ce/Al<sub>2</sub>O<sub>3</sub>, Pt/Rh/CeO<sub>2</sub> and Pt/CeO<sub>2</sub> catalysts was potentially beneficial for hydrocarbon oxidation in a synthetic exhaust mixture, after catalyst activation in the exhaust stream. Activation was associated with in-situ catalyst reduction by the low levels of H<sub>2</sub> present. In agreement with the present study, TPR profiles revealed the existence of a direct noble metal-CeO<sub>2</sub> interaction which was found to correlate with improved light-off performance after activation (7). It was concluded that Pt migrated selectively to CeO<sub>2</sub> during preparation and that direct interaction between the two metals led to dramatic improvements in catalyst light-off activity following in-situ reduction. The authors (7) believed that the main benefit of CeO<sub>2</sub> was in enhanced CO oxidation activity after activation, which prevented CO inhibition effects and, thereby, allowed more effective hydrocarbon removal. Improvements in CO oxidation activity over Pt-Ce/Al<sub>2</sub>O<sub>3</sub> catalysts have been reported after pre-reduction (5, 8) and in a reducing environment (11). This has been associated with oxidation of CO adsorbed on the noble metal by lattice oxygen donated from neighbouring ceria particles (4, 5, 11, 61). However, in the current study, improvements in the performance of Pt-Ce/Al<sub>2</sub>O<sub>3</sub> and Pt/CeO<sub>2</sub> catalysts, relative to Pt/Al<sub>2</sub>O<sub>3</sub>, for i-C<sub>4</sub>H<sub>10</sub> oxidation, cannot be attributed to increased CO oxidation activity. It appeared that the existence of a Pt-Ce interaction was potentially beneficial for the oxidation of i-C<sub>4</sub>H<sub>10</sub>, even in the absence of CO in the reactant stream.

Yu-Yao (9) found that the activity of Pt-Ce/Al<sub>2</sub>O<sub>3</sub> catalysts for the oxidation of alkanes was improved following reduction by the hydrocarbon at 350°C. This was attributed to a belief that reduced precious metal was more active for alkane oxidation, while oxidised precious metal was less active (9). Present results would appear to suggest that reduction of surface Pt to a more metallic state may not have been the primary reason for improved activity of Ce-containing catalysts after reduction. Reduction of 0.5% Pt/Al<sub>2</sub>O<sub>3</sub> and some Pt-Ce/Al<sub>2</sub>O<sub>3</sub> catalysts was found to cause a loss of oxidation activity, indicating that for these samples reduced Pt was less active. One possible explanation for this apparent discrepancy, may be that reduced Pt may be more active for i-C<sub>4</sub>H<sub>10</sub> oxidation provided that strong interaction between Pt and Al<sub>2</sub>O<sub>3</sub> does not occur during reduction. As discussed previously, strong interaction between Pt and Al<sub>2</sub>O<sub>3</sub> has been proposed to explain losses of surface Pt observed after catalyst reduction (46, 52-54). This might be expected to result in lower activity if the interaction involved loss of

Pt to less exposed sites in the alumina matrix (46). In the present study, reduction of samples PA and PC10A at 500°C was found to cause some loss of H<sub>2</sub> chemisorption capacity. As mentioned previously, TPR profiles obtained immediately prior to high temperature reduction indicated that deactivation was associated with the presence of some form of Pt-Al<sub>2</sub>O<sub>3</sub> interaction. Thus, the existence of a Pt-Ce interactive species may have prevented catalyst deactivation during reduction by stabilising surface Pt against strong interaction with the Al<sub>2</sub>O<sub>3</sub> support.

The existence of a Pt-Ce interactive surface species certainly appeared to be associated with improved activity after reduction. Diwell et al. (12) found that the pre-reduction of a 0.9 wt.% Pt/CeO<sub>2</sub> catalyst resulted in enhanced conversion of CO, NO, H<sub>2</sub>, and C<sub>3</sub>H<sub>6</sub> components of a simulated exhaust gas mixture. However, in contrast to the current study, alkane oxidation activity was adversely affected. This discrepancy may have been associated with the more stringent reduction temperatures of 600 or 900°C employed by Diwell et al. (12). The authors (12) noted that the low temperature activity changes, which were observed upon pre-reduction, could not be explained by a simple reduction of Pt to a more metallic state as proposed by Yu-Yao (8, 9). Instead, Diwell and co-workers (12) believed that an induced Pt-CeO<sub>2</sub> interaction occurred during reduction which greatly affected the nature and activity of the catalytic sites. TPR profiles also indicated the existence of a Pt-CeO<sub>2</sub> interaction upon reduction. This was tentatively proposed to involve Pt encapsulation by partially reduced CeO<sub>2</sub>, with increased CO and NO removal being associated with the formation of ionised vacancies in the support. The role of the metal particles was to act as an electron donor or sink. Loss of alkane oxidation was explained in terms of loss of surface Pt, but it was noted that the proposed model could not explain increases in alkene oxidation activity after reduction (12).

As mentioned previously, improvements in the CO oxidation activity of noble metals have been ascribed to the donation of lattice oxygen from CeO<sub>2</sub> for participation in the oxidation of adsorbed CO to CO<sub>2</sub> (3, 4, 5, 11, 61, 62). Recently, Hardacre et al. (44) proposed that, in some circumstances, CeO<sub>2</sub> can behave as a very active CO oxidation catalyst, with the noble metal acting as a promoter. In apparent agreement with the theory of Diwell et al. (12), Hardacre et al. (44) found that in some cases Pt, which was fully encapsulated by CeO<sub>2</sub>, was more active than a clean Pt surface. This was attributed to enhanced conversion of CO by CeO<sub>2</sub>, due to interaction of the oxide with the underlying Pt. It was noted that in supported catalysts, partial rather than complete encapsulation may be more favourable allowing greater participation of Pt in the catalytic process (44).

In the present study, a similar phenomenon may have occurred with a Pt-CeO<sub>2</sub> interactive species, with Pt sites available for hydrocarbon adsorption and subsequent oxidation to CO<sub>2</sub> being enhanced by lattice oxygen donation from neighbouring CeO<sub>2</sub> sites. XPS analysis of calcined samples pointed towards the possibility of a slight increase in the oxidation state of Pt in samples PC and PC10A. As proposed by Serre et al. (39), a small increase in the metal oxidation state might be related to charge transfer from metal to ceria, resulting in cerium being slightly reduced, and leading to a decrease in Ce-O bond strength. As discussed in section 3.3.1, TPR experiments revealed that Pt promoted the reduction of surface CeO<sub>2</sub> by H<sub>2</sub>. Thus, it may be possible that the reduction of surface CeO<sub>2</sub> by i-C<sub>4</sub>H<sub>10</sub> may also have been accelerated by the presence of Pt. Previous studies have reported that the reduction of surface CeO<sub>2</sub>, by both CO (39) and H<sub>2</sub> (36-38), is promoted by the presence of Pt. Hardacre et al. (44) believed that such studies supported the theory that lattice oxygen donation from CeO<sub>2</sub> when in close contact with Pt could bring about CO oxidation. However, based on the results obtained in the present study, the possibility that i-C<sub>4</sub>H<sub>10</sub> oxidation on reduced Pt-Ce/Al<sub>2</sub>O<sub>3</sub> and Pt/CeO<sub>2</sub> catalysts was assisted by lattice oxygen from surface ceria sites, due to destabilisation of Ce-O bonds by Pt, is highly speculative. Mendelovici and Steinberg (63) have previously reported evidence for the participation of lattice oxygen in the oxidation of C<sub>2</sub>H<sub>4</sub> on a Pt/CeO<sub>2</sub> catalyst, using Electron Spin Resonance (ESR). This was supported by pulse reactor experiments performed in the absence of O<sub>2</sub>. However, the role of lattice oxygen was restricted to reaction temperatures above 300°C (63). No such direct evidence for participation of lattice oxygen from CeO<sub>2</sub> in the oxidation of i-C<sub>4</sub>H<sub>10</sub> over Pt-Ce/Al<sub>2</sub>O<sub>3</sub> and Pt/CeO<sub>2</sub> catalysts was found in the present study. At the same time, the results obtained strongly suggested that Pt-CeO<sub>2</sub> interactive surface sites were more active than Pt-Al<sub>2</sub>O<sub>3</sub> species after equivalent reduction treatments.

In general, it can be stated that Ce, when present at an atomic ratio of Ce:Pt ≥ 8:1 or as the support material, resulted in poorer initial activity relative to Pt/Al<sub>2</sub>O<sub>3</sub> after calcination in air at 630°C, but improved oxidation activity after pre-reduction at 500°C. In reaching this conclusion, it should be stated that improvements in the low temperature activity of some of the calcined Ce-containing catalysts, after exposure to the reactants, were greater than that for Pt/Al<sub>2</sub>O<sub>3</sub>. However, the latter sample was more active during the initial test run. Similarly, in a study of CO oxidation on precious metal catalysts, Yu-Yao and Kummer (2) reported that for CeO<sub>2</sub>-containing catalysts, a strong Pt-CeO<sub>2</sub> interaction was observed which was characterised by deactivation in an oxidising environment and a sharp increase in activity after reduction.

TPR profiles for Pt-Ce/Al<sub>2</sub>O<sub>3</sub> samples after Activity Tests A and B indicated that the stability of Pt-Ce surface interaction on exposure to the iso-butane : air

stoichiometric reaction mixture increased with increasing Ce concentration at least up to 3.6wt.%. For the lower Ce contents, PC0.5A, PC1A, and to a lesser extent PC8A, use of the calcined catalysts for the oxidation reaction seemed to result in loss of Pt-Ce interaction and the formation of a Pt-Al<sub>2</sub>O<sub>3</sub> interactive species. For samples PC1A and PC8A, this species appeared to be slightly more difficult to reduce than the corresponding species in the Pt-only sample PA. The reduction peak temperature for samples PC1A and PC8A was ca.430-450°C compared to ca.420°C in PA i.e. the characteristic Pt-Al<sub>2</sub>O<sub>3</sub> reduction feature was shifted to slightly higher temperatures in the presence of Ce. Migration of Pt between CeO<sub>2</sub> and Al<sub>2</sub>O<sub>3</sub> phases was found to be possible during thermal treatment by Yu-Yao and Kummer (2), which was thought could lead to dynamic redistribution of Pt on use in an oxidising environment, as was found in the present study. For higher Ce contents in samples PC10A and PC17A, and for samples SPC8A and SCP8A, surface Pt appeared to remain in close proximity to the Ce component and Pt-Ce interaction was still evident in the TPR profiles obtained even after exposure to the reaction mixture at temperatures of up to 350°C. For samples PC8A, SPC8A, SCP8A, PC10A, PC17A and PC, exposure to the reaction mixture seemed to result in the loss of surface reducible species, while for samples PA, PC0.5A, and PC1A, the H<sub>2</sub> uptake increased after reaction. The reasons for these changes in H<sub>2</sub> uptake are unknown.

### 3.3.3 Effects of Aging on Activity and Surface Features

In this section, the effects of high temperature (800°C) aging on the activity and surface properties of samples PA, PC10A, PC and PZ are discussed.

After aging of the calcined catalysts, the available Pt surface area of each was reinvestigated using H<sub>2</sub> chemisorption. The H<sub>2</sub> chemisorption uptakes of the fresh and aged catalysts are compared in Table 3.11.

**Table 3.11** : H<sub>2</sub> Chemisorption Measurements after Aging in Various Atmospheres

Sample	Parameter	Fresh*	Air-Aged	Air:i-C <sub>4</sub> H <sub>10</sub> Aged	Argon-Aged
PA	H <sub>2</sub> Uptake (cm <sup>3</sup> g <sup>-1</sup> )	0.336	0.026	0.015	0.011
	S <sub>Pt</sub> (m <sup>2</sup> g <sup>-1</sup> )	1.45	0.11	0.06	0.05
PC10A	H <sub>2</sub> Uptake (cm <sup>3</sup> g <sup>-1</sup> )	0.327	0.002**	0.021	0.007
	S <sub>Pt</sub> (m <sup>2</sup> g <sup>-1</sup> )	1.41	0.01**	0.09	0.03
PC	H <sub>2</sub> Uptake (cm <sup>3</sup> g <sup>-1</sup> )	0.055	0.054	0.029	ND
	S <sub>Pt</sub> (m <sup>2</sup> g <sup>-1</sup> )	0.24	0.23	0.12	ND
PZ	H <sub>2</sub> Uptake (cm <sup>3</sup> g <sup>-1</sup> )	0.009	ND	ND	ND
	S <sub>Pt</sub> (m <sup>2</sup> g <sup>-1</sup> )	0.04	ND	ND	ND

\* Fresh i.e. after impregnation and calcination at 630°C.

\*\* determined after activity testing.

S<sub>Pt</sub> = Pt Surface Area.

ND = not determined.

From Table 3.11, it can be seen that the chemisorption capacity of the Al<sub>2</sub>O<sub>3</sub>-supported samples, PA and PC10A, was considerably depleted after aging in the various environments. As discussed in section 2.3.3, the most probable reason for the apparent loss of Pt surface area in the aged samples was sintering of dispersed Pt to form larger particles in which only the outer Pt atoms are capable of H<sub>2</sub> adsorption. Sintering of Al<sub>2</sub>O<sub>3</sub>-supported Pt in an O<sub>2</sub>-containing atmosphere at temperatures above 500°C has been previously reported by several studies (12, 16, 17, 52, 55, 56). XRD results from

this laboratory have also indicated that aging of Pt/Al<sub>2</sub>O<sub>3</sub> in air, under the conditions employed here, causes an increase in Pt particle size (60). Aging in Ar, as well as in air and in air : i-C<sub>4</sub>H<sub>10</sub>, also caused a considerable loss of Pt surface area for samples PA and PC10A, as shown in Table 3.11. Again, this was probably associated with Pt sintering, rather than metal encapsulation by the support material, since no loss of activity (see Tables 3.12-3.14) was observed for Ar-aged PA or PC10A samples relative to the fresh calcined catalysts (56). The driving force behind the sintering processes is the minimisation of surface energy by the maximisation of the number of Pt - Pt bonds (64). Two types of mechanisms have been proposed for the growth of supported metal particles. These involve growth via the migration of particles leading to particle collisions and coalescence, or growth via some form of atomic or molecular interparticle transport (64, 65).

The presence of Ce, at a Ce:Pt atomic ratio of 10:1, in sample PC10A, did not appear to have any major stabilising effect on Pt dispersion under the aging conditions employed, when compared with the Pt-only sample PA. Diwell et al. (12) reported that the presence of CeO<sub>2</sub> resulted in the stabilisation of Pt dispersions after aging of 0.9 wt.% Pt/Al<sub>2</sub>O<sub>3</sub> and 0.9 wt.% Pt/75% Al<sub>2</sub>O<sub>3</sub>-25% CeO<sub>2</sub> catalysts in air for 2h at temperatures between 600-800°C. CO chemisorption studies indicated that Pt dispersion was more stable in the CeO<sub>2</sub> containing sample. The ability of CeO<sub>2</sub> to stabilise Pt dispersion was attributed to a Pt-Ce interaction which maintained the Pt in a higher oxidation state that was more resistant to sintering (12). The lower level of CeO<sub>2</sub> employed in the present study may not have been sufficient to stabilise Pt dispersion in sample PC10A under the stringent aging conditions employed.

Otto et al. (20) reported that redispersion of sintered Pt/Al<sub>2</sub>O<sub>3</sub> catalysts occurred during C<sub>3</sub>H<sub>8</sub> oxidation measurements at 275°C. The H<sub>2</sub> chemisorption uptake of sample PC10A, aged in air, was measured after subsequent testing in the stoichiometric air : i-C<sub>4</sub>H<sub>10</sub> oxidation mixture at temperatures of up to 350°C. The H<sub>2</sub> uptake measured was ca.0.002cm<sup>3</sup>g<sup>-1</sup> which corresponds to an apparent Pt surface area of ca.0.01m<sup>2</sup>g<sup>-1</sup>. Although the H<sub>2</sub> uptake prior to reaction was not measured for this sample, it might be inferred that no significant redispersion effects occurred. Alternatively, if redispersion had occurred it may have been masked by C-deposition during testing which would be expected to prevent H<sub>2</sub> chemisorption.

An attempt to redisperse air-aged PA at 450°C in air for 4.5h was also made. After this treatment, H<sub>2</sub> uptake for the aged sample increased from 0.026cm<sup>3</sup>g<sup>-1</sup> to 0.036 cm<sup>3</sup>g<sup>-1</sup>. As discussed in section 3.3.2, the H<sub>2</sub> uptake of calcined samples was depleted dramatically after exposure to the air : i-C<sub>4</sub>H<sub>10</sub> oxidation mixture in Activity Tests A-C

but could be partially recovered by treatment in flowing air at 450°C. The increase in H<sub>2</sub> uptake of the sintered PA sample was considerably less than that obtained for samples used in the oxidation mixture. Thus, the recovery of H<sub>2</sub> uptake for the latter samples can be attributed mainly to the removal of C-residues, rather than redispersion effects, as was expected.

For the Pt/CeO<sub>2</sub> sample, PC, aging in air at 800°C did not appear to cause any loss of available Pt surface area. The apparent Pt surface area for the air-aged sample was 0.23m<sup>2</sup>g<sup>-1</sup> which compares with a value of 0.24m<sup>2</sup>g<sup>-1</sup> measured for the fresh calcined sample. Murrell et al. (66) reported that ceria had the ability to form isolated Pt-O complexes at the metal-support interface. The existence of such Pt-O groups was found to stabilise Pt surface area on calcination at high temperatures in an oxidising environment. Even after calcination at 1000°C, the Pt-O surface structure was still retained in high concentration on the CeO<sub>2</sub> surface in spite of considerable loss of CeO<sub>2</sub> surface area (66). In the present study, CeO<sub>2</sub> also appeared to be able to maintain Pt surface area upon aging in air, under conditions in which Al<sub>2</sub>O<sub>3</sub> -supported samples showed dramatic losses of surface area. Murrell et al. (66) reported that aging under cyclic redox conditions at 850°C caused severe Pt sintering. This was presumed to be due to decomposition of the Pt-O groups during the reducing swings of the aging cycle with sintering of Pt metal then occurring (66). From Table 3.11, it can be seen that some loss of Pt surface area did occur on aging in the stoichiometric air : i-C<sub>4</sub>H<sub>10</sub> reaction mixture. This may have been associated with a reducing effect of the i-C<sub>4</sub>H<sub>10</sub> which resulted in Pt sintering. Alternatively, the possibility that C-deposition during reaction contributed to the loss of H<sub>2</sub> chemisorption capacity for the samples aged in the oxidation mixture must be considered (57).

As discussed previously, the Pt dispersion in sample PZ after calcination was very low. No chemisorption measurements were made on this catalyst after aging.

TPR profiles obtained for samples PA and PC10A, after aging in air at 800°C, are illustrated in Fig. 3.41 and 3.42, respectively. Aging appeared to result in the decomposition of oxidised surface Pt species, as indicated by the lack of characteristic reduction peaks when compared to the profiles of unaged samples in Fig. 3.20(a) and 3.21(c).

After aging, catalyst PA showed no peaks in the region 20-500°C (Fig. 3.41(a)). This indicates the absence of reducible Pt oxides on the catalyst surface which is in correlation with XPS results discussed below. The profile for sample PC10A (Fig. 3.42(a)) exhibits a peak at ca.360°C which may have been due to Pt reduction but could also have been associated with surface Ce reduction. A feature at approximately this

temperature in the calcined sample was previously attributed to the reduction of a surface Ce species as discussed in section 3.3.1.

Use of the aged sample PA for activity testing in the stoichiometric air : i-C<sub>4</sub>H<sub>10</sub> mixture led to the apparent reoxidation of surface Pt, with a peak apparent at ca.450°C in the profile obtained after testing (Fig. 3.41(b)). As discussed in section 3.3.1, a reduction peak in this temperature region appeared to be associated with some form of Pt-Al<sub>2</sub>O<sub>3</sub> interactive species. After testing, the aged sample of catalyst PC10A again exhibited a peak at slightly below 400°C with a slight increase in peak temperature (Fig. 3.42(b)). The assignment of this peak is uncertain.

The TPR profiles of sample PZ before and after aging in air at 800°C are illustrated in Fig. 3.43(a) and (b). The lack of any discernible reduction peaks for sample PZ prior to aging may indicate the presence of larger Pt particles, relative to those in Pt/Al<sub>2</sub>O<sub>3</sub> and Pt/CeO<sub>2</sub> samples, after calcination at 630°C. The lack of surface reducible Pt in the unaged sample supports the chemisorption data for PZ which indicated the presence of larger Pt particles even before aging. Similarly, the TPR profile obtained after aging indicates a lack of surface reducible species with no reduction features apparent.

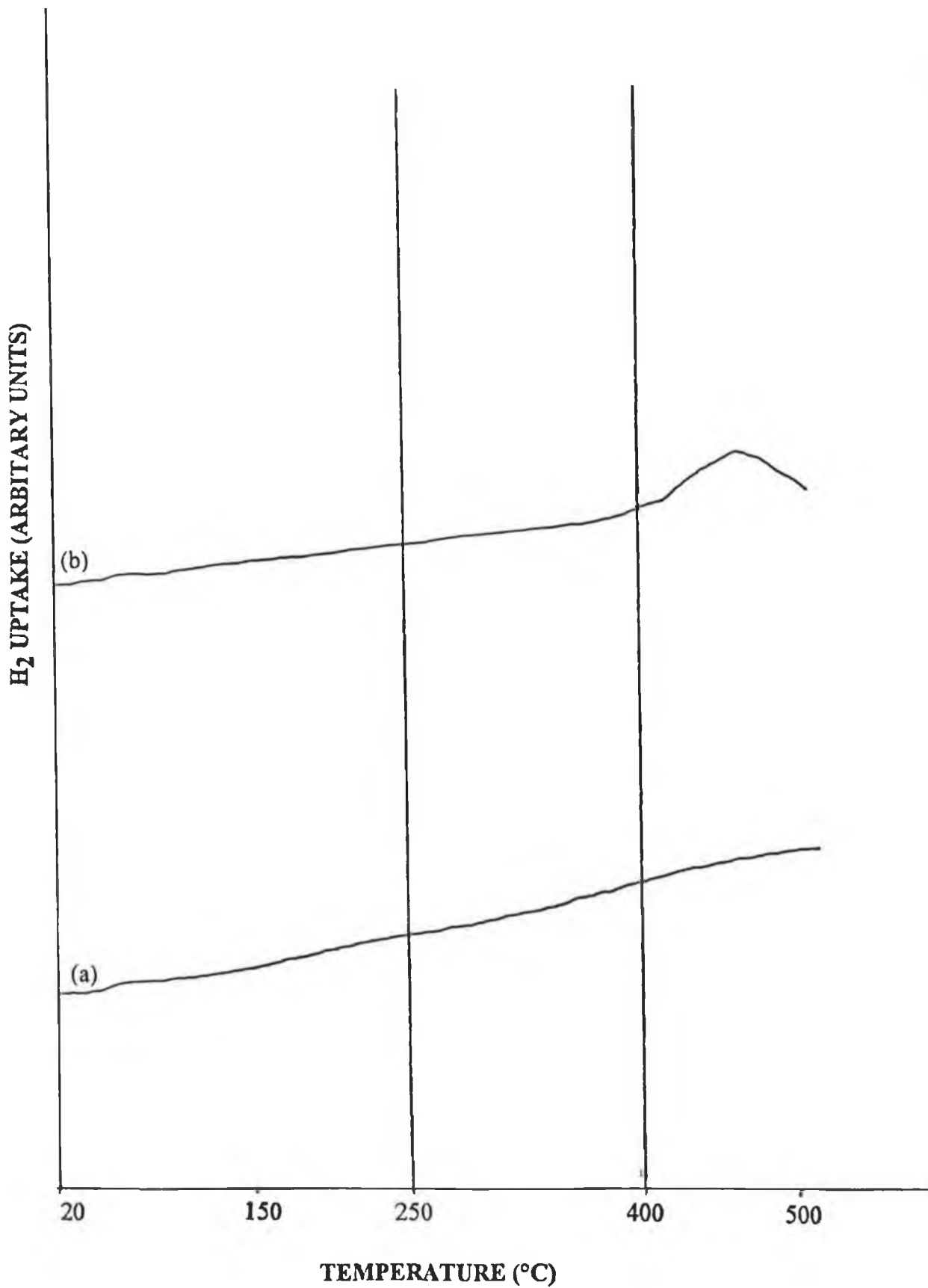


**Fig. 3.41 : TPR profiles of air-aged PA, (a)-before and (b)-after, testing for  $i\text{-C}_4\text{H}_{10}$  oxidation activity.**

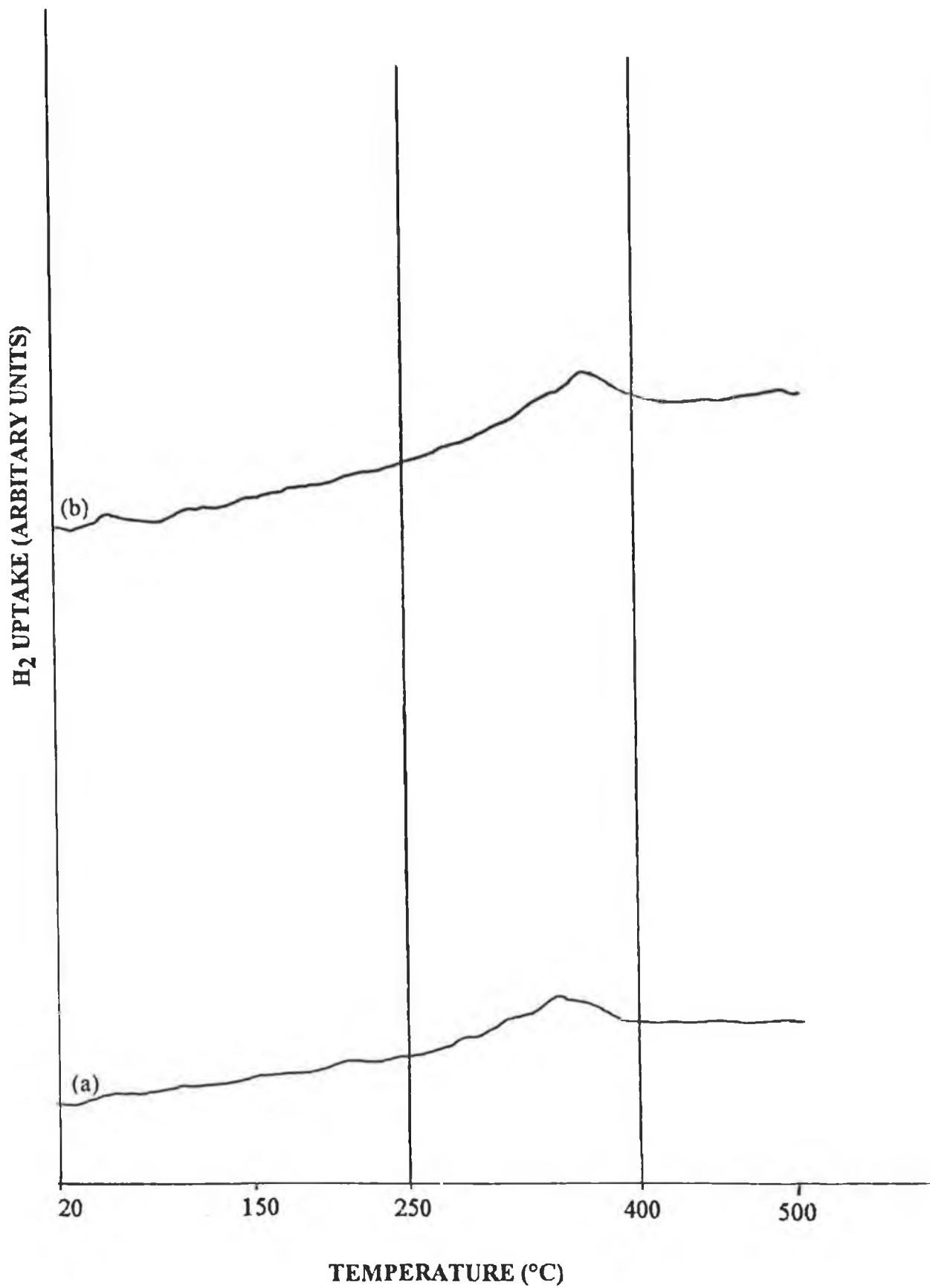


Fig. 3.42 : TPR profiles of air-aged PC10A, (a)-before and (b)-after, testing for  $i\text{-C}_4\text{H}_{10}$  oxidation activity.

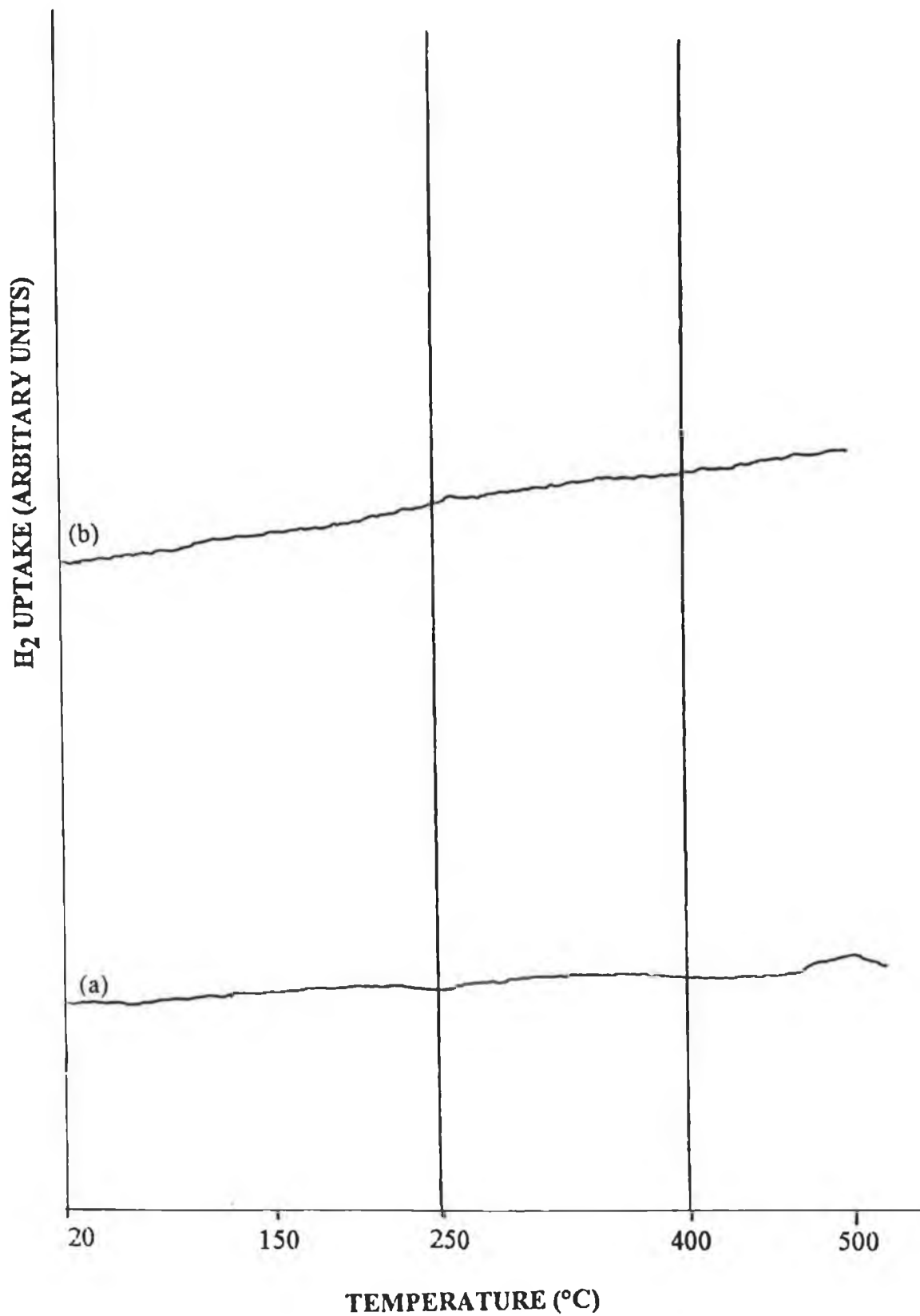


Fig. 3.43 : TPR profiles of sample PZ, (a)-before and (b)-after, aging at 800°C in air.

The XPS survey scan for sample PA, after aging in air at 800°C, is illustrated in Fig. 3.44(a). The surface elemental composition was similar to that before aging (see Fig. 3.13(a)), with Al, Si, C, O, and F all present. However, after aging the Cl peak at ca.200eV was not as prominent which indicates that removal of residual Cl from the  $\text{H}_2\text{PtCl}_6$  precursor salt may have occurred during the aging procedure. An expanded scan of the Pt 4d region is shown in Fig. 3.44(b) with peaks attributable to the Pt 4d<sub>5/2</sub> and Pt 4d<sub>3/2</sub> levels evident at 319.9eV and 337.1eV, respectively. After correction for sample charging, Pt 4d<sub>5/2</sub> and Pt 4d<sub>3/2</sub> binding energies of 314.5eV and 331.7eV were measured. These compare with values of 315.6eV and 332.9eV measured for the calcined sample before aging (see section 3.3.1). Shyu and Otto (45) reported a Pt 4d<sub>5/2</sub> binding energy of  $314.2 \pm 0.3\text{eV}$  for Pt metal, and Nunan et al. (7) deemed that a binding energy of lower than 315.5eV for Pt 4d<sub>5/2</sub> peaks was evidence that surface Pt was reduced and present as Pt<sup>0</sup>. Thus, it appears that surface Pt in sample PA was in a more metallic state after high temperature aging in air, presumably due to the decomposition of Pt oxide species (21). This is in agreement with the TPR profile for the aged sample (Fig. 3.41(a)) which revealed an absence of any distinct peaks associated with Pt reduction. Mc Cabe et al. (32) reported that larger Pt crystallites are less oxidised than more dispersed Pt particles because it was believed that only the surface Pt atoms become oxidised (32).

As discussed above, H<sub>2</sub> chemisorption was severely reduced for all samples after aging in air which was concluded to be due to sintering of dispersed Pt to produce larger Pt particles. In contrast to the H<sub>2</sub> chemisorption results, the XPS spectrum for aged PA revealed no decrease in the surface atomic Pt content. Pt concentrations were determined as ca.0.06 atomic% for both the aged and the calcined sample. The Pt 4d features were, if anything, a little more distinct for the aged sample. Previous results in this laboratory (60), have also showed a slight increase in the intensity of Pt XPS peaks in Pt/Al<sub>2</sub>O<sub>3</sub> samples, after aging under the same conditions as those employed in the present study, even though H<sub>2</sub> chemisorption and BET surface area measurements indicated that Pt sintering had occurred during aging.

Quantification of the C 1s peak for the aged PA sample revealed a slight increase in C content from 8.8% for the calcined sample to 11.5%. This might be attributed to adsorption of carbon from the static air atmosphere during aging.

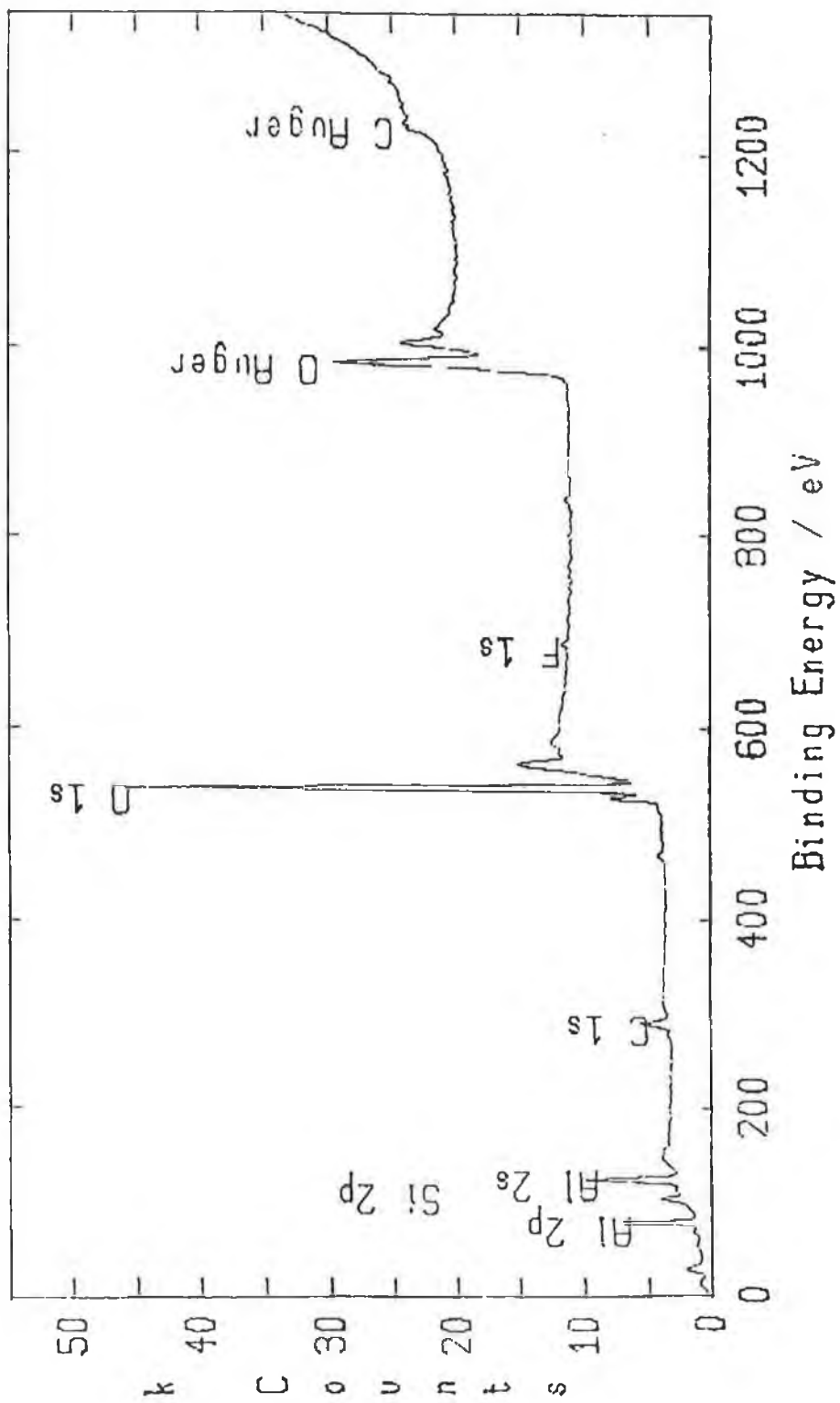


Fig 3.44(a) : XPS spectrum of air-aged PA.

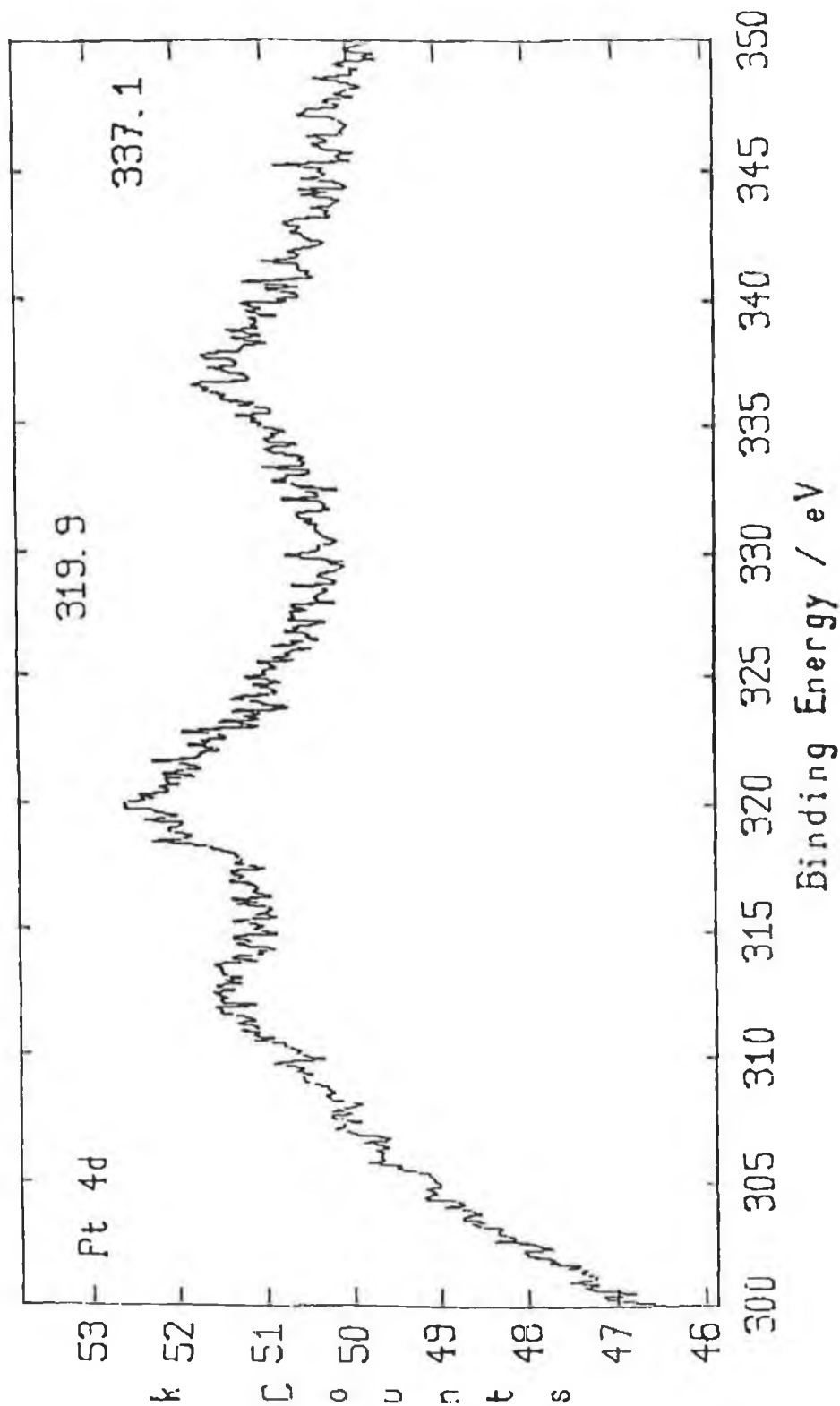


Fig 3.44(b) : XPS spectrum showing an expanded energy range scan in the Pt 4d region for air-aged PA. Charge correction = 5.4eV.

After aging in different atmospheres, the conversion of  $i\text{-C}_4\text{H}_{10}$  as a function of temperature is shown for samples PA, PC10A, and PC in Fig. 3.45-3.47. In addition, the activity curves for sample PZ, both before and after aging, are illustrated in Fig. 3.48. The performance of the fresh and aged samples are compared in Tables 3.12-3.14, in terms of the temperatures at which 10, 50 and 90% conversion of  $i\text{-C}_4\text{H}_{10}$  was achieved.

**Table 3.12 : Temperatures (°C) of 10% Iso-Butane Conversion over Catalyst Samples after Aging in Various Atmospheres.**

Sample	Fresh*		Air-Aged		Air: $i\text{-C}_4\text{H}_{10}$ -Aged		Argon-Aged	
	Run 1	Run 2	Run 1	Run 2	Run 1	Run 2	Run 1	Run 2
PA	215	185	105	105	105	105	190	170
PC10A	265	165	155	200	150	125	135	150
PC	240	205	265	265	245	250	245	275
PZ	150	105	150	105	150	150	ND	ND

**Table 3.13 : Temperatures (°C) of 50% Iso-Butane Conversion over Catalyst Samples after Aging in Various Atmospheres.**

Sample	Fresh*		Air-Aged		Air: $i\text{-C}_4\text{H}_{10}$ -Aged		Argon-Aged	
	Run 1	Run 2	Run 1	Run 2	Run 1	Run 2	Run 1	Run 2
PA	260	255	125	125	130	130	260	220
PC10A	285	250	175	220	175	170	210	215
PC	285	230	315	300	295	290	320	325
PZ	175	125	175	125	175	170	ND	ND

**Table 3.14 : Temperatures (°C) of 90% Iso-Butane Conversion over Catalyst Samples after Aging in Various Atmospheres.**

Sample	Fresh*		Air-Aged		Air: $i\text{-C}_4\text{H}_{10}$ -Aged		Argon-Aged	
	Run 1	Run 2	Run 1	Run 2	Run 1	Run 2	Run 1	Run 2
PA	270	270	145	150	150	150	290	270
PC10A	300	290	195	245	200	200	245	245
PC	295	270	350	>350	345	345	350	>350
PZ	195	145	190	145	195	195	ND	ND

\* Fresh i.e. After impregnation and calcination at 630°C

ND = not determined

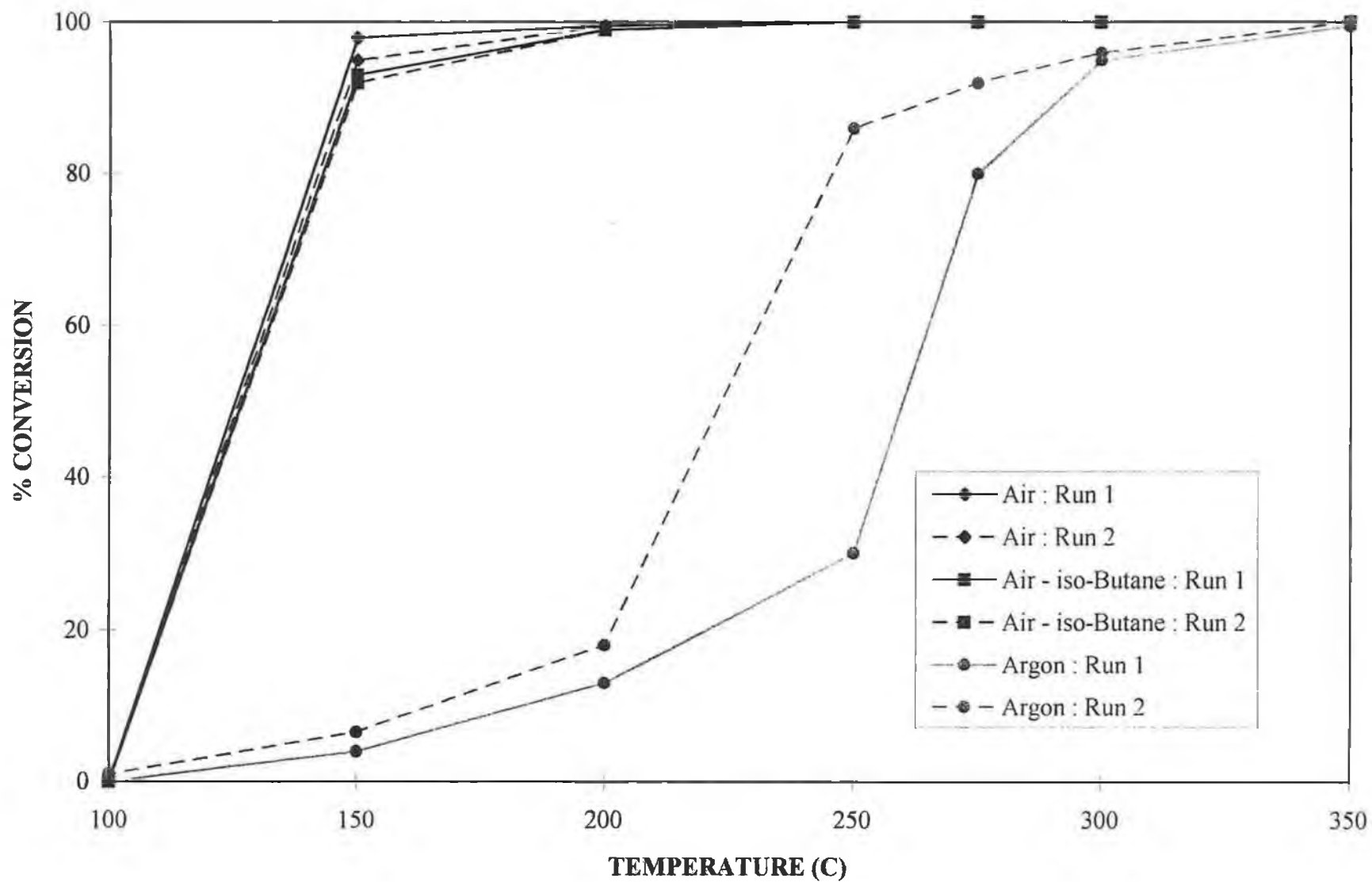


Fig. 3.45 : % iso-Butane Conversion versus Temperature for Sample PA after aging in different atmospheres.

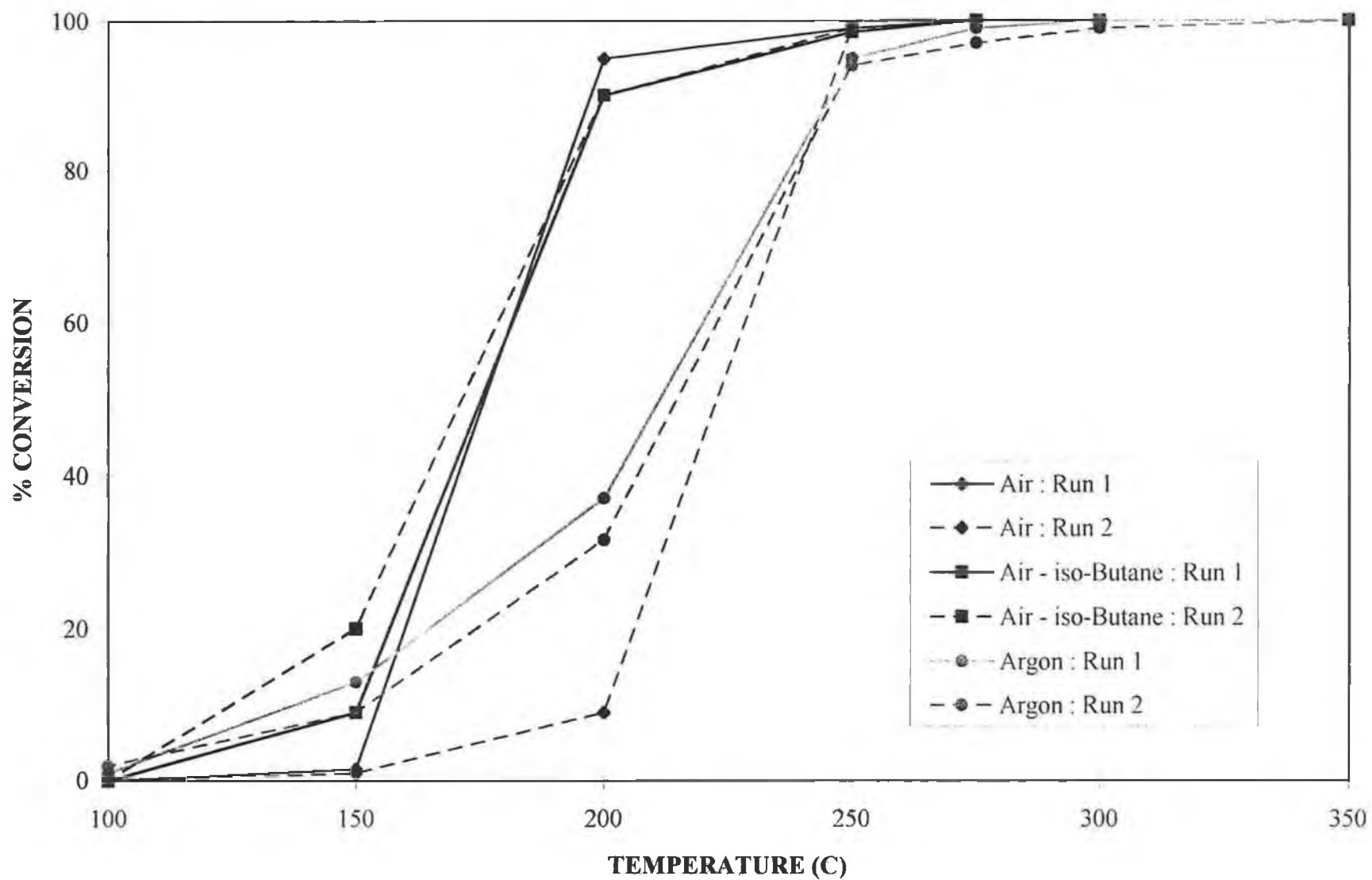


Fig. 3.46 : % iso-Butane Conversion versus Temperature for Sample PC10A after aging in different atmospheres.

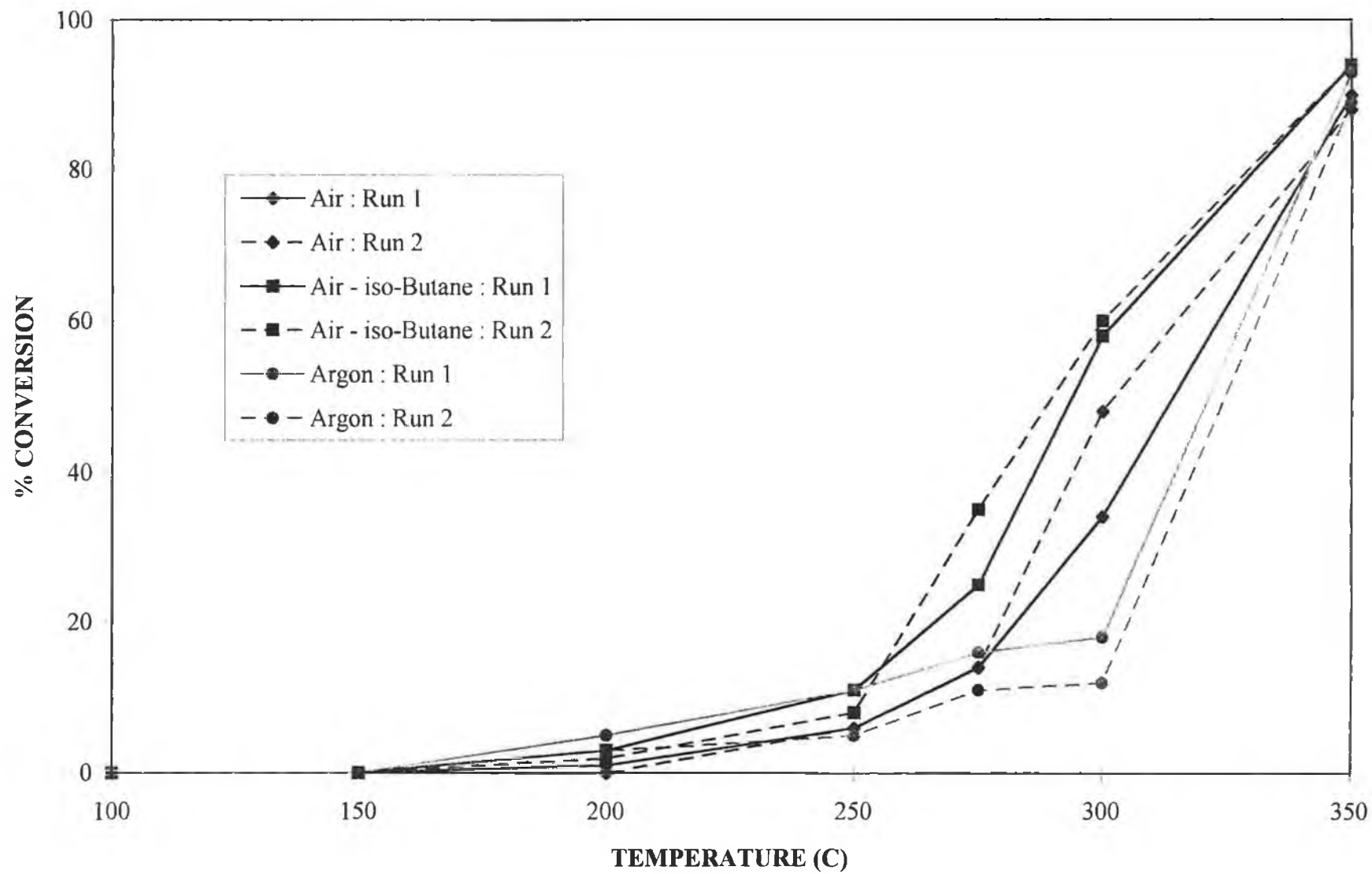


Fig. 3.47 : % iso-Butane Conversion versus Temperature for Sample PC after aging in different atmospheres.

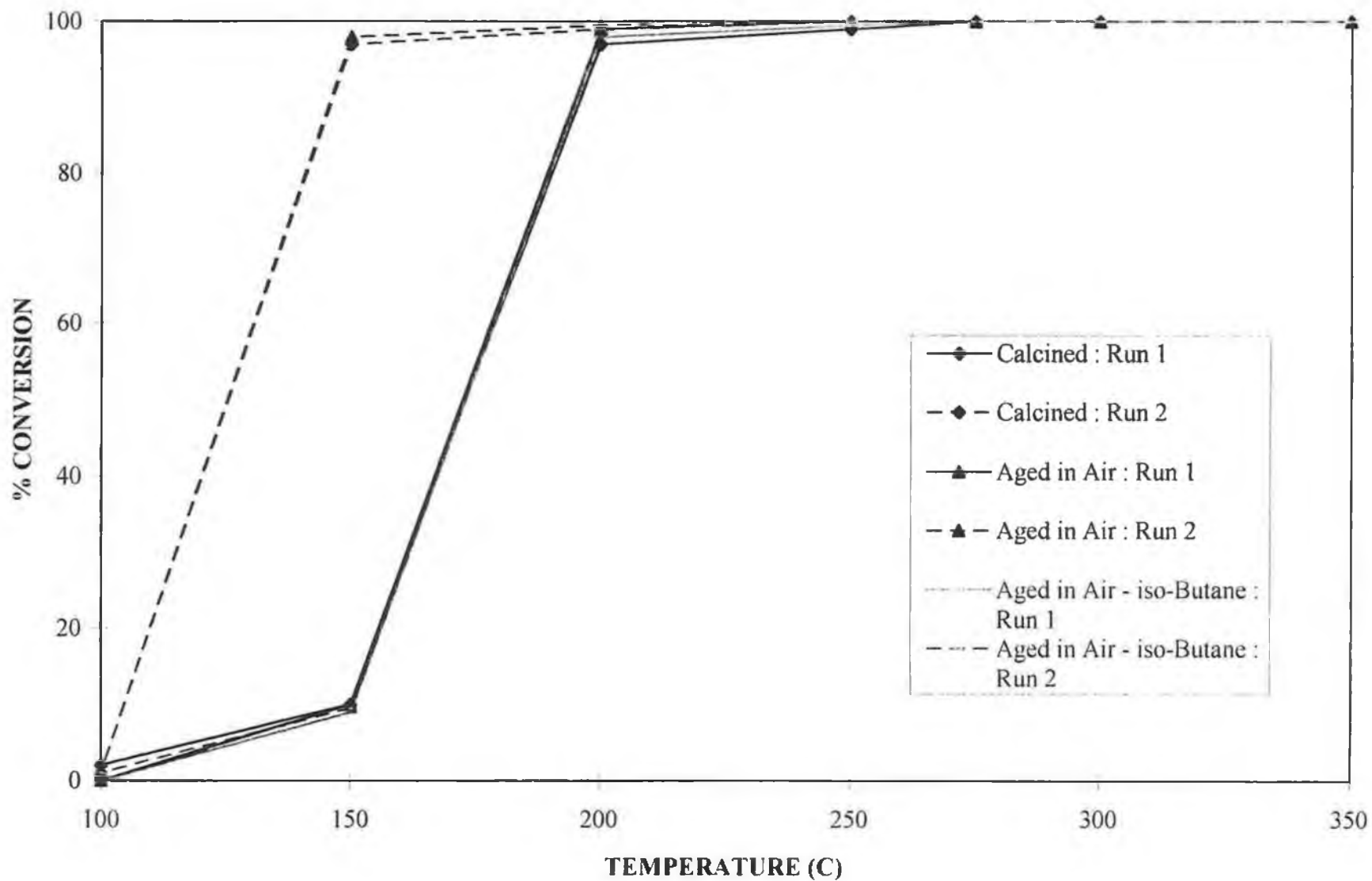


Fig. 3.48 : % iso-Butane Conversion versus Temperature for Sample PZ after various treatments.

A dramatic increase in the activity of sample PA was observed after high temperature aging in air. For example,  $T_{50}$  was lowered by 135°C relative to the fresh calcined sample (see Table 3.13). This indicates that larger Pt particles, present in the aged sample, were considerably more active than the highly dispersed Pt present in the fresh sample. Thus, it appears that  $i\text{-C}_4\text{H}_{10}$  oxidation over Pt/Al<sub>2</sub>O<sub>3</sub> catalysts is a structure sensitive reaction. In agreement with this observation, several previous studies have reported that alkane oxidation on Pt/Al<sub>2</sub>O<sub>3</sub> is a structure sensitive catalytic reaction with larger Pt crystallites showing greater activity than highly dispersed Pt (9, 16-20).

Otto et al. (20) reported that sintering of Pt/Al<sub>2</sub>O<sub>3</sub> catalysts caused an increase in activity for C<sub>3</sub>H<sub>8</sub> oxidation, but found that excessive sintering defeated the benefit of increased site activity due to considerable loss of surface metal. In the present study, loss of surface Pt during aging was more than compensated for by increased site activity, since, not only was the activity per surface site increased but the activity per gram of catalyst was also considerably enhanced even though H<sub>2</sub> chemisorption indicated a substantial decrease in available Pt surface area.

In order to indicate the extent of the changes observed in Pt site activity after aging, the activity per surface Pt atom in the fresh and air-aged catalysts was calculated using the H<sub>2</sub> chemisorption results in Table 3.11. Turnover numbers (TON) for the different samples at 150°C and 275°C are compared in Tables 3.15 and 3.16 in terms of the percentage iso-butane conversion per surface Pt atom. These values were calculated by dividing the percentage  $i\text{-C}_4\text{H}_{10}$  conversion per gram of catalyst sample, by the number of determined Pt surface sites per gram of sample. The number of Pt surface atoms per gram of catalyst was calculated from the volume of H<sub>2</sub> adsorbed in chemisorption measurements using equation (8) in Appendix B.

Comparisons of site activity in the different samples on the basis of TONs calculated in this manner assumes that each Pt atom on the surface is an active site. It should also be noted that for aged samples and for sample PZ the low level of H<sub>2</sub> chemisorption will have introduced a sizeable error into the determination of the number of available Pt surface sites which will have been translated into the TON values obtained for these samples. In addition, C-deposition during aging in the reaction mixture may have introduced further error into the determination of the number of Pt surface sites which could participate in the reaction and the calculated TON values for such samples may be overestimated. Therefore, particular care must be taken in comparing TON values for aged samples. However, the increases in TON values for Al<sub>2</sub>O<sub>3</sub>-supported samples after aging help to give some indication of the structure-sensitive nature of the

reaction. For example, Table 3.15 indicates that the activity of each surface Pt site in sample PA, at 150°C was increased by a factor of at least 250 after aging in air at 800°C.

**Table 3.15** : Turnover Numbers for Catalysts after Aging in Various Atmospheres. [(% conversion per surface Pt atom at 150°C) × 10<sup>-17</sup>]

Sample	Fresh*		Air-Aged		Air:i-C <sub>4</sub> H <sub>10</sub> -Aged		Argon-Aged	
	Run 1	Run 2	Run 1	Run 2	Run 1	Run 2	Run 1	Run 2
PA	0.00	0.09	23.31	22.60	38.42	38.01	2.25	3.66
PC10A	0.00	0.09	---	---	2.65	5.89	11.51	7.97
PC	0.00	0.00	0.00	0.00	0.00	0.00	---	---
PZ	6.88	66.74	---	---	---	---	---	---

**Table 3.16** : Turnover Numbers for Catalysts after Aging in Various Atmospheres. [(% conversion per surface Pt atom at 275°C) × 10<sup>-17</sup>]

Sample	Fresh*		Air-Aged		Air:i-C <sub>4</sub> H <sub>10</sub> -Aged		Argon-Aged	
	Run 1	Run 2	Run 1	Run 2	Run 1	Run 2	Run 1	Run 2
PA	1.76	1.84	23.79	23.79	41.31	41.31	45.07	51.84
PC10A	0.25	1.61	---	---	29.46	29.46	87.68	85.90
PC	3.15	10.58	1.61	1.61	5.34	7.47	---	---
PZ	68.80	68.80	---	---	---	---	---	---

\* Fresh i.e. After impregnation and calcination at 630°C

Structure sensitivity in alkane oxidation on Pt/Al<sub>2</sub>O<sub>3</sub> has been reported to be related to an increased reactivity of adsorbed oxygen on larger Pt particles due to a lowering of Pt-O bond strength (16, 19). Alternatively, the improved performance with larger Pt particles may reflect a requirement for several adjacent Pt sites to allow hydrocarbon adsorption and reaction (8, 9). The possible existence of particular site ensembles of high reactivity has also been suggested (18, 20). Carballo and Wolf (56) related increased C<sub>3</sub>H<sub>6</sub> oxidation activity for pre-sintered Pt/Al<sub>2</sub>O<sub>3</sub> catalysts to the fact that increasing crystallite size was expected to decrease the fraction of Pt atoms in edges and kinks and increase the fraction of atoms in terrace sites. It was concluded that C<sub>3</sub>H<sub>6</sub> was oxidised more readily on crystallite terraces due to a decrease in bond strength between the metal and reactants which led to higher specific reaction rates (56).

Similarly, for CH<sub>4</sub> oxidation, Briot et al. (16) reported that turnover frequency for Pt/Al<sub>2</sub>O<sub>3</sub> increased with decreasing dispersion of the metallic phase and this was attributed to the fact that the reactivity of adsorbed oxygen was higher on large rather than small Pt particles. Increased reactivity of adsorbed oxygen for larger Pt particles was confirmed by microcalorimetric measurements and by H<sub>2</sub> titration of adsorbed oxygen. Sintering of a Pt/Al<sub>2</sub>O<sub>3</sub> catalyst in the reaction mixture was found to cause a decrease in the apparent activation energy for CH<sub>4</sub> oxidation from ca.24 to ca.17 kcal.mol<sup>-1</sup>. It was noted that the interaction of CH<sub>4</sub> with the Pt particles could also have been a function of particle size (16). In contrast, Otto et al. (20) found no evidence for a change in the activation energy for C<sub>3</sub>H<sub>8</sub> oxidation on Pt/Al<sub>2</sub>O<sub>3</sub> with increasing Pt particle size and hence, could not relate increased activity with changes in the energy associated with the rate determining step. Instead, structure sensitivity was thought to be related to a change in reaction-site density (20). It cannot be determined from the results obtained in the present study as to whether increased activity for sintered samples was due to geometric or electronic effects, with the former involving a change in reaction site density (8, 20) and the latter involving a change in the strength of interaction between metal and reactants due to changes in the electronic properties of surface metal (16, 19, 56, 67). Yu-Yao (9) also reported that the activity of Pt/Al<sub>2</sub>O<sub>3</sub> in the oxidation of C<sub>1</sub>-C<sub>4</sub> alkanes varied with Pt particle size. Pt wires were found to be more active than supported Pt, and larger Pt particles appeared to be more active than highly dispersed isolated Pt ions or atoms. The fact that deactivation by the Al<sub>2</sub>O<sub>3</sub> support, compared to Pt wire, was less for CH<sub>4</sub> than for the larger alkanes, indicated a possible requirement of adjacent metal sites for alkane adsorption i.e. geometric effects. It was noted, however, that decreased activity for supported Pt may have also been related to a greater tendency of dispersed Pt to be oxidised (9).

Völter et al. (17) reported that the total oxidation of n-C<sub>7</sub>H<sub>16</sub> on 0.5% Pt/Al<sub>2</sub>O<sub>3</sub> was affected by the relative amounts of crystalline and dispersed Pt species present. Treatment of a chloride-containing catalyst in air at temperatures above 500°C was found to cause a decrease in the dispersion of Pt which was attributed to the decomposition of a highly dispersed Pt<sup>4+</sup> surface complex into poorly dispersed metallic crystalline Pt. With increasing calcination temperature, in the range 500-900°C, the conversion of n-C<sub>7</sub>H<sub>16</sub> was increased. This was explained in terms of the formation of greater amounts of active crystalline Pt<sup>0</sup> as the calcination temperature increased. Dispersed Pt was believed to be less active because of a greater tendency to become oxidised to less active Pt<sup>4+</sup>. Treatment in Ar, as opposed to air, at 900°C was found to cause an even greater improvement in catalyst activity. This was attributed to the formation of even more metallic Pt during heat treatment in the absence of O<sub>2</sub> (17). Such a theory is in disagreement with results in the present study. It can be seen from Tables

3.12-13 that sample PA was considerably more active for  $i\text{-C}_4\text{H}_{10}$  oxidation after aging in air as opposed to Ar.  $T_{50}$  was reached at  $135^\circ\text{C}$  lower over the air-aged sample (Table 3.13).. After aging in Ar,  $T_{50}$  was initially at the same temperature as for the fresh calcined sample. However, the activity of the Ar aged sample increased after exposure to the reaction mixture. TON values were greater on the Ar aged sample than on the fresh calcined sample (see Tables 3.15-3.16). This supports the theory that larger Pt particles were more active than highly dispersed Pt. The results obtained also indicate the need for some degree of oxidation of the sintered Pt to achieve optimum performance, with heat treatment in an inert atmosphere being less effective than in air. XPS and TPR results indicated that Pt was in a strongly metallic state after aging in all environments but it may be possible that some chemisorbed oxygen on the large Pt crystallites might have been undetected by these techniques. Assuming heat treatment in Ar at  $800^\circ\text{C}$  caused the decomposition of Pt oxides to metallic Pt, exposure to the air : iso-butane reaction mixture during Run 1 may have been expected to cause some degree of reoxidation of surface Pt and this may have been associated with increased activity during Run 2 for this sample.

As reported by Völter and co-workers. (17), Hicks et al. (19) also reported the existence of two different Pt phases in supported catalysts as evidenced by changes in the IR stretching frequency of adsorbed CO. Structure sensitivity was explained in terms of crystalline Pt being more active for  $\text{CH}_4$  oxidation than dispersed Pt due to the existence of more reactive adsorbed oxygen on the former phase. This was supported by the finding that the activation energy for  $\text{CH}_4$  oxidation was higher on dispersed Pt than crystalline Pt. It was proposed that dispersed Pt became oxidised to  $\text{PtO}_2$  during reaction, while Pt crystallites became covered with more reactive chemisorbed oxygen (19). This theory was thought to be supported by the TPR study of Niwa et al. (33) who found that the activity of supported Pt catalysts for  $\text{CH}_4$  oxidation increased as the reactivity of surface oxygen towards  $\text{H}_2$  increased. Hicks et al. (19) reported that the relative amounts of the two phases, i.e. crystalline and dispersed Pt, depended more on the support material used than on the degree to which Pt was actually dispersed over the support.  $\text{Al}_2\text{O}_3$  was deemed to be capable of stabilising Pt in a highly dispersed state, while less reactive supports such as  $\text{ZrO}_2$  did not stabilise the Pt dispersion and Pt crystallites were formed (19).

Hubbard et al. (68, 69) reported a similar strong effect by the support material in the  $\text{C}_3\text{H}_8$  oxidation activity of Pt catalysts. For  $\text{Pt}/\text{Al}_2\text{O}_3$  catalysts, the specific rate constant was found to increase with increasing particle size, while for  $\text{Pt}/\text{ZrO}_2$  smaller particles were at least as active as larger particles (68). It was thought that highly dispersed Pt was more active than larger Pt crystallites for  $\text{C}_3\text{H}_8$  oxidation provided that

the metal was supported on an inert material such as  $ZrO_2$ . Greater activity of Pt/ $ZrO_2$  compared to Pt/ $Al_2O_3$  at low Pt concentrations was attributed to deactivation of small Pt particles by the  $\gamma$ - $Al_2O_3$  support (68). At higher Pt loadings, the larger Pt particles present did not experience as close a contact with the support material and reaction rates were not as affected by the support material employed (68, 69). In the present study, 0.5% Pt/ $ZrO_2$  was found to be considerably more active than 0.5% Pt/ $Al_2O_3$  after calcination at 630°C (see Tables 3.12-3.16). The activity of the calcined PZ sample was comparable to that of sample PA after aging in air at 800°C. This may have indicated a deactivating effect by  $Al_2O_3$  on highly dispersed Pt in the calcined PA sample which did not influence the larger particles present after aging (68, 69). However, an alternative explanation is that large Pt particles were present on the lower surface area  $ZrO_2$  support even after initial calcination at 630°C, which were responsible for the high activity of calcined PZ. This latter theory is supported by  $H_2$  chemisorption results (see Table 3.11) and by the fact that the activity of sample PZ was apparently unaffected by aging in air at 800°C which indicates the presence of large crystallites even prior to aging. Thus, higher activity for PZ relative to PA after calcination, may have been simply due to decreased Pt dispersion in the former sample rather than an effect of the support material on inherent Pt activity.

Studies of  $CH_4$  oxidation over Pd/ $Al_2O_3$  catalysts have reported that considerable activation of the catalysts can occur on exposure to the reaction mixture (58, 59, 70, 71). This has been associated with the possibility of morphological changes during reaction which may have resulted in the exposure of more favourable crystal planes (58, 59, 70, 71). Unless both reactants were present, no such activation was achieved (58, 59, 70, 71). Hicks et al. (19) reported that morphological changes for both supported Pt and Pd catalysts were indicated by changes in the IR band of adsorbed CO during  $CH_4$  oxidation and could be correlated with changes in oxidation activity. Briot et al. (16) noted that improved  $CH_4$  oxidation activity for a Pt/ $Al_2O_3$  catalyst after aging in the reaction mixture may have been related to the existence of preferentially exposed crystal planes after exposure to the reactants as well as increased particle size. Morphological changes were indicated by TEM which showed that larger Pt particles were not spherical and many were faceted (16). In the current study, examination of calcined samples also indicated improvements in  $i-C_4H_{10}$  oxidation activity on exposure to the reaction mixture as discussed in section 3.3.2. Thus, it was of interest to examine the effect of high temperature aging in the stoichiometric reaction mixture on catalyst activity. After aging of sample PA in the air : iso-butane mixture, a considerable improvement in catalyst activity occurred when compared to the calcined fresh sample, as illustrated in Tables 3.12-3.16. However, activation of Pt/ $Al_2O_3$  was similar after aging in both air and air :  $i-C_4H_{10}$  atmospheres with similar  $T_{10}$ ,  $T_{50}$  and  $T_{90}$  values.

This indicates that activation was associated with increased Pt particle size and the presence of  $i\text{-C}_4\text{H}_{10}$  was not required. TON values (Tables 3.15-3.16) were greater for the sample aged in the reaction mixture but this was solely due to a lower  $\text{H}_2$  uptake on this sample which was probably affected by C-deposition during aging. Thus, comparison of site activity for samples aged in air and in the reaction mixture by TON values, as calculated in Tables 3.15 and 3.16, is deemed inappropriate. The possibility that particle morphology changed with increasing particle size after heat treatment cannot, however, be discounted as a possible contributing factor in the observed structure sensitivity of iso-butane oxidation on  $\text{Pt}/\text{Al}_2\text{O}_3$  (16, 55).

From Tables 3.12-3.16, it can be seen that the activity of the  $\text{Pt-Ce}/\text{Al}_2\text{O}_3$  sample, PC10A, also increased after high temperature aging. Again, this can be attributed to an increased Pt particle size as indicated by  $\text{H}_2$  chemisorption measurements. As for the calcined samples, the activity of sample PC10A was lower than that of sample PA after aging in static air at  $800^\circ\text{C}$  (Tables 3.12-3.14). As discussed previously in section 3.3.2, decreased activity for  $\text{Pt-Ce}/\text{Al}_2\text{O}_3$ , relative to  $\text{Pt}/\text{Al}_2\text{O}_3$ , after treatment in an oxidising environment may have been associated with a bimetallic interaction which affected the oxidation properties of surface Pt (8, 9, 12). The possibility that Ce stabilised the Pt dispersion during aging and thereby resulted in lower activity due to decreased particle size relative to the Pt-only sample, PA, was not suggested by  $\text{H}_2$  chemisorption results. As mentioned previously, Gandhi and Shelef (10) found that addition of Ce to a 0.07%  $\text{Pt}/\gamma\text{-Al}_2\text{O}_3$  sample resulted in a decrease in activity for  $\text{C}_3\text{H}_8$  oxidation which was associated with stabilised Pt dispersion in the presence of Ce. Similarly, Diwell et al. (12) attributed decreased  $\text{C}_3\text{H}_8$  oxidation activity for  $\text{Pt-Ce}/\text{Al}_2\text{O}_3$  relative to  $\text{Pt}/\text{Al}_2\text{O}_3$  to the existence of a Pt-Ce interaction which stabilised Pt dispersion on aging in air between  $700\text{-}800^\circ\text{C}$  possibly by maintaining Pt in a more oxidised state. No such improvements in Pt dispersion were apparent in the present study (see Table 3.11).

From Fig. 3.46, it can be seen that the low temperature activity of PC10A after aging in the stoichiometric air :  $i\text{-C}_4\text{H}_{10}$  mixture was higher than that after aging in air. This may have been associated with a reducing effect of the hydrocarbon in the reaction mixture, since reduction was seen in section 3.3.2 to cause increased oxidation activity for Pt-Ce catalysts. Sample PC10A was, again, less active than sample PA after aging in the air : iso-butane mixture. However, after aging in Ar, sample PC10A was more active than sample PA (see Tables 3.12-3.14). This would appear to suggest that the presence of Ce promotes the  $i\text{-C}_4\text{H}_{10}$  oxidation activity of  $\text{Pt}/\text{Al}_2\text{O}_3$  after pretreatment in the absence of  $\text{O}_2$ , since  $\text{Pt-Ce}/\text{Al}_2\text{O}_3$  samples were also more active than  $\text{Pt}/\text{Al}_2\text{O}_3$  after pre-reduction in  $\text{H}_2/\text{Ar}$  (see section 3.3.2) but were less active after treatment in air or in the air : iso-butane mixture.

As can be seen from Tables 3.12-3.14, the activity of sample PC decreased after aging in air, air : i-C<sub>4</sub>H<sub>10</sub>, or Ar. The reasons for deactivation of the Pt/CeO<sub>2</sub> sample are unknown. There was no apparent relationship between Pt surface area, in the fresh and aged samples, and catalyst activity. Loss of oxidation activity in the air-aged sample can definitely not be attributed to loss of Pt surface area (see Table 3.11). However it can be stated that, in applications where the catalyst are likely to be exposed to high operating temperatures, use of Ce as an additive in Pt/Al<sub>2</sub>O<sub>3</sub> catalysts appears to be more advisable than use of CeO<sub>2</sub> as a support, even in spite of improved Pt dispersion in the latter case.

### **3.4 Conclusions**

TPR and XPS studies indicated differences in the nature of the Pt and Ce surface species present in the Pt/Al<sub>2</sub>O<sub>3</sub>, Pt-Ce/Al<sub>2</sub>O<sub>3</sub> and Pt/CeO<sub>2</sub> catalysts examined. Even though all catalysts had the same Pt loading (0.5 wt.%), there was also a considerable variation in catalyst activity for i-C<sub>4</sub>H<sub>10</sub> combustion.

XPS analysis indicated a difference in the nature of Ce species present in Pt-Ce/Al<sub>2</sub>O<sub>3</sub> samples relative to Pt/CeO<sub>2</sub>. For Pt/CeO<sub>2</sub>, the typical Ce 3d spectral features of CeO<sub>2</sub> (Ce<sup>4+</sup>) were exhibited. However, for Al<sub>2</sub>O<sub>3</sub>-supported samples, the Ce 3d spectra obtained more closely resembled that of Ce<sup>3+</sup> than Ce<sup>4+</sup>. This may indicate the presence of some form of Ce-alumina interactive species which stabilises dispersed Ce in a more reduced state than that in CeO<sub>2</sub>. Analysis of the Pt oxidation state in the different catalysts was complicated due to the low level of Pt present and overlap of the most sensitive Pt 4f lines with the Al 2p feature for Al<sub>2</sub>O<sub>3</sub>-supported samples. The Pt 4d lines were analysed instead which are comparatively broad and less sensitive. Because of these problems the elucidation of Pt oxidation state(s) was difficult. Pt appeared to be oxidised and exist as Pt<sup>2+</sup> (PtO) rather than Pt<sup>4+</sup> (PtO<sub>2</sub>) in both Pt/Al<sub>2</sub>O<sub>3</sub> and Pt/CeO<sub>2</sub> after calcination. The addition of Ce to Pt/Al<sub>2</sub>O<sub>3</sub> resulted in a shift in Pt 4d<sub>5/2</sub> binding energy indicating the existence of an electronic interaction between Pt and Ce. The effect of Ce appeared to vary depending on its loading. For a Pt-Ce/Al<sub>2</sub>O<sub>3</sub> (Ce:Pt = 0.5:1 atomic ratio) catalyst, the Pt 4d features were shifted to more electronegative values relative to Pt/Al<sub>2</sub>O<sub>3</sub> indicating decreased oxidation of surface Pt in the presence of low levels of Ce. For a higher level of Ce in a Pt-Ce/Al<sub>2</sub>O<sub>3</sub> (Ce:Pt = 10:1 atomic ratio) catalyst, Pt appeared to be slightly more oxidised relative to Pt/Al<sub>2</sub>O<sub>3</sub> with a slight electropositive shift in Pt 4d<sub>5/2</sub> peak position for the former sample. This may also have been the case for the Pt/CeO<sub>2</sub> catalyst, but electronic transfer from the noble metal to the rare earth could not be concluded solely on the basis of the limited XPS data obtained. However, such a conclusion would be supported by TPR experiments and by thermodynamic consideration of redox potentials for the two metals.

TPR experiments also indicated the existence of electronic interaction between Pt and Ce in Pt-Ce/Al<sub>2</sub>O<sub>3</sub> and Pt/CeO<sub>2</sub> catalysts. Comparison of the TPR profiles for Pt/CeO<sub>2</sub> and CeO<sub>2</sub> samples indicated that the presence of Pt promoted more facile reduction of surface CeO<sub>2</sub> sites, with a downward shift in the temperature of the dominant reduction peak from ca.500°C to ca.265°C. In addition, the TPR profiles for Pt-Ce/Al<sub>2</sub>O<sub>3</sub> samples were not a direct superimposition of those for monometallic Pt/Al<sub>2</sub>O<sub>3</sub> and Ce/Al<sub>2</sub>O<sub>3</sub> samples. This indicated the existence of a Pt-Ce surface

interaction. Profiles obtained for uncalcined samples indicated that this interaction affected the reduction properties of both metals even prior to calcination.

A reduction feature at ca.420-440°C in TPR profiles was concluded to be characteristic of a Pt-Al<sub>2</sub>O<sub>3</sub> interactive species. For Pt-Ce/Al<sub>2</sub>O<sub>3</sub> samples, a feature at ca.250°C was assigned to the reduction of a Pt-Ce interactive surface species. For samples prepared by co-impregnation of the two metals, Pt appeared to interact preferentially with Ce rather than with Al<sub>2</sub>O<sub>3</sub> even at low Ce levels ( $\leq 0.29$  wt.% Ce). This was also true for a Pt-Ce/Al<sub>2</sub>O<sub>3</sub> (Ce:Pt =8:1 atomic ratio) sample in which Ce was deposited on the Al<sub>2</sub>O<sub>3</sub> prior to impregnation with Pt. However for a sample with the same metal loadings, but prepared by the reverse sequence of impregnation (pre-deposition of Pt prior to the addition of Ce) both Pt-Ce and Pt-Al<sub>2</sub>O<sub>3</sub> interactive species were evident in TPR profiles. For Pt-Ce/Al<sub>2</sub>O<sub>3</sub> samples, the stability of Pt-Ce interaction on exposure to the i-C<sub>4</sub>H<sub>10</sub>:air oxidation mixture increased with increasing Ce concentration, at least up to 3.6 wt.% i.e.Ce:Pt = 10:1.

The activity of the Pt catalysts for the complete oxidation of i-C<sub>4</sub>H<sub>10</sub> in a stoichiometric reaction mixture was affected by the presence of Ce. For Al<sub>2</sub>O<sub>3</sub>-supported samples, the activity varied depending on the level of Ce and the sequence of impregnation of the two metals. For calcined catalysts, the presence of Ce, at Ce:Pt  $\geq 8$ :1 atomic ratio, resulted in poorer performance relative to Pt/Al<sub>2</sub>O<sub>3</sub> with higher temperatures required to achieve the same level of i-C<sub>4</sub>H<sub>10</sub> conversion. The only exception to this general trend was a Pt-Ce/Al<sub>2</sub>O<sub>3</sub> (Ce:Pt = 8:1 atomic ratio) sample in which Pt impregnation preceded that of Ce. Pt/CeO<sub>2</sub> was also less active than Pt/Al<sub>2</sub>O<sub>3</sub> after calcination in air. However, at lower Ce loadings (Ce:Pt = 0.5:1 or 1:1), oxidation activity was not so adversely affected and one sample, containing 0.29 wt.% Ce, was found to be noticeably more active than monometallic Pt/Al<sub>2</sub>O<sub>3</sub>.

The effects of Ce addition on the activity of Pt can be attributed to the existence of bimetallic interaction, which affected the activity of the noble metal, since Ce/Al<sub>2</sub>O<sub>3</sub> did not appreciably catalyse i-C<sub>4</sub>H<sub>10</sub> oxidation in the temperature range investigated. The differences in activity for different Ce loadings are in line with XPS data which showed that the nature of Pt-Ce interaction in the calcined catalysts may vary depending on Ce concentration.

The activity of the calcined catalysts was altered upon testing in the stoichiometric oxidation mixture at temperatures of up to 350°C. In general, exposure of the catalysts to the reactants resulted in improved activity during subsequent testing. This was particularly true in terms of light-off performance and low temperature activity with 10 and 50% conversion of i-C<sub>4</sub>H<sub>10</sub> being achieved at lower temperatures over most

catalysts after initial testing. Activation was greater for some Ce-containing samples than for Pt/Al<sub>2</sub>O<sub>3</sub> with the result that Pt/CeO<sub>2</sub>, and some Pt-Ce/Al<sub>2</sub>O<sub>3</sub> catalysts, were more active than Pt/Al<sub>2</sub>O<sub>3</sub> at certain temperatures during retesting even though they may have been less active initially.

Activity data, for catalysts which were pre-reduced in a 5% H<sub>2</sub>-95% Ar mixture, strongly suggested that Pt-Ce interactive surface sites were more active than Pt-Al<sub>2</sub>O<sub>3</sub> sites, after equivalent reduction treatments. After TPR from 20-500°C, the activity of Pt/Al<sub>2</sub>O<sub>3</sub> decreased while that of most Ce-containing samples increased. In addition, interaction between Pt and Ce was somehow important in preventing loss of activity after prolonged reduction at 500°C. Significant loss of activity occurred for most samples in which Pt was in greater interaction with the Al<sub>2</sub>O<sub>3</sub> surface rather than with Ce, as indicated by TPR profiles obtained immediately prior to reduction. Catalysts whose TPR profiles did not show the characteristic Pt-Al<sub>2</sub>O<sub>3</sub> reduction feature above 400°C were, in general, considerably more active after reduction.

Loss of surface Pt during activity testing and reduction experiments was indicated by XPS and H<sub>2</sub> chemisorption tests. This may have been due to Pt sintering and/or coke deposition during reaction of the air : i-C<sub>4</sub>H<sub>10</sub> mixture. Migration of Pt to less exposed sites due to strong interaction with the support material during reduction at 500°C may also have contributed to the apparent loss of surface Pt.

Aging of calcined Pt/Al<sub>2</sub>O<sub>3</sub> and Pt-Ce/Al<sub>2</sub>O<sub>3</sub> (Ce:Pt = 10:1 atomic ratio) samples in static air, or in the stoichiometric air : i-C<sub>4</sub>H<sub>10</sub> reaction mixture under flow conditions, at 800°C resulted in a considerable increase in activity for i-C<sub>4</sub>H<sub>10</sub> oxidation. For example, the turnover number for Pt/Al<sub>2</sub>O<sub>3</sub> at 150°C, increased by a factor of more than 250 after aging in air at 800°C. TPR profiles indicated that aging in air resulted in the decomposition of surface Pt oxide species and XPS analysis of the air-aged Pt/Al<sub>2</sub>O<sub>3</sub> sample indicated that Pt was in a more metallic, reduced state compared to the unaged sample. The H<sub>2</sub> chemisorption capacity of the samples decreased considerably after aging. This was most probably associated with sintering of dispersed Pt to produce larger Pt particles under the aging conditions.

It was concluded that the oxidation of i-C<sub>4</sub>H<sub>10</sub> on Al<sub>2</sub>O<sub>3</sub>-supported Pt is a structure sensitive reaction with larger Pt particles being more active than highly dispersed Pt. In support of this conclusion, a 0.5% Pt/ZrO<sub>2</sub> catalyst was found to be considerably more active than 0.5% Pt/Al<sub>2</sub>O<sub>3</sub> after calcination at 630°C. The activity of the calcined Pt/ZrO<sub>2</sub> sample was comparable to that of Pt/Al<sub>2</sub>O<sub>3</sub> after aging in air at 800°C and did not improve upon aging. This may have been due to the presence of large

poorly dispersed Pt particles on the lower surface area  $\text{ZrO}_2$  support even prior to high temperature aging as indicated by the  $\text{H}_2$  chemisorption uptake on the calcined sample.

The activity of  $\text{Pt}/\text{Al}_2\text{O}_3$  was greater after aging in air or in the reaction mixture than after aging in Ar. This may indicate a need for  $\text{O}_2$  in the aging atmosphere to achieve optimum activation even though XPS and TPR both indicated that an increase in the metallic character of surface Pt after aging in  $\text{O}_2$ -containing atmospheres at  $800^\circ\text{C}$  was concomitant with a considerable increase in activity.

For samples aged in air, or in the oxidation reaction mixture,  $\text{Pt}/\text{Al}_2\text{O}_3$  was more active than  $\text{Pt-Ce}/\text{Al}_2\text{O}_3$  (Ce:Pt = 10:1 atomic ratio). However after aging in an inert (Ar) atmosphere, the latter catalyst was more active indicating a beneficial effect of Ce. Therefore, it could be concluded that Pt-Ce interaction in the  $\text{Al}_2\text{O}_3$ -supported samples generally resulted in higher activity for  $i\text{-C}_4\text{H}_{10}$  oxidation after pre-reduction or aging in an inert atmosphere and resulted in decreased activity after calcination or aging in an  $\text{O}_2$ -containing atmosphere.

Aging of  $\text{Pt}/\text{CeO}_2$  in various atmospheres at  $800^\circ\text{C}$  resulted in significant activity losses even though  $\text{H}_2$  chemisorption measurements indicated that the  $\text{CeO}_2$  support had a greater ability than  $\text{Al}_2\text{O}_3$  to stabilise Pt dispersion on exposure to high temperature conditions.

## REFERENCES

- (1) Summers, J. C. and Ausen, S. A., *J. Catal.* **58**, 131 (1979).
- (2) Yu-Yao, Y. F. and Kummer, J. T., *J. Catal.* **106**, 307 (1987).
- (3) Oh, S. H. and Eickel, C. C., *J. Catal.* **112**, 543 (1988).
- (4) Lööf, P., Kasemo, B., Björnkvist, L., Andersson, S. and Frestad, A., in “*Catalysis and Automotive Pollution Control II*” (Crucq, A., ed.), Studies in Surface Science and Catalysis, Vol. 71, 253-274, Elsevier, Amsterdam, 1991.
- (5) Serre, C., Garin, F., Belot, G. and Maire, G., *J. Catal.* **141**, 9 (1993).
- (6) Engler, B., Koberstein, E. and Schubert, P., *Appl. Catal.* **48**, 71 (1989).
- (7) Nunan, J. G., Robota, H. J., Cohn, M. J. and Bradley, S. A., *J. Catal.* **133**, 309 (1992).
- (8) Yu-Yao, Y. F., *J. Catal.* **87**, 152 (1984).
- (9) Yu-Yao, Y. F., *Ind. Eng. Chem. Prod. Res. Dev.* **19**, 293 (1980).
- (10) Gandhi, H. S. and Shelef, M., in “*Catalysis and Automotive Pollution Control I*” (Crucq, A. and Frennet, A., eds.), Studies in Surface Science and Catalysis, Vol. 30, 199-214, Elsevier, Amsterdam, 1987.
- (11) Oh, S. H., Mitchell, P. J. and Siewert, R. M., *J. Catal.* **132**, 287 (1991).
- (12) Diwell, A. F., Rajaram, R. R., Shaw, H. A. and Truex, T. J., in “*Catalysis and Automotive Pollution Control II*” (Crucq, A., ed.), Studies in Surface Science and Catalysis, Vol. 71, 139-152, Elsevier, Amsterdam, 1991.
- (13) Pirault, L., El Azami El Idrissi, D., Marécot, P., Dominguez, J. M., Mabilon, G., Prigent, M. and Barbier, J., in “*Catalysis and Automotive Pollution Control III*” (Frennet, A. and Bastin, J.-M., eds.), Studies in Surface Science and Catalysis, Vol. 96, 193-202, Elsevier, Amsterdam, 1995.
- (14) Shyu, J. Z., Otto, K., Watkins, W. L. H., Graham, G. W., Belitz, R. K. and Gandhi, H. S., *J. Catal.* **114**, 23 (1988).
- (15) Silver, R. G., Summers, J. C. and Williamson, W. B., in “*Catalysis and Automotive Pollution Control II*” (Crucq, A., ed.), Studies in Surface Science and Catalysis, Vol. 71, 167-180, Elsevier, Amsterdam, 1991.
- (16) Briot, P., Auroux, A., Jones, D. and Primet, M., *Appl. Catal.* **59**, 141 (1990).
- (17) Völter, J., Lietz, G., Spindler, H. and Lieske, H., *J. Catal.* **104**, 375 (1987).
- (18) Otto, K., *Langmuir* **5**, 1364 (1989).
- (19) Hicks, R. F., Qi, H., Young, M. L. and Lee, R. G., *J. Catal.* **122**, 280 (1990).
- (20) Otto, K., Andino, J. M. and Parks, C. L., *J. Catal.* **131**, 243 (1991).
- (21) Huizinga, T., Van Grondelle, J. and Prins, R., *Appl. Catal.* **10**, 199 (1984).
- (22) Kapteijn, F., Moulijn, J. A. and Tarfaoui, A., in “*Catalysis*” (Moulijn, J. A., van Leeuwen, P. W. N. M. and van Santen, R. A., eds.), Studies in Surface Science and Catalysis, Vol. 79, 401-417, Elsevier, Amsterdam, 1993.
- (23) Anderson, J. R. and Pratt, K. C., “*Introduction to Characterization and Testing of Catalysts*”, 203-256, Academic Press, Australia, 1985.
- (24) Hurst, N. W., Gentry, S. J., Jones, A. and Mc. Nicol, B. D., *Catal. Rev. Sci. Eng.* **24(2)**, 233 (1982).
- (25) Yao, H. C., Sieg, M. and Plummer Jr., H. K., *J. Catal.* **59**, 365 (1979).
- (26) Johnson, M. F. L. and Keith, C. D., *J. Phys. Chem.* **67**, 200 (1963).
- (27) Yao, H. C., Gandhi, H. S. and Shelef, M., in “*Metal-Support and Metal-Additive Effects in Catalysis*” (Imelik, B., Naccache, C., Coudurier, G., Praliaud, H.,

- Meriaudeau, P., Gallezot, P., Martin, G. A. and Vedrine, J. C., eds.), *Studies in Surface Science and Catalysis*, Vol. 11, 159-169, Elsevier, Amsterdam, 1982.
- (28) Lieske, H., Lietz, G., Spindler, H. and Völter, J., *J. Catal.* **81**, 8 (1983).
- (29) Lietz, G., Lieske, H., Spindler, H., Hanke, W. and Völter, J., *J. Catal.* **81**, 17 (1983).
- (30) Mc. Nicol, B. D. and Short, R. T., *J. Electroanal. Chem.* **92**, 115 (1978).
- (31) Ebitani, K. and Hattori, H., *Bull. Chem. Soc. Jpn.* **64**, 2422 (1991).
- (32) Mc. Cabe, R. W., Wong, C. and Woo, H. S., *J. Catal.* **114**, 354 (1988).
- (33) Niwa, M., Awano, K. and Murakami, Y., *Appl. Catal.* **7**, 317 (1983).
- (34) Johnson, M. F. L. and Mooi, J., *J. Catal.* **103**, 502 (1987).
- (35) Shyu, J. Z., Weber, W. H. and Gandhi, H. S., *J. Phys. Chem.* **92**, 4964 (1988).
- (36) Yao, H. C. and Yu-Yao, Y. F., *J. Catal.* **86**, 254 (1984).
- (37) Shyu, J. Z. and Otto, K., *J. Catal.* **115**, 16 (1989).
- (38) Harrison, B., Diwell, A. F. and Hallett, C., *Plat. Met. Rev.* **32**, 73 (1988).
- (39) Serre, C., Garin, F., Belot, G. and Maire, G., *J. Catal.* **141**, 1 (1993).
- (40) Niemantsverdriet, J. W., in “*Catalysis*” (Moulijn, J. A., van Leeuwen, P. W. N. M. and van Santen, R. A., eds.), *Studies in Surface Science and Catalysis*, Vol. 79, 363-400, Elsevier, Amsterdam, 1993.
- (41) Anderson, J. R. and Pratt, K. C., “*Introduction to Characterization and Testing of Catalysts*”, 353-433, Academic Press, Australia, 1985.
- (42) Scholten, J. J. F., Pijpers, A. P. and Hustings, A. M. L., *Catal. Rev. Sci. Eng.* **27**, 151 (1985).
- (43) Le Normand, F., Hilaire, L., Kili, K., Krill, G. and Maire, G., *J. Phys. Chem.* **92**, 2561 (1988).
- (44) Hardacre, C., Ormerod, R. M. and Lambert, R. M., *J. Phys. Chem.* **98**, 10901 (1994).
- (45) Shyu, J. Z. and Otto, K., *Appl. Surface Sci.* **32**, 246 (1988).
- (46) Bouwman, R. and Biloen, P., *J. Catal.* **48**, 209 (1977).
- (47) Wagner, C. D., Riggs, W. N., Davis, L. E., Moulder, J. F. and Mullenberg, G. E., “*Handbook of X-ray Photoelectron Spectroscopy*”, Perkin-Elmer Co., Eden Prairie, Minnesota, 1979.
- (48) Briggs, D. and Seah, M. P., “*Practical Surface Analysis*”, Wiley, Chichester, 1984.
- (49) Geus, J. W. and van Veen, J. A. R., in “*Catalysis*” (Moulijn, J. A., van Leeuwen, P. W. N. M. and van Santen, R. A., eds.), *Studies in Surface Science and Catalysis*, Vol. 79, 335-360, Elsevier, Amsterdam, 1993.
- (50) Park, S. H., Tzou, M. S. and Sachtler, W. M. H., *Appl. Catal.* **24**, 85 (1986).
- (51) Anderson, J. R. and Pratt, K. C., “*Introduction to Characterization and Testing of Catalysts*”, 1-53, Academic Press, Australia, 1985.
- (52) Dautzenberg, F. M. and Wolters, H. B. M., *J. Catal.* **51**, 26 (1978).
- (53) Den Otter, G. J. and Dautzenberg, F. M., *J. Catal.* **53**, 116 (1978).
- (54) Ren-Yuan, T., Rong-An, W. and Li-Wu, L., *Appl. Catal.* **10**, 163 (1984).
- (55) Harris, P. J. F., *J. Catal.* **97**, 527 (1986).
- (56) Carballo, L. M. and Wolf, E. E., *J. Catal.* **53**, 366 (1978).
- (57) Kooh, A. B., Han, W. J., Lee, R. G. and Hicks, R. F., *J. Catal.* **130**, 374 (1991).
- (58) Baldwin, T.R. and Burch, R., *Appl. Catal.* **66**, 337 (1990).
- (59) Baldwin, T. R. and Burch, R., *Appl. Catal.* **66**, 359 (1990).
- (60) Curley, J. W., Doctoral Thesis, “*Oxidation Studies on Supported Metal Catalysts*”, Dublin City University, March 1995.

- (61) Jin, T., Okuhara, T., Mains, G. J. and White, J. M., *J. Phys. Chem.* **91**, 3310 (1987).
- (62) Bunluesin, T., Cordatos, H. and Gorte, R. J., *J. Catal.* **157**, 222 (1995).
- (63) Mendelovici, L. and Steinberg, M., *J. Catal.* **93**, 353 (1985).
- (64) Wynblatt, P., in "*Growth and Properties of Metal Clusters*"(Bourdon, J., ed.), Studies in Surface Science and Catalysis, Vol. 4, 15-33, Elsevier, Amsterdam 1980.
- (65) Flynn, P. C. and Wanke, S. E., *J. Catal.* **37**, 432 (1975).
- (66) Murrell, L. L., Tauster, S. J. and Anderson, D. R., in "*Catalysis and Automotive Pollution Control II*" (Crucq, A., ed.), Studies in Surface Science and Catalysis, Vol. 71, 275-289, Elsevier, Amsterdam, 1991.
- (67) Chou, P. and Vannice, M. A., *J. Catal.* **105**, 342 (1987).
- (68) Hubbard, C. P., Otto, K., Gandhi, H. S. and Ng, K. Y. S., *J. Catal.* **139**, 268 (1993).
- (69) Hubbard, C. P., Otto, K., Gandhi, H. S. and Ng, K. Y. S., *J. Catal.* **144**, 484 (1993).
- (70) Briot, P. and Primet, M., *Appl. Catal.* **68**, 301 (1991).
- (71) Ribeiro, F. H., Chow, M. and Dalla Betta, R. A., *J. Catal.* **146**, 537 (1994).

## **CHAPTER 4**

### **Study of Pt-Mn/Al<sub>2</sub>O<sub>3</sub>, Pt-Cr/Al<sub>2</sub>O<sub>3</sub> and Pt-Zr/Al<sub>2</sub>O<sub>3</sub> Catalysts**

## **4.1 Introduction**

In this chapter, the surface characterisation and combustion activity of Al<sub>2</sub>O<sub>3</sub>-supported Pt-Mn, Pt-Cr and Pt-Zr catalysts is discussed. The techniques used for characterisation were Temperature Programmed Reduction (TPR) and H<sub>2</sub> Chemisorption. The activity of the samples for the oxidation of i-C<sub>4</sub>H<sub>10</sub>, both before and after TPR, was investigated. The effects of different aging treatments on the activity and surface properties of the catalysts were also examined.

As discussed in section 1.2, the oxides of Cr and Mn have been reported to be amongst the most active metal oxides for the combustion of hydrocarbons (1-7). Kummer (3) reviewed the potential use of metal oxides as automotive exhaust catalysts and reported that the most active oxides for the oxidation of paraffins included MnO<sub>2</sub> and Cr<sub>2</sub>O<sub>3</sub>.

Anderson et al. (4) examined the oxidation of CH<sub>4</sub> on a variety of supported and unsupported oxides and supported Pt and Pd samples. Supported samples were prepared by impregnation with aqueous nitrate solutions followed by drying and heating in air at 250°C. For Al<sub>2</sub>O<sub>3</sub>-supported metal oxide samples, the activity per gram of active metal was compared. On this basis, Cr<sub>2</sub>O<sub>3</sub> and Mn<sub>2</sub>O<sub>3</sub> were found to be the most active oxides tested. Co<sub>3</sub>O<sub>4</sub> was found to be the most active single component catalyst tested but its' activity decreased when impregnated on alumina, possibly because of the formation of CoAl<sub>2</sub>O<sub>4</sub> (4).

Stein et al. (5) studied the oxidation of eight different C<sub>5</sub> and C<sub>6</sub> hydrocarbons, and reported that oxides of Cr and Mn were amongst the most active catalysts tested with only Co and Ni oxides being more effective. Samples were prepared by precipitation from an aqueous solution of the metal nitrate by adding potassium carbonate solution. The precipitate was then filtered, washed free of potassium salts, dried and sintered in air at 600°C. The phases present were then identified by XRD which showed the oxide formula for the Cr catalyst to be Cr<sub>2</sub>O<sub>3</sub>, while the Mn catalyst was a mixture of Mn<sub>2</sub>O<sub>3</sub> and Mn<sub>3</sub>O<sub>4</sub> (5).

Morooka et al. (7) examined the activity of eight metal oxide catalysts for C<sub>3</sub>H<sub>8</sub> oxidation. Samples were prepared by impregnation of silicon carbide pellets with an aqueous solution of the respective nitrate followed by drying and calcination at either 450 or 600°C. Of the catalysts tested only Co<sub>3</sub>O<sub>4</sub> was more active than Cr<sub>2</sub>O<sub>3</sub> with

MnO<sub>2</sub> and CuO also being considerably more active than the oxides of Ni, Fe, Ce and Th (7).

In light of these findings, potential benefits associated with the addition of the transition metals Cr and Mn, to Pt/Al<sub>2</sub>O<sub>3</sub> catalysts were envisaged in the present study of i-C<sub>4</sub>H<sub>10</sub> oxidation.

The addition of Zr to Pt/Al<sub>2</sub>O<sub>3</sub> was also investigated in view of the high activity of a Pt/ZrO<sub>2</sub> catalyst discussed in section 3.3.3.

Insulators such as ZrO<sub>2</sub> are generally not active oxidation catalysts (1), and Stein et al. (5) reported that ZrO<sub>2</sub> was one of least active of the seventeen different oxides tested for the oxidation of C<sub>5</sub>-C<sub>6</sub> hydrocarbons.

Summers and Ausen (8) investigated the effects of the addition of 0.2 to 8.5 wt.% Zr on the CO oxidation activity of a 0.05 wt.% Pt/Al<sub>2</sub>O<sub>3</sub> catalyst. The catalysts were prepared by impregnation of  $\gamma$ -Al<sub>2</sub>O<sub>3</sub> spheres with solutions of H<sub>2</sub>PtCl<sub>6</sub> and ZrO(NO<sub>3</sub>)<sub>2</sub>. Zr impregnation preceded that of Pt with calcination carried out at 500°C in air for 4 hours after each impregnation step. Thermal aging was performed in air for 6 hours at 900°C. The performance of fresh and thermally aged samples for CO oxidation are compared in Table 4.1.

**Table 4.1 : CO Conversion Data for Fresh and Air-Aged 0.05 wt.% Pt - Zr/Al<sub>2</sub>O<sub>3</sub> Catalysts (8).**

Zr (wt.%)	Pt : Zr*	T <sub>30</sub> ** (°C)	
		Fresh	Aged
0	---	200	280
0.2	1 : 8.5	205	285
0.7	1 : 30	200	285
2.8	1 : 120	200	285
8.5	1 : 356	190	270

\* atomic ratio

\*\* T<sub>30</sub> = temperature of 30% CO conversion

As can be seen from Table 4.1, the presence of Zr at Pt : Zr atomic ratios of 1 : 8.5 to 1 : 356 had no apparent effects on the CO oxidation activity of the Pt catalyst. The authors concluded that ZrO<sub>2</sub> did not interact strongly with the noble metal and therefore had no apparent effects on the activity of the catalysts (8).

## **4.2 Experimental**

### **[a] Activity/TPR Tests.**

The activity and reducibility of catalysts PMn10A, PCr10A and PZr10A were investigated using the sample analysis procedures previously described in section 3.2.5(a). TPR and activity tests were performed as described in sections 3.2.3 and 3.2.4, respectively.

The activity and TPR of calcined samples of PMn1A and PCr1A, and the non-Pt containing samples, Mn10A, Cr10A and Zr10A, were also investigated.

### **[b] Aging Tests**

Samples of the catalysts PMn10A, PCr10A and PZr10A were artificially aged in various environments as described in section 3.2.5(b). The activity of the aged samples was investigated and the effects of aging on Pt surface area determined using H<sub>2</sub> chemisorption.

### **4.3 Results and Discussion**

The TPR profiles (TPR1) of the samples investigated before testing for  $i\text{-C}_4\text{H}_{10}$  oxidation activity are illustrated in Fig. 4.1-4.3. As mentioned previously, quantification of reduction peaks was not attempted due to problems with detector stability and baseline drift. Interpretation was restricted to qualitative purposes.

The reduction profiles obtained for samples Zr10A, Mn10A and Cr10A are shown in Fig. 4.1(a)-(c). For the 2.3 wt.% Zr/ $\text{Al}_2\text{O}_3$  sample, Zr10A, no reduction features were apparent in the temperature range investigated (Fig. 4.1(a)). For the 1.4 wt.% Mn/ $\text{Al}_2\text{O}_3$  sample, Mn10A, a shoulder peak at ca. 410°C is apparent in Fig. 4.1(b), while the profile for 1.33 wt.% Cr/ $\text{Al}_2\text{O}_3$  shows a large reduction peak at ca. 350°C (Fig. 4.1(c)). These features are attributable to the reduction of Mn and Cr species since the  $\text{Al}_2\text{O}_3$  support material showed no  $\text{H}_2$  uptake in the temperature range investigated (see Fig. 3.17(a)).

The profile obtained for PCr10A (i.e. Pt-Cr/ $\text{Al}_2\text{O}_3$ , Pt:Cr = 1:10 atomic ratio) is shown in Fig. 4.2(c) and is clearly not a linear combination of those for samples PA (Fig. 3.20(a)) and Cr10A (Fig. 4.1(c)). This indicates the existence of a bimetallic interaction which affected the surface reduction of the metals (9). After calcination at 630 °C, the TPR profile consists of a large reduction feature centred at ca. 275°C with a small shoulder evident on the low temperature side at ca. 220°C. This peak may be attributable to the combined reduction of both Pt and Cr surface species. Comparison of the profiles obtained for Cr10A and PCr10A indicates that the presence of Pt promoted the reduction of surface Cr species with a shift in the temperature of the main reduction feature from ca.350 to ca.275°C. One possible explanation for the profile obtained for PCr10A is that the shoulder feature at ca. 220°C might be attributable to Pt reduction which then catalyses the subsequent reduction of neighbouring Cr on the catalyst surface (9).

The profile obtained for sample PMn10A after calcination is shown in Fig. 4.2(b) and again indicates the existence of a bimetallic interaction on the  $\text{Al}_2\text{O}_3$  surface since the profile obtained is clearly not a direct superimposition of those for PA (Fig. 3.20(a)) and Mn10A (Fig. 4.1(b)). Instead, the profile consists of a completely new feature at ca. 240°C with shoulders evident at ca. 210°C and ca. 260°C. Again, this feature may be attributable to the combined reduction of Pt and Mn with the shoulder on the low temperature side possibly associated with Pt reduction.

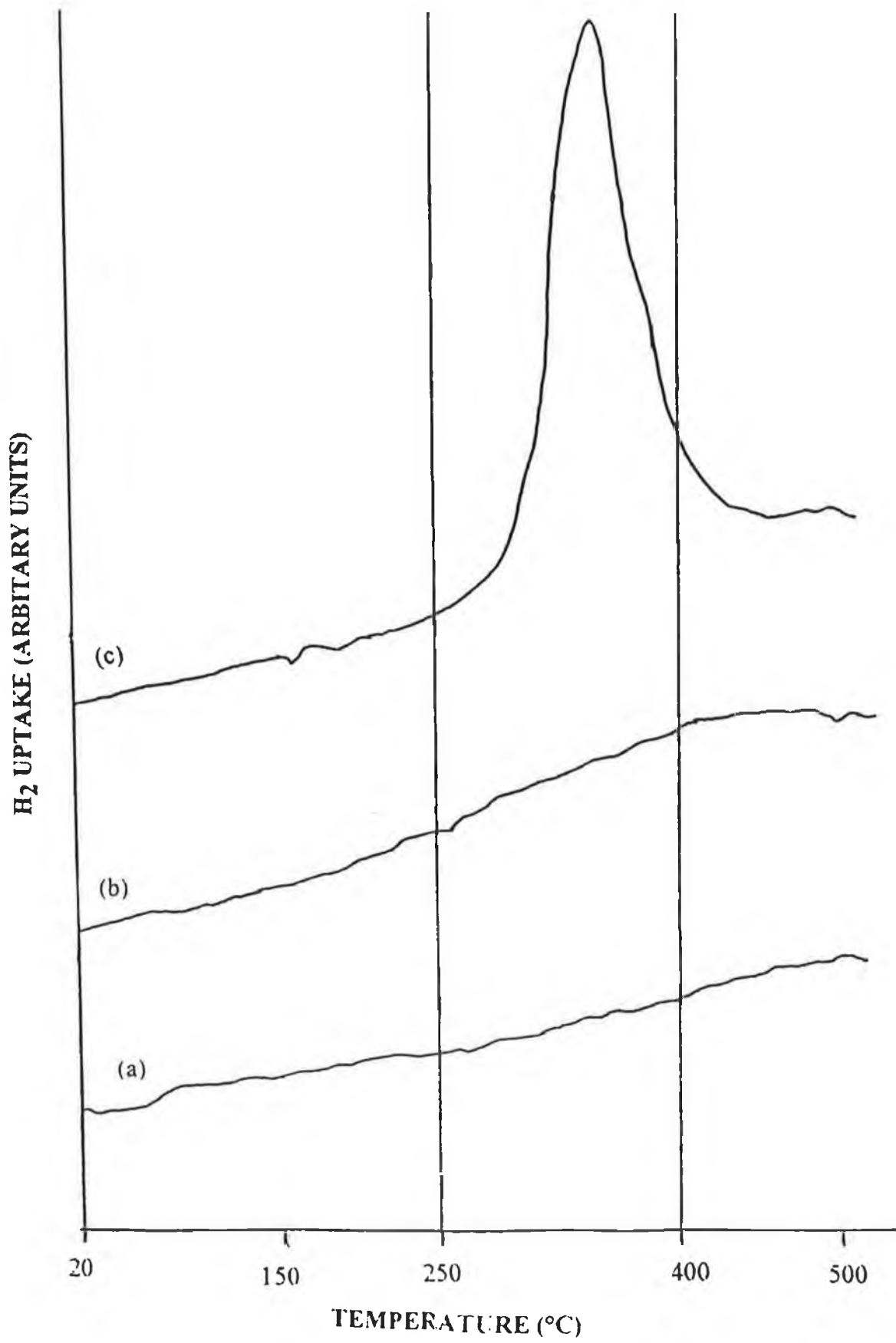


Fig. 4.1 : TPR profiles of calcined samples, (a)-Zr10A, (b)-Mn10A, (c)-Cr10A.

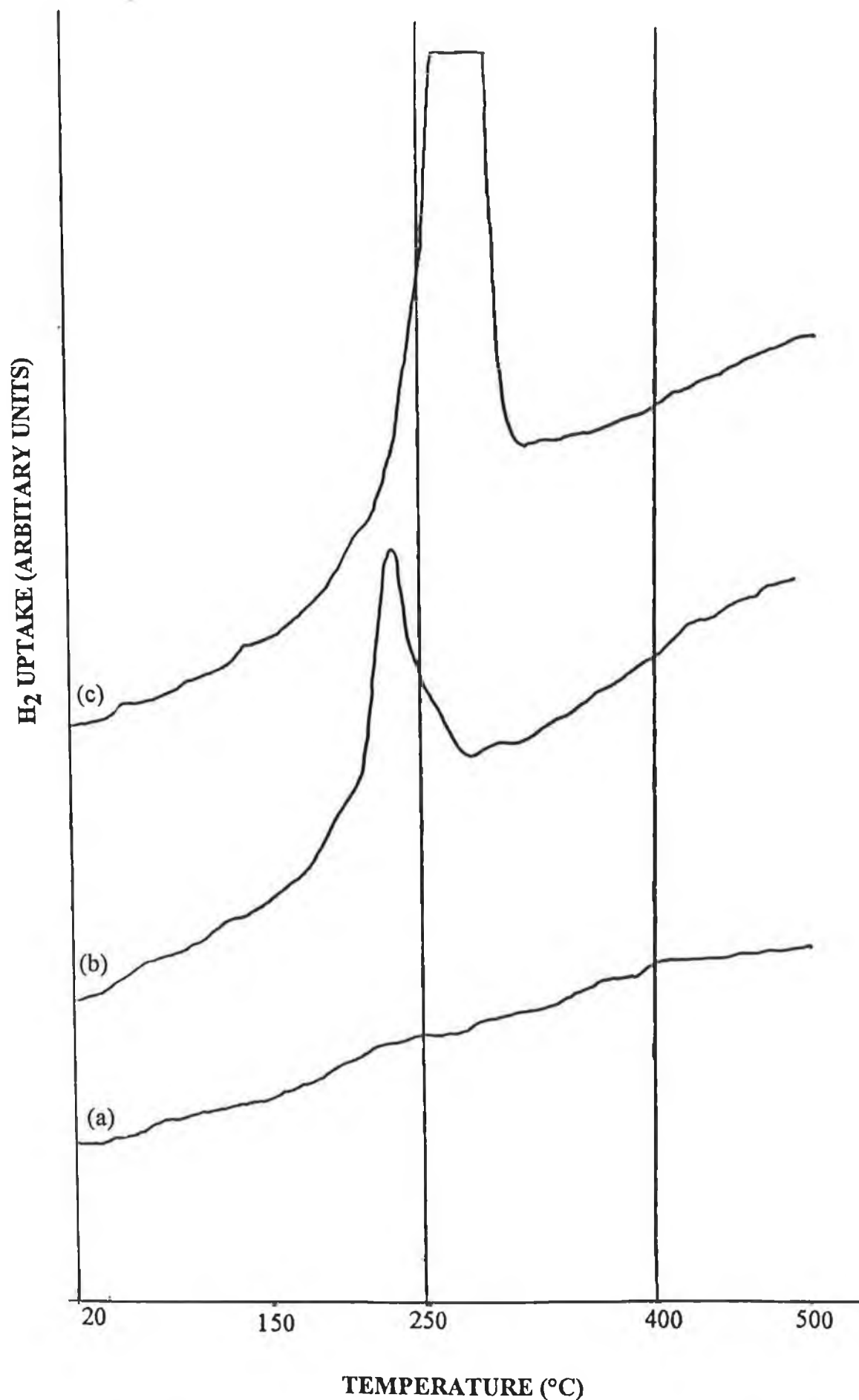


Fig. 4.2 : TPR profiles of calcined samples, (a)-PZr10A, (b)-PMn10A, (c)-PCr10A.

As can be seen from Fig. 4.2(a), the TPR profile for sample PZr10A shows no reduction features in the temperature range 20-500°C. The lack of reduction peaks indicates that Zr appears to have affected either the oxidation or reduction of surface Pt sites since atomic absorption spectroscopy (see section 2.3.2) and H<sub>2</sub> chemisorption results (see section 2.3.3) revealed that the presence of Zr did not appear to significantly affect the uptake of Pt on the support or the number of Pt surface sites.

The TPR profiles obtained for samples PMn1A and PCr1A are illustrated in Fig 4.3. For PMn1A (Fig. 4.3(a)), the lack of reduction features in the profile obtained might be attributed to an interaction between Mn and Pt which inhibited Pt reduction when compared with sample PA in which Pt reduction appeared to occur at ca. 420°C (see Fig. 3.20(a)). However, the profile obtained for PMn1A shows a considerable baseline drift which may have masked any small reduction features present. For PtCr1A, the profile obtained (Fig. 4.3(b)) consists of a peak at ca. 250°C with a shoulder apparent at ca.220°C. This indicates the existence of a Pt-Cr surface interaction similar to that at the higher level of Cr in PCr10A (see Fig. 4.2(c)) with a smaller reduction feature apparent at a slightly lower temperature for PCr1A. At the lower level of Cr in PCr1A, the size of the shoulder feature at ca.220°C relative to the main peak at ca. 250°C was increased compared to sample PCr10A. This supports a theory that the shoulder feature may be due to Pt reduction which then catalyses the subsequent reduction of neighbouring Cr species with the size of the main peak proportional to the amount of Cr present.

Figures 4.4-4.6 illustrate the conversion of i-C<sub>4</sub>H<sub>10</sub> as a function of temperature in Activity Tests A-C for the catalysts PCr10A, PMn10A and PZr10A. The conversion curves for samples PCr1A and PMn1A in Activity Test A are shown in Fig. 4.7. The extent of butane conversion is given in terms of a percentage of the overall amount of butane present prior to reaction. None of the catalysts showed any activity at room temperature and, therefore, only measurements made between 100-350°C are illustrated. For most of the samples examined, the extent of conversion of i-C<sub>4</sub>H<sub>10</sub> increased as the temperature was raised. Total conversion (>99%) was achieved, in most cases, below 350°C. From each curve, the light-off temperature (LOT) was measured as the temperature at which 2.5% conversion of i-C<sub>4</sub>H<sub>10</sub> was achieved. The LOT values for each sample, in the different activity test runs, are shown in Table 4.2. Similarly, the temperatures at which 10% conversion was achieved (T<sub>10</sub> values) are shown in Table 4.3. The temperatures of 50%, T<sub>50</sub>, and 90%, T<sub>90</sub>, conversion are compared in Tables 4.4 and 4.5, respectively. For samples PCr1A, PMn1A, Cr10A, and Mn10A only Activity Test A was performed. For comparison purposes LOT, T<sub>10</sub>, T<sub>50</sub> and T<sub>90</sub> values for samples PA and PZ are also shown in Tables 4.2-4.5.

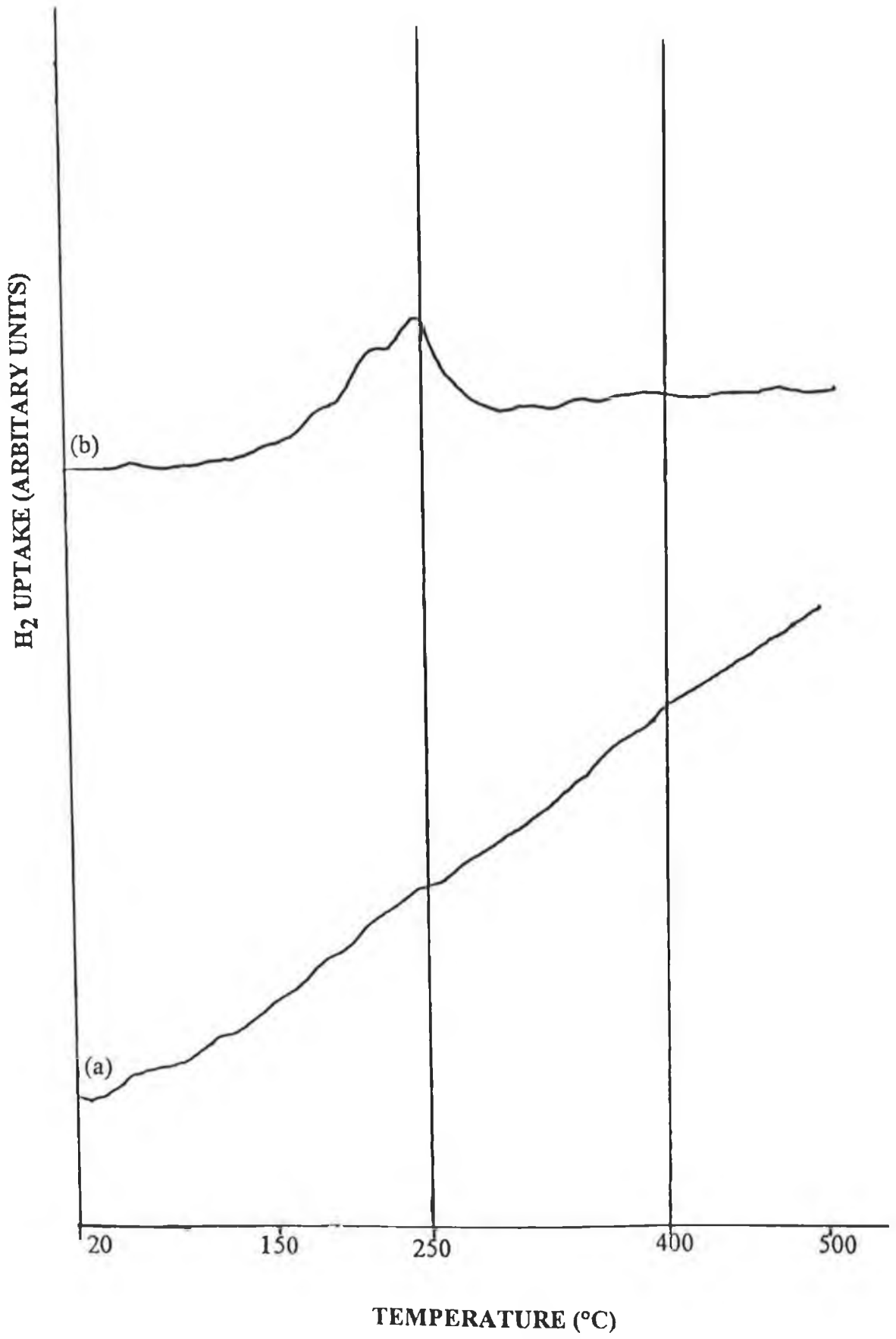


Fig. 4.3 : TPR profiles of calcined samples, (a)-PMn1A, (b)-PCr1A.

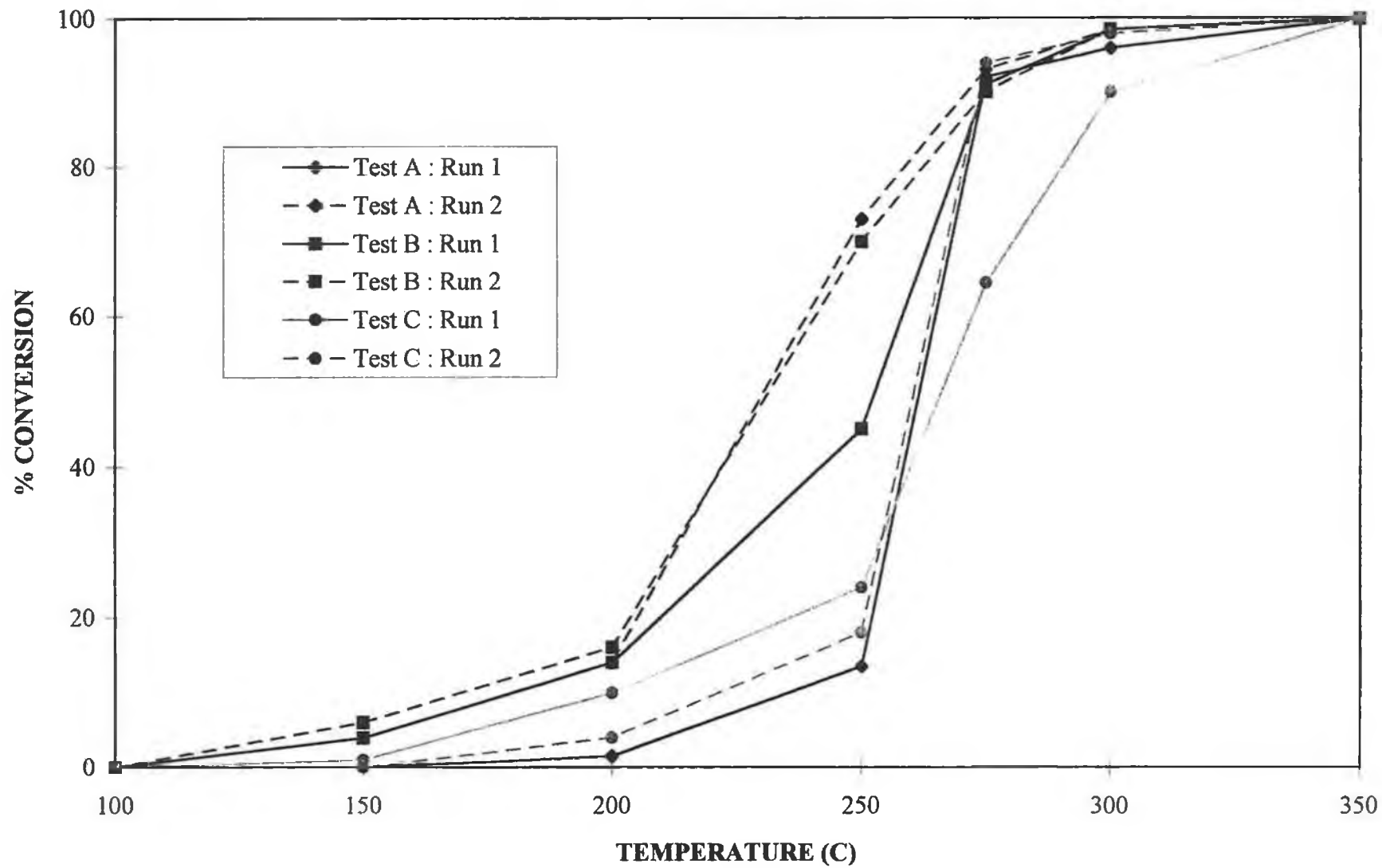


Fig. 4.4 : % iso-Butane Conversion versus Temperature for Sample PCr10A.

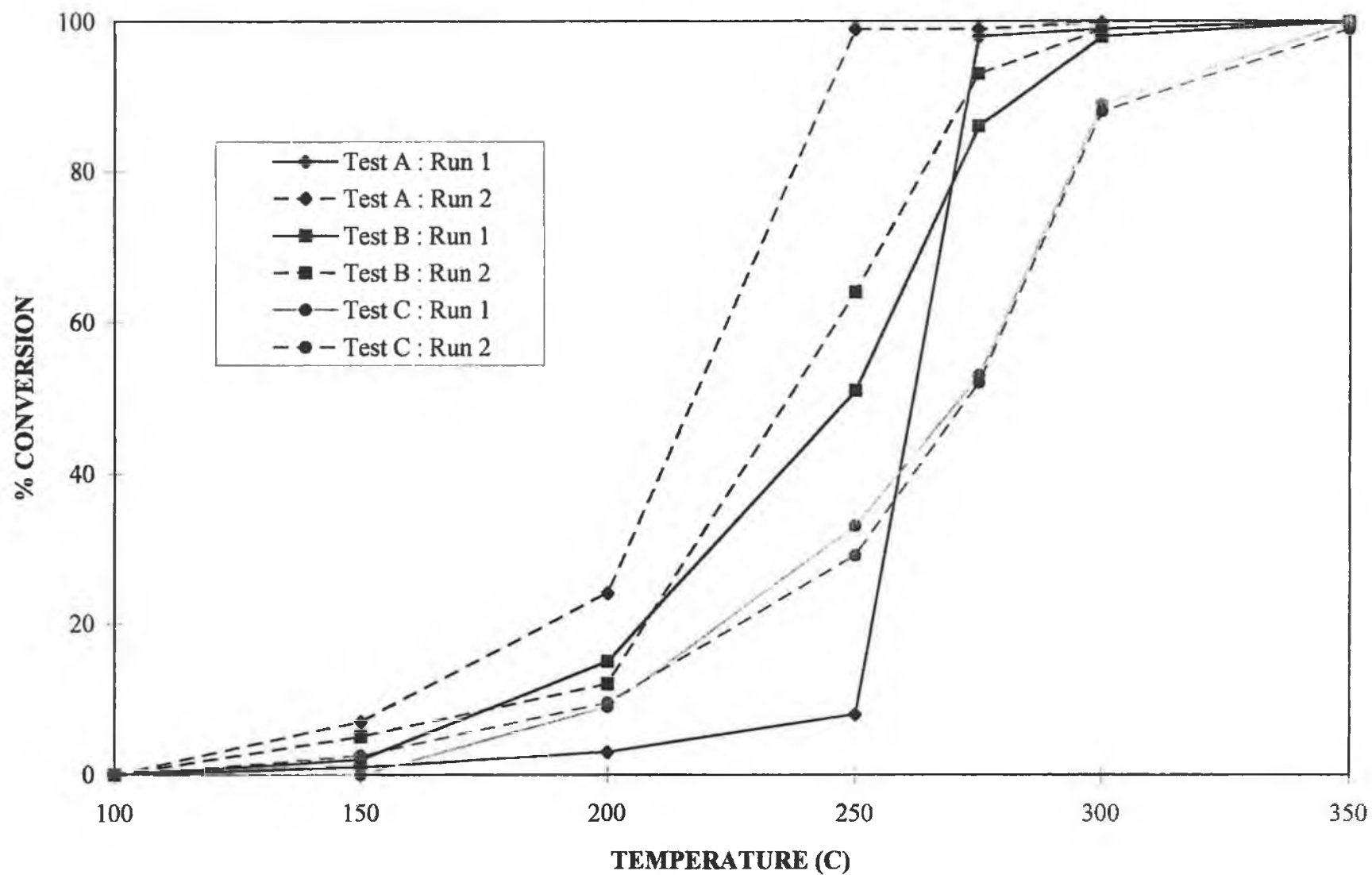


Fig. 4.5 : % iso-Butane Conversion versus Temperature for Sample PMn10A.

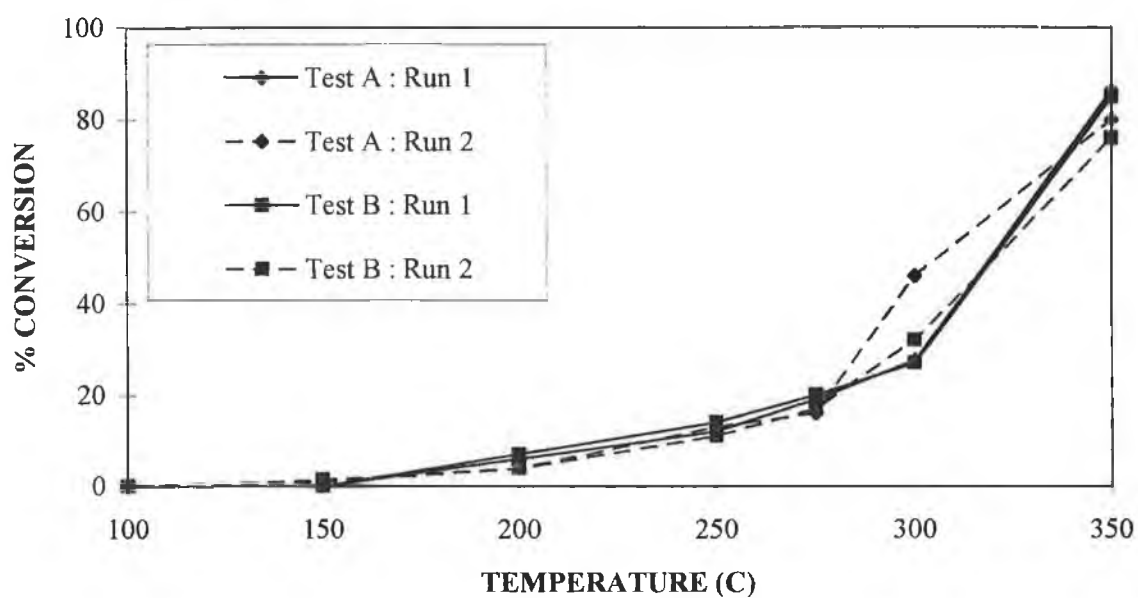


Fig. 4.6 : % i-C<sub>4</sub>H<sub>10</sub> Conversion versus Temperature for Sample PZr10A.

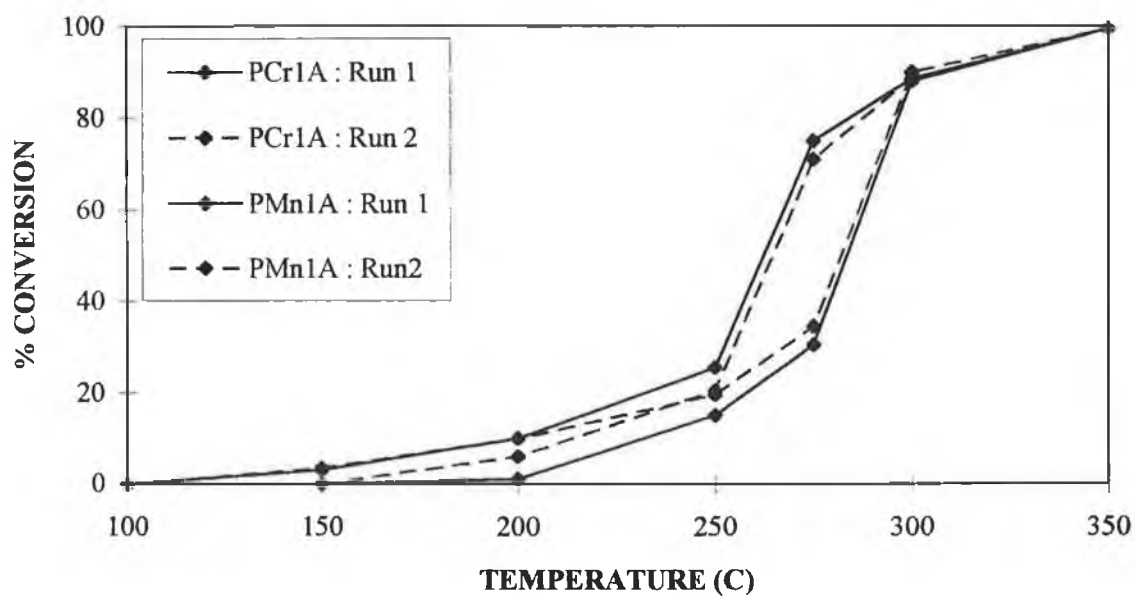


Fig. 4.7 : % i-C<sub>4</sub>H<sub>10</sub> Conversion versus Temperature for Samples PCr1A and PMn1A

**Table 4.2 : Light-off Temperatures (°C) for Iso-Butane Oxidation.**

Sample	Activity Test A		Activity Test B		Activity Test C	
	Run 1	Run 2	Run 1	Run 2	Run 1	Run 2
PA	175	130	140	130	180	215
PZ	100	100	---	---	---	---
PCr1A	205	175	---	---	---	---
PMn1A	150	145	---	---	---	---
PCr10A	205	135	135	125	160	190
PMn10A	205	125	155	135	170	155
PZr10A	170	175	165	175	---	---
Mn10A	225	200	---	---	---	---
Cr10A	200	220	---	---	---	---

**Table 4.3 : Temperatures (°C) of 10% Iso-Butane Conversion (T<sub>10</sub> Values).**

Sample	Activity Test A		Activity Test B		Activity Test C	
	Run 1	Run 2	Run 1	Run 2	Run 1	Run 2
PA	215	185	200	180	295	300
PZ	150	105	---	---	---	---
PCr1A	235	220	---	---	---	---
PMn1A	200	200	---	---	---	---
PCr10A	235	175	175	170	200	220
PMn10A	250	160	180	190	200	200
PZr10A	235	235	225	245	---	---
Mn10A	270	260	---	---	---	---
Cr10A	235	265	---	---	---	---

**Table 4.4 : Temperatures (°C) of 50% Iso-Butane Conversion (T<sub>50</sub> Values).**

Sample	Activity Test A		Activity Test B		Activity Test C	
	Run 1	Run 2	Run 1	Run 2	Run 1	Run 2
PA	260	255	280	275	330	320
PZ	175	125	---	---	---	---
PCr1A	285	265	---	---	---	---
PMn1A	260	280	---	---	---	---
PCr10A	260	230	255	235	265	260
PMn10A	260	215	250	240	270	275
PZr10A	320	305	320	320	---	---
Mn10A	335	340	---	---	---	---
Cr10A	320	330	---	---	---	---

**Table 4.5 : Temperatures (°C) of 90% Iso-Butane Conversion (T<sub>90</sub> Values).**

Sample	Activity Test A		Activity Test B		Activity Test C	
	Run 1	Run 2	Run 1	Run 2	Run 1	Run 2
PA	270	270	290	>300	>350	340
PZ	195	145	---	---	---	---
PCr1A	305	305	---	---	---	---
PMn1A	305	300	---	---	---	---
PCr10A	275	270	275	275	300	275
PMn10A	270	245	285	275	300	305
PZr10A	>350	>350	>350	>350	---	---
Mn10A	>350	400	---	---	---	---
Cr10A	350	>350	---	---	---	---

On initial testing of the calcined samples, oxidation activity was slightly improved in the low temperature region for sample PMn1A (Pt : Mn = 1 : 1) relative to sample PA, with LOT (Table 4.2) and  $T_{10}$  (Table 4.3) values shifted to slightly lower temperatures. However, the  $T_{90}$  value (Table 4.5) was higher for PMn1A relative to PA. On increasing the level of Mn to a Pt : Mn atomic ratio of 1 : 10, low temperature activity disimproved relative to the Pt-only sample while both PA and PMn10A had equivalent  $T_{50}$  and  $T_{90}$  values. Thus, it appeared that the effects of Mn on Pt activity varied depending on the level of Mn present. As discussed above, the TPR profiles for samples PMn1A (Fig. 4.3(a)) and PMn10A (Fig. 4.2(b)) both indicated the existence of a Pt-Mn interaction on the catalyst surface. However, the nature of Pt-Mn interaction at the two levels may have been different as indicated by differences in the TPR profiles in Fig. 4.2(b) and Fig. 4.3(a). A contribution of Mn to the overall activity of both samples cannot be discounted. The  $Al_2O_3$ -supported Mn sample, Mn10A, was less active than the Pt-containing sample, PMn10A, at all temperatures. Although a physical mix of samples PA and Mn10A was not investigated, the activity of PMn10A was less than that expected from the combined activity of PA and Mn10A. For example, at 250°C, 6 and 24% conversion of  $i-C_4H_{10}$  was achieved with samples Mn10A and PA, respectively. For sample PMn10A, conversion was only 8% at the same temperature. This indicates that Pt-Mn interaction in PMn10A had an inhibiting effect on the activity of one or both metals.

Cr had a detrimental effect on the low temperature activity of Pt/ $Al_2O_3$ . In terms of LOT and  $T_{10}$  values, the activity of PCr1A and of PCr10A was less than that of sample PA. For sample PCr1A,  $T_{50}$  and  $T_{90}$  values were also disimproved. However, 50 and 90% conversion of  $i-C_4H_{10}$  were achieved at similar temperatures over PCr10A and PA. In terms of LOT and  $T_{10}$  values, the activity of sample Cr10A was similar to that of the Pt-containing sample, PCr10A. However, 50 and 90% conversion of  $i-C_4H_{10}$  required considerably higher temperatures over Cr10A than over PCr10A establishing the importance of the noble metal for achieving complete conversion at lower temperatures. As for PMn10A, the activity of sample PCr10A was certainly less than that calculated for a linear combination of the activity for samples PA and Cr10A, indicating the existence of Pt-Cr interaction which had a detrimental effect on the activity of one or both metals.

Although the LOT values over samples PA and PZr10A were similar, the activity of the Zr-containing sample was slow to increase with temperature (see Fig. 4.6) and  $T_{50}$  and  $T_{90}$  values were considerably higher than over PA.

Comparison of light-off temperatures for the various samples (Table 4.2) on Activity Test A, Run 1 showed the following order of activity:

PMn1A > PZr10A > PA > Cr10A > PCr1A ≈ PCr10A ≈ PMn10A > Mn10A.

Light-off temperatures were in the range 150-225°C. The order of activity in terms of T<sub>10</sub> (Table 4.3) was as follows:

PMn1A > PA > PZr10A ≈ Cr10A ≈ PCr1A ≈ PCr10A > PMn10A > Mn10A.

T<sub>10</sub> values varied from 200-270°C. T<sub>50</sub> (Table 4.4) values were in the range 260-335°C and showed the following activity trend:

PMn1A ≈ PA ≈ PCr10A ≈ PMn10A > PCr1A > PZr10A ≈ Cr10A > Mn10A.

Finally, T<sub>90</sub> (Table 4.5) values ranged from 270°C to above 350°C and catalyst activity decreased in the order:

PA ≈ PMn10A > PCr10A > PCr1A ≈ PMn1A > Cr10A > PZr10A > Mn10A

Although Mn improved the low temperature activity of Pt/Al<sub>2</sub>O<sub>3</sub> when present at a Pt : Mn atomic ratio of 1 : 1, it can be seen that, in general, the presence of the additive metals did not have any beneficial effects when compared to the oxidation activity of the calcined Pt/Al<sub>2</sub>O<sub>3</sub> sample. As discussed in section 2.3.3, the presence of Cr or Zr did not appear to have any effects on Pt dispersion. Therefore, the effects of Cr and Zr on Pt activity cannot be related to changes in Pt dispersion.

Turnover numbers (TON) values were calculated for the fresh samples at 250°C using the H<sub>2</sub> chemisorption measurements in Table 2.7. The H<sub>2</sub> uptake of each sample was used to calculate the number of surface Pt atoms present and Pt site activity (TON) was calculated in terms of the percentage iso-butane conversion per surface Pt atom. The values calculated are shown in Table 4.6. It should be noted that the Pt site activity calculated for the Cr-containing samples PCr1A and PCr10A in Table 4.6, may be overestimated due to a contribution of Cr to the overall activity. TON values were not calculated for samples PMn1A and PMn10A as no H<sub>2</sub> chemisorption analysis was performed on these samples.

**Table 4.6 : Turnover Numbers for Calcined Catalysts [(% conversion per surface Pt atom at 250°C) × 10<sup>-17</sup>]**

Sample	TON* (% per Pt atom) × 10 <sup>-17</sup>
PA	0.47
PCr1A	0.37
PMn1A	ND
PCr10A	0.32
PMn10A	ND
PZr10A	0.30

ND = not determined.

\* Based on initial activity of the fresh samples.

With the exception of PZr10A, low temperature oxidation activity (LOT) was improved for all Pt-containing samples following initial testing in the stoichiometric air : i-C<sub>4</sub>H<sub>10</sub> mixture (compare Activity Test A, Run 1 and Activity Test A, Run 2 in Table 4.2). Similarly, most Pt catalysts exhibited lower T<sub>10</sub> and T<sub>50</sub> values during Run 2. LOT, T<sub>10</sub> and T<sub>50</sub> values were particularly lowered for samples PCr10A and PMn10A. For example, 10% conversion of i-C<sub>4</sub>H<sub>10</sub> was achieved at 90°C lower for sample PMn10A and 60°C lower for sample PCr10A during Run 2. High temperature performance (T<sub>90</sub>) was enhanced most for sample PMn10A, improved slightly for PCr10A and PMn1A, and remained almost unaffected for samples PA, PCr1A and PZr10A. The pronounced activation of samples PCr10A and PMn10A on exposure to the air : i-C<sub>4</sub>H<sub>10</sub> mixture was due to the presence of both Pt and the transition metals. For sample Mn10A, low temperature activity was improved during Run 2 but the lowering of LOT and T<sub>10</sub> values was not nearly as pronounced as for sample PMn10A. In addition, high temperature activity was disimproved for the non-Pt containing Mn sample, with T<sub>50</sub> and T<sub>90</sub> values shifted to higher temperatures on retesting. The activity of sample Cr10A disimproved during Run 2 with higher temperatures required to achieve 2.5, 10, 50 and 90% conversion of i-C<sub>4</sub>H<sub>10</sub>. Therefore, activation after initial testing was greatest for samples containing both Pt and either Mn or Cr. Activation was larger for the higher levels of the transition metals i.e. samples PCr10A and PMn10A rather than samples PCr1A and PMn1A.

During Activity Test A, Run 2, the presence of Mn at ten times the atomic level of Pt resulted in improved activity relative to Pt/Al<sub>2</sub>O<sub>3</sub> at all temperatures. PCr10A was also more active than PA in terms of the temperature required for 10 and 50%

conversion and both samples had similar LOT and  $T_{90}$  values. All the other samples were less active than PA.

The order of decreasing activity in terms of LOT during Run 2 was:

PMn10A > PA > PCr10A > PMn1A > PCr1A  $\approx$  PZr10A > Mn10A > Cr10A

LOT values were in the range 125-220°C.

$T_{10}$  values were between 160-265°C and followed the activity trend:

PMn10A > PCr10A > PA > PMn1A > PCr1A > PZr10A > Mn10A > Cr10A.

$T_{50}$  values of between 215-340°C were found and catalyst activity decreased in the order:

PMn10A > PCr10A > PA > PCr1A > PMn1A > PZr10A > Cr10A > Mn10A.

$T_{90}$  was achieved in the range 245 to above 350°C and catalyst activity decreased according to:

PMn10A > PCr10A  $\approx$  PA > PMn1A > PCr1A > PZr10A  $\approx$  Cr10A > Mn10A.

TPR profiles (TPR2) obtained for the catalysts PMn10A, PCr10A and PZr10A after Activity Test A are illustrated in Fig. 4.8.

The profile obtained for sample PCr10A (Fig. 4.8(a)) after testing contains a reduction feature at ca.270°C with a shoulder evident on the low temperature side at ca.235°C. The TPR profile of the calcined sample (Fig. 4.2(c)) contained a similar feature in the same temperature region but the  $H_2$  uptake was decreased considerably after exposure to the oxidation mixture. As discussed previously, this feature may be associated with the reduction of a Pt-Cr interactive surface species. The profile obtained after testing contains an additional peak above 400°C. This latter feature is at approximately the same temperature as that associated with the reduction of a Pt- $Al_2O_3$  interactive species (420-450°C) in Pt/ $Al_2O_3$  and Pt-Ce/ $Al_2O_3$  catalysts after exposure to the stoichiometric air : i- $C_4H_{10}$  mixture as discussed in section 3.3.2. The appearance of this feature in the profile of PCr10A after testing may indicate that migration of some Pt to surface sites where it experienced closer interaction with the  $Al_2O_3$  support rather than the Cr additive had occurred. The decrease in the size of the proposed Pt-Cr reduction feature at ca.270°C after testing would support such a theory.

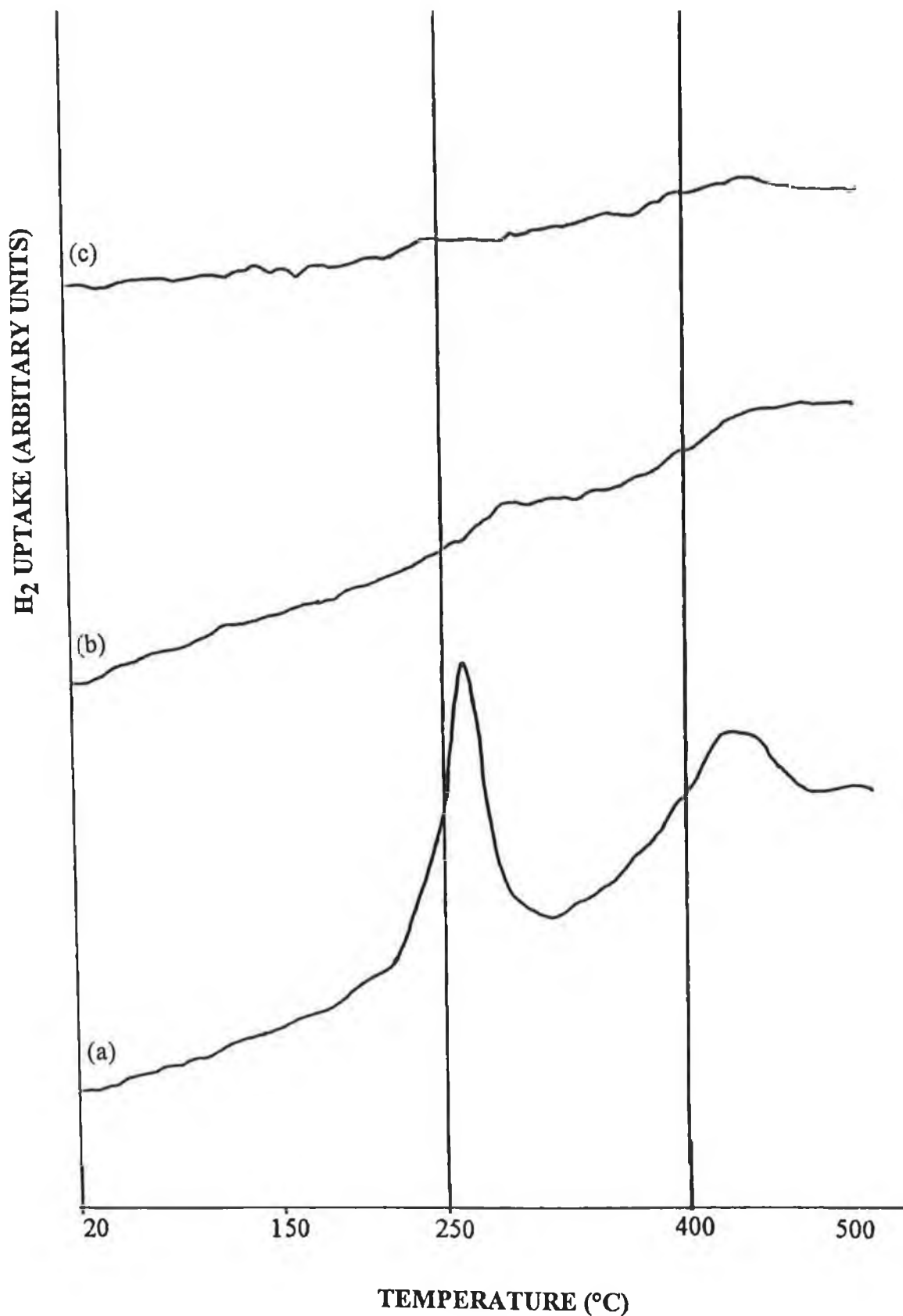


Fig 4.8 : TPR profiles of samples after Activity Test A, (a)-PCr10A, (b)-PMn10A, (c)-PZr10A.

The TPR profile obtained for sample PMn10A after Activity Test A (Fig. 4.8(b)) indicates that a distinct loss of reducible surface sites had occurred when compared with the calcined sample (see Fig. 4.2(b)). Comparison of the profiles for samples PMn10A (Fig. 4.8(b)) and PA (Fig. 3.34(a)) after Activity Test A indicates that the presence of Mn still affected Pt reducibility after testing. This was presumably due to some form of Pt-Mn interaction. The profile obtained in Fig. 4.8(b) shows small reduction features at ca.300°C and above 400°C. The former may correspond with the feature at ca.240°C in the calcined sample, shifted to a higher temperature after testing. As discussed previously, this feature in the calcined sample was possibly attributable to the combined reduction of Pt and Mn in an interactive surface species. The small peak above 400°C may be associated with either Pt or Mn on Al<sub>2</sub>O<sub>3</sub> as TPR profiles of PA and Mn10A both exhibited reduction features in this temperature region.

The profile obtained for sample PZr10A after Test A is shown in Fig. 4.8(c) and, as for the calcined sample (Fig. 4.1(a)), shows no major reduction features in the temperature range 20-500°C. The lack of reduction peaks indicates that Zr affected the reduction characteristics of surface Pt.

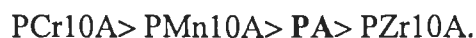
The activity of samples PMn10A, PCr10A and PZr10A was reinvestigated after TPR in Activity Test B. Comparison of catalyst activity in Test A, Run 2, and Test B, Run 1, shows that the effect of TPR varied depending on the catalyst. From Fig. 4.5, it is evident that the activity of the Pt-Mn sample was lower after reduction. As discussed in section 3.3.2, the activity of sample PA also decreased after TPR with higher temperatures required to achieve 2.5, 10, 50 and 90% i-C<sub>4</sub>H<sub>10</sub> conversion (see Tables 4.2-4.5). For PCr10A, LOT, T<sub>10</sub> and T<sub>90</sub> values were almost unaffected by TPR while T<sub>50</sub> disimproved. The low temperature activity of sample PZr10A was improved slightly with LOT and T<sub>10</sub> values lowered by 10°C. However, T<sub>50</sub> was disimproved after TPR.

From Tables 4.2-4.5, it can be seen that during Test B, Run 1, sample PCr10A was more active than PA in terms of LOT, T<sub>10</sub>, T<sub>50</sub> and T<sub>90</sub>. Sample PMn10A was also more active than sample PA in terms of T<sub>10</sub>, T<sub>50</sub> and T<sub>90</sub>, but light-off was achieved at a lower temperature over the Pt-only sample. Sample PZr10A was the least active catalyst at all temperatures tested.

During Test B, Run 1, the order of activity in terms of LOT in the region 135-165°C was:



T<sub>10</sub> was reached between 175-225°C and catalytic activity decreased as follows:



In relation to T<sub>50</sub> values in the range 250-320°C, the activity trend was:



90% conversion of i-C<sub>4</sub>H<sub>10</sub> required temperatures ranging from 275°C to above 350°C, with the order of activity being:



On remeasuring the activity of the reduced samples in Activity Test B, Run 2, sample PCr10A was again more active than PA at all temperatures. PMn10A was also more active than PA in terms of T<sub>50</sub> and T<sub>90</sub>, but was less active than the Pt-only sample at lower temperatures with slightly higher temperatures required for light-off and 10% i-C<sub>4</sub>H<sub>10</sub> conversion. Again, sample PZr10A was the least active sample tested.

During Test B, Run 2, LOT values varied from 125-175°C. In this temperature region, catalyst activity was in the same order as for Test B, Run 1. In terms of T<sub>10</sub>, catalyst activity decreased in the same order in the temperature range 170-245°C. T<sub>50</sub> values varied from 235-320°C with catalytic activity decreasing as follows:



For T<sub>90</sub>, which varied from 275°C to above 350°C, the order of activity was:



TPR profiles (LTPR) obtained for the samples PCr10A and PMn10A after Activity Test B are illustrated in Fig. 4.9.

The profile obtained for sample PCr10A is shown in Fig. 4.9(a) and consists of a peak at ca.285°C with a larger feature evident at ca.450-470°C. The former feature is probably associated the feature seen at ca.270-275°C in Figures 4.2(c) and 4.8(a) and decreased in size during Tests A and B. As discussed previously, this peak might be attributed to the presence of a Pt-Cr surface interaction. The higher temperature peak may be associated with the reduction of a Pt-Al<sub>2</sub>O<sub>3</sub> interactive surface species and

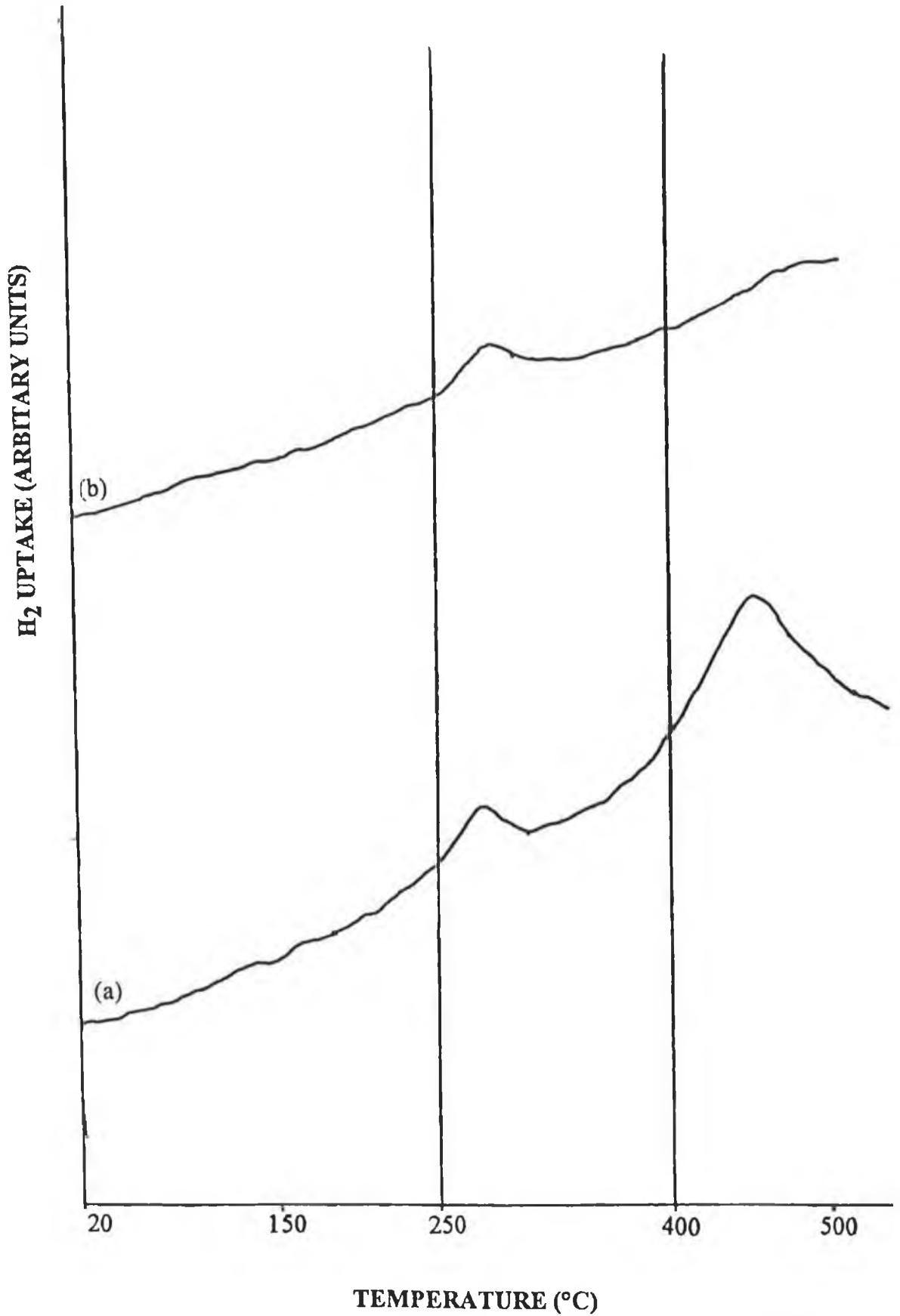


Fig 4.9 : TPR profiles of samples after Activity Test B, (a)-PCr10A, (b)-PMn10A.

increased in size with increasing time in the reaction mixture (compare Figures 4.2(c), 4.8(a) and 4.9(a)). The change in the relative size of the two reduction features after testing may indicate migration of Pt from sites where it was in strong interaction with Cr to surface sites of greater interaction with the Al<sub>2</sub>O<sub>3</sub> support.

The LTPR profile for sample PMn10A after Test B is shown in Fig. 4.9(b) and is similar to that obtained after Test A (see Fig. 4.8(b)) with small reduction features evident at ca. 285°C and above 400°C. As discussed previously, the former might be attributed to the reduction of a Pt-Cr interactive species and the latter feature to Pt-Al<sub>2</sub>O<sub>3</sub> or Mn-Al<sub>2</sub>O<sub>3</sub> species.

The activity of samples PA, PCr10A and PMn10A was retested after LTPR and the conversion curves determined in Activity Test C are shown in Figures 3.23, 4.4 and 4.5, respectively. It is evident that the activity of all three samples was adversely affected by reduction at 500°C. As for Ce-containing samples (see section 3.3.2), the presence of Cr or Mn appeared to help prevent loss of activity upon reduction. Comparison of LOT, T<sub>10</sub>, T<sub>50</sub> and T<sub>90</sub> values for Activity Test B, Run 2, and Activity Test C, Run 1, shows that deactivation was less significant for samples PCr10A and PMn10A than for PA.

In Activity Test C, the Pt-Cr/Al<sub>2</sub>O<sub>3</sub> and Pt-Mn/Al<sub>2</sub>O<sub>3</sub> samples were more active than Pt/Al<sub>2</sub>O<sub>3</sub> in terms of LOT, T<sub>10</sub>, T<sub>50</sub> and T<sub>90</sub> values in both Run 1 and Run 2. In Run 1, PCr10A was more active than PMn10A in terms of LOT and T<sub>50</sub> with the same temperatures required for 10 and 90% conversion on both catalysts. In Run 2, PMn10A was more active than PCr10A in terms of LOT and T<sub>10</sub>, but the activity order was reversed in terms of T<sub>50</sub> and T<sub>90</sub> values.

To summarise the activity results for the calcined samples, it appeared that the i-C<sub>4</sub>H<sub>10</sub> oxidation activity of calcined Pt/Al<sub>2</sub>O<sub>3</sub> was affected by the addition of Cr, Mn or Zr. TPR profiles indicated the existence of bimetallic surface interactions which may have been associated with the effects of the additive metals on the activity of Al<sub>2</sub>O<sub>3</sub>-supported Pt. The activity of the various catalysts depended on the loading of the additive metal and was affected by testing in the stoichiometric air : iso-butane mixture. Reduction in a 5% H<sub>2</sub>/95% Ar mixture also affected catalyst activity. The presence of Mn or Cr was potentially beneficial depending on all of these variables.

On initial testing of the calcined catalysts, the effect of Mn on the i-C<sub>4</sub>H<sub>10</sub> oxidation activity of Pt/Al<sub>2</sub>O<sub>3</sub> depended on the loading of Mn and also on catalyst temperature. At a Pt : Mn atomic ratio of 1 : 1 in PMn1A, low temperature activity was improved relative to sample PA with 10% conversion achieved at lower temperatures on

the former sample. However, Pt/Al<sub>2</sub>O<sub>3</sub> was at least as active as both Mn-containing samples at higher temperatures. For samples PCr1A and PCr10A, no beneficial effects of the presence of Cr were observed compared with Pt/Al<sub>2</sub>O<sub>3</sub>. The Pt-only sample was at least as active as, and generally more active than, both Pt-Cr catalysts during initial testing after calcination. Turnover numbers calculated at 250°C indicated that Pt site activity was greatest in the Pt-only sample.

Although the activity of some catalysts decreased at certain temperatures after initial testing, exposure of the Pt-catalysts to the stoichiometric air : iso-butane reaction mixture generally resulted in improved activity during subsequent testing. This was particularly true in terms of LOT, T<sub>10</sub> and T<sub>50</sub> values. T<sub>90</sub> was also significantly improved for sample PMn10A.

Possible explanations for the activation of the calcined Pt catalysts during initial testing have been previously discussed in section 3.3.2. These include the removal of a deactivating chloride species (10, 11), a favourable change in Pt particle morphology induced during reaction (12, 13) or the sintering of dispersed Pt to produce more active larger metal particles.

Activation of calcined samples in the reaction mixture was most pronounced for samples containing Pt and either Mn or Cr at a Pt : TM (TM = transition metal) atomic ratio of 1 : 10. Activation was not as significant for samples PCr1A or PMn1A with lower levels of TM or for the TM-only samples Cr10A and Mn10A. On this basis, it is concluded that activation was most pronounced for Pt-TM interactive sites with a certain level of TM required. For the Pt-Zr sample, PZr10A, no significant improvements in i-C<sub>4</sub>H<sub>10</sub> conversion occurred following exposure to the reaction mixture. Pt-Zr interaction appeared to inhibit activation of Pt/Al<sub>2</sub>O<sub>3</sub> at low temperatures.

After initial activation of the calcined samples in the air : i-C<sub>4</sub>H<sub>10</sub> mixture, sample PMn10A was more active than the Pt-only sample PA. In addition, the presence of Cr at ten times the atomic ratio of Pt in PCr10A led to increased activity at certain temperatures after initial testing. However, sample PA was more active than all the other bimetallic samples.

After reduction in 5% H<sub>2</sub>/95% Ar, increases in the activity of Pt/Al<sub>2</sub>O<sub>3</sub> on addition of Mn or Cr at ten times the atomic level of Pt were still evident.

After TPR from 20 to 500°C, PCr10A was more active than PA at all temperatures tested. PMn10A was also more active than PA after TPR, particularly at

higher temperatures with 50 and 90% conversion of  $i\text{-C}_4\text{H}_{10}$  achieved at lower temperatures.

The activity of samples PCr10A, PMn10A and PA all decreased after prolonged reduction in the 5%  $\text{H}_2/95\%$  Ar mixture at  $500^\circ\text{C}$  for 2.5h in the LTPR step of the analysis procedure. However, the transition metals appeared to help reduce the extent of deactivation and the bimetallic samples were more active than  $\text{Pt}/\text{Al}_2\text{O}_3$  during subsequent tests.

On the basis of the results obtained, it is only possible to speculate on the reasons for the beneficial effects of Mn and Cr on the activity of  $\text{Pt}/\text{Al}_2\text{O}_3$  observed after activation in the oxidation mixture and after pre-reduction. A contribution of Mn and Cr to the overall activity of the bimetallic samples was expected since samples Mn10A and Cr10A both catalysed  $i\text{-C}_4\text{H}_{10}$  conversion in the temperature range investigated. TPR experiments showed the existence of bimetallic surface interactions in Pt-Cr and Pt-Mn samples. The exact nature of these interactive species is unknown. However, this bimetallic interaction had a detrimental effect on the activity of calcined samples and may also have been involved in the increased activity of samples PCr10A and PMn10A relative to PA after reduction.

The Pt-Zr/ $\text{Al}_2\text{O}_3$  (Pt : Zr = 1 : 10) catalyst tested was less active than  $\text{Pt}/\text{Al}_2\text{O}_3$  both before and after TPR from 20- $500^\circ\text{C}$ . This may be related to a slightly lower Pt content in sample PZr10A (0.40 wt.%) compared with sample PA (0.53 wt.%) as measured by atomic absorption spectroscopy (see Table 2.5). However, this was not the sole reason for the lower activity of sample PZr10A. Turnover numbers (see Table 4.6) for calcined samples PA and PZr10A showed that Pt site activity was lower in the Zr-containing sample. Samples PCr10A (0.41 wt.% Pt) and PMn10A (0.41 wt.% Pt) had similar Pt contents but were also generally more active than PZr10A. The negative effect of Zr on the  $i\text{-C}_4\text{H}_{10}$  oxidation activity of  $\text{Pt}/\text{Al}_2\text{O}_3$  contrasts with the results of a previous study of CO oxidation (8). As discussed previously, Summers and Ausen (8) reported that the presence of Zr at Pt : Zr atomic ratios of 1 : 8.5 to 1 : 356 had no apparent effects on the dispersion or CO oxidation activity of a  $\text{Pt}/\text{Al}_2\text{O}_3$  catalyst. The authors concluded that  $\text{ZrO}_2$  did not interact strongly with the noble metal and therefore had no apparent effects on the activity of the catalysts (8). In the present study, the addition of 2.3 wt.% Zr to a 0.5 wt.%  $\text{Pt}/\text{Al}_2\text{O}_3$  did not have any effect on Pt dispersion as measured by  $\text{H}_2$  chemisorption (see Table 2.7). However, the reducibility of surface Pt in TPR experiments was affected by some form of Pt-Zr interaction which also resulted in decreased activity for  $i\text{-C}_4\text{H}_{10}$  oxidation. One possible explanation for the

discrepancy between the results obtained in the present study and those obtained in (8) might be the difference in preparation conditions employed.

As discussed previously,  $ZrO_2$  has been reported to be a less reactive support than  $Al_2O_3$  towards Pt (10, 14, 15). Hubbard et al. (14) thought that the low reactivity of  $ZrO_2$  towards supported Pt could explain the greater  $C_3H_8$  oxidation activity found for highly dispersed Pt when supported on  $ZrO_2$  rather than on  $Al_2O_3$ . For Pt/ $Al_2O_3$  samples, lower activity for highly dispersed Pt relative to larger Pt crystallites was attributed to deactivation of smaller well dispersed Pt particles due to interaction with the support material. No such effects were reported for Pt/ $ZrO_2$  samples (14). In view of these studies (8, 10, 14, 15), the considerable effects of Zr on the TPR and oxidation activity of Pt/ $Al_2O_3$  in the current study are difficult to explain. However the results obtained do indicate that the higher activity of 0.5 wt.% Pt/ $ZrO_2$  relative to 0.5 wt.% Pt/ $Al_2O_3$  after calcination (see section 3.3.3) is likely to be due to the presence of larger Pt particles on the lower surface area  $ZrO_2$  support material rather than a lower reactivity of  $ZrO_2$  compared to  $Al_2O_3$  as reported in the study by Hubbard and co-workers (14).

As discussed in section 3.3.3,  $i-C_4H_{10}$  oxidation over Pt/ $Al_2O_3$  and Pt-Ce/ $Al_2O_3$  catalysts was found to be a structure sensitive reaction with larger Pt particles more active than highly dispersed Pt. In order to investigate the possibility of structure sensitivity in the bimetallic catalysts being investigated in this section of the study, samples PCr10A, PMn10A and PZr10A were artificially aged under conditions expected to induce sintering of surface Pt. After aging of the calcined catalysts in air at  $800^\circ C$ , the available Pt surface area of each was reinvestigated using  $H_2$  chemisorption. The  $H_2$  chemisorption uptakes of fresh and aged catalysts are compared in Table 4.7.

From Table 4.7, it can be seen that the chemisorption capacity of the  $Al_2O_3$ -supported samples was considerably depleted after aging in air. As discussed in section 3.3.3, the most probable reason for the apparent loss of Pt surface area in the aged samples was sintering of dispersed Pt to form larger particles in which only the outer Pt atoms are capable of  $H_2$  adsorption. From Table 4.7, it is seen that aging of sample PA in the stoichiometric air :  $i-C_4H_{10}$  mixture and in Ar also resulted in a significant decrease in available Pt surface area which indicates that sintering of  $Al_2O_3$ -supported Pt also occurred in these atmospheres. Although the  $H_2$  chemisorption uptakes of the bimetallic samples after aging in the reaction mixture or in Ar were not measured it is expected that Pt sintering will also have occurred for these samples.

**Table 4.7 : H<sub>2</sub> Chemisorption Measurements after Aging in Various Atmospheres**

Sample	Parameter	Fresh*	Air-Aged	Air:i-C <sub>4</sub> H <sub>10</sub> -Aged	Argon-Aged
PA	H <sub>2</sub> Uptake (cm <sup>3</sup> g <sup>-1</sup> )	0.336	0.026	0.015	0.011
	S <sub>Pt</sub> (m <sup>2</sup> g <sup>-1</sup> )	1.45	0.11	0.06	0.05
PCr10A	H <sub>2</sub> Uptake (cm <sup>3</sup> g <sup>-1</sup> )	0.259	0.005	ND	ND
	S <sub>Pt</sub> (m <sup>2</sup> g <sup>-1</sup> )	1.11	0.02	ND	ND
PMn10A	H <sub>2</sub> Uptake (cm <sup>3</sup> g <sup>-1</sup> )	ND	0.020	ND	ND
	S <sub>Pt</sub> (m <sup>2</sup> g <sup>-1</sup> )	ND	0.09	ND	ND
PZr10A	H <sub>2</sub> Uptake (cm <sup>3</sup> g <sup>-1</sup> )	0.251	0.014	ND	ND
	S <sub>Pt</sub> (m <sup>2</sup> g <sup>-1</sup> )	1.08	0.06	ND	ND

\* Unaged sample i.e. after impregnation and calcination at 630°C.

S<sub>Pt</sub> = Pt Surface Area.

ND = not determined.

After aging in the different atmospheres, the conversion of i-C<sub>4</sub>H<sub>10</sub> as a function of temperature is shown for samples PCr10A, PMn10A and PZr10A in Fig. 4.10-4.12. The performance of the fresh and aged samples are compared in Tables 4.8-4.10, in terms of the temperatures at which 10, 50 and 90% conversion of i-C<sub>4</sub>H<sub>10</sub> was achieved. For comparison purposes, T<sub>10</sub>, T<sub>50</sub> and T<sub>90</sub> values for sample PA are also shown.

**Table 4.8 : Temperatures (°C) of 10% Iso-Butane Conversion over Catalyst Samples after Aging in Various Atmospheres.**

Sample	Fresh*		Air-Aged		Air:i-C <sub>4</sub> H <sub>10</sub> -Aged		Argon-Aged	
	Run 1	Run 2	Run 1	Run 2	Run 1	Run 2	Run 1	Run 2
PA	215	185	105	105	105	105	190	170
PCr10A	235	175	155	165	140	140	155	185
PMn10A	250	160	155	150	110	105	205	200
PZr10A	235	235	155	155	ND	ND	165	185

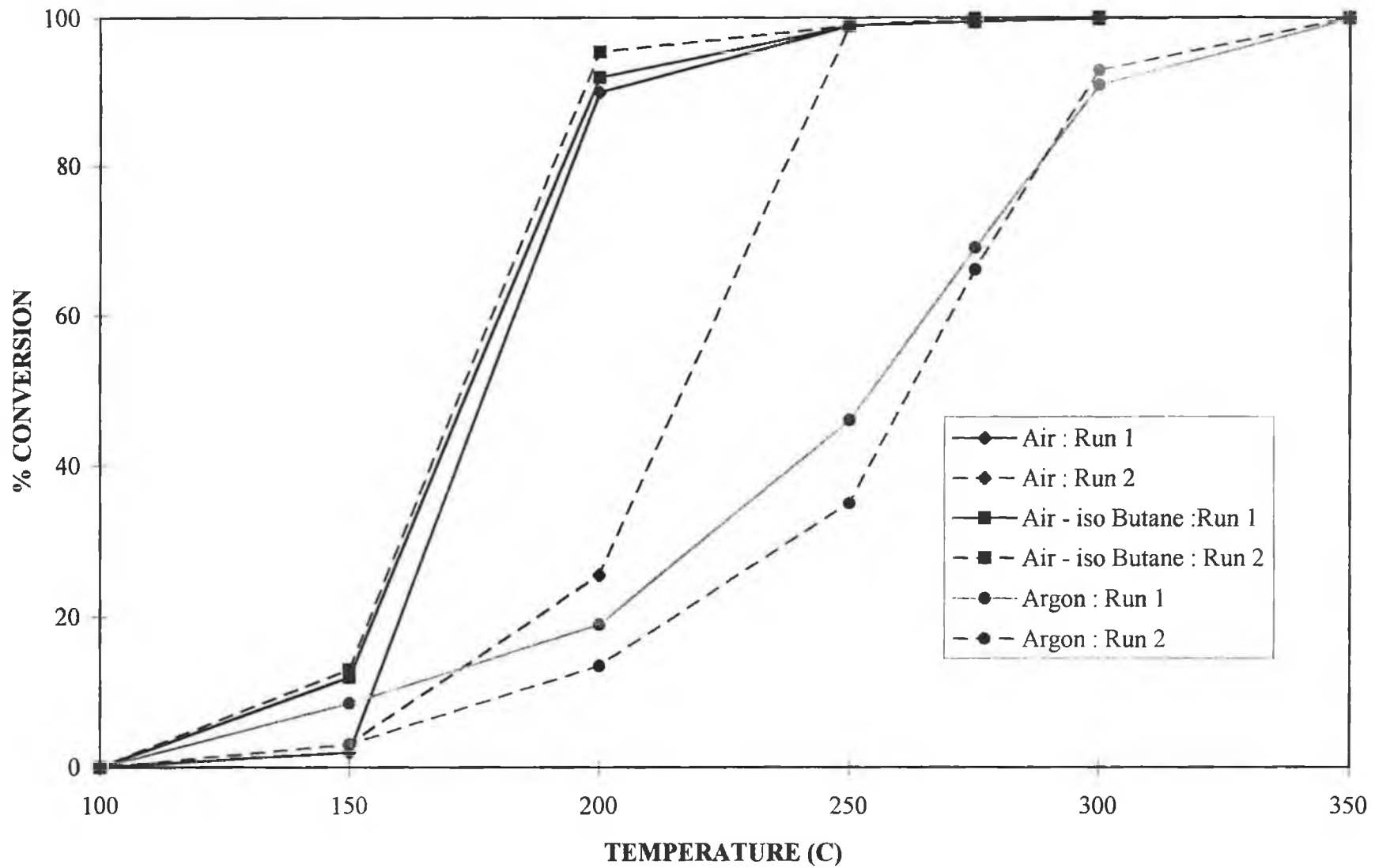


Fig. 4.10 : % iso-Butane Conversion versus Temperature for Sample PCr10A after aging in various atmospheres.

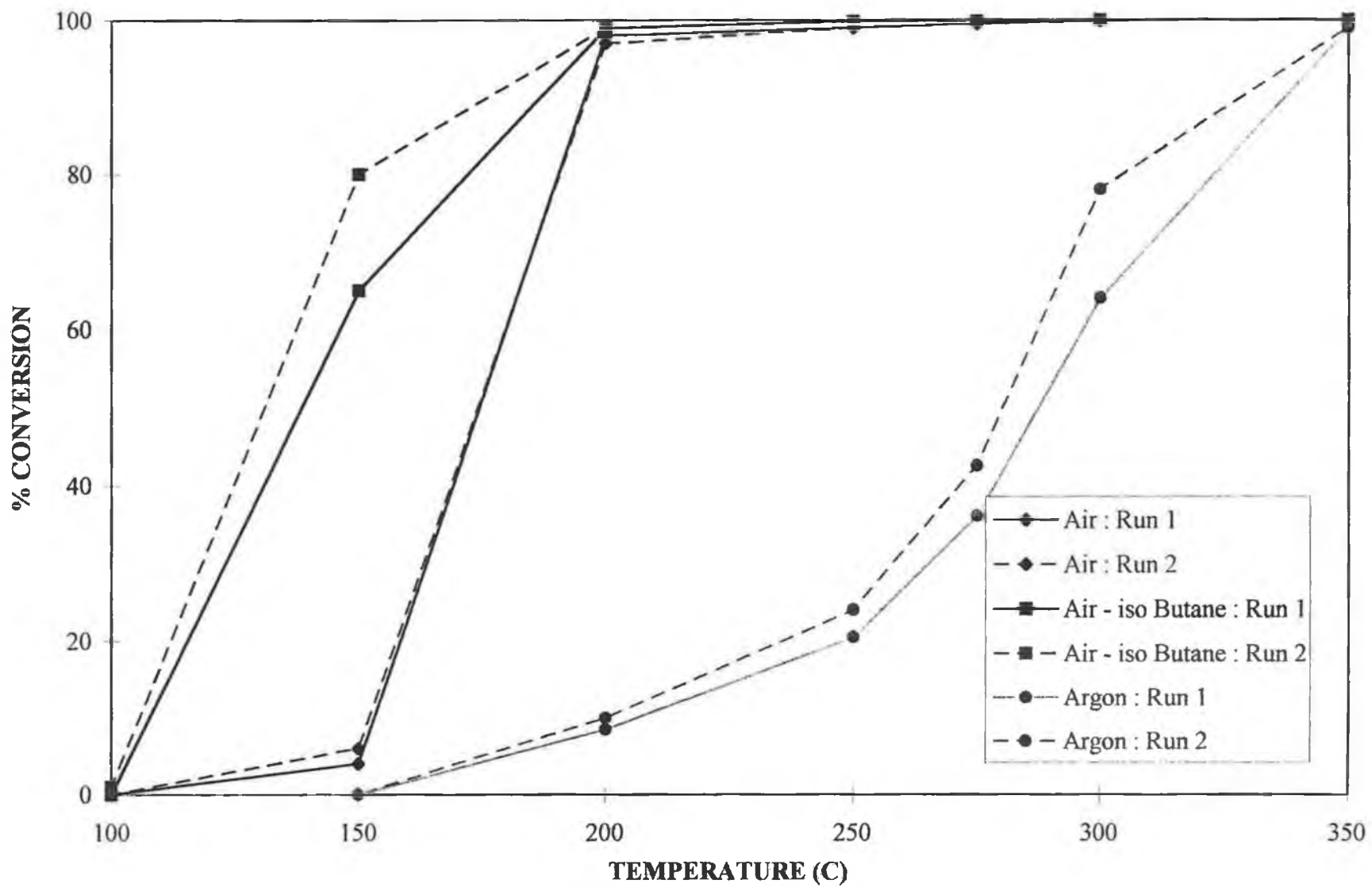


Fig. 4.11 : % iso-Butane Conversion versus Temperature for Sample PMn10A after aging in various atmospheres.

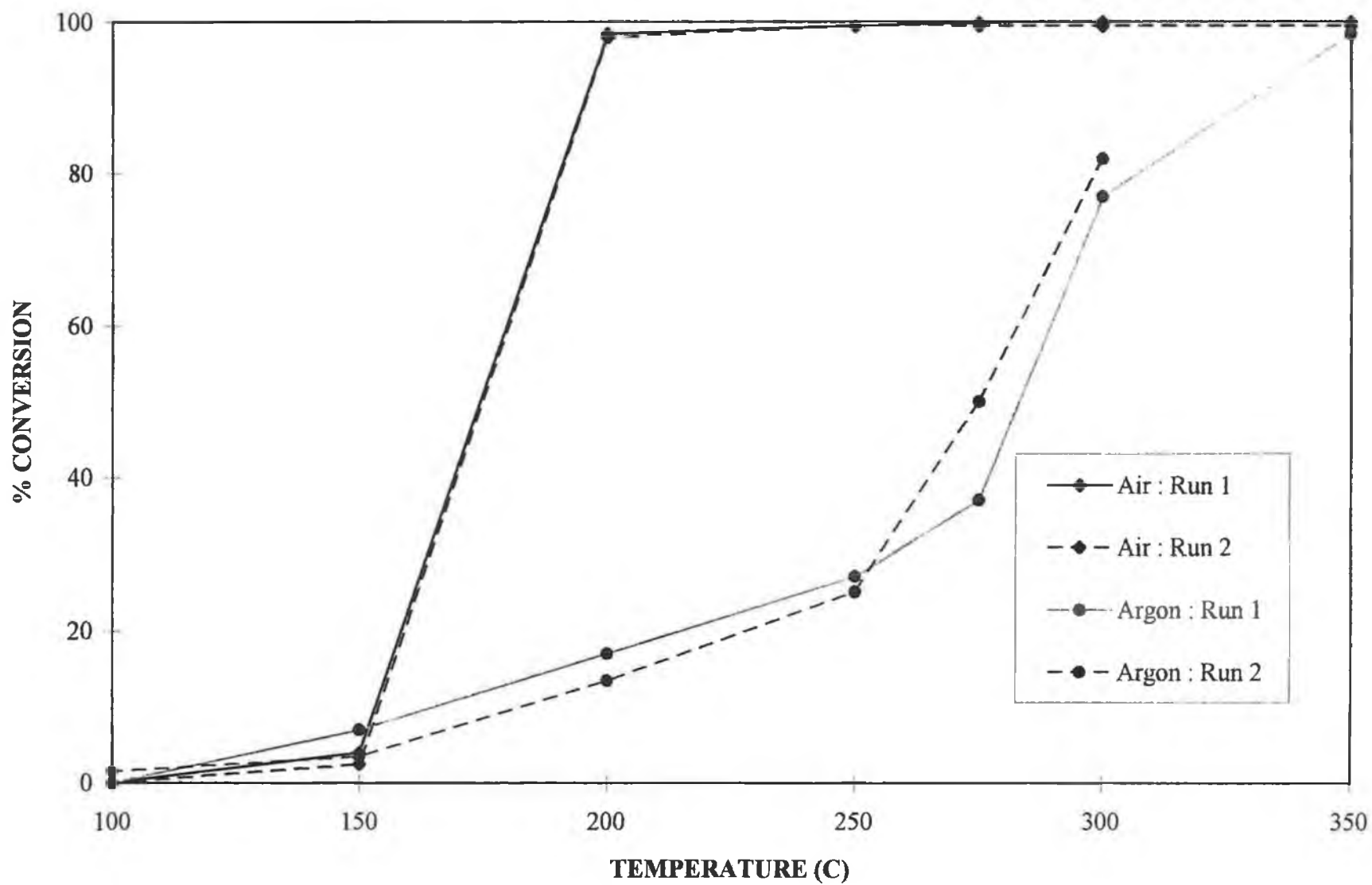


Fig. 4.12 : % iso-Butane Conversion versus Temperature for Sample PZr10A after aging in various atmospheres

**Table 4.9 :** Temperatures (°C) of 50% Iso-Butane Conversion over Catalyst Samples after Aging in Various Atmospheres.

Sample	Fresh*		Air-Aged		Air:i-C <sub>4</sub> H <sub>10</sub> -Aged		Argon-Aged	
	Run 1	Run 2	Run 1	Run 2	Run 1	Run 2	Run 1	Run 2
PA	260	255	125	125	130	130	260	220
PCr10A	260	230	180	215	165	165	255	260
PMn10A	260	215	175	175	140	130	290	280
PZr10A	320	305	175	175	ND	ND	285	275

**Table 4.10 :** Temperatures (°C) of 90% Iso-Butane Conversion over Catalyst Samples after Aging in Various Atmospheres.

Sample	Fresh*		Air-Aged		Air:i-C <sub>4</sub> H <sub>10</sub> -Aged		Argon-Aged	
	Run 1	Run 2	Run 1	Run 2	Run 1	Run 2	Run 1	Run 2
PA	270	270	145	150	150	150	290	270
PCr10A	275	270	200	245	200	195	300	295
PMn10A	270	245	195	195	190	180	340	330
PZr10A	>350	>350	195	195	ND	ND	335	>300

\* Fresh i.e. After calcination at 630°C

ND = not determined

From Tables 4.8 to 4.10, it can be seen that the activity of all Al<sub>2</sub>O<sub>3</sub>-supported samples increased after aging in air with lower temperatures required for 10, 50 and 90% conversion of i-C<sub>4</sub>H<sub>10</sub> compared with the fresh calcined catalysts. The results obtained indicate that larger Pt particles in the air-aged samples were more active than the highly dispersed Pt present after calcination at 630°C. Thus, it can be concluded that the oxidation of i-C<sub>4</sub>H<sub>10</sub> on Pt/Al<sub>2</sub>O<sub>3</sub> is a structure sensitive reaction both in the presence and absence of Cr, Mn or Zr additives. As discussed in section 3.3.3, the oxidation of alkanes on Pt/Al<sub>2</sub>O<sub>3</sub> catalysts has been previously reported in several studies to be a structure sensitive reaction with larger Pt crystallites showing greater activity than highly dispersed Pt (10, 11, 16-19).

The activity of air-aged PA was higher than that of air-aged PCr10A, PMn10A and PZr10A. Thus, the presence of Mn, Cr or Zr at ten times the atomic ratio of Pt had an adverse effect on the activity of 0.5 wt.% Pt/Al<sub>2</sub>O<sub>3</sub> after aging in air. The conversion curves for all three air-aged bimetallic samples were similar during initial testing in Run

1. However, the activity of PCr10A (Fig. 4.10) decreased during Run 2, while that of PMn10A (Fig. 4.11) and PZr10A (Fig. 4.12) was unchanged after the initial run.

Turnover numbers (TON) for the fresh and air-aged samples at 150°C and 275°C are compared in Tables 4.11 and 4.12 in terms of the percentage iso-butane conversion per surface Pt atom. As discussed in section 3.3.3, particular care must be taken in comparing TON values for aged samples due to considerable error margins introduced into the determination of the number of surface Pt sites by the low levels of H<sub>2</sub> chemisorption after aging. This is particularly true for the TON values in Table 4.12 because almost 100% conversion of i-C<sub>4</sub>H<sub>10</sub> was achieved on all air-aged samples at 275°C. Thus, differences in Pt site activity for the air-aged samples at 275°C are solely due to variations in H<sub>2</sub> uptake. However, the increases in TON values for Al<sub>2</sub>O<sub>3</sub>-supported samples after aging help to give some indication of the structure-sensitive nature of the reaction. For example, Pt site activity for sample PCr10A at 150°C was increased by a factor of at least 25 after aging in air.

**Table 4.11 : Turnover Numbers for Catalysts after Aging in Various Atmospheres. [(% conversion per surface Pt atom at 150°C) × 10<sup>-17</sup>]**

Sample	Fresh*		Air-Aged	
	Run 1	Run 2	Run 1	Run 2
PA	0.00	0.09	23.31	22.60
PCr10A	0.00	0.10	2.47	3.71
PMn10A	---	---	1.24	1.86
PZr10A	0.00	0.02	1.77	1.11

\* Fresh i.e. After impregnation and calcination at 630°C

**Table 4.12 : Turnover Numbers for Catalysts after Aging in Various Atmospheres. [(% conversion per surface Pt atom at 275°C) × 10<sup>-17</sup>]**

Sample	Fresh*		Air-Aged	
	Run 1	Run 2	Run1	Run 2
PA	1.76	1.84	23.79	23.79
PCr10A	2.20	2.23	123.29	123.29
PMn10A	---	---	30.99	30.99
PZr10A	0.47	0.40	44.28	44.10

After aging in the stoichiometric air :  $i\text{-C}_4\text{H}_{10}$  mixture, the activity of samples PCr10A and PMn10A was also increased relative to that of the unaged samples. Again, the aged samples were less active than sample PA after equivalent pretreatment. This was particularly true for sample PCr10A. The activity of sample PMn10A was comparable to that of PA in terms of  $T_{10}$  and  $T_{50}$ , but the bimetallic sample was less active at higher temperatures (see Tables 4.8-4.10).

As discussed in section 3.3.3, aging in the stoichiometric oxidation mixture at  $800^\circ\text{C}$  was expected to cause Pt sintering which was probably associated with the increased activity after aging for samples PCr10A and PMn10A. However for both catalysts, and in particular for PMn10A, samples aged in the oxidation mixture were more active than those aged in air as can be seen from Fig. 4.10 and Fig. 4.11. This suggests that the presence of iso-butane in the aging mixture was important in achieving maximum activation. This was not the case with sample PA which had similar activity after aging in air and in the air :  $i\text{-C}_4\text{H}_{10}$  mixture (see Fig. 3.45). As discussed above, the activity of fresh calcined samples of PCr10A and PMn10A was also improved after initial testing in the air :  $i\text{-C}_4\text{H}_{10}$  mixture, with greater activation seen for PMn10A. A similar order was seen after aging in the test mixture (see Tables 4.8-4.10). The increased activity for the Pt-Mn and Pt-Cr samples after exposure to the air :  $i\text{-C}_4\text{H}_{10}$  reactants may be related to a change in the Pt particle morphology which resulted in the exposure of more favourable crystal faces for the oxidation reaction as well as an increase in Pt particle size. As discussed in section 3.3.3, changes in Pd particle morphology during reaction have been previously proposed to explain increases in  $\text{CH}_4$  oxidation activity during testing (12, 13, 20, 21). Baldwin and Burch (12, 13) noted that C-deposition may also have affected changes in Pd activity observed during reaction. However, C-deposition has been reported by other authors to result in decreased activity of noble metal catalysts during hydrocarbon oxidation (22, 23) and therefore would be an unlikely explanation for the increases in activity observed on exposure to the air :  $i\text{-C}_4\text{H}_{10}$  reaction.

The low temperature activity of samples PMn10A, PCr10A and PZr10A was increased after aging in Ar with 10%  $i\text{-C}_4\text{H}_{10}$  conversion achieved at lower temperatures over all samples during Run 1 after aging compared with the initial activity of the calcined samples.  $T_{50}$  and  $T_{90}$  values were also improved for sample PZr10A after aging in the inert atmosphere. However, the activity of samples PCr10A, and in particular PMn10A, were adversely affected at higher temperatures with  $T_{90}$  shifted to higher values for PMn10A, PCr10A and PZr10A relative to PA.

Further investigation of the catalysts using surface sensitive techniques, and in particular XPS and XRD, would have been required to allow more speculation on the nature of the proposed bimetallic interactions in these catalysts. For example, it would be interesting to elucidate the effects, if any, of the additive metals on the oxidation state of surface Pt sites. TPR profiles indicated that Pt promoted surface reduction of Mn and Cr oxides. It would, therefore, be interesting to investigate the possibility of involvement of redox reactions of the metal oxides in the enhanced conversions of  $i\text{-C}_4\text{H}_{10}$  observed under certain conditions. The possibility of electron transfer from Pt to the additive metal which would be expected to promote reduction of the latter and promote the involvement of lattice oxygen in the reaction can not be discounted. However in the absence of XPS analysis, any such theory would be highly speculative especially as the Mn and Cr oxide phases present were not determined. XRD analysis would be needed to identify the additive oxide phases present (i.e. the values of  $x$  and  $y$  in the metal oxide formula  $\text{M}_x\text{O}_y$ ). It would then be possible to predict the possible direction of any electron transfer expected between Pt and the additive metal based on the reduction potentials for the metal ions.

## **4.4 Conclusions**

The effects of the metal oxide (Cr, Mn, Zr) additives on the  $i\text{-C}_4\text{H}_{10}$  oxidation activity of  $\text{Pt}/\text{Al}_2\text{O}_3$  varied for the different metals. For a given oxide, the effects on catalyst activity depended on the loading used and the conditions to which the catalysts were exposed prior to testing. In general, the activity of the Pt catalysts increased after initial testing in the reactant mixture which may have been associated with a change in the nature of catalytic sites on the catalyst surface during reaction.

TPR profiles of  $\text{Al}_2\text{O}_3$ -supported Pt-Cr, Pt-Mn and Pt-Zr catalysts indicated the existence of an interaction between Pt and the additive metal which affected the reducibility of surface species by  $\text{H}_2$ . Further investigation of the samples using other surface-sensitive techniques such as XPS and XRD would be required to gain more information about the nature of such interactions.

After impregnation and calcination at  $630^\circ\text{C}$ , monometallic  $\text{Pt}/\text{Al}_2\text{O}_3$  was at least as active as the bimetallic samples and was generally more active. The only exception to this general trend was a Pt-Mn (atomic ratio = 1 : 1) sample which was more active than the Pt-only sample in terms of light-off and the temperature required for 10% conversion of  $i\text{-C}_4\text{H}_{10}$ .  $\text{Mn}/\text{Al}_2\text{O}_3$  and  $\text{Cr}/\text{Al}_2\text{O}_3$  samples both catalysed  $i\text{-C}_4\text{H}_{10}$  oxidation in the temperature range investigated. Hence, contributions of the transition metals to the overall activity of Pt-Mn and Pt-Cr samples were expected. The initial activity of Pt-Cr and Pt-Mn samples was lower than that predicted from the individual activity of  $\text{Pt}/\text{Al}_2\text{O}_3$ ,  $\text{Mn}/\text{Al}_2\text{O}_3$  and  $\text{Cr}/\text{Al}_2\text{O}_3$  catalysts containing the same metal loadings. This indicated the existence of detrimental effects of bimetallic interaction in the calcined catalysts.

Activation of  $\text{Pt-Mn}/\text{Al}_2\text{O}_3$  and  $\text{Pt-Cr}/\text{Al}_2\text{O}_3$  samples with a Pt : TM (TM = transition metal) atomic ratio of 1 : 10 was greater than that of  $\text{Pt}/\text{Al}_2\text{O}_3$  during testing of the calcined samples. Because of this, these bimetallic samples were more active than  $\text{Pt}/\text{Al}_2\text{O}_3$  at certain temperatures during retesting even though they may have been less active initially. The presence of Mn and Cr at ten times the atomic level of Pt also led to improvements in activity after pre-reduction in a 5%  $\text{H}_2/95\%$  Ar mixture. The activity of  $\text{Pt}/\text{Al}_2\text{O}_3$ ,  $\text{Pt-Mn}/\text{Al}_2\text{O}_3$  and  $\text{Pt-Cr}/\text{Al}_2\text{O}_3$  samples decreased upon reduction at  $500^\circ\text{C}$ . However, deactivation was most significant for the Pt-only sample.

The activity of a  $\text{Pt-Zr}/\text{Al}_2\text{O}_3$  (atomic ratio, Pt : Zr = 1 : 10) catalyst was lower than that of  $\text{Pt}/\text{Al}_2\text{O}_3$  both before and after catalyst reduction.

The effects of aging in various atmospheres on the activity of the catalysts was examined. The oxidation of  $i\text{-C}_4\text{H}_{10}$  on Pt-Mn, Pt-Cr and Pt-Zr (Pt : TM = 1 : 10) samples was found to be a structure sensitive reaction. Sintered Pt crystallites present after aging in an  $\text{O}_2$ -containing atmosphere were more active than highly dispersed smaller Pt particles present in the unaged samples. The activity of the aged bimetallic samples was less than that of Pt/ $\text{Al}_2\text{O}_3$  after equivalent aging treatment. For Pt-Mn and Pt-Cr catalysts, aging in the stoichiometric air :  $i\text{-C}_4\text{H}_{10}$  reaction mixture produced a greater increase in activity than aging in static air which may have been associated with a strong change in the nature of surface active sites for these samples during the oxidation reaction.

## REFERENCES

- (1) Spivey, J. J., in "Catalysis" (Bond, G. C. and Webb, G., eds.), The Royal Society of Chemistry, Cambridge, UK, 1989.
- (2) Zwinkels, M. F. M., Järås, S. G. and Menon, P. G., *Catal. Rev. Sci. Eng.* **35**, 319 (1993).
- (3) Kummer, J. T., *Prog. Energy Combust. Sci.* **6**, 177 (1980).
- (4) Anderson, R. B., Stein, K. C., Feenan, J. J. and Hofer, L. J. E., *Ind. Eng. Chem.* **53**, 809 (1961).
- (5) Stein, K. C., Feenan, J. J., Thompson, G. P., Shultz, J. F., Hofer, L. J. E. and Anderson, R. B., *Ind. Eng. Chem.* **52**, 671 (1960).
- (6) Morooka, Y. and Ozaki, A., *J. Catal.* **5**, 116 (1966).
- (7) Morooka, Y., Morikawa, Y. and Ozaki, A., *J. Catal.* **7**, 23 (1967).
- (8) Summers, J. C. and Ausen, S. A., *J. Catal.* **58**, 131 (1979).
- (9) Anderson, J. R. and Pratt, K. C., "Introduction to Characterization and Testing of Catalysts", 203-256, Academic Press, Australia, 1985.
- (10) Hicks, R. F., Qi, H., Young, M. L. and Lee, R. G., *J. Catal.* **122**, 280 (1990).
- (11) Völter, J., Lietz, G., Spindler, H. and Lieske, H., *J. Catal.* **104**, 375 (1987).
- (12) Baldwin, T. R. and Burch, R., *Appl. Catal.* **66**, 337 (1990).
- (13) Baldwin, T. R. and Burch, R., *Appl. Catal.* **66**, 359 (1990).
- (14) Hubbard, C. P., Otto, K., Gandhi, H. S. and Ng, K. Y. S., *J. Catal.* **139**, 268 (1993).
- (15) Hubbard, C. P., Otto, K., Gandhi, H. S. and Ng, K. Y. S., *J. Catal.* **144**, 484 (1993).
- (16) Yu-Yao, Y. F., *Ind. Eng. Chem. Prod. Res. Dev.* **19**, 293 (1980).
- (17) Briot, P., Auroux, A., Jones, D. and Primet, M., *Appl. Catal.* **59**, 141 (1990).
- (18) Otto, K., *Langmuir* **5**, 1364 (1989).
- (19) Otto, K., Andino, J. M. and Parks, C. L., *J. Catal.* **131**, 243 (1991).
- (20) Briot, P. and Primet, M., *Appl. Catal.* **68**, 301 (1991).
- (21) Ribeiro, F. H., Chow, M. and Dalla Betta, R. A., *J. Catal.* **146**, 537 (1994).
- (22) Kooh, A. B., Han, W. J., Lee, R. G. and Hicks, R. F., *J. Catal.* **130**, 374 (1991).
- (23) Carballo, L. M. and Wolf, E. E., *J. Catal.* **53**, 366 (1978).

## **CONCLUSIONS**

## 5 Conclusions

The main focus of this thesis was on the investigation of supported Pt (0.5 wt.%) and bimetallic catalysts for the combustion of iso-butane. A variety of catalysts were investigated and attempts were made to associate particular surface characteristics with combustion efficiency. In particular, the effects of Ce addition to Pt/Al<sub>2</sub>O<sub>3</sub> systems was investigated.

The use of Ce, Cr or Mn additives was found to be potentially beneficial for the iso-butane oxidation activity of Pt/Al<sub>2</sub>O<sub>3</sub>. The effects of the different metal oxide additives varied. For a given oxide, the effects on catalyst activity depended on the loading used, the sequence of impregnation of the two metals and the conditions to which the catalysts were exposed prior to testing. In general, the activity of the Pt catalysts increased after initial testing in the reactant mixture which may have been associated with a change in the nature of catalytic sites on the catalyst surface during reaction. The oxidation of i-C<sub>4</sub>H<sub>10</sub> on Al<sub>2</sub>O<sub>3</sub>-supported Pt was found to be a structure sensitive reaction with sintered Pt crystallites more active than highly dispersed smaller Pt particles. This was true both in the presence or absence of Ce, Mn, Cr and Zr.

TPR showed that addition of Ce, Cr, Mn or Zr to Pt/Al<sub>2</sub>O<sub>3</sub> resulted in a bimetallic surface interaction which affected the reduction profiles obtained. For Pt-Ce catalysts, XPS analysis of the Pt 4d spectra indicated that the nature of this electronic interaction varied depending on the level of Ce. At a Ce : Pt atomic ratio of 10 : 1, Pt surface sites appeared to be more oxidised relative to monometallic Pt/Al<sub>2</sub>O<sub>3</sub>, while the presence of Ce at an atomic ratio of 0.5 : 1 resulted in decreased oxidation of surface Pt. XPS spectra indicated that Pt was oxidised on the surface and was present as Pt<sup>2+</sup> (PtO) rather than Pt<sup>4+</sup> (PtO<sub>2</sub>) in both Pt/Al<sub>2</sub>O<sub>3</sub> and Pt/CeO<sub>2</sub> catalysts after calcination at 630° C. For Pt/CeO<sub>2</sub>, the typical spectral features of Ce<sup>4+</sup> were exhibited. However, for Al<sub>2</sub>O<sub>3</sub>-supported samples, the Ce 3d spectra obtained more closely resembled that of Ce<sup>3+</sup> than Ce<sup>4+</sup> indicating strong interaction of dispersed Ce with the support material.

After impregnation and calcination, the presence of Ce, at atomic Ce : Pt ≥ 8 : 1, resulted in poorer performance relative to Pt/Al<sub>2</sub>O<sub>3</sub> with higher temperatures required to achieve the same level of i-C<sub>4</sub>H<sub>10</sub> conversion.. The only exception to this general trend was a Pt-Ce/Al<sub>2</sub>O<sub>3</sub> (Ce : Pt = 8 : 1) sample in which Pt impregnation preceded that of Ce. Pt/CeO<sub>2</sub> was also less active than Pt/Al<sub>2</sub>O<sub>3</sub> after calcination in air. However, at lower Ce loadings (Ce : Pt ≤ 1 : 1), oxidation activity was not so adversely affected and one sample, containing 0.29 wt.% Ce, was found to be noticeably more active than monometallic Pt/Al<sub>2</sub>O<sub>3</sub>. The effects of Ce addition on the activity of Pt can be attributed to the existence of a bimetallic interaction, which affected the activity of the noble metal,

since Ce/Al<sub>2</sub>O<sub>3</sub> did not appreciably catalyse i-C<sub>4</sub>H<sub>10</sub> oxidation in the temperature range investigated. Activation of the calcined catalysts during testing was greater for some Ce-containing samples than for Pt/Al<sub>2</sub>O<sub>3</sub> with the result that Pt/CeO<sub>2</sub> and, some Pt-Ce/Al<sub>2</sub>O<sub>3</sub>, catalysts were more active than Pt/Al<sub>2</sub>O<sub>3</sub> at certain temperatures during retesting even though they may have been less active initially. Activity data, for catalysts which were pre-reduced in a 5% H<sub>2</sub>-95% Ar mixture, strongly suggested that Pt-Ce interactive surface sites were more active than Pt-Al<sub>2</sub>O<sub>3</sub> sites, after equivalent reduction treatments. The stability of the Pt-Ce interaction during i-C<sub>4</sub>H<sub>10</sub> oxidation tests increased with increasing Ce concentration, at least up to 3.6 wt.% (Ce : Pt = 10 : 1).

The most active Pt/Al<sub>2</sub>O<sub>3</sub> catalysts were obtained after aging in the stoichiometric air : i-C<sub>4</sub>H<sub>10</sub> oxidation mixture or in a static air atmosphere at 800°C. H<sub>2</sub> chemisorption results suggested that the main effect of aging was to increase Pt particle size. The reaction was concluded to be structure sensitive with sintered Pt crystallites being more active than highly dispersed Pt. The activity of Pt/Al<sub>2</sub>O<sub>3</sub> was greater after aging in air or in the reaction mixture than after aging in Ar. This indicated a need for O<sub>2</sub> in the aging atmosphere to achieve optimum activation even though XPS and TPR both indicated that an increase in the metallic character of surface Pt after aging in O<sub>2</sub>-containing atmospheres at 800°C was concomitant with a considerable increase in activity. For samples aged in air, or in the oxidation reaction mixture, Pt/Al<sub>2</sub>O<sub>3</sub> was more active than Pt-Ce/Al<sub>2</sub>O<sub>3</sub>, Pt-Mn/Al<sub>2</sub>O<sub>3</sub>, Pt-Cr/Al<sub>2</sub>O<sub>3</sub> or Pt-Zr/Al<sub>2</sub>O<sub>3</sub> catalysts at an additive metal : noble metal atomic ratio of 10 : 1. However after aging in an inert (Ar) atmosphere, the Pt-Ce/Al<sub>2</sub>O<sub>3</sub> catalyst was more active than Pt/Al<sub>2</sub>O<sub>3</sub>. The Pt-Mn catalyst was the most active of the bimetallic samples after aging in the air : i-C<sub>4</sub>H<sub>10</sub> oxidation mixture.

After impregnation and calcination at 630°C, a 0.5 wt.% Pt/ZrO<sub>2</sub> catalyst was considerably more active than 0.5 wt.% Pt/Al<sub>2</sub>O<sub>3</sub>. After aging in air, both catalysts had similar activity. The Al<sub>2</sub>O<sub>3</sub>-supported sample was more active after aging in the oxidation mixture. Addition of 2.3 wt.% Zr to a 0.5 wt.% Pt/Al<sub>2</sub>O<sub>3</sub> had a detrimental effect on catalyst activity. Therefore, it was concluded that the greater activity of unaged Pt/ZrO<sub>2</sub> relative to that of Pt/Al<sub>2</sub>O<sub>3</sub> was due to the presence of larger Pt particles on the former support due to its' considerably lower surface area.

The results of the present study show that the use of Ce, Mn and Cr additives in Pt/Al<sub>2</sub>O<sub>3</sub> catalysts can have a beneficial effect on alkane oxidation activity. The use of Mn and Cr additives was only briefly investigated in the present study but the potential benefits observed for both of these systems, as well as for Ce, warrants further study. The

long term aim of such studies would involve attempts to find practical applications where catalyst performance can be enhanced by the incorporation of the additives at certain defined levels in the catalyst composition.

From this study, it can be concluded that the presence of metal oxides can enhance the  $i\text{-C}_4\text{H}_{10}$  oxidation activity of unaged Pt catalysts particularly after activation in the reaction mixture or after pre-reduction. The oxidation of  $i\text{-C}_4\text{H}_{10}$  is a structure sensitive reaction which was favoured on larger Pt crystallites rather than highly dispersed Pt. The presence of Ce, Mn, Cr and Zr additives in Pt/ $\text{Al}_2\text{O}_3$  catalysts at an additive : noble metal atomic ratio of 10 : 1 appeared to prevent the achievement of the optimum activity of these larger Pt crystallites under the conditions used for catalyst preparation, aging treatments and oxidation activity tests. The effects of the additive metals on the performance of sintered samples may, however, be different if alternative loadings of the additive metal were employed or under different reaction or pretreatment conditions as was the case for unaged samples. It would be particularly interesting to determine if catalyst reduction prior to aging had an effect on the activity of the aged catalysts. A more detailed analysis of the catalysts using XPS and other surface-sensitive techniques may also provide more information on the effects of the additive metals, and of pretreatment conditions, on the nature of the catalytic sites involved. It is believed that further investigation of the supported Pt catalysts for the combustion of other reactants is warranted. For example, the effects of the different aging treatments on catalyst activity for  $\text{CH}_4$  activity might be different to those observed for the more facile oxidation of higher alkanes such as  $i\text{-C}_4\text{H}_{10}$ . In addition, it would be interesting to see if there are any beneficial effects of Ce, Cr and Mn additives on the oxidation of  $\text{CH}_4$  over Pt catalysts.

## Appendix A

### Basis of Surface Area Determination by N<sub>2</sub> Physisorption

The physical adsorption of a gas on a solid surface can be described by the BET equation (1), one form of which reads as follows:

$$(P/P_0)/V[1-(P/P_0)] = [1/(V_m C)] + [(C-1)/(V_m C)]P/P_0 \quad (1)$$

where  $V$  = volume of gas adsorbed at STP,

$P$  = gas pressure,

$P_0$  = saturated vapour pressure of liquified gas at the adsorbing temperature,

$V_m$  = volume of gas (at STP) required to form an adsorbed monolayer,

$C$  = a constant related to the energy of adsorption.

The surface area,  $S$ , of a sample which has a monolayer of adsorbed gas of volume,  $V_m$ , can be calculated from:

$$S = V_m AN/M \quad (2)$$

where  $A$  = Avogadro's number =  $6.023 \times 10^{23}$  molecules/mole of gas,

$N$  = area of each adsorbed gas molecule =  $16.2 \times 10^{-20}$  m<sup>2</sup>/molecule for N<sub>2</sub>,

$M$  = molar volume of gas = 22414 cm<sup>3</sup>/mole.

### Multipoint Surface Area Determination

From equation (1), it can be seen that by plotting values for  $(P/P_0)/V[1-(P/P_0)]$  on the ordinate against  $P/P_0$  on the abscissa, the slope and intercept of the resulting straight line, gives values for  $(C-1)/(V_m C)$  and  $1/(V_m C)$  respectively. The surface area,  $S$ , can be obtained using equation (2):-

$$S = 6.023 \times 10^{23} \times 16.2 \times 10^{-20} / (22414 \times (\text{slope} + \text{intercept}))$$

This allows for multipoint surface area determinations from physisorption data.

### Single Point Surface Area Determination

Previous results from this laboratory (2) have shown that the use of a single point physisorption measurement allows the determination of sample surface areas which are in good agreement with values measured using the multipoint procedure. The use of a single point procedure also allows for considerable savings in time and effort and was therefore employed in the current study.

The constant C in equation (1) is typically a relatively large number, i.e.  $C \gg 1$ ; using this assumption equation (1) approximates to:

$$(P/P_0)/V[1-(P/P_0)] = (1/V_m)[(1/C) + (P/P_0)]$$

If  $P/P_0 \gg 1/C$ , this equation reduces to:

$$(P/P_0)/V[1-(P/P_0)] = (1/V_m)(P/P_0)$$

Rearranging for  $V_m$  leads to:

$$V_m = V[1-(P/P_0)].$$

Substituting this equation for  $V_m$  into equation (2) leads to:

$$S = VAN[1-(P/P_0)]/M.$$

Taking into account standard temperature and pressure, i.e. STP, the surface area of a given volume of  $N_2$ , V, can be calculated as follows:

$$S = \frac{V \times 273.2 \times \text{Atm.Press.} \times 6.023 \times 10^{23} \times 16.2 \times 10^{-20} \times [1-(\%N_2/100)] \times \text{Atm.Press.}}{\text{Room Temp.} \times 760 \times 22414 \times \text{Saturated Press.}}$$

$$= V \times \text{constant.}$$

This is the basis for the single point surface area determination used in this study.

For calibration purposes, this means that a volume,  $V = 1 \text{ cm}^3$ , of  $N_2$  injected at  $22^\circ\text{C}$  and 760 mmHg results in a constant having a value of 2.76 at a  $\%N_2$  of 30%, assuming a saturation pressure of 775 mmHg. The value of the constant changes with changes in ambient temperature and pressure. Hence the instrument has to be recalibrated prior to each surface area analysis by injection of  $1 \text{ cm}^3$  of  $N_2$  under the prevailing conditions of room temperature and pressure. In this manner, the surface area of a sample can be calculated using only one pressure of  $N_2$ . In this study, a 30%  $N_2/\text{He}$  mix was used as the analysis gas.

## REFERENCES

- (1) Scholten, J. J. F., in "*Catalysis*" (Moulijn, J. A., van Leeuwen, P. W. N. M. and van Santen, R. A., eds.), *Studies in Surface Science and Catalysis*, Vol. 79, 419-438, Elsevier, Amsterdam, 1993.
- (2) Curley, J. W., Doctoral Thesis, "*Oxidation Studies on Supported Metal Catalysts*", Dublin City University, March 1995

## Appendix B

### Calculation of Pt Surface Area, Dispersion and Particle Size from H<sub>2</sub> Chemisorption Measurement

The free metal surface area, % metal dispersion, and metal particle size can be calculated from H<sub>2</sub> chemisorption measurements using the following equations, assuming that one hydrogen atom is adsorbed by each surface Pt atom. Another factor which must be assumed is the number of Pt surface atoms per unit area of the polycrystalline surface being investigated. If the surface consists of equal proportions of (111), (110), (100) planes, then there are  $1.25 \times 10^{19}$  Pt particles per m<sup>2</sup>. This is the surface assumed by most investigators (1, 2). It has also been postulated that the morphology of face-centred cubic metals of small crystallite size corresponds to the exposition of 70% (111) planes, 25% (100) planes, and 5% (110) planes (2). For this latter supposition, there are  $1.42 \times 10^{19}$  Pt surface atoms per m<sup>2</sup> of the polycrystalline surface. For the purpose of this study, a value of  $1.25 \times 10^{19}$  Pt particles per m<sup>2</sup> was assumed to allow comparison of Pt surface areas in the different catalyst samples.

#### Pt Surface Area

The Pt surface area was calculated using the relationship;

$$S_{Pt} = n_m \cdot X_m \cdot A \cdot n_s^{-1} \quad (1)$$

where,  $S_{Pt}$  = Pt surface area,

$n_m$  = number of moles of H<sub>2</sub> adsorbed,

$X_m$  = average number of moles of surface Pt associated with adsorption of each mole of H<sub>2</sub> i.e.  $X_m = 2$ ,

$A$  = Avogadro's number =  $6.023 \times 10^{23}$  atoms/mole of Pt,

$n_s$  = number of Pt atoms per unit area of surface =  $1.25 \times 10^{19}$  atoms m<sup>-2</sup>.

In order to calculate  $n_m$ , the volume of  $H_2$  adsorbed i.e.  $V_{ads}$  must firstly be calculated. Under the conditions used,

$$V_{ads} \text{ (cm}^3\text{)} = [101\% \text{ of P.A.1} - \text{P.A.2} / 101\% \text{ of P.A.1}] \times 0.053 \quad (2)$$

where P.A.1 = entrance peak area

P.A.2 = exit peak area

101% = (average ratio of exit peak area to entrance peak area in blank reactor tests)  $\times$  100.

0.053 = loop volume (cm<sup>3</sup>).

As the measurements were performed at room temperature and pressure,

$$V_{ads}g^{-1} \text{ S.T.P (cm}^3g^{-1}\text{)} = (V_{ads}/w)(273/R.T.)(R.P./760) \quad (3)$$

where  $V_{ads}g^{-1} \text{ S.T.P}$  = volume of  $H_2$  adsorbed per gram of catalyst sample at standard temperature and pressure

w = final sample weight (g)

R.T. = room temperature (K)

R.P. = atmosphere pressure (mmHg).

The number of moles of  $H_2$  adsorbed,  $n_m$ , is then given by,

$$n_m \text{ (molesg}^{-1}\text{)} = V_{ads}g^{-1} \text{ S.T.P} / 22414 \quad (4)$$

where 22414 = volume occupied by one mole of gas at S.T.P (cm<sup>3</sup>mole<sup>-1</sup>).

Substituting for  $n_m$  into equation (1) yields,

$$S_{Pt} \text{ (m}^2\text{Ptg}^{-1}\text{catalyst)} = (V_{ads}g^{-1} \text{ S.T.P} / 22414)(2 \times 6.023 \times 10^{23} / 1.25 \times 10^{19}) \quad (5)$$

Equation (5) was used to calculate the Pt surface areas in this study.

### % Dispersion

The state of subdivision of a supported metal is often defined in terms of the ratio of the total number of surface metal atoms to the total number of metal atoms present, referred to as the metallic dispersion,  $D_m$ , i.e.

$$D_m = P_{t_s}/P_{t_t} \quad (6)$$

$$\%D_m = [P_{t_s}/P_{t_t}] \times 100 \quad (7)$$

where  $P_{t_s}$  = number of Pt surface atoms

$P_{t_t}$  = total number of Pt atoms present.

Using the relations described above,  $P_{t_s}$  can be calculated as follows,

$$\begin{aligned} P_{t_s} (\text{atoms g}^{-1} \text{catalyst}) &= (V_{\text{ads}} \text{g}^{-1} \text{S.T.P}/22414)(X_m \cdot A) \\ &= (V_{\text{ads}} \text{g}^{-1} \text{S.T.P} \times 2 \times 6.023 \times 10^{23})/22414 \quad (8) \end{aligned}$$

$P_{t_t}$  can be calculated using the % Pt loading determined by Atomic absorption Spectroscopy. The number of grams of Pt per gram of catalyst is given by,

$$(1\text{g}/100) \times \% \text{ Pt} \quad (9)$$

The number of Pt atoms in one gram of Pt is equal to,

$$A/m = 6.023 \times 10^{23}/m \quad (10)$$

where  $m$  = molecular weight of Pt = 195.09 gmole<sup>-1</sup>.

Combining equations (9) and (10) leads to,

$$P_{t_t} (\text{atoms g}^{-1} \text{catalyst}) = (0.01 \times \% \text{ Pt})(6.023 \times 10^{23}/195.09) \quad (11)$$

Substituting for  $P_{t_t}$  and  $P_{t_s}$  into equation (7) yields,

$$\begin{aligned} \%D_m &= [(V_{\text{ads}} \text{g}^{-1} \text{S.T.P} \times 2 \times 6.023 \times 10^{23}/22414)/(0.01 \times \% \text{ Pt} \times 6.023 \times 10^{23} \\ &\quad /195.09)] \times 100 \quad (12) \end{aligned}$$

Equation (12) was used to calculate the dispersion of Pt in catalyst samples.

### Average Pt Particle Diameter

The average size of Pt particles was calculated by assuming that the supported particles were spherical in shape (1). The equation for the diameter,  $d$ , of a sphere is,

$$d = 6 \times (\text{volume})/(\text{surface area}) \quad (13)$$

The average Pt particle diameter was calculated using,

$$d (\text{\AA}) = (6 \times 10^4 / 21.5 \times S_{\text{Pt}}) \quad (14)$$

where  $21.5 =$  density of Pt in  $\text{g/cm}^3$  at  $25^\circ\text{C}$

$S_{\text{Pt}} =$  surface area of Pt in  $\text{m}^2\text{g}^{-1}$  of Pt.

### REFERENCES

- (1) Anderson, J.R. and Pratt, K.C., "*Introduction to Characterization and Testing of Catalysts*", Academic Press, Australia, 1985
- (2) Scholten, J.J.F., Pijpers, A.P. and Hustings, A.M.L., *Catal. Rev. -Sci. Eng.* **27**, 151 (1985)